IN-PLANE SHEAR BEHAVIOUR OF COMPOSITE WALLING WITH PROFILED STEEL SHEETING

A DISSERTATION SUBMITTED TO THE DEPARTMENT OF CIVIL ENGINEERING AND THE COMMITTEE FOR POSTGRADUATE STUDIES OF THE UNIVERSITY OF STRATHCLYDE, GLASGOW, FOR THE DEGREE OF DOCTOR OF PHILOSOPHY

BY

Khandaker Muhammed Anwar Hossain

B.Sc. Engineering (BUET, Dhaka)

M.Sc. Engineering (BUET, Dhaka)

December, 1995

Abstract

This thesis introduces a novel form of double skin composite walling with profiled steel sheeting and an infill of concrete. This is a logical extension of research on composite slabs with profiled steel sheeting currently known as popular " Fastrack" construction. The composite walling is thought to be specially applicable as shear or core walls in steel frame buildings. The profiled steel sheeting will act as a temporary shear bracing to stabilise the frame against wind and destablising forces during construction and also act as a form work for infill of concrete. In the service stage, they will act as a reinforcement to carry axial, lateral and in-plane forces.

This thesis investigates the behaviour of composite walls under in-plane shear so that they can be used as shear elements in buildings. The investigation includes analytical, numerical and small scale model tests. Design recommendations for the composite walls are the final aim of the research.

The investigation is based on the concept that the in-plane shear strength and stiffness of the composite wall will be derived from the individual sheeting, concrete core and from the interaction between the two. Based on above, individual behaviour of the sheeting and concrete core was studied before considering the composite wall as a whole. A shear rig has been designed and fabricated to carry out the model tests of approximately 1/6 th scale using very thin sheeting (profiled in house) and micro-concrete.

Analytical equations for the shear strength and stiffness of the sheeting, profiled concrete and composite wall are derived. These equations are validated by model tests and finite element analysis. Finite element analysis included modelling of composite walling with full composite action and some parametric studies using interface elements. The stiffness of the composite wall is found to be greater than the individual summation of stiffness of the sheeting and concrete core. The profiled steel sheeting will provide sufficient shear bracing to the frame during construction. The composite wall is capable of taking high in-plane shear loads which is greater than the summation of individual capacity of the sheeting and concrete and confirms its potential to be used as shear elements in buildings.

Simple equations for the calculation of shear strength and stiffness of the composite wall are derived which can safely be used for design purposes. Further research directions are also outlined.

Acknowledgements

I would like to thank my supervisor, Professor Howard D. Wright, for his support and encouragement throughout this project. His guidance and encouragement were invaluable in focusing the project on achievable goals.

I also like to thank Professor K. Z. Andrawes, Professor I.A. Macleod, Dr. W. Duncan, Dr. P. Ridgeway and Dr. Bimal Kumar for their affections and advice during my study.

I greatly appreciate the contributions of the technical staff whose helpful and practical assistance enabled the smooth running of the laboratory experiments. Mr. Jack Morrin, Mr. Joe Mclean, and Mr. John Harper showed their patience and sincerity in all the stages of my experiments. Mr. Chris Bonner provided a lot of effort in sieving fine sand for micro-concrete. I like to thank both Mr. Chris Bonner and Mr. Andy Baillie for their helping hands during my experiments. I like to acknowledge Mr. Ron Baron for his assistance in the computer room.

I would like to thank my wife Popy for her invaluable moral support and patience during this work and also my two sons, Julkar and Shabbeer for their patience. I also like to acknowledge my father and mother who provided me the basic foundation of my success.

I like to thank my colleagues Mr. Mahmoud Essawy, Dr. Stewart Gallocher, Mr. Benny Raphael, Mrs. Sun Liqing and Ms. Avril Neilson for their assistance and co-operation during the period of my study in the University of Strathclyde.

Finally I like to thank Commonwealth Scholarship Commission in UK for providing full financial support.

CONTENTS

Note: All the graphs are pasted within the text and the photographs are provided at the end of each chapters

NOTATION

Unless otherwise stated the following notation applies

b depth of panel

a width of the panel

A cross sectional area of edge member or purlins

p pitch of sheet to purlin fastener

n_s no. of seam fasteners per side laps

n_{sc} number of side fasteners or shear connector

n_f total number of sheet-purlin fasteners per sheet width

n_{sh} number of sheet widths per panel

s_s slip per seam fastener per unit load.

s slip per sheet to purlin fastener per unit load

s_{pr} slip at purlin-rafter connections per unit load

s_{sc} slip per sheet to shear connector fastener per unit load

F_s ultimate load of one of seam fastener

n_s no. of seam fasteners per side lap

F_p ultimate load of one sheet-purlin fastener

n_e no. of sheet-purlin fasteners

n_p number of purlins

s slip per sheet to purlin fastener per unit load

s_s slip per seam fastener per unit load

F_{sc} the ultimate load of individual shear connector fastener

V applied shear load

δ shear deformation

I_c moment of inertia of concrete core

E the elastic modulus of the material

t thickness

Iy the moment of inertia of one repeating corrugation about its neutral axis

ν poisson's ratio of the material of sheeting

ϕ angle of inclination of the tension field

δ_e limiting elastic shear displacement

J yield function

k_2 post-buckling stiffness

σ_t tension field stress

k_1 pre-buckling stiffness

τ_y shear yield stress of web material

f_y yield stress of the material

λ scale factor

C_t ratio of compressive to tensile strength of concrete

f'_c cylinder strength

f_{cu} cube strength

f'_t splitting tensile strength

f_r modulus of rupture

CHAPTER ONE

GENERAL INTRODUCTION

1. 1. The Development of Composite Walling

The development of composite walling using profiled steel sheeting is a logical progression from the current popular and economic use of profiled steel sheets in composite floors. Composite slabs are most commonly used in multi-storey steel-framed buildings although they may be incorporated in concrete, masonry or wood structures. They are normally located internally where corrosion is unlikely to occur under normal conditions. Maximum spans range from 2m to over 4m with deep profiles or where temporary supports are provided. Since the early 1980's the use of composite slabs in the construction industry has grown rapidly, replacing traditional reinforced concrete flooring system. For the historical development the reader is referred to papers by Viest (1960), Schuster (1976) and more recently Wright (1987).

Their present widespread popularity in "Fastrack" construction arises from the advantages of this type of construction:

The decking can be installed quickly (approximately 800m^2 per person per day) and easily poured which decreases construction time.
The sheeting provides temporary working platform that eliminates or reduce the need for temporary supports.
The sheeting acts as tensile reinforcement on the soffit of the slab, reducing substantially the overall requirements. The mesh reinforcement normally required can be easily fixed in position.
Services. The geometry of the re-entrant decking ribs allow simple installation of suspended ceilings and ventilation.
Wind bracing. Once the decking is fixed in position it provides in-plane stability to the frame.
Weight reductions. Composite slabs are normally lighter than the equivalent reinforced flooring providing savings in material, and reductions in foundation and column costs.

The profiled decks can be with re-entrant ribs and those with trapezoidal ribs as shown in figure1.1. The thickness of the decks range from 0.75mm to 1.5mm protected on both faces by 20 micron zinc coating. Embossments are pressed into the surface of the ribs and upper flanges, which provide longitudinal shear resistance at the steel concrete interface (figure 1.1).

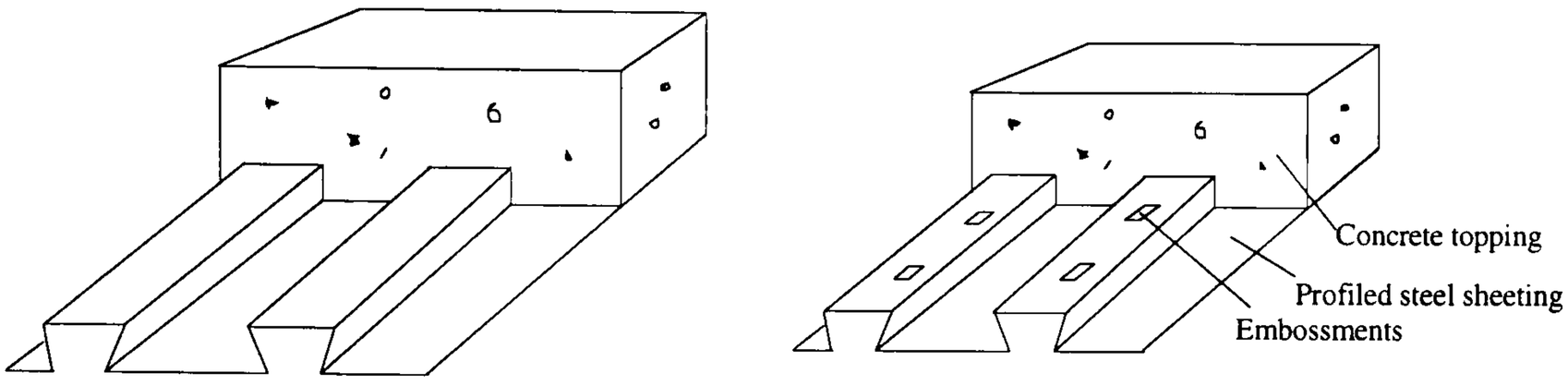

Figure 1.1 (a) Re-entrant Profile Deck with or without embossments

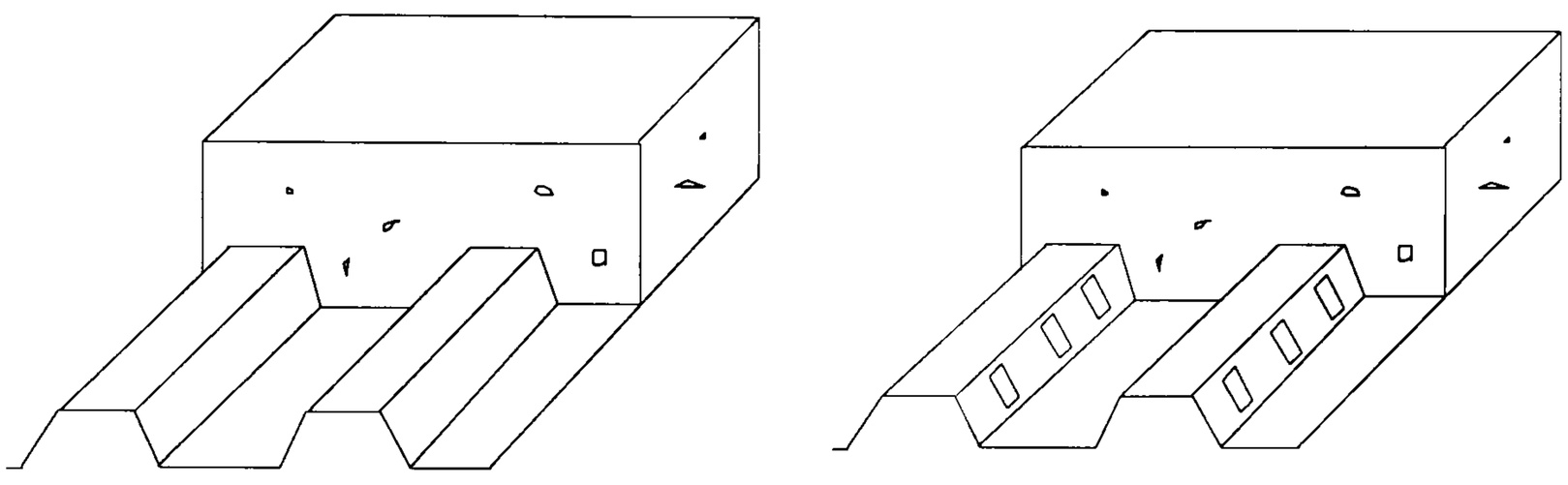

Figure 1.1(b): Trapezoidal Profile Deck with or without embossments

Based on the advantages of composite slabs, Wright, Evans and Gallocher (1992) and Gallocher (1993) proposed the concept of composite walling. Figure 1.2 shows a schematic diagram of the walling system which comprises vertically aligned profiled steel sheeting and an infill of concrete. The whaling supports are temporary and may be removed after casting.

Composite walling has many advantages when used in conjunction with composite flooring and is thought to be especially applicable to shear or core walls in steel framed buildings. The advantages of the system are thought similar to those of composite slabs:

- The steel sheeting will act as permanent form work obviating the need for expensive rebuilding of shutters

- The steel sheeting will act as reinforcement to the wall and allows the concrete to be placed without the infringing clutter of reinforcing bars associated with a reinforced concrete wall.

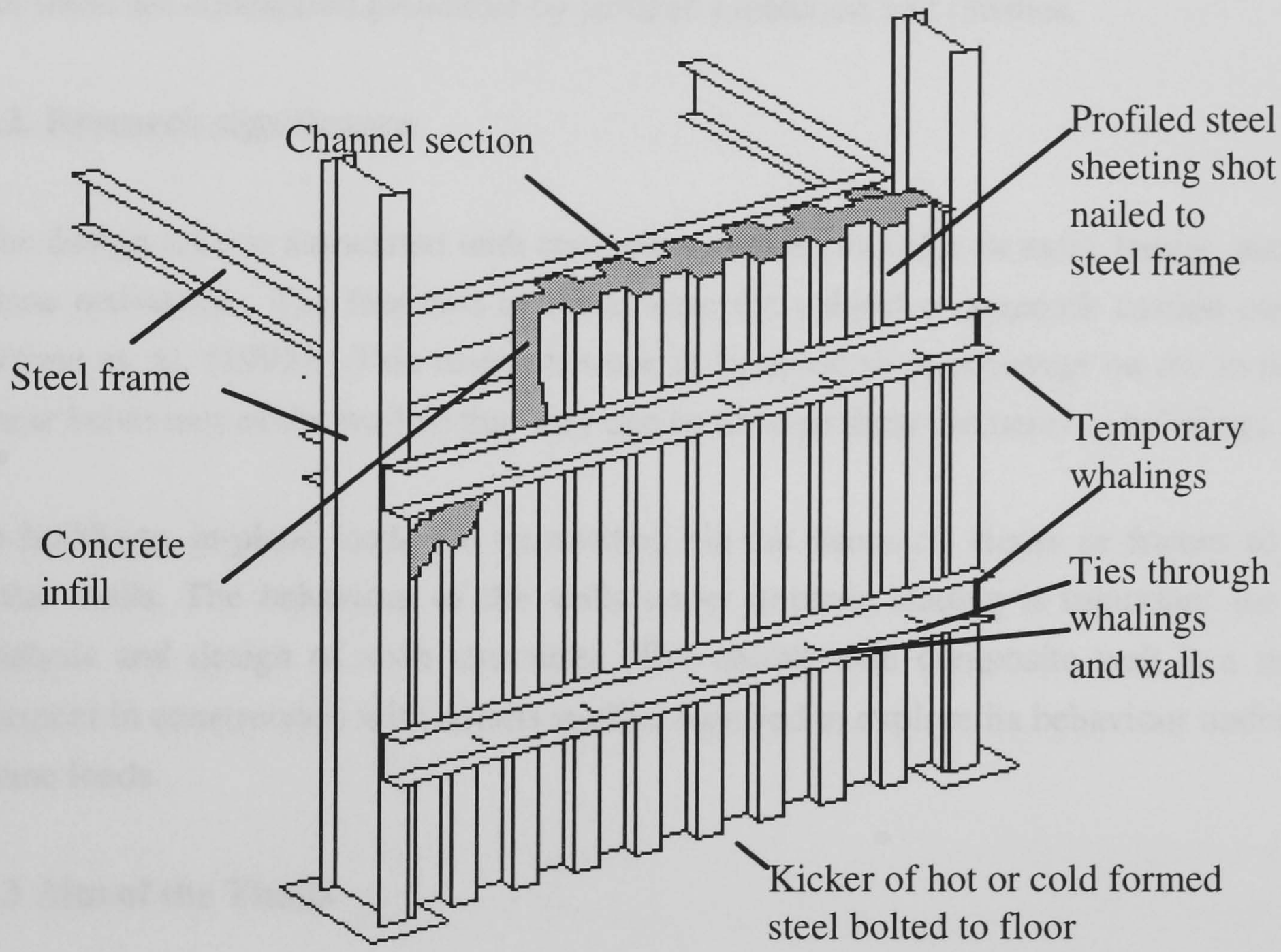

Figure 1.2 : Schematic of composite walling system

- The profiling of the steel sheets results in less concrete required for the same inertia, with a consequent weight saving, especially where slenderness is a factor.

- The bond between the concrete and steel can be improved by using embossments or by providing shear connectors.

- For steel framed buildings, the walls must be formed either before or after the steel frame is erected. In the latter case, the steel sheeting will provide temporary bracing to wind and destabilising forces during construction.

- Overall construction costs, as in composite slabs are reduced.

Certain disadvantages have also been identified such as fire and corrosion resistance but these are considered avoidable by suitable protection and finishes.

1.2. Research significance

The design criteria associated with composite walling includes its axial, lateral and in-plane resistance. The first two of these were the subject of research carried out by Wright et. al. (1992). This research work is intended to concentrate on the in-plane shear behaviour of the wall so that they can be used as shear elements in buildings.

In buildings, in-plane loads are transmitted via the structural floors or frames to the shear walls. The behaviour of the walls under in-plane loading is important for the analysis and design of such structures. The double skin composite wall is a novel element in construction with details studied required to explore its behaviour under in-plane loads.

1.3 Aim of the Thesis

An extensive research study consisting of theoretical and experimental investigation has been planned and carried out by the author studying the in-plane shear behaviour of composite wall. Design recommendations for the composite wall under in-plane shear are the final aim of the current thesis.

The theoretical and experimental investigations will be based on the concept that the composite walls resist shear loading in three ways: i. shear resistance of the profiled steel sheeting as a skin, ii. shear resistance of the concrete core and iii. shear resistance arising from the interaction of the sheeting and core. Consequently both theoretical

and experimental investigations have concentrated upon the individual behaviour of the component parts before considering the composite wall as a whole.

Analytical model for shear strength and stiffness of the sheeting, concrete core and composite wall have been developed. Numerical analyses using a finite element program have been carried out to model the behaviour. To validate the analytical and numerical work a series of model tests have been carried out. The experimental work has been based upon an approximate scaling factor of 1/6th full scale and involves the testing of specially formed profiled steel sheeting and formed concrete cores consisting of micro-concrete as well as combinations representing the composite wall. A shear rig was designed to ensure that pure shear loading could be imparted to the specimens. The heavily instrumented model tests are designed to give information on strength and stiffness, load transfer mechanism, strain characteristics and hysteretic behaviour of the test panels.

The design and construction of shear rig is given in chapter 2 . The performance of the rig was validated by testing a flat sheet plate and comparing this with test and theoretical data found from the literature.

The detailed small scale modelling of composite wall with micro-concrete is described in chapter 3. The performance of the chosen micro-concrete was also validated by testing a flat slab and several parameters such as the shear retention factor to be used in numerical simulation of micro-concrete was determined from this test.

The chapter 4 is devoted to the analytical, numerical and experimental behaviour of the profiled concrete core. The strength, stiffness and strain characteristics are focused.

The individual behaviour of the profiled steel sheeting under in-plane shear is described in chapter 5. Analytical model for the strength and stiffness of the profiled sheeting are derived based on the previous associated works. Finite element modelling of profiled steel sheeting for various boundary conditions are also carried out. Both numerical and analytical results are compared to the small scale model tests. Design equations for strength and stiffness of sheeting under practical situations of composite walling are suggested.

The behaviour of the composite wall is described in chapter 6. The study includes small scale model tests on composite wall along with analytical model developments for strength and stiffness. The numerical analysis was carried out assuming full connection between sheeting and concrete core. Parametric studies are also carried out with various interface elements available in finite element program LUSAS. Design equations for strength and stiffness of the composite wall are developed based on model tests and numerical analysis.

Although the current research is mainly concentrated on pure shear behaviour of the walls. Some work has also been carried out on the behaviour of composite wall as a beam subjected to a concentrated load at the centre span in chapter 7. The limited number of tests (mainly two tests) provided information on ultimate strength of the wall beam and distribution of bending and shearing strain. Analytical models for shear and moment capacity are described with some finite element analysis.

Chapter 8 describes the design and potential application of composite shear wall in buildings. The design of a framed composite shear wall is described with design equations for strength and stiffness both in service and construction stages.

Chapter 9 summarises the major findings of the thesis with recommendations for further research.

CHAPTER TWO

DESIGN OF A SHEAR TESTING RIG

2.1. Introduction

The design of a shear testing rig required early attention in order to allow the experimental small scale model investigation to proceed on schedule.

The Heavy Structures Laboratory located in the John Anderson Building at Strathclyde University had a Dartec loading machine capable of applying tensile, compressive and dynamic loading to specimens. This machine could be used with two cylinders to apply a load of between 25 kN and 250 kN. The Dartec was therefore, used as the loading device for a purpose made shear testing frame. The shear testing frame was connected to the Dartec via special head details and the model panels were tested by applying load through head details. The shear frame simulated in-plane shear in the model panels.

Various factors related to cost, model scale, simplicity and feasibility, use of existing facility, previous research experience and performance were considered in the design and selection of a particular shear testing rig.

2.2. Design alternatives

A literature review revealed some information on the shear testing rigs used in previous research. A number of shear rigs with different systems of applying loads to generate in-plane shear were critically examined before a choice of rig was finalised. A brief reference of those will be mentioned here.

Vechio F.J. and Collins M. P. (1986) used a membrane element tester to study the response of rectangular reinforced concrete element subjected to in-plane shear and combination of in-plane shear and axial stresses. The 37 double acting hydraulic jacks, the network of links, the shear keys, a steel box -section reaction frame to house jack-

and-link assembly and a lateral support frame to resist any out of plane displacement made the rig costly and unfeasible for the author's model tests.

The idea of the rig designed for the current research was taken from the following Researchers. Rocky K.C., Anderson R.G. and Cheung Y.K. (1969) studied the shear buckling behaviour of webs having central circular holes. Easely J.T. (1975) used a rig to study the behaviour of corrugated metal deck shear diaphragms. Davies J.M. and Fisher, J. (1979) constructed a rig to study the diaphragm action of cantilever square composite slabs with profiled steel sheeting. Zaras J. et. al (1983) devised a rig to study the behaviour of rectangular plates under complex loading including in-plane shear. Roberts T.M. and Sabouri-Ghomi (1992) studied the hysteric behaviour of steel plate shear panels. The basic idea of generating in-plane shear in all the rigs was same.

The problems of testing panels of micro-concrete and panels of composite walling were not faced by previous researchers. The designed shear testing rig has proved cost effective, simple in fabrication and incorporates the Dartec machine with simple head details.

2.3. Design of Shear Frame

The frame was designed to be capable of applying a tensile or compressive force of 200 kN across a diagonal. This allowed sufficient capacity of the rig to carry out all model tests. The design was carried out at the ultimate limit state according to the recommendations of BS 5950: 1984 with a serviceability check performed at working load levels to ensure that the yield was not reached. The general details of the shear frame assembly is shown in figure 2.1 and also in photograph 2.1. The shear rig has the following components:

a. Test Frame

The details of the test frame is shown in figure 2.1(a) and 2.1(b). The test frame was consisted of four pairs of frame members. The frame members were made from 16 mm thick and 60 mm wide steel plates. The internal dimension of square test frame was 500 mm x 500 mm which provided an effective dimension of 560 mm x 560 mm for the model panels under test. The panels were clamped between pairs of frame members by one row of 10 mm diameter high tensile bolts. These bolts were designed to provide sufficient clamping force for shear forces to be transferred from the test

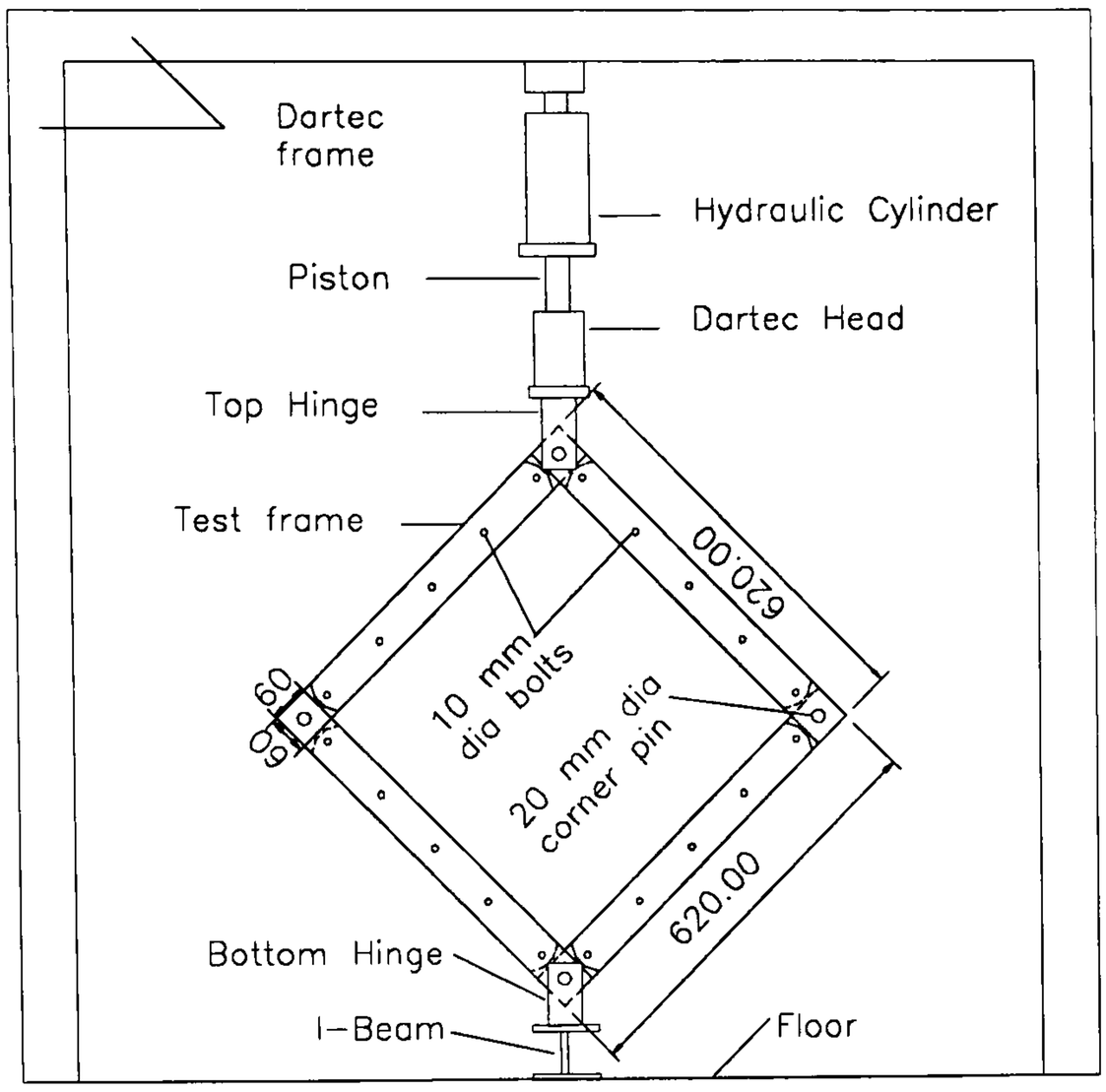

Figure 2.1(a): Detail of shear frame assembly

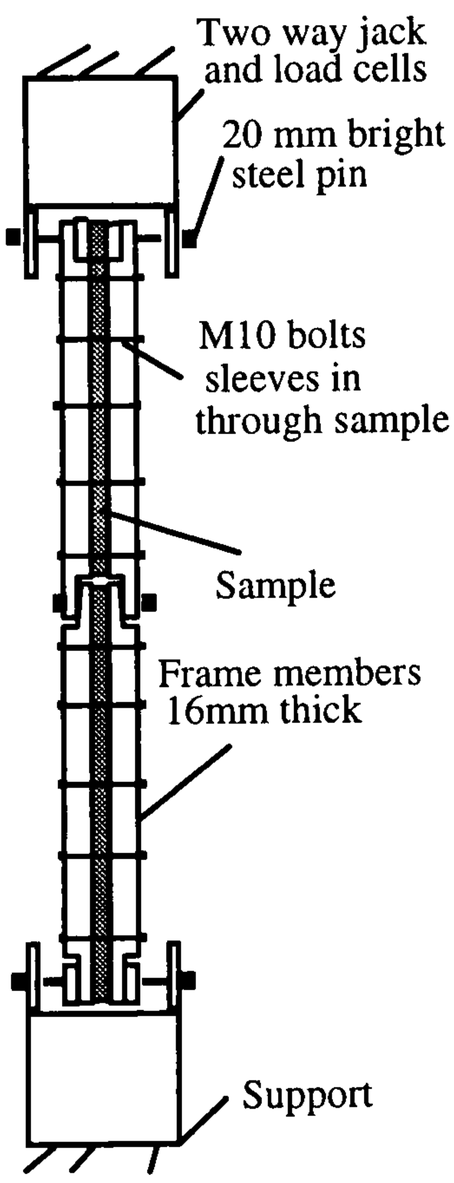

Fig. 2.1 (b)Side elevation of shear frame

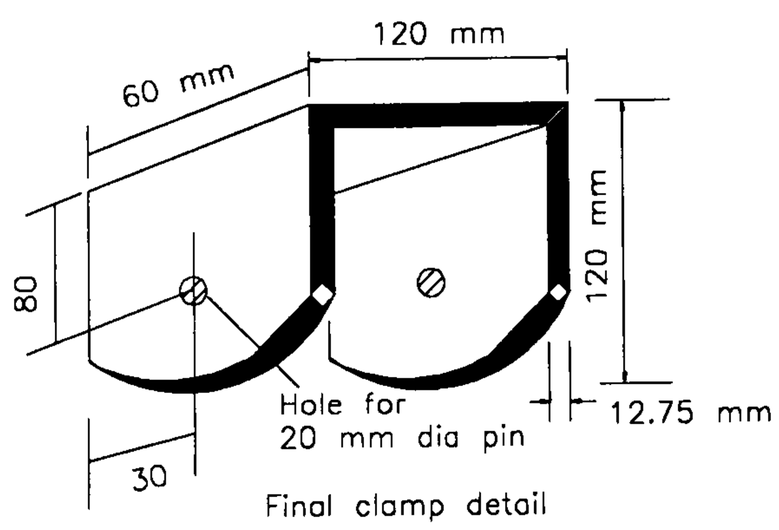

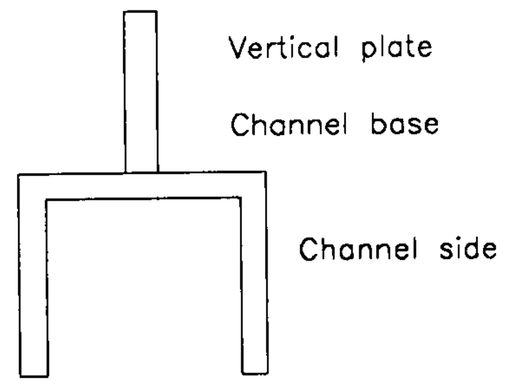

Figure 2.3(a) and (b): Clamp details

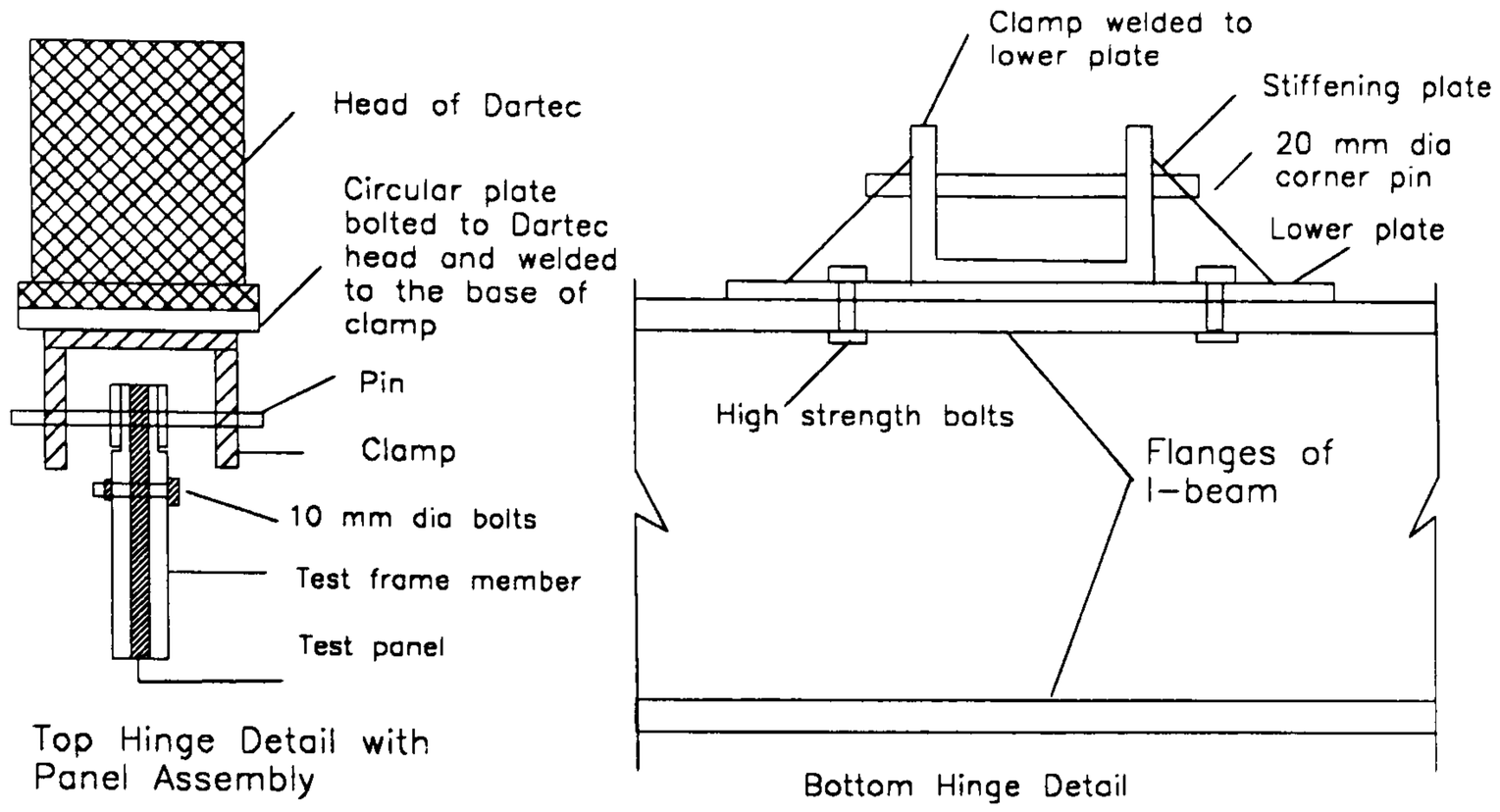

Figures 2.2 and 2.4: Top and Bottom hinge details

frame to the panels by friction with no slip. The boundary frame members were pinned at their corner with 20 mm diameter high strength pins. These corner pins were designed so that they could safely transfer loads to the test frame whilst maintaining hinge action.

b. Top Hinge

The test frame was connected to the Dartec head through the top hinge, details of which are shown in figure 2.2. This consisted of a clamp welded to a specially made circular plate. The circular plate was bolted to the Dartec head through high strength bolts. The detail of the clamp initially used (figure 2.3(a)) was different than its final form (figure 2.3(b)). Initial clamp consisted of a channel and a vertical plate welded to the channel base. Vertical plate was removed due to the possible bending and twisting. The final form consisted of only a channel welded to circular plate at its base. Holes were made at the sides of the channel for 20 mm dia corner pin. The test frame was connected to the top hinge through the corner pin.

c. Bottom Hinge

The final detail of the bottom hinge is shown in figure 2.4. It consisted of a channel section welded to a rectangular plate at the base. The rectangular plate was bolted to

the strong I-beam bolted to the strong floor. The sides of the channel were stiffened to avoid bending and twisting by using stiffening plates. Provision was made for the holes at the sides of the channel to allow the corner pin to make connection between bottom hinge and test frame.

2.4. Loading System

The general details of the experimental set up including the shear testing rig is presented in figure 2.1. Two diagonally opposite pinned corners of the test frame were connected to the Dartec head (through top hinge) at the top and I-beam at the bottom (through bottom hinge). The rig was capable of testing in-plane shear and hysteretic behaviour of the panels.

The shear panels were tested by applying tensile or compressive forces across a diagonal of the test frame. Since the boundary members of the test frame were pinned at their corner, they formed a mechanism and did not contribute to the load carrying capacity of the system as a rigid framework. All components of the pinned joints and hinges were machined as accurately as possible to minimise slack during loading and unloading.

The general method of realisation of shear loading is shown in figure 2.5. The diagonal force P applied to the top hinge was transmitted through corner pin to the frame members and produced the components V_a and V_b which were then transmitted on to the panels. The equilibrating resultant P acting at the bottom hinge also produced V_a and V_b in the similar way. The required stress system may be converted into a system of self equilibrating forces via the following relationships:

$P = \bar{V}_a + \bar{V}_b$; $V_a = \tau at$ and $V_b = \tau bt$ where

$V_a : V_b$ = Shear forces along a and b edges respectively

t = Thickness of the panel and

τ = Shearing stress

Due to application of diagonal load, P, the test panel abcd undergoes shear deformation and assumed deformed configuration ab'c'd' as shown in figure 2.5. If the deformed shape ab'c'd' is rotated clockwise so that ab' coincides with ab (as shown in figure 2.5), the diagonal force P and corresponding diagonal deformation Δ can be

related to the panel shear force V and shear displacement δ by the following equations :

$V = P \cos\theta_d$ and $\delta = \Delta / \cos\theta_d$ .....(2.1)

where θ_d is the angle of loaded diagonal

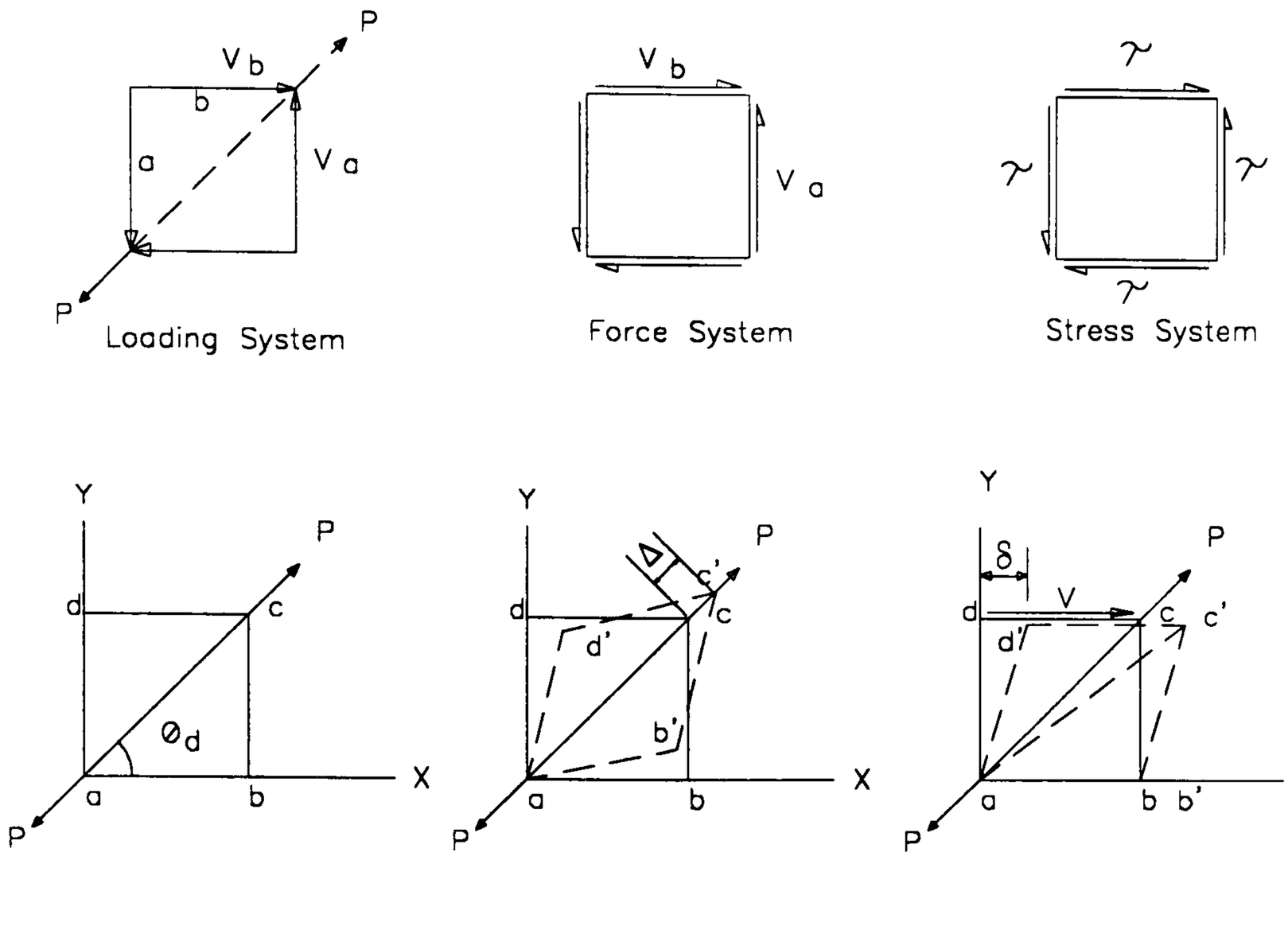

Figure 2.5: Load and deformation realisation in shear rig

The equation(1) needed the following assumptions :

- 0 Rotation of test frame members at the hinges should be same at each load increment throughout the loading history.
- 0 The boundary members were assumed very rigid and test frame behaved as a mechanism.
- 0 Slip at the interior bolts was negligible.
- 0 No overall out of plane movement of the whole rig.
- 0 Non-linear variation of shearing stress along the boundary frame should not affect the value of resultant shear force,V, along the boundaries.
- 0 For square panels, magnitude of resultant shear forces, V, along each of the boundaries were same.

The above assumptions were deemed to be reasonable and particular attention was given to attain the required conditions during testing of the panels.

2.5. Shake Down Trials

Preliminary tests were conducted to check the performance of the rig. The shear rig alone was tested to study whether the frame behaved as mechanism or not. It was found that the frame behaved as a mechanism and no load was recorded for a diagonal displacement of up to 60 mm.

2.5.1. Preliminary Test on Plain Steel Sheet

A model test on a very thin steel sheet was performed to validate the shear rig. The same type of steel sheet was used latter for making profiled steel sheet and composite wall models.

2.5.1.1 Material Test

Tensile tests were performed on specimens of the steel sheet to determine the properties of the sheet. The load-extension curves from coupon tests are shown in figure 2.6. The general shape of the curves are similar to the typical stress-strain curve (BS5950: Part 1, 1988) for steel as shown in figure 2.7. The curves show well defined yield plateau extending more than six times the strain at first yield. Table 2.1 summarises the properties of the steel sheet derived from the coupon tests.

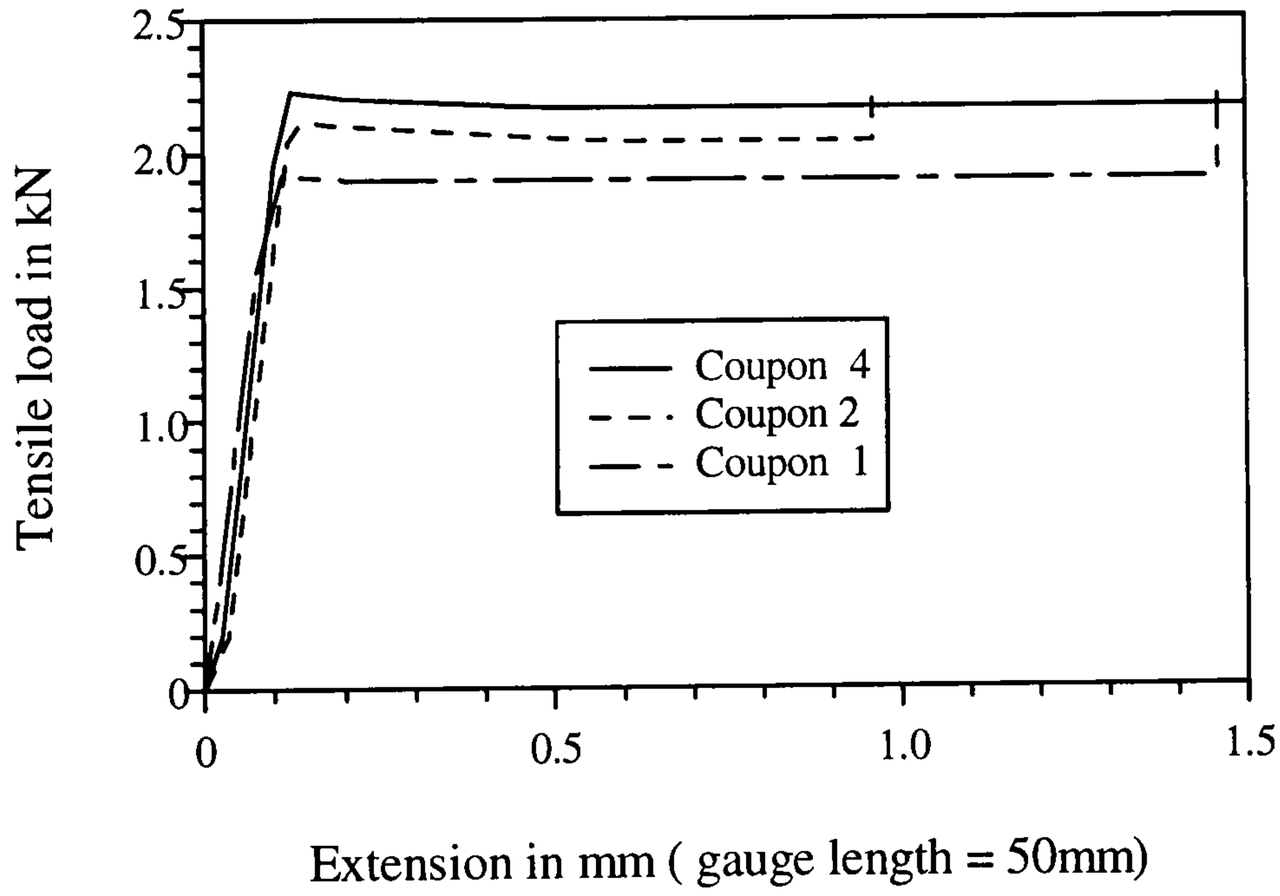

Figure 2.6: Load-extension curves from coupon tests 1, 2 and 4

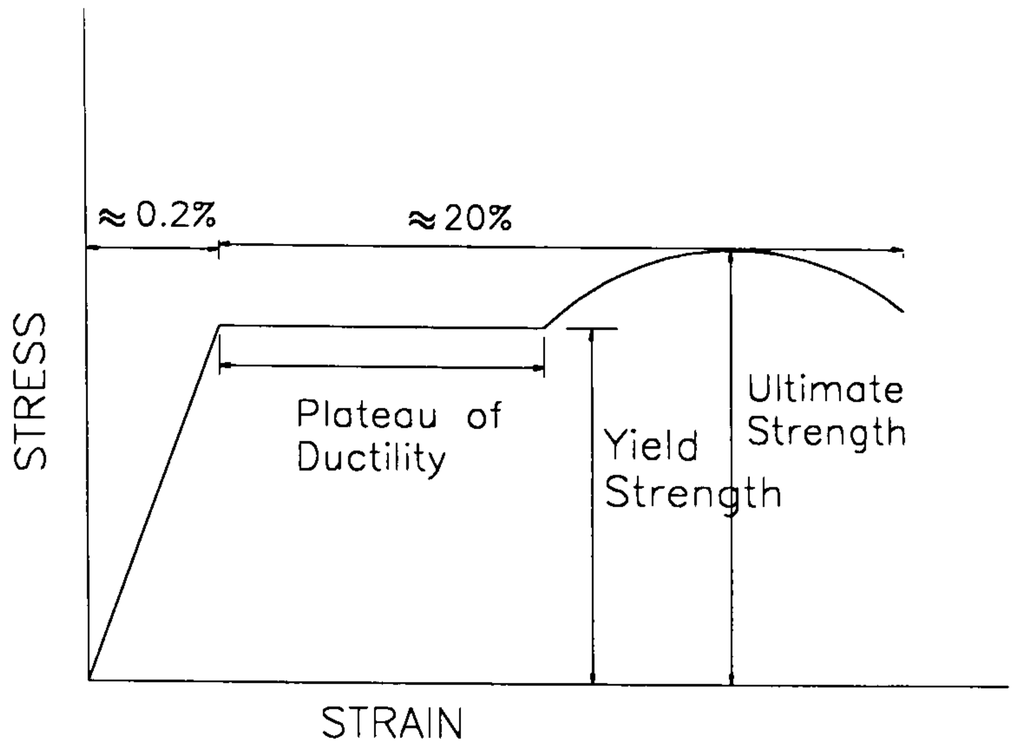

Figure 2.7: Typical stress-strain curve for steel

Table 2.1: Summary of steel sheet properties

Coupon Number	Yield Load kN	Ultimate Load kN	Yield Strength kN/mm^2	Ultimate Strength kN/mm^2	Modulus of Elasticity (E) kN/mm^2	% Elonga-tion
1	1.92	2.20	0.338	0.387	201.10	21.0
2	2.10	2.24	0.372	0.397	192.74	20.0
3	2.20	2.30	0.375	0.392	200.79	22.0
4	2.16	2.28	0.377	0.398	205.00	20.0
Average			0.375	0.394	200.00	20.75

[1]

2.5.1.2. Detailing and Instrumentation

The overall dimension of the square panel was 620 mm x 620 mm providing an effective dimension of 560 mm x 560 mm square once the frame had been fixed. The panel was placed between the pair of frame members at each side of the square frame and bolted strongly to avoid any slip at bolt locations.

Electrical strain gauges were used at key locations, as shown in figure 2.8 to determine the stress-strain characteristics within the panel. As the sheet was very thin, the strain gauges were used only on one side of the sheeting. Linear voltage

---

1 Average thickness of the sheet = 0.45 mm (deducting 0.04 mm galvanised coating)
Average yield strain (calculated) = 0.0024
Poisson's ratio, $\upsilon = 0.25$

displacement transducer (LVDT) and dial gauges were used to measure diagonal deformation. A micro-computer based data acquisition system (SPECTRA DAS) which linked strain gauges, load cell and LVDT was used to monitor strains, deformation and load. The strains, load and displacement values were simultaneously printed and stored in diskette at each load increment throughout the entire range of loading.

2.5.1.3. Loading and Test Observations

The steel sheet panel was subjected to tensile load along the diagonal and tested under displacement control. The experimental set-up with steel sheet panel is presented in

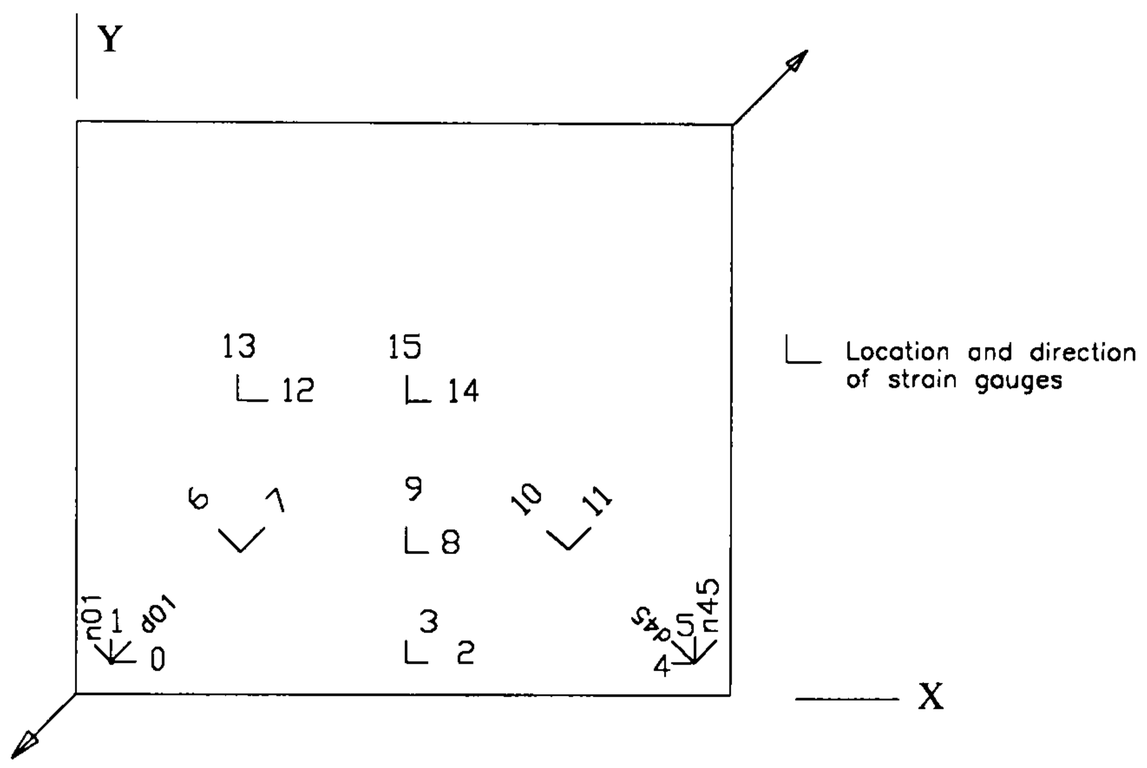

Figure 2.8: Strain gauge location for plain steel sheet panel

photograph 2.2. Initially loading and unloading was carried out for several times up to a load of 4 kN to minimise the possible slack that may exist in pin and bolt locations. Then the load was applied incrementally and at each load increment strains and deformations were measured. Strain gauge-15 was not working at the time of experiment.

As the sheet was very thin, its shear buckling load was very small. Buckling of the sheeting was observed at a very low load. No attempts were made to measure the out-of-plane displacement. As the load increases, the gradual development of a tension field was observed. The sheet showed a substantial post-buckling strength before it failed at about 57 kN by tearing at bolts near the bottom corner pins of the loaded diagonal.

Unfortunately at the later stages of loading bottom hinge began to bend and twist causing possibly a stress concentration at the bottom corner. The bending of the lower beam was also observed. The hinge details at the top and bottom were modified to minimise those effects in the later tests. A large I-beam replaced the comparatively smaller beam used in this test.

2.5.1.4. Experimental Strain Analysis

a. Strains, along and normal to diagonals

Loaded Diagonal

Figure 2.9 shows the variation of strain along and normal to the loaded diagonal with shear load. Strains along the loaded diagonal (d01 and 7) were mainly tensile. The diagonal strain close to the corner (d01) was always higher than those at gauge 7 away from the corner. Corner gauge (d01) yielded first and yielding proceeded towards the centre subsequently yielding gauge 7.

Strain normal to the diagonal at no1 (near the corner) was in compression for most of the time whereas gauge-6 showed tensile strain.

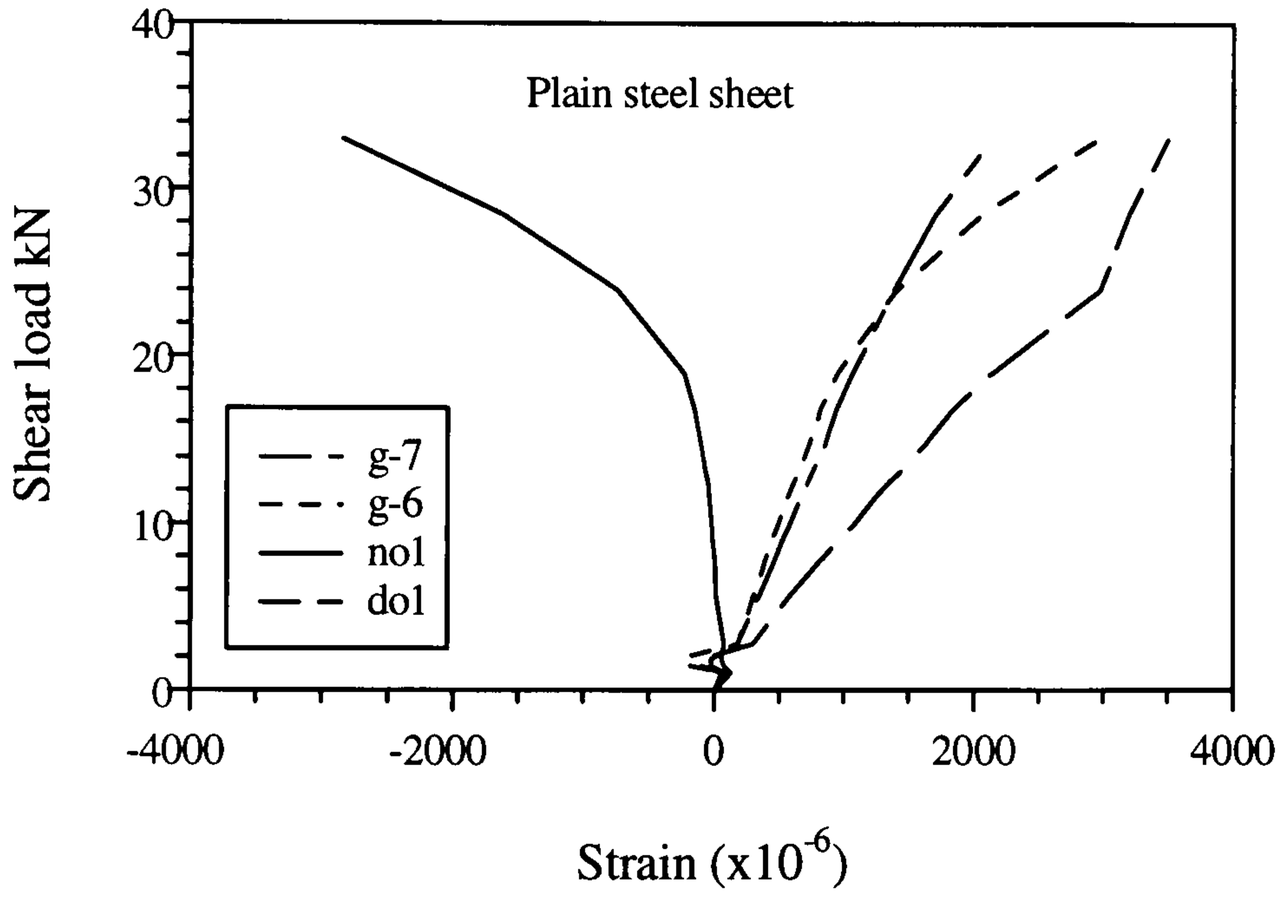

Figure 2.9: Variation of strain along the loaded diagonal

Off-diagonal

Figure 2.10 shows the variation of strain along and normal to the off-diagonal. Gauge-10 was initially (up to 12 kN) under tension and then subjected to compression. Same thing happened for gauge-d45. But the compressive strains at gauge-10 were always higher than those at gauge-d45.

Normal strains at n45 and 11 were tensile all the time and strains at 11 were always higher than those at n45. It gives an indication of increase in compressive stress from the corners towards the centre of the panel.

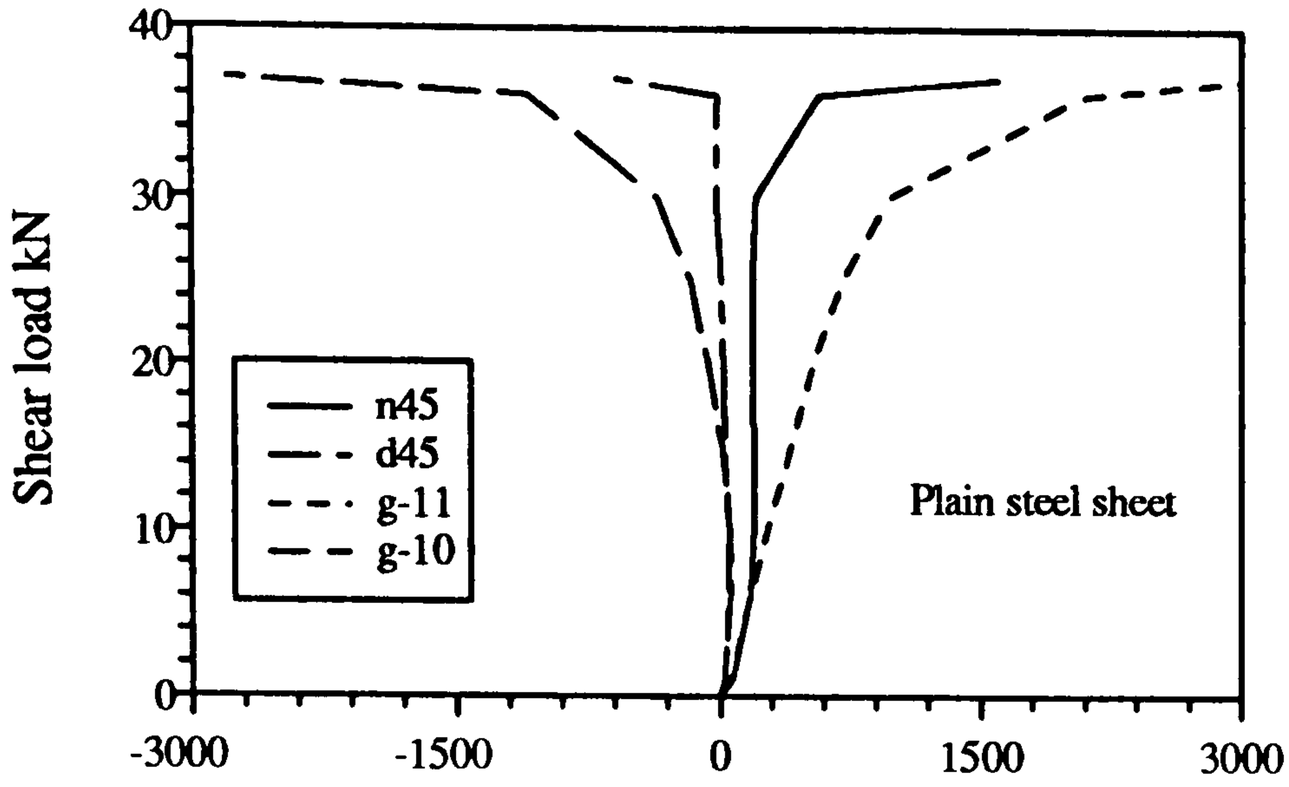

Figure 2.10: Variation of strain along the off-diagonal

Comparison of strains related to two diagonals

Figures 2.11 compare the strains along and normal to diagonals for the loaded and off-diagonal. Diagonal strain at gauge-7 (loaded diagonal) was tensile and much higher than the predominant compressive strain at gauge-10. Diagonal strain at d01 was tensile and much higher than those at d45. It clearly defined that the loaded diagonal was subjected predominantly to tensile stress and subsequently yielded in tension. The off-diagonal was under compression but magnitude of strain was small up to about 80% of ultimate load.

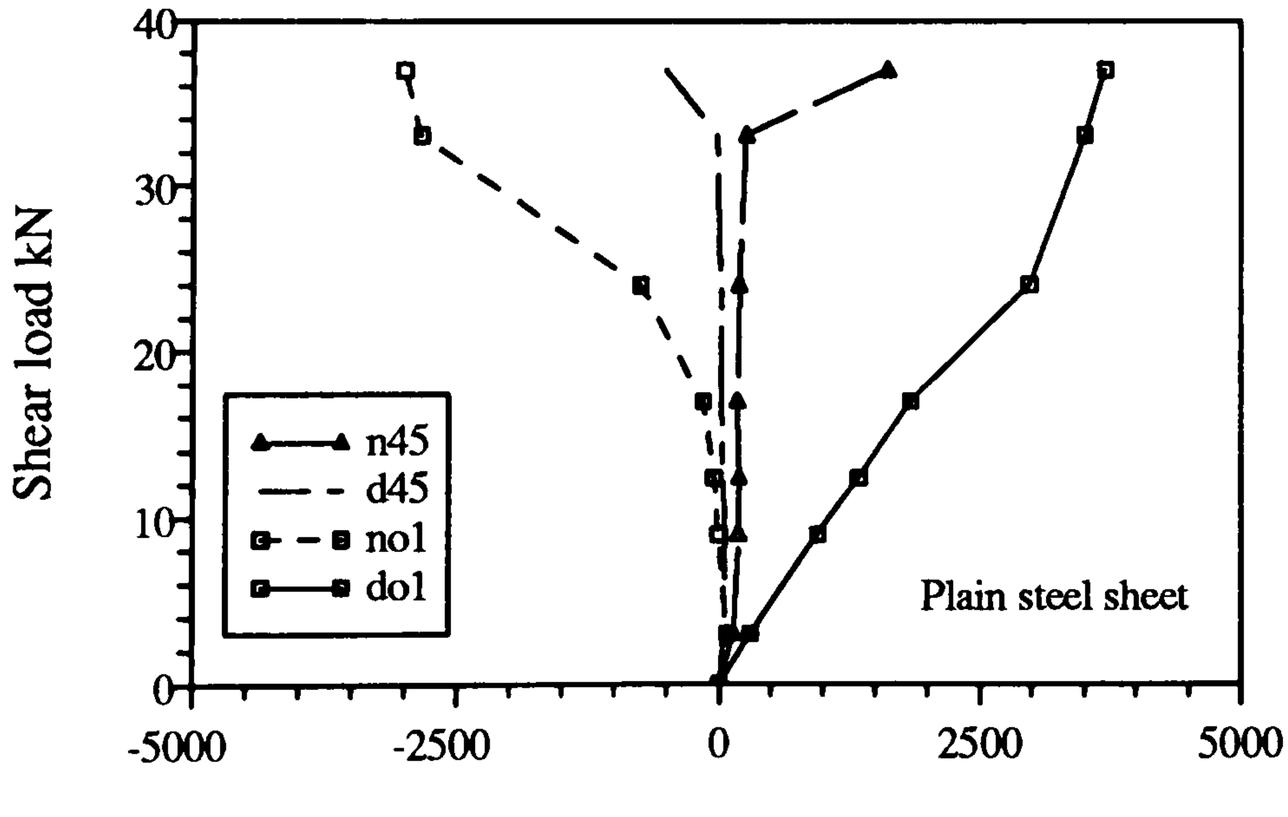

Figure 2.11(a)

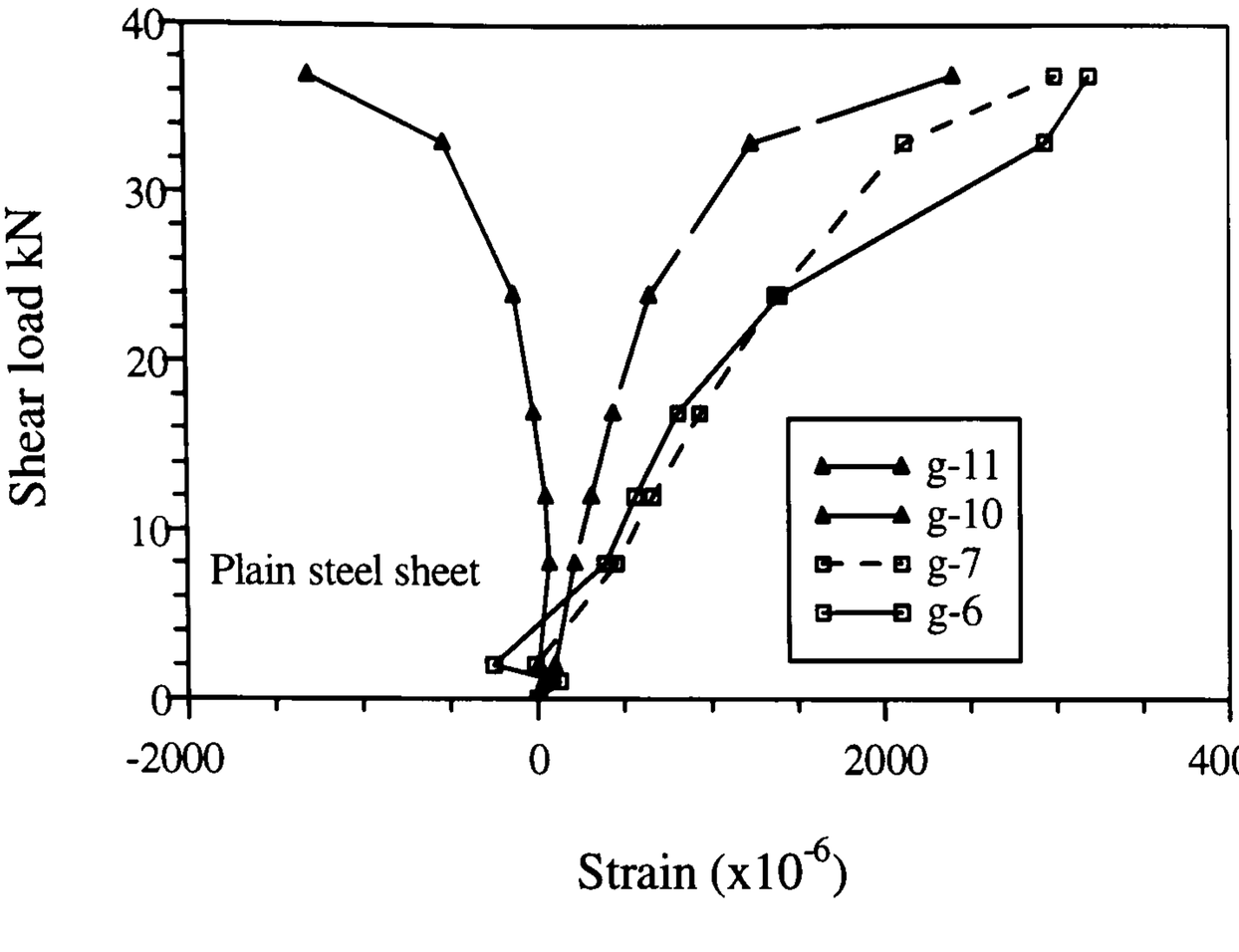

Figure 2.11(b)

Figure 2.12: Comparison of strains in loaded and off-diagonals

b. Strains along and normal to boundary frame member

The variation of X and Y strain along the boundary is similar to each other as shown in figures 2.12 and 2.13, with higher strains at the loaded corner.

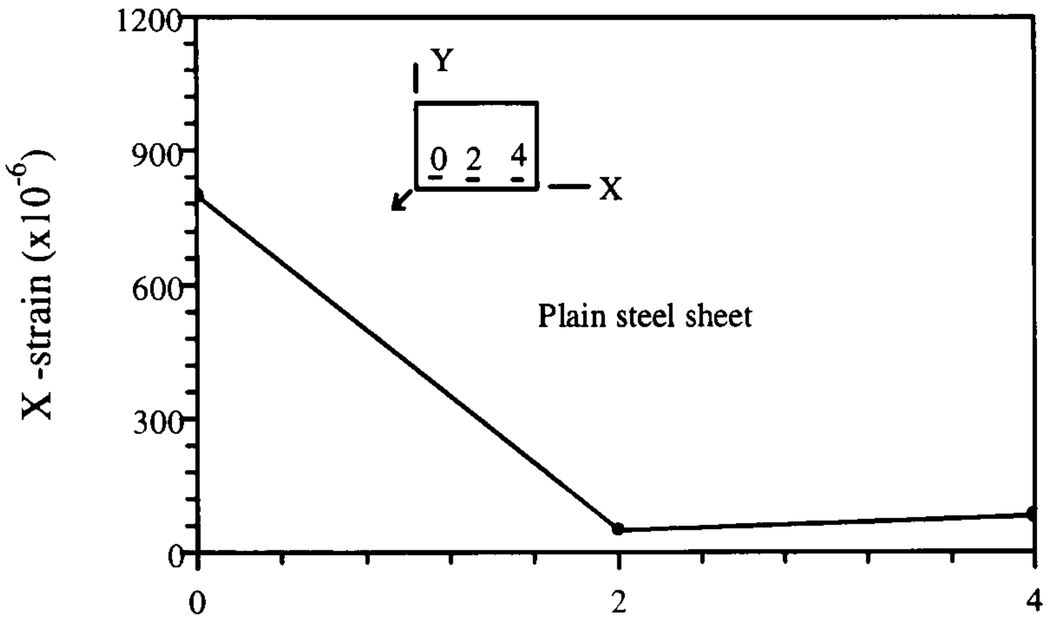

Figure 2.12: Variation of X strain along the boundary

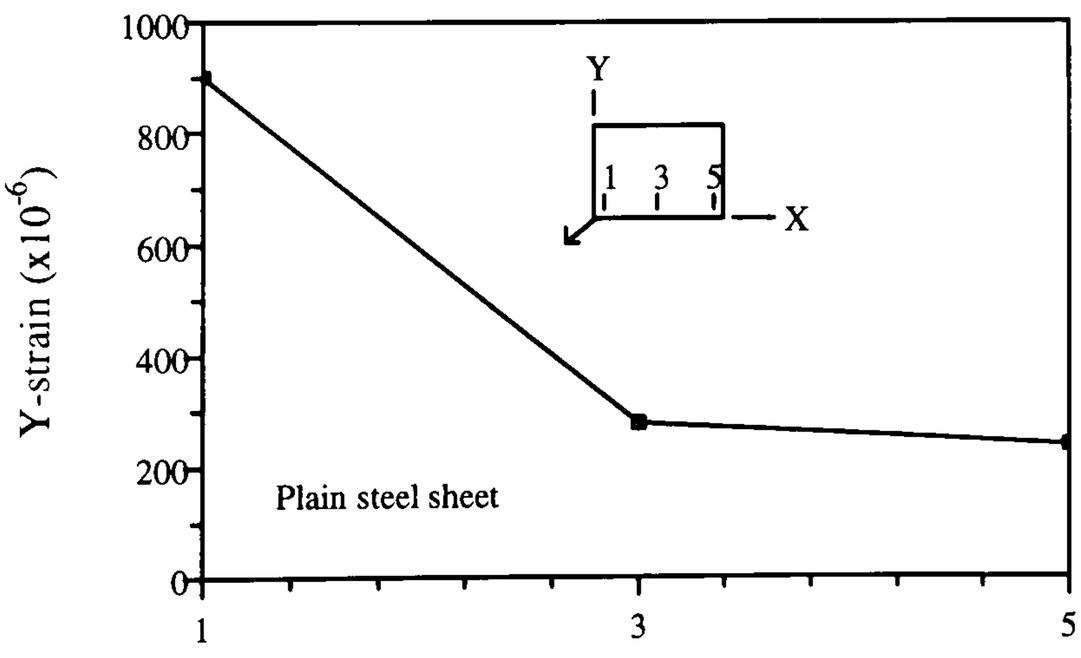

Figure 2.13: Variation of Y-strain along the boundary

2.5.1.5. Development of Tension field

Photograph 2.2 shows the development of tension field and subsequent failure of the panel. The gradual yielding of the panel along the loaded diagonal was confirmed from the strain analysis as a consequence of the tension field action. The yielding started from the corner of the loaded diagonal and gradually proceed towards the centre until whole diagonal yielded in tension. After yielding of the loaded diagonal, yielding extended towards the other region to form a yield band.

2.5.2. Analytical Model for the plain steel sheet panel

The shear strength and stiffness of the sheeting are the important factors in the evaluation of their behaviour under in-plane shear. Analytical models for strength and stiffness will be derived on the basis of existing models.

2.5.2.1 Literature Review

Numerous research studies on the behaviour of steel plate shear panels have been carried out in the past. Those comparing closely with the present study will be described here.

Buckling behaviour of plates in shear, with different boundary conditions was investigated by many researchers and detailed information can be obtained from Timoshenko, S.P. and Gere, J.M. (1961).

The shear behaviour of web in plate girders was studied by Basler(1961). It was considered that the web will be in pure shear in pre-buckling stage and after buckling load will be resisted by the development of a diagonal tension band. Flanges of girder were assumed so flexible that they could not withstand any load and the web failed when it develops an off-diagonal yield band. The ultimate load (V_{ult}) calculated by Basler was given by equation 2.2.

$$V_{ult} = \tau_{cr}.at + \sigma_{ty}.at/(2\sqrt{1+\alpha^2}) \quad \text{.....(2.2)}$$

where $\sigma_{ty} = f_y(1-\tau_{cr}/\tau_y) = \sqrt{3}(\tau_y-\tau_{cr})$ = Tension field stress,

α = a/b ; a,b = Dimensions of web,

t = Thickness of the web,

τ_y = Shear yield stress of web material = $f_y/\sqrt{3}$ and

f_y = Yield stress of the web material

Gaylord(1963) and Fuji(1969) modified ultimate load resistance of the Baslar model.

Rockey and Skaloud(1968) showed that the ultimate load carrying capacity of the girder web was greatly influenced by the flexural rigidity of the flanges. The collapse mode involved the development of plastic hinges in the tension and compression flanges in addition to the diagonal tensile stress which cause the web to yield. Ultimate load of the model was found closer to the experimental failure load. The weakness of the model was the assumption that the inclination of tensile band coincides with the inclination of the panel diagonal.

Porter, Rockey and Evans(1975) presented a model for the failure of a girder web loaded primarily in shear. They assumed that the effect of flange bending stresses on the shear buckling stress of the web and the variation of tension field stress over the web can be ignored. This "Cardiff " model described a pure shear state in pre-buckling stage, development of a tension membrane field in the post-buckling stage and in the ultimate stage, failure occurred when plastic hinges formed in the flanges together with a yielded band of web forming a plastic mechanism. Under the action of tension field, the flanges bend and inclination of the tension field (ϕ) was greatly influenced by the rigidity of the flanges. The optimum value of ϕ (ϕ_m, normally lies between $\phi_d/2 < \phi_m < 45^o$) can be calculated using an iterative equation proposed in the model. It was found that the value of ultimate load was not sensitive to small changes in angle from the optimum value, ϕ_m, which was around 30^o.

Bryan and El-Dakhakhni (1964) made an attempt to calculate the shear stiffness of panels taking into consideration the flexibility of the edge members. They pointed out that the effect of flexibility on the stress redistribution in the sheeting and bending strain energy of the edge members were much more important. These two factors, based on assumption of rigid edge members, may modify the shear stiffness many times as confirmed from their model tests.

Wagner (1931) as reported by Bryan and El-Dakhakhni, first made attempt to determine a theoretical value of ϕ taking into consideration the longitudinal extension or contraction of edge members but not of their bending flexibility. However, he made allowances for bending flexibility in the form of a flexibility parameter.

Kulak (1986) gave an expression to calculate the value of ϕ for panel with boundary frames. The expression for ϕ is

$$\tan^4 \phi = \frac{2/ta + 1/A}{2/ta + 2b/Aa + b^4/180Ia^2}$$

where a and b are height and width of the panel respectively,
A is the cross sectional area of boundary frame and
I is the moment of inertia of boundary frame

For a very rigid boundary frame, the above equation gives the value of ϕ equal to 45^0 which was suggested and assumed by all researcher prior to this.

Review Conclusion

The overall behaviour of shear panel can be summarised as shown in the flow diagram 2.1.

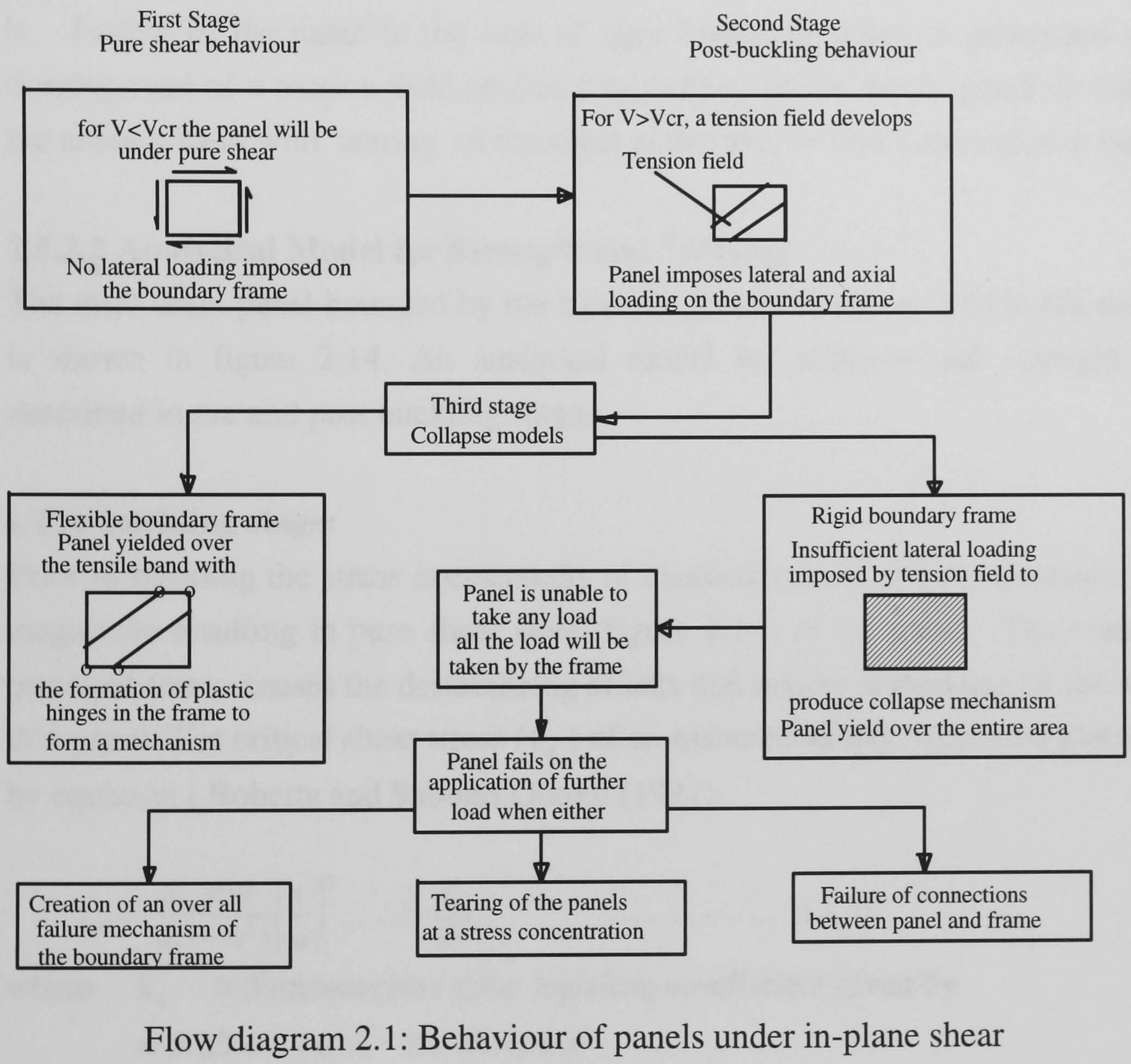

Flow diagram 2.1: Behaviour of panels under in-plane shear

The following are the basic points on the behaviour of shear panels:

0 Pure shear behaviour occurs in the pre-buckling stage with buckling being dependent upon the slenderness (b/t). Following elastic buckling a pure tension or in-

complete tension field will be developed in the post buckling stage. Pure shear is associated with uniformly distributed shear stresses along the boundaries but in post-buckling stage the stress distribution is non-linear.

0 The stiffness of the boundary frame has marked influence on the angle of tension field. It is reasonable to assume ϕ as 45^0 in the case of rigid boundary frame and 35^0-40^0 for practical flexible boundary frame.

0 The shear resistance contribution of a surrounding pin ended rigid frame (pinned beam-column frame in building) is negligible but shear resistance of fixed ended frame (beam-column frame in building or flanges in girders) may be significant and should be taken into account.

0 Failure of panels with flexible boundary frame is associated with the development of tension field and subsequent formation of plastic hinges in the frame forming a mechanism.

0 Failure of the panel in the case of rigid boundary frame is associated with the development of a tension field resulting in yielding of the whole panel or yielding of the tension band with tearing of the sheet at the rivet or bolt connection at the edges.

2.5.2.2 Analytical Model for Strength and Stiffness

The steel sheet panel bounded by the rigid pin jointed frame as used in the model test is shown in figure 2.14. An analytical model for stiffness and strength will be described in pre and post buckling stages.

i. Pre-buckling stage:

Prior to buckling the stress is essentially of diagonal tensile and compression of equal magnitude resulting in pure shear state (figure 2.14) of the panel. The compressive principal stress causes the destabilizing effects that results in buckling of the relatively thin panel. The critical shear stress (τ_{cr}) of an assumed simply supported plate is given by equation (Roberts and Sabouri Ghomi (1991):

$$\tau_{cr} = \frac{K_\tau . \pi^2 E}{12(1-\upsilon^2)}\left[\frac{t}{a}\right]^2 \ldots\ldots \leq \frac{f_y}{\sqrt{3}} \qquad \ldots\ldots\ldots\ldots\ldots\ldots (2.3)$$

where k_τ = dimensionless shear buckling co-efficient given by

$= 5.35 + 4\ (a/b)^2$ for $a/b \geq 1.0$

$= 4 + 5.35\ (a/b)^2$ for $a/b \leq 1.0$

a,b = dimensions of the panel and , t = thickness of the panel

E = modulus of elasticity and υ = poisson's ratio of the panel material

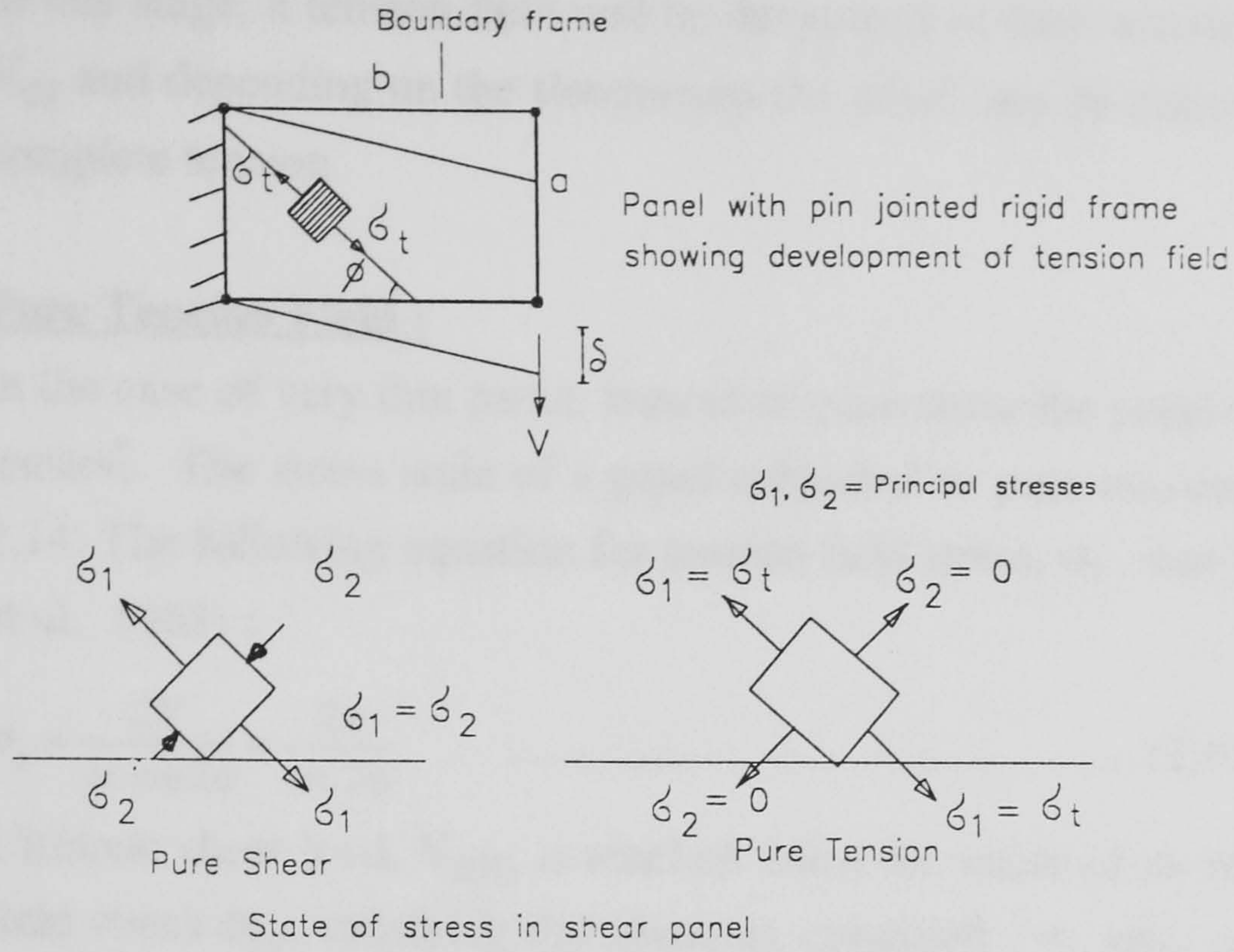

Figure 2.14: Panel with pin jointed frame

Shear stress,τ, will be uniformly distributed along the boundaries to give a shear load ,V, and corresponding shearing strain,γ, according to equation :

$$V = \tau . at ....0 \leq V \leq V_{cr} \quad ....(2.4)$$

$$\gamma = \frac{\tau}{G} = \frac{2V(1+\nu)}{Eat} \quad ....(2.5)$$

where V_{cr} is the critical buckling load of the panel which is given by

$$V_{cr} = \tau_{cr} . at \quad ....(2.6)$$

Maximum shear load in this stage will be V_{cr} and shear deflection at any stage of loading within this stage can be obtained from the equation:

$$\delta = \gamma a = 2V(1+\nu)b/(atE) \quad ....(2.7)$$

Shear flexibility of the panel in the pre-buckling stage, c_1 , is given by :

$$c_1 = \frac{\delta}{V} = \frac{2b(1+\nu)}{Eat} = \frac{1}{k_1} \quad ....(2.8)$$

where k_1 is pre-buckling stiffness of the panel

ii. Post-buckling stage:

In this stage, a tension field will be developed to take account of any load more than V_{cr} and depending on the slenderness the panel may be either in pure tension or in in-complete tension.

Pure Tension Field :

In the case of very thin panel, instead of pure shear the panel will be subjected to pure tension. The stress state of a panel subjected to pure tension field is shown in figure 2.14. The following equation for tension field stress, σ_t , can be derived (Timoshenko et al, 1961) :

$$\sigma_t = \frac{2V}{at.\sin 2\phi} = \frac{2\tau}{\sin 2\phi} \qquad \text{.....(2.9)}$$

Ultimate shear load, V_{ult}, is reached when the value of σ_t reaches yielding tension field stress σ_{ty}, satisfying the plasticity condition : $\sigma_t = \sigma_{ty} = f_y$. The ultimate load can be derived from the equation (2.9), assuming $\phi = 45^0$ for the rigid boundary frame as:

$$V_{ult} = \frac{f_y.at}{2} \qquad \text{.....(2.10)}$$

The shearing strain,γ, can be derived from energy consideration using figure (2.14) and equation (2.9) as:

$$\gamma = \frac{4V}{Eat\sin^2 2\phi} \qquad \text{.....(2.11)}$$

Shear flexibility ,c_2, can be derived from equation :

$$c_2 = \frac{\delta}{V} = \frac{\gamma.b}{V} = \left[\frac{4V}{Eat\sin^2 2\phi}\right].b \text{.....} V_{cr} \le V \le V_{ult} \qquad \text{.....(2.12)}$$

The above equation can be modified for the case of rigid boundary frame assuming $\phi = 45^0$ as :

$$c_2 = \frac{4b}{Eat} = \frac{1}{k_2} \qquad \text{.....(2.13)}$$

where k_2 is the post-buckling stiffness of the panel.

In-complete Tension Field

In the case of panels which are not very thin they will act partially in shear and partially in tension. This is the intermediate case of pure shear and pure tension. The analytical model described here, is based on equilibrium solution developed by Porter, Rockey and Evans (1975). It is assumed that during post buckled stage, a tension

field inclined at an angle ϕ to the horizontal as shown in figure 2.15, gradually develops throughout the entire panel.

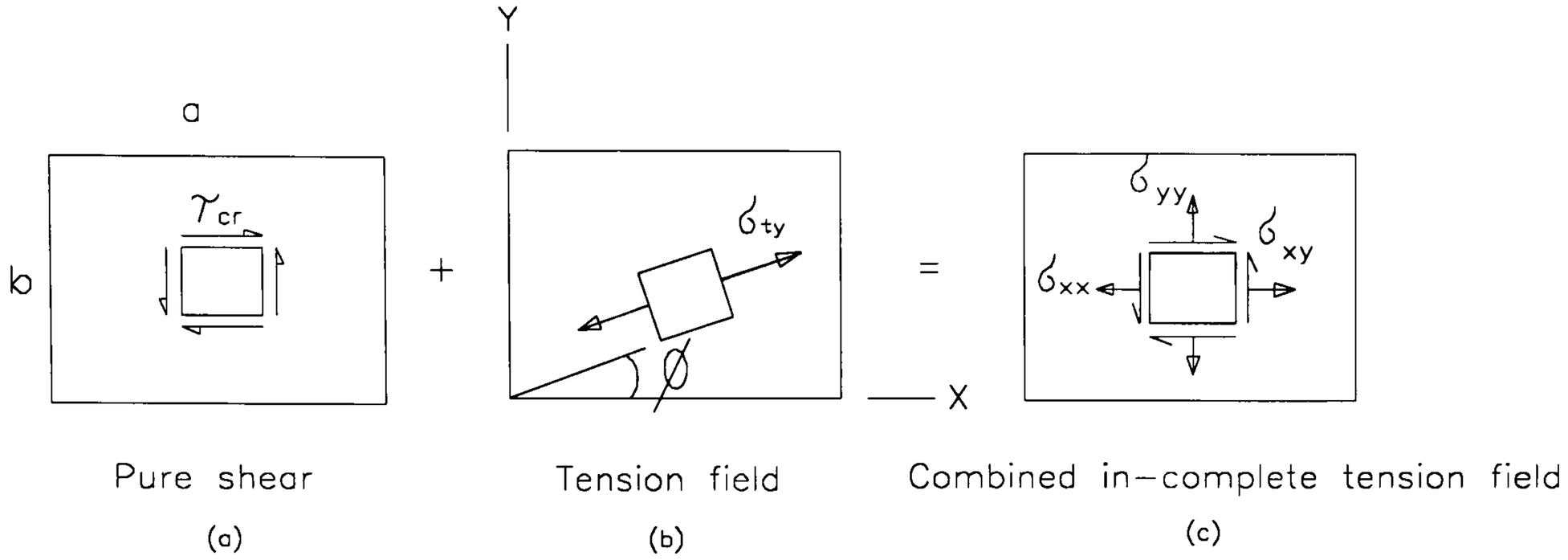

Figure 2.15: In-complete tension field

If σ_{ty} denotes the tension field stress at which yielding occurs, the total state of stress in the plate at yield, shown in figure 2.15 is defined by:

$$\sigma_{xx} = \sigma_{ty}\cos^2\phi\ldots;..\sigma_{yy} = \sigma_{ty}\sin^2\phi..and..\sigma_{xy} = \tau_{cr} + \frac{\sigma_{ty}.\sin 2\phi}{2}$$

The boundary stress, σ_{xy}, is a maximum when $\Phi = 45^0$ and hence

$$\sigma_{xx} = \sigma_{yy} = \frac{\sigma_{ty}}{2}.....and..\sigma_{xy} = \tau_{cr} + \frac{\sigma_{ty}}{2} \qquad .....(2.14)$$

According to Von-Misses yield criterion, yielding of the panel occurs when Yield function J is

$$J(\sigma)=(\sigma_{xx}-\sigma_{yy})^2+(\sigma_{yy}-\sigma_{zz})^2+(\sigma_{zz}-\sigma_{xx})^2+6\sigma_{xy}^2+6\sigma_{yz}^2+6\sigma_{zx}^2-2f_y^2=0.0 \quad .....(2.15)$$

For this particular case $\sigma_{zz} = \sigma_{yz} = \sigma_{zx} = 0.0$

Hence substituting equations (2.14) into equation (2.15), the value of tension field stress can be derived as

$$\sigma_{ty} = -1.5\tau_{cr} \pm \frac{\sqrt{4.f_y{}^2 - 3.\tau_{cr}{}^2}}{2} \qquad .....(2.16)$$

Ultimate shear load of the panel can be obtained from :

$$V_{ult} = \sigma_{xy}.at = \left[\tau_{cr} + \frac{\sigma_{ty}}{2}\right].at \qquad .....(2.17)$$

If the sheet is very thin, τ_{cr} can be neglected and equation (2.17) reduces to equation (2.10) derived for pure tension field.

The limiting elastic shear displacement (δ_e) can be determined approximately by equating the work done by post buckled component of shear force to the strain energy of the tension field, i.e.,

$$\frac{(\sigma_{xy}-\tau_{cr})(\delta_e-\delta_{cr})at}{2}=\frac{\sigma_{ty}{}^2.abt}{2E}$$

After simplification expression for limiting elastic shear displacement becomes :

$$\delta_e=\delta_{cr}+\frac{2\sigma_{ty}.b}{G}=\frac{\tau_{cr}.b}{G}+\frac{2\sigma_{ty}.b}{E}$$

where δ_{Cr} is critical shear displacement and G is the modulus of rigidity of panel material.

The post-buckling flexibility, c_2, or stiffness, k_2, of the panel can be derived approximately from the limiting elastic shear displacement as :

$$c_2=\frac{1}{k_2}=\frac{\delta_e}{V_{ult}}=\frac{4b\left[\tau_{cr}(1+\nu)+\sigma_{ty}\right]}{Eat\left(2\tau_{cr}+\sigma_{ty}\right)} \quad \text{.....} \quad (2.18)$$

For the case of pure tension field, assuming τ_{Cr}=0.0, the equation (2.18) reduces exactly to equation (2.13) derived for pure tension field.

2.5.2.3 Modelling of Shear-Load Deflection Curves

An approximate elastic model for the behaviour of a thin plate surrounding by a rigid pin jointed frame subjected to shear loading is presented in the previous article. The idealised load-deflection relationship can be approximated from the strength and stiffness of the panel as shown in figure 2.16.

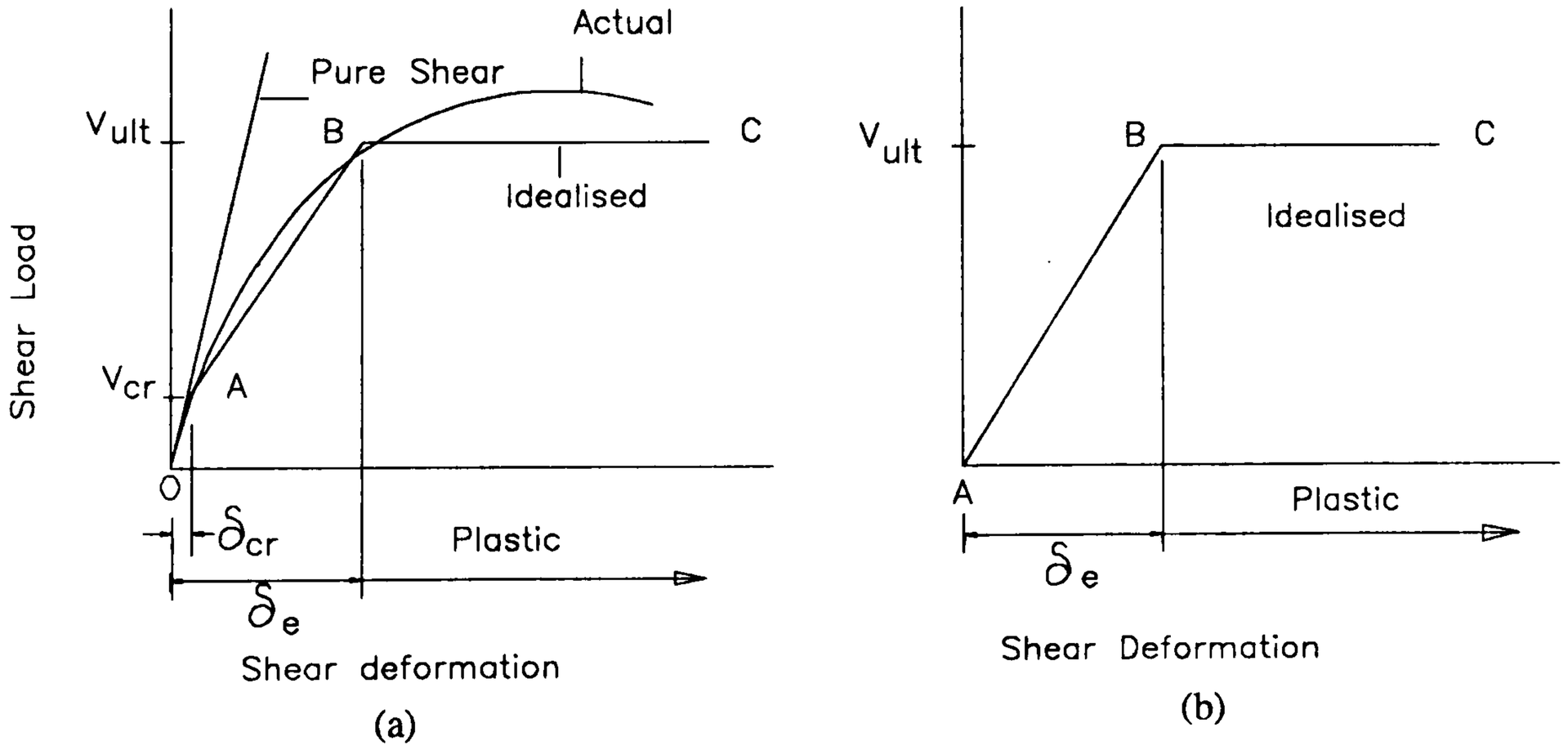

Figure 2.16: Idealisation of load-deflection curves

Idealised load -deflection curve follows a straight line (OA) until the critical buckling load (V_{cr}) is reached and then follows another straight line of lower stiffness(AB) in

the post-buckling stage. The reduction in stiffness is due to the buckling of the compression diagonal in the panel. The actual relationship, however, is non-linear. This is caused by two factors: (i) the buckling of the compression diagonals is restrained by the tautness of the tension field. Thus compressive stress will increase and the load -deflection curve in the post-buckling stage follow a curve as shown in figure 2.16(a) like experimental curve (figure 2.19) and (ii) The second non-linear factor is due to plasticity. It was found from the experiment that the stress concentration occurred at the corners of the loaded diagonal causing the region to yield at a load which was much smaller than the yield load calculated from uniform stress distribution. As a result although the ultimate load of the panel may not be affected the stiffness will be affected to some extent.

The line OA, representing pure shear can be approximated by estimating V_{cr} from equation (2.6) and the stiffness, k_1, from equation (2.8). For the current case of very thin steel sheeting V_{cr} is negligible, the part OA can be neglected and an idealised curve may be represented as shown in figure 2.16(b). It is assumed that the response is elastic and linear from points A to B even though the sheet will buckle at a shear force much smaller than V_{ult}. After buckling an inclined tension field gradually develops and yields when the shear force equals V_{ult}. The line AB can be approximated by estimating V_{ult} using equation (2.10) or (2.17) or (2.2) and k_2 using equation (2.13) or (2.18). From B to C the sheet is assumed to strain plastically and can be approximated from the flow theory of plasticity. This is not included in the present study and is approximated only by a straight line.

2.5.3 Finite Element Modelling

Finite element programme LUSAS was used to model the shear behaviour of the plain steel sheet. Pre and post-buckling behaviour were modelled from different approach.

Pre-buckling behaviour:

Pure shear behaviour before buckling was modelled by using 8-noded iso-parametric plane membrane elements. A typical finite element idealisation of the sheet is shown in figure 2.17. Trials with different number of elements (8,16,24 and 32) were done and results were found satisfactory with 16 elements. The load was applied in the form of prescribed displacement in x-direction to simulate the shear deflected shape as shown in figure 2.17. At each load increment shear load V and displacement δ were

calculated from LUSAS output to have load-deformation response and stiffness values.

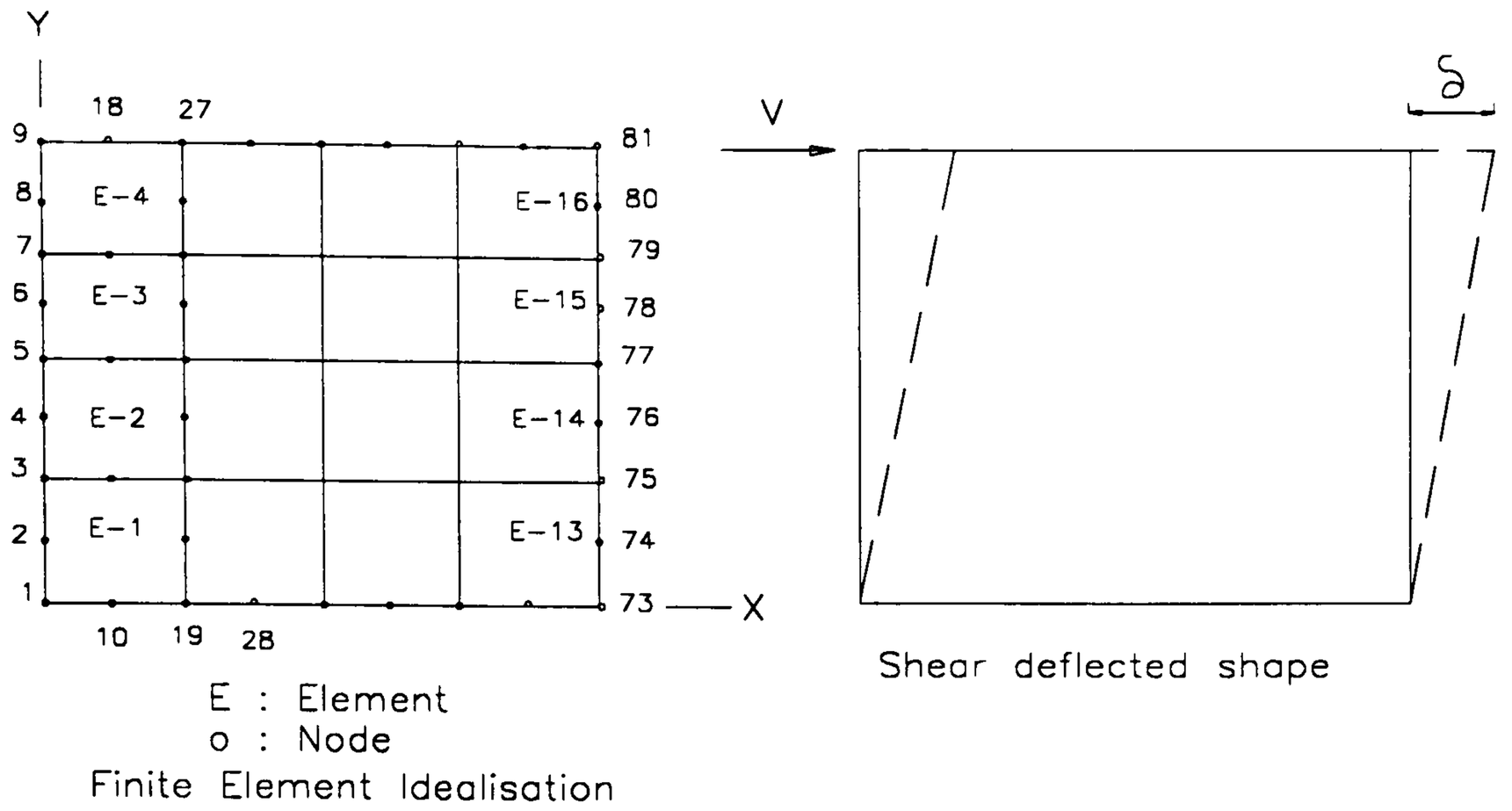

Figure 2.17: Typical finite element idealisation with shear deformation

Post-buckling behaviour:

An inclined bar model was employed to analyse the post-buckling response including tension field action of the sheet. A number of simplifying assumptions were made:

0 Shear buckling capacity of the sheet was neglected.

0 The tension field was modelled as a series of inclined strips.

0 The limit of action of a single strip was that corresponding to tension yield strength. This neglected the effects of strain hardening and ignored the effect of compressive stresses acting on the strips.

0 Bending of the boundary frame due to action of tension field was assumed to be nil.

0 The angle of inclination of the tension field,ϕ, was assumed to be 45^0.

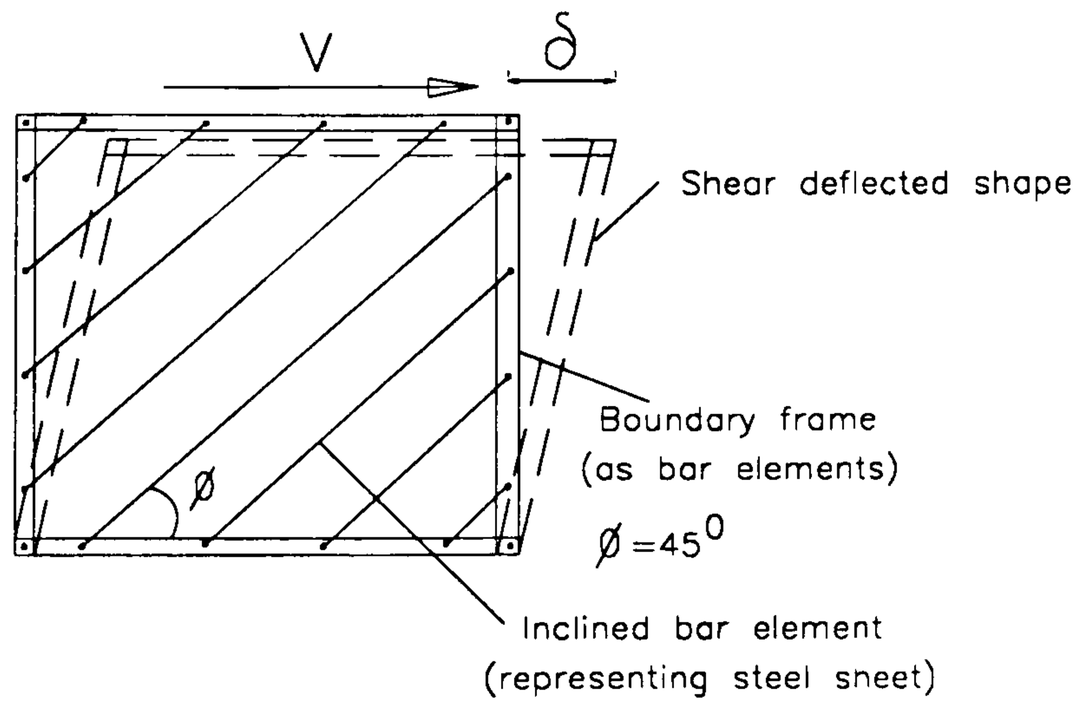

Figure 2.18: Inclined bar model for post-buckling analysis

Figure 2.18 shows the assembly of the model where tension field was represented by a series of bars inclined at an angle of 45^0. The bars were obtained by dividing the sheet into a series of inclined strips of equal width. The area of the bars were equal to the product of the width of the strip and thickness of the sheeting.

The model was incorporated into the LUSAS non-linear finite element programme using 3-noded bar elements for both inclined bars and boundary frame. The bars were assumed to be pin connected to the surrounding frame and were capable of transmitting axial force only. Loads were applied so that the complete assembly undergoes shear deformation as shown in the figure 2.18. From the finite element analysis shear load, V, and corresponding shear deformation ,δ, were found out. The ultimate load of the panel was reached when the inclined truss members were yielded.

2.5.4 Comparison of different analysis

Figure 2.19 has been presented to compare shear load-deflection curves from experimental, FEA and analytical studies. Analytical and FEA curves show an excellent agreement throughout the whole loading history.

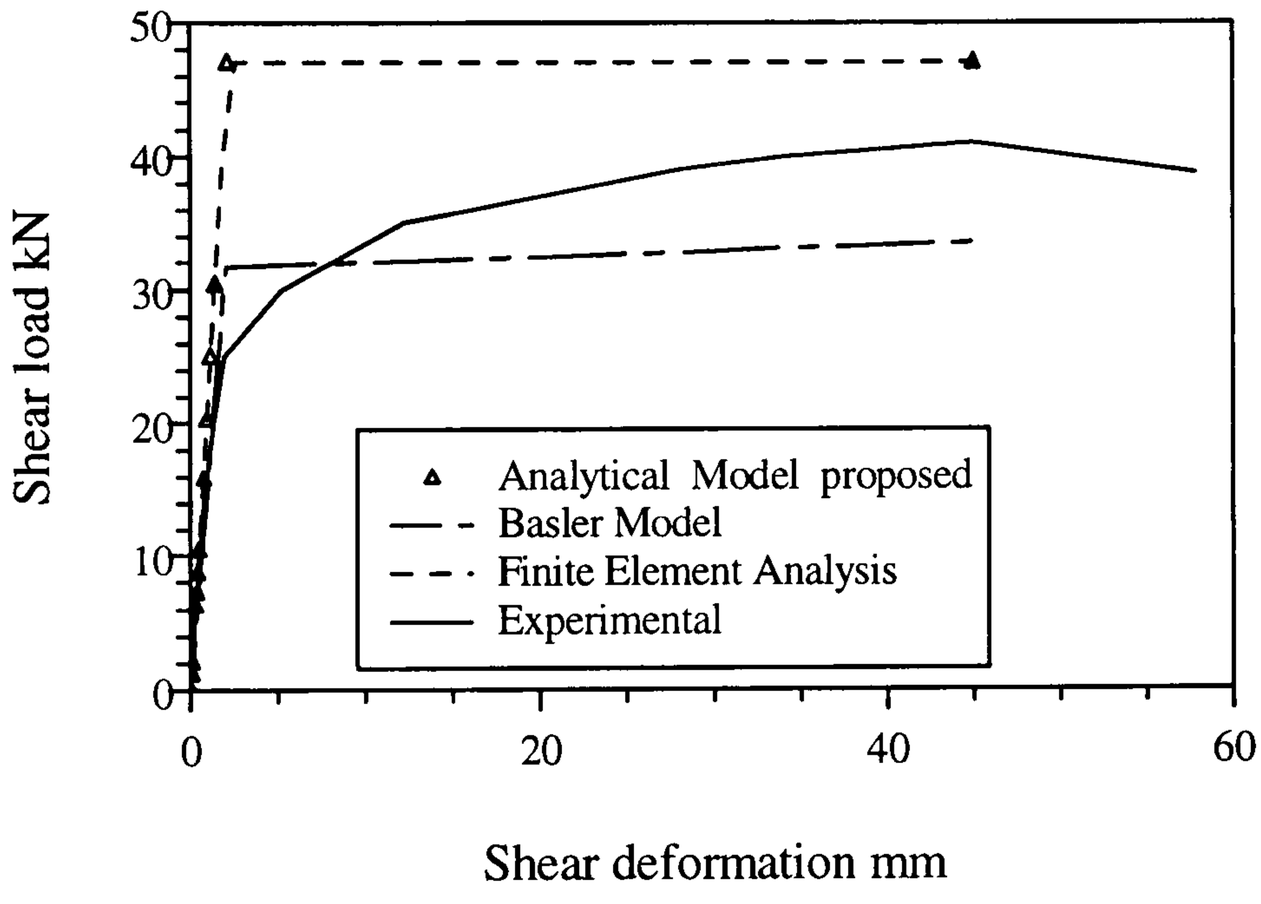

Figure 2.19: Comparison of load-deformation responses

It was not possible to study the pre-buckling behaviour of the thin sheet as bucking load was very small (only 0.27kN). However excellent agreement was found between analytical and finite element analysis in the pre-buckling stage when buckling load and stiffness were compared.

Table 2.2 is presented to compare overall behaviour of the panel.

Table 2.2: Comparative study of different approach

Analysis	Pre buckling stage				Post- buckl. stage				
	Vcr (kN)	c1 mm/kN	k1 (kN/ mm)	Diffe- rence k1 (%)	c2 mm/kN	k2 (kN/ mm)	Diffe- rence k2 (%)	Vult (kN)	Diffe- rence (%)
Model Test	–	–	–	–	0.053	18.87		4062	
Analytical Model Proposed	0.27	0.028	35.71		0.044	22.73	20.45	4704	15.80
Basler	-	-	-	-	0.063	15.87	15.90	3350	17.53
Finite Element	_	0.028	35.71	0.0	0.046	21.74	15.21	4727	16.37

Experimental post-buckling stiffness is 20.45% and 15.21% lower than those from analytical model and FEA analysis showing reasonable agreement. But 15.90% higher than Basler model.

Experimental load was 15.80% and 16.37% lower than those from analytical and FEA analysis but 17.53% higher than the Basler model.

The Basler ultimate load is lower due to the assumption that sheet failed when a diagonal tension band yield rather than whole panel as assumed in the proposed analytical model. Model sheet failed at stress concentration near the corner of the loaded diagonal by tearing of the sheet at bolt locations and yielding was observed in a substantial part of the sheet but not whole. Basler model may therefore be used as a lower bound and proposed model may be used as upper bound for the ultimate load of the panel. Experimental ultimate load is therefore in reasonable agreement with those from analytical models.

2.5.5 Study Conclusion on the significance of thin plain sheet test

The instrumented plain sheet test provided useful information on the variation of stress-strain within the panel throughout the loading history. It confirms the development of a pure tension field in the post-buckling stage and subsequent failure of the panel due to yielding of diagonal band as well as tearing of the sheeting at the

boundary. The variation of strains near the boundary edges is also revealed. The reasonable agreement of test result with analytical and numerical analysis validate the performance of the rig to model in-plane shear behaviour.

2.6 Conclusions

The following conclusions can be drawn regarding the performance of the shear rig:

- the shear rig will be able to model the overall in-plane shear behaviour of panels to be tested.

- the effect of corner pin deflections on the diagonal deformation of the panel is an important factor and to be carefully sorted out if they are included in the diagonal deformation measurement.

- linear load-deformation response of the corner pins was evaluated from test observations and their contribution to the overall diagonal deformation can be adjusted.

- The test frame behaved purely as a mechanism and did not contribute to the load carrying capacity of the panel tested.

- the performance of the shear rig can be considered as satisfactory.

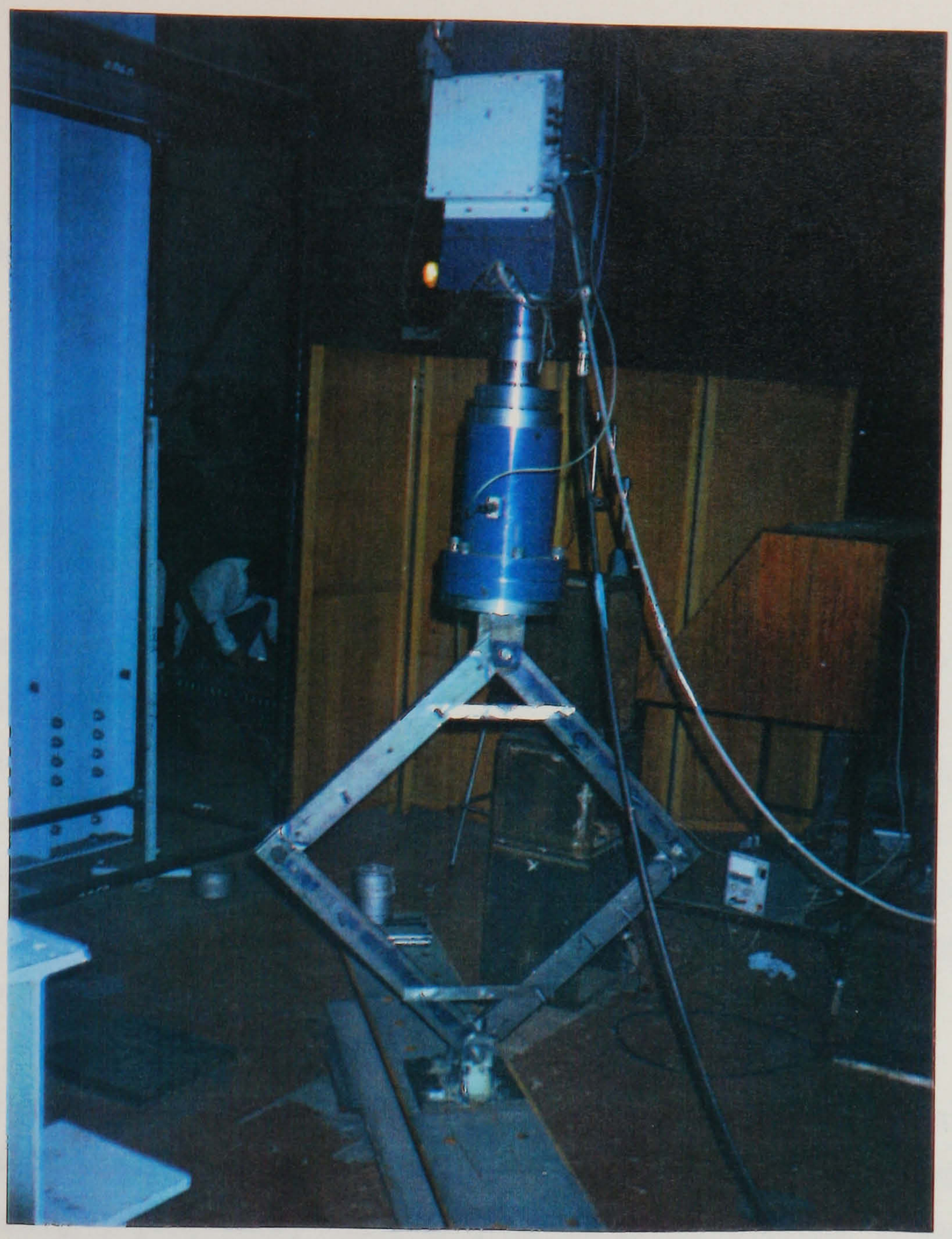

Photograph 2.1: Shear Rig

Photograph 2.2: Experimental set-up with plain steel sheet panel

CHAPTER THREE

SMALL SCALE MODELLING OF COMPOSITE WALLING WITH MICRO-CONCRETE

3.1 Introduction

Small scale model tests are designed to study the in-plane shear behaviour of the composite wall. This chapter will describe the modelling of the composite wall with micro-concrete. Model codes and derivation of the laws of similitude will be reviewed. Micro-concrete properties and its modelling will be described from an extensive literature review of the past research. The criteria for the selection of a gap-graded micro-concrete will be highlighted. Modelling of the profiled steel sheeting will also be described.

A model test on plain micro-concrete panel will be described to check the performance of the concrete. Numerical simulation of the behaviour of micro-concrete will be done using a proprietary finite element program, LUSAS. Finite element simulation of the actual test assembly will be described. Analytical model for strength and stiffness of plain concrete panel will be derived. Finally analytical, numerical and experimental results will be compared.

3.2. Model Analysis and Testing

Model studies are being established as acceptable methods for the direct design of structures in addition to providing data on general patterns of structural behaviour and checking experimentally, the results of analytical procedures.

Successful use of small-scale models in the analysis, design and constructions of building structures has been reported in the literature over the past two decades. Examples of scale models have been mentioned in ACI Committee 444's State-of-the-Art Report (1979). Sabnis,G.M.; White,R.N.; Harris, H.G.; and Mirza, S.M. (1982) presented specific applications in design study (The TWA hanger structures, Missouri and The Three Sister's Bridge, Washington) and in research (Cornell and Drexel

Universities projects). Recent advances in the areas of instrumentation, model materials and computer-controlled testing devices have further added to an increasing use of model studies for various kinds of structures subjected to dynamic, earthquake, wind, blast , thermal and other unusual types of loading. The examples of such studies are presented by Clarke, J.L.; Garas, F.K.; and Armer, G.S.T. (1985), ACI special publication (1982) and Armer, G.S.T., and Garas, F.K. (1982).

For large and complex structures, it is hardly practicable to test to destruction full size components and in these circumstances the designer must be content with the predictions of analytical procedures and /or model studies. Experimental methods are able to take into account many of the secondary effects and indeterminate factors which have to be neglected in analytical procedures in order to make them tractable. Model investigations are able to avoid many of the difficulties encountered in theoretical studies and are particularly advantageous when used to predict the behaviour of structures of unusual shapes or geometry, material properties and complex loading which are difficult to define in mathematical terms.

3.2.1 Model Codes of Practice

This section reviews the use of models in various codes, in Britain and other countries.

The ACI Building Code (1989) provides for the use of elastic models as an alternative for design of shell structures. It specifies a suitable methodology in the code and describes model analysis as a tool in the structural analysis and design in the Commentary. Some of the empirical formulas in the ACI Building Code (1989), for example , are based mainly on experimental results of reduced-scale model tests.

Australian Code (1974) was one of the first to allow model testing as an alternative to design calculations and code provision is reflected in the relatively large number of model-aided designs completed in Australia.

American National Standard ANSI A58.1 (ASCE A7-88, 1982) has also recognised models mainly for wind loads and to measure response of the structure to such loads using scale models. Specific guidelines are given for such applications.

The New York City Building code (1985) provides a more detailed statement and model analysis is permitted as a means of establishing the structural design.

The National Building Code of Canada (1985) permits the use of model analogues by a specially qualified person; however, no specific modelling procedures or limitations are specified.

The British Code of Practice for Bridges, BS 5400 (1984) permits the use of prototypes and models to define the load effects in a structure or to verify a proposed theoretical analysis. It specifies that model must be representative of the prototype, and model tests must be conducted and interpreted by experienced engineers. Guidelines are provided to establish the reliability of the test results and the safety factor based on the number of tests and the method of testing. In addition the BS 8110 (1985) has detailed provisions for the use of models in structural design.

Members of ACI Committee 444 (ACI Structural Journal, 1991) believe that the results obtained from a well-conducted structural model study, where scaling materials and geometry are properly considered, can be more reliable than those obtained from conventional analysis and design of a structure where the calculation accuracy is affected by many uncertainties in loading and material properties and also simplifications and approximations used. They made recommendations for ACI Building Code (ACI 318-89) to include models as a viable tool for design of structures. This recommendation encourages the proper use of physical models in a more positive manner in the ACI Building Code.

In summary, it can be stated that model analysis and testing have been accepted and recommended as a useful design alternatives in British Standard and in many different countries. The model tests and interpretation of the test results for the purpose of design must be carried out under the direction of expert in the relevant area. The modelling material may be glass, plastic, micro-concrete or other material which adequately approximates the behaviour of the prototype. The selection of model scale is important and its effect must be considered. The reliability of test results shall be assessed from the consideration of the following:

i. Model and prototype material properties,
ii. Relation between model and prototype loading,
iii. Methods of measurements,
iv. Equilibrium of loads and reactions and
v. Boundary conditions.

The interpretation of the test results for the purpose of design shall be based on :

i. Number of tests

ii. Similitude requirements

iii. Test procedures and loading history

iv. Methods used to derive load effect from measurements.

3.2.2 Model and Model Rules

Models may be classified as direct and indirect models irrespective of the objectives of the study. In indirect models, the actual loading of the prototype is not reproduced to scale and is used to model linear behaviour of the structures such as to obtain influence lines. The assumption of linear behaviour considerably simplifies the similarity requirements and a wide range of materials may be used for constructing the models. In the case of direct models the pattern of loading applied to the model is similar to that acting on the prototype. They may be used to simulate complete similarity of behaviour up to collapse. The choice of scales and suitable model materials are of paramount importance for the simulation of all aspects of the structural behaviour.

In model analysis certain rules must be fulfilled, to predict the behaviour of full scale structure from the model tests. The scaling factors by which any quantity in the model must be multiplied in order to obtain the corresponding quantity in the prototype, must be known. These scaling factors are obtained from the laws of similitude, which can be determined in one of two ways. The first approach is to consider the laws of structural mechanics, i.e. static equilibrium, compatibility of deformations, and stress-strain relationships. This approach is applicable only to static conditions or very slowly moving load system. The second approach is to use the method of dimensional analysis as described by Buckingham (Langhar, H.L (1967)), which can be applied quite generally to include any required phenomena, including dynamic or time-dependent effects.

If an equation is dimensionally homogeneous, i.e. the physical dimensions of each term in the equation must be identical to one another, it can be reduced to a relationship among a complete set of dimensionless products of the variables in the equation. This is known as Buckingham's pi theorem and is the fundamental basis of any dimensional analysis. The steps in dimensional analysis of any problem are :

i. The variables which are assumed to influence the structural behaviour are listed and their dimensions are determined.

ii. From these dimensions, the number of dimensionless products in a complete set is found.

iii. According to the theorem, some unknown function of the dimensionless products in this set must be zero. To determine the laws of similitude, the function need not be known, the only necessary condition being that the numerical value of each of the dimensionless products should be the same for the model or for the prototype.

3.3 Modelling of Double Skin Composite Wall

Small-scale modelling of composite walling is a new addition to the model investigation. The geometry of the wall having two skins of profiled steel sheeting and a core of concrete makes the model construction and testing more complicated. Small-scale model tests are designed to study the pure shear as well as bending plus shear behaviour of the wall. The simulation of pure shear behaviour using designed shear rig was a challenging task due to complex boundary condition of the problem. The use of micro-concrete with scaled profiled steel sheeting needed much care and attention during the whole sequence of fabrication, moulding, casting, curing and testing fulfilling the required boundary conditions.

Model tests also included the study of the pure shear behaviour of profiled steel sheet and profiled and plain concrete core alone.

The following steps will describe the modelling procedure and derivation of the laws of similitude:

i. Selection of Prototypes,
ii. Selection of model scale,
iii. Detail dimensioning of the scale models,
iv. Derivation of laws of similitude,
v. Selection of model steel sheet and profiling,
vi. Selection of micro-concrete and
vii. Planning of the model test program

3.3.1 Selection of prototypes

The full scale prototypes for the composite wall is shown in figure 3.1 for pure shear model tests. Square composite wall of dimension 3300mm x 3300mm x 180 mm (at crest) is selected for pure shear and 3300mm x 1500mm x 180mm (at crest) is selected for beam tests. The detail of prototype profiled sheet cross-section is also shown in figure 3.1.

3.3.2 Selection of model scale

The following factors are taken into account in the selection of model scale :

i. Complexity of the prototype and its boundary conditions,

ii. Availability of equipment for loading and monitoring behaviour and best use of existing facilities in the laboratory,

iii. Feasibility of providing appropriately scaled micro-concrete and availability of steel sheet of required thickness,

iv. Simple construction of shear rig,

v. Making model construction and testing simpler and

v. Costs

Considering all these factors, a 1/6th model was chosen. The scaled down model will have a minimum thickness of 14mm compared to 80mm in the prototype.

3.3.3 Detail dimensioning of the scale models

Complete geometric similarity between model and prototypes were maintained. The dimensions of the models were derived by using scale factor of 6 to the prototype dimensions. The detail dimensions of the composite wall models are shown in figure 3.2. The thickness of the sheeting was determined from the equality of the shear stiffness maintaining similitude requirement between model and prototype.

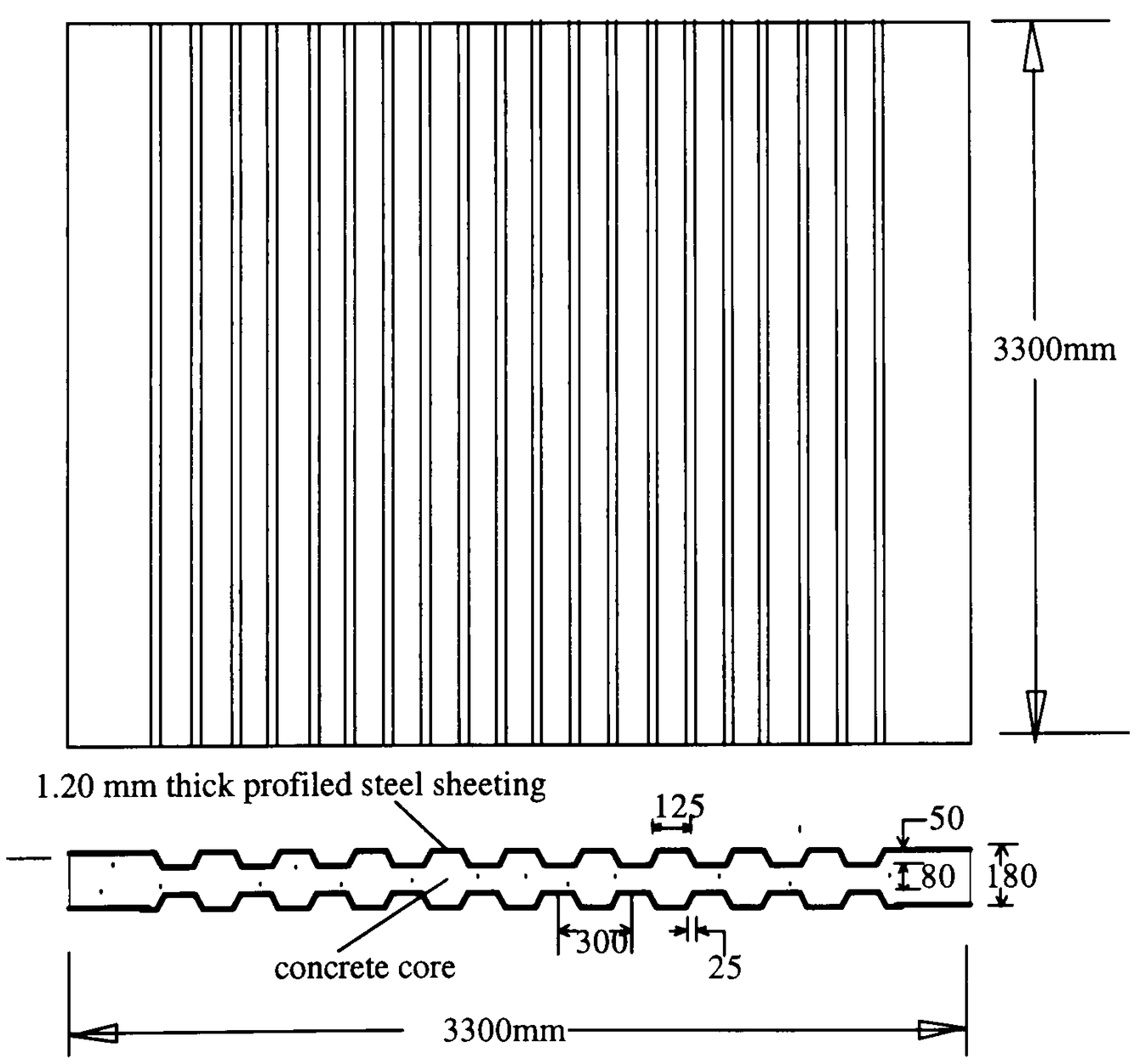

Figure 3.1: Composite wall full scale prototype

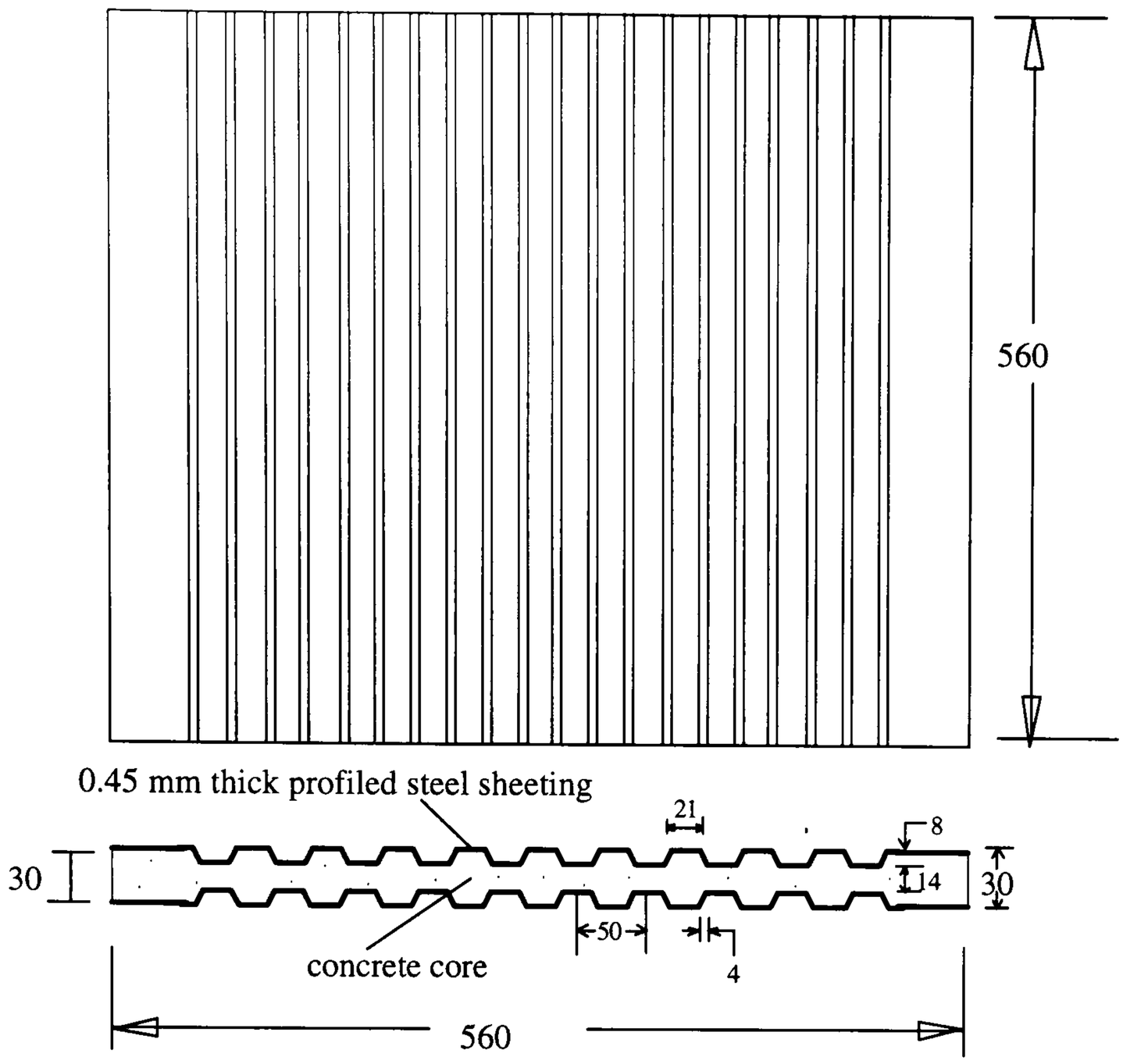

Figure 3.2: Composite wall model (Scale factor λ=6)

3.3.4 Derivation of the laws of structural similitude

The formulation of the variables which affect the behaviour of the composite wall was the main and difficult part in the dimensional analysis. The variables taken under consideration includes the material properties, physical dimensioning of the structure and the variables which influence the structural response such as shear stiffness of the profiled steel sheeting.

From the dimensional analysis (Preece, B.W. and Davies, J.D.,1964), the following laws can be summarised:

Complete geometric similarity between model and prototype is required. Apart from the equality of strains(ε), poisson's ratio (υ) and the co-efficient of linear expansion, the laws of structural similitude require that for the model, the displacement (u_m) and stress (σ_m), at any point, and the Modulus of elasticity (E_m) and density (ρ_m) of the material, should be in the following relationship to the corresponding prototype values (with suffix 'p').

$u_m = (1/S_l).u_p$

$\sigma_m = (1/S_f).\sigma_p$

$E_m = (1/S_f).E_p$

$\rho_m = (S_l/S_f).\rho_p$

where S_l and S_f are the length scale and the stress scale factors. The applied load relationships should be as follows:

Pressure or udl: $p_m = (1/S_f).p_p$

Point loading: $P_m = (1/S_f.S_l2).P_p$

The forces should be applied in exact magnitude and direction. The distribution of loads in model and prototype has to be the same.

When study of non-linear behaviour of the structure is considered, the geometric similarity is still required but the behaviour of the material can no longer be represented by E and υ. In this case complete similarity of the stress-strain relationship is required both for compression and tension. For composite wall, this should be satisfied for both concrete and steel.

The practical problems in the applicability of this rules will be described later in micro-concrete modelling.

3.3.5 Selection of model steel sheet and its profiling

The thickness of the profiled steel sheet is calculated from the equality of the shear stiffness of the model and prototype sheet. The shear stiffness equation of the profiled steel sheeting due to shear and bending distortion is taken. The full details of the equation is described in chapter 5. The stiffness (k) or flexibility(c) due to bending and shear deformation can be written as in table 5.1:

$c = 1/k = 0.144Kd^4/(Et^3ab) + 2b(1+\upsilon)(d+2h)/(atdE)$

= bending or distortion + Shear deformation

Using the equality of stiffness for model and prototype and applying the laws of similitude, the following relationships between model and prototype thickness can be derived:

Case 1: Only bending or distortion

Equality of stiffness of model and prototype sheeting :

$$k_p = \frac{E_p t_p^3 a_p b_p}{0.144 d_m^4 K} = \frac{E_m t_m^3 a_m b_m}{0.144 d_m^4 K} = k_m \quad \text{..... (3.1)}$$

$a_m=\lambda a_p$, $b_m=\lambda b_p$, $d_m=\lambda d_p$ where λ= scale factor .....(3.2)

Using equation 3.2 in equation 3.1, the relation between model and prototype sheet thickness can be derived as : $t_m = \lambda^{-.667}.t_p$

Case 2: Considering shearing deformation only

Equality of stiffness of model and prototype sheeting :

$$k_m = \frac{a_m t_m E_m}{2b_m(1+\upsilon_m)\left[1+\frac{2h_m}{d_m}\right]} = k_p = \frac{a_p t_p E_p}{2b_p(1+\upsilon_p)\left[1+\frac{2h_p}{d_p}\right]} \quad \text{.....(3.3)}$$

$a_m=\lambda a_p$, $b_m=\lambda b_p$, $d_m=\lambda d_p$, $\upsilon_m=\upsilon_p$ and $E_m=E_p$ . .....(3.4)

using equation 3.4 equation 3.3, the relation can be derived as:

$t_m = \lambda.t_p$ .....(3.5)

Case 3: Considering combined bending and shear

Equality of stiffness of model and prototype sheeting :

$$k_m = \frac{E_m t_m{}^3 a_m b_m d_m}{0.144 d_m{}^5 K + 2b_m{}^2 t_m{}^2(1+\upsilon_m)(d_m+2h_m)} = k_p = \frac{E_p t_p{}^3 a_p b_p d_p}{0.144 d_p{}^5 K + 2b_p{}^2 t_p{}^2(1+\upsilon_p)(d_p+2h_p)} \quad \text{..(3.6)}$$

Using equation 3.4 and 3.5 in equation 3.6, The relation between model and prototype sheet thickness can be derived as : $t_m = \lambda^{-.667}.t_p$ .....(3.7)

For 1/6th scale model, the equation 3.7 relating thickness of model sheeting (t_m) to that of prototype sheeting (t_p) becomes: $t_m = .3027.t_p$

From this equation, for a prototype sheet thickness of 1.20 mm, a 0.363mm thickness model sheet is required.

It was difficult to get a properly scaled down thin sheet and profiling it according to its dimension. The thin sheet also cause problem in profiling due to its brittle properties. It was decided to use locally available steel sheet of minimum thickness. A galvanised plain steel sheet having an effective thickness of 0.45 mm was used.

Profiling of sheeting

A pair of fly press steel dyes were fabricated. Profiling of the sheet was done by pressing the sheet between the dyes. The whole set up showing the profiling of the sheet is shown in the photograph 3.1. The movement of the two dyes relative to each other was controlled by using guide bolts at the ends so that the both dyes can move in the same vertical plane during pressing maintaining uniform cross-section of the profile. The profiled steel sheets were found to be distorted due to residual stresses developed as a results of profiling. The effect of residual forces was minimised by pressing the sheeting three times (at the ends and in the middle) in each profile.

3.3.6 Selection of micro-concrete

The selection of suitable model material for a structural model depends upon several requirements. The material must meet the laws of similitude and certain practical requirements. The choice of suitable micro-concrete was an important aspect of our model investigation. An extensive literature review on previous micro-concrete research has been done and a brief description is presented here:

Micro-concrete and its essential properties

A suitable material with which to simulate the behaviour of concrete structures has been sought for years by many investigators. A bibliography by White and Sabnis (1966) is a comprehensive tabulation of the research conducted on structural models. Micro-concrete is widely accepted as the material to model reinforced concrete structures. Micro-concrete can simulate most of the properties of the actual concrete because : a) stress-strain curves up to failure, b) the ratio of tensile to compressive strength (C_t), c) poisson's ratio and d) E-value can be made homologous to that of actual concrete.

Micro-concrete is not really a scaled down concrete as it is not feasible to scale cement and fine aggregate of actual concrete, to exact model scale. When aggregates (both coarse and fine) are scaled, it requires a large amount of aggregate finer than 100 or 200 U.S. sieve and there remains no existence of coarse aggregate. The model material would then consist only of cement, water and fine aggregate. Therefore, it would be designated as mortar. Since the gradation curve of the total aggregate should be scaled down in accordance with the geometric scale factor, this mortar might be designated as a 'micro-concrete'.

To avoid large amount of air voids in micro-concrete, White, Sabnis and Harries (1966) limit the amount of aggregate finer than no. U.S. 100 sieve to less than 10% besides modifying the entire aggregate gradation curve which results in steeper gradation curve for aggregate. They also recommended maximum aggregate size for a given minimum model dimension.

Most of the researchers used locally available sand with the coarsest particles removed with the geometric scale factors and minimum model size. Besides some researcher used Ottawa sand, Geneva filter sand, Leighton Buzzard sand and crushed lime stone with proper gradation. Ordinary portland cement or high early strength was used.

Sommervile,G.; Roll,F. and Caldwell,J.A.D (1965), Waldron,P.; Pinkey,M.W. and Perry,S.H. (1980) used gap-graded sand to increase workability without using excess water or an admixtures.

It is known that the ratio of compressive to tensile strength (C_t) decreases as the aggregate of the mix are reduced in size and for micro-concrete it is therefore low. As a result, the cracking loads are high and crack widths too broad. It is therefore, necessary to develop a micro-concrete of less tensile strength without affecting the E-value or the compressive strength. Investigations were conducted on C_t ratio as this is the convenient parameter for modelling both tensile strength and ductility. This can be made possible by suitably adjusting the water-cement ratio, nature and size of aggregates, aggregate-cement ratio and by using additives. For practical building purposes, C_t for normal concrete lie above 9.0. This value of C_t was achieved by Muller, R.K.(1985) and Majlessi, Noor and Newman (1985) only by adjusting the amount of cement, aggregate, sand and water without using any additives. A gap-graded mix, used by Noor, F.A. and Khalid, M. (1980), of favourable workability gives the values of C_t about 13.0. For greater reduction of tensile strength, Muller(1985) coated larger fraction of the aggregates with a separating agent on a silicon base which interferes in the contact region between cement and aggregate. Noor,F.A. and Wijayasri (1982) found that a gap-graded mix in which more than 50% of the 2mm single size aggregate was replaced by 2mm glass beads produce the value of C_t as high as 16.0. Hughes (1966) came to the conclusion that the size and shape of the aggregate also affect the C_t ratio. Larger rounded particles produce reduction in bond between aggregate and cement paste.

Micro-concrete of low strength and workability can be obtained by replacing a large amount of cement by pulverised fuel ash (Kumar and Dupuch (1980)).

One way, used by Swamy, R.N. and Faisal, M.F. (1985), to minimise bleeding and to improve bond with steel is to use fly ash and premixing water with aggregate so that aggregate particle can be coated with layer of cement paste.

Casting and curing

Methods of mixing, compaction and curing were different for different Researchers. Some Researchers preferred hand mixing for small batches and machine mixing for large batches. Specimens were compacted on vibrating table or with a small poker. For workability assessment slump, third scale slump or spread measurements were

used. Under water curing or moist curing was used. Johnson,R.P.(1962) found that a scaled-down slump test is unsuitable for use with scale down mixes of low workability.

Testing

A large number of investigations were performed to study the size effects in control specimens. Majlessi, Noor and Newman (1985) suggested that the differential compaction in micro-concrete is one of the sources of variation in strength. Fresh density method of compaction control was proved to be suitable. It was found that the strength of cubes with similar wet densities were close for all cube sizes proofing that the compressive mechanism of failure in concrete is independent of size of control specimens provided all the boundary conditions are controlled. For practical purposes 50mm cube is recommended as the smallest size for most model work.

Similar type of research by Sabnis,G.M.; Harries,H.G.; White,R.N. and Mirza,S.M.(1982) confirmed that differential density and differential moisture content were the critical factors in size effects. An extensive series of test on cylinders proved that the size effects in uniaxial compression and in split cylinder strength disappeared when compaction procedures were used that produced uniform density in the cylinders of all sizes and when drying conditions were controlled to provide the same moisture content in all sizes cylinder.

ACI models committee (Long,A.(1980)) suggested that as well as testing properly scaled specimens it is advisable to test 100x50mm cylinders in addition as datum.

Tests of the specimens can be done in accordance with B.S.1881:1952. It could be desirable to use lower rates of loading for smaller specimens as Wright,P.J.F(1952) found that increased rate of loading increases the apparent strength of the test specimens. Johnson,R.P.(1962) suggested that little error will be introduced by using 4000psi per minute for compression and 200psi per minute for split tension. He also suggested that the width of the plywood packing strips for split tensile test should be 1/12th of the cylinder diameter. Long,A (1980) reduced the width from 1 inch to 1/4 inch and found that the tensile strength was reduced by around 30%. To avoid this dilemma for micro-concrete, most sensible option is not to use plywood strip at all. This has been done by White and Clark (1977).

Reinforcement for Micro-concrete

The availability of reinforcement which is ideal for use in micro-concrete models is difficult to model. The characteristics of prototype reinforcement that must be considered are the shape of the stress-strain curve, yield strength and bond characteristics. The failure of ductile material usually implies either initiation of yielding or the development of plastic hinge or mechanism. Therefore, the stress-strain curves need be homologous only up to and into the yield range. The selection of reinforcement is also governed by the cementitious material because the stress and strain scale factors must be the same for both concrete and reinforcement. The simplest way of achieving this is to use steel although it may require some annealing or cold working for the equality of stress-strain curve.

Bond Characteristics

It is relatively simple to satisfy the requirements for stress and strain similitude but it is considerably harder to meet the bond requirement. In search for proper reinforcement material for micro-concrete, Maisel, E (1980) found that hot dipped galvanised plain steel wires give the best bonding. Rusted or threaded or deformed bars were found to give better bond than plain diameter round bar. Investigations by White and Clark (1977) confirmed that coarse aggregate mixes give higher ultimate bond strength than fine aggregate mixes. Aggregate size has greater influence on bond but aggregate shape has little influence when used in conjunction with deformed rather than plain reinforcement.

Crack simulation

The cracking behaviour of model depends mainly upon two parameters namely the tensile strength of concrete and the bond properties of reinforcement. Clark (1980) tested slab models to simulate cracks in reinforced micro-concrete. The test data indicated that cracking does not scale and this is due to the material properties and size rather than scale of the model. Model crack spacings are relatively greater than those for the prototype.

Time effects

As the mechanical properties of concrete are a function of time, tests generally have to be carried out when the concrete has obtained the required strength. The shrinkage of the concrete -although also a function of time - is mainly determined by the linear dimensions, so for the model the time scales for strength and shrinkage are different. Waldron, P and Perry, S.H.(1980) found that the initial shrinkage rates are relatively

much larger for smaller specimens, but became less important with age.

Micro-concrete and similitude requirement

As micro-concrete is composed of the original materials but more or less linearly scaled down, poisson's ratio, density, strain, co-efficient of linear expansion, damping ratio and modulus of elasticity are the same for model and prototype. Equality of modulus of elasticity makes the stress and strain scale factors unity for micro-concrete.

The main advantage of the use of micro-concrete as a model material is the possibility of a full simulation of the real structure at relatively low cost. The main disadvantage is that the equality of modulus of elasticity needs the density of model concrete equal to the length scale factor times density of the prototype concrete. In practice, density simulation is achieved by imposing additional load by some means to the model.

Review conclusion

The following basic guidelines for micro-concrete modelling can be summarised:

a. Models should be made as big as practically possible to minimise scale effect.
b. Micro-concrete should have a properly scaled maximum aggregate size and compressive to tensile strength ratio representative of prototype concrete.
c. A properly controlled micro-concrete can simulate most of the laws of similitude and is ideal for modelling full scale concrete.
d. Care should be taken to maintain uniformity in casting and curing procedures for all model tests.
e. Control specimens should be tested for each of the model tests to take care of the variability of micro-concrete properties.
f. Reinforcement should have satisfactory bond characteristics and well defined yield point.
g. Modelling should be simplified by using locally available materials for micro-concrete and reinforcement.

3.3.6.1 Micro-concrete used for small scale tests

A gap-graded micro-concrete suitable to the model scale has been tested in the laboratory and selected for use in model tests. The micro-concrete has aggregate-cement ratio of 3.0 and water-cement ratio of 0.6 by weight. Portland cement and locally available sand (B.S. Sieve 7-14 = 50% and B.S. Sieve 52-100= 50%) are used.

The following points were considered in selection :

0 gap-graded mix has the advantage of increasing workability without using excess water or an admixture.

0 the mix approximates to a 1/8th scale concrete based on 19mm maximum size aggregate. Maximum size of the aggregate in the mix is 2.41mm which satisfy the recommended maximum aggregate size (White,R.N., Sabnis, JM,and Harries, HG (1966)) for minimum model dimension (14mm in our models).

0 the aggregate finer than B.S. 100 (maximum recommended is only 10%) is absent which may have favourable effect in reducing the amount of air voids and water requirements for mortar

0 this is a slightly modified version of a well known micro-concrete used by many Researchers - Waldron, P; Pinkney,M.W. and Perry, S.H. (1980), Waldron, P. and Perry, S.H. (1980) and Sommervile,G; Roll, F. and Caldwell, J.A.D. (1965), and widely used for 1/4th to 1/16th scale mixes.

The performance of the micro-concrete and its properties will be analysed in the next section.

3.3.7 Small-scale model test program

The model tests are planned from the assumption that the strength and stiffness of the composite wall will be derived from the individual strength and stiffness of concrete core and sheeting and also from the interaction between sheeting and core. Therefore, tests are planned to investigate the behaviour of sheeting and core individually besides composite wall tests. The tests are designed to give information on strength, stiffness, stress-strain characteristics, failure and also hysteretic behaviour of the system. The model test program is presented below:

1. ***Design and fabrication of a shear rig***
   (described in Chapter 2)
2. ***Pure shear test on***
   - Plain steel sheet
   - Plain concrete
   - Profiled concrete
   - Profiled steel sheet
   - Composite wall (load applied to both concrete and steel)
   - Composite wall (load applied to concrete only)
   - Plain composite wall

3. ***Hysteretic test on***
   - Profiled concrete
   - Profiled steel sheet
   - Composite wall
4. ***Beam test*** : Composite wall

3.4 Analysis of Micro-concrete properties

In this article, the properties of micro-concrete obtained from model tests will be described along with the properties of typical concrete.

Stress-strain curve

A typical uniaxial tension or compression stress-strain curve for concrete is shown in figure 3.3. This stress-strain curve is linearly elastic up to 30% of the maximum compressive strength (f_{cu}). Above this point the stress increases gradually until it reaches f_{cu}. Immediately after the peak value, the stress-strain curve descends and crushing failure occurs at an ultimate strain ε_{cu}. The descending part is called softening. The stress-strain curve for micro-concrete is shown in figure 3.4. The curve is similar to the typical concrete curve but it was not possible to record the softening part from the compression test of cylinder due to the manual monitoring of strains by demec gauges.

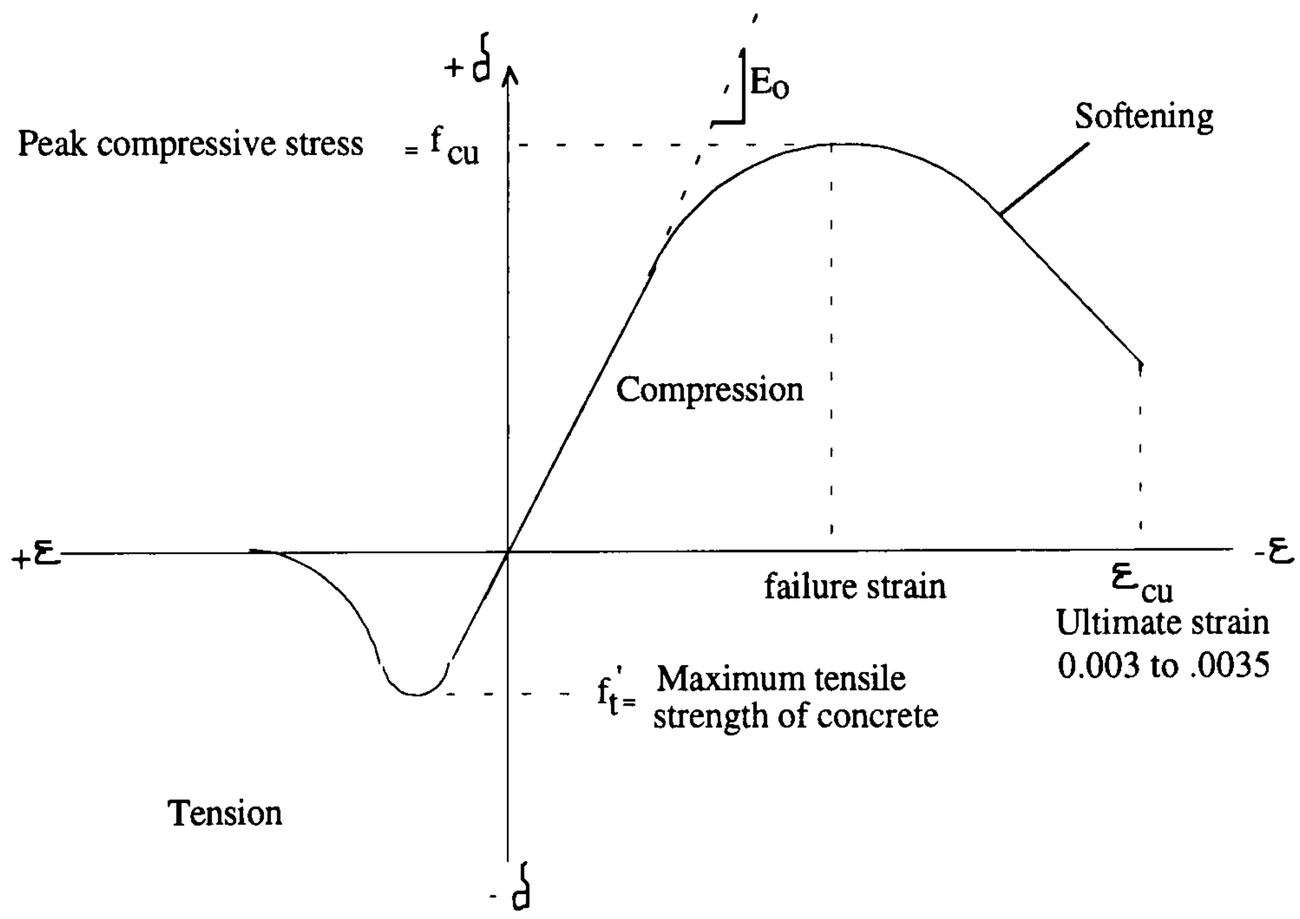

Figure 3.3: Typical stress-strain curve for concrete

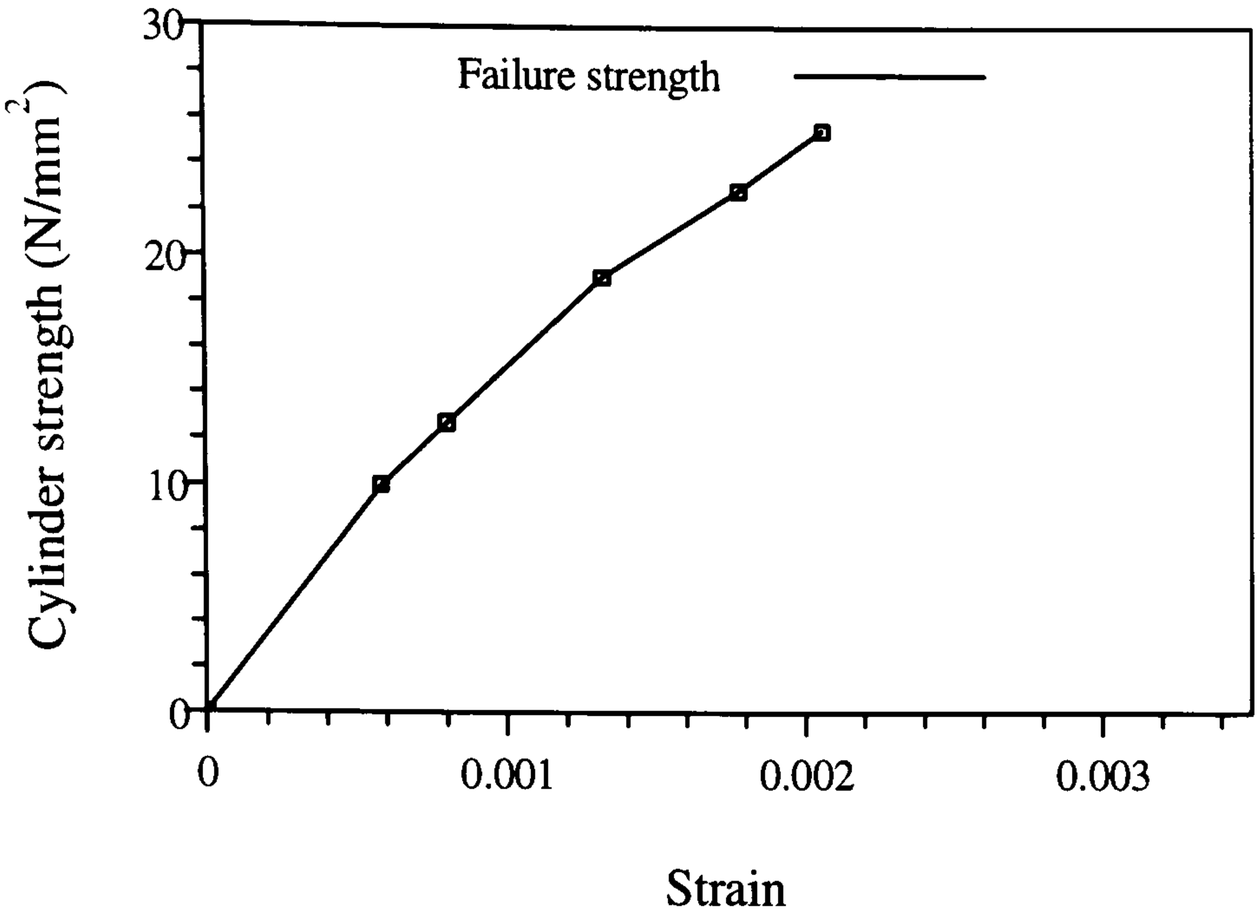

Figure 3.4 : Typical stress-strain curve for micro-concrete

Modulus of Elasticity

Cylinders of size 100x200mm have been tested in the laboratory according to B.S.1881,1970 to determine stress-strain curves, E-values and peak compressive strain. The results are presented in table 3.1.

Table 3.1: Modulus of Elasticity of micro-concrete

Sample No.	Age days	E kN/mm^2	f'_c N/mm^2	Peak Compressive strain
1	20	15.10	20.50	-
2	33	17.59	28.01	0.0022 *
3	40	18.20	28.37	0.0017 **

* measured at 91% of the ultimate stress

** measured at 82% of the ultimate stress

The modulus of elasticity of micro-concrete is well within the range of normal concrete.

Strength of micro-concrete

Concrete generally shows variable properties which are difficult to predict. The prediction of micro-concrete properties needs much more attention. For this reason, control specimens have been cast for each test. Cubes (70x70x70), cylinders (100x200) and beams(230x50x50) were cast to determine compressive cylinder strength (f'_c), cube strength (f_{cu}), splitting tensile strength (f'_t) and modulus of rupture from centre point beam bending (f_r). The table 3.2 has been prepared from these tests on plain and profiled concrete.

Table 3.2: Properties of micro-concrete

Test	Age	f_{cu}	f'_c	f'_t	Wet density	C_t
	days	N/mm^2	N/mm^2	N/mm^2	kg/m^3	
Plain	23	29.00	27.00	2.40	2326.5	11.2
Profiled						
1	40	21.00	----	2.323	2356.0	
2	21	31.73	21.00	2.467	2300.0	8.5
	33	----	28.01	2.665		10.5
3	40	28.37	23.42	2.39	2260.0	9.8
4	30	24.00	23.30	2.48	2360.00	9.4
5	35	24.68	22.00	2.45	2300.00	8.98

The mean wet density of the micro-concrete is 2317 kg/m^3 which is close to the 2400 kg/m^3 of plain concrete according to CEB-FIP Model code (1990). Wet density of the micro-concrete was taken as the measure of compaction control in the specimen.

The compressive to tensile strength ratio C_t (f'_c/f'_t) for micro-concrete varies from 8.5 to 11.2 which satisfy the normal requirement of above 9.0.

The table 3.3 shows the relation between tensile strength from splitting cylinder and centre point beam test. The relation is similar to that for normal concrete.

Table 3.3: Tensile strength of micro-concrete

Test	Split cylinder	Modulus of rupture	f_r/f'_t	Age
No.	f'_t	f_r		days
	N/mm2	N/mm2		
1	2.323	4.92	2.12	40
2	2.467	5.94	2.40	21
3	2.865	6.60	2.30	33

3.5. Small-scale model test on plain micro-concrete panel

A model test was carried out on a plain micro-concrete panel to study its behaviour under in-plane shear. This test will also check the performance of micro-concrete and the ability of the shear rig to handle small-scale concrete. The panel has a square

effective dimension of 560 x 560 x 22 mm.

Casting and Curing

The panel was cast in a vertical wooden mould in which provision has been made for making holes at the boundary of the casted panel. During casting, plastic spacers were used between the two ply wood boards of the mould. The micro-concrete was machine mixed and then poured into the mould by hand using a spatula. During casting, the micro-concrete was compacted by hand with a rod having square cross-section and also compacted by vibration in different layers on a vibrating table. After 24 hours the panel was removed from the mould and the plastic spacers from the holes were taken off. The panel was then cured under dry condition.

Testing and observation

After curing, the panel was fitted to the test frame of the shear rig using bolts across the holes. Plastic paddings were used between frame members and the panel to have a plane surface. The bolts were made tight so that there was no relative in-plane movement between the frame members and the panel. The complete experimental set-up showing the position of LVDT's to measure diagonal deformation is shown in the photograph 3.2.

The panel was then tested to failure by applying tensile force along a diagonal. Diagonal load deformation response was monitored by computer aided data acquisition system. The panel failed due to the formation of a major diagonal crack along the off-diagonal at about 32kN as shown in photograph 3.2. The test was satisfactory as the panel failed in a manner demonstrating pure shear behaviour.

3.6. Analytical model for plain concrete panel

Analytical model for strength of the plain micro-concrete panel will be derived based on bi-axial stress condition in normal concrete. A large number of failure criteria have been proposed by many investigators. The failure criteria proposed by Kupfer and Gerstle (1973) and Balakrishnan and Murray (1988) will be adopted in this study.

Failure criteria (Kupfer and Gerstle)

Material failure is referred to a stress envelope formulated in terms of the principal stress components (σ_1 , σ_2); figure 3.5.

1. Tensile failure

For tension-tension region, Kupfer and Gerstle suggest a constant tensile strength equal to the tensile strength of concrete (f'_t). The stress criteria can be written as :

$\sigma_1 - f'_t \leq 0$ and $\sigma_2 - f'_t \leq 0$

For tension-compression region : the boundary is defined as

$\sigma_1 / f'_c = (f'_t / f'_c)(1 - \sigma_1 / f'_c)$ and

$\sigma_2 / f'_c = (f'_t / f'_c)(1 - \sigma_2 / f'_c)$ ..... (3.8)

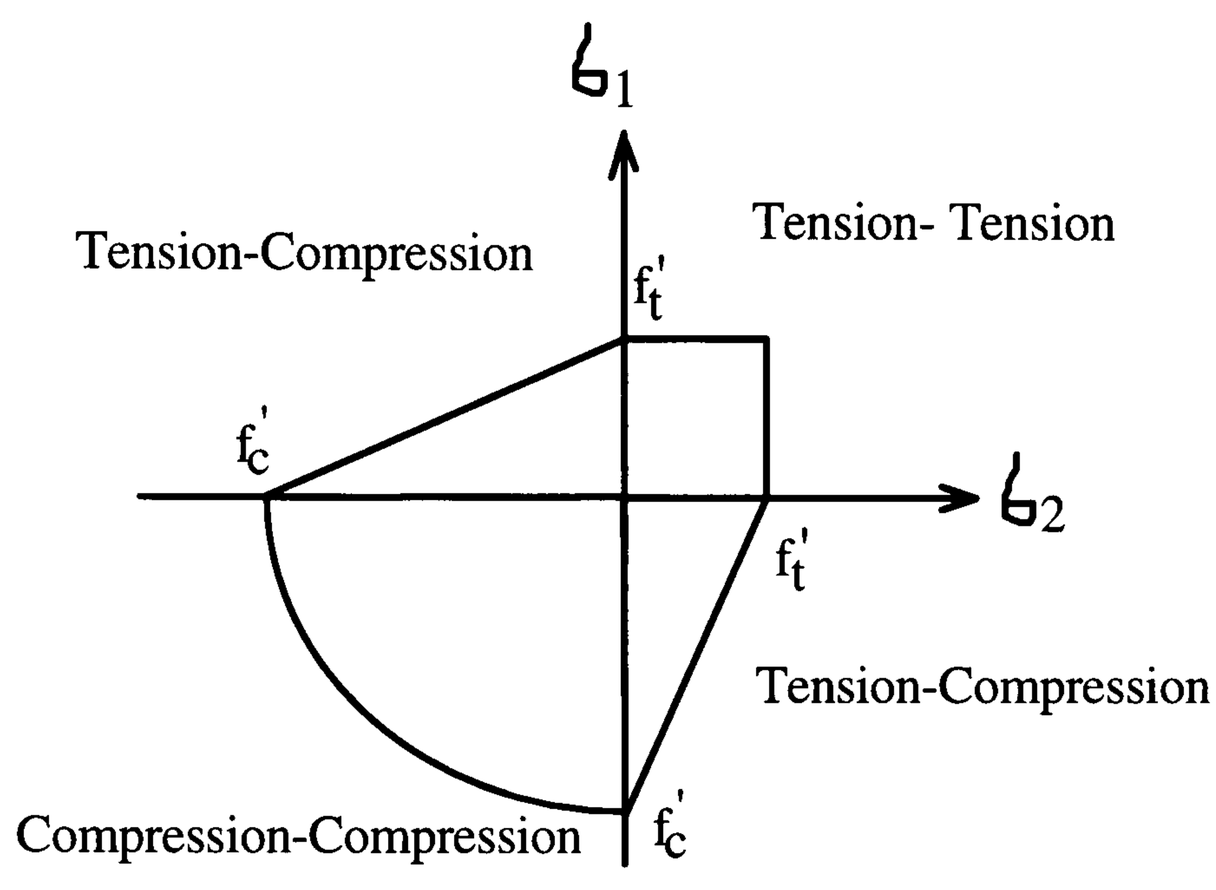

Figure 3.5: Bi-axial failure envelope (Kupfer and Gerstle, 1973)

2. Compressive failure

In the compression-compression region the peak principal stress is defined by the expressions

$\sigma_1 = f'_c(1+3.65\,\alpha)/(1+\alpha)^2$ and $\sigma_2 = \alpha\, f'_c(1+3.65\,\alpha)/(1+\alpha)^2$

where $\alpha = \sigma_1 / \sigma_2$ and f'_c is compressive strength of concrete.

Balakrishnan and Murray described that concrete cracks in tension compression region if

$\left|\frac{\sigma_2}{\sigma_1}\right| < \left|\frac{2 f'_c}{f_t}\right|$ and

$\sigma_1 = 2 f'_c / (\sigma_2 / \sigma_1 + 2f'_c/f_t)$ ....(3.9)

Analytical model for strength

Figure 3.6 shows a panel subjected to pure shear stress. For a square panel under pure shear, the direction of principal stresses should coincide with the direction of the panel diagonals. This is confirmed by the model test which showed a pure shear failure. The panel failed due to the development of diagonal tension. For the case of pure shear, the principal stresses (σ_1, σ_2) can be written as $\sigma_1 = \sigma_2 = \tau = V/bt = V/at$.

Ultimate load for the panel can be written as:

$$V = \sigma_1 at = \left[\frac{f_c' f_t'}{f_c' + f_t'}\right] at \quad \text{Kupfer and Gerstle}$$

$$= \frac{2f_c'}{\frac{\sigma_2}{\sigma_1} + \frac{2f_c'}{f_t}} at \quad \text{Balakrishnan and Murray} \qquad \text{.....(3.10)}$$

where for the tension-compression zone of failure the σ_1 and σ_2 can be derived from equations 3.8 and 3.9.

Analytical model for shear stiffness (k_c)

The linear (pre-cracking) shear-load deformation response and shear stiffness can be derived considering the concrete as a linear elastic material. If a panel subjected to shear force, V, undergoes shear deformation, δ, as shown in figure 3.7, then by applying strain energy approach as described in section 2.5.2.2 of chapter 2, the shear stiffness (k_c) for plain concrete panel can be written as

$k_c = V/\delta = E_c at/(2b(1+\nu_c)$ .....(3.11)

The pre-cracking shear load-deformation response can be written as $V=k\delta$.

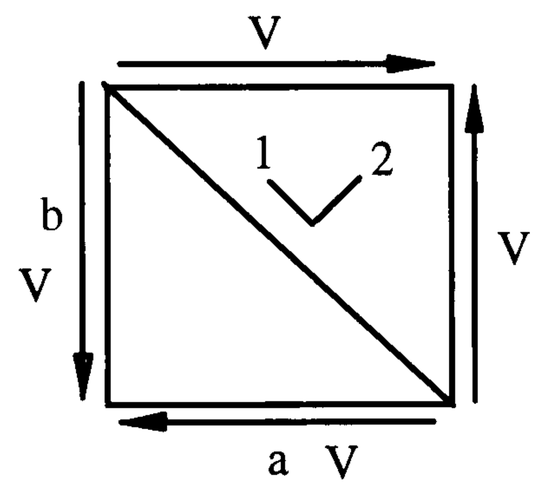

1, 2: Principal directions

Figure 3.6: Square panel under pure shear

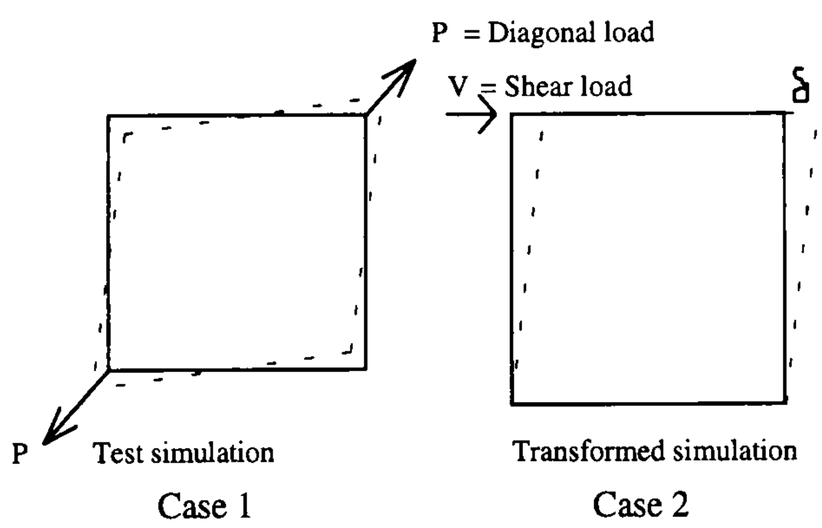

Figure 3.7 : Panel subjected to shear deformation

3.7 Numerical Modelling of Micro-concrete

As a gap-graded micro-concrete is used to represent the concrete in small-scale model test program of composite wall research, the finite element analysis of the behaviour

of concrete core and composite wall using proprietary program LUSAS requires proper simulation of micro-concrete behaviour. The application of the LUSAS concrete model to represent micro-concrete needs the adjustments of variables affecting the properties of concrete so that the numerical load-deformation response matches closely that from model tests. The data from the model plain concrete panel test has been used to simulate micro-concrete behaviour using LUSAS.

3.7.1 The features of the LUSAS concrete model

The concrete model in LUSAS (1987) has been developed for plane stress applications and can be used to study the non-linear response of the reinforced concrete structures. Concrete failure criteria used was that proposed by Kupfer and Gerstle (1973). A Smeared cracking model is used to represent cracks in concrete. Cracking is assumed to occur when one or both, of the principal stresses are in violation of the cracking criterion defined by the tensile failure envelope. Shear transfer across a crack is modelled using a shear retention factor,β, whose values varies from 0 and 1. Constant or variable shear retention models are available but in this case the constant model was used. Strain-softening or tension stiffening is implemented as a descending branch of the tensile stress-strain relationship for concrete, which gradually releases the stress normal to the crack. The numerical value (ranges between 5 to 50) of the softening parameter is uncertain, problem dependent and may be critical for problems with brittle failure. The LUSAS concrete model has some limitations: it gives load-deformation response in the form a straight line rather than a curve with continously decreasing slopes as the cracking continues and no definite indication of failure load as it is based on cracking.

3.7.2 Numerical simulation of plain micro-concrete panel test (case 1)

Finite element idealisation (shown in figure 3.8(a)) of the complete test assembly of the model is by 2D, 8-noded plane membrane elements having two degrees of freedom at each node for concrete panel, 2D,2-noded beam elements having 3 degrees of freedom at each node for boundary frame and 2D joint elements having two degrees of freedom to connect the frame and panel. Appropriate boundary conditions have been given so that hinges can be simulated at the corners and the frame can act as a mechanism. The stiff connection between frame and panel is achieved by providing very high stiffness to the joints. The structure is then restrained at one corner and the loads in the form of prescribed displacements are applied at the diagonally opposite corner simulating exact model test condition. The load is then applied incrementally until failure of the panel to obtain complete diagonal load-deformation response.

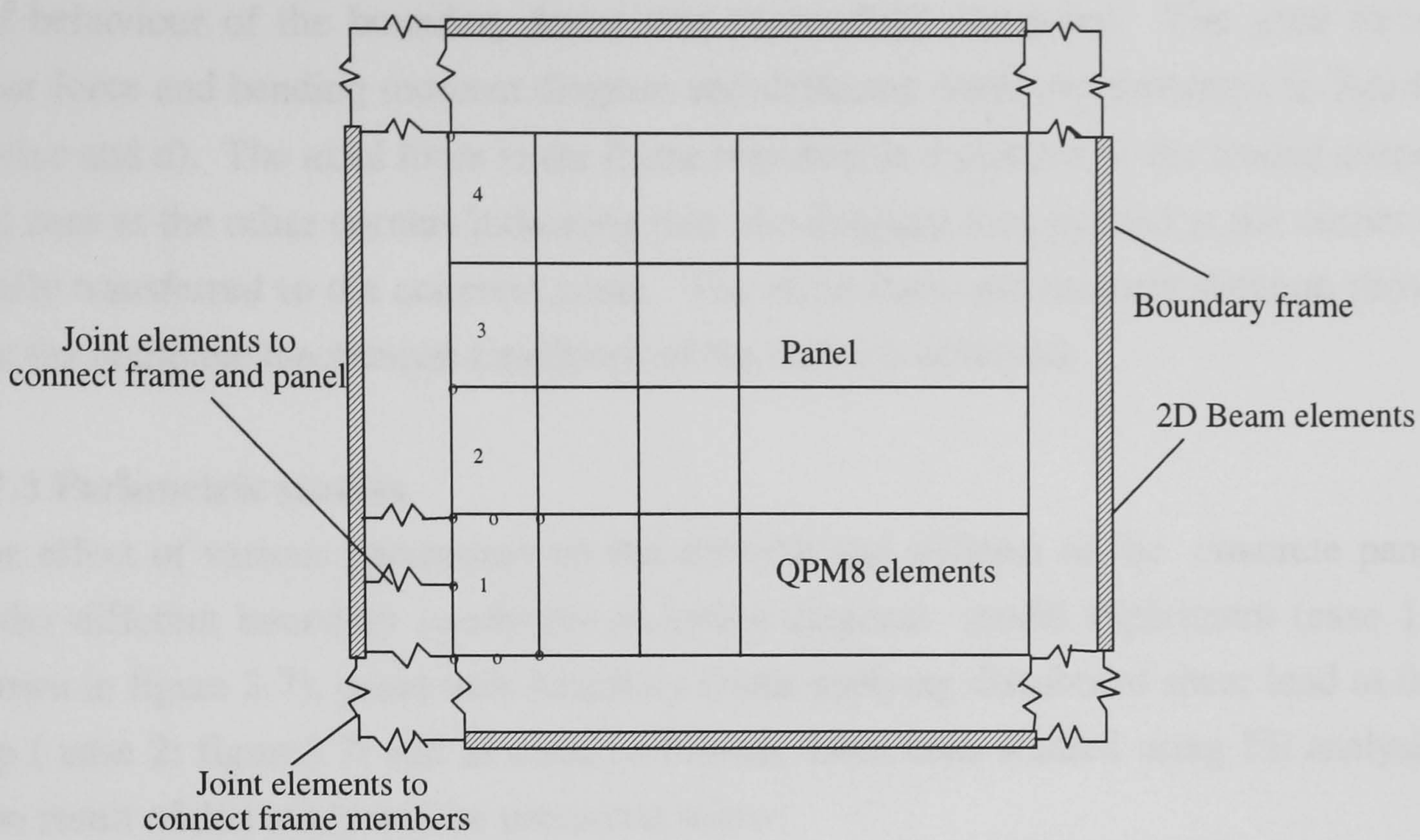

Figure 3.8(a): Finite element idealisation of model test simulation

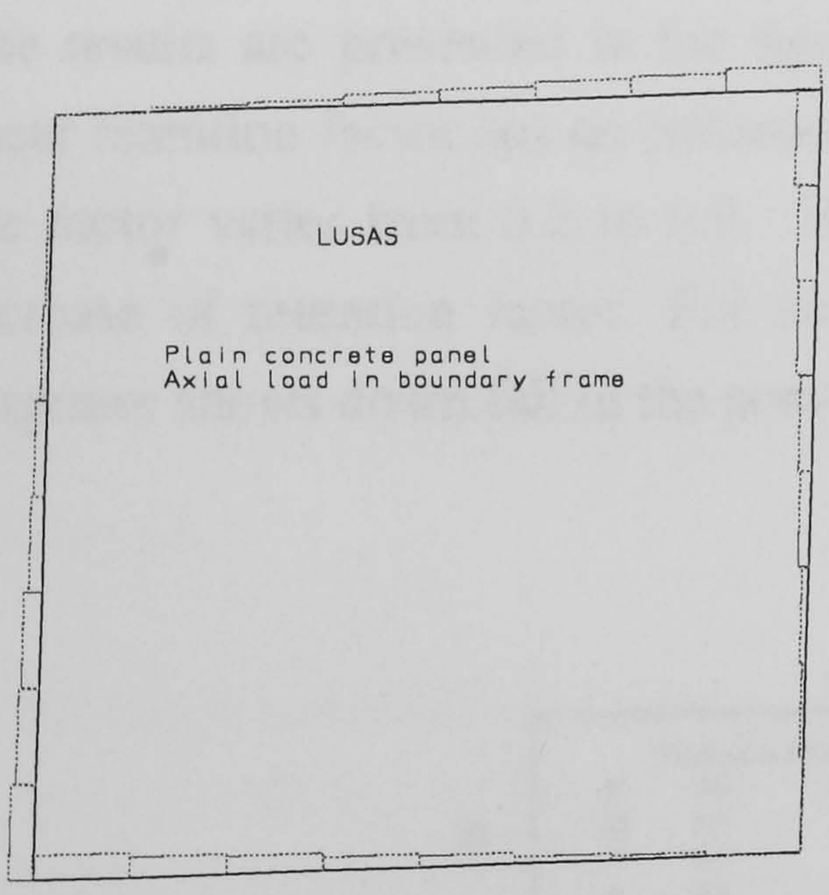

Figure 3.8(b)

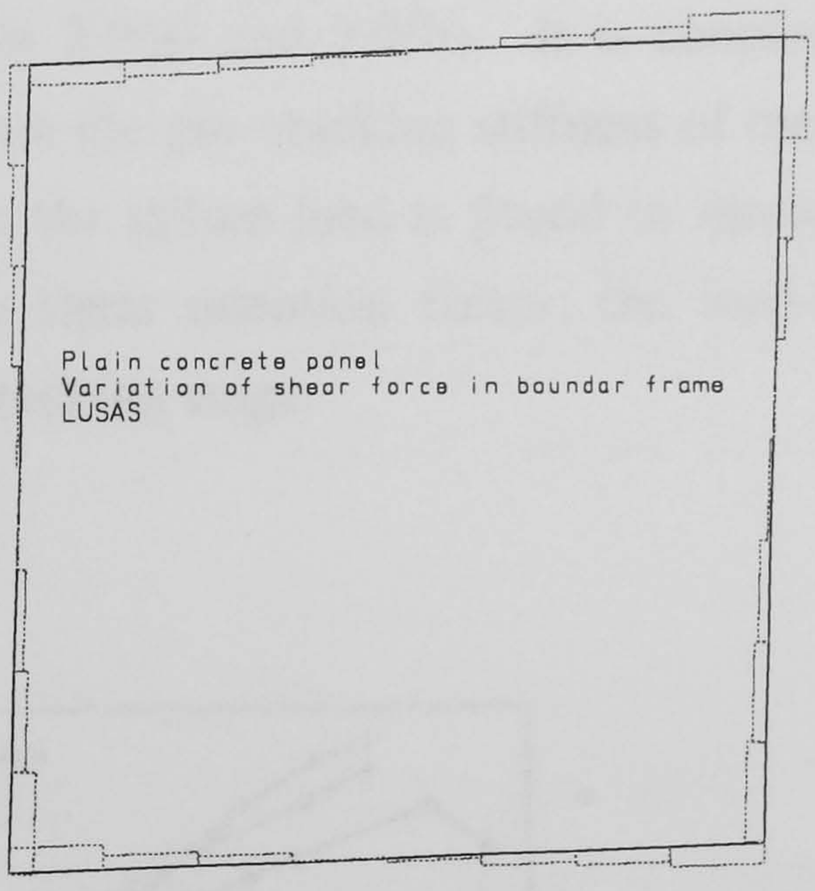

Figure 3.8(c)

Figure 3.8(d)

Figure 3.8 (b,c and d): Simulation of boundary frame

The behaviour of the boundary frame was successfully simulated. The axial force, shear force and bending moment diagram and deflected shape are presented in figures 3.8(b,c and d). The axial force in the frame members is maximum at the loaded corner and zero at the other corners indicating that the diagonal load applied at the corner is totally transferred to the concrete panel. The shear force and moment diagram prove that the complete mechanism conditions of the frame is achieved.

3.7.3 Parametric studies

The effect of various parameters on the strength and stiffness of the concrete panel under different boundary conditions including diagonal model experiment (case 1 : shown in figure 3.7), panel with boundary frame applying distributed shear load at the top (case 2: figure3.7) and as cantilever beam have been studied using FE analysis. The result of this study will be presented below:

Shear retention factor

The results are presented in the figures 3.9(a) and 3.9(b). It is concluded that the shear retention factor has no influence on the pre-cracking stiffness of the panel when the factor varies from 0.2 to 0.9. But the failure load is found to increase with the increase of retention factor. For zero shear retention factor, the load-deformation response shows down fall in the post-cracking stage.

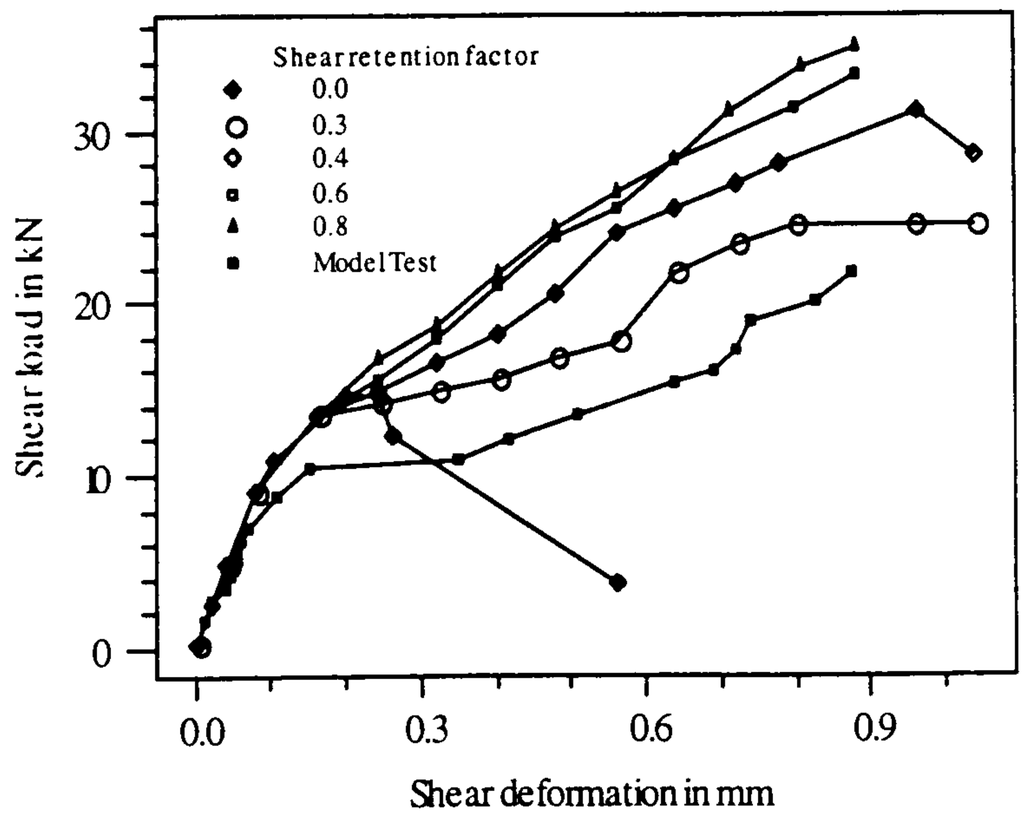

Figure 3.9(a): Shear-load deformation responses

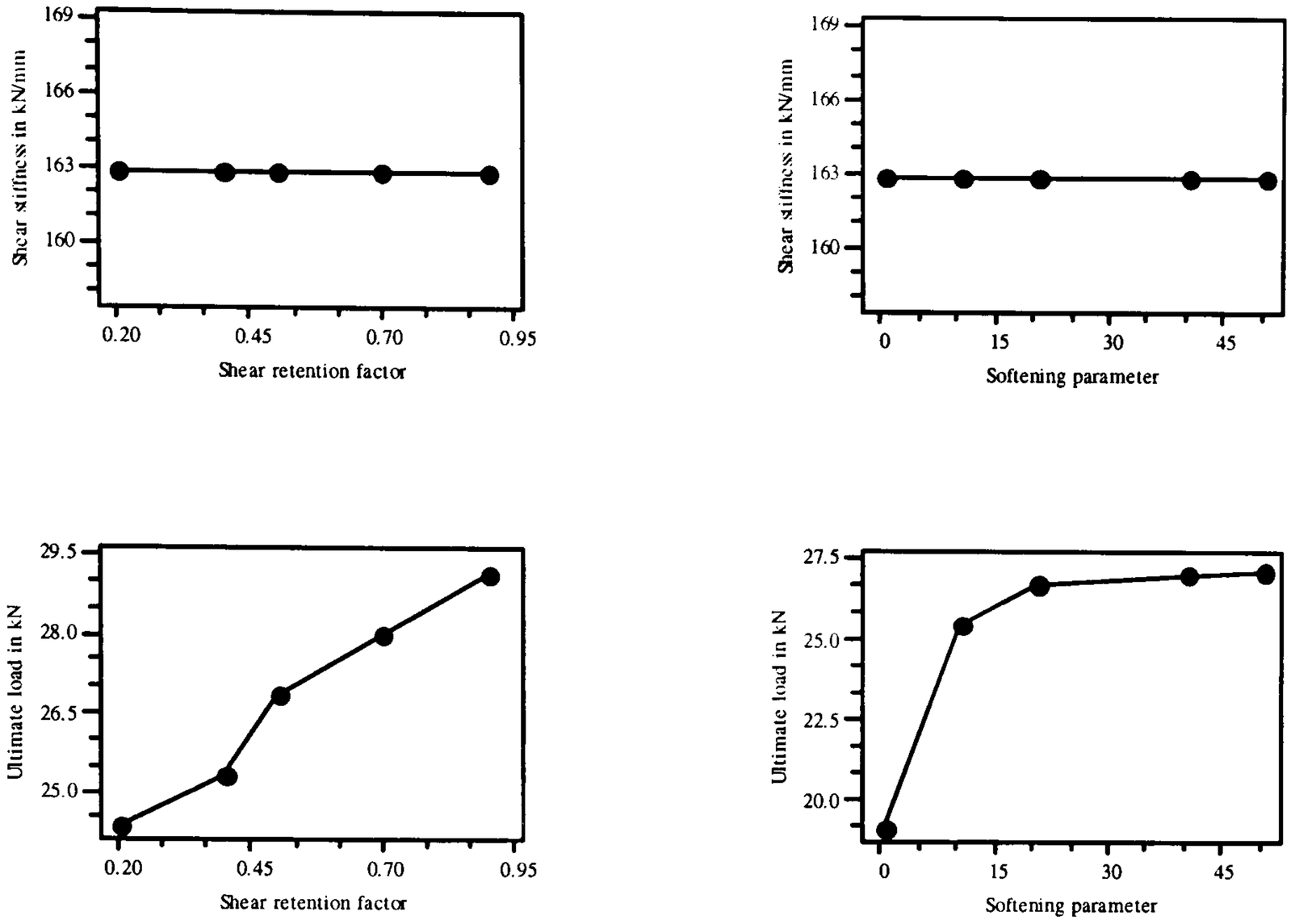

Figure 3.9(b): Effect of shear retention factor and softening parameter

Softening parameter

The results are presented in figure 3.9(b). No influence on pre-cracking stiffness is found when the values ranges from 0 to 50. The ultimate load is increased when the value is increased from 0 to 10. After that no significant increase in ultimate load is observed.

Maximum compressive strain

The pre-cracking stiffness is not affected by the compressive strain. The effect of maximum compressive strain on the ultimate strength is not so pronounced when varied from 0.002 to 0.0036

Tensile strength

Tensile strength has marked influence on the ultimate strength but has no influence on the pre-cracking stiffness. The failure load is found to be increased with the increase of tensile strength.

Conclusion

It is very difficult to model the entire experimental load-deformation behaviour with LUSAS. This is due to the uncertainties in the post-cracking behaviour of micro-concrete which is influenced by so many factors coming from its material

characteristics and experimental conditions. But the pre-cracking behaviour and ultimate load of the panel can be simulated. It is concluded (Hossain and Wright (1994)) that the behaviour of the chosen micro-concrete can be numerically modelled by using shear retention factor and softening parameter within the range 0.25-0.4 and 20-30 respectively. This conclusion is identical to normal concrete where lower values of shear retention factor (<0.5) and softening parameter are recommended for shear dominated failures.

3.7.4 Analysis of finite element results

Finite element analysis of the plain concrete panel has been carried out using shear retention factor of 0.3, softening parameter of 30, maximum compressive strain of 0.0026, poisson's ratio of 0.18 and other properties derived from control specimens of micro-concrete.

Load-deformation response

The shear load-deformation response from Case 1 (shear retention factor=0.3) and experimental model is shown in figure 3.9(a). Satisfactory agreement is found between diagonal stiffness and ultimate diagonal load.

Stress characteristics and crack pattern

The contour diagram for maximum principal stress and its direction are shown in figures 3.10. The principal stress is higher near the loaded corners and the direction varies between 44.24 to 45.75 degrees in the pre-cracking stage (diagonal load = 12.89 kN). The higher principal stress at the loaded corner confirms the formation cracks parallel to the off-diagonal. This also confirms the simulation of pure shear behaviour of the panel.

The variation of stress normal to the boundary and in direction parallel to the boundary is shown in figures 3.11. The variation of shearing stress as shown in figure 3.12 shows uniform variation before cracking.

The crack patterns are shown in figure 3.13. Cracks started from the corner of the loaded diagonal. The crack pattern shows the formation of off-diagonal cracks as found in the model test.

The finite element simulation of actual experimental model test is found to closely simulate the in-plane shear behaviour of the panel.

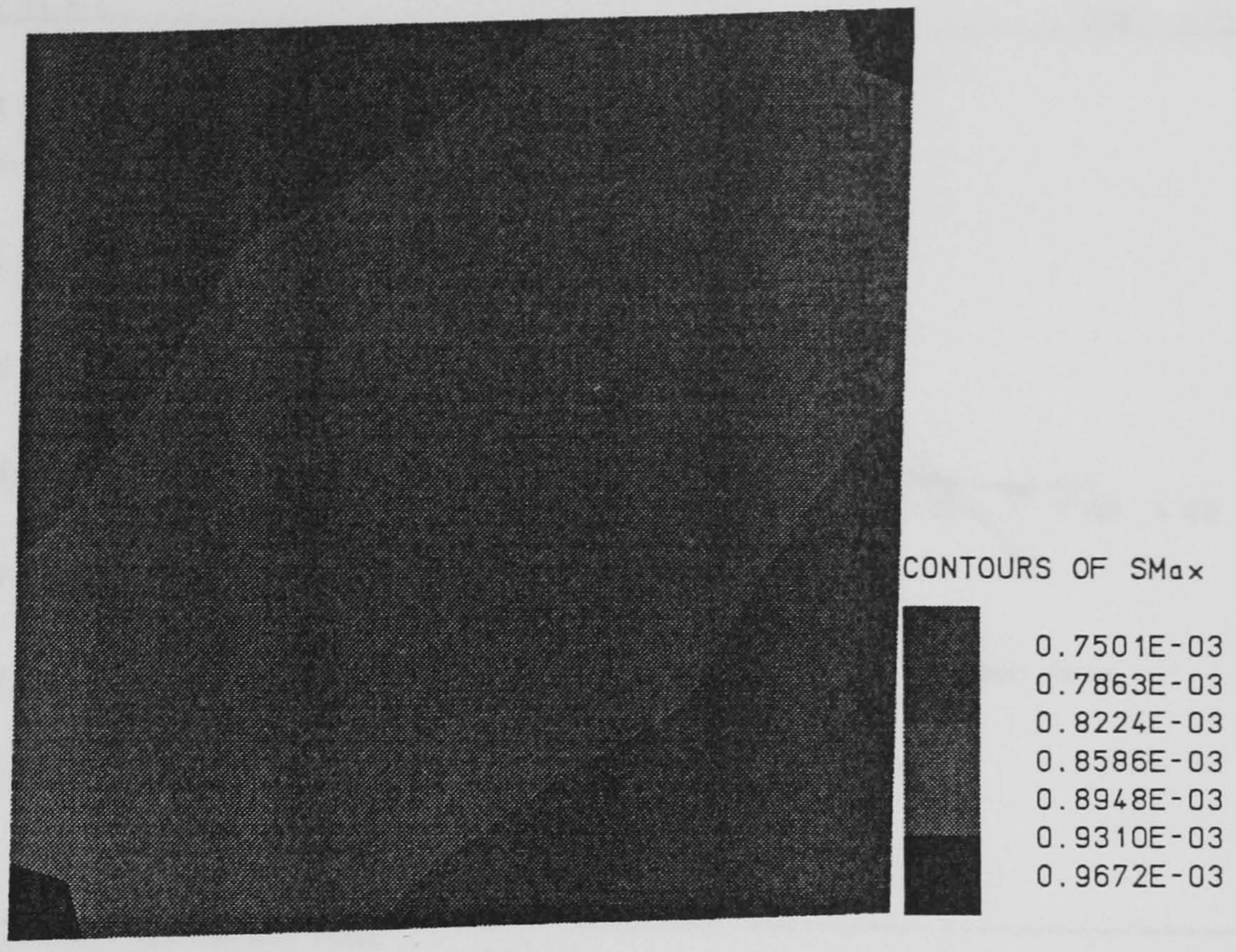

Figure 3.10(a): Contour diagram of principal stress (kN/mm^2)

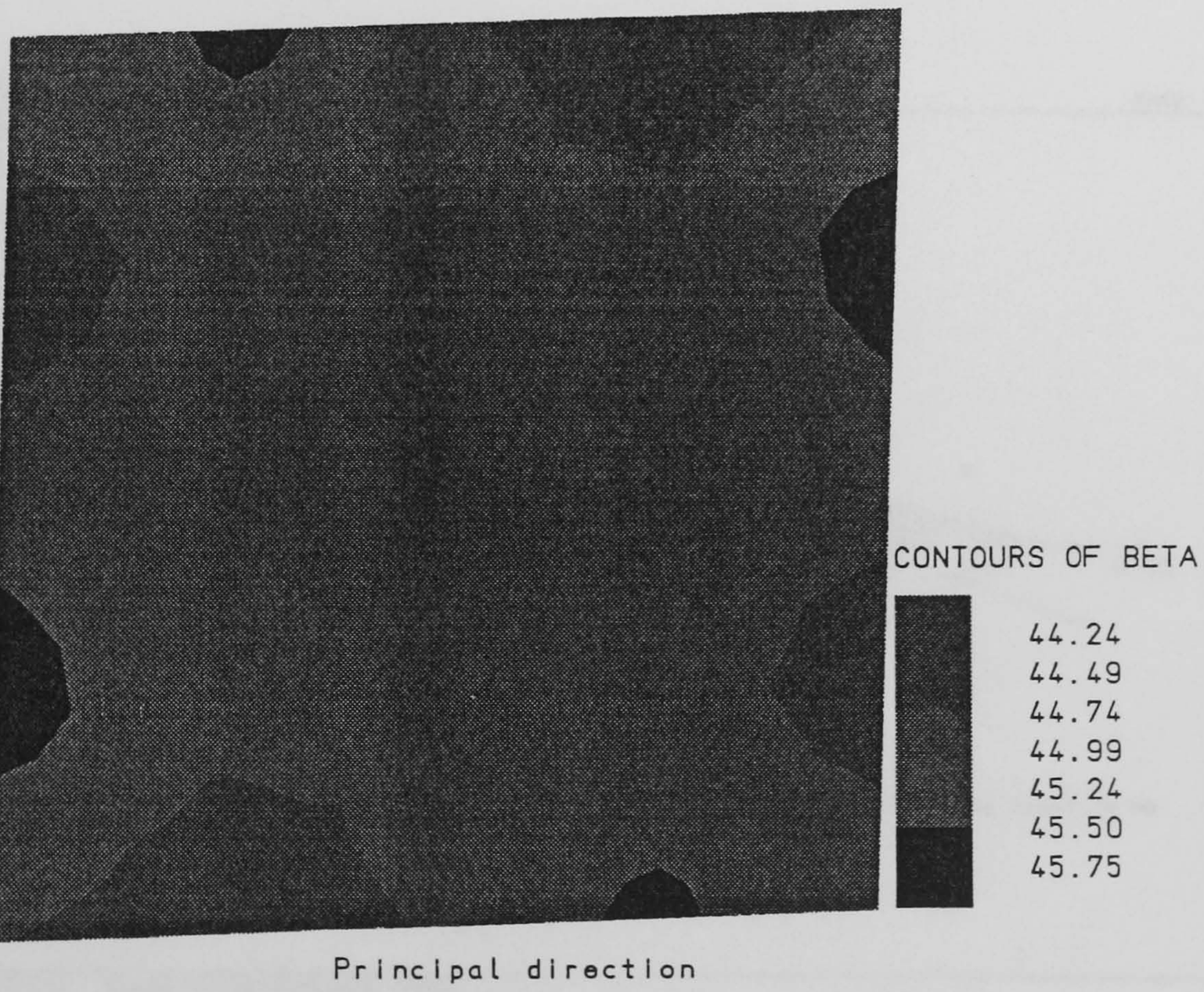

Figure 3.10(b): Contour diagram of principal direction

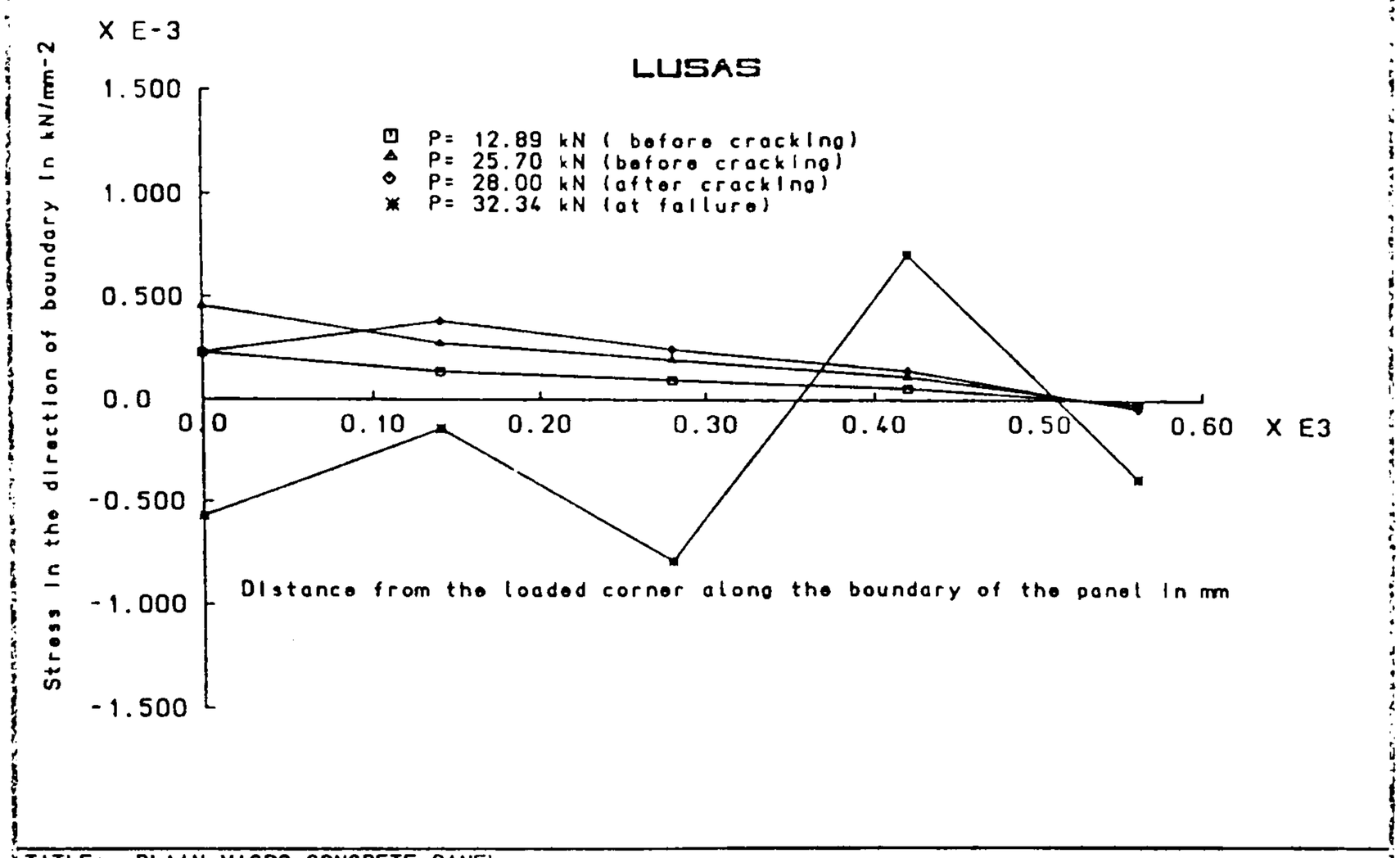

Figure 3.11(a): Variation of stress parallel to the boundary

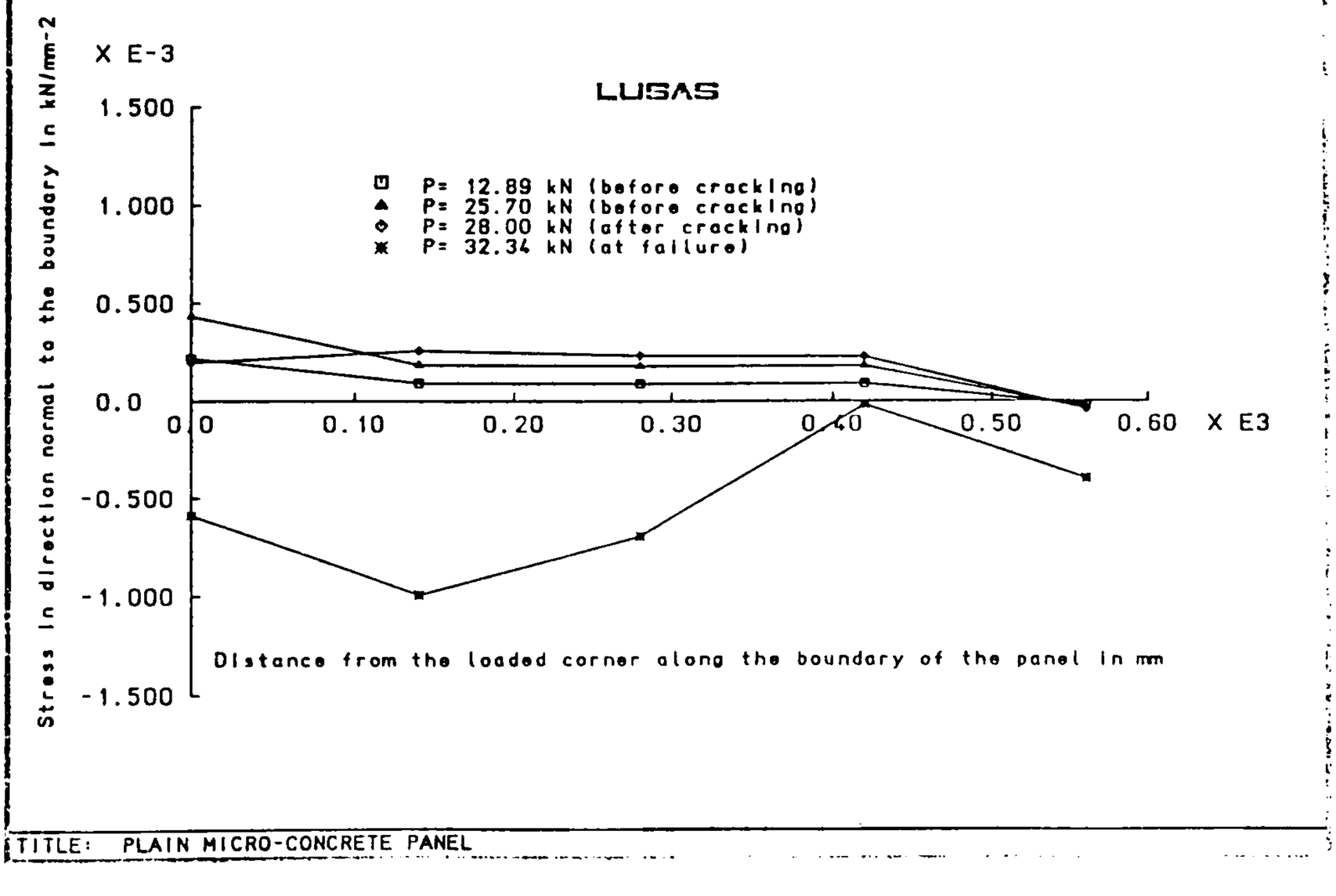

Figure 3.11(b): Variation of stress normal to the boundary

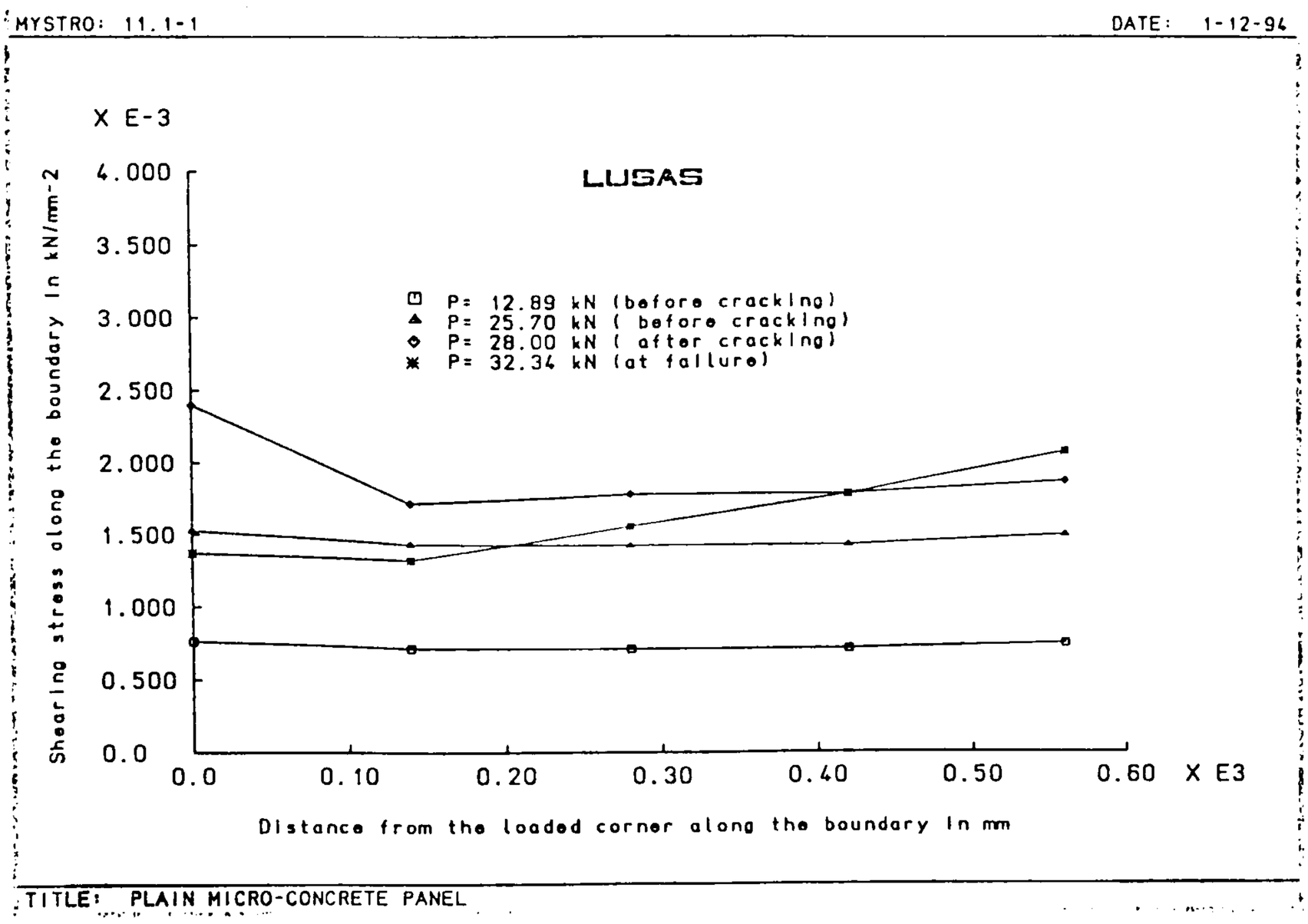

Figure 3.12: Variation of shearing stress

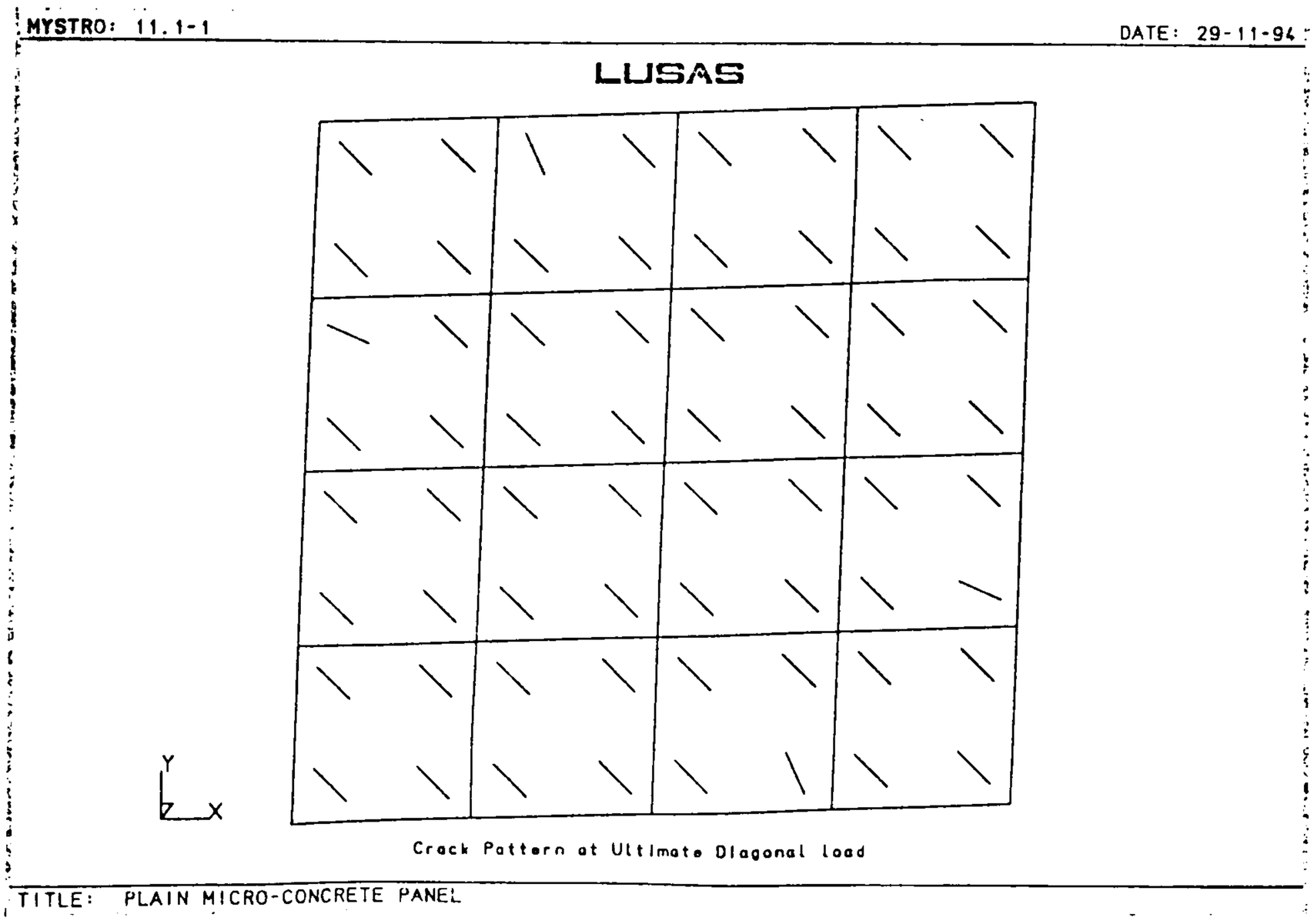

Figure 3.13: Crack pattern in plain concrete panel

3.7.5 Comparative study of analytical, experimental and numerical results

The table 3.4 has been prepared to compare the shear stiffness and failure load of the panel. The satisfactory agreement has been found among analytical, experimental and finite element models.

Table 3.4: Analytical , numerical and model test comparison

Plain micro-concrete panel	Diagonal stiffness kN/mm	Shear stiffness kN/mm	Ultimate Diagonal load (kN)	Ultimate shear load kN
Model Test	308	154	31	22
Analytical: Kupfer and Gerstle	----------	165	-----	27
Balakrishnan & Murray	----------	165	-----	28
FE analysis : Case 1	326	163	32	22.62
Case 2	----------	171	-----	25

3.8 Conclusions

Small-scale modelling of the composite walling under in-plane shear needs special care to tackle the problems associated with the complex geometry of the wall, micro-concrete and simulation of actual boundary condition of the problem. The performance of the micro-concrete was satisfactory and its numerical simulation using LUSAS is found to be reasonable. The analytical models for strength and stiffness are in reasonable agreement with the numerical and model test results.

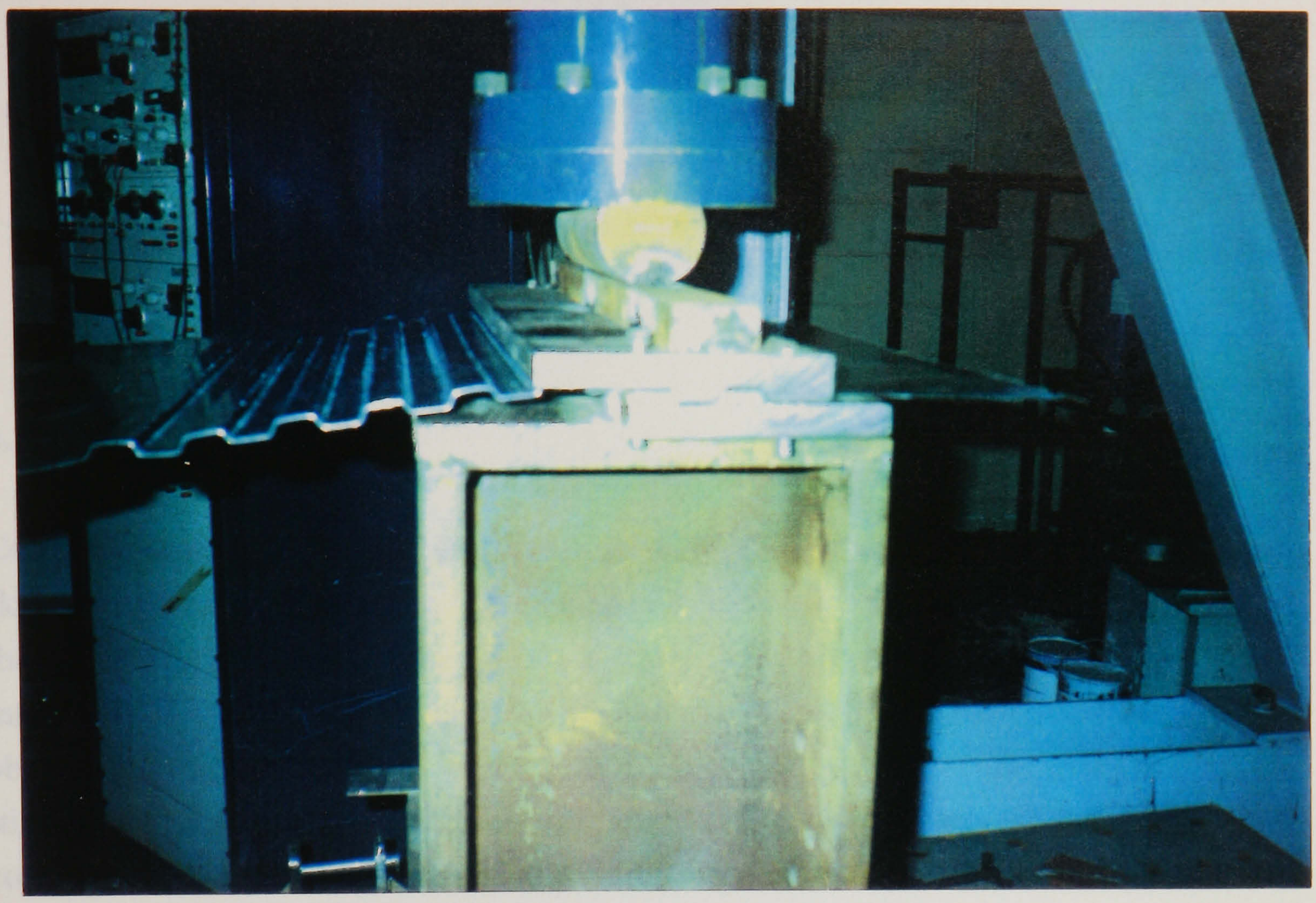

Photograph 3.1: Fly press showing profiling of steel sheeting

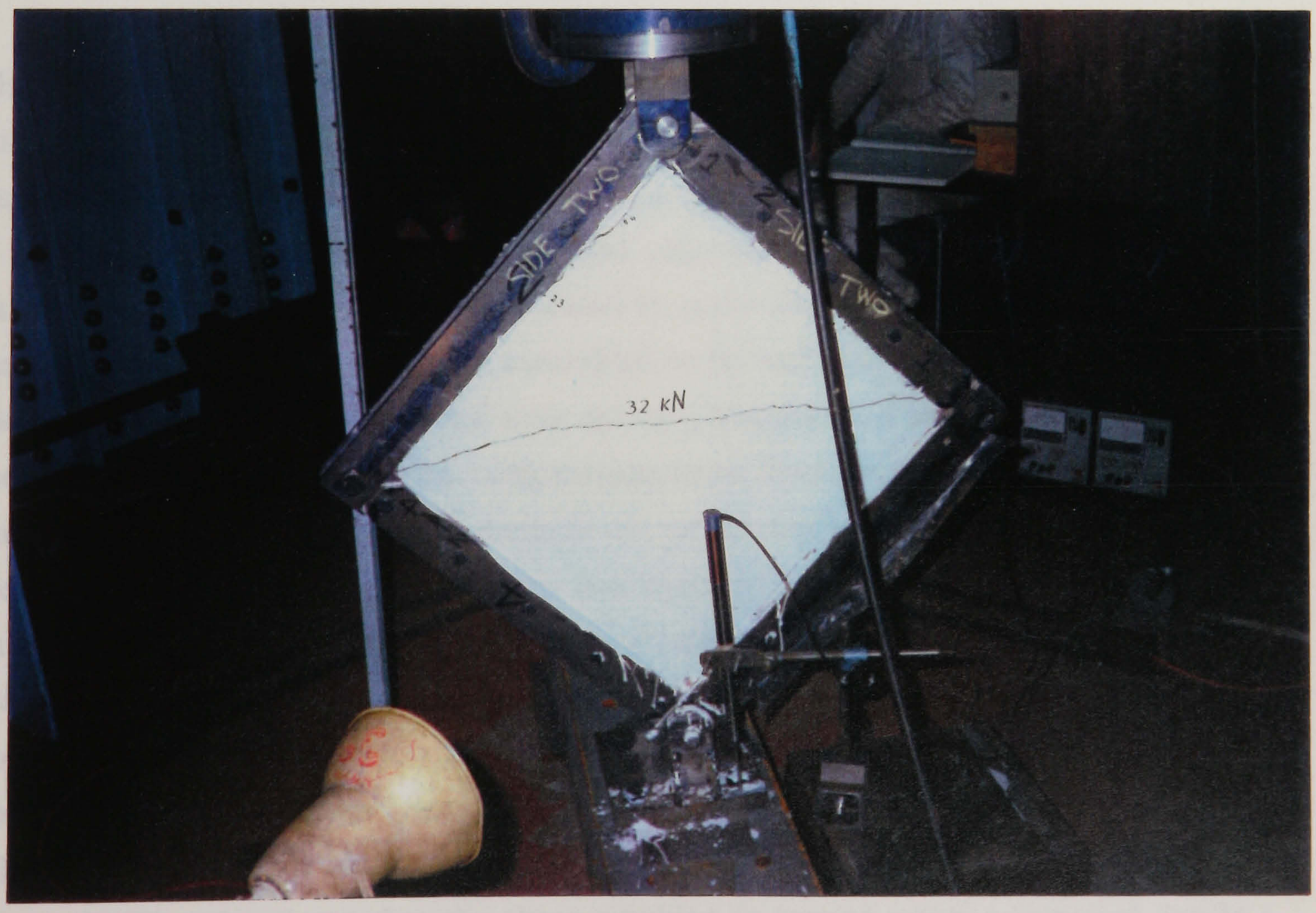

Photograph 3.2: Experimental set-up showing failed plain concrete panel

CHAPTER FOUR

BEHAVIOUR OF PROFILED CONCRETE CORES UNDER IN-PLANE SHEAR

4.1 Introduction

Composite walling is formed with a core of profiled concrete along with two outer skins of profiled steel sheeting. This chapter will describe the individual behaviour of the profiled concrete core under in-plane shear. Detailed description of the heavily instrumented small scale model tests using micro-concrete and the associated observations and results will be presented. An analytical model for strength and stiffness of the panel will be described. Finite element modelling of the profiled concrete panel simulating actual model tests will also be described. Comparison between experimental and theoretical results will be made.

4.2 Literature Review

Much research has been carried out in the past to study the shear resistance of concrete and reinforced concrete panels. Before the cracking of concrete, shear can be transmitted by the concrete continuum. After cracking plain concrete walls have little, if any, stiffness or strength. In reinforced concrete structures subjected to shear, various internal mechanisms can be created to resist shear loading. In regions where the reinforcement causes the crack conditions to be well distributed, the predominant mechanism of resistance is internal truss action (Vecchio and Nieto 1991). Through the formation of diagonal cracks, compression struts develop in the concrete while the longitudinal and transverse reinforcement act as tension ties. In the case where the well-distributed crack condition does not exist (this can occur, for example, in structural components under high direct shear) strength can be governed by behaviour along a single plane or a dominant crack. Here the mechanism of shear transfer is commonly seen as relying less on the formation of compression fields, and more on contributions from shear friction, dowel action and aggregate interlock (Vecchio and Nieto 1991).

Regan(1969) pointed out that the shear cracking is caused when a principal tensile

stress due primarily to shear exceeds the resistance of concrete. Many experiments have since been carried out to investigate shear transfer and shear strength, e.g. Hofbeck, et al. (1969), Taylor(1974), Swamy and Andriopoulos (1974), Mattock (1974), Pauly and Loeber (1974), Vecchio and Collins (1986), Balakrishnan and Murray (1988).

Pauly and Loeber (1974) concluded that the crack width has the largest influence on the shear stiffness, and the maximum size and shape of the coarse aggregate does not seem to influence the shear stress-shear strain relationship. Other factors such as the amount of reinforcement crossing the cracks and the orientation of the reinforcement with respect to the crack, also have significant influence on both the ultimate shear strength and shear stiffness (Mattock 1974).

Vecchio and Collins (1986) presented an analytical model for predicting the load-deformation response of reinforced concrete elements subjected to in-plane shear and normal stresses.

Cracking and failure envelopes for concrete have been developed by many Researchers (e.g. Kupfer and Gerstle (1973), Balakrishnan and Murray (1988)) to evaluate the ultimate strength of the concrete and reinforced concrete panels.

The in-plane shear behaviour of composite slabs with profiled steel sheeting have been studied by researchers e.g. Luttrell (1971), Davies and Fisher (1979), Easterling and Porter (1994). They have all presented analytical models for strength and stiffness for composite slabs.

Review conclusion

Theoretical models have been developed to predict the behaviour of plain and reinforced concrete panels. These models can be used with simplicity to asses the in-plane shear behaviour of the profiled concrete core. The profiled concrete core in composite wall is geometrically similar to that of profiled concrete part in composite slab. However until now, the individual in-plane shear behaviour of the profiled concrete core or panel in composite slabs and walls has not, to the author's knowledge, been reported anywhere. The stress-strain condition within the panel is also not known definitely. Therefore, the behaviour of the profiled concrete core alone has been studied experimentally, analytically and numerically and will be reported in the subsequent articles.

4.3 Features of model tests

Six small scale models of profiled concrete core were tested under pure shear condition. The models had effective dimension of 560mm x 560mm. The model tests include the following steps:

4.3.1 Mould preparation for casting of concrete

The test frame of the shear rig was used to construct the mould. Two profiled steel sheeting panels were assembled in the test frame using bolts passing through the holes in both frame members and sheeting. Steel spacers of required diameter and length were used to maintain the sheeting in their exact position so that the geometric dimensions of the panel could be secured. However it was not possible to use spacers and bolts through all the holes in the profiled boundaries because of the spacing of the holes in the test frame dictated some holes to be on the inclined face of the profile. But at least two bolts were used in each of those two profiled boundaries. The assembled test frame was then made to stand up on a wooden base. Two pairs of base plates made from steel angle were used to fix the test frame firmly to the wooden base. The connection of the base plate to the frame was carried out by using bolts through the corner holes of the frame and the base plate. The complete mould assembly is shown in photograph 4.1. The entire assembly needed accurate fabrication of each part of the mould. Two side plates of the mould were made of perspex so that the level of concrete in the mould can be identified during casting. The side plates were clamped to the frame. Transverse wooden stiffeners were used at mid height of the sheeting during casting so that the sheeting would not deform due to concrete pressure and compaction. The mould was sealed properly using rubber padding at the bottom and by using plastic tapes. The two profiled steel sheets were greased properly before they were assembled in the frame.

4.3.2 Casting of micro-concrete

The casting of micro-concrete is similar to that described in section 3.5. Control specimens, cylinders and cubes, for each panels were cast at the same time.

4.3.3 Curing

After casting, the panels were cured in air with a polythene cover. After four or five days the panels were demoulded. Special cares were taken so that the sample did not suffer any damage whilst removing bolts through the holes and dismantling of the test frame and sheeting. The panels were then preserved safely and cured in air until they

were tested. Control specimens were taken out of the mould after 24 hours and then cured in air.

4.3.4 Casting Resins

To fulfil the required boundary condition of the problem and to secure proper transfer of force from the frame to the panel, it was necessary to fill the profiled gap between panel boundary and the frame. A risk assessment had been carried out to identify the problems in using hazardous material like mould release, methyl ethyl ketone peroxide and polyester resin in styrene. The following precautions were put forward:

- 0 Hand protection measures (use of plastic gloves) should be taken to avoid direct contact.
- 0 A fume cabinet should be used to avoid irritation of eyes and respiratory system.

The casting of resins to fill the gap between test frame member and the profiled boundary of the panel has the following steps:

Assemble of panels to the test frame and Drilling holes

The use of spacers, to a great extent, remove the difficulties of drilling holes through the micro-concrete. As mentioned earlier that it was not possible to use bolts through all the holes along the profiled boundary. To fully assemble the panel in the test frame, it was therefore necessary to drill holes at those locations. During tightening of the bolts, great care was taken so that the panel did not suffer any damage. Panel-2 did crack slightly during this process. The boundary surfaces of the panel (specially the profiled ones) were not level and there was always some gap between frame members and the panel. Tightening of the bolts caused concentration of pressure at some location of the panel and the panel cracked due to flexure. To avoid this problem, the bolts were made finger tight during drilling (if it was done before casting resins) or during the preparation of mould for casting resins. After casting and curing of resins, the bolts were then tightened properly as a level surface was then ensured. A masonry drill was used for drilling the micro-concrete.

Preparation of mould for resin casting

The test frame with panel was then assembled in a similar manner as described in the section on the casting of concrete. Special mould release oil was applied thoroughly to the test frame members, bolts, corner pins and all other parts of the mould which

might come in contact with resins. This was done very carefully to avoid the damage of the panels. Panel-3 was damaged due to inadequate measures taken during this process. In that case, resin came into the holes of the corner pins and bolts and formed a strong bond between spacers and the pin and bolts. It was not possible to take out the corner pins without breaking of the panel. To avoid this problem, sufficient mould release was applied to all parts of the mould including frame, spacers, pins and bolts coming in contact with resin. The pins and bolts were first covered with a layer of plaster seal and then mould release oil was applied over the layer. These measures solved the problem. The complete assembly of the mould is shown in photograph 4.2.

Making and Casting

The making and casting of resins were conducted in a fume cabinet. 500 grams of polyester resin was taken in a glass jar. 5ml of Methyl Ethyl Ketone was then poured in to the jar from a test tube. A filler material (Talc powder) white in colour was then added and the mix was constantly stirred until the colour becomes uniform and sticky to such a state that it can be poured into the profiled gap between panel and frame members. A specially made steel plate was used to pour the resin into the gaps. After casting, the material was allowed to cure for 24 hours in the fume cabinet until it had hardened. The same procedures were adopted to cast the resins on the opposite profiled boundary. Therefore for each specimen the entire sequence of casting resins was carried out two times.

4.3.5 Final assemble

After casting and curing of resins, the test frame with panel was taken out from the mould. The drilling of the holes the profiled boundary was carried out. The bolts were then loosened so that the pair of frame members in each boundary could be separated from the panel. The frame members and corners holes were then cleaned from hardened resins and plaster seals especially on the profiled boundary so that they would not interfere with the movement of corners pins and frame members in the hinge condition. The resin was very sticky when not properly cured and became brittle when it was hardened. So it was necessary to allow sufficient time for hardening (at least 24 hours) and this made it easy to clean the brittle resins. The panel was then finally assembled in between the pairs of frame members and the bolts were tightened properly. Rough paper padding was used between frame members and panel to secure proper contact surface in the plain boundary of the panel.

4.3.6 Instrumentation

The profiled micro-concrete panel was then made ready for installing the strain gauges. The procedure followed was similar to that used for normal concrete. Steel strain gauges (rosettes and single gauges) were installed on the surface of micro-concrete and they were found to work satisfactorily.

The test frame assembly was then connected to the loading frame through the corner pins along one of the two diagonals. The experimental set up with profiled concrete panel is shown in Photograph 4.3. LVDT's and dial gauges were used to measure the diagonal load-deformation response of the panel. They also gave the deflections of bottom beam and pins.

4.3.7 Loading and monitoring

A computer aided data acquisition system as mentioned in the earlier chapters was used to monitor the load-deformation response and strains during testing. Panel-1, panel-2 and panel-4 were tested by applying tensile force along the loaded diagonal. While panel-6 were tested to study the hysteretic behaviour of the system.

4.4 Small scale profiled micro-concrete model panel testing

In this article the model tests will be described and results and test observations will be presented. The detail dimensions of the panels and the location of strain gauges are shown in figure 4.1.

4.4.1 Test-1

The panel was tested by applying tensile force along the loaded diagonal. The load was applied incrementally until failure of the panel. The loading and unloading was done several times up to the cracking load at 8kN intervals. At each load increment diagonal load-deformation and strains were monitored through the data logger.

The first crack was developed at 23 kN near the bottom pin and was parallel to the off-diagonal. At about 29.5 kN another crack developed near the top pin. Then a series of cracks parallel to the off-diagonal were gradually developed one after the other starting from top corner towards the centre during subsequent loading. The panel failed at about 52 kN. The gradual development of the cracks are shown in photograph 4.3. Cracks parallel to the corrugation profile were also found to develop near the boundary frame along the trough where the cross section of the

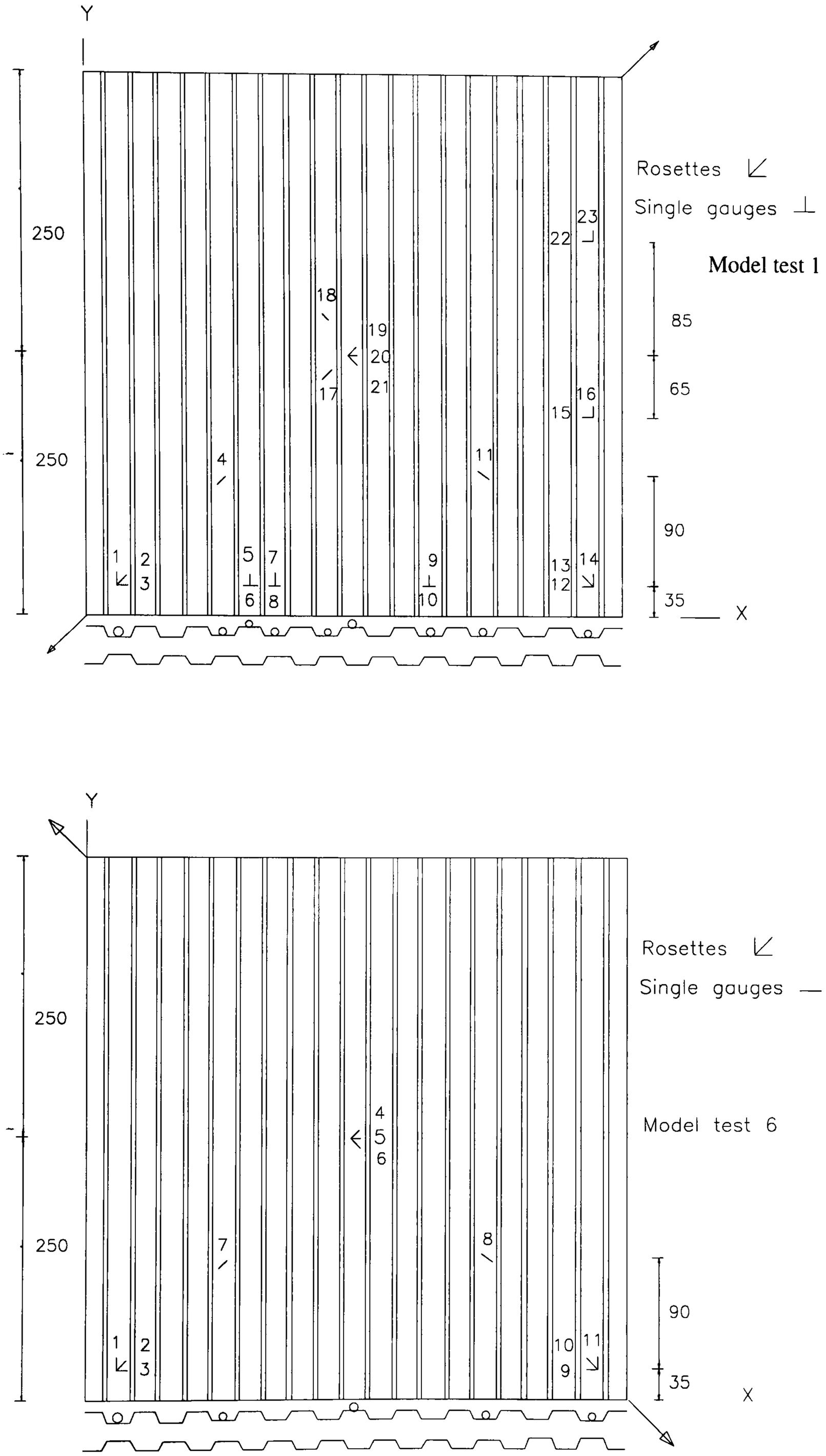

Figure 4.1: Detail dimensions and strain gauge locations

panel was smaller. The cracks were extended from one side to another representing similar crack patterns on both sides. The development of cracks parallel to the off-diagonal represented to a great extent the pure shear condition within the panel. The boundary condition of the panel was therefore assumed to behave properly.

4.4.1.1 Analysis of strains within the panel

i. Diagonal strain along the off-diagonal

Figure 4.2 shows the variation of strain throughout the loading history. From the figure it is concluded that the diagonal was under compression throughout the loading history.

ii. Diagonal strain along the loaded diagonal

Figure 4.3 revealed that the diagonal was under tension up to the initial cracking of the panel but after that compressive strains were pronounced.

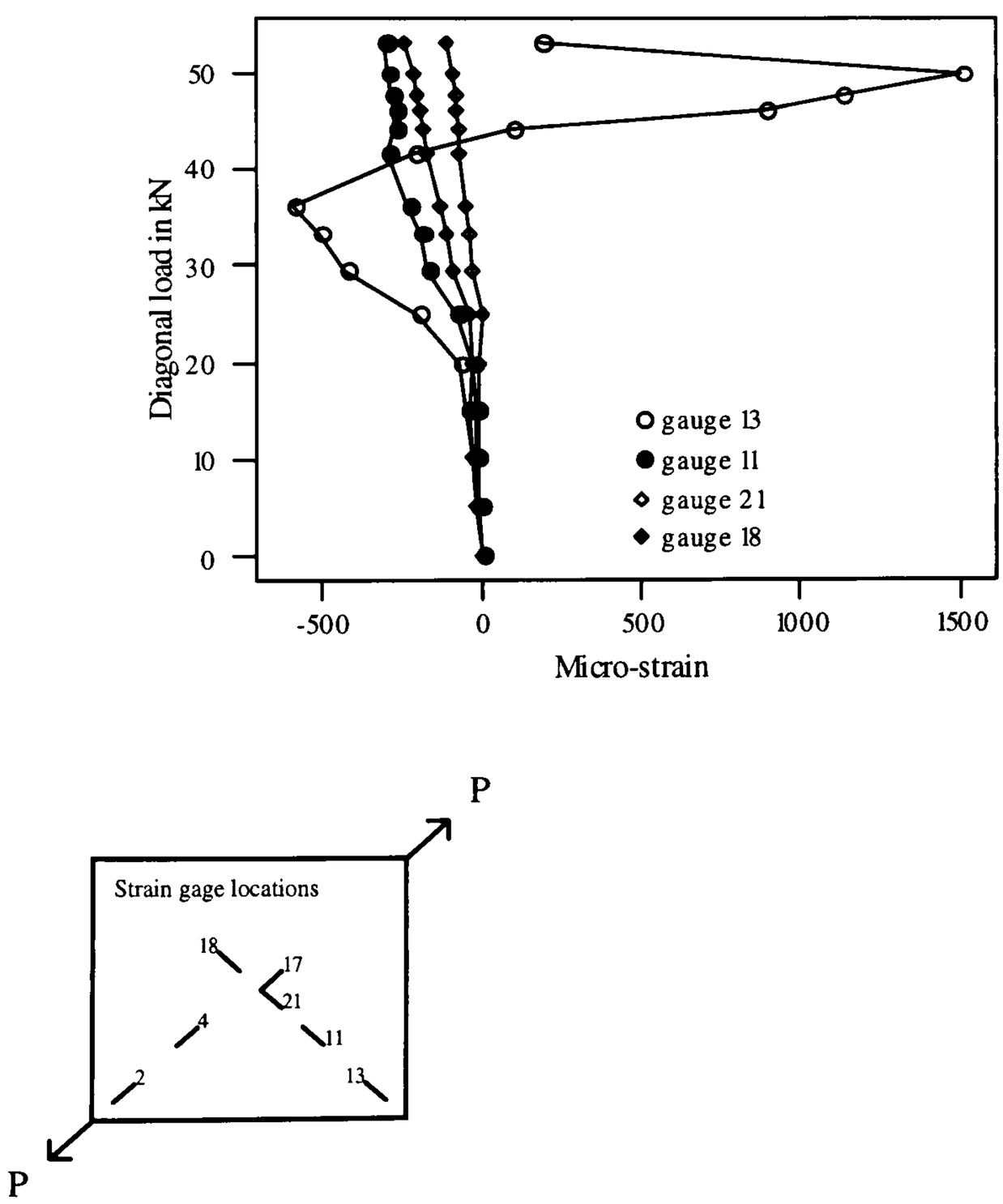

Figure 4.2 : Variation of strain along the off-diagonal

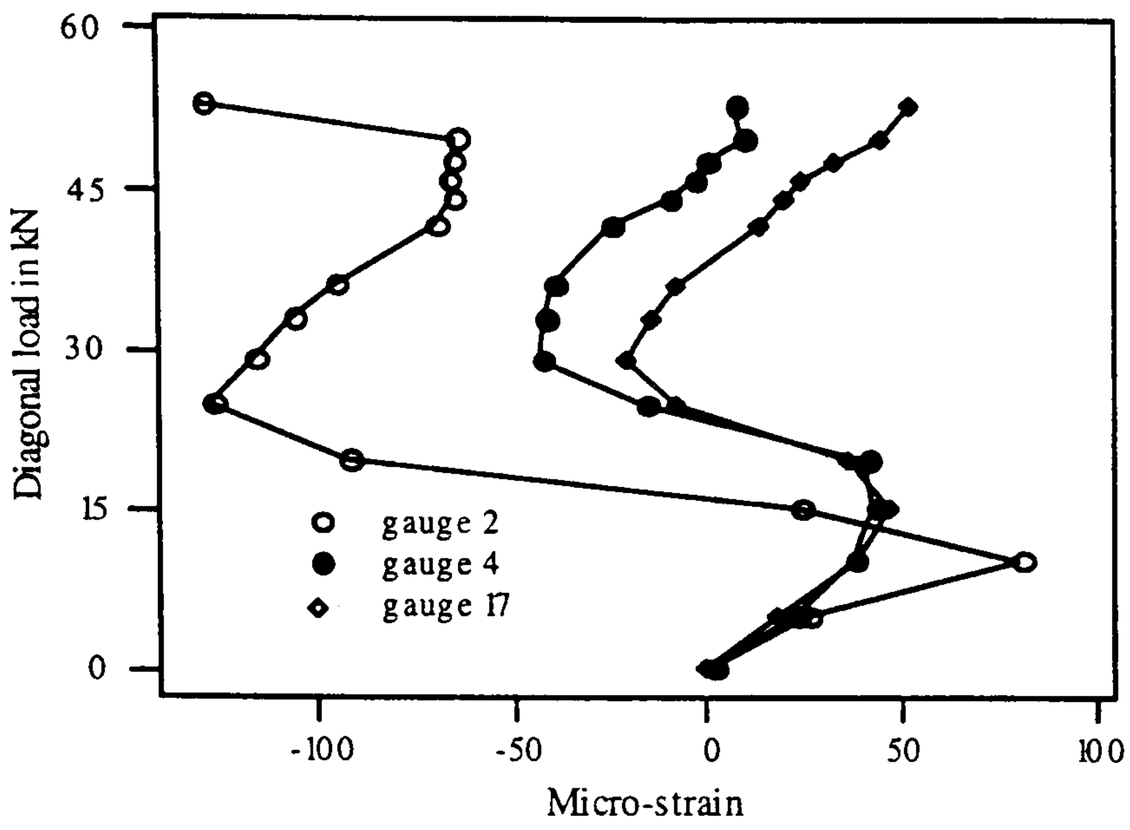

Figure 4.3: Variation of strain along the loaded diagonal

iii. Variation of principal stress

Figure 4.4 shows the variation of principal stresses at the rosette location. The solid line indicates the micro-concrete tensile strength and it intersects the principal tensile stress graph at about 25 kN. This confirms the load (about 23.5 kN) at which initial cracking of the panel started. The principal direction is also shown in the figure. The major principal direction makes an angle with +X-axis which varies from 46-49 degrees before cracking. This confirms the direction of principal tensile stress of approximately perpendicular to the off-diagonal causing cracks parallel to off-diagonal and hence justifies the experimental findings.

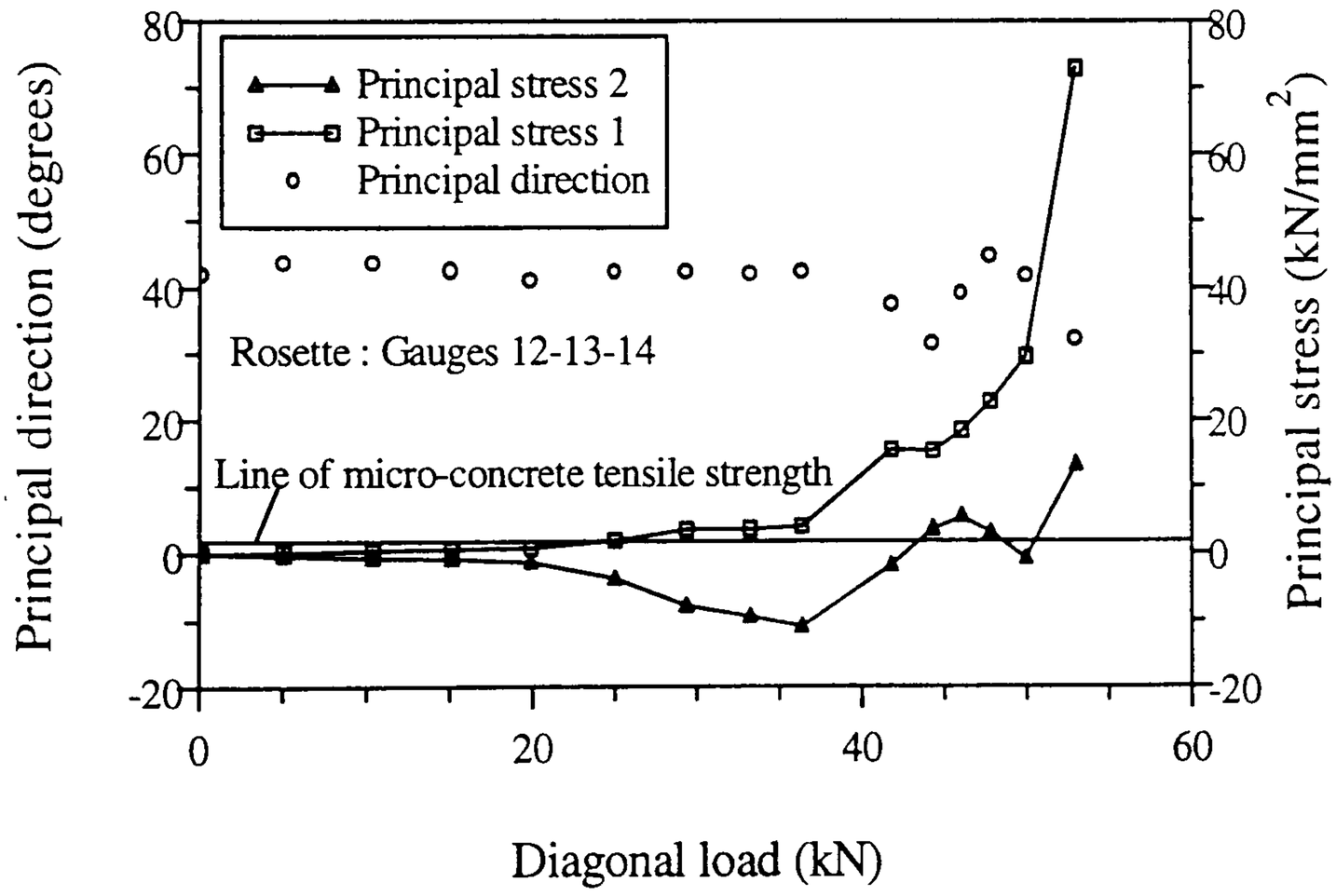

Figure 4.4 : Variation of principal stress at rosette 12-13-14

An attempt has been made to compare the principal strain at rosette location with the diagonal strain at that location and is shown figure 4.5. The diagonal strain in gauge-13 is found to match with principal compressive strain almost throughout the loading history.

The variation of principal stresses at the centre of the panel is shown in figure 4.6. The stresses are found to be less than those shown in figure 4.4. This is due to the fact that this rosette location is at the crest section where the thickness of the panel is higher by about 30mm compared to 14mm of the other rosette location at trough section. This proves the development of higher stresses in the trough sections of the panel. Figure 4.7 compares the principal direction at the two rosette locations.

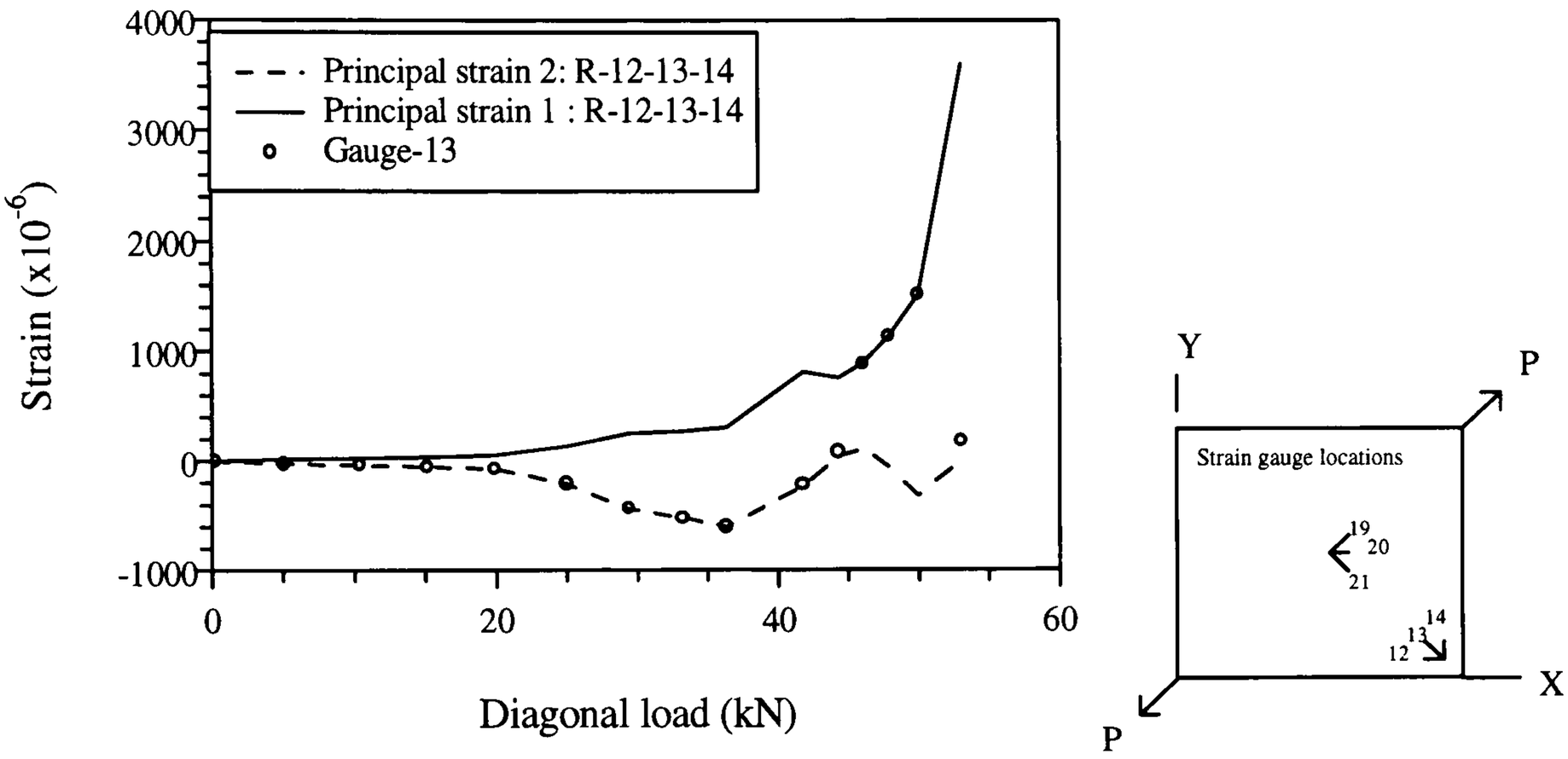

Figure 4.5: Variation of principal strain at rosette 12-13-14

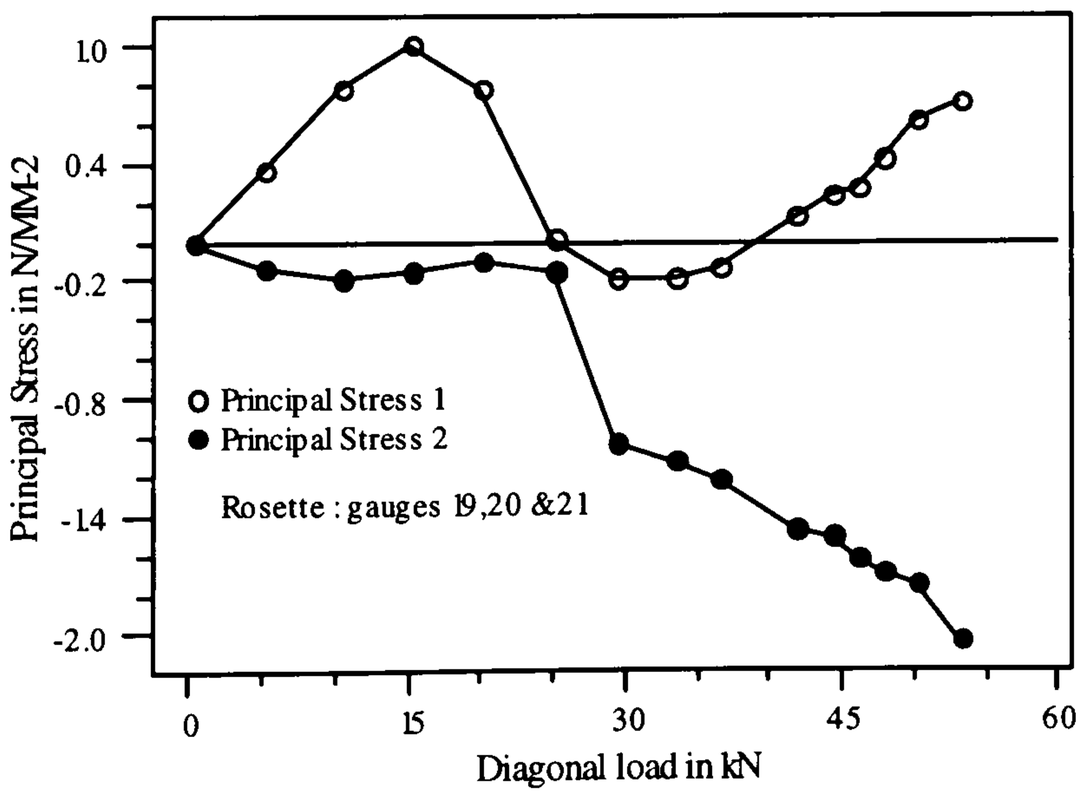

Figure 4.6: Variation of principal stress at rosette 19-20-21

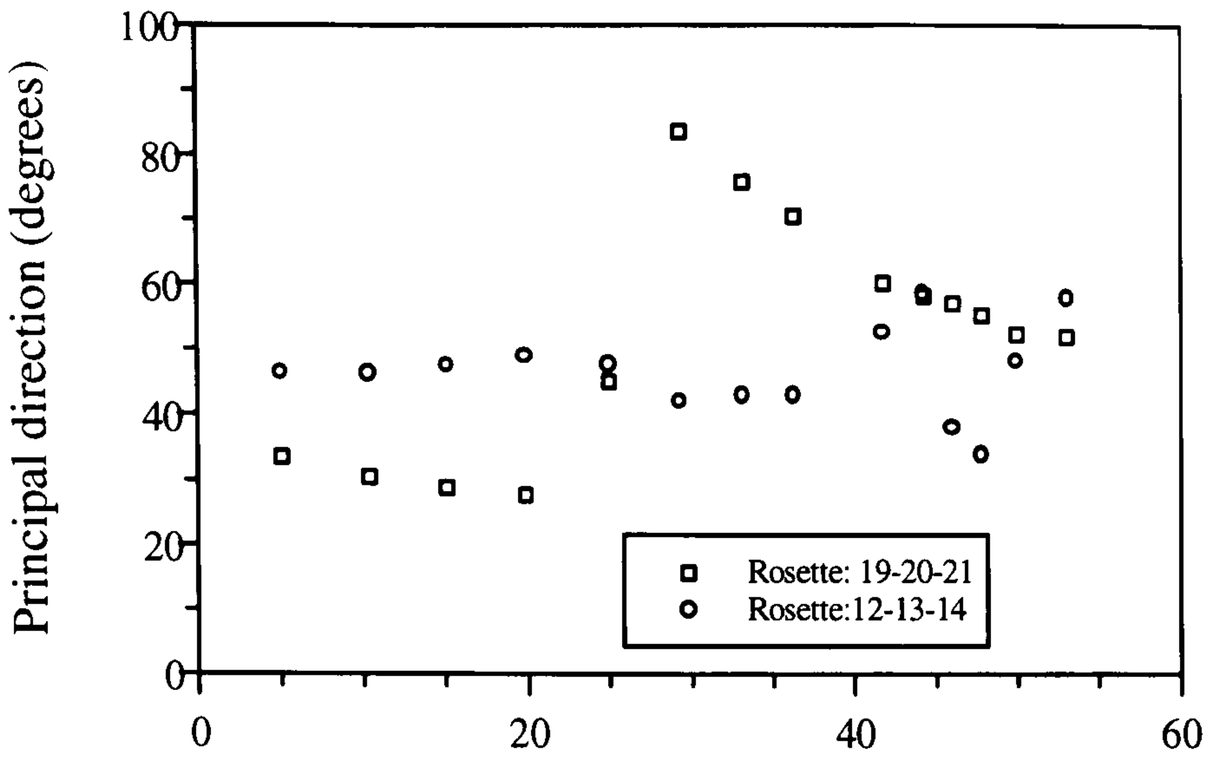

Figure 4.7: Variation of principal direction

iv. Strains at crest and trough sections

Figure 4.8 compares the strain at trough and crest sections of the profile. Trough sections are strained higher than the crest sections.

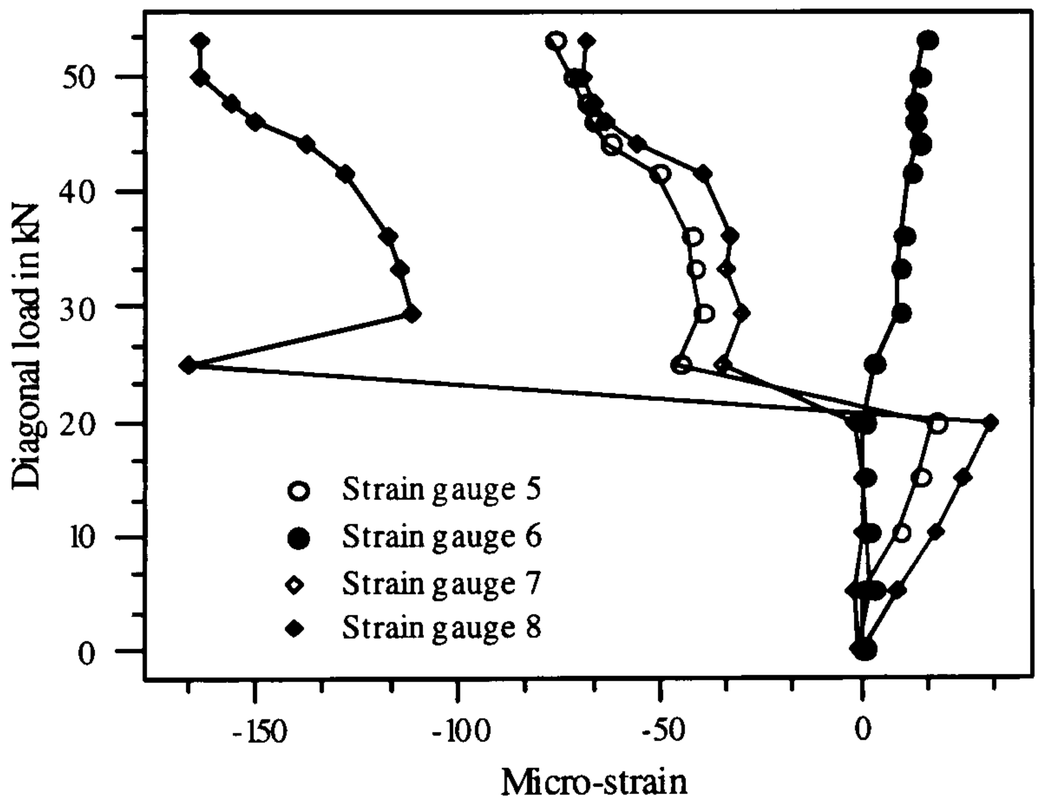

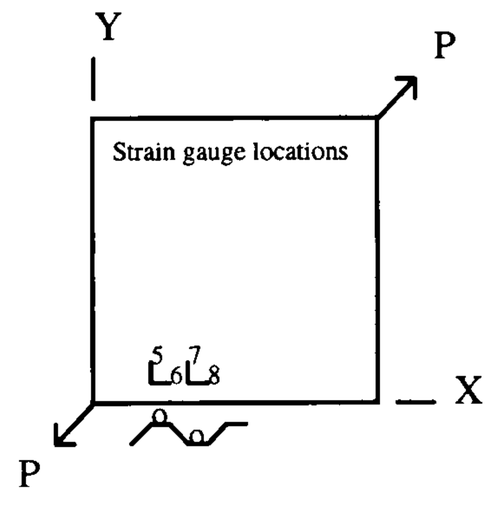

Figure 4.8: Strain at adjacent trough and crest section

v. Variation of strain along the profiled and plain boundaries

Figures 4.9 show the variation of X and Y-strain along the profiled and plain boundaries respectively. The typical variation in the pre-cracking stage is shown as dotted lines while the solid line connecting square symbols shows the variation in the post-cracking stage. The variation in the post-cracking stage does not follow any pattern.

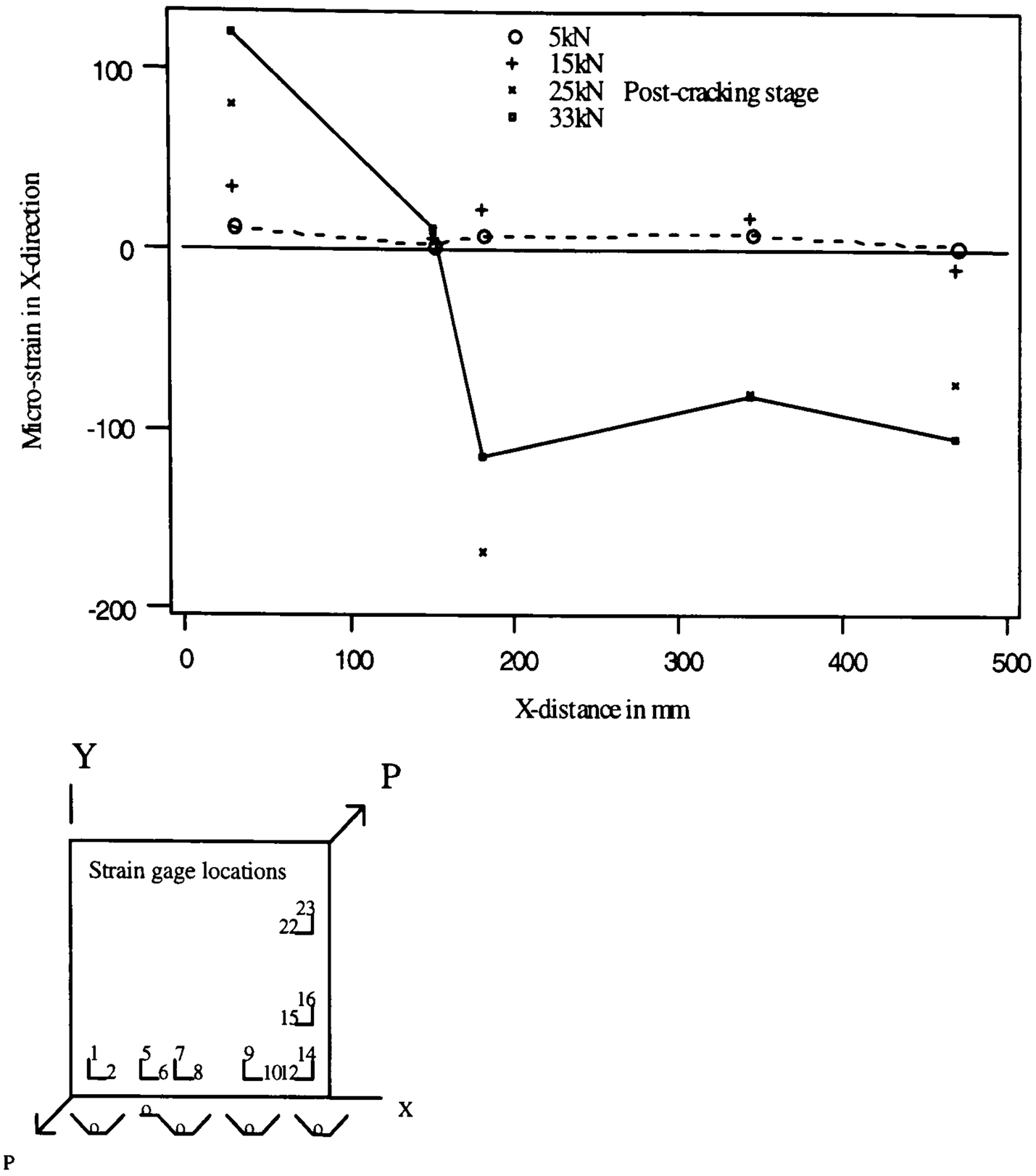

Figure 4.9(a): Variation of X-strain along the profiled boundary

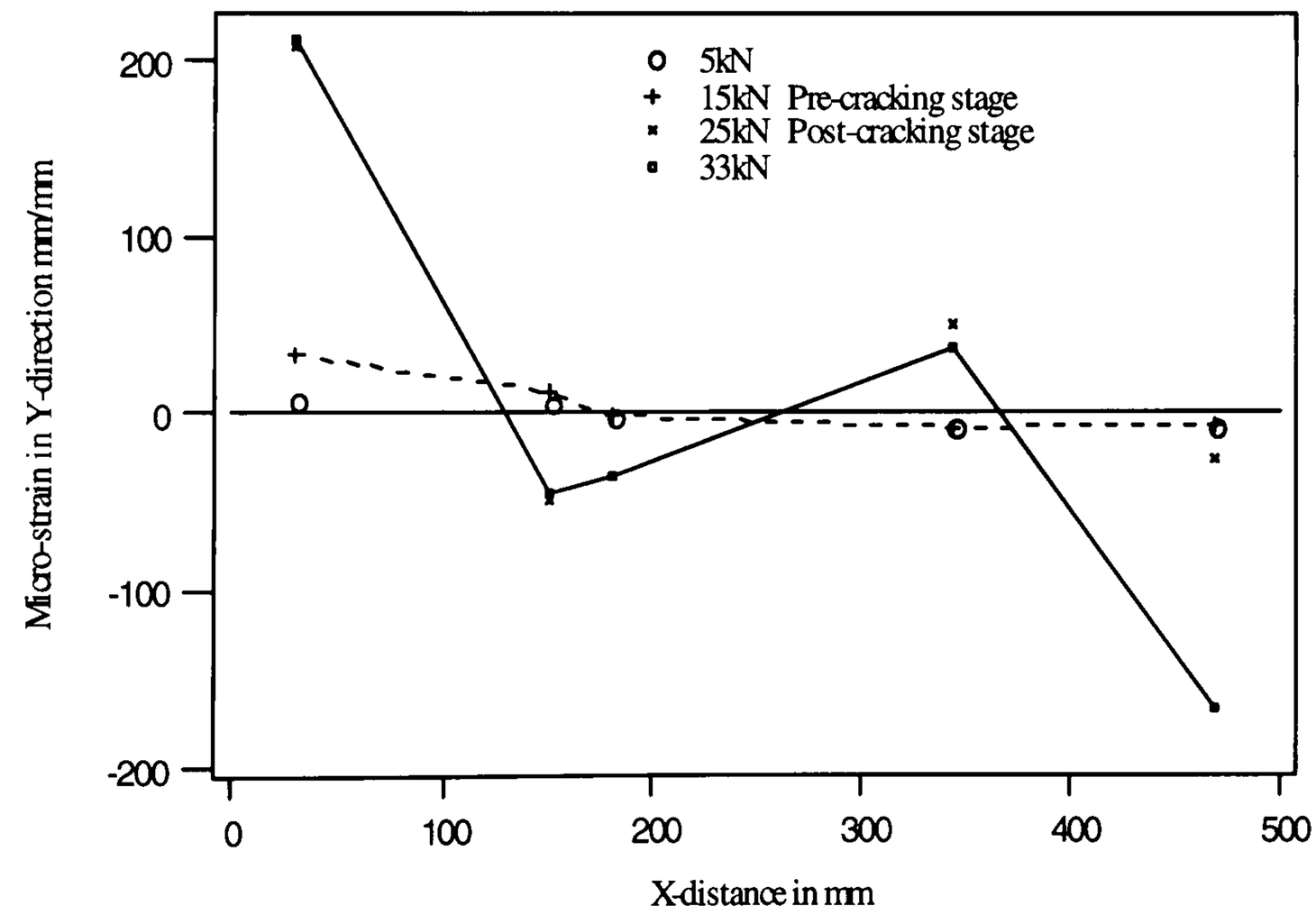

Figure 4.9(b): Variation of Y-strain along the profiled boundary

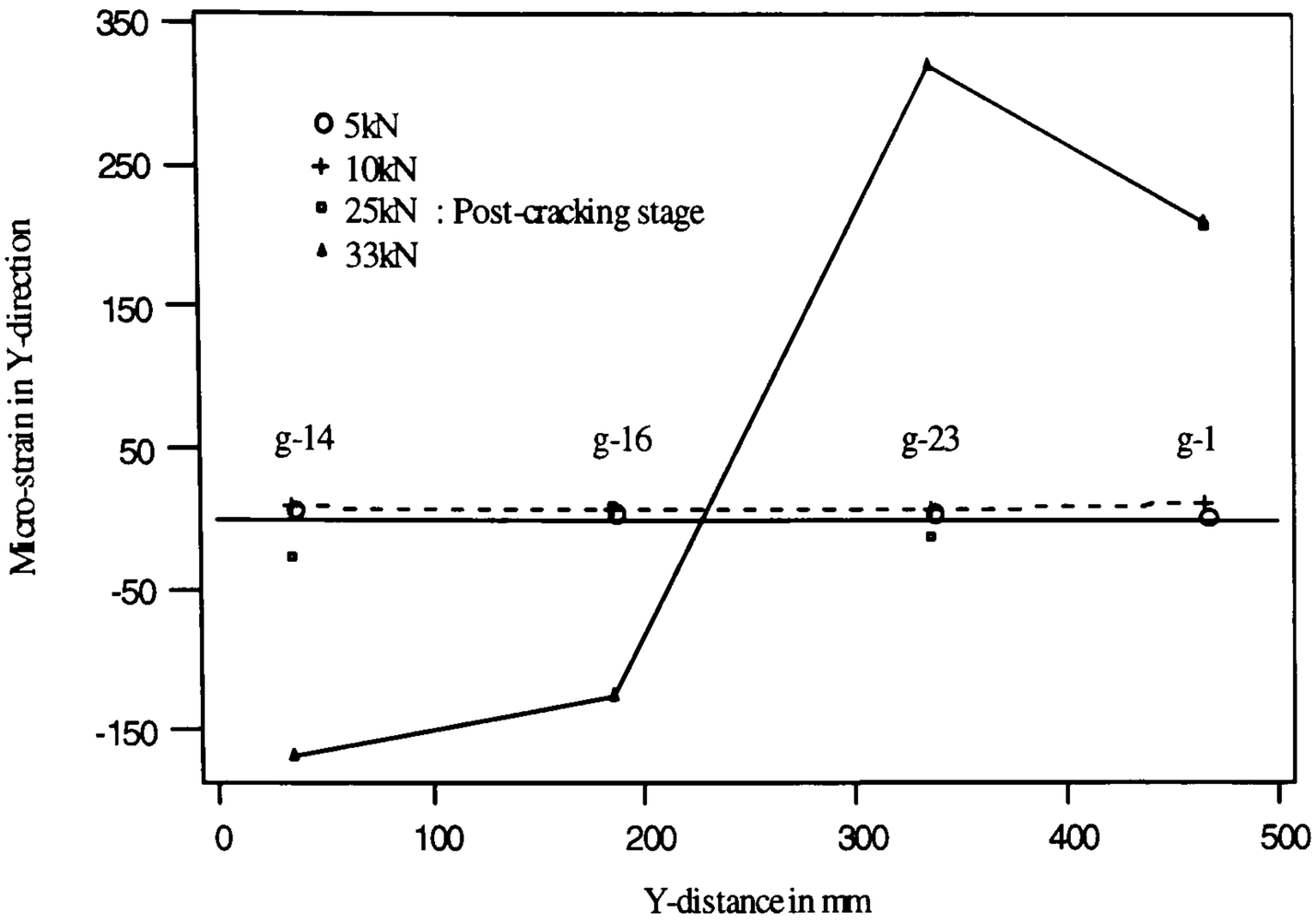

Figure 4.9(c): Variation of Y-strain along the plain boundary

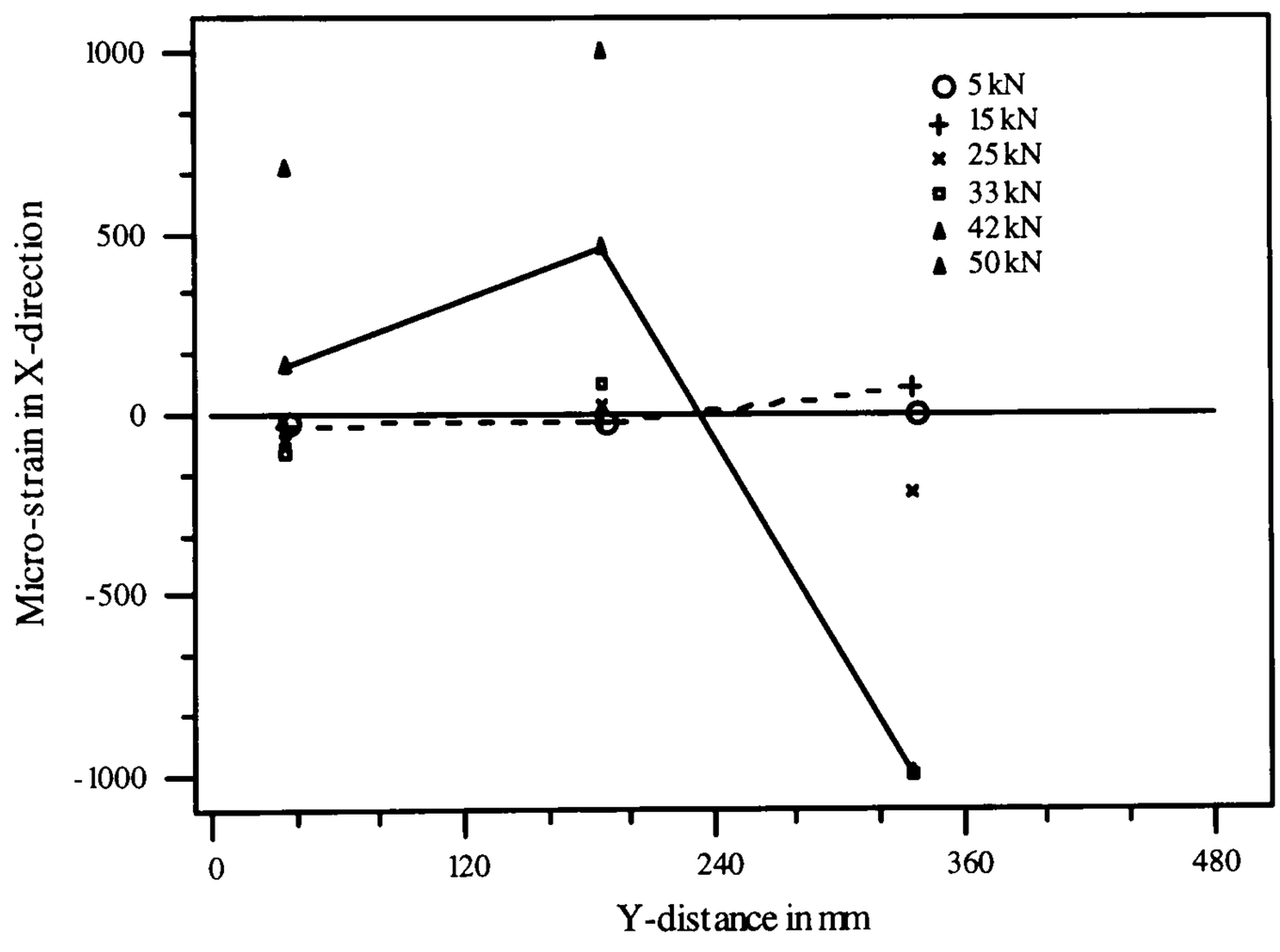

Figure 4.9(d): Variation of X-strain along the plain boundary

4.4.1.2 Analysis of crack diagrams

Figure 4.10 shows the main crack lines A,B,C,D and E and corresponding points on the crack lines at the centre of crest and troughs.

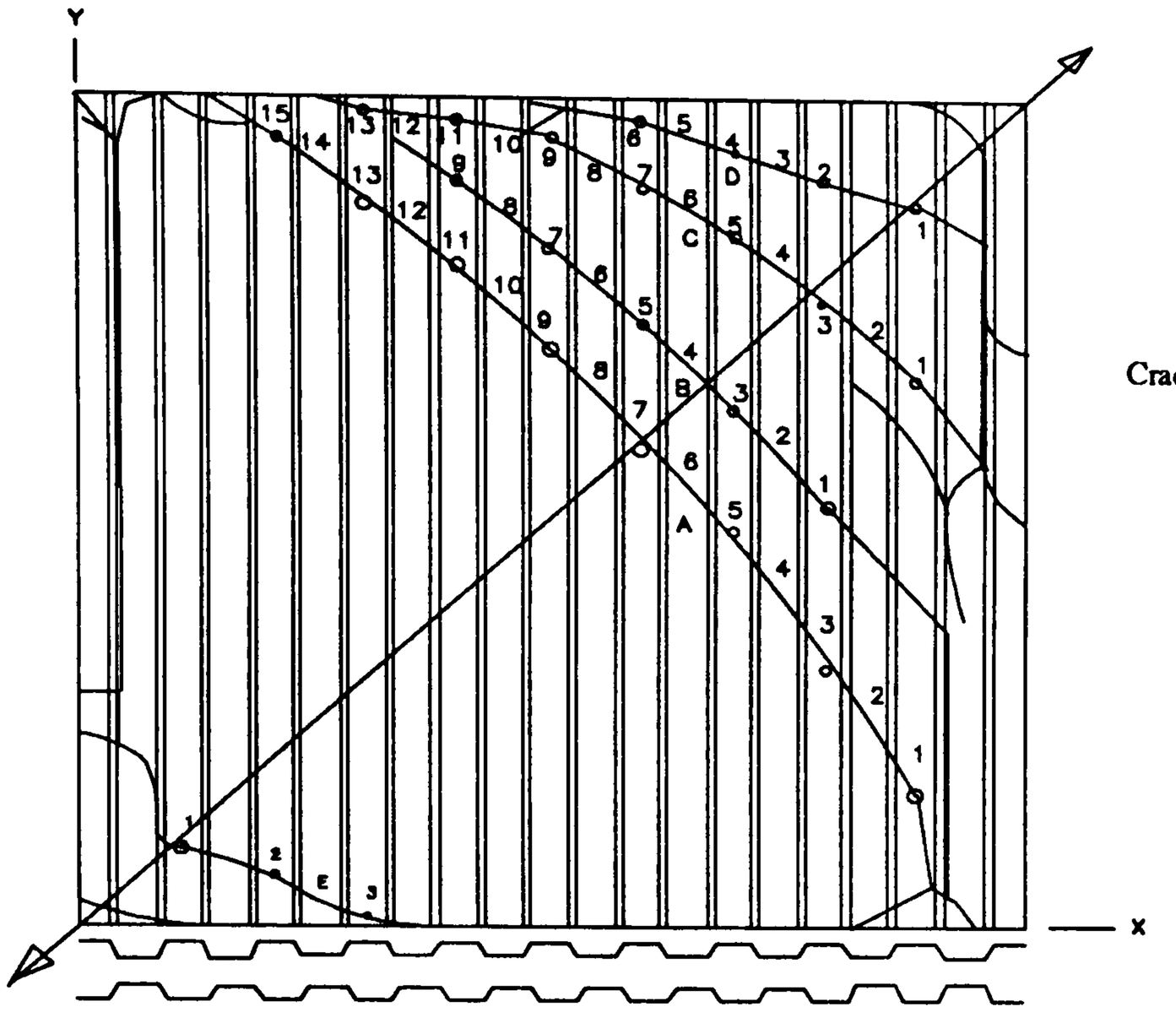

Crack line	Cracking load
E	23kN
D	29.5kN
C	31kN
B	45kN
A	50kN

Figure 4.10: Crack pattern

The orientation of cracks in failed panel is shown in tabular form in table 4.1. Crack angle seems to be decreased from central cracks towards the corner cracks in both trough and crests. Crack angle ranges between 37 to 56 degrees along the loaded central diagonal band as shown by bold figures in the table.

Table 4.1: Crack analysis

Crackline	Crack angles at points on crack lines														
	1	2	3	4	5	6	7	8	9	10	11	12	13	14	15
A Crest	48		57		**44**		**38**		**37**		45		32		**26**
A Trough		62		62		**44**		**52**		45		36		35	
B Crest	46		**43**		**41**		36		32						
B Trough		**56**		**47**		45		52							
C Crest	32		**38**		31		27		27		16		7		
C Trough		**44**		**43**		34		28							
D Crest	**34**		19		14										
D Trough		24		17											

* Crack angles measured with respect to X-axis

4.4.2 Test 2

The panel was cracked initially during its assembling operation in the frame due to bending. The panel was tested without casting resins to fill the profiled gap between panel and frame. Initial cracks were found to dictate the failure pattern and failure load of the panel. The panel failed at about 20 kN with the formation of several cracks. At the bottom corner of the panel where there was no initial cracks, two cracks parallel to off-diagonal were formed.

4.4.3 Test 4

This panel was tested in a similar manner to that of test-1. No strain gauges were used. The panel was cracked at about 25 kN and failed at about 46 kN. The crack pattern and failure were almost similar to that of test-1 but in this case two major cracks parallel to the off-diagonal were observed.

4.4.4 Test 5

This panel was damaged during testing due to machine failure. A machine fault caused a rapid increase in tensile force along the diagonal and it was not possible to monitor the diagonal load-deformation response or strains from the strain gauges. However it represented similar testing conditions to test-1 and the crack pattern and failure mode of the panel were similar to those of test-1 and test-3.

4.4.5 Test-6 (Hysteretic behaviour)

4.4.5.1 Introduction

This panel was tested to study the hysteretic behaviour of the panel. The panel was subjected to tensile force up to a certain load along the loaded diagonal and then load released to zero. Then the panel was subjected to compression force along the loaded diagonal to the same magnitude of load as applied before in tension and then released to zero. The alternating application of tensile and compressive force along the loaded diagonal was continued for several cycles until the panel cracked. After cracking the panel was subjected to failure by applying tensile forces along the diagonal.

4.4.5.2 Testing and observation

The panel was first loaded to a tensile force of +2.0 kN and then load was released to zero. Then the panel was loaded to a compressive force of -2.0 kN and then load was released to zero to complete one cycle. In this way the panel was subjected to several cycles of loading and in each cycle the load was increased by 2.0 kN. The panel cracked at about +13 kN after 7 cycles of loading with the formation of a crack

parallel to the off-diagonal near the lower pin. Several cracks parallel to the off-diagonal were formed as the panel was loaded to failure under tension. Crack patterns, as shown in photograph 4.4, were found to be similar to those from other tests. The diagonal failure load of the panel was around +40 kN.

4.4.5.3 Analysis of strain results

Figures 4.11 show typical hysteresis loops for the diagonal strain gauges (7 and 8) show clearly the reversal of strains along the diagonal during the cycles of loading. The similar behaviour is shown by the other diagonal gauges.

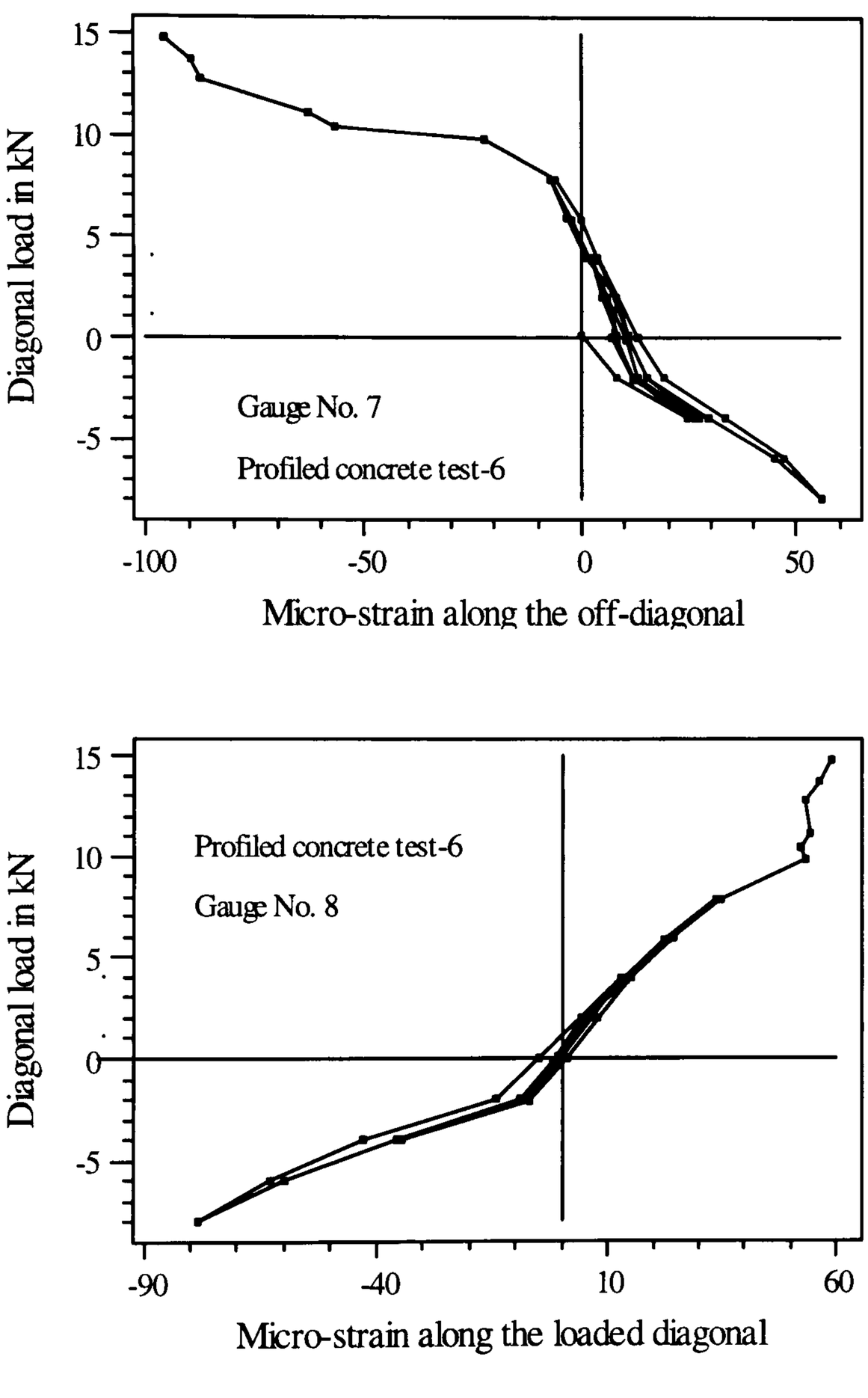

Figure 4.11: Hysteretic variation of strain

Strain along the diagonals

The variation of strain along the off-diagonal is shown in figure 4.12(a). All three gauges are in compression under tensile diagonal load and in tension under

compression diagonal load which is reasonable. The variation of strains along the loaded diagonal is shown in figure 4.12(b). All three gauges are in tension under tensile diagonal load and in compression under compressive diagonal load up to the cracking load which is just opposite to those of the other diagonal. However, the diagonal strains at the rosette 4-5-6 are found to be less than those of the other rosettes as it is in the crest section where thickness of the panel is highest.

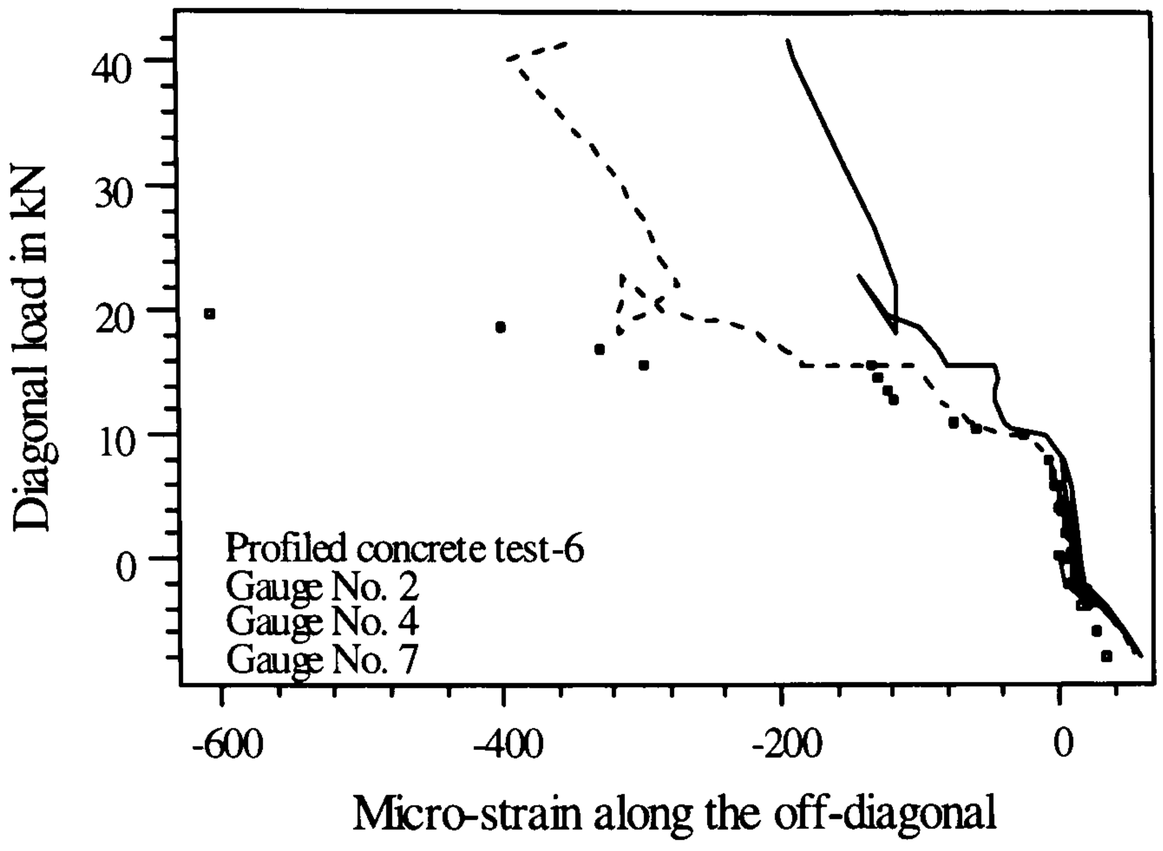

Figure 4.12(a): Strain along the off-diagonal

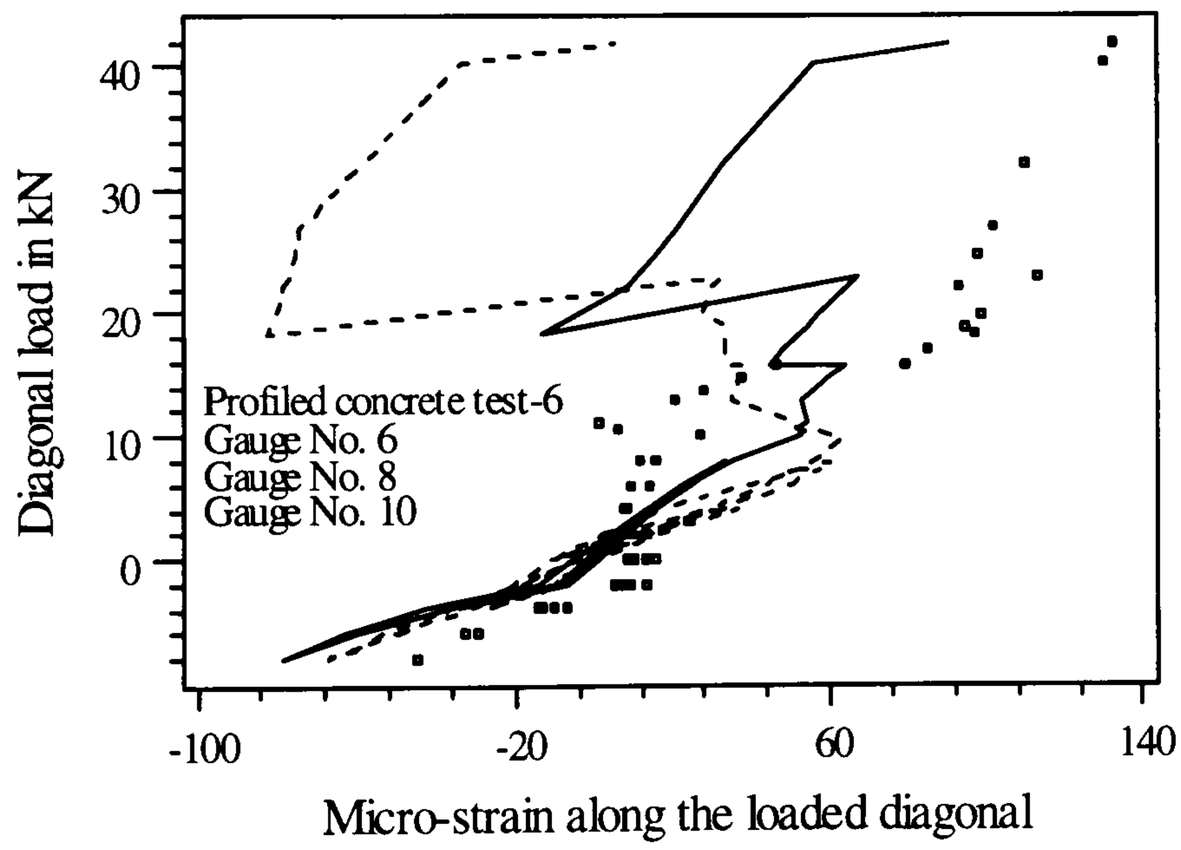

Figure 4.12(b): Strain along the loaded diagonal

Principal strain

The variation of principal strains at three rosette locations throughout the loading history is shown in figure 4.13. Pre-cracking major and minor principal strains are found to be approximately the same specially in each of the rosette locations 1-2-3

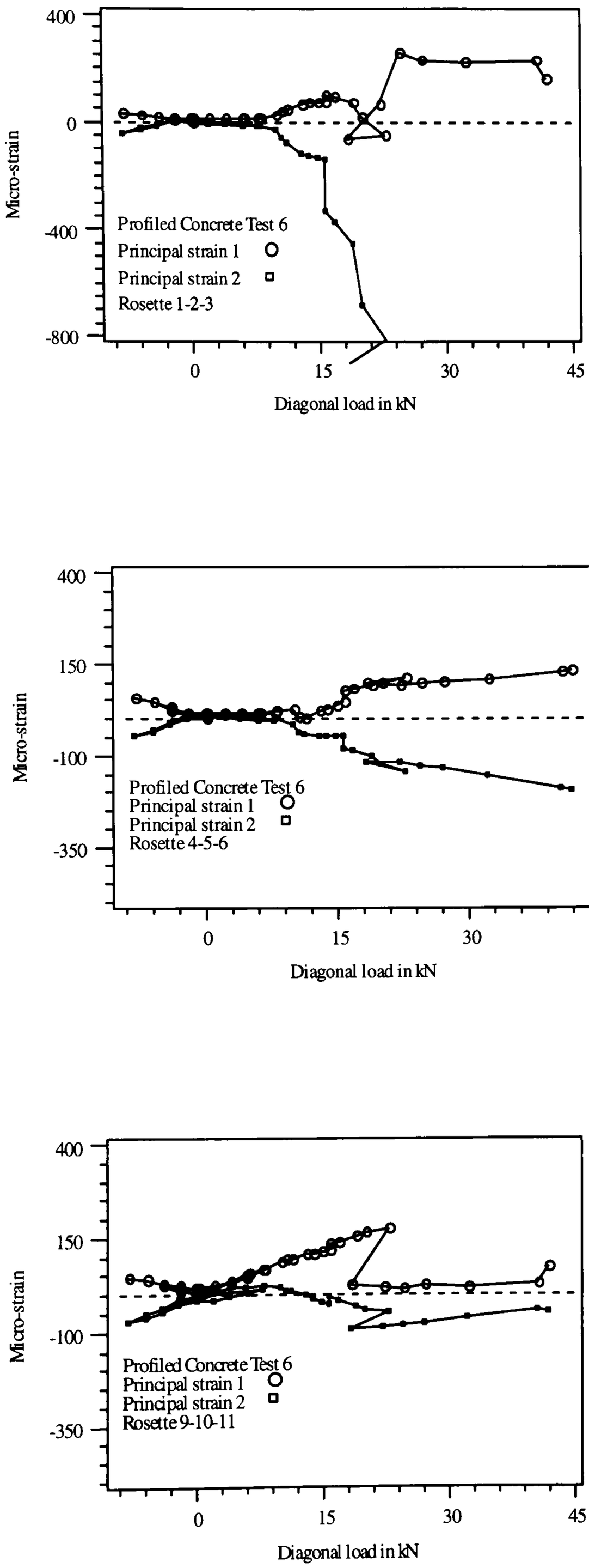

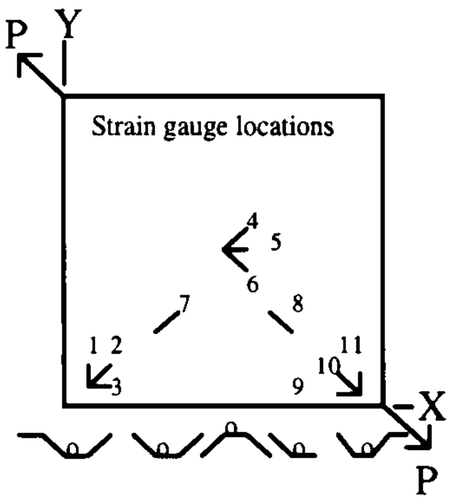

Figure 4.13: Principal strain variation

and 4-5-6. The principal micro-strain in the rosette locations just before cracking at a diagonal load of 12.85 kN are 78 (R1-2-3), 38 (R4-5-6) and 111 (R 9-10-11). The principal stresses or strain at R-4-5-6 are less than the others due to the thicker cross-section at the crest location. The principal stress and strain at rosette 9-10-11 (near the bottom corner) exceeds the ultimate tensile stress and strain of concrete earlier which justifies the formation of the first diagonal crack near the bottom corner.

4.4.6 Comparison of results between Panel tests

Principal strain

The principal strains at R-1-2-3 of test 6 and R-12-13-14 of test 1 are compared in figure 4.14. The table 4.2 below shows the exact values of the stress and strain in the pre-cracking stage. They are found to be in good agreement up to the pre-cracking stage which proves consistency and repeatability of the model tests.

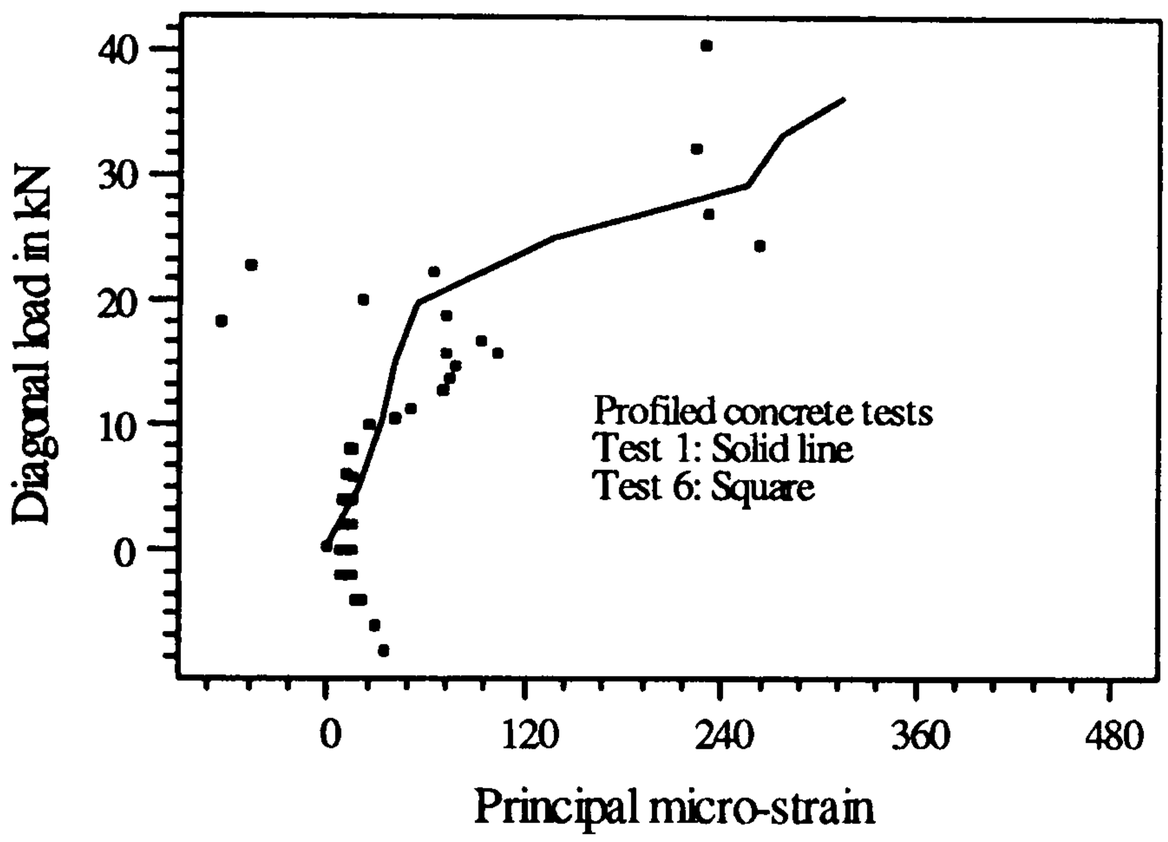

Figure 4.14: Comparison of principal strain

Table : 4.2: Comparison of principal stress-strain

	Diagonal load 5kN		Diagonal load 10kN	
	Test 1	Test 6	Test 1	Test 6
Principal stress N/mm^2	0.31	0.32	0.54	0.58
Principal micro-strain	19	18	33	40

Load -deformation and stiffness

The properties of micro-concrete for the panel tests are summarised in table 4.3. The diagonal load-deformation responses of the all the model test panels are shown in figures 4.15. The slopes of the initial and re-loading parts will be used to determine

the average stiffness of the panel. The cracking point can be identified from the sudden decrease in stiffness of load-deformation responses.

The load and stiffness values are summarised in table 4.4. The pre-cracking stiffness of the panels are found to be in good agreement to each other except for panel 2 which was cracked initially. The cracking load seems to be decreased by 30% compared to panel test 4 & 1 due to the application of hysteretic load in panel test 6. The hysteretic effect also reduced the ultimate load by about 18%.

Table 4.3: Material properties

Test no	Cylinder strength	Cube strength	Splitting
1		21	2.323
2	21	31	2.467
4	23.3	24	2.48
6	18-22	24.68	2.45

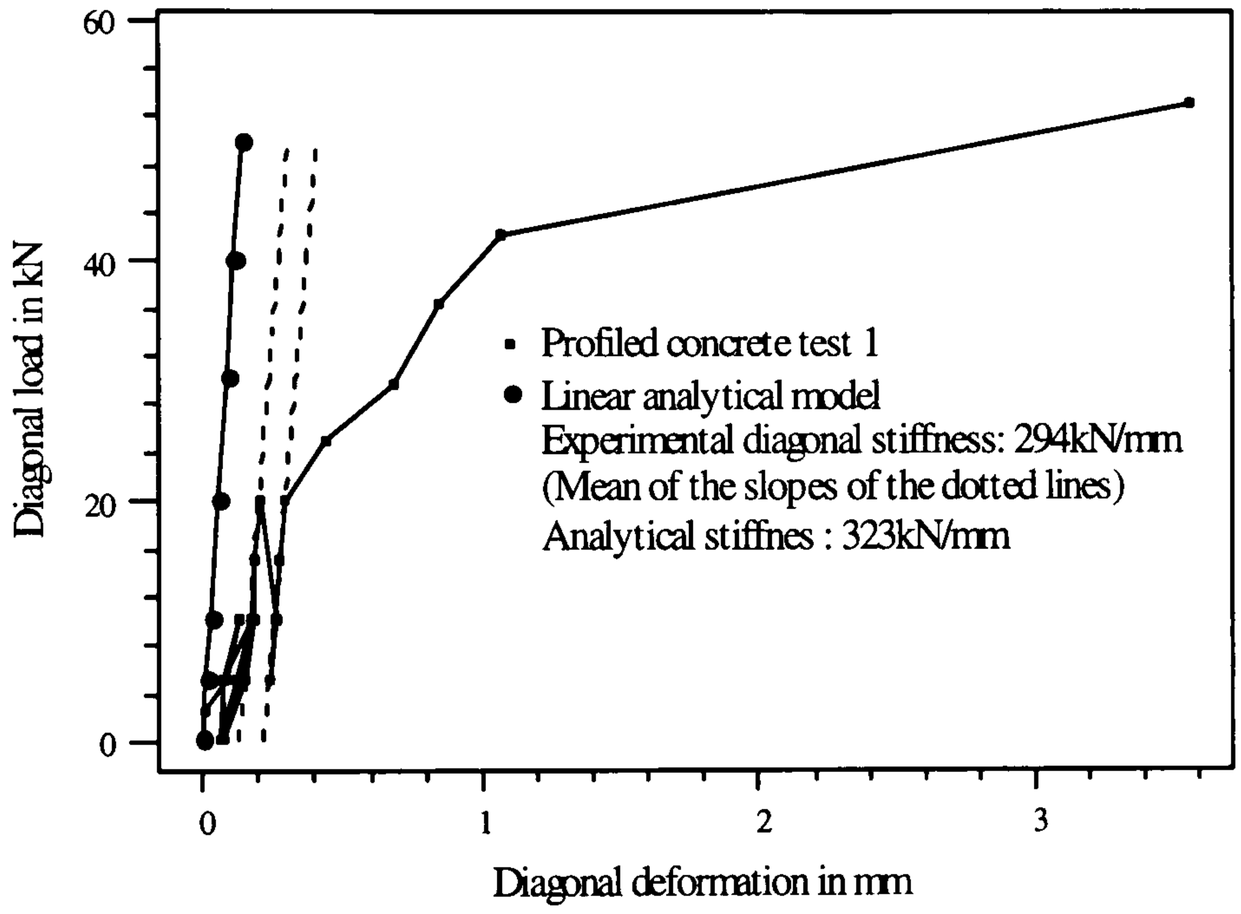

Figure 4.15(a)

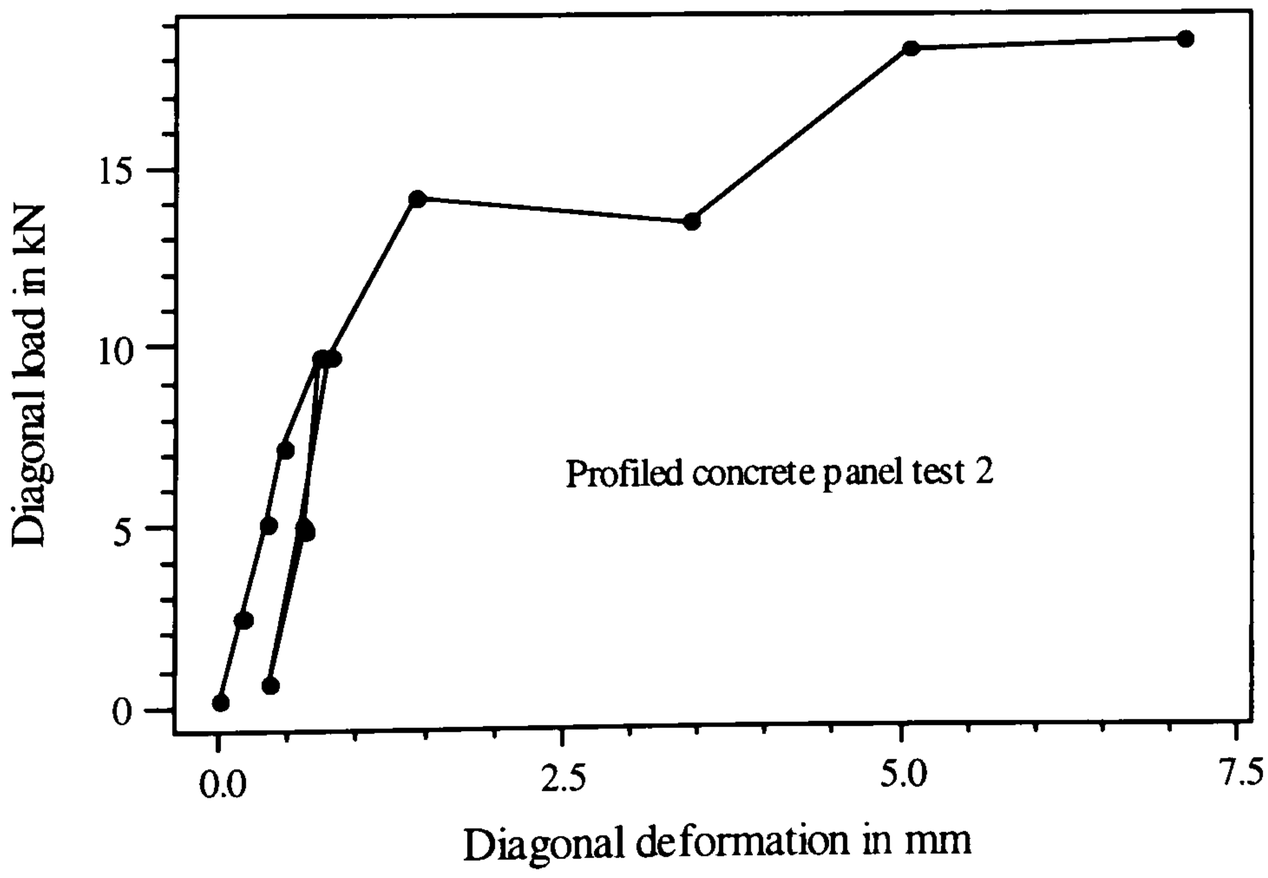

Figure 4.15(b)

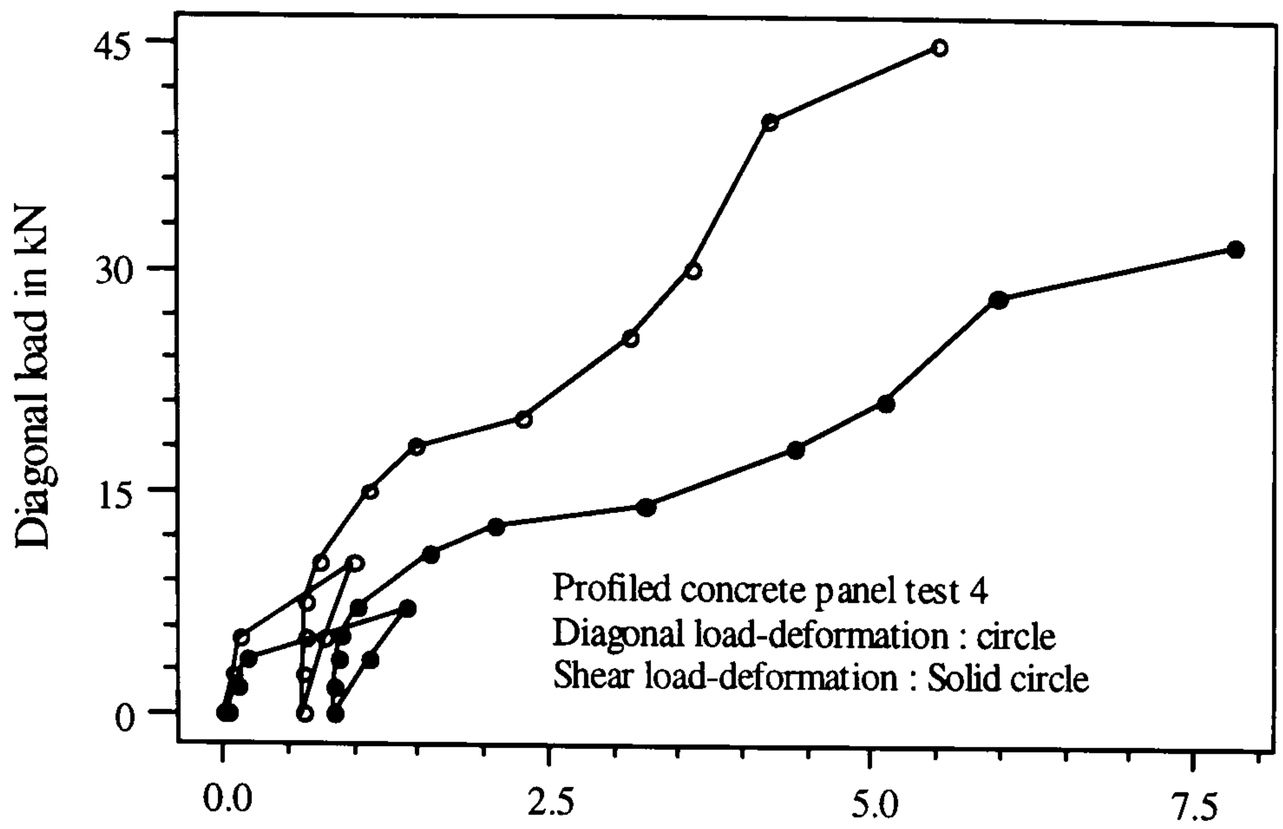

Figure 4.15(c)

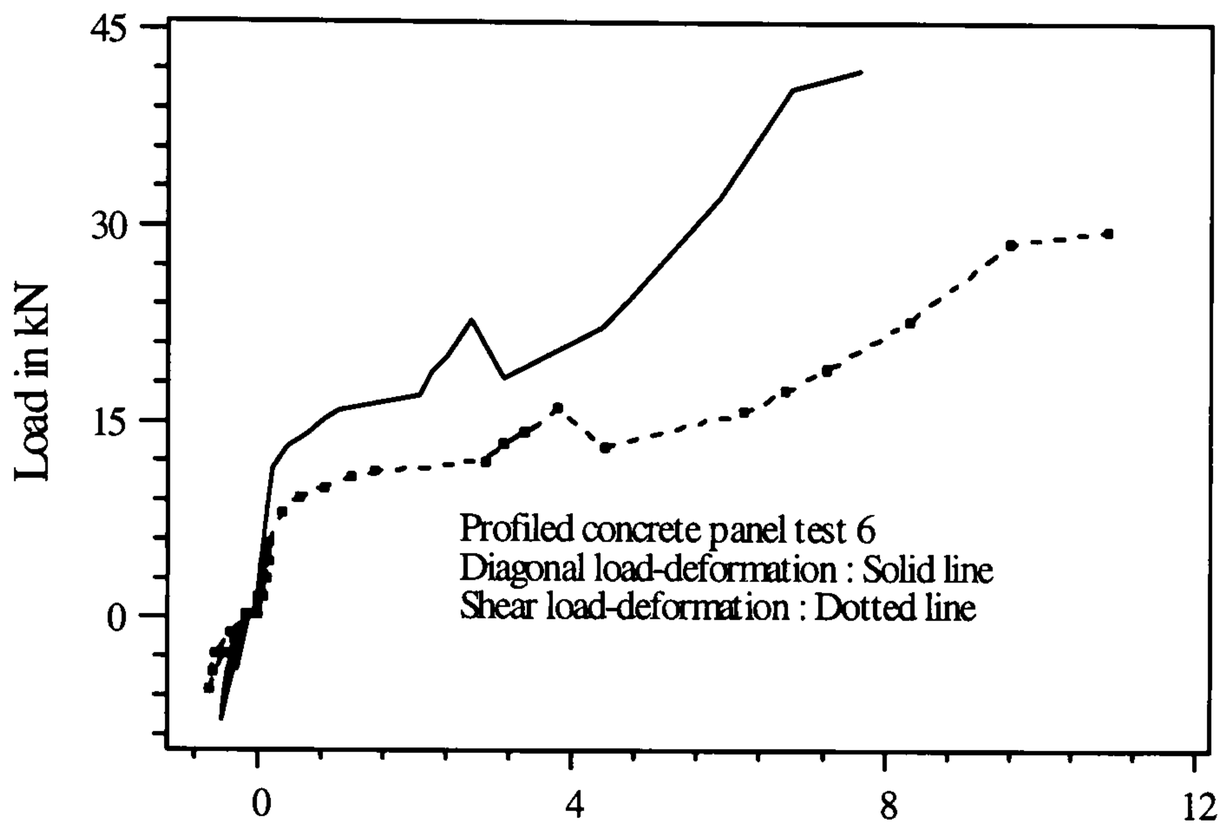

Figure 4.15(d)

Figure 4.15: Load-deformation response for the model tests

Table 4.4: Summary of strength and stiffness

Test no.	Stiffness kN/mm		Cracking load kN		Ultimate load kN	
	Diagonal	Shear	Diagonal	Shear	Diagonal	Shear
1	294	147	22	15.5	48	34
2	--	--	---	---	18.5	13
4	257	129	19	13.43	44	31
6	282	141	13	9.19	36	25.5

4.5 Finite Element modelling

The symmetric half profiled concrete panel was idealised with 3D semi-loof shell element. The boundary frame of the panel was represented by semi-loof beam elements. The panel and the boundary frame was connected through compatible joint elements. The joint properties were assigned in such a way that the boundary frame could simulate the actual model test condition. Finite element idealisation of the panel with boundary frame is shown in figure 4.16.

Exact boundary conditions have been given so that hinges can be simulated at the corners and the frame can act as a mechanism. The structure was then restrained at one corner and the load in the form of prescribed displacements were applied at the diagonally opposite corner simulating exactly model test condition. The load was then applied incrementally until failure of the panel so that diagonal load-deformation response could be found.

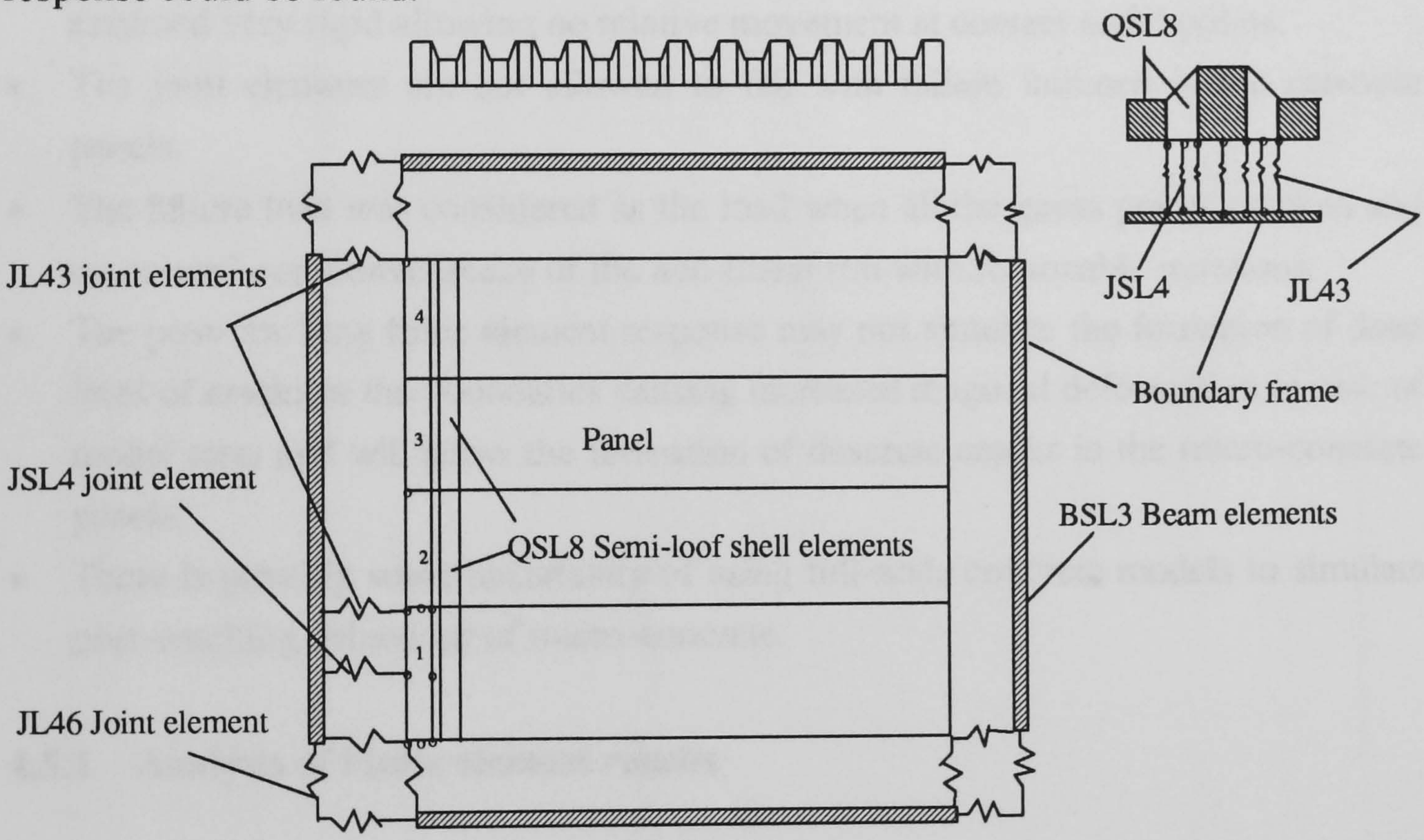

Figure 4.16: Finite element idealisation

To validate the equation (2.1 of chapter 2) for transformation of diagonal response to shear response for profiled concrete panel, finite element analysis for both cases were carried out. The shear load deformation response obtained from test simulation using transformed equation is compared with that from shear simulation in figure 4.17. The pre-cracking stiffness, cracking load and ultimate load are found to be in good agreement.

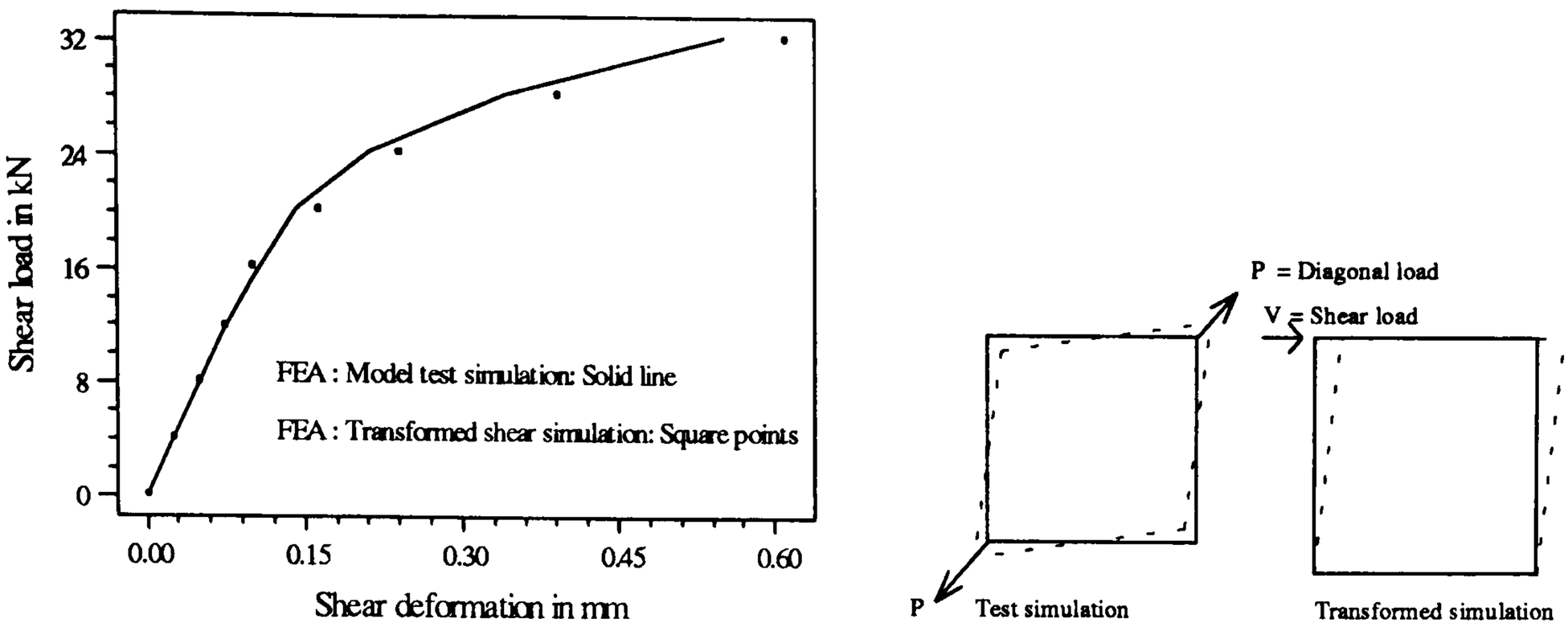

Figure 4.17: Validation of transform equation

Assumptions and limitations of FE analysis

- The connections between profiled concrete core and the boundary frame were assumed very rigid allowing no relative movement at contact nodal points.
- The joint elements are not allowed to fail with failure initiated in the concrete panels.
- The failure load was considered as the load when all the gauss points cracked and associated non-convergence of the non-linear run with reasonable iterations.
- The post-cracking finite element response may not simulate the formation of deep lines of cracks at the boundaries causing increased diagonal deformation in case of model tests and will allow the formation of descrete cracks in the micro-concrete panels.
- There is possibly some uncertainty of using full-scale concrete models to simulate post-cracking behaviour of micro-concrete.

4.5.1 Analysis of Finite element results

Finite element analysis of the panel had been carried out using shear retention factor of 0.3, softening parameter of 30, maximum compressive strain of 0.0026, poisson's ratio of 0.18 and other parameters derived from actual control specimens of micro-concrete.

Strain along the boundary of the panel

Variation of shearing strain along the boundaries are as shown in figure 4.18 and 4.19. The shearing strain in the crest points are found to be lower than those of trough

points. The shearing strain is found to be higher at the loaded corner and gradually decreased towards the off-diagonal corner. But the variation ranges between 77-80 micro-strain for most of the crest points and 96-102 micro-strain for most of the trough points which seems to be more or less uniform. The variation of shearing strain along the plain boundary is found to be more or less uniform.

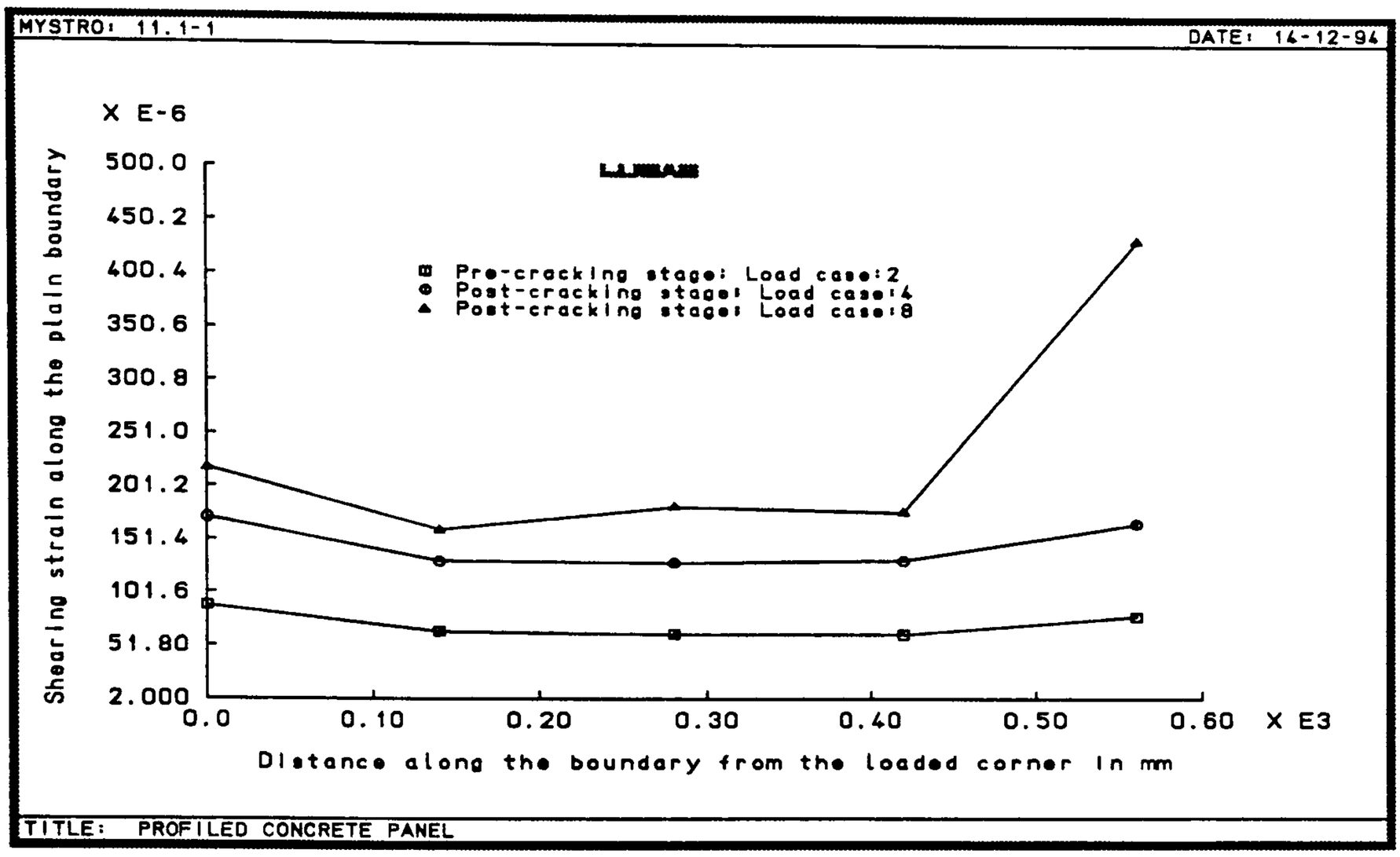

Figure 4.18: Shearing strain along the plain boundary

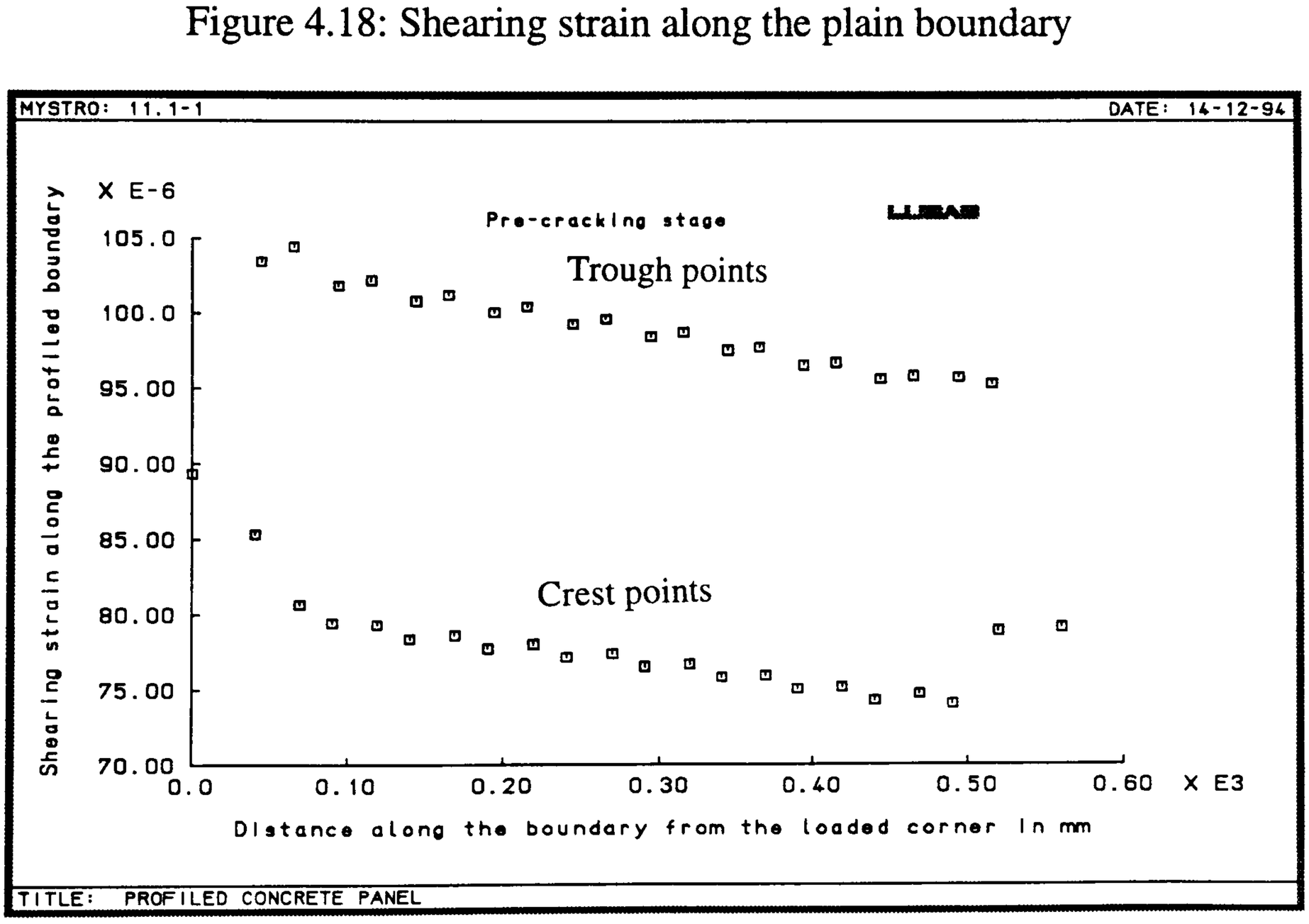

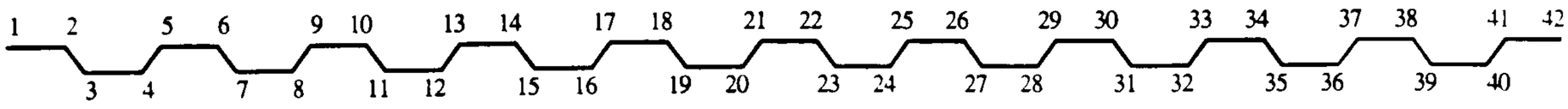

Crest and trough points in the profiled boundary

Figure 4.19: Shearing strain along the profile boundary

Variation of X and Y-strain along the plain boundary is shown in figure 4.20. The variation of strains seems to be more or less similar to those of model tests shown in figures 4.9(c) and (d) although the model gauges are placed in the trough section adjacent to the boundary.

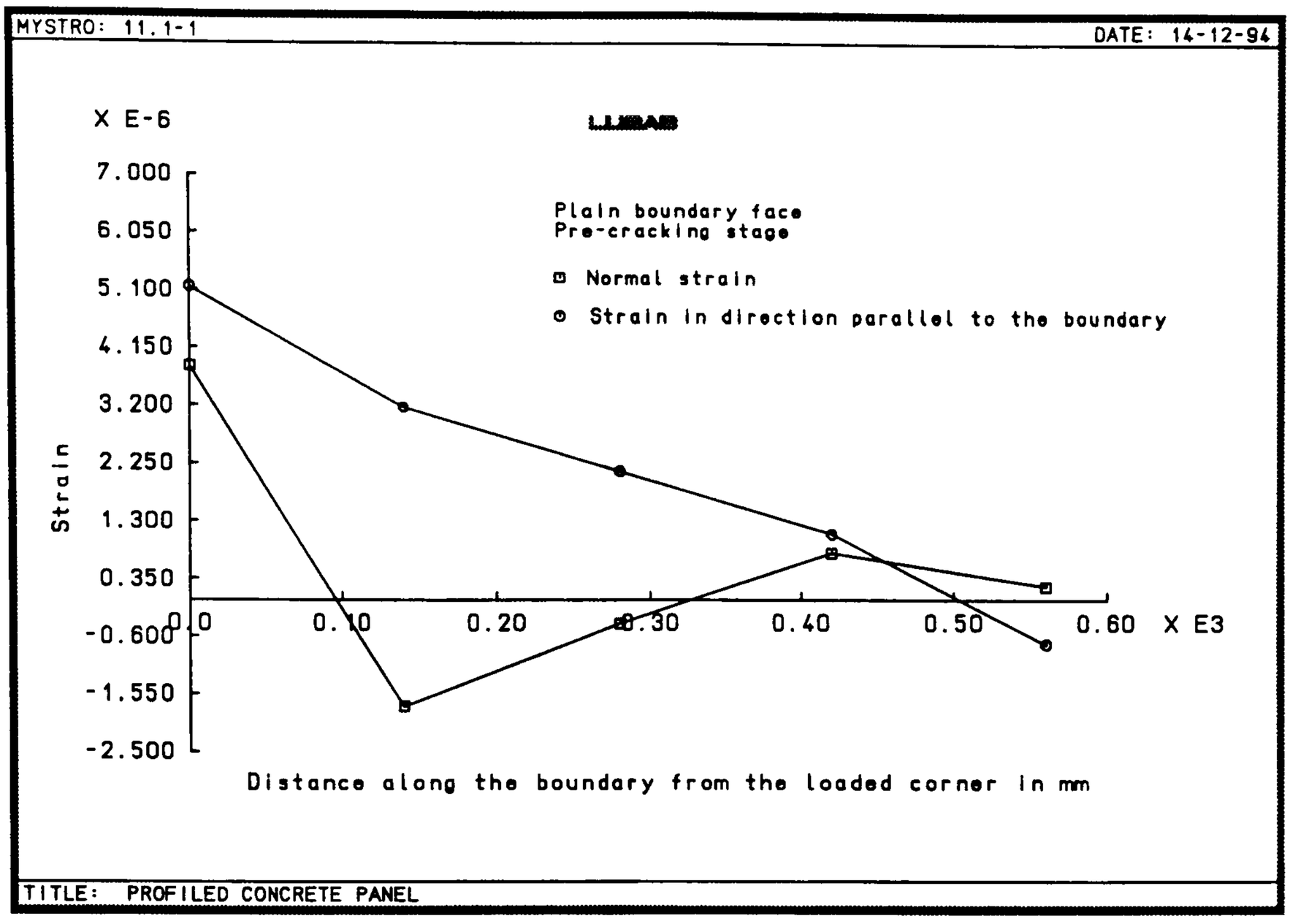

Figure 4.20: Variation of Xand Y strain along the plain boundary

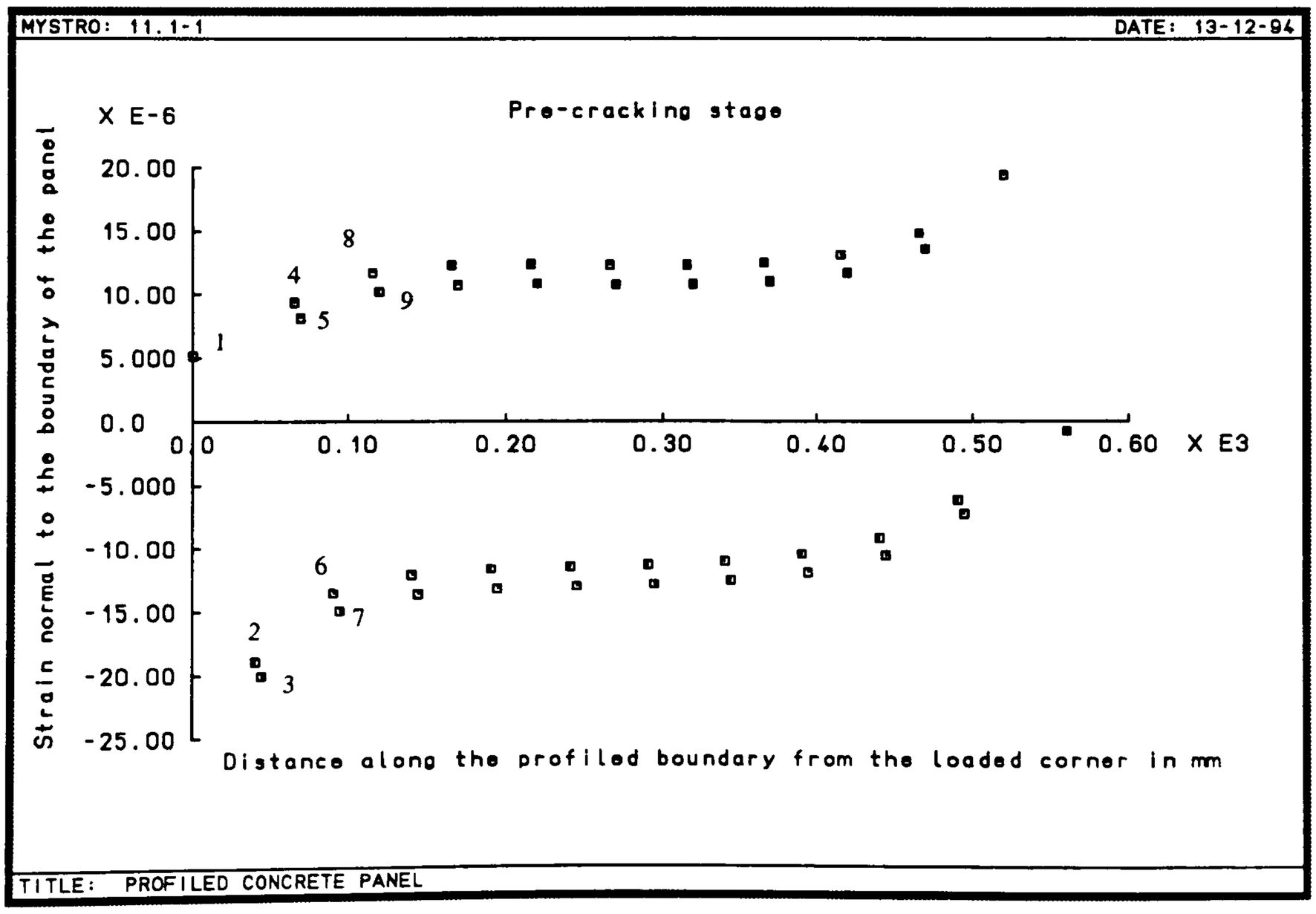

Figure 4.21: Variation of Y strain along the profile boundary

Variation of Y strain along the profiled boundary is shown in figure 4.21. The strains seems to be dependent on the position of points on the inclined face of the profile. The exact variation of X,Y and shearing strains (ε_x,ε_y and γ_{xy}) along a section of profile on the boundary for a particular load case is presented in the table 4.5.

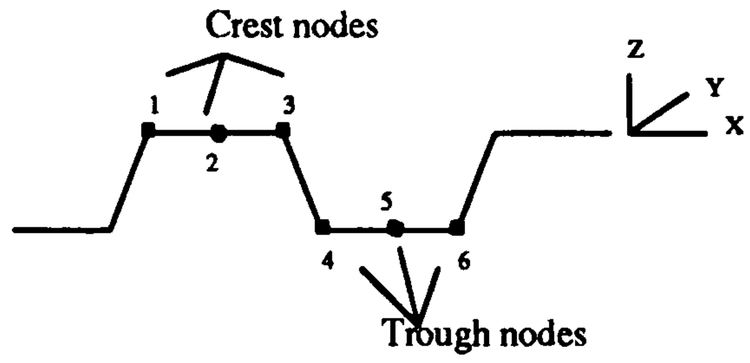

Table 4.5

Micro-strain	Nodes					
FE analysis	1	2	3	4	5	6
ε_x	0.94	0.89	0.84	1.59	1.46	1.33
ε_y	4.65	-0.20	-5.03	-5.69	-0.17	5.33
γ_{xy}	31.74	31.6	31.3	49	49	49

The ε_x and γ_{xy} seem to be not changing along the crest or trough nodes but strains in trough nodes are higher than those at crest nodes. ε_y change sign between end nodes in both crest and trough sections with nearly zero values at the mid nodes.

Strains along the loaded and off-diagonals

The variation of principal strains along the loaded and off-diagonals are shown in figures 4.22 and 4.23. The crests points are found to be strained less than trough points on both diagonals. In the pre-cracking stage, the variation of principal strains is found to be uniform at both trough and crest points along the most part of the diagonals except near the corners. The principal strains along both the diagonals are equal to each other. For the particular case considered, the major and minor principal strain for crest points can be averaged as + 28 and -28 micro-strain while those for trough points can be averaged as +65 and -65 micro-strains. The major and minor principal strains can be considered as equal to each other.

The variation of principal direction along the both diagonals in pre-cracking and just after cracking stages is shown in figures 4.24 and 4.25. The direction falls in the band 42-46 degrees. But in the failure stage, the principal direction ranges between 38 to 55 degrees. The equality of the principal strains in both diagonals and the equality of major and minor principal strains and their direction confirm the simulation of pure shear condition within the panel.

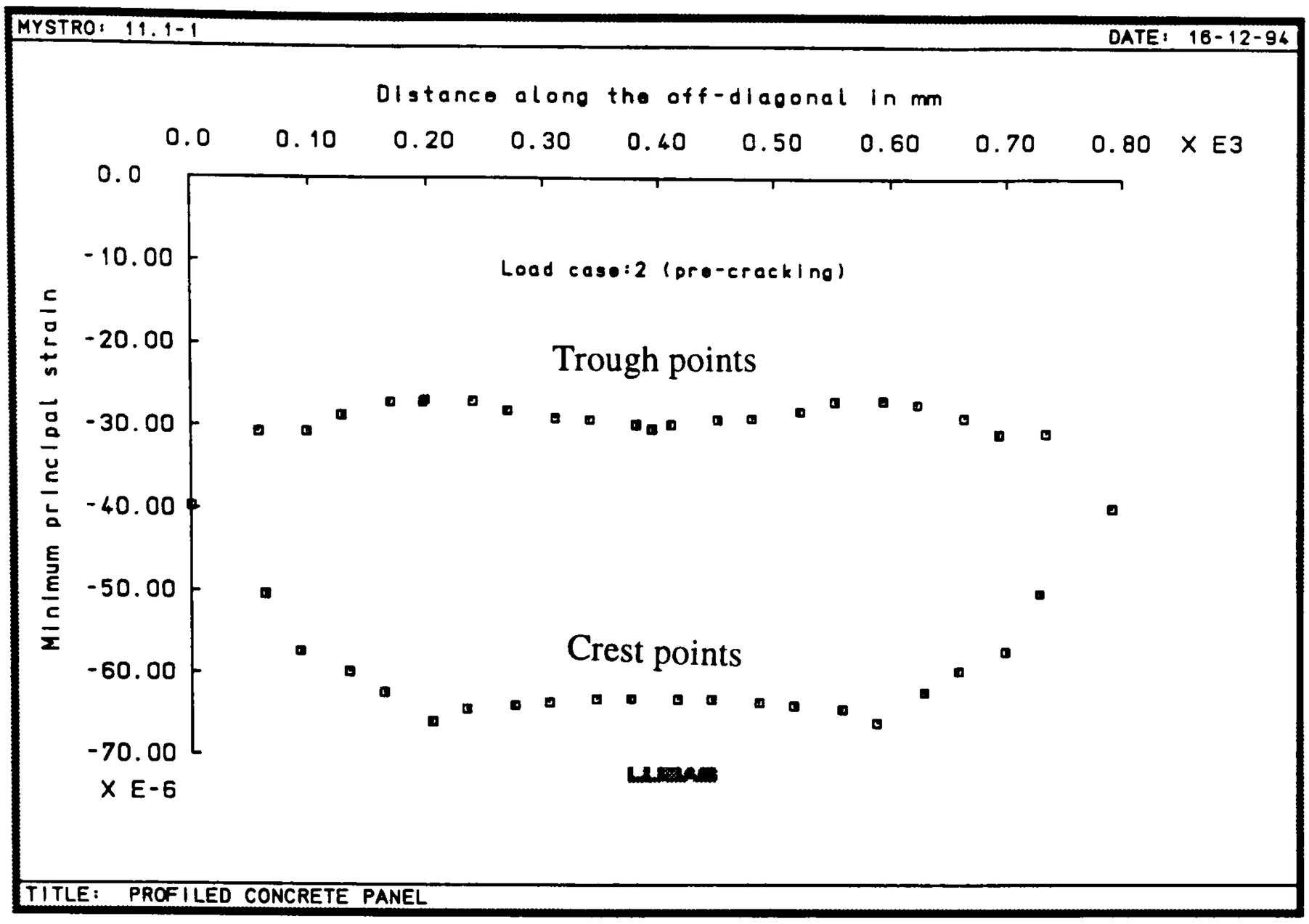

Figure 4.22: Variation of principal strain along the off-diagonal

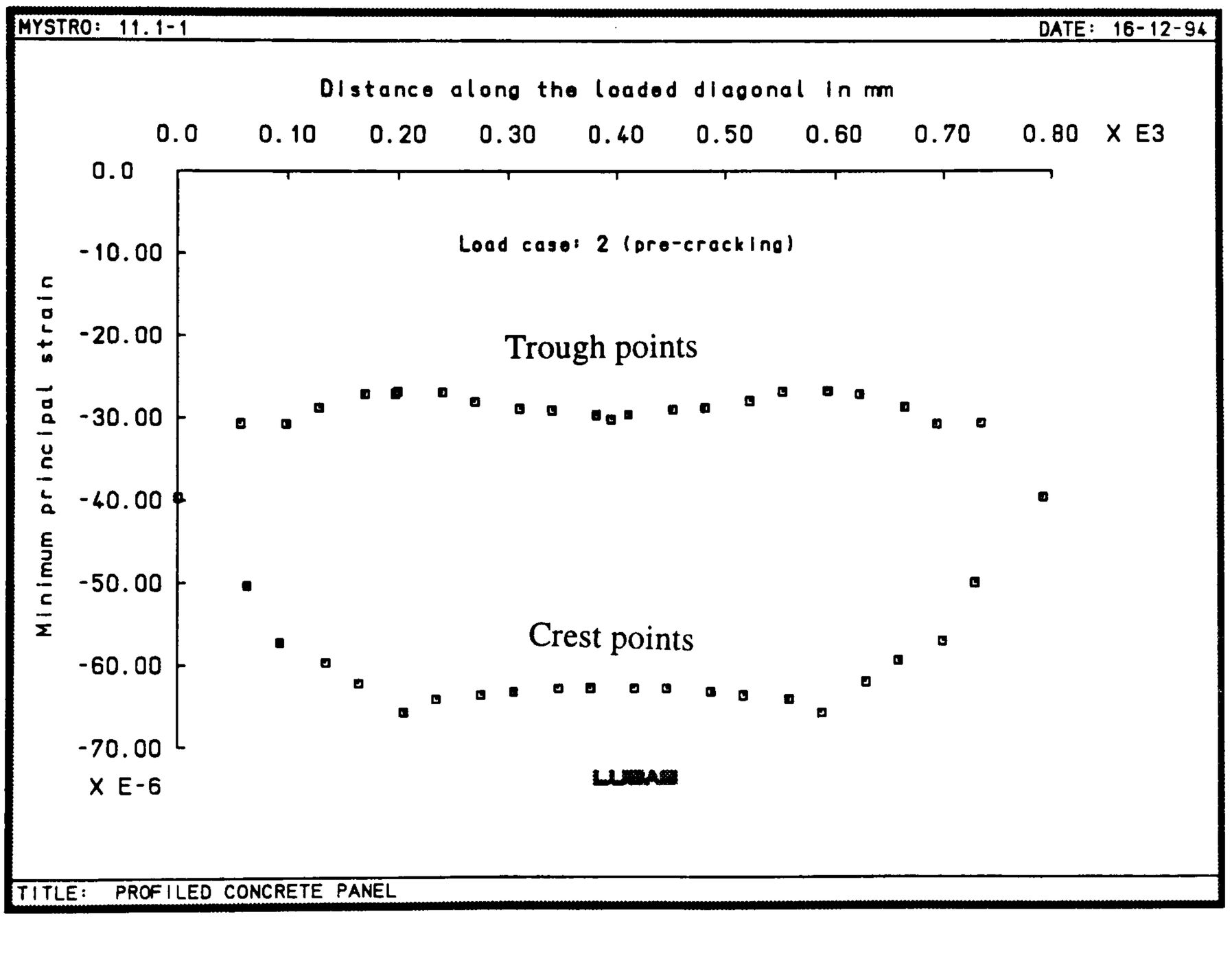

Figure 4.23: Variation principal strain along the loaded diagonal

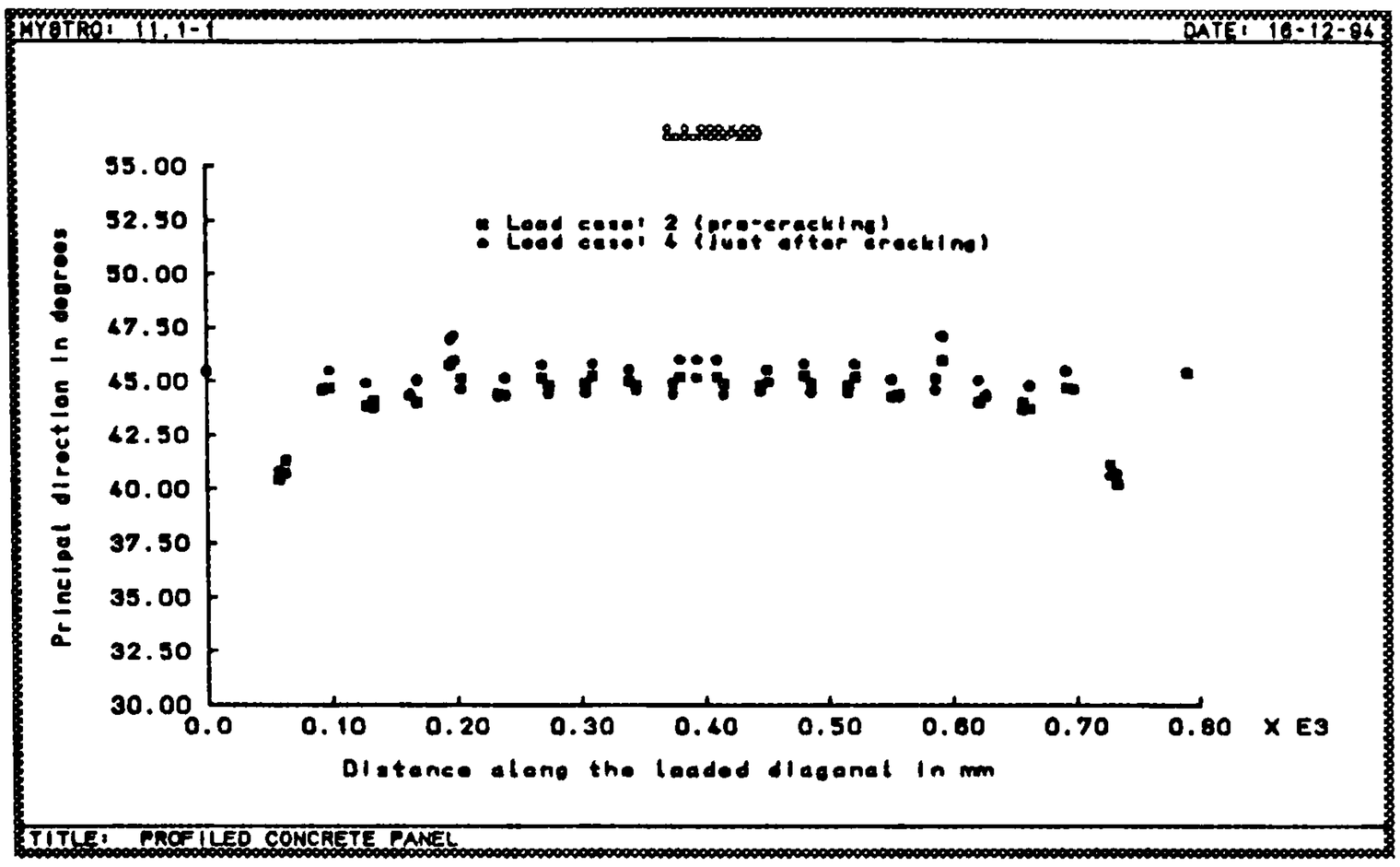

Figure 4.24: Variation of principal direction along the loaded diagonal

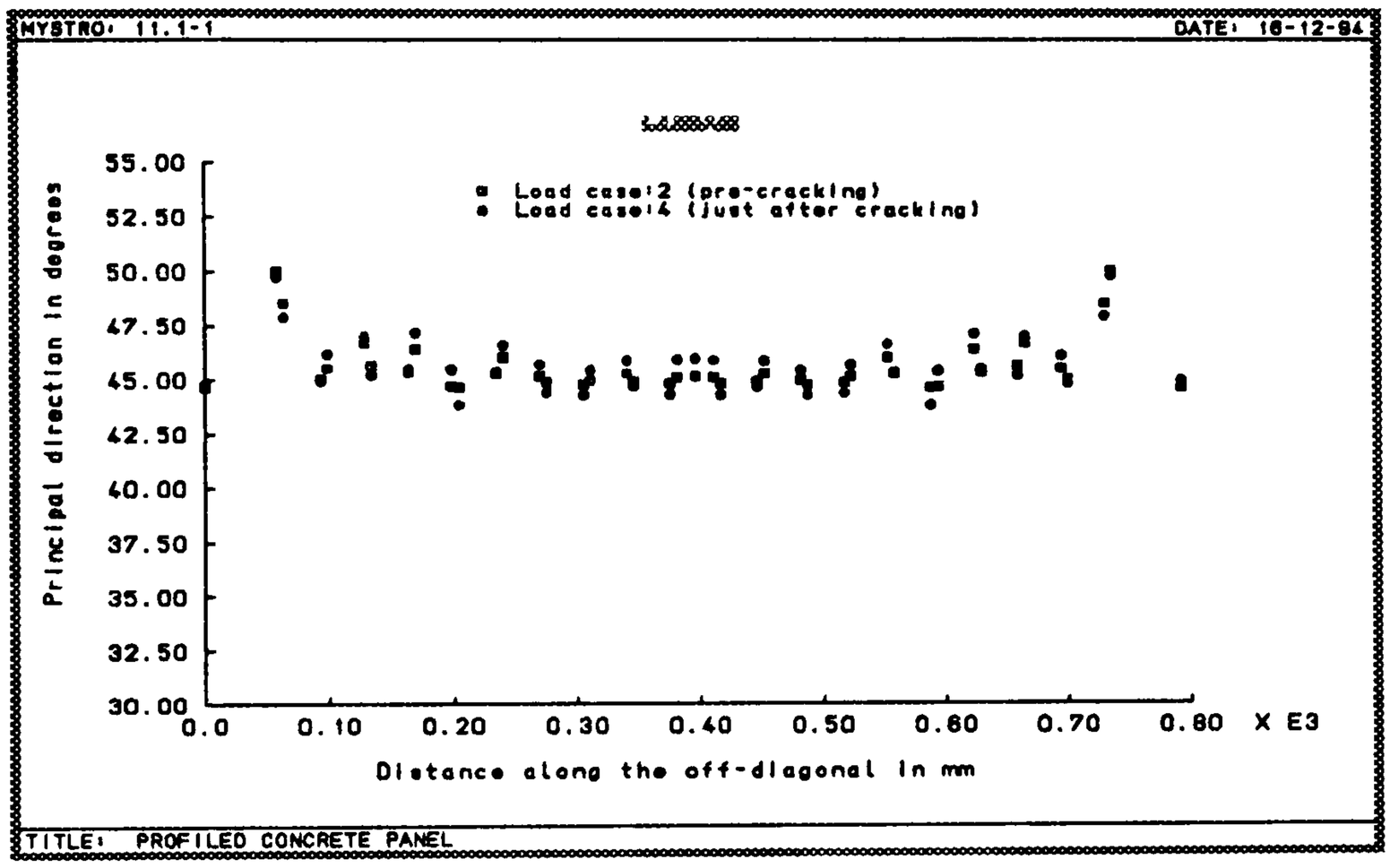

Figure 4.25: Variation of principal direction along the off-diagonal

Principal strain and direction within the panel

Figures 4.26 and 4.27 show the contour maps for the variation of principal strain and its direction. The principal strain in the trough is found to be higher that in the crest where the thickness of the panel is greater. The principal direction varies from 38-52 degrees. The formation of diagonal tension along the loaded diagonal and compression strut along the off-diagonal are confirmed from the direction of principal strain. The formation of a series of cracks perpendicular to the loaded diagonal is also justified. The formation of cracks along the trough line near the boundary as found in the crack diagram of model tests confirms the high stress concentration along the trough.

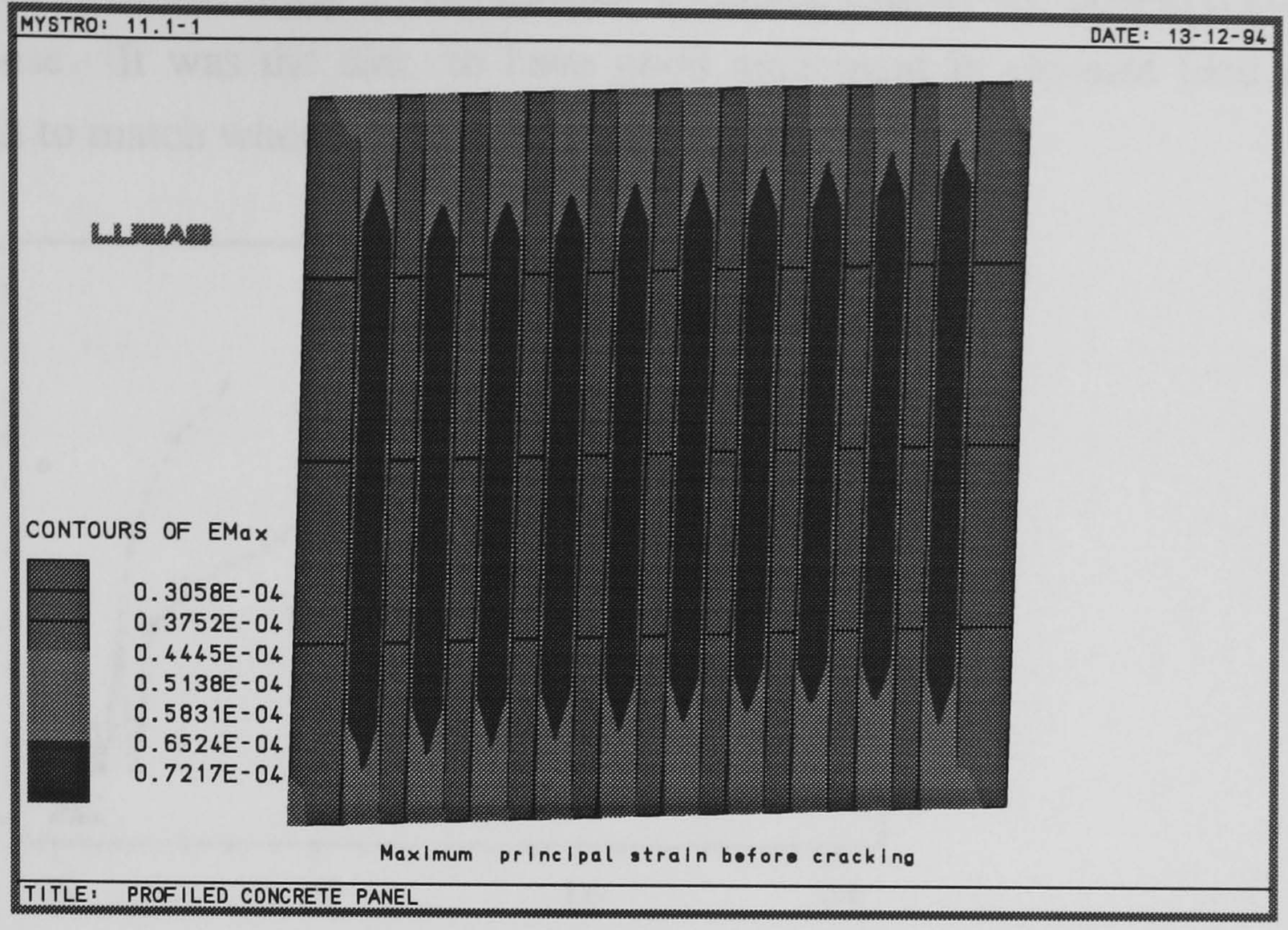

Figure 4.26: Contour diagram of principal strain

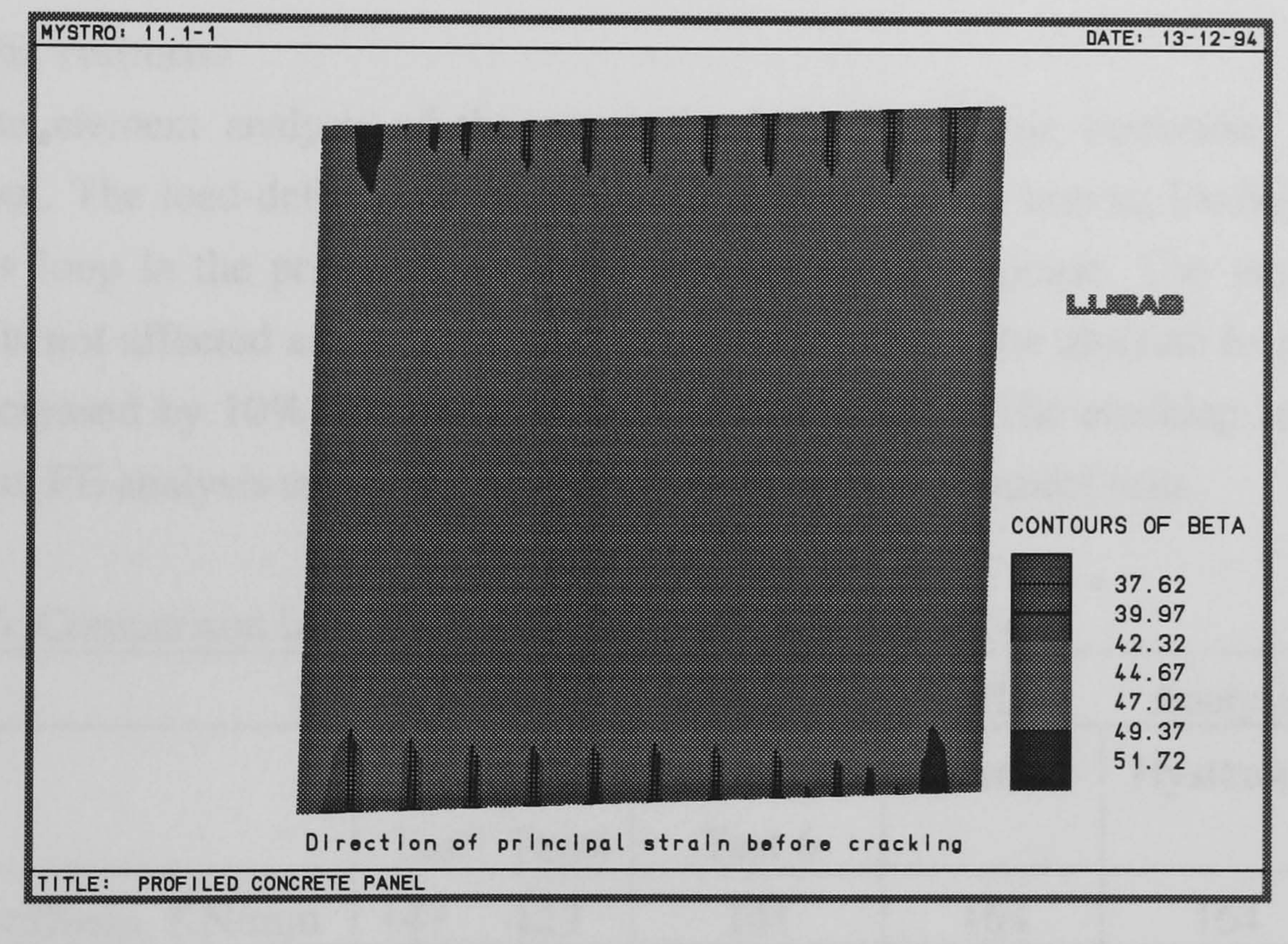

Figure 4.27: Contour diagram of principal direction

4.5.2 Comparison of FEA and model tests

Load-deformation response

The load -deformation responses from the model test 1 and finite element analysis are compared in figure 4.28. The pre-cracking parts with pre-cracking stiffness and cracking load show good agreement. The assumptions in simulation by FEA and

actual test conditions made it very difficult to match exactly the post-cracking part of the response. It was the aim to have good agreement in ultimate load prediction rather than to match whole post-cracking response.

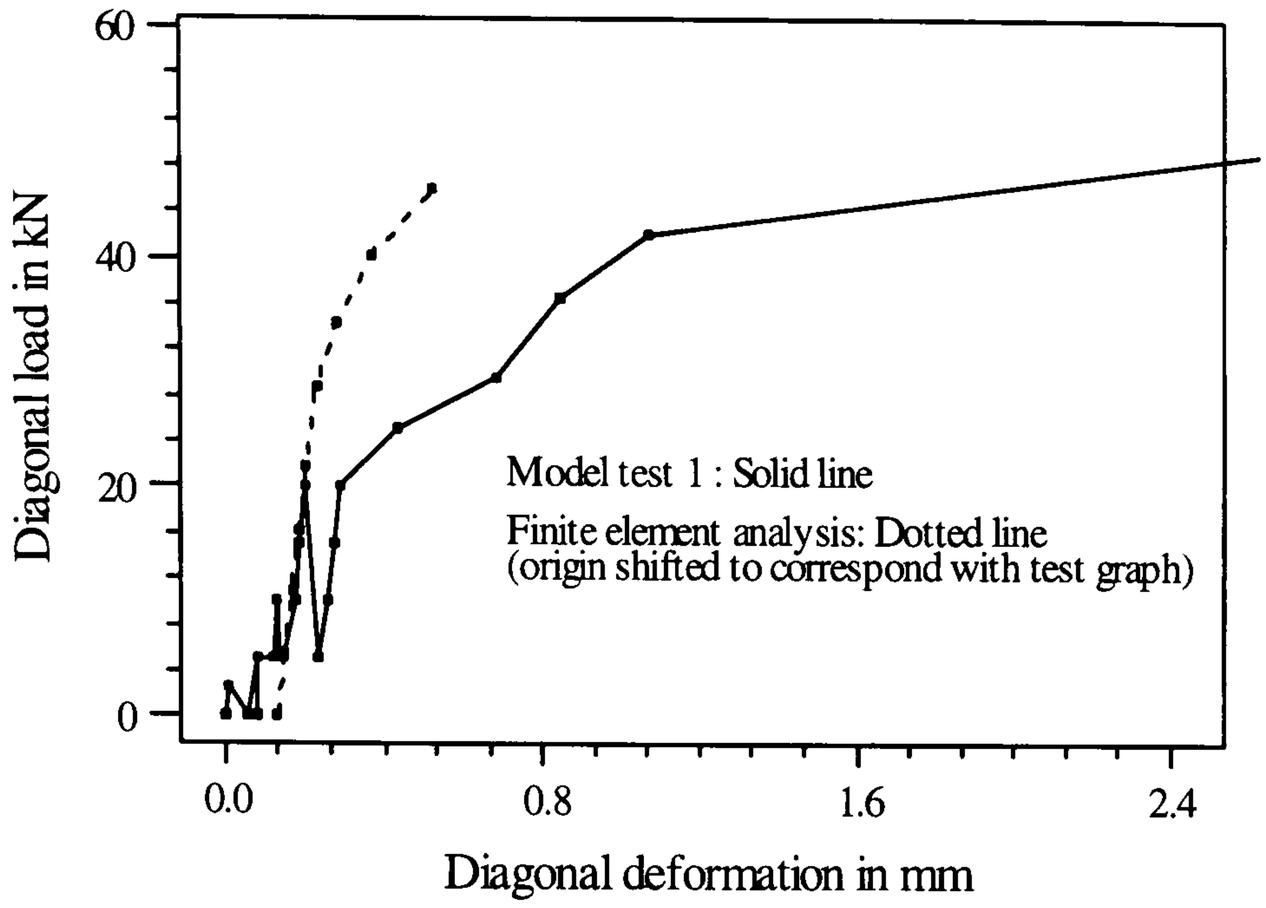

Figure 4.28: Comparison of FEA and Model test load-deformation response

Hysteretic response

The finite element analysis of the panel simulating hysteretic behaviour has been carried out. The load-deformation response is identical to the normal loading with no hysteresis loop in the pre-cracking stage showing linear response. The pre-cracking stiffness is not affected as found in model tests (table 4.6). The ultimate load is found to be decreased by 10% compared to 20% in model tests. The cracking load is not affected in FE analysis compared to about 30% reduction in model tests.

Table 4.6: Comparison between normal and hysteretic analysis

	Model Tests		FE Analysis	
	Normal Test1 Test4	Hysteretic Test 6	Normal	Hysteretic
Shear stiffness, KN/mm	147 129	141	164	164
Cracking load , kN	15.5 13.43	9.19	16.18	16.18
Ultimate load, kN	33 31	25	30	27

Boundary strains at strain gauge locations

An attempt has been made to compare the boundary strains measured from the model tests with those from the finite element analysis. It is difficult to compare the strain in direction perpendicular to the profiled boundary (Y-strains) because of the sensitivity of the strains to change with the position of the points (nodal or gauss) as observed in

FEA within the cross-section of the profile. The X-strains seems not to be changing to much at nodal or gauss points along each trough or crest sections. So it is possible to take the strain gauge readings across the whole trough or crest sections as an average of the nodal or gauss points strains in that section. Figure 4.29 shows a comparison of the variation of X-strain along the profiled boundary in pre-cracking stage from model test and FE analysis. The pattern of variation is identical but the model strains are higher than those from FEA. The strain in trough section is found to be higher than that in crest section.

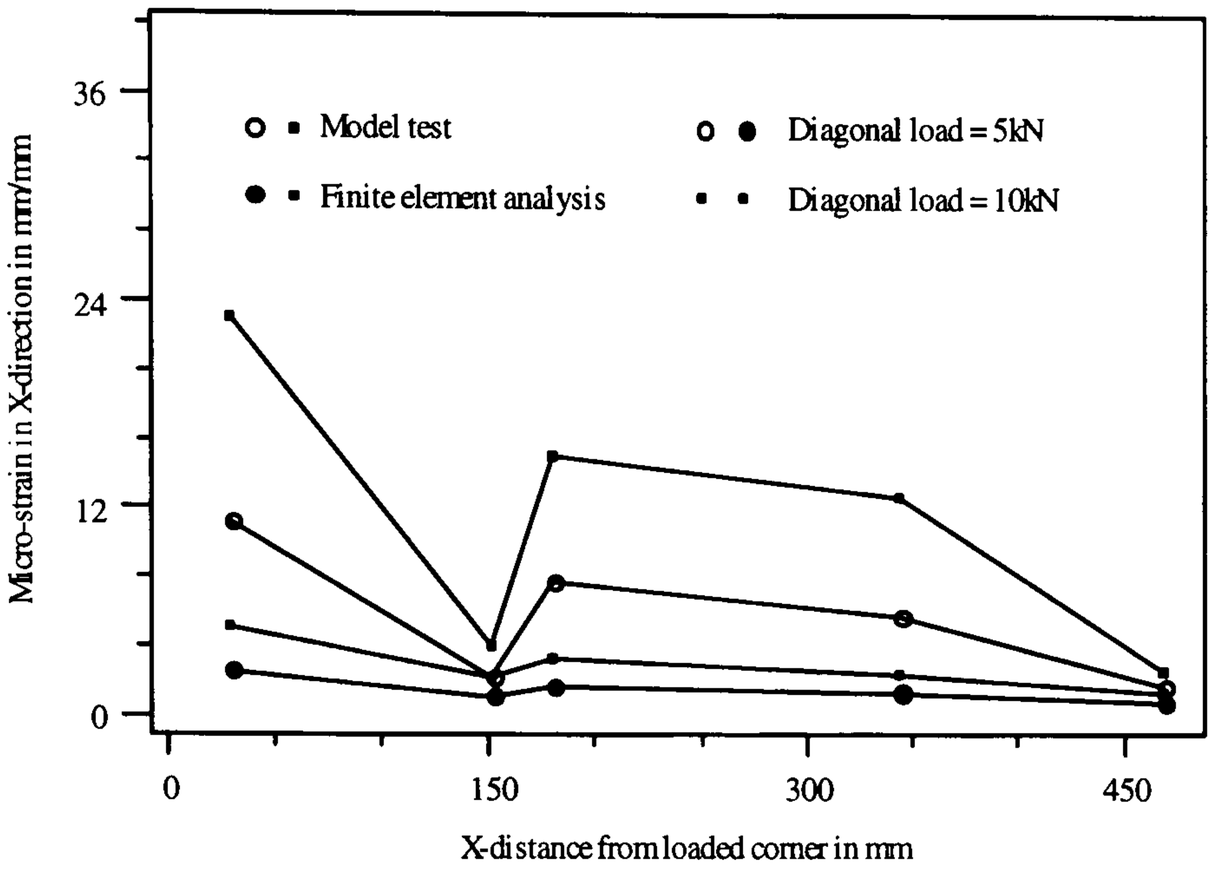

Figure 4.29: Comparison of X strain

Figure 4.30 compares the variation of Y-strain along the plain boundary from model test and FE analysis. Both show similar type of variation with model strain values higher than those from FE analysis. Strains at midside node and middle gauss point of the elements are averaged.

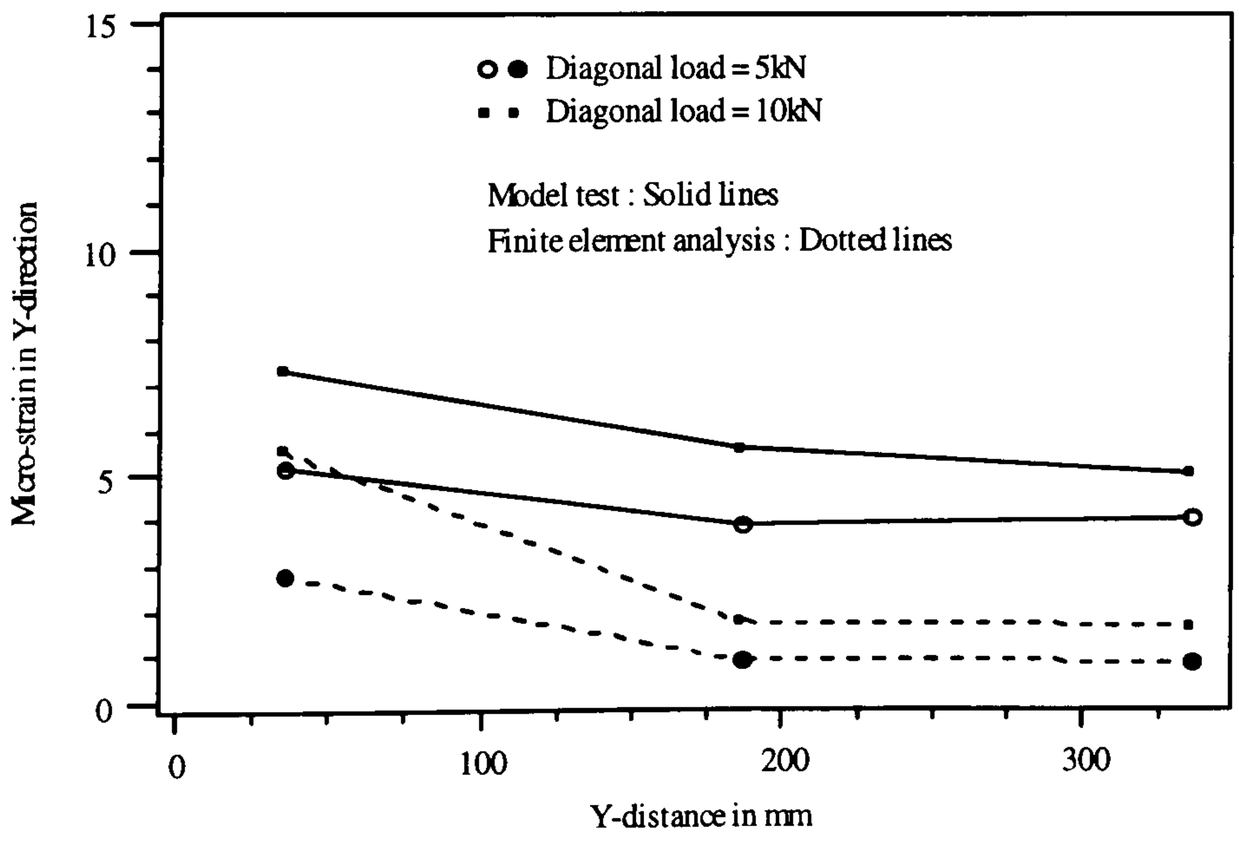

Figure 4.30: Comparison of Y strain

Principal strains at rosette locations

Principal strains from model test 1 & 6 and finite element analysis are compared and presented in figures 4.31. They showed identical variation specially in the pre-cracking stage. Considering the position of strain gauges on the surface of the concrete and finite element simulation of micro-concrete, the agreement may be considered as satisfactory.

A comparison has been made in figure 4.32 between FEA and model test 1 for the principal direction. The principal direction at rosette locations from FEA ranges between 43-46 degrees while that in the rosette 12-13-14 ranges between 41-44 degrees in the pre-cracking stage representing a good agreement.

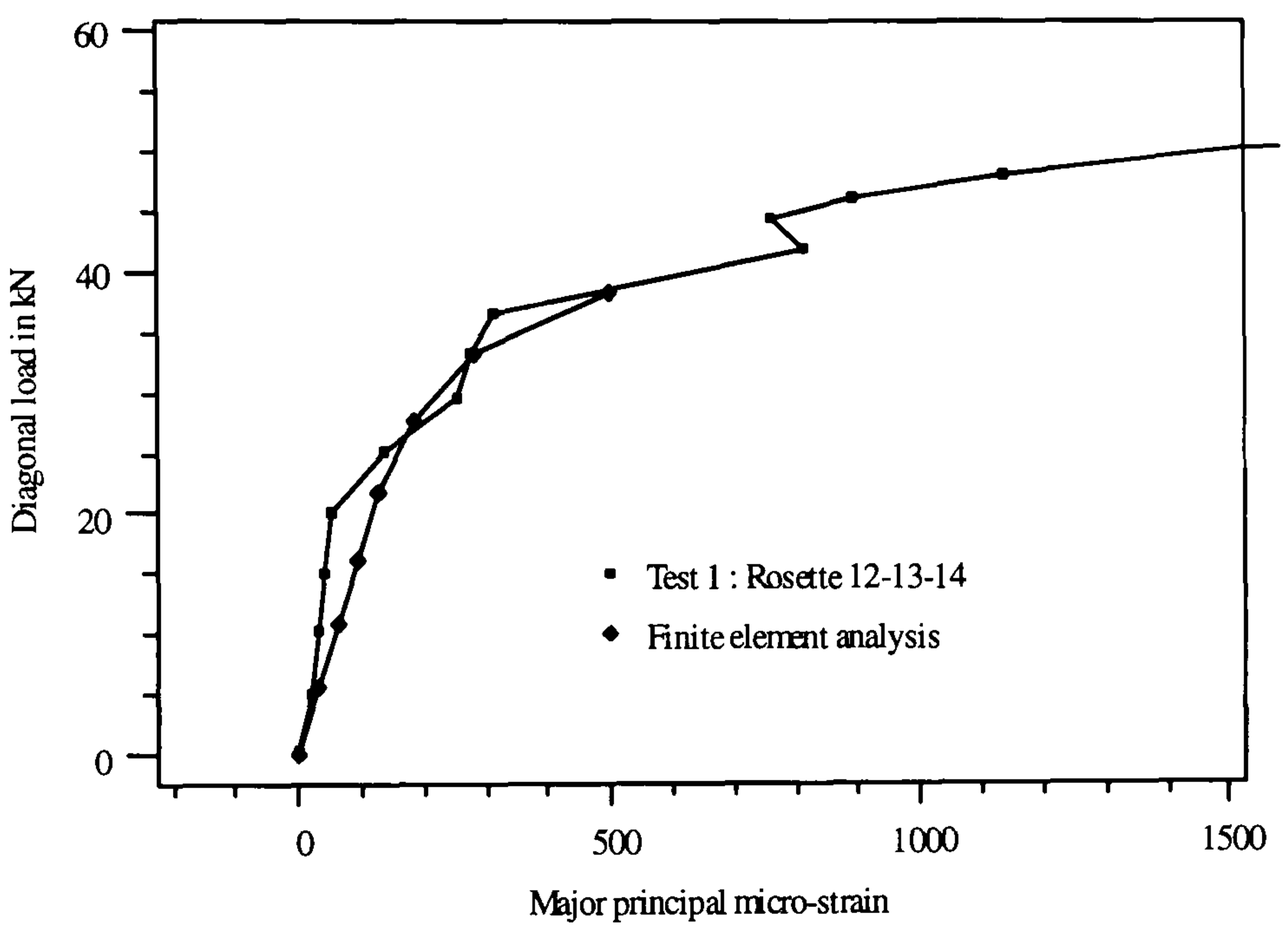

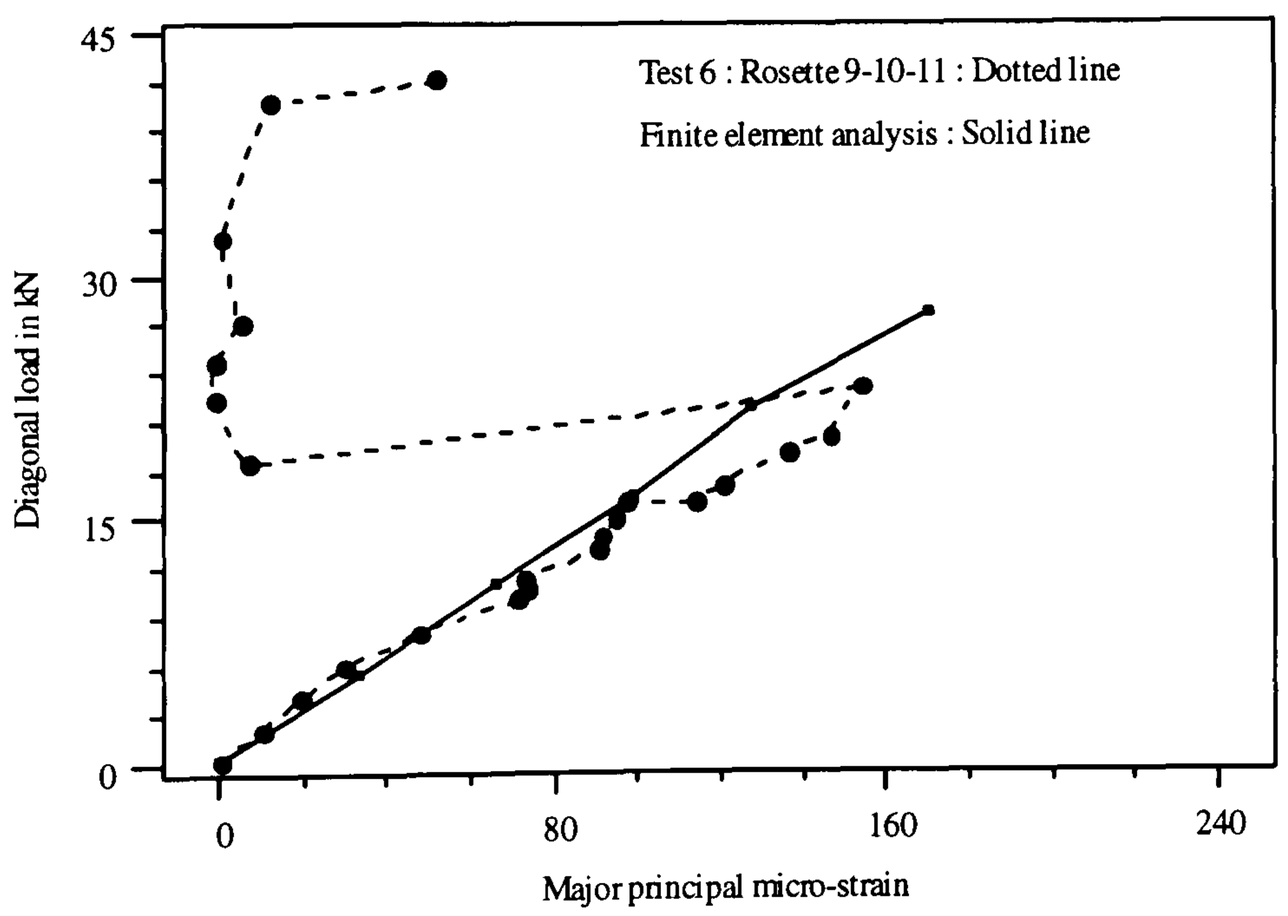

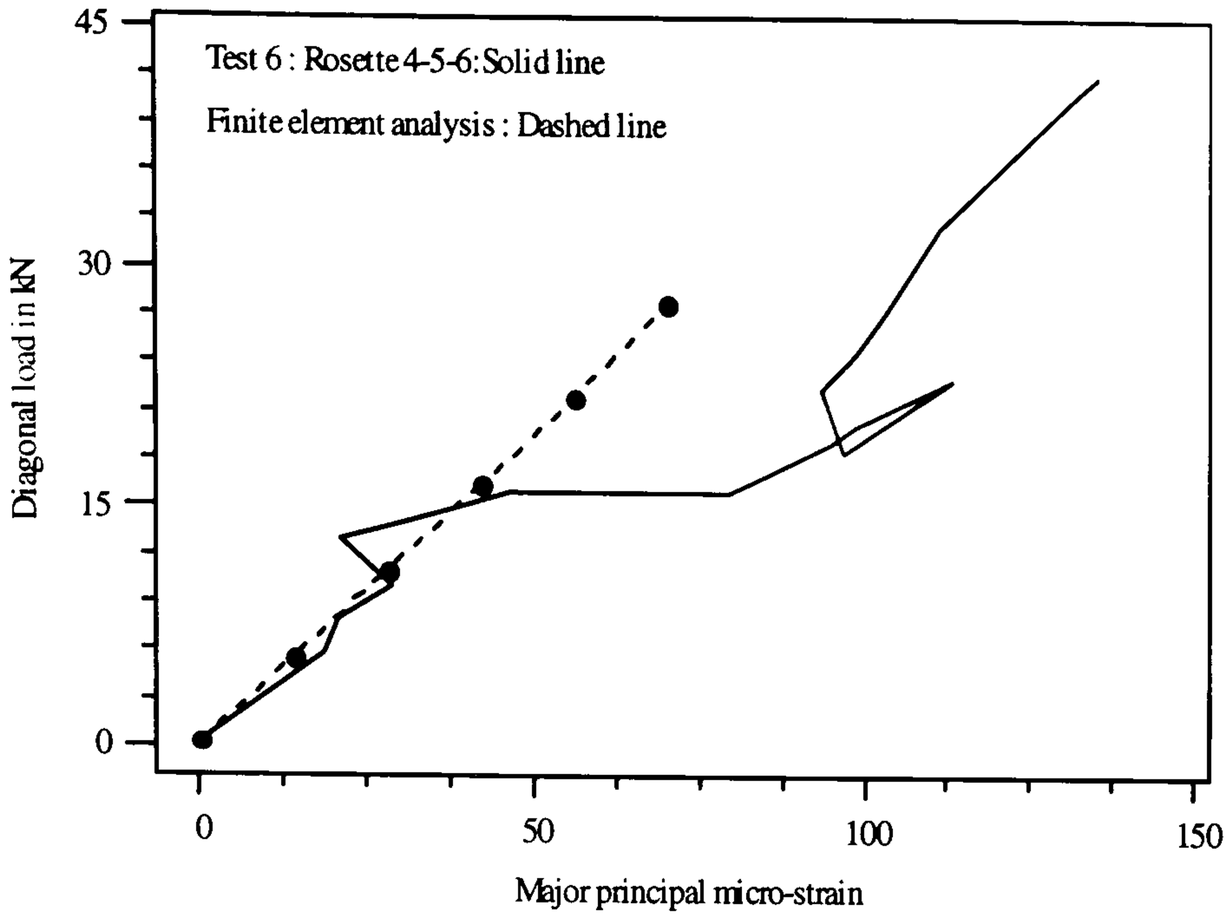

Figure 4.31: Comparison of principal strains from FE and model tests

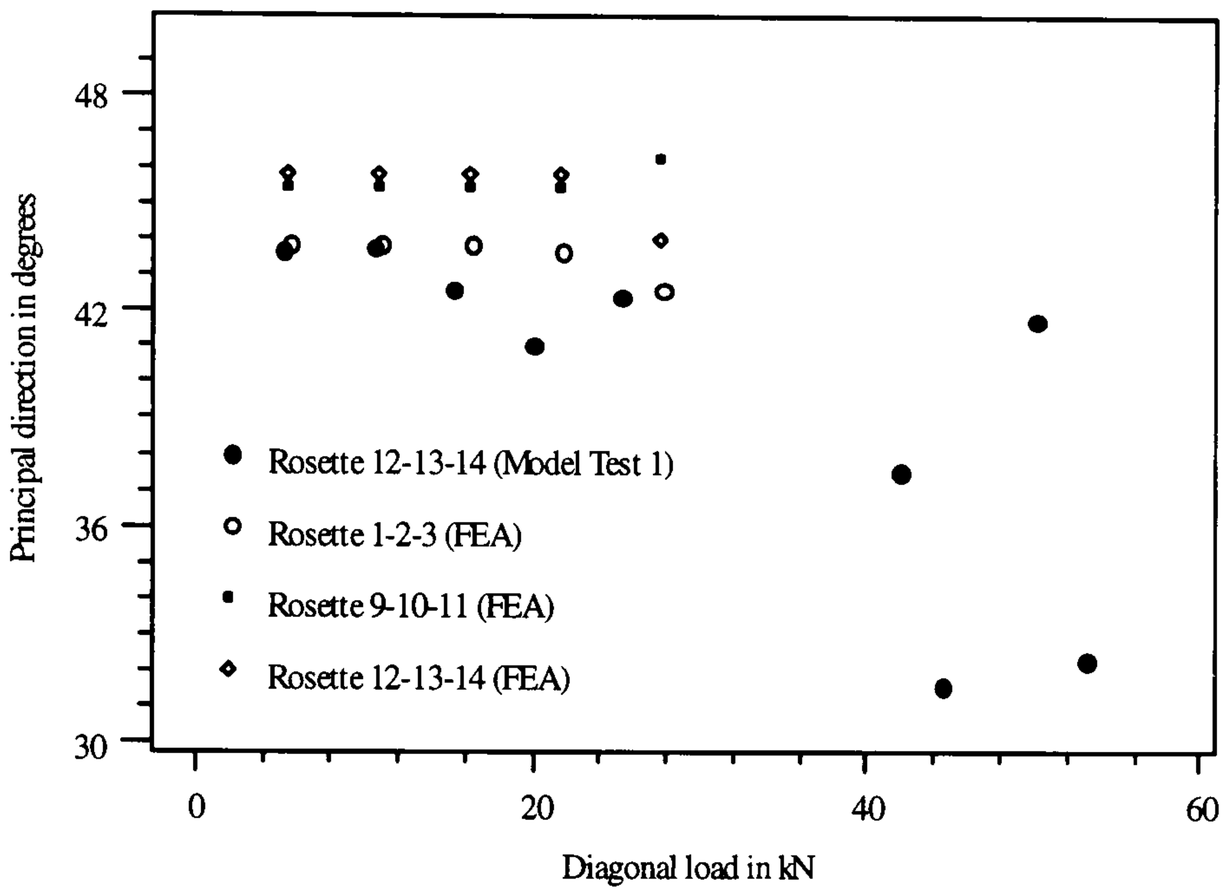

Figure 4.32: Comparison of principal directions

Crack Pattern

Cracked model panels are presented in photographs 4.3 and 4.4 to compare with crack patterns shown in figure 4.33(a). The first crack was formed near the loaded corners of the model panel conforming to the first crack in FE analysis. A series of main cracks was then formed one after the other from the corner towards the centre of the panel. The directions of the cracks were approximately parallel to the off-diagonal again conforming to the direction of distributed cracks in FE analysis. The formation of distributed cracks rather than single lines of crack as found in model tests is one of the main problems in the simulation of post-cracking response.

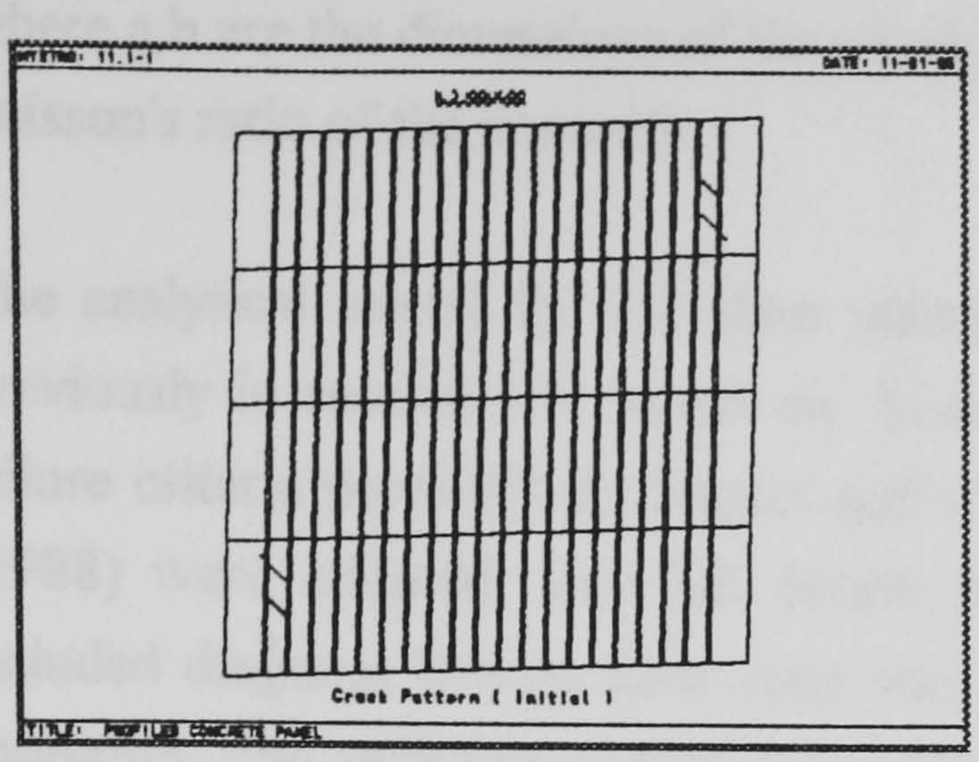

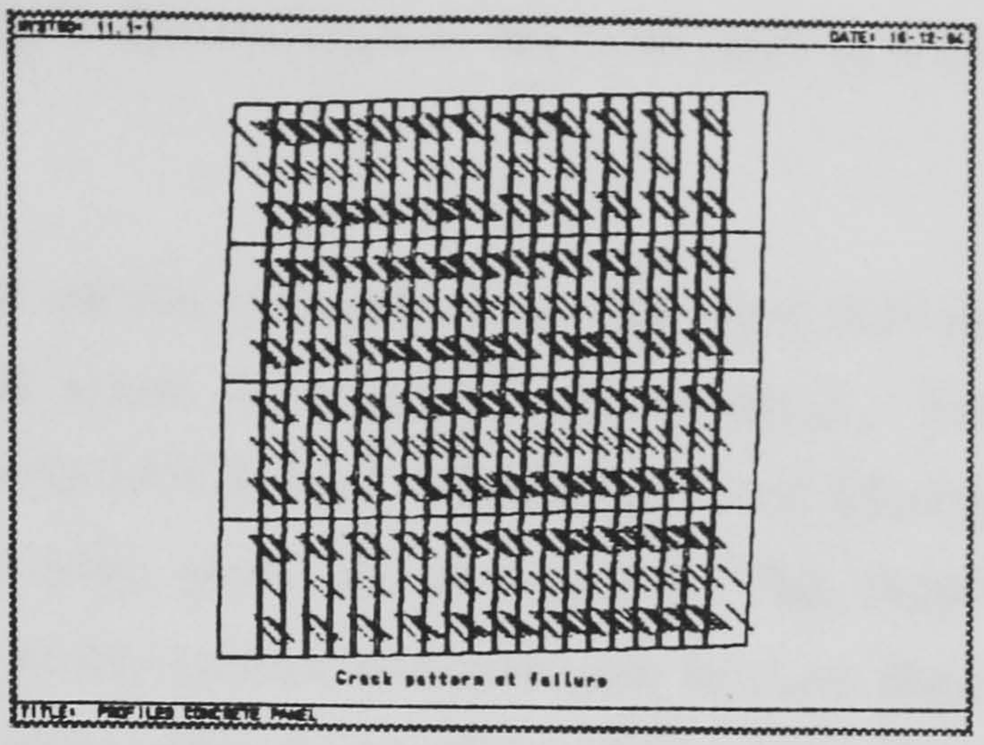

Diagonal load= +9.06kN Diagonal load = +19.76kN

* Load based on symmetric half of the panel

Figure 4.33(a): Crack pattern from FEA analysis

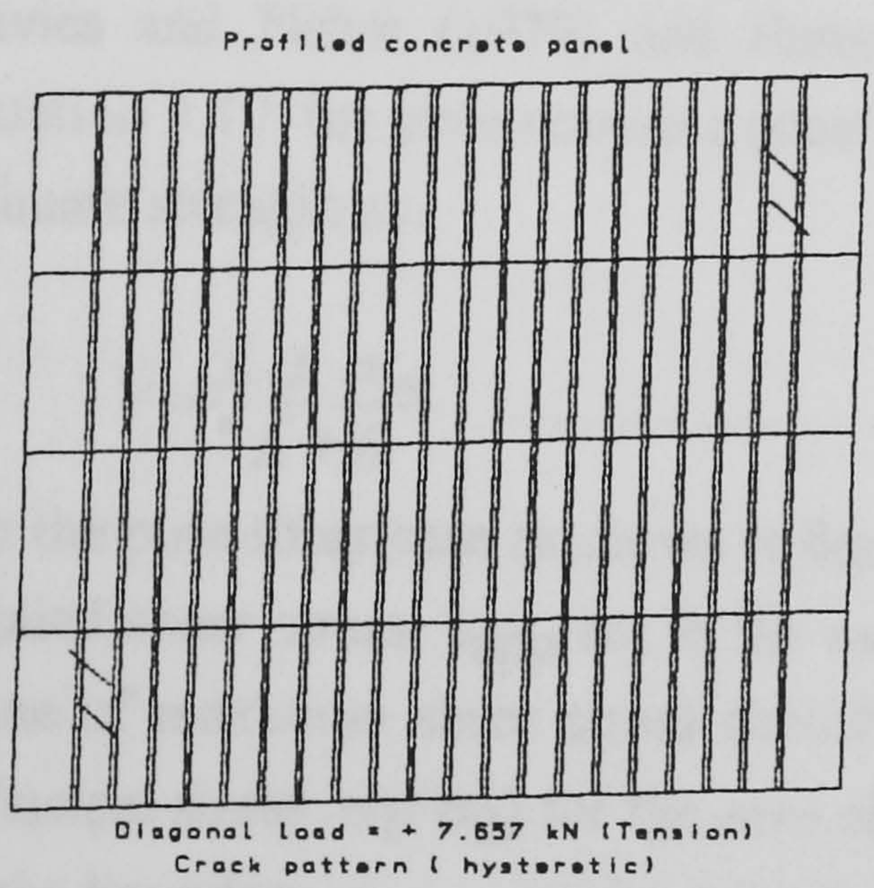

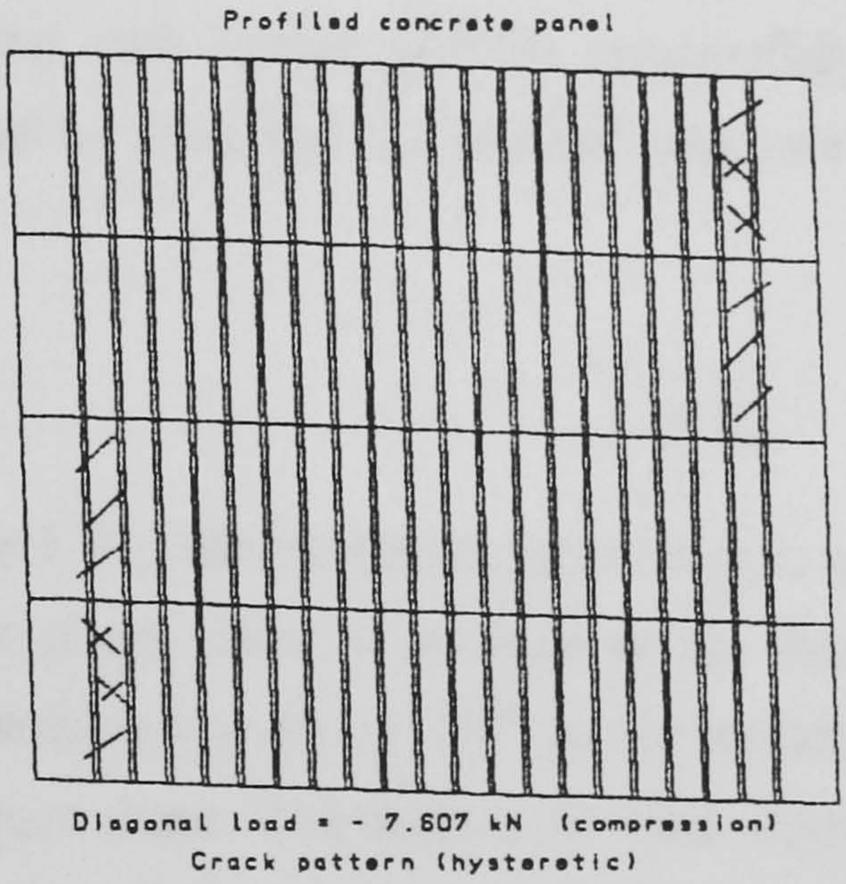

Figure 4.33(b): Crack pattern under hysteretic load

The crack pattern under hysteretic load (figure 4.33(b)) shows the formation of cracks approximately perpendicular to each other. This confirms the reversal of principal stress due to consecutive application of cyclic loading.

4.6. Analytical Model for strength and stiffness

Analytical model for strength and stiffness of the panel will be derived based on the model developed for plain micro-concrete panel as described in section 2.5.2.2 of chapter 3. The profiled concrete panel is considered to be as an equivalent plain concrete panel of same dimensions but having an average thickness of t_{eq}. The pre-cracking shear stiffness of the panel can be derived as

$$k = \frac{E_c . a t_{eq}}{2b(1+\upsilon_c)} \quad \text{.....(4.1)}$$

where a,b are the dimensions of the panel, E_c is the modulus of elasticity and ν_c is the poisson's ratio of the concrete.

The analytical model for the shear strength of the concrete core has been derived previously in section 3.6 based on bi-axial stress conditions in the concrete. The failure criteria proposed by Kupfer and Gerstle (1973) and Balakrishnan and Murray (1988) were adopted. The full details has been given in section 3.6. The model included diagonal tension limit state which is the normal phenomenon in pure shear condition. The analytical model derived for plain concrete panel in section 3.6 will be adopted for profiled concrete panel with some modification to take into account profiled cross section. The model included the idea of transforming the profiled concrete core into an equivalent plain concrete core of rectangular cross-section having an average thickness of t_{eq}. This simplified the problem and was used by Davies and Fisher (1979) and Easterling and Porter (1994) successfully. The equation 3.10 for plain concrete panel can be modified for profiled concrete panel for ultimate strength as:

$$V = \frac{f_c' . f_t' . a t_{eq}}{f_c' + f_t'} \quad \text{.....(4.2)}$$

For the pure shear case as shown in figure 4.34, the maximum shear stress, τ_{max} and applied shear stress, τ_{app} act in the same plane. This is because of the fact that the plane of maximum shear stress should make an angle of 45^0 to the principal plane (principal stress: σ_1, σ_2) for the case of pure shear. The analytical shear stress applied to the boundary, τ_{app}, can be related to the maximum shearing stress, τ_{max}, within the panel for pure shear by the equation 4.3.

$$\tau_{max} = \frac{\sigma_1 - \sigma_2}{2} = \sigma_1 \text{ or } \sigma_2 \quad \text{(Willems, N. , Easely, J.T. and Rolfe, S.T. (1981)}$$

$$\frac{V}{at_{eq}} = \tau_{app}$$

and

$$\tau_{max} = \frac{\sigma_1 - \sigma_2}{2} = \sigma_1 \text{ or } \sigma_2 = \frac{V}{at_{eq}} = \tau_{app} \quad \text{.....(4.3)}$$

Therefore, if τ_{max} obtained from model tests rosette analysis equals the analytically calculated τ applied at the boundary, it will validate the pure shear simulation by shear rig and analytical approach.

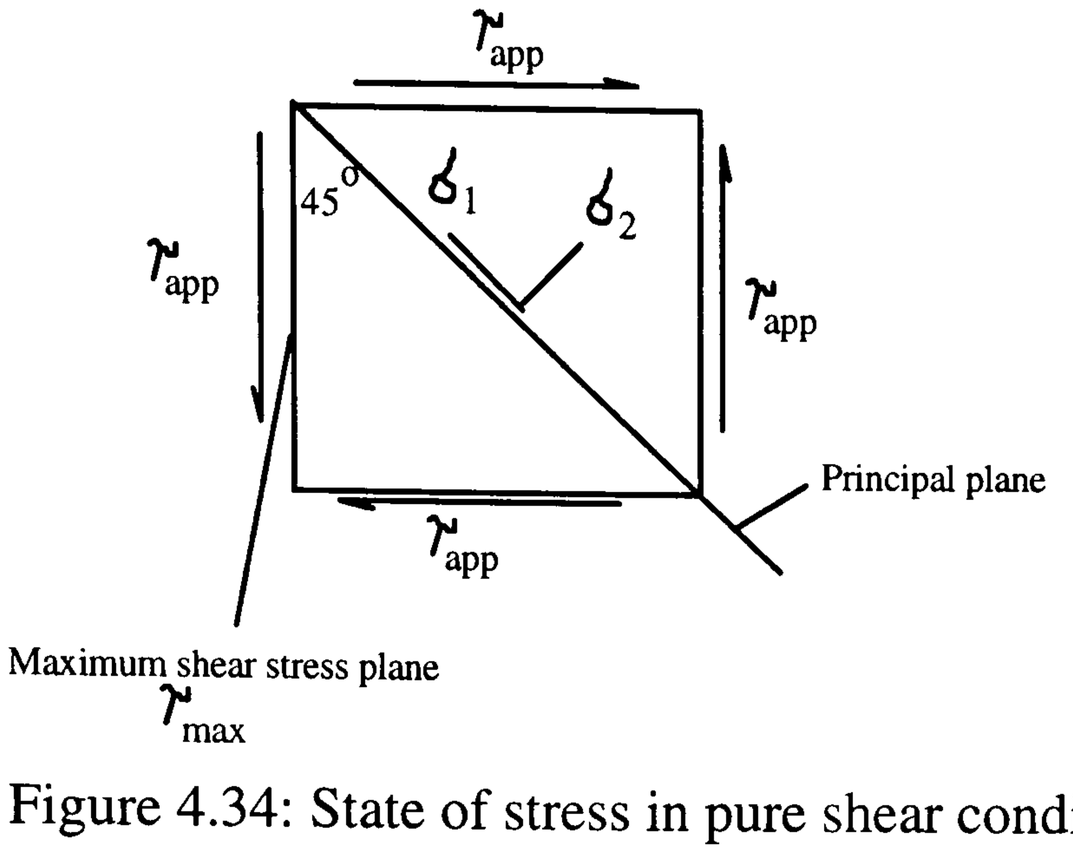

Figure 4.34: State of stress in pure shear condition

4.7 Comparison of analytical, model tests and FE analysis

Analytical, model tests and FE analysis results for strength and stiffness are summarised in table 4.7. The ratio of model test stiffness to analytical stiffness ranges between 0.8 and 0.913. The corresponding strength ratio ranges between 0.95 to 1.26. They are supposed to be in reasonable agreement. The analytical models can therefore be used safely to predict ultimate strength of the profiled concrete panel.

Table 4.7: Comparison of different analysis

Test No.	Shear Stiffness in kN/mm					Ultimate Shear load in kN				
.	Model test	FEA	Ratio	Analytical	Ratio	Model test	FEA	Ratio	Analytical	Ratio
1	147	164	0.896	161	0.913	34	30	1.13	27	1.26
4	129	164	0.787	161	0.800	31	30	1.03	27.6	1.12
6	141	164	0.86	161	0.875	25.5	30	0.85	26.89	0.95

The ratio of model test stiffness to FE stiffness ranges between 0.787 to 0.896 and the corresponding strength ratios ranges between 0.85 to 1.13. The finite element analysis predicted pre-cracking stiffness and ultimate strength of the profiled concrete panel showing reasonably good agreement with model test and analytical approach.

Figures 4.35 compare maximum shear stress from model tests and FE analysis with the analytical shear stress (τ_{ap}) calculated from equation 4.3.

It is clear from the graphs that the maximum shear stress at the rosette locations

coincide throughout the pre-cracking stage with the analytical shearing stress applied to the boundary. This proves the fulfilment of equation 4.3 and hence validate the performance of the shear rig and analytical approach.

The shearing stress from FEA are less than those predicted from model tests. However, pre-cracking responses are considered as satisfactory.

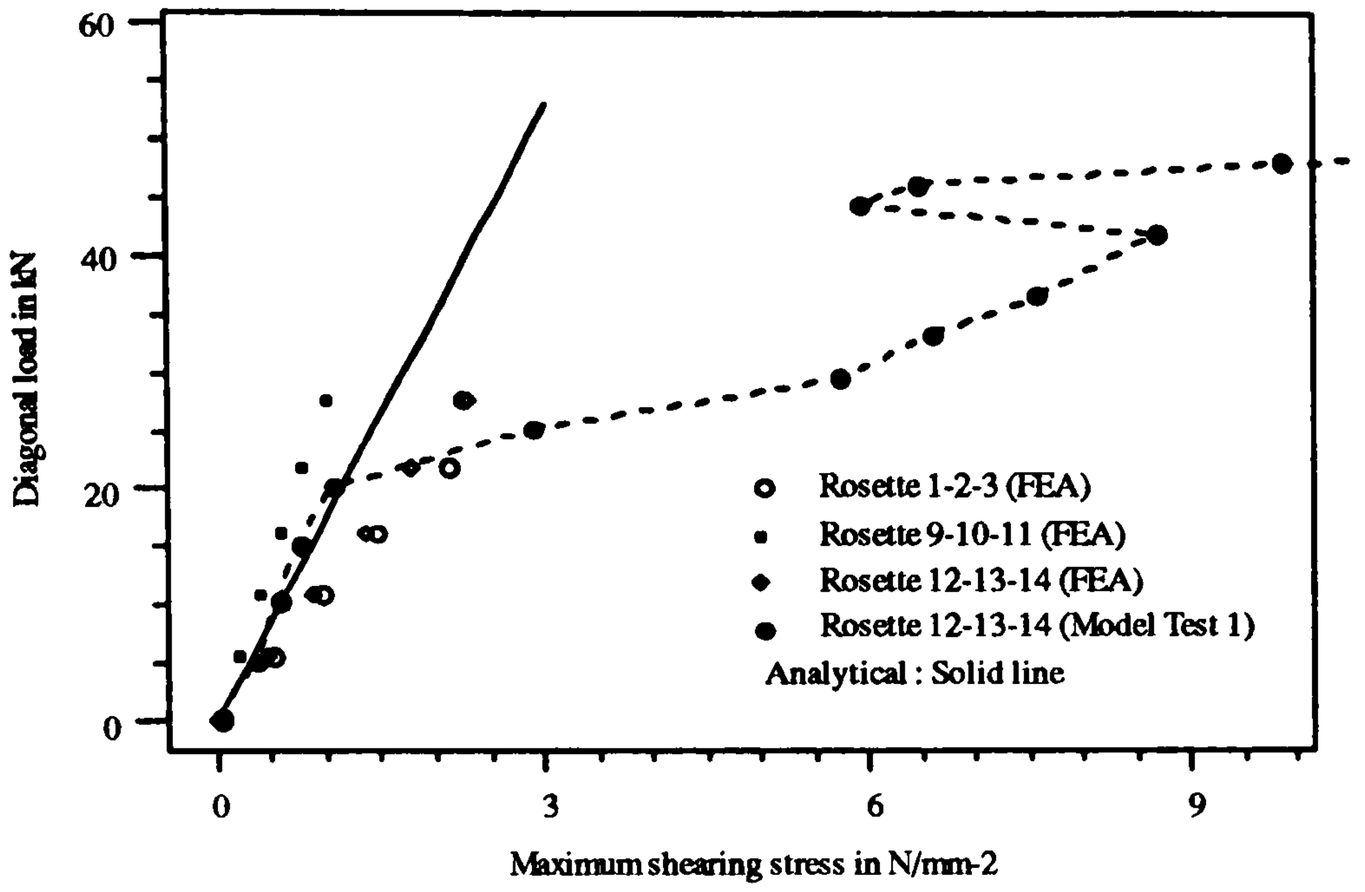

Figure 4.35: Comparison of shearing stress from different analysis

4.8 Comparative study of profiled and plain concrete panel

The profiled concrete panel is quite different than the plain concrete panel due to its geometry. The trough sections of the profiled concrete acts as a weaker section in the panel. This is confirmed from the model and finite element analysis. The comparison will be made on the following conditions:

Strain condition: In both cases the development of diagonal tension is observed. If the contour diagrams for both cases are compared, it can be seen that the trough section shows higher strain (figure 4.26) for the case of profiled concrete while a uniform stress are found to prevail along the diagonal in the case of plain concrete panel (figure 3.10).

Crack pattern: Plain concrete panel failed by the formation of a major diagonal crack approximately along the off-diagonal (photograph 3.2). But in the case of profiled concrete panel, cracks parallel to the trough sections are formed along with diagonal cracks (photographs 4.3 and 4.4). This weak trough section near the boundary may reduce the strength of the profiled concrete panel.

The analytical formulation of strength and stiffness of profiled concrete panel based on the equivalent plain concrete panel is proved to be good.

4.9 Conclusions

This chapter described the analytical, numerical and experimental investigations on the individual behaviour of the profiled concrete core under in-plane shear. The model tests provided consistent and repeatable results although it was not an easy task to perform small scale test with micro-concrete panels. The development of diagonal tension state in the panels are confirmed from both analytical and numerical investigations. The strength and stiffness equation suggested for the profiled concrete panel based on an equivalent plain concrete panel can be used for the design purposes. The next chapter will described the individual behaviour of the profiled steel sheeting.

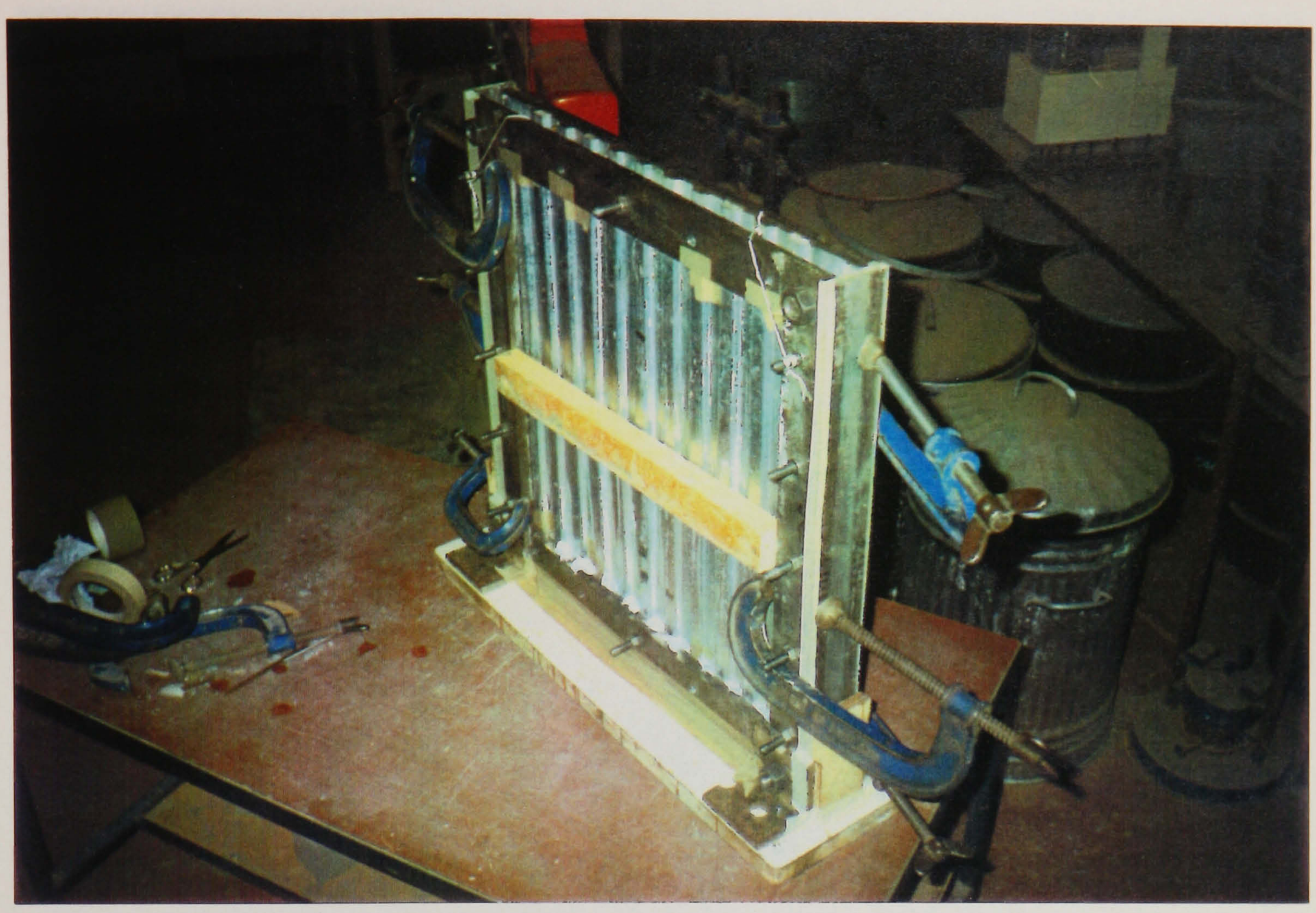

Photograph 4.1: Complete Mould Assembly

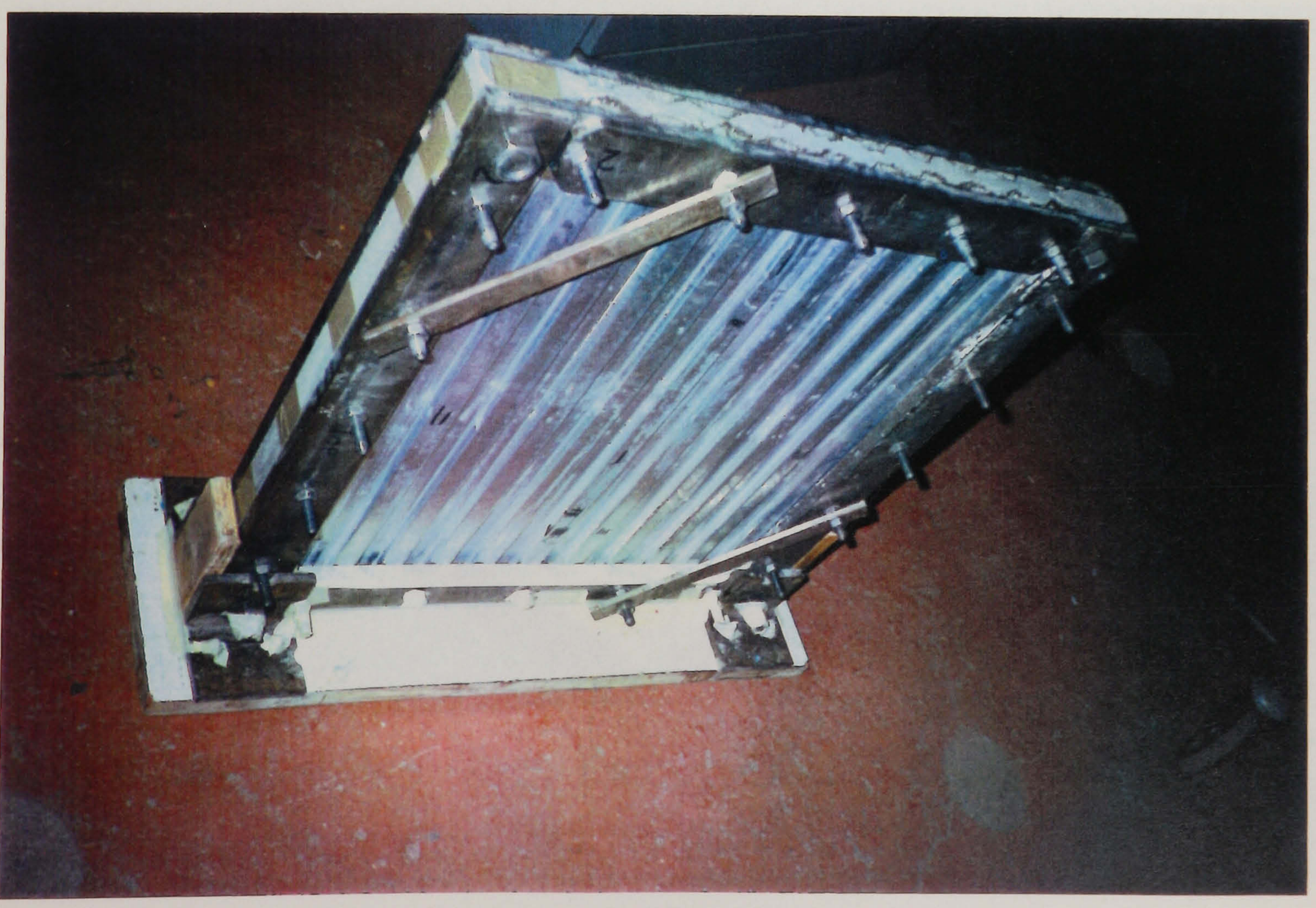

Photograph 4.2: Mould Assembly for casting resin (one side casted)

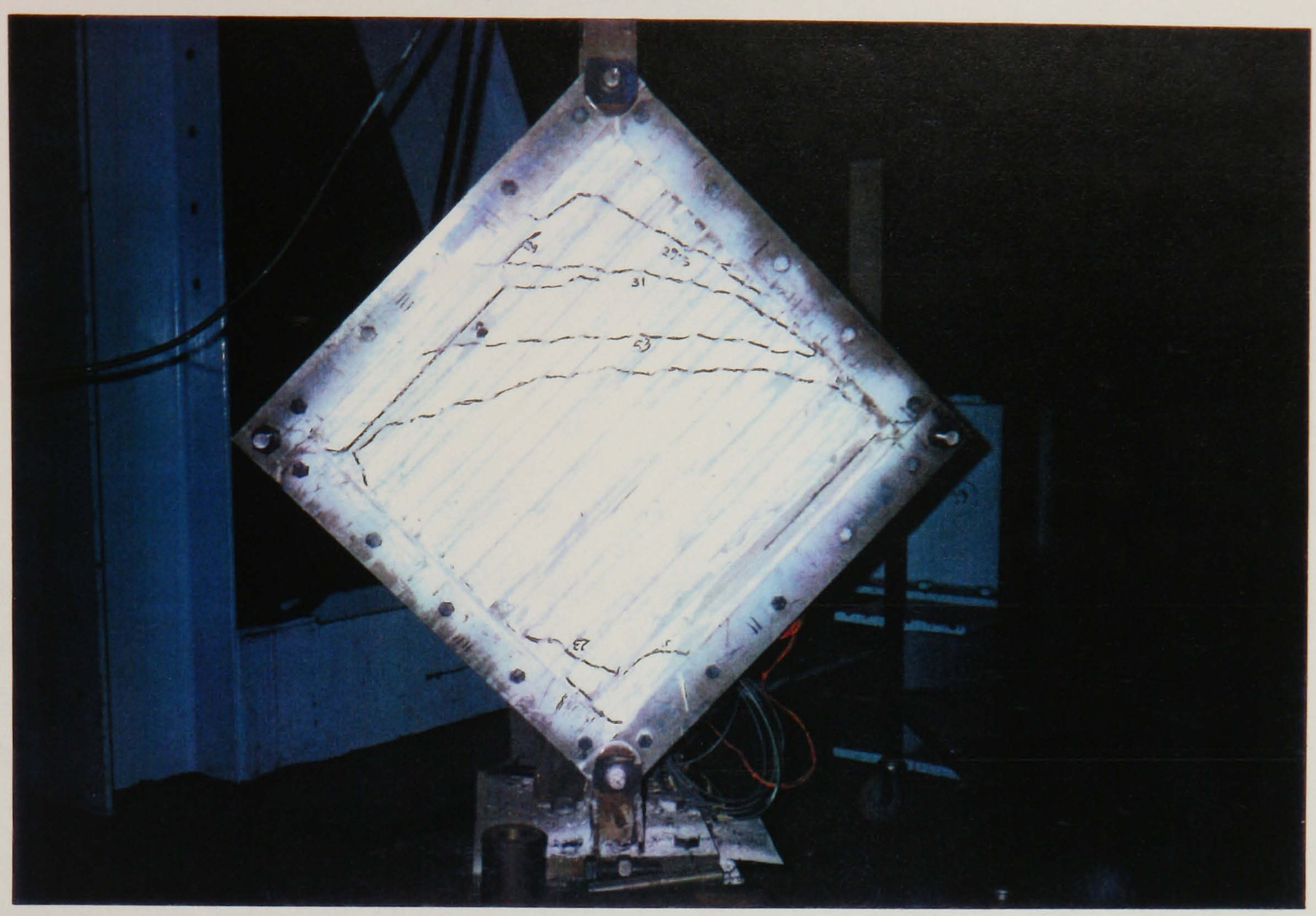

Photograph 4.3: Experimental set-up showing cracking of profiled concrete panel

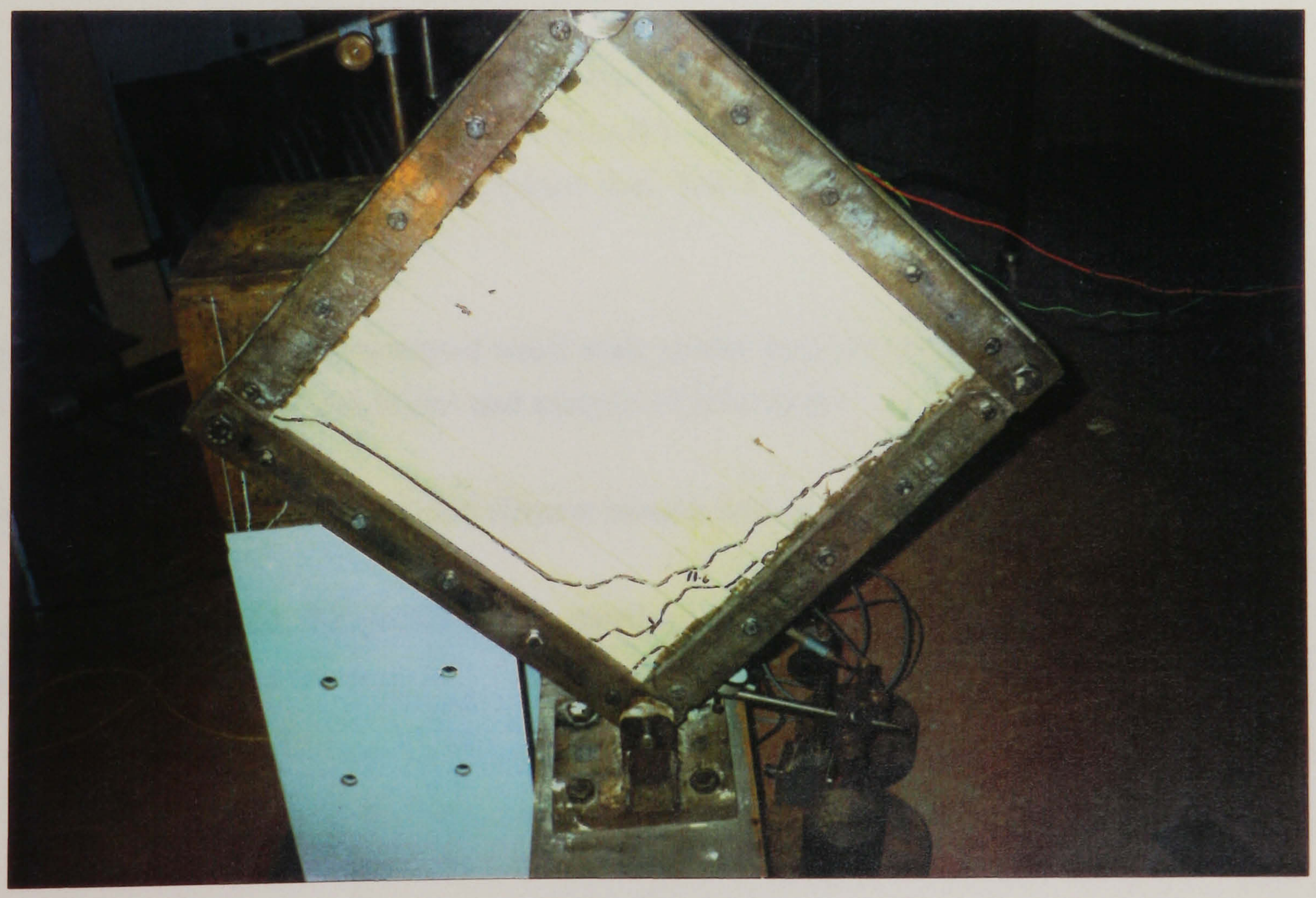

Photograph 4.4: Cracking of profiled concrete panel 6

CHAPTER FIVE

STUDY OF THE IN-PLANE SHEAR BEHAVIOUR OF PROFILED STEEL SHEETING

5.1 Introduction

When used in combination with steel frames, cold formed light-gauge steel corrugated panels offer considerable shear resistance to lateral loads. To predict the true behaviour of frames having such panels, it is necessary to consider the integrated behaviour of the clad frames, and for this purpose, the shear strength and stiffness of these panels must be known. Two skins of profiled steel sheeting will resist in-plane shear forces when the composite wall is used as shear or core walls in steel framed buildings. The behaviour of the profiled steel sheeting in composite wall can be related to the light gauge corrugated steel diaphragms that act in shear to resist horizontal and seismic forces on the building. This chapter will describe the following:

A literature review of the shear diaphragm behaviour and the development of simplified analytical models for strength and stiffness of the profiled steel sheeting that can be applied in the design of composite wall based on the available models from previous research.

Description of heavily instrumented small scale model tests on profiled steel sheeting with different boundary conditions and analysis of test results.

Comparison of analytical and finite element models with small scale model tests.

A design problem for the profiled steel sheeting connected with different boundary conditions to the steel frame.

5.2 Shear diaphragm behaviour

Light gauge steel diaphragms and the use of diaphragm actions in structural design gained widespread acceptance in America and Britain. A typical isolated diaphragm comprises of corrugated steel sheeting (of variety of shapes), primary supporting members (rafters), secondary supporting members(purlins), shear connectors and a variety of stiffeners is shown in figure 5.1.

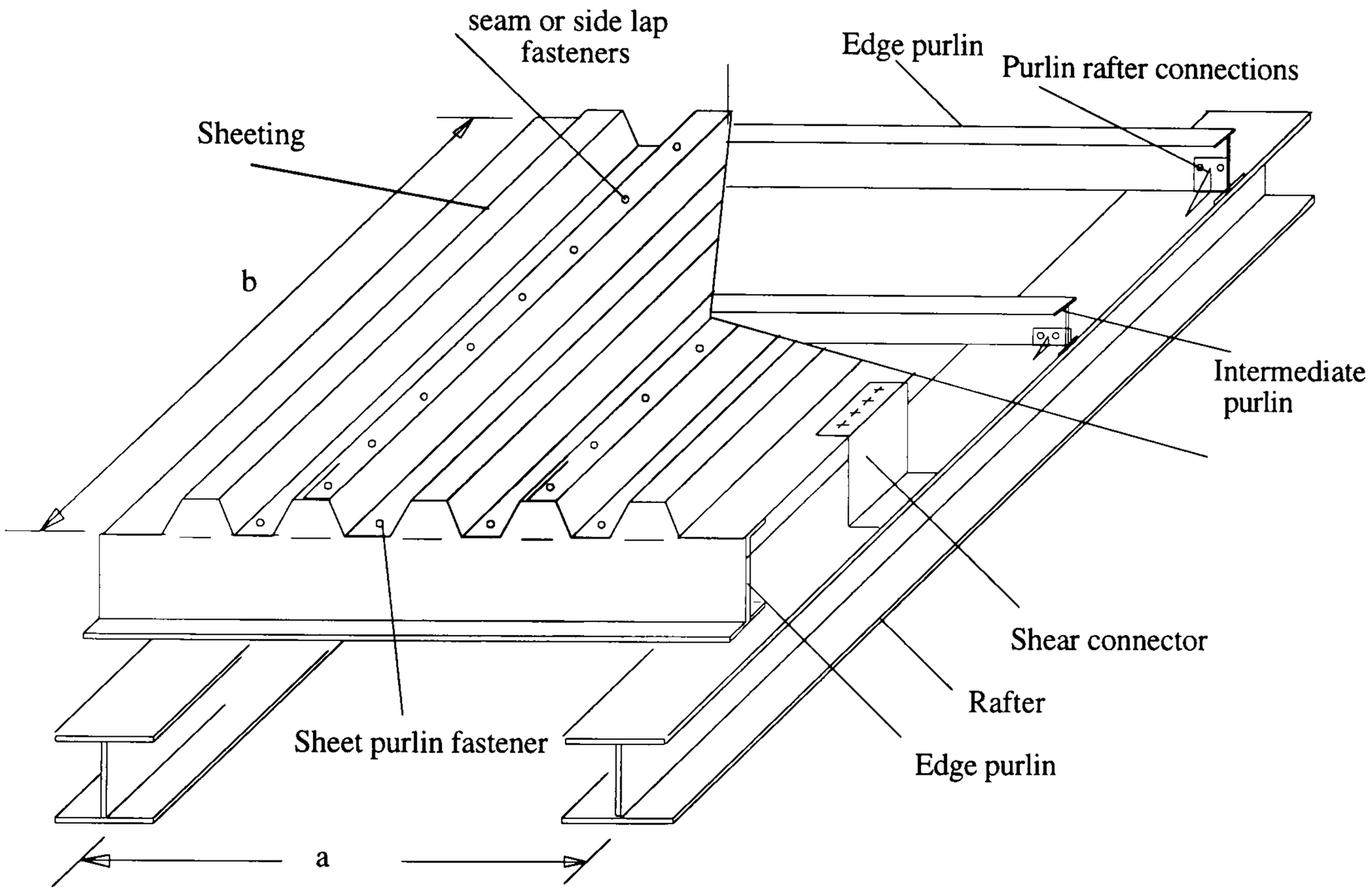

Figure 5.1: Schematic of a shear diaphragm

In the United States a considerable amount of work on shear diaphragm have been carried out. Much of the early experimental work on the shear diaphragms was conducted on a proprietary basis for various manufacturers of metal deck. Limited tests of an actual structure was carried out in 1950. Nilson(1960) at Cornell University in 1954 laid down the foundations of the work, mainly for Fenestra, Inc., and for the H.H. Robertson Co.. These, together with subsequent tests by others, done under the sponsorship of AISI, catalogued the behaviour of more than 100 shear diaphragms. The Cornell tests provided the basis for publication by AISI of the manual Design of Light Gauge Steel Diaphragms (1967). But it would seen to be apparent that no suitable general theory for determining diaphragm stiffness and strength has been developed.

Meanwhile, work has proceeded in related directions in England under the direction of Bryan at Manchester and later at Salford. El-Dakhakhni and others, working with Bryan made significant contributions (1968a,1968b). This work culminated in the production of a manual for the design of stressed skin structures (1972). The most important property of light gauge diaphragm that appears in the analysis and design is its shear flexibility. Bryan and others developed a general theory for predicting the flexibility of practical shear diaphragms. This theory was verified by extensive testing on component parts as well as on large scale panels.

Bryan's approach has been improved and extended by Davies (1976) and fully justified by comparison with finite element results. Bryan's method is not able to deal with irregular situations such as diaphragm with large openings, so Davies (1977) also described a simplified computer oriented method which requires nothing more elaborate than a plane frame analysis. Davies (1976a) also extended his work on folded plate structures and derived simplified formulas for determining flexibility of roofs.

El-Dakhakhni (1976) described a method for calculating the shear flexibility of light gauge partitions using a strain energy approach.

Behaviour of corrugated plates in shear was studied by Hussain and Libove (1976). The study included the theoretical and experimental prediction of stiffnesses of discretely attached corrugated plates in shear.

Horne and Raslan (1971a, 1971b) presented a finite difference approach and an energy solution to the problem of shear deformation of corrugated panels.

Significant contributions to the knowledge of buckling behaviour of shear diaphragm have been made by Easely and McFarland (1969) and Easley(1975). Previously Bergmann and Reissner as reported by Easely (1975) and than later Hlavacek (1968) also derived different sets of formulas applicable to such shear diaphragms.

5.2.1 Shear flexibility of diaphragm

Properly fastened steel sheeting lends considerable strength and stiffness to panels which are subject to in-plane or shear displacement. In elastic design, the stiffening of steel sheeting depends on the flexibility of a panel of roof sheeting in shear relative to

the flexibility of an unclad frame. A panel is regarded as being the area of sheeting, complete with all attachments between two adjacent rafters and between two extreme purlins. The shear flexibility is defined as the shear displacement 'c' of the panel subjected to a unit shear load (figure 5.2).

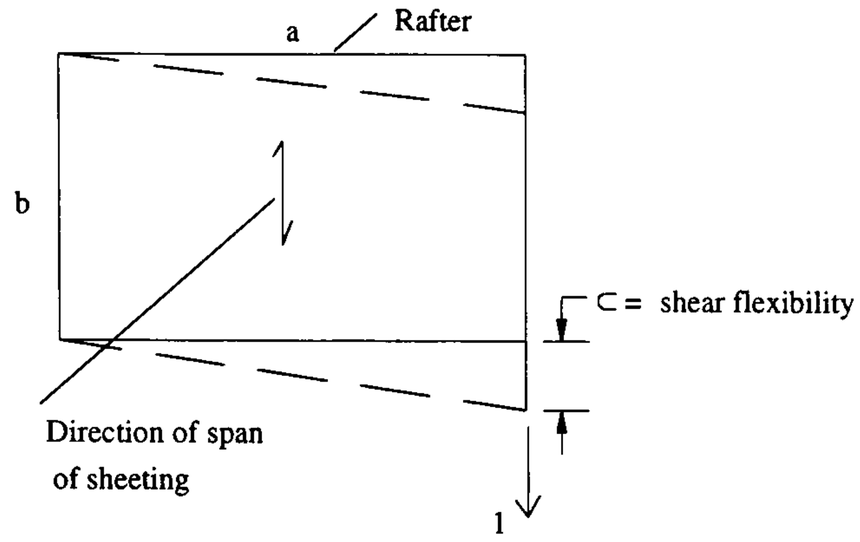

Figure 5.2: Definition of shear flexibility

A typical panel of sheeting complete with attachments is shown in figure 5.1. The overall shear flexibility 'c' (displacement under unit shear load) is almost entirely due to the flexibility of the following items (Bryan(1972) and Davies(1976):

a) Flexibility because of sheet deformation (c_1): This includes the following effects :

- i. flexibility because of bending of corrugation profile ($c_{1.1}$) taking into account the effect such as fasteners at every corrugations, effect of intermittent fasteners and effect of intermediate purlins,
- ii. shear strain in sheet ($c_{1.2}$) taking into account the effect of intermediate purlins,
- iii. torsion of the sides of the corrugations ($c_{1.3}$),
- iv. membrane stress ($c_{1.4}$) and
- v. axial strain in the purlins ($c_{1.5}$) taking into account the effect of intermediate purlins.

Therefore $c_1 = c_{1.1} + c_{1.2} + c_{1.3} + c_{1.4} + c_{1.5}$

Bending and distortional flexibilities arises because the centre of shear resistance of the profile is eccentric to the plan of application of the applied shear force and the corrugation is twisted out of shape by its own shear flow. The individual plates, whilst moving laterally, also rotate and bend in plane thus giving rise to longitudinal warping with accompanying shear displacement of the sheeting. So it will be appreciated that items $c_{1.1}$, $c_{1.3}$ and $c_{1.4}$ must always be considered together because it is impossible for one to occur without the others. Again in an actual

diaphragm items $c_{1.3}$ and $c_{1.4}$ are normally negligible and item $c_{1.1}$ may be considered alone.

b) Flexibility because of slip at the sheet fasteners(c_2):

Because of lack of fit at the sheet fasteners or because of local crushing or tearing of the sheeting, there will be a flexibility in the sheeting. This includes the following effects:

i. slip at the sheet-purlin fasteners ($c_{2.1}$) taking into account the effect under pure shear only and under combined bending and shear;

ii. slip at seam fasteners ($c_{2.2}$) under pure shear only and under combined bending and shear;

iii. slip at sheet rafter fasteners ($c_{2.3}$).

So $c_2 = c_{2.1} + c_{2.2} + c_{2.3}$

c) Flexibility because of purlin rafter connections (c_3)

Therefore, the total flexibility $c = c_1 + c_2 + c_3$

5.2.1.1 Comparison between Bryan's (1972) and Davies'(1976) approach

According to the type of construction, Bryan(1972) has classified diaphragms into two major types: (1) diaphragms with panels connected to the framing members on all four sides (**Direct Shear Transfer Case**); and (2) diaphragms with panels connected to the purlins, which in turn connected to the rafters (**Indirect Shear Transfer Case**). Table 5.1 presents a summary of the shear flexibilities derived from two approaches. Derivations of these expressions are fully given Bryan (1972) and Davies(1976).

Davies'(1977) approach can be considered a modification of Bryan's based on improvements in the assumed internal force distribution. Changes are proposed only for $c_{2.1}$, $c_{2.2}$ and $c_{2.3}$ with remaining components of flexibility unchanged.

Davies' equation for $c_{2.1}$ is identical to that given by Bryan for the direct shear transfer case but herein it is proposed that it should apply for both direct and indirect shear transfer case. Davies expression for $c_{2.2}$ has three important differences :

i. It applies for both direct and indirect shear transfer cases,

Table 5.1

Shear flexibility due to	Factor	Bryan's method: Basic Expression Sheeting fixed to purlins and shear connectors	Bryan's method: Basic Expression Sheeting fixed to purlins only	Davies method: Basic expression sheeting fixed to purlins with or without connections
1. Sheet deformation	Bending of corrugation	$c_{1.1} = n_c \frac{144 K h^3 l^2 f_1}{E t^3 b^3}$ $c_{1.1} = \frac{0.144 a d^4 f_1 K}{E t^3 b^3} mm / kN$	Same	Same
	Shear strain	$c_{1.2} = \frac{2 a f_2 (1+\nu)(1+\frac{2h}{d})}{btE}$	Same	Same
	Axial strain in purlins	$c_{1.5} = \frac{2 a^3 f_3}{3 b^2 AE}$	Same	Same
2. Slip at sheet fasteners	Sheet/Purlin fasteners Seam fasteners Sheet connector fasteners	$c_{2.1} = \frac{2 a s p f_3}{b^2}$ $c_{2.2} = \frac{(n_{sh}-1) s_s}{n_s}$ $c_{2.3} = \frac{2 s_{sc}}{n_{sc}}$	$c_{2.1} = \frac{2sp}{a}\left[\frac{6}{n_p} + \frac{a^2 f_3}{b^2}\right]$ $c_{2.2} = \frac{n_{sh} s_s}{n_s}$ Not applicable	$c_{2.1} = \frac{2 a s p f_3}{b^2}$ $c_{2.2} = \frac{2 s_s s (n_{sh}-1)}{2 n_s s + g_1 n_p s_s}$ $c_{2.3} = \frac{2 s_{pr}}{n_p} + \frac{2s}{g_2 n_p}\left[\frac{2 n_s s + g_2 n_p s_s}{2 n_s s + g_1 n_p s_s}\right]$ * $c_{2.3} = \frac{2 s_{sc}}{n_{sc}}$ **
3. Purlin -rafter connections		Not applicable	$c_3 = \frac{2 s_{pr}}{n_p}$	
		Sheeting fixed on all four sides (Direct shear transfer)	Indirect shear transfer	

* without shear connectors ** with shear connectors

ii. It recognises the influence of a distribution of lateral fastener forces along the purlins by the factor g_1. Bryan ignored this distribution for the direct shear transfer case and postulated a quiet different distribution for the indirect shear transfer case. Davies presented the values of g_1 for both quadratic and linear variation of fastener forces.

iii. It recognises that along a given seam the sheet-purlin fasteners act as though both sheets are connected separately to each purlin giving rise to approximately twice the flexibility of a single fastener connecting a thin sheet to a thicker member.

Davies expression for $c_{2.3}$ is different than that of Bryan for indirect shear transfer case and introduces another factor g_2 with g_1 to represent a quadratic variation of displacement and force. The values of g_2 are also tabulated by Davies (1976).

The expression for $c_{1.1}$ contains a dimensionless constant, K, which is a property of the cross-section of the sheeting and depends on the mode of attachment of the

sheeting to surrounding structure. The value of , K, (Bryan and El-dakhakhni (1968)) for fastener in every corrugation can be calculated from the equation:

$K = \frac{(l+2h+2e)(l^2 - 2le + 4e^2)}{12h(l+2e)^2}$, where l, e and h are the sheet cross-sectional properties as shown in figure 5.3 . But to take into account the effect of intermittent fasteners (such as one fastener in two or three or four or more corrugations) the expressions for $c_{1.1}$ should be modified as:

$(c_{1.1})_{modified} = c_{1.1}\left[1 + \frac{(N-1)^2 d^2 (3l+2h)}{6Kl^2 hN}\right]$ with fasteners 1 in N corrugations .....(5.1)

The value of reduction factors f_1, f_2 and f_3 for intermediate purlins are tabulated by Bryan (1972).

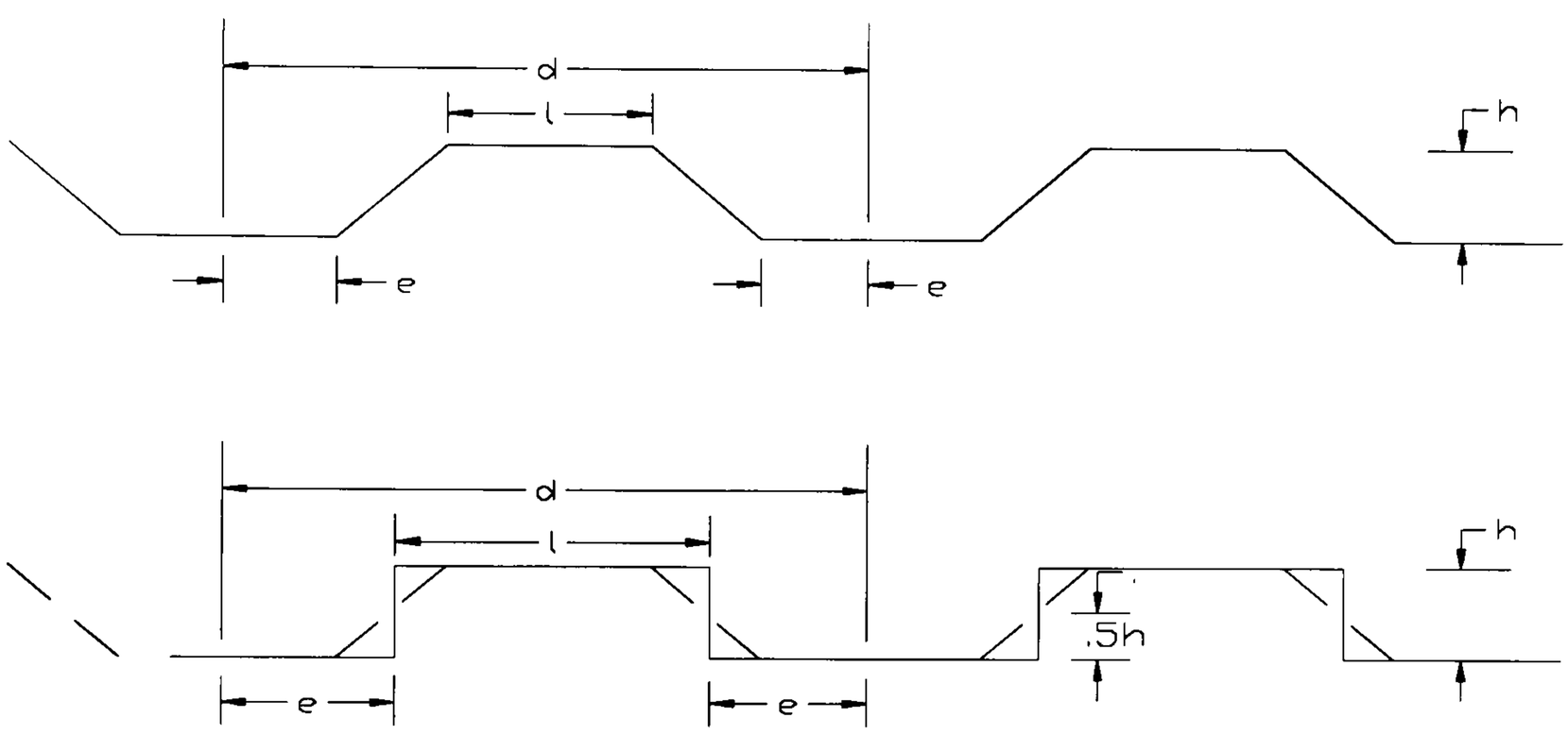

Figure 5.3 Profiled steel sheet cross-sectional properties

5.2.2 Shear strength of diaphragm

Analytical methods have been developed from the observed behaviour and failure modes of diaphragms by Bryan(1972), Davies(1976) and Easley(1977) where the fasteners other than welds (screws, rivets or bolts) are used. However, it has been claimed that the theories could be readily applied for welded diaphragms also. Fazio, Kinh and Chockalingam (1978) extended Easley's theory and developed simple formulas to predict shear capacity of diaphragms with any type of fasteners, whether weld, rivets, or screws. Only Bryan's and Davies approaches will be highlighted here.

Bryan's approach

For both direct and indirect shear transfer cases a uniform distribution of the fasteners forces is assumed and the load that first causes failure in any of the fasteners (seam, sheet-purlin or sheet-connector) is taken as the shear capacity of the diaphragm. For

diaphragm connected on all four sides, the shear capacity, V_u, per unit length can be taken as the minimum of the two expressions:

$V_u = F_S.n_S/b$: Strength from seam fasteners

$V_u = Fp_.n_e/a$: Strength from sheet-purlin fasteners

Davies approach

Simple distribution of fastener forces as proposed by Bryan would yield results in gross error, especially when the diaphragm fasteners are of widely different strengths and stiffnesses, such as with welds and mechanical clinches. Davies employed an improved internal force distribution for the fasteners based on finite element analysis and test observations to overcome the deficiencies in Bryan's expressions. By assuming that each panel in a diaphragm would resist equal load and failure would occur because of tearing of the sheeting along a vertical line of fasteners (parallel to corrugation), Davies(1976) proposed the following equations for the shear strength Vult when the diaphragm capacity is controlled by the capacity of seam fasteners:

Case i : Failure at internal seam

Assuming a sheet-purlin fastener in line with the seam fasteners

$$V_{ult} = \frac{(n_S F_S + n_p F_p)(2n_S s + g_1 n_p s_S)}{(2n_S s + n_p s_S)}$$

and assuming no sheet-purlin fasteners in line with the seams the expression reduced to the form: $$V_{ult} = \frac{n_S F_S (2n_S s + g_1 n_p s_S)}{2n_S s}$$

Case ii. Failure at end of panel (Direct Shear Transfer Case)

$V_{ult} = n_{sc} F_{sc}$

Review conclusion

The failure of the diaphragm may occur due to the buckling of sheeting or by shearing of the seam fasteners (most undesirable, as failure is sudden and is progressive) or by tearing at the seam or sheet-purlin fasteners (more desirable as this type of failure ensures that large deformation can take place without significant reduction in the collapse load). Both Bryan's and Davies approaches calculated ultimate shear load from the lowest tearing strength of the seam, sheet-purlin or sheet-connector fasteners. This is the case also for Easley and Fazio's approaches. The shear strength of the diaphragm is based on the strength and characteristics of fasteners rather than buckling of the diaphragm.

5.2.3 Fastener Characteristics

Analytical prediction of strength and stiffness of a diaphragm depends primarily on the behaviour of the fasteners governing the internal and external boundary conditions of the diaphragm. The load-slip or deformation curves for the fasteners must be obtained accurately from separate tests. For seam fasteners Bryan (1972) used pop rivets. Fazio et al (1978) used mechanical clinching (button punching)where ultimate strength varies from 1.29-2.09kN and initial slope of load-deformation curve varies from (0.25-0.44kN/mm) for 18 gauge sheet. For end fasteners (sheet-purlin or sheet-rafter) Bryan used self tapping screws with washers. Fazio used 19mm puddle weld where ultimate load of 24.5 kN and stiffness of 13.13 kN/mm were achieved.

5.2.4 Buckling of shear diaphragm

In the case where the number of fasteners is sufficient so that localised failure at the fasteners does not occur first, elastic buckling becomes the mode of failure and is important in diaphragm design since it represents the maximum possible strength. Light gage diaphragms are usually thin and flexible enough and of sufficient length, for buckling to occur well before the onset of any plastic behaviour. Since most corrugated shear diaphragms can be classified as thin orthotropic plates, the buckling loads of orthotropic plates loaded by pure in-plane shear forces are applicable to them. In the buckling analysis, the significant orthotropic constants (D_x, D_y, $D_1$and D_2) that are needed are those relating bending (M_x, M_y) and twisting moments(M_{xy}, M_{yx}) in a buckled diaphragm to the local curvatures (θ_x and θ_y)and local twist(θ_{xy}) of the diaphragm. According to Easely and McFarland(1969,1975), the relations between bending and twisting moments per unit length, which act on a qxq element of the diaphragm (shown in figure 5.4(a)) and curvatures are :

$$M_x = D_x\theta_x + D_1\theta_y, \cdots M_y = D_2\theta_x + D_y\theta_y \cdots and \cdots M_{xy} + M_{yx} = D_{xy}\theta_{xy}$$

For corrugated sheets of any cross-section, the constants are

$$D_x = \frac{q}{s}\frac{Et^3}{12}\cdot\cdot, D_y = \frac{EI_y}{q}, D_1 = D_2 = 0 \ldots and \ldots D_{xy} = \frac{s}{q}\frac{Et^3}{6(1+\upsilon)} \qquad \ldots\ldots\ldots(5.2)$$

where E= the elastic modulus of the material of the sheet; t= its thickness, s= the arc length of one repeating corrugation shape and I_y= the moment of inertia of one repeating corrugation about its neutral axis and ν= poisson's ratio of the material of sheeting.

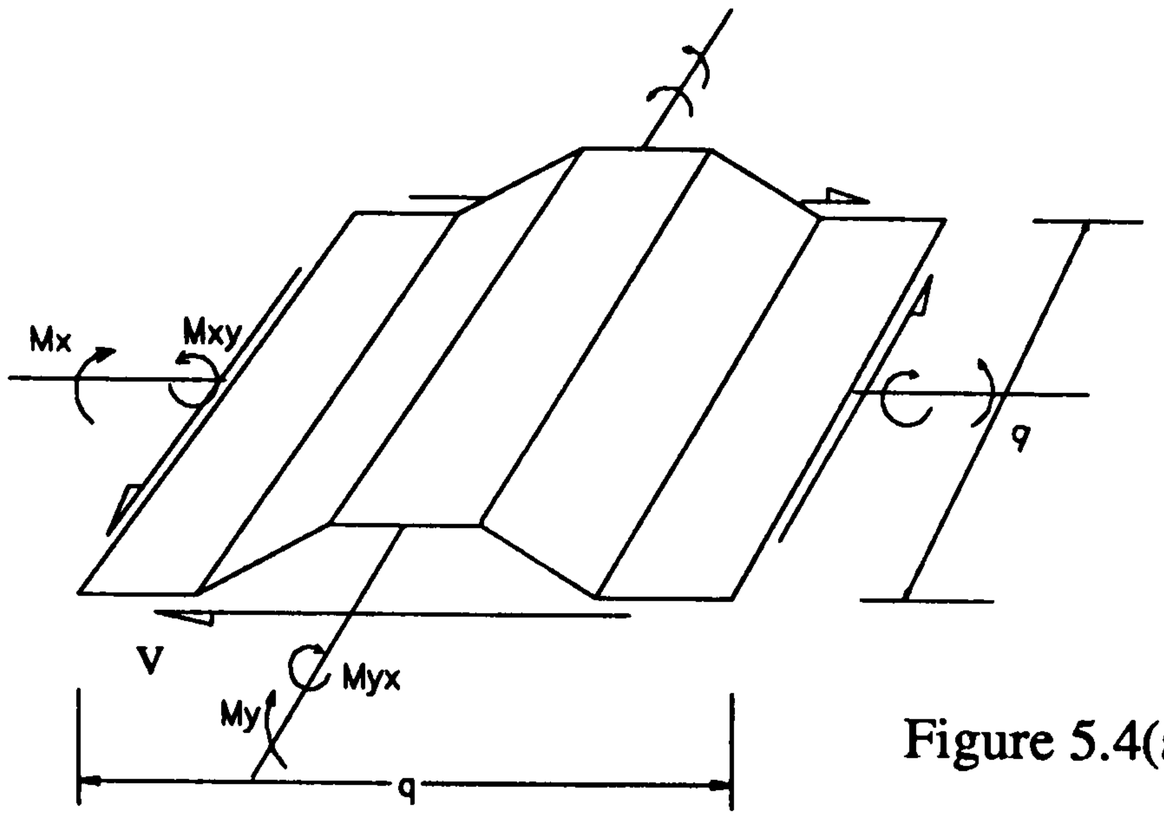

Figure 5.4(a)

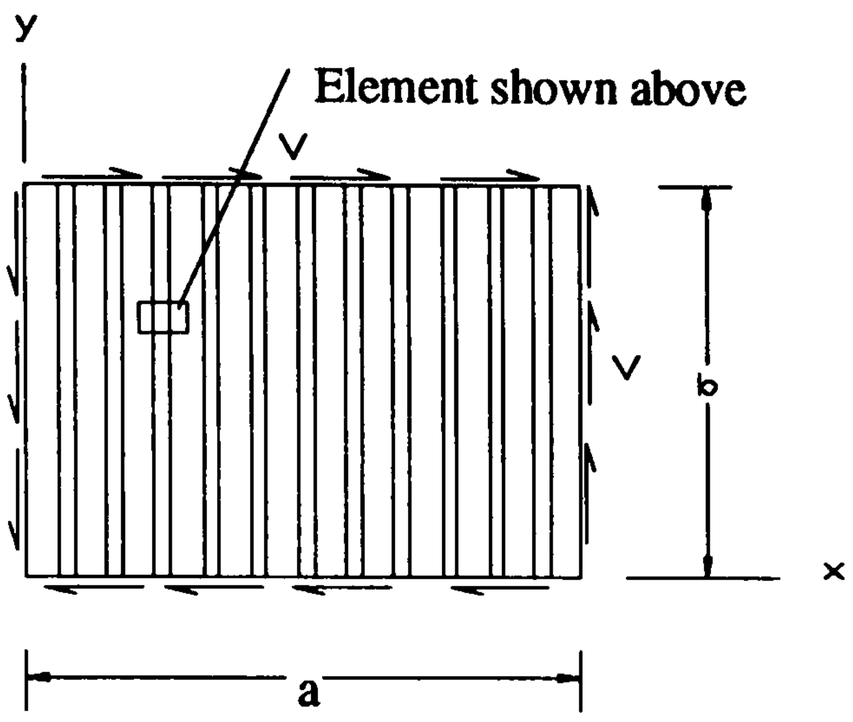

Figure 5.4(b)

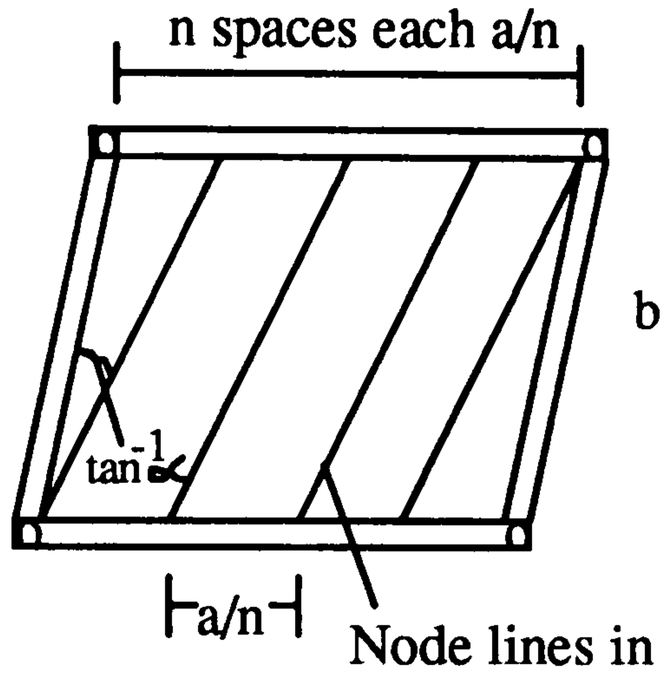

Figure 5.4(c)

The condition $D_1=D_2=0$ is an approximation that is valid only when $D_y>>D_x$ and this is usually true for all types of corrugated sheets that are commonly used. A reasonable limiting condition for its applicability should be $D_y>50D_x$.

5.2.4.1 Existing buckling formulas and comparison

Three different sets of formulas for elastic buckling loads are available and will be described here:

Easley and McFarland (1969,1975)formula:

Easely and McFarland investigated the general buckling behaviour of light gauge corrugated shear diaphragms subjected to in-plane shear loads V per unit length (figure 5.4(b)) treating them as plates having flexural rigidities in two perpendicular directions. They derived formulas for buckling load, V_{cr}, per unit length and formulas for the post-buckling load-deflection relations of a shear diaphragm. For the buckling load they obtained:

$$V_{cr} = D_y\pi^2\left(\frac{a^2}{2\alpha n^2 b^4}+\frac{3\alpha}{b^2}+\frac{\alpha^3 n^2}{2a^2}\right)+D_x\pi^2\frac{n^2}{2\alpha a^2}+D_{xy}\pi^2\left(\frac{1}{2\alpha b^2}+\frac{\alpha n^2}{2a^2}\right)$$

Using simplified expressions for n (= $\frac{a}{b}\left(\frac{D_y}{D_x}\right)^{\frac{1}{4}}$) and α (=$\left(\frac{D_x}{11D_y}\right)^{\frac{1}{4}}$) in the above equation , they derived simplified buckling load as: $V_{cr} = 36\frac{D_x^{1/4}D_y^{3/4}}{b^2}$

Bergmann and Reissner(1929)Formulas:(as quoted from Easley 1975)

The buckling load in shear was derived treating corrugated plates as orthotropic plates having different flexural rigidities in two perpendicular direction. They derived the formula:

$V_{cr} = 4\lambda\frac{D_x^{1/4}D_y^{3/4}}{b^2}$ in which λ is a multiplier dependent upon θ and ϕ derived from expressions $\theta = \frac{(D_xD_y)^{0.5}}{D_{xy}}$ and $\Phi = \frac{b}{a}\left(\frac{D_x}{D_y}\right)^{0.5}$. The dependence of θ and ϕ is given in the form of curves by Timoshenko and Gere (1961). It was found from those curves that if $D_y \rangle\rangle D_x$ and D_{xy} then the co-efficient, 4λ, becomes 36 which makes the formula similar to that of Easely and McFarland.

Hlavacek Formulas(1968,1970)

Hlavacek investigated the buckling behaviour in shear of flat sheets reinforced by separate equally spaced stiffeners symmetrically attached to both faces of the sheet, but intended that his results be applicable to corrugated metal diaphragm as well. Analysis of his formulas showed that for light gauge corrugated metal diaphragms, the formula for buckling load can be expressed as :

. $V_{cr} = 41\frac{D_x^{1/4}D_y^{3/4}}{b^2}$

It has the same form as Easley and McFarland but the numerical co-efficient is 1.14 times higher.

Critical review of buckling formulas

Bergmann-Reissner formula was the more rigorous and considered buckled deflection, w, in the form $w = \sum_{i=1}^{\infty}\sum_{j=1}^{\infty} A_{ij}\sin\frac{i\pi x}{a}\sin\frac{j\pi y}{b}$, in which Aij could be adjusted to satisfy the governing differential equation and within the framework of orthotropic plate theory, this formula should give a highly accurate value of V_{cr} for simply supported diaphragm. For the case of diaphragm the co-efficient, 4λ, becomes 36 which makes the formula exactly similar to that of Easely and McFarland.

Easely and McFarland (1969) and Hlavacek(1968), both used approximate energy methods in their derivatives, assuming the buckled deflection in the form of equation

$w = A\sin\frac{n\pi}{a}(x-\alpha y)\sin\frac{\pi y}{b}$, which satisfied simply supported condition on the ends of diaphragms (edges y=0 and y=b) but not on the sides. This less rigorous development was used to treat more mathematically complicated post buckling behaviour of diaphragms. Hlavacek additionally assumed the half wave number, n, and the wave inclination, α,(figure 5.4(c)) to be related to the diaphragm dimensions by $n=a/\alpha b$ whereas Easely-McFarland treated these two parameters as independent. This is the one reason why the two formulas differ by about 20%.

A second smaller difference in Hlavacek's method was the use of bending stiffness of flat sheet for D_x which is equal to $\frac{Et^3}{12(1-\upsilon^2)}$ while Easely and McFarland derived equation for D_x specifically for profiled sheet as in equation (5.2). Hlavacek used equation (5.2) for D_y and neglected the twisting stiffness, D_{xy}, of his flat sheet model.

Lawson(1976) derived from Easely and McFarland formula that $V_{cr} \propto h^{3/4}/S$ that is the section which maximises the buckling load must maximise the depth, h, and minimise the corrugation parameter (S).

Theoretical and experimental analysis by Easely (1975), strongly indicate that Easely and McFarland formula is the correct one for simply supported diaphragm when the correction for the effect of end restraint is taken into account. Easely (1975) generalised the Easely Mcfarland formula to apply for practical cases taking into account the effect of end restraint against rotation as :

$$V_{cr} = 36\beta\frac{D_x^{1/4}D_y^{3/4}}{b^2} \quad \text{in which } 1 \le \beta \le 1.90. \quad \text{.....(5.3)}$$

where β is a co-efficient dependent on boundary condition. For the simply supported condition (no end restraint against rotation) β=0.0 and according to Bergmann and Reissner, for clamped condition (full restraint against rotation) β=1.90. However, true variation of β with diaphragm end restraint is unknown which demands further investigations.

5.2.4.2 Post-buckling behaviour

As we have seen, buckling of the sheeting is not a design criteria for the shear strength of the diaphragm as failure is initiated in the fasteners. But if the connections of the sheeting to the boundary frames is very rigid then buckling of the sheeting will be a design criteria. In that case, the critical shear buckling load and subsequent post-buckling response of the sheeting is very important.

Small deflection theory of orthotropic plates used by Easely and McFarland (1969) to derive buckling load of a diaphragm gives no information concerning post-buckling behaviour. Information concerning post-buckling behaviour can only be obtained from a large deflection theory. Easely and McFarland (1969) carried out large deflection analysis and derived post-buckling load-deflection relationship. The smallest value of load for which a laterally deflected equilibrium configuration can exist is given by V_{min} which in no case is significantly smaller than V_{cr}. They indicated that V_{min} should be equal to or greater than $0.95V_{cr}$ in all cases.

The girders with trapezoidal profiled web have been found to be advantageous and economical over plate girders with flat stiffened webs. Luo (1995) studied the behaviour of steel plate girders with trapezoidal profiled webs. The web slenderness is so large that one should pay attention to the risk of buckling. Experiments conducted on such girders under shear loading showed an unstable post-buckling behaviour, which usually occurs in a rapid and sudden process leading to a sudden snap-through type buckling. Luo and Edlund(1995) also carried out finite element analysis to model post-buckling behaviour taking into account the effect of large deflection.

ECCS-Technical Committee (1986) reported that for girders with trapezoidal profile web, it easy to reach the condition $\tau_{cr} \geq \tau_y$ whereτ_{cr} is the shear buckling stress and τ_y is shear yield stress. This means that shear yield stress not the shear buckling stress will govern the design.

Due to the very sudden transition (snap through) to the tension field action, ASCE-AASHTO TASK COMMITTEE(1977) recommended not to consider the post buckling shear reserves in the design. This recommendation is quite logic as confirmed from the tests by Gachon (ECCS-Technical Committee,1986), Luo(1995) and Luo and Edlund(1995).

5.2.5 Review conclusion

The shear flexibility or stiffness of the diaphragm depends mainly on the manner of attachment of the sheeting to the surrounding frame or boundary members.
The flexibility equations from Bryan and Davies for shear diaphragms can be used to derive flexibility of profiled steel sheeting connected to steel beam-column frame in steel framed building. The co-efficient, K, in flexibility equations representing manner of attachment of sheeting to the frame needs to be studied to verify analytical expressions for determining K.

The shear strength of the diaphragm due to Bryan, Davies, Easley and Fazio is a function of fastener characteristics. The failure is assumed to be due to the failure of connections to the frame and not due to buckling of sheeting. These models can be adopted in actual case of composite wall when boundary connections failure is desired.

For rigid connections where buckling load will govern the design, the generalised buckling load equation by Easely(1975) can be used taking into consideration the boundary co-efficient β. The variation of β due to various boundary conditions needs further investigations.

Post-buckling shear reserves of the profiled steel sheeting should not be considered in the design and hence it would be wise and realistic not to study deeply the post-buckling response.

It is possible to make the critical shear buckling stress of the profiled steel sheeting higher than the shear yield stress by adjusting the physical dimension of the geometry of the profile.

The stress-strain characteristics within the profiled steel sheeting under in-plane shear is not yet reported any where until now. Investigation on this matter may provide some useful information regarding the development of tension field within the panel and the variation of stress or strain along the boundary.

The hysteretic behaviour of the profiled steel sheeting is also not yet studied. This needs to be studied as the sheeting in building frame may be subjected to wind and earthquake forces causing cyclic application of load which may effect the stress distribution within the panel and also the buckling load.

5.2.6 Aim of study:

0 The development of an analytical model for stiffness and strength of the profiled steel sheet for various boundary conditions representing actual building application and small scale model tests.

0 Description of small scale model tests, analysis of test results, comparison of results between model tests.

0 Model test to study the hysteretic behaviour of the system.

0 Finite element simulation of actual model tests and comparison of Model test results and FE analysis.

0 The validation of analytical expressions for the factor, K, and its validation by FEA and Model tests.

0 FE analysis of buckling load for different boundary condition and to find the value of β from the comparison of FEA and Model tests.

5.3 Analytical Model Developments

A diagrammatic arrangement of the profiled steel sheeting considering the practical use of composite wall in building frame is shown in figure 5.5. The sheets are installed with profile generator vertically up right position and connected to the frame beam-column boundary by fasteners. In practice although sheets are produced in lengths which satisfies the normal storey height requirements but they are available only in standard widths that vary from 0.6m to 0.9 m. Therefore individual sheets have to be fastened together along the seam.

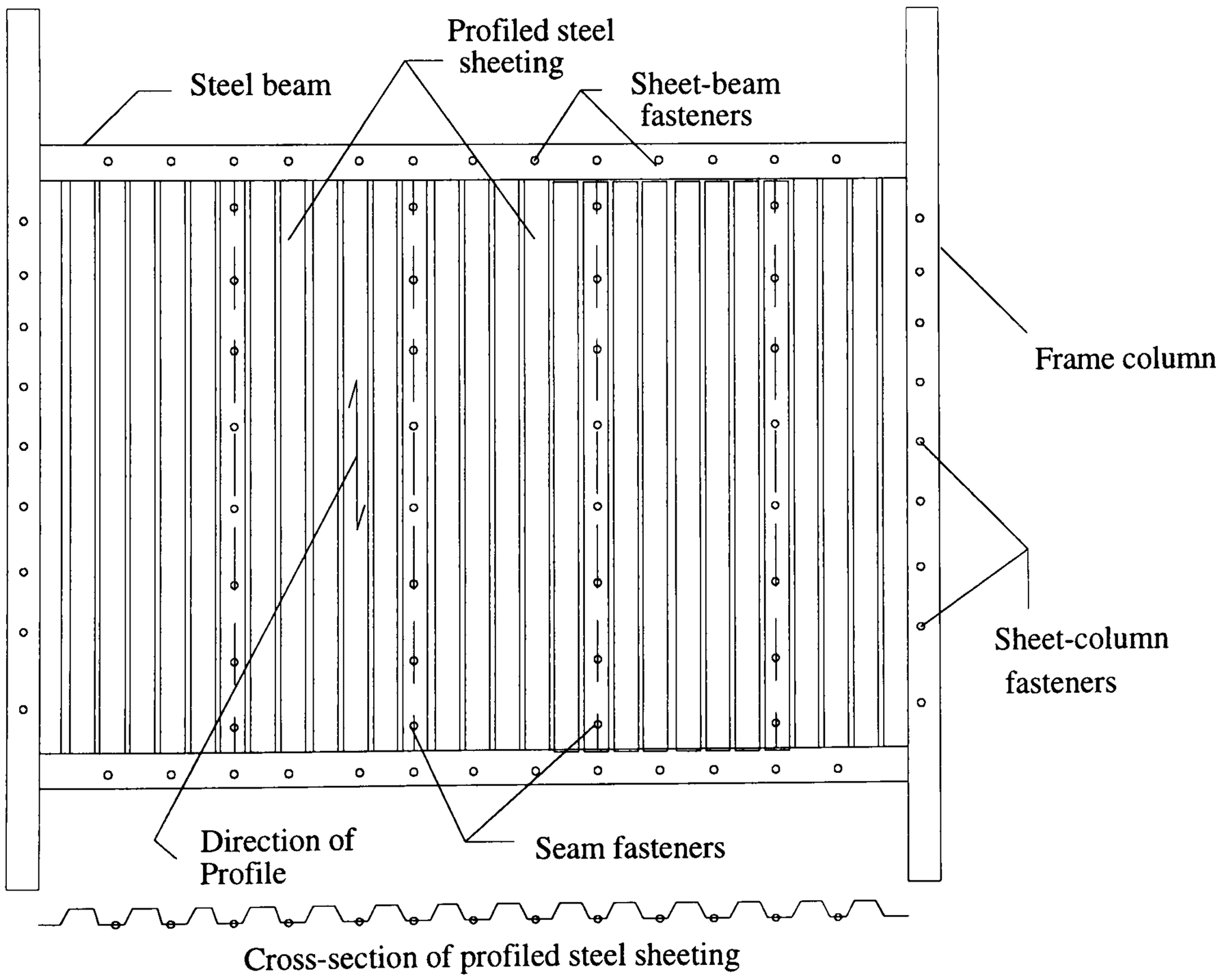

Figure 5.5: Schematic of profiled steel sheeting in building frame

The following assumptions can be considered to simplify the analytical developments:
1. The beam to column connections are pinned so that the frame allows shear transfer from the frame to the profiled sheeting maintaining the sheet in pure shear.
2. The sheeting does not interfere with flexure of the boundary frame beams and columns.
3. The frame will transfer uniform shearing forces to the sheeting boundaries.

5.3.1 Analytical approach for shear flexibility and stiffness of profiled steel sheet

The flexibility will be dependent on the boundary condition of the wall, especially how it is attached to the frame. The main difference between profiled sheet panel used for decks or roofs and that used for composite walls are :

-The shear flexibility of the profiled sheet is the displacement per unit shear load (δ/V) applied normal to the direction of profile generator (line condition) (figure5.6) instead of parallel to the profile generator (gable condition) as used in deck or roof panel.

Total shear flexibility of the profiled sheet, c_s, will be described as the summation of components of the various factors involved. The main components considered are due to : Shear deformation of sheet (c_1) , bending or distortion of corrugation profile (c_2), axial deformation of the beam-column frame (c_3) and local deformation of sheet at the sheet-frame and seam connections(c_4,c_5).

Therefore, $c_s = c_1 + c_2 + c_3 + c_4 + c_5 = 1/k_S$ .....(5.4)

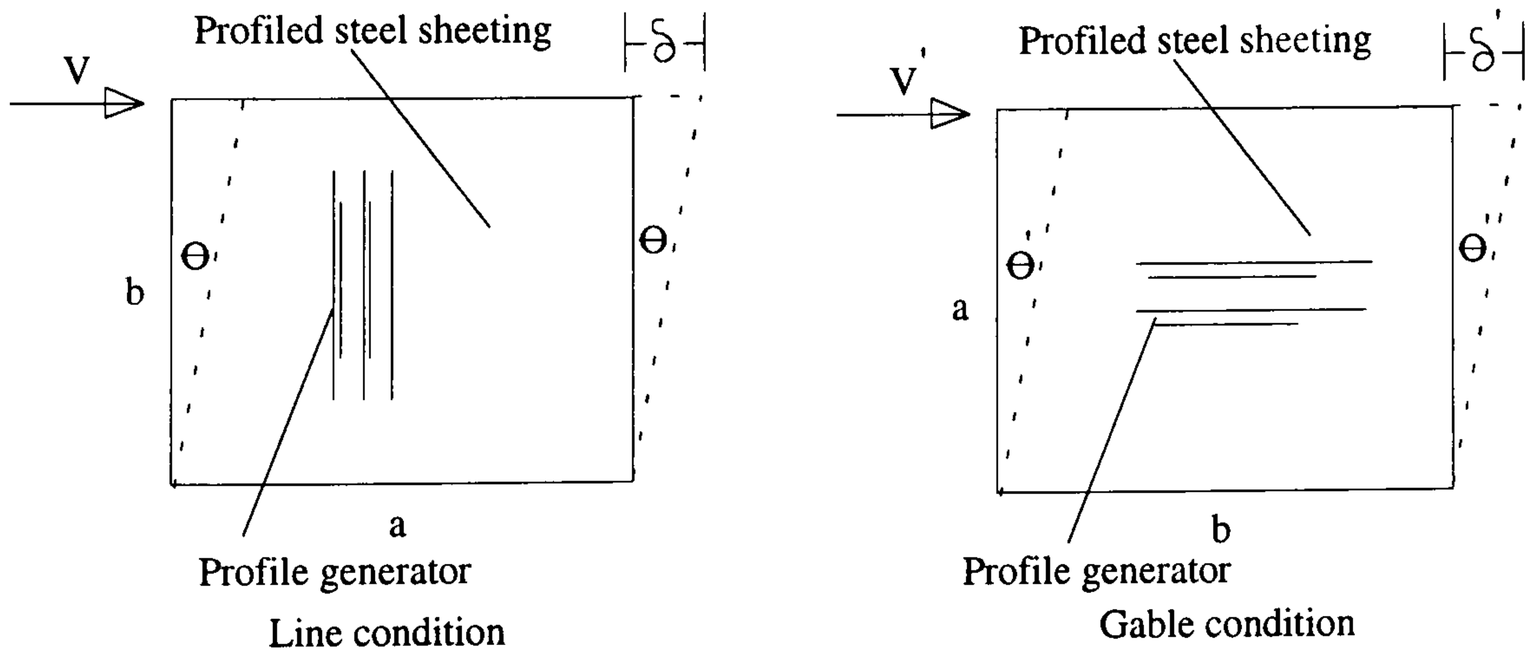

Figure 5.6: Shear flexibility conditions

Flexibility due to shear deformation of sheet(c_1):

Let us consider a profiled sheet panel and let it be subjected to a shearing force V as shown in figure 5.6. Assuming that no bending of corrugation profile takes place, then the shear displacement, δ , will be only due to shear deformation in the sheet.

Applying strain energy approach : The total shear strain energy, U, due to shearing stress, v (=V/at$_S$), can be written as

$U = \frac{v^2}{2G_S}(a\alpha b t_S) = \frac{\alpha b V^2}{2G_S at} = \frac{\alpha b V^2(1+\upsilon_S)}{E_S a t_S}$, where G_S, E_S, υ_S are shear modulus, modulus of elasticity and poisson's ratio of material of sheeting respectively, is the sheet thickness mater and α = ratio of developed length of a profile to its projected length. Equating total strain energy, U, to the external work done (0.5Vδ), the flexibility due to shear deformation of sheet can be expressed as :

$$c_1 = \delta / V = 2\alpha b(1+\upsilon_S)/(E_S.a.t_S) \quad \text{.....(5.5)}$$

This equation is similar to the expression of $c_{1.2}$ derived by Bryan (1972) and Davies (1976) presented in table 5.1.

For plain steel sheet the equation can be written as :

$$c_1 = \delta / V = 2b(1+\upsilon_S)/(E_S.a.t_S) \quad \text{.....(5.6)}$$

Flexibility due to bending of corrugation profile (c_2) :

This flexibility will be dependent on the manner of attachment of the sheeting to the surrounding frame. If the sheet is fastened to the frame in such a manner (such as fastened to the edge member on one face only) that it allows bending and torsion of corrugation profile, then the shear displacement will occur due to these two effects. The flexibility expression for $c_{1.1}$ derived by Bryan (1972) and Davies (1976) neglecting the torsional effect are for the gable condition and needs to be transformed to line condition for its application to this problem. Let c_2 and c_2' are the flexibilities in line and gable condition respectively. The shear distortion in a direction perpendicular to the line of profile is equivalent to the shear distortion in a direction parallel to the profile. From the figure 5.6 , it can be derived that

$$V = \frac{\delta}{c_2} = \frac{b\theta}{c_2} \text{ and } V' = \frac{\delta'}{c_2'} = \frac{a\theta}{c_2'} \text{ and also } Vb = V'a$$

putting the values of V and V' from the first two equations into the third one, the relationship between flexibilities in line and gable conditions can be found as:

$$c_2 = \frac{b^2}{a^2} c_2'$$

Putting $c_2' = c_{1.1}$ (Bryan and Davies, Table 5.1) in the above equation the flexibility due to bending of corrugation profile , c_2 , for the present problem can be expressed as : $c_2 = c_2' \frac{b^2}{a^2} = c'_{1.1} \frac{b^2}{a^2} = \frac{144 K h^3 l^2}{E_S t_S^3 abd}$ .....(5.7)

The factor, K, represents the mode attachment of the sheeting to the frame and the general formula (equation 5.1) given by Bryan and El-Dakhakhni (1968b) can be used. If the sheet is welded to the edge members at the centre of valley as shown in figure 5.26(a), the value of K can be obtained by putting N=1 in the general formula (equation 5.1) as :

$$K = \frac{(d+2h)(d^2 - 3ld + 3l^2)}{12hd^2} \quad \text{.....(5.8)}$$

If the sheet is continuously welded along the lower face (may be used for composite wall) or just at the toes as shown in figure 5.26(b), K , can be expressed as (El-Dakhakhni (1976):

$$K = \frac{2l+3h}{12(l+6h)} \quad \text{.....(5.9)}$$

If the sheeting is attached to the boundary members in such a way that the bending or distortion of the profile is not allowed, then c_2 can be neglected.

Flexibility due to Axial deformation of frame beam column

The axial force in the frame beams and columns is triangular (figure 5.7) varying linearly from a maximum value at one end to zero at the other end . The strain energy approach will be used to derive expression for flexibility due to axial deformation (c_3) of frame members.

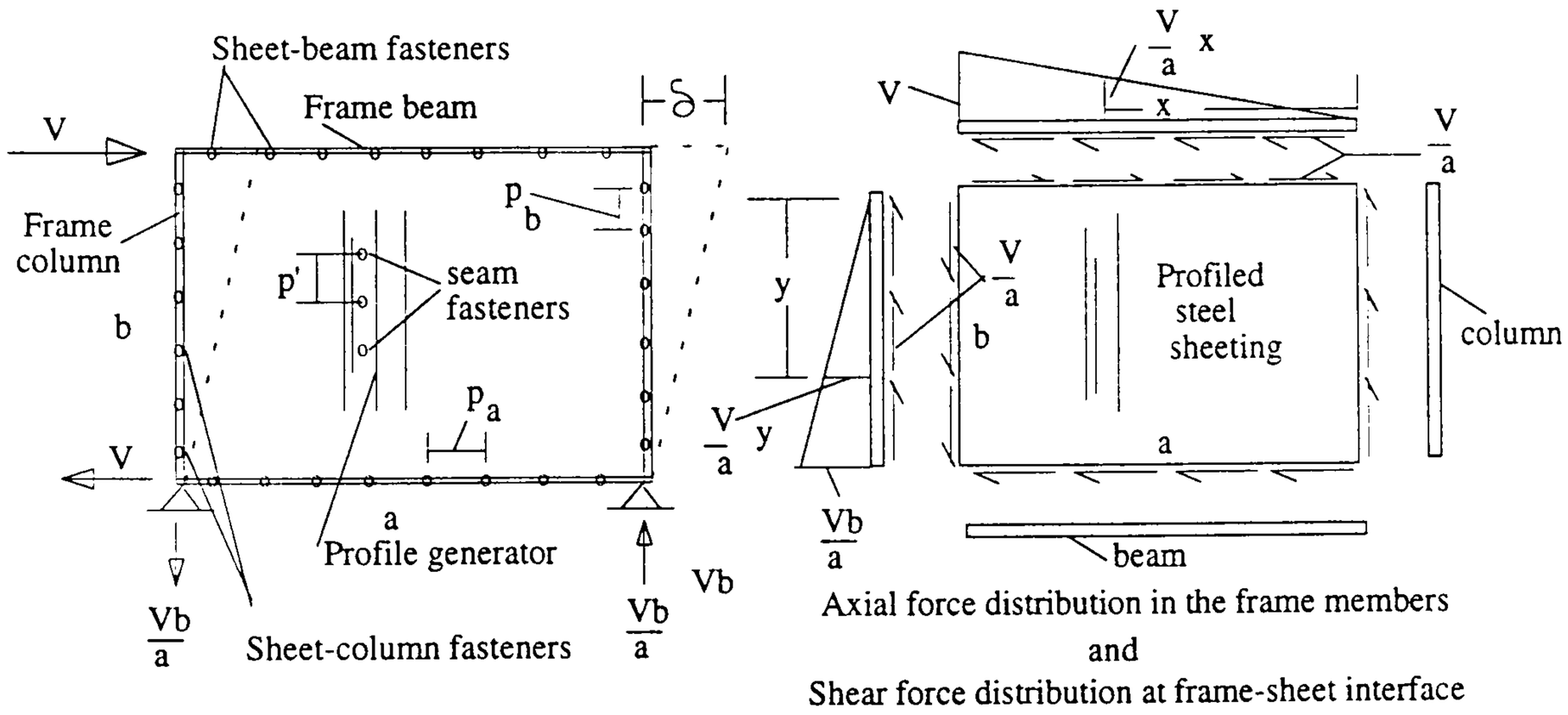

Figure 5.7: Distribution of forces in the frame

The strain energy of a beam member, U_b, and column member, U_c, can be derived as :

$$U_b = \int_0^a \frac{1}{2E_s A_b}\left(\frac{Vx}{a}\right)^2 dx = \frac{V^2 a}{6E_s A_b} \quad \text{and} \quad U_c = \int_0^b \frac{1}{2E_s A_c}\left(\frac{Vy}{a}\right)^2 dy = \frac{V^2 b^3}{6E_s A_c a^2}$$

Equating the strain energy of the two pairs of beam and column to the external work done (0.5Vδ), The expression for c_3 can be derived as:

$$c_3 = \frac{\delta}{V} = \frac{2}{3E_s}\left[\frac{a}{A_b} + \frac{b^3}{A_c a^2}\right] \quad \text{.....(5.10)}$$ where A_b and A_c are the cross sectional area of beam and column respectively. This expression is similar to the expression of $c_{1.5}$ (table 5.1) of Bryan and Davies.

Flexibility due to local deformation at sheet-frame fasteners (c_4):

The shear transfer between the sheet and the frame members at the fastener points cause stress concentration which results in local deformation of light gauge material. This is known as crimping at sheet-frame fasteners and contribute to the sheet flexibility. Let the p_a and p_b are the spacing of beam and column fasteners respectively as shown in figure 5.7 and s is the relative movement due to sheet crimping at each fastener per unit load .

Work done at all fasteners along the pair of beam members = Force per fastener x movement per fastener x no. of fasteners = $\frac{1}{2}.\frac{Vp_a}{a}.\frac{sVp_a}{a}.\frac{2a}{p_a} = \frac{sp_a V^2}{a}$

Similarly, work done at all fasteners along pair of columns = $\frac{sp_b b V^2}{a^2}$

Equating the work done at all fasteners to the external work done leads to

$c_4 = \frac{2s}{a^2}\left[P_a a + P_b b\right]$ .....(5.11),

this formula is also an extension of expression for $c_{2.1}$ (Bryan and Davies). If the sheet is continuously welded instead of spot welded, c_4 can be neglected.

Flexibility due to crimping at seam fasteners (c_5)

Crimping in seam fasteners results in additional flexibility. Let p' is the spacing of fasteners along each lap joint and s' is the relative movement due to sheet crimping at each fastener per unit load. Work done at all fasteners = force per fastener x movement per fastener x no. of fastener in each seam x no. of profiled sheet = $\frac{Vp'}{a}.\frac{Vp's'}{a}.\frac{b}{p'}.\frac{a}{a_o}.\frac{1}{2} = \frac{V^2 bs'p'}{2aa_o}$

Equating the work done at all fasteners to the external work done, the flexibility expression for c_5 becomes:

$c_5 = \frac{\delta}{V} = \frac{bs'p'}{aa_o}$ .....(5.12), where a_o = average width of individual profiled sheet.

Summary of analytical flexibility and stiffness

Models for practical use

Analytical model for flexiblity(c_s)and stiffness(k_S) of profiled steel sheeting based on contribution from sheeting, boundary frame, sheet-frame fasteners and seam fasteners is presented as: $c_s = c_1 + c_2 + c_3 + c_4 + c_5 = 1/k_S$. .....(5.13)

For practical case, building frame may be considered as rigid with axial deformation negligible and in that case c_3 can be neglected and the flexibility and stiffness will be:

$c_s = c_1 + c_2 + c_4 + c_5 = 1/k_S$. .....(5.14)

If the sheet is connected to the boundary frame in such a way that it does not allow bending of corrugation profile (continuously welded or connected along both faces of the profile to the frame) then c_2 can be neglected and the flexibility equation reduces to:

$c_s = c_1 + c_4 + c_5 = 1/k_S$. .....(5.15)

5.3.2 Analytical model for ultimate strength

The ultimate shear strength of the profiled steel sheeting connected to steel frame can be derived from the shear strength of diaphragm for direct shear transfer case due to Bryan (1972) and Davies (1976) as explained in section 5.2.2, if the failure is desired in the fasteners. Then the ultimate strength (V_u) will be minimum of : (figure 5.7)

Strength due to seam fasteners : $V_u = F_s . b/p'$..... (5.16)

Strength due to sheet-beam or sheet -column fasteners:

$V_u = F_{sb} . a/p_a = F_{sc} . b/p_b$.. ..... (5.17)

where F_s= ultimate strength of one seam fastener, F_{sb} and F_{sc} are the ultimate strength of one sheet-beam or sheet-column fastener respectively.

If the number of fasteners is sufficient, so that localised failure does not occur first at fasteners, elastic buckling becomes the mode of failure. In this case, as the post-buckling shear reserves can not be considered in design as discussed in section 5.2.5.2, the ultimate load can be taken as the critical buckling load calculated from generalised equation (5.3) due to Easely (1975). The ultimate load per unit width can be taken as :

$$V_u = V_{cr} = 36\beta \frac{D_x^{1/4} D_y^{3/4}}{b^2} \quad \text{in which } 1 \le \beta \le 1.90. \quad \text{.....(5.18)}$$

where β is a co-efficient dependent on boundary condition.

5.4 Small scale model tests

Three small scale model tests have been performed to study the behaviour of profiled steel sheeting under shear loading. Model tests also provide information on the effect of boundary condition and hysteretic load. The model tests had the following stages:

Manufacturing of model profiled sheet

The model sheet have been manufactured in the house from flat sheet of 0.45mm thickness using a fly press. The detailed modelling of profiled steel sheeting and manufacturing of sheeting have been presented in chapter 3.

Assembling of the sheeting in test frame

The assembly of the sheeting to the boundary frame depends on the intended boundary conditions of the tests. Test 1 and Test 2 have the same boundary conditions. For these tests sheeting is placed in between the pair of frame members and then drilled and bolted to the frame. To fill the gaps as shown in figure 5.8 between profiled boundary of the sheeting and the frame members, resin has been cast in the gaps following the steps and necessary precautions described in section 4.3.4 of chapter 4. Extra steel plates have been used along the plain boundaries of the sheeting to fill the gaps due to the depth of profiles.

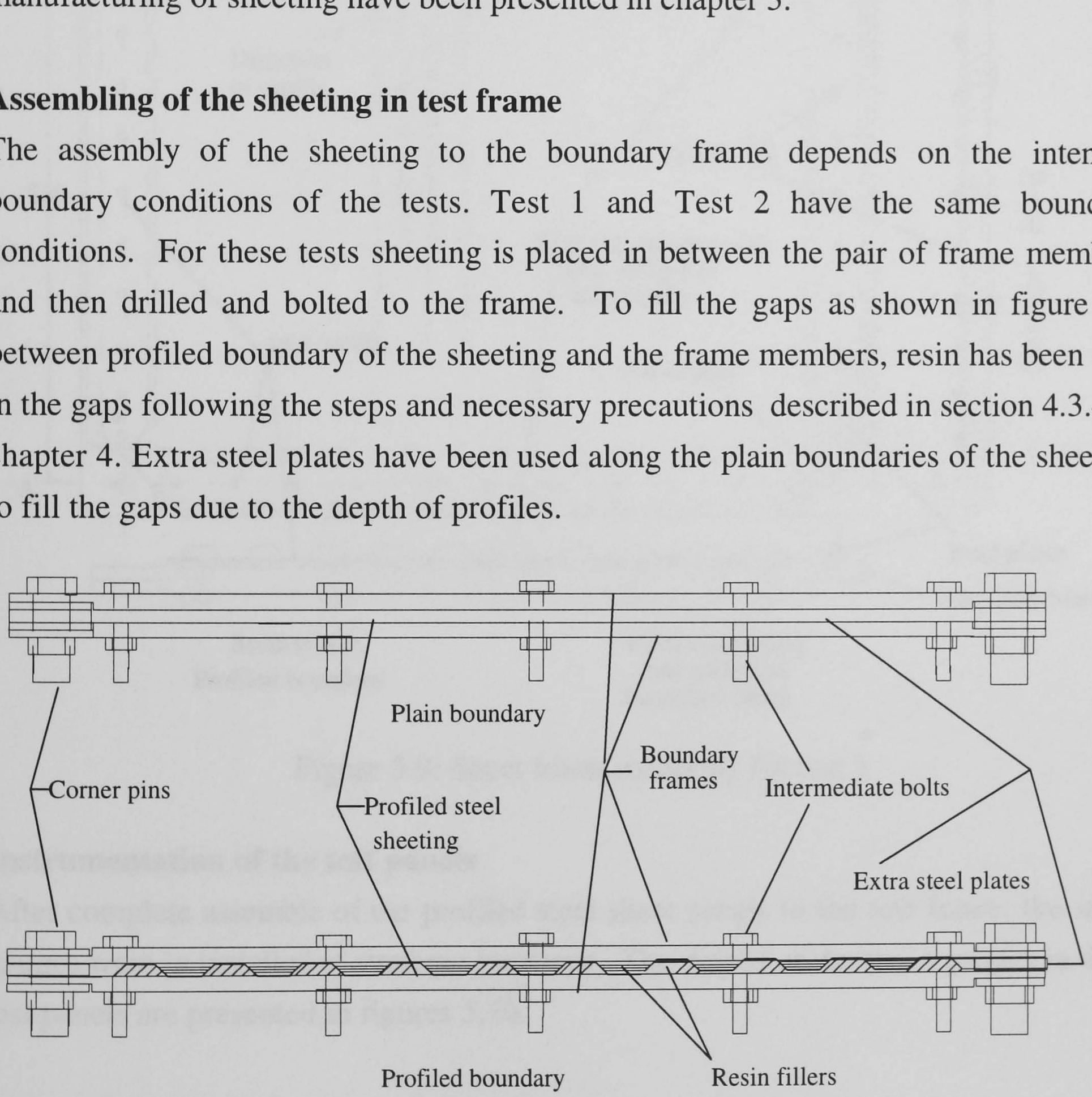

Figure 5.8: Schematic of resin filler in profiled boundary

Test 3 was performed with sheeting spot welded to the boundaries. The profiled steel sheeting is first spot welded to steel plates of 5mm thickness at the boundaries . The spot welding process and sheet-plate assembly is shown in photograph 5.1. The whole

sheeting and plate assembly is then connected to the test frame boundary by using bolts which connect the steel plates to the boundary frame. The detail is shown in figure 5.9. The lines of spot welds coincide with the central line of corners pins in the test frame assembly.

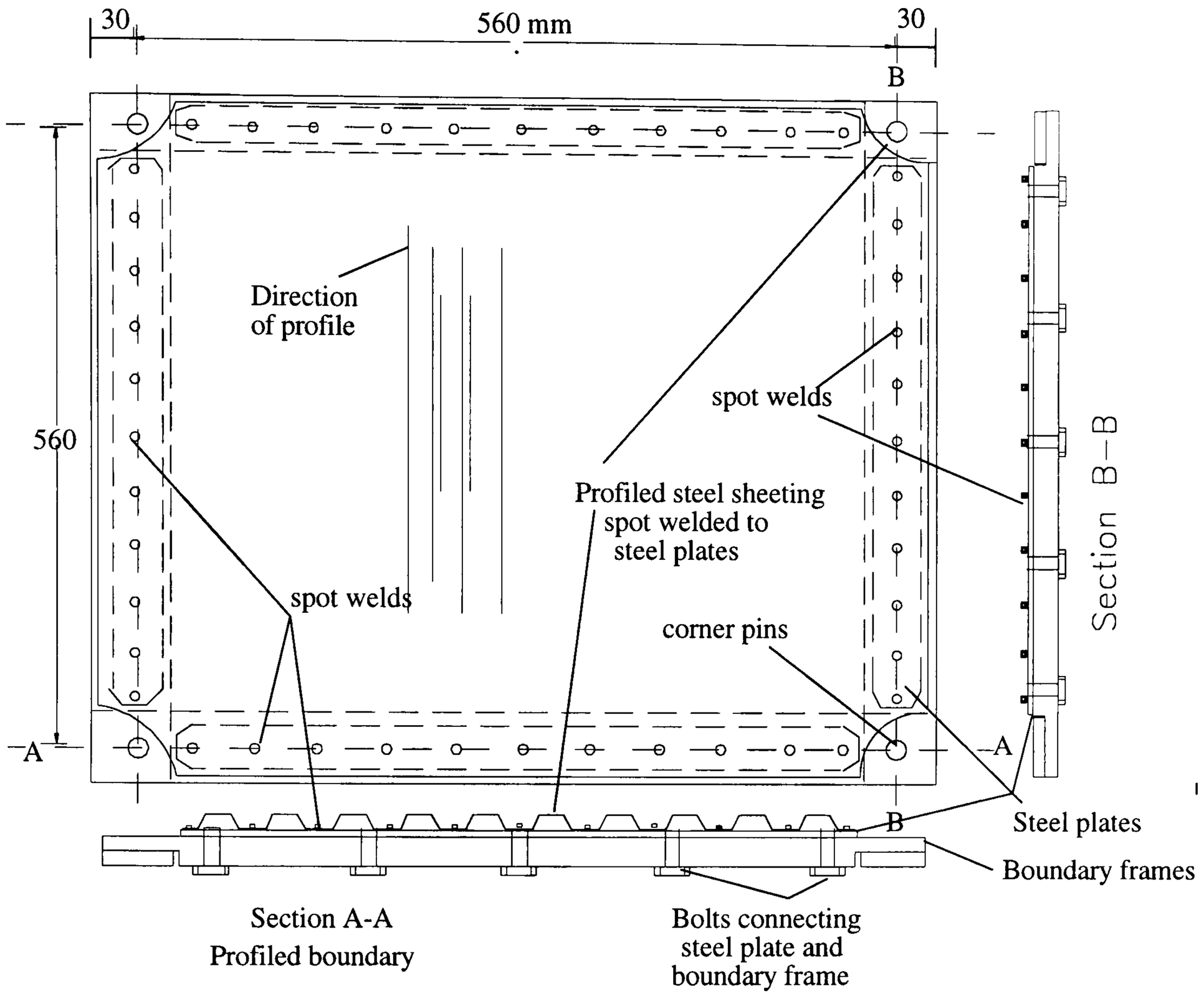

Figure 5.9: Sheet frame assembly for test 3

Instrumentation of the test panels

After complete assemble of the profiled steel sheet panels to the test frame, the strain gauges were in installed at strategic locations. The details of the strain gauges in three test panels are presented in figures 5.10.

Painting and marking of red line grids

After strain gauging, the panel was turned upside down to paint the other side white. When the paint became dry, grids of red lines were formed using thin strips of red plastic liner. These red line grids on white background were very effective in showing the buckling and distortion of the profiles as shown in photograph 5.3.

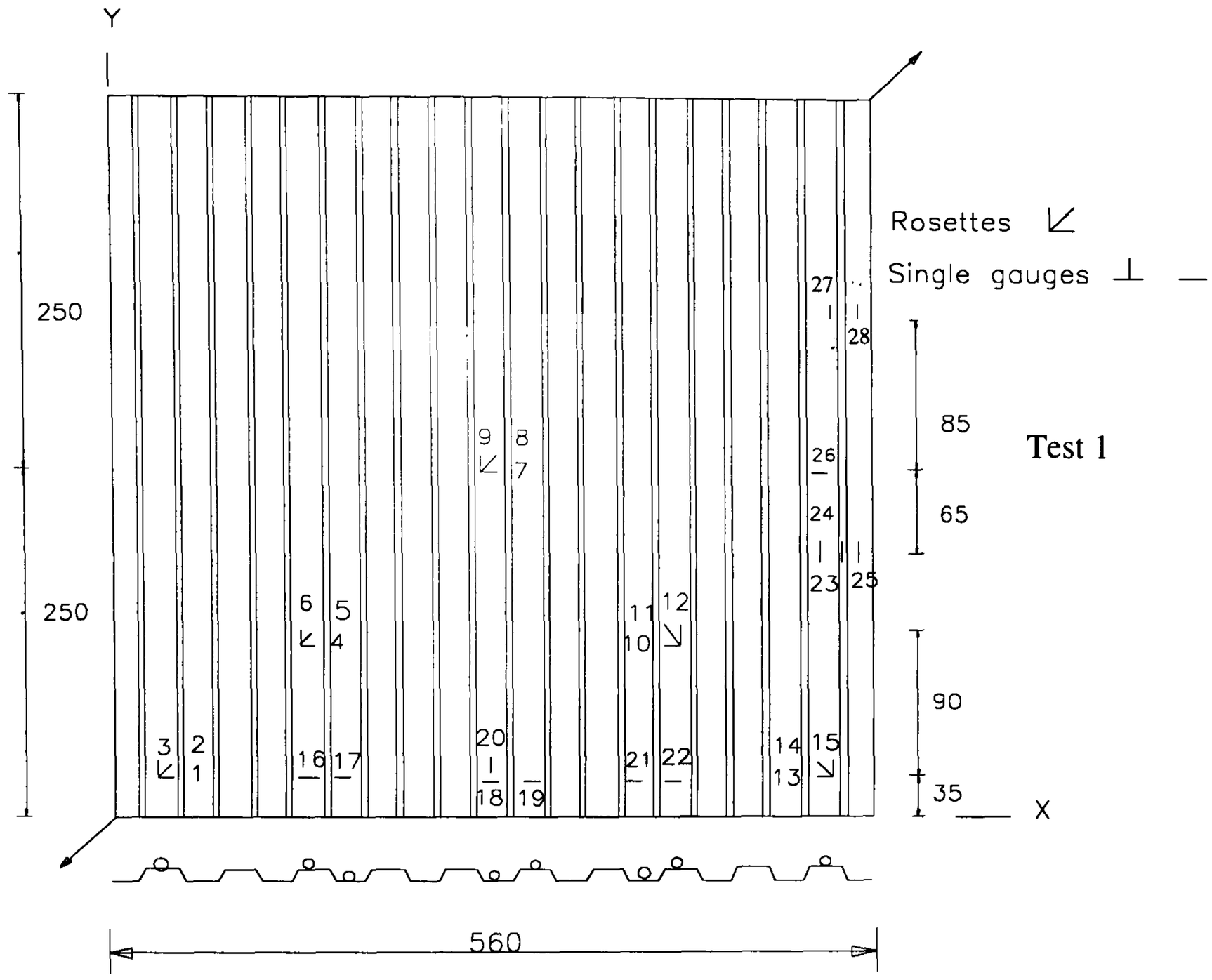
Y
250
250
560
Rosettes
Single gauges
Test 1
27
28
85
65
90
35
X
9
8
7
6
5
4
3
2
1
16
17
20
18
19
11
10
12
21
22
26
24
23
25
14
13
15

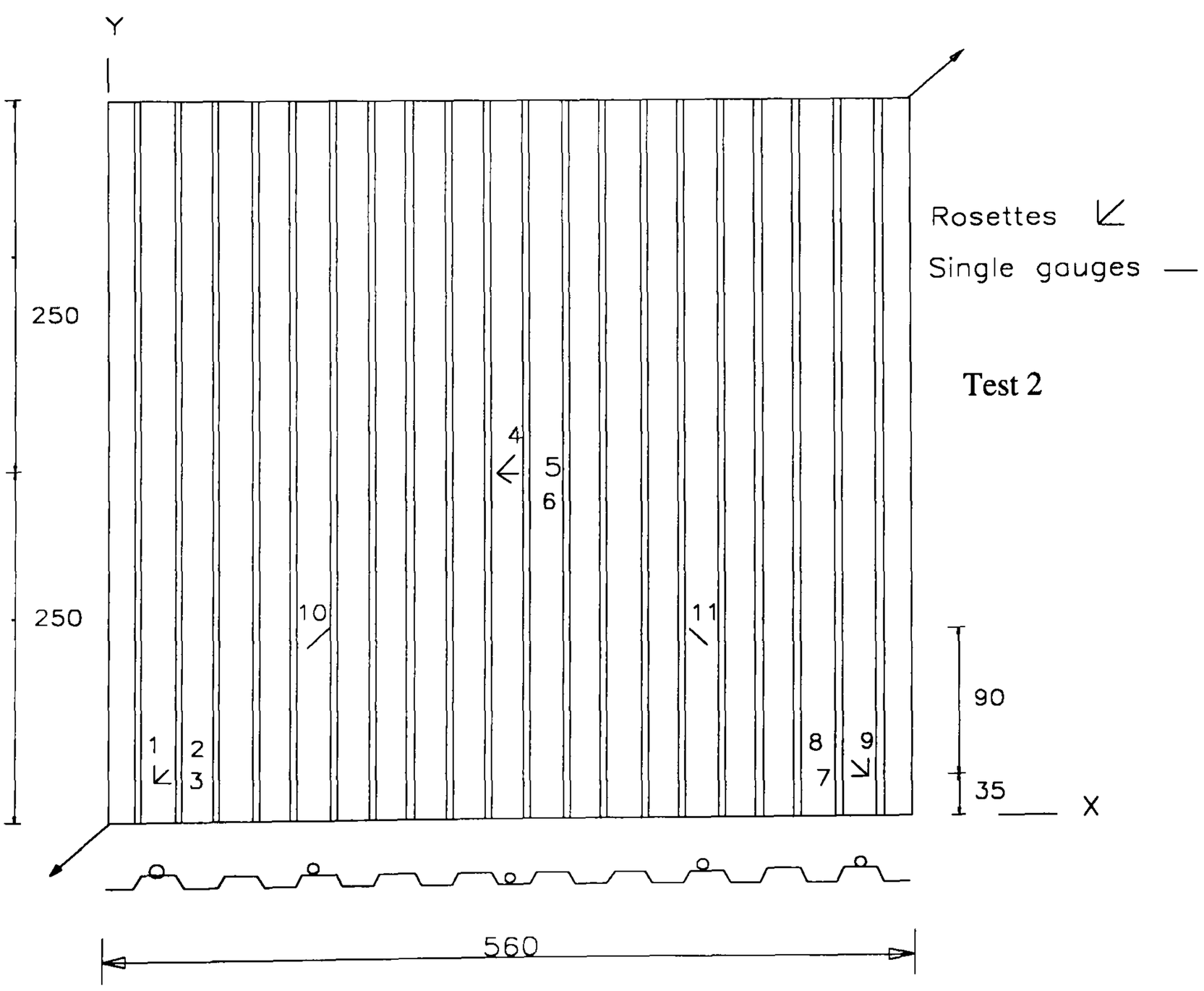
Y
250
250
560
Rosettes
Single gauges
Test 2
90
35
X
1
2
3
10
4
5
6
11
8
9
7

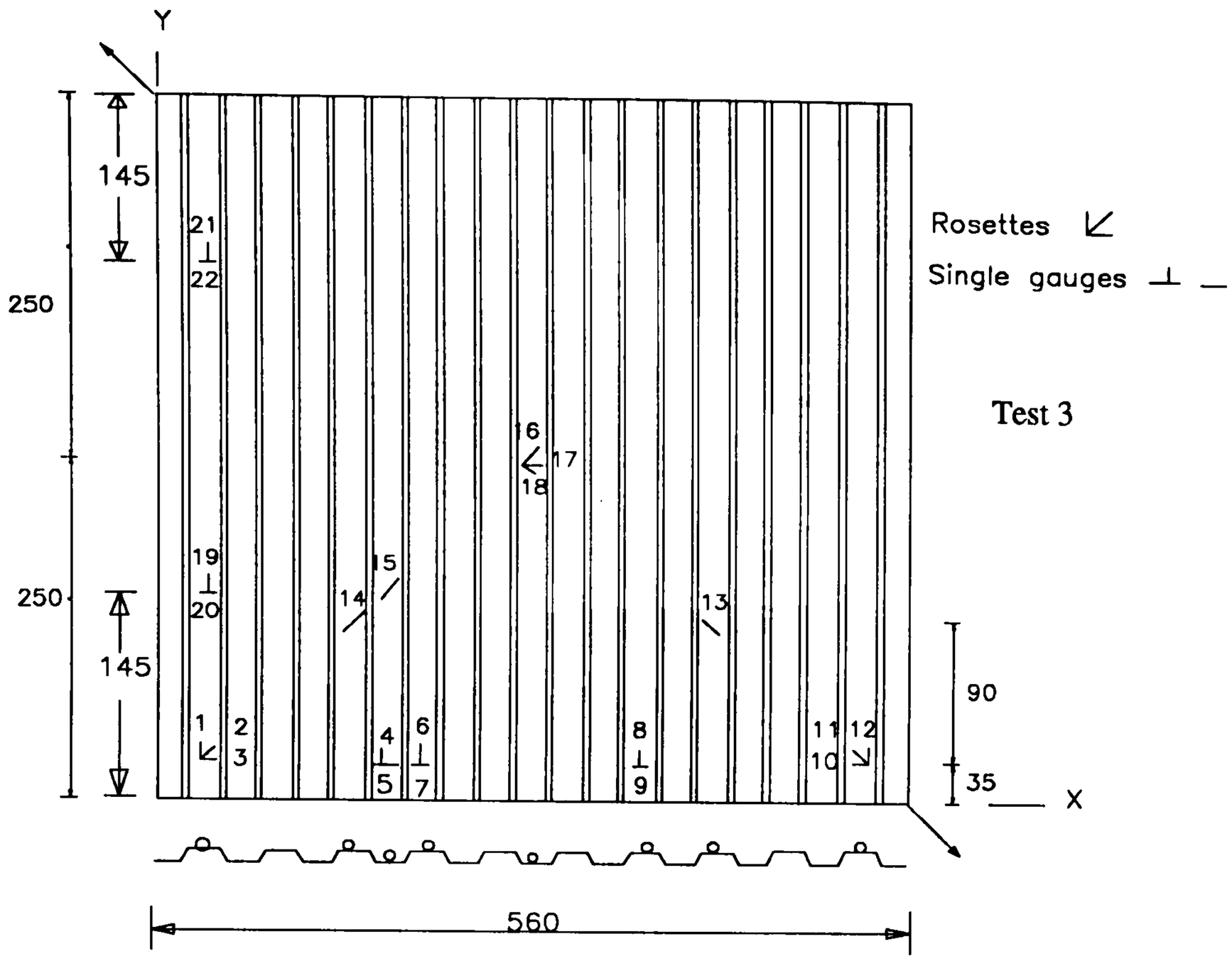

Figure 5.10: Instrumentation of profiled steel sheet panels

Test set-up

The test set-up is similar to those described in earlier chapters with an additional arrangements to measure the out-of plane displacements along the trough lines of the profile. The arrangements provided the facility for an LVDT to travel along an inclined direction so that it can record the lateral displacement along the trough lines of the profiled steel sheeting. The movement of the device which hold the LVDT was controlled by a motor and it could be stopped at any point on the trough lines to record the displacement at that point. Only one trough line of the panel was selected for displacement recording and displacements were recorded only at some specific points on that chosen trough line. The displacement recording was continued until the movement of the LVDT was restricted by the distorted profile. The computer aided data acquisition system was used as before to monitor the diagonal load-deformation response, strains and displacements throughout the loading history. The complete experimental set-up is shown in photograph 5.2 as taken from composite wall test.

5.4.1 Loading and Test observations

Test 1

This test was performed by applying tensile forces along the loaded diagonal of the panel. The loading and unloading were done several times during the whole loading history. The load was applied incrementally and at each load increment displacements and strains were recorded. The panel failed at a diagonal load of about 52kN. The failure was mainly due to buckling of the sheeting. No yielding or tearing of the sheet at intermediate bolts of the boundaries and no cracking or splitting of the resin filler at the profiled boundaries were observed. The load-deformation response for the test is shown in figure 5.11(a). From the graph, the diagonal buckling load can be clearly identified to be around 40kN where a change in slope of the graph occurred. Up to the buckling load, the stiffness of the panel remains almost constant as shown in figure and reduced in the post-buckling stage.

Before the buckling load, no distortion of the sheeting was observed. Post-buckling behaviour was characterised by the formation of localised tension field or buckles parallel to the direction of the applied load at trough or crest sections of the profiles. At the failure stage, tension fields were extended over some length of the trough and crest profiles accompanied by severe distortion and bending of profile with the loss of profile geometry. The failure mode of the panel is shown in photograph 5.3. The failure was sudden due to the sudden transition to tension field action.

Test 2 (hysteretic behaviour)

The boundary condition of this test is similar to that of test 1. The panel was loaded diagonally under alternate tension and compression to simulate hysteretic effect. The hysteretic application of load was started with tension and then load released to zero to follow compression. In this way several cycles of loading were completed before the failure of the panel was initiated under compressive diagonal load. The load was increased at an increments of 5 kN in each cycle. The failure of the panel was similar to that of test 1 with the formation of extended tension fields and localised buckling. The panel failed at about 45kN. The load -deformation response of the panel is shown in figure 5.11(b).

Test 3

The loading condition of this test was similar to that of test 1 but the boundary condition was different as the sheeting was spot welded to the boundary. The failure of the panel was initiated at a centre weld of one of the profiled boundary (crest line

10) where the weld failed at about 20kN diagonal load (figure 5.11(c)). The load increased with subsequent buckling and twisting of the profile. Local crimping of the sheeting occurred at almost all the points of spot weld and was pronounced on the profiled boundaries. Finally the panel failed at about 25 kN due to tearing of the sheeting at almost all the spot welds on the profiled boundary where the failure started first. No weld failure or tearing of the sheeting occurred on the plain boundaries. The failed panel is shown in photograph 5.4(a) and 5.4(b).

5.4.2 Test results, analysis and comparison

5.4.2.1 Load-deformation response and stiffness

The load-deformation response for test 1 are shown in figure 5.11(a). The stiffness in the pre-buckling stage can be averaged as 56.5kN/mm.

The hysteretic load deformation response of the panel test 2 is shown in figure 5.11(b). The tensile part of the response shows linear variation of up to a load of around 35kN but in the compression zone loops are clearly visible. The stiffness in the tension zone can be averaged as 53 kN/mm while the stiffness under compression can be averaged as 40 kN/mm. This difference of about 24% may be due to the effect of hysteretic load.

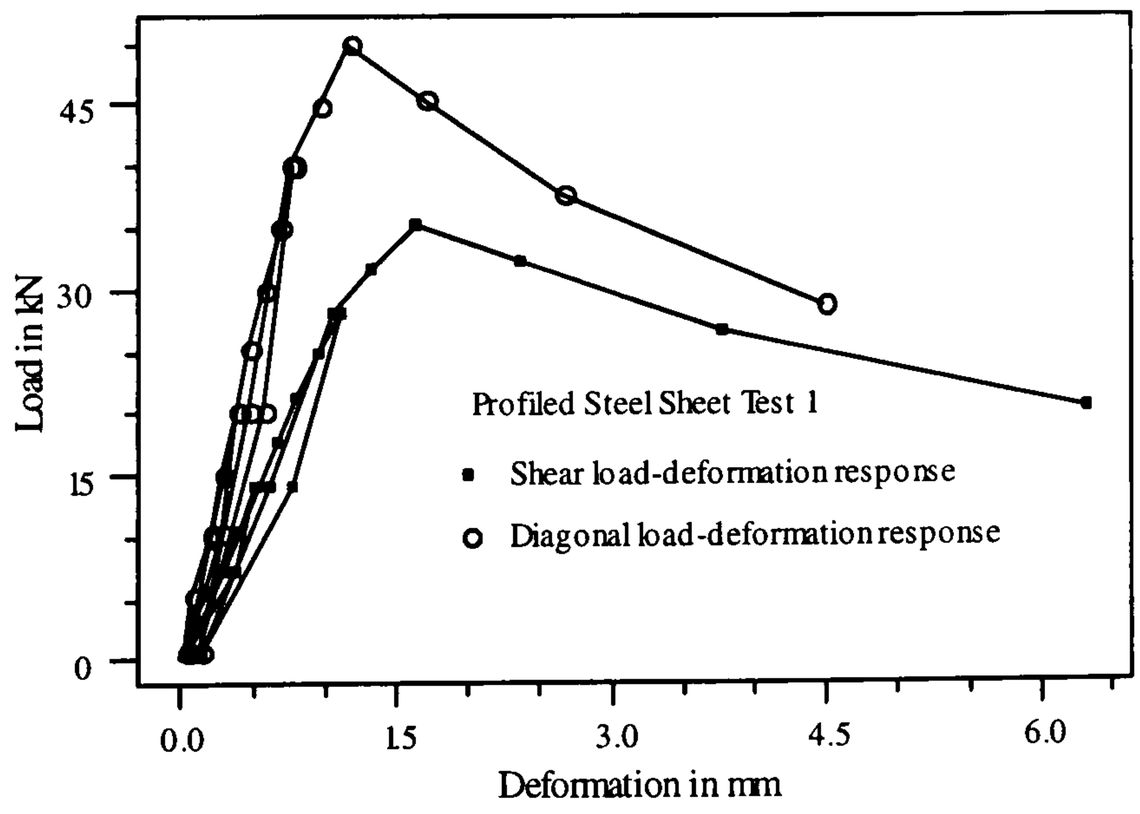

Figure 5.11(a) : Load-deformation response for test 1

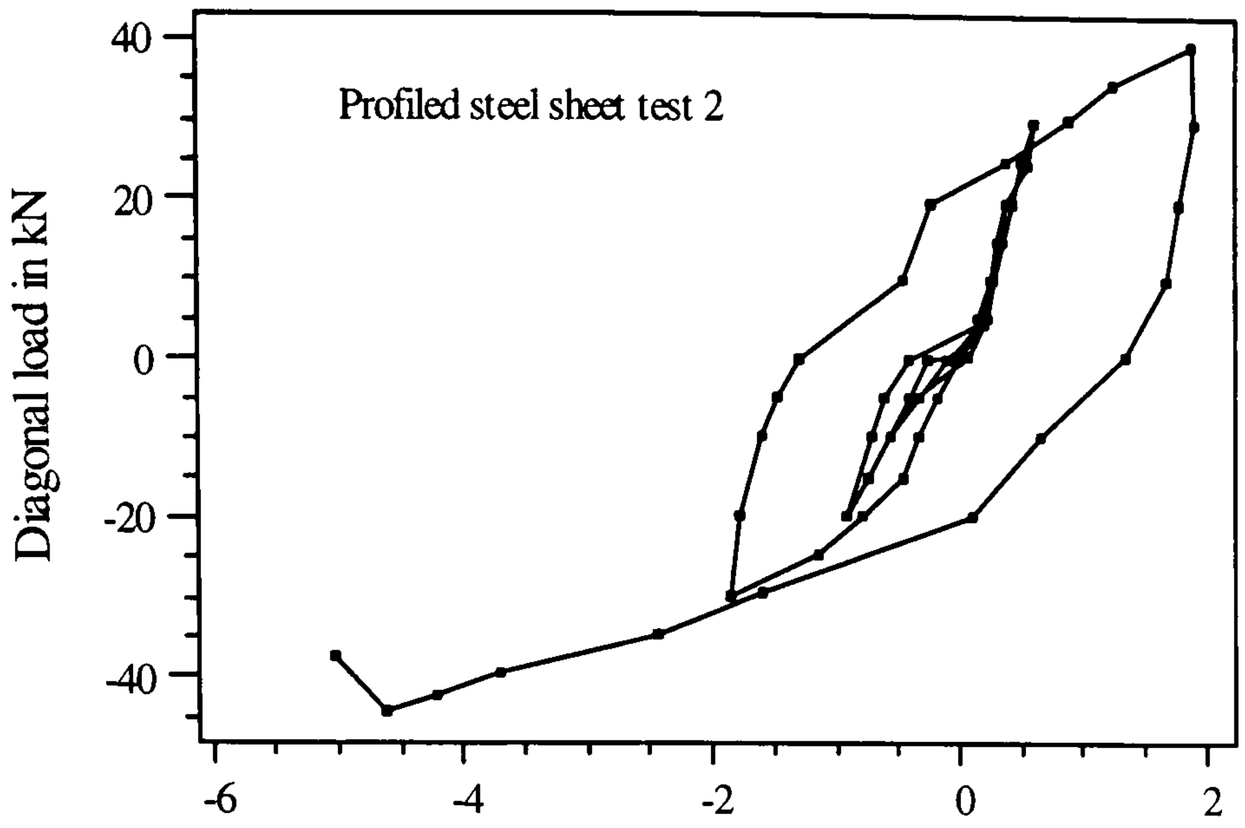

Figure 5.11(b): Load-deformation response

The load -deformation response from test 3 is shown in figure 5.11(c). The stiffness of the panel varies between 16.96 to 18.93 kN/mm before the failure of spot weld at about 20kN and averaged as 17.87. A typical load-deformation response of spot weld is presented in figure 5.11(d) from sample tests. The test specimens of sheeting spot welded to steel plate were tested under tensile load.

The movement (s) due to sheet deformation at the weld can be taken as 0.1236mm/kN. The ultimate load depends on the type of failure. The ultimate strength of the weld where failure was due to tearing of sheeting was around 4.48kN. But in cases when weld failed before tearing of the sheeting. The ultimate strength ranges from1.7-2.5kN as shown in figure 5.11(d).

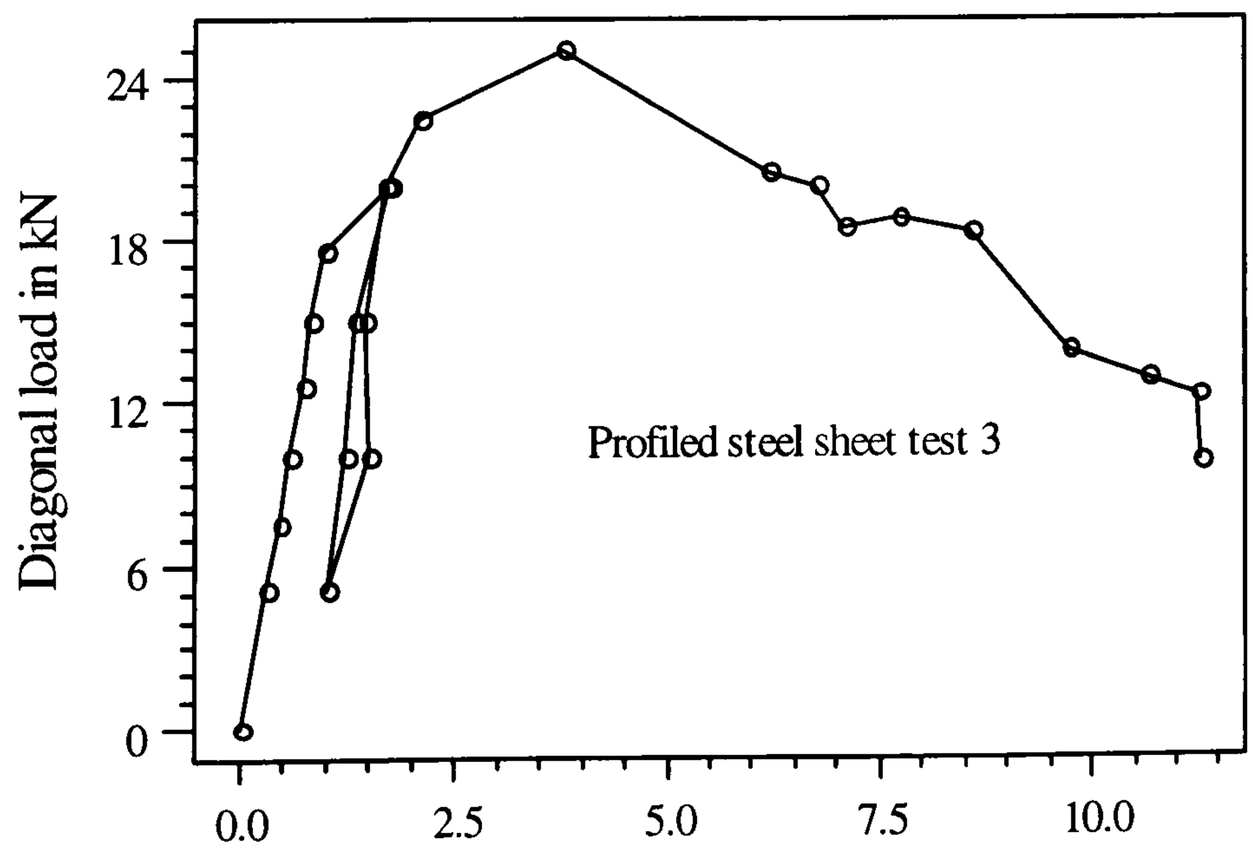

Figure 5.11(c): Load-deformation response

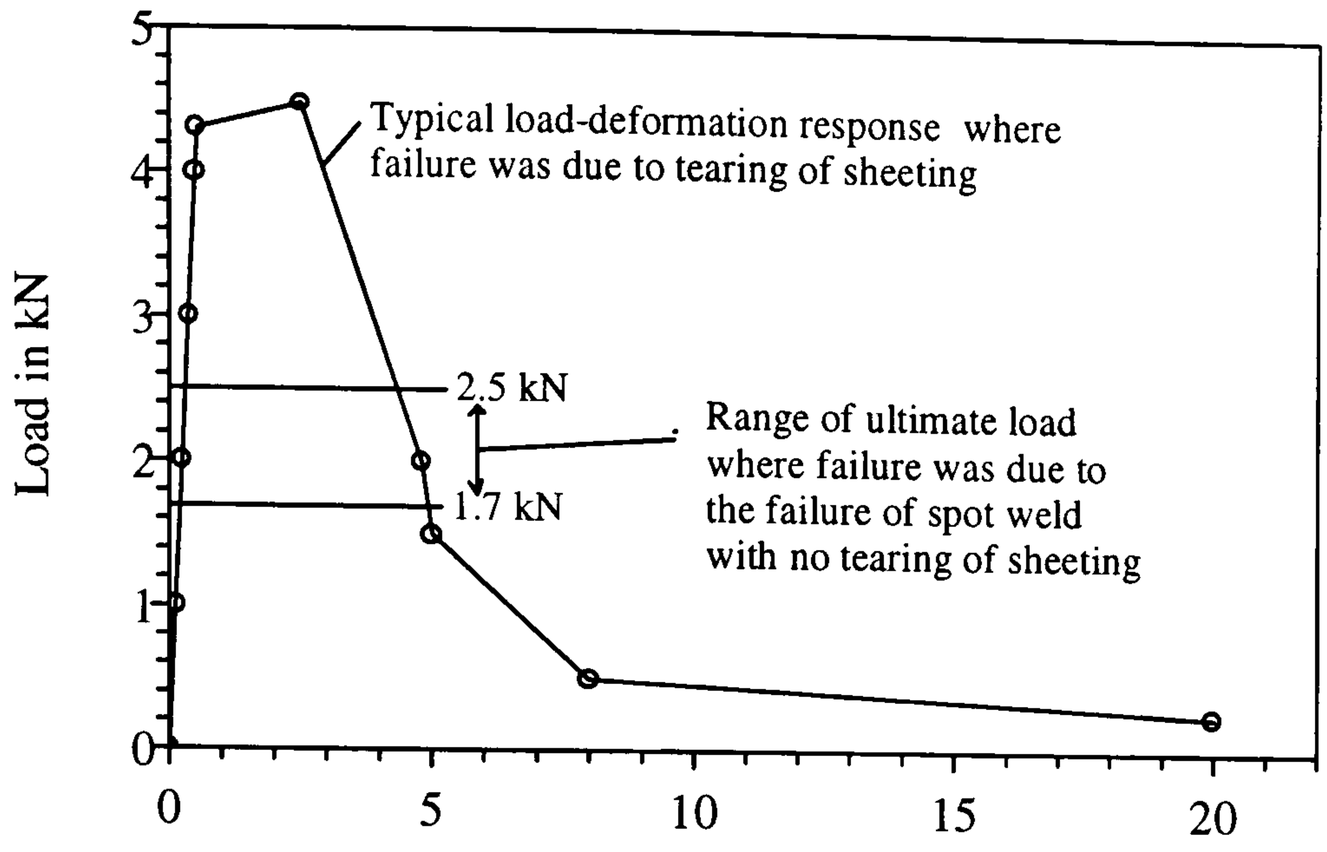

Figure 5.11(d): Typical spot weld response

The stiffness and ultimate load are summarised in table 5.2. The ultimate load from test 2 is 14% lower than that from test1. The stiffness (tensile part) are found to be in good agreement. The ultimate load of test 3 is around half of test 1 & test 2 while the stiffness is found to be around one third.

The post-critical shear reserves are not taken under consideration according to section 5.2.4.2 and 5.3.2 in the proposed analytical model and as a result the buckling load will be considered as the ultimate load of the panel. This will give a factor of safety of around 1.20 for test 1.

Table 5.2: Ultimate load and stiffness values

Test No.	Boundary condition	Buckling load kN		Ultimate load kN		Stiffness kN/mm	
		Diagonal	Shear	Diagonal	Shear	Diagonal	Shear
1	clamped	42.0	29.70	52.0	36.80	56.5	28.25
2	clamped	40.0	28.20	-45.0	-31.80	53.0	26.50
3	spot welded			25.0	17.68	17.87	8.935

5.4.2.2 Failure modes

Test 1

Figure 5.12(a) shows the location of localised buckling and extended tension field for the test panel 1. From table 5.3 it is found that the locations on the crest buckled

downward and most of the trough locations buckled upward. The tension fields extended up to 20 to 35% of the total length at failure.

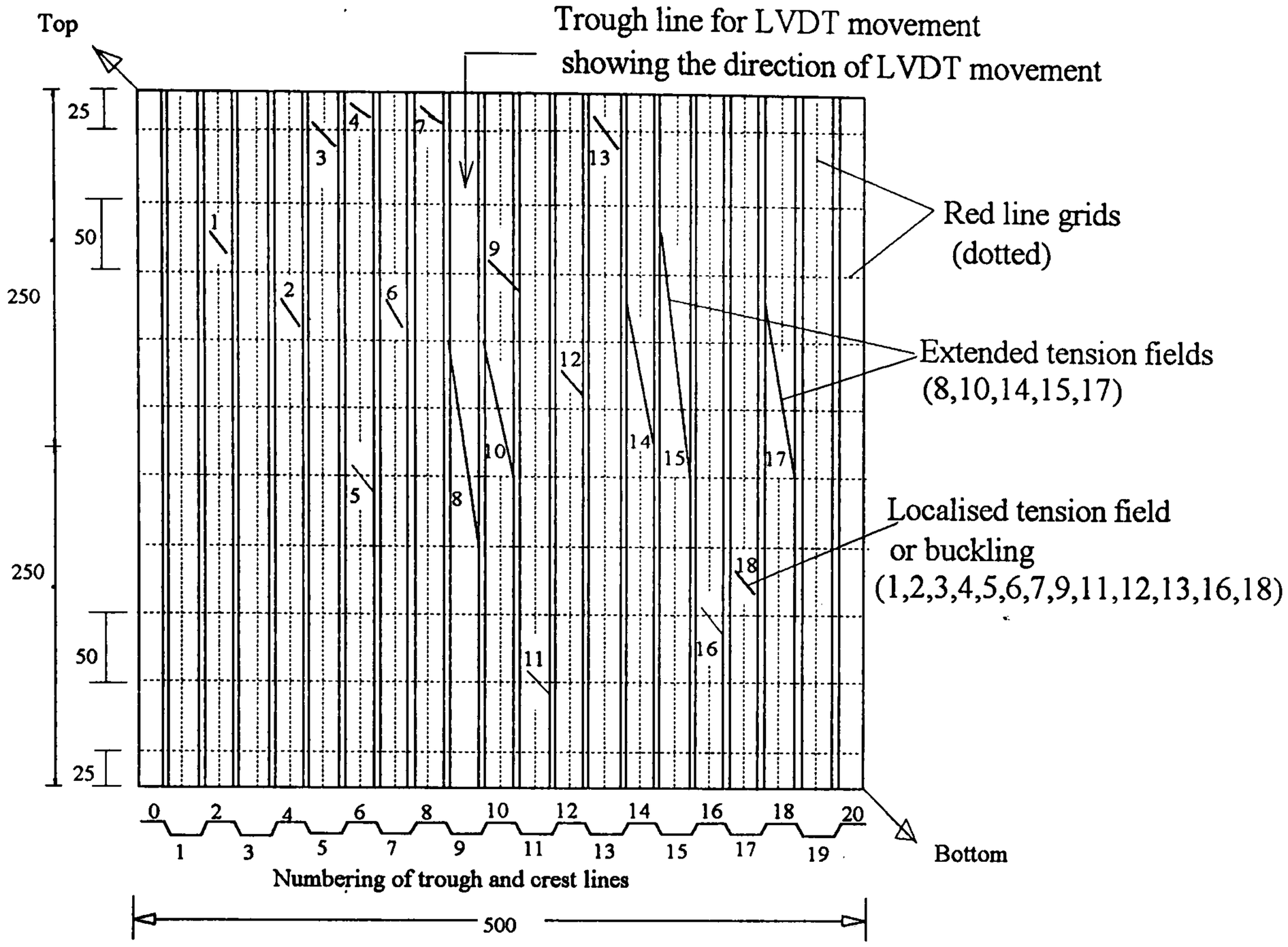

Figure 5.12(a) : Tension field diagram (Test 1)

Table 5.3: Analysis of tension field

Test no.	Localised buckling downward		upward		Extended tension field downward	length	ratio	upward	Length	ratio
1	1c	9c	3t	13t	10c	100	0.2	8t	150	0.3
	2c	12c	4c	16c	14c	100	0.2	15t	175	0.35
	5c		6t	18t 7c				17c	125	0.25
2			3t		1c	150	0.3	2t	150	0.3
3	4c				2c	200	0.4	1t	100	0.2
	5c				6c	100	0.2			
					3t	350	0.7	3t	350	0.7
'c' indicates crest points ' t' indicates trough points					ratio=tension field length/length of trough or crest lines length in mm					

Test 2

The extended tension field and local buckling of the panel at failure is shown in figure 5.12(b). The panel was failed under compression diagonal load rather than tension in test 1 and as a result the direction of the tension field is different. They may actually follow the direction of major principal direction. The tension fields are analysed in table 5.3 and they seem to be extended up to 30% of the total length of trough or crest lines.

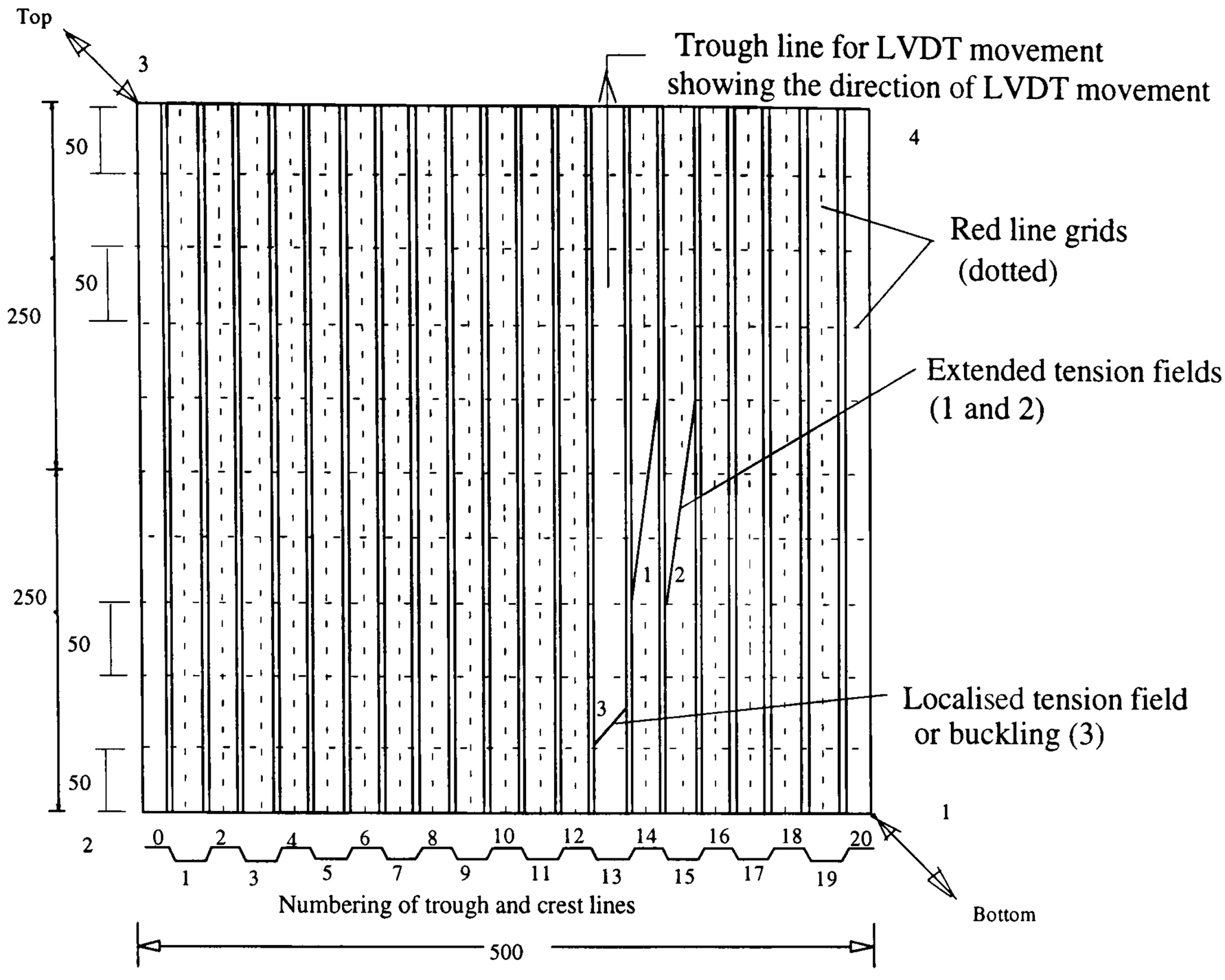

Figure 5.12(b): Tension field diagram (Test 2)

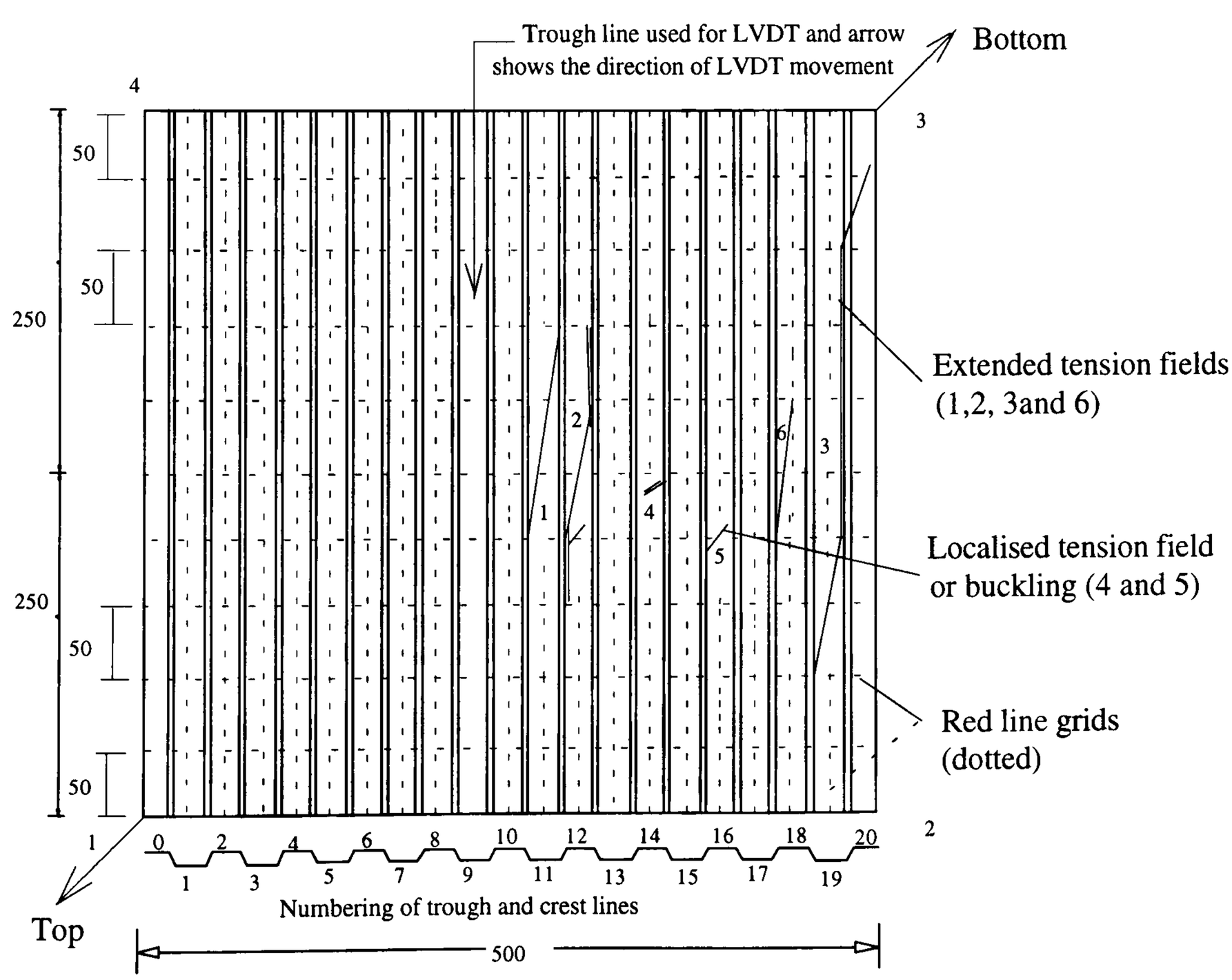

Figure 5.12(c): Tension field diagram (Test 3)

Test 3

The locations of tension fields are shown figure 5.12(c) . The direction is similar to that of test 1 as both panels were tested under tensile diagonal load. The extended length of the tension fields (table 5.3) ranges between 20 to 70% of the total length of trough or crest lines of the panel.

Remarks

Test 1 and test 2 showed an unstable post-buckling behaviour leading to a sudden snap-through type buckling. As a result, the failure of the panel was noticed immediately after buckling which suggests that post-critical shear reserves should not be considered in design.

The failure of the panel in test 3 was due to the failure of spot weld and tearing of the sheeting at the weld location along the profiled boundaries with subsequent buckling and twisting of the sheeting.

The failure of all the panels are characterised by the formation of local and extended tension fields associated with local and global buckling. Local buckling seems to be restricted to the plane part of the folds of the cross section. Extended tension fields while crossing the folds forced the sheeting to loose its geometric shape. As a result the sheet yielded and lost its stiffness very rapidly in the post -buckling stage.

The direction of tension fields seems to follow the principal direction. The length of the extended tension fields in test 3 is supposed to be higher (maximum up to 70%) than those in test 1 and 2 (maximum 35%)

5.4.2.3 Analysis of buckling pattern

Test 1

The failure of the model panel was associated with the formation of waves of buckles. Figures 5.13 show the typical pattern of buckling of trough and crest lines of profile. Most of the buckles are half waves besides some full waves.

Test 2

The buckled waves at trough and crest lines 13,14 and 15 is presented in figure 5.14. As in test 1 , maximum of them are supposed to be half waves.

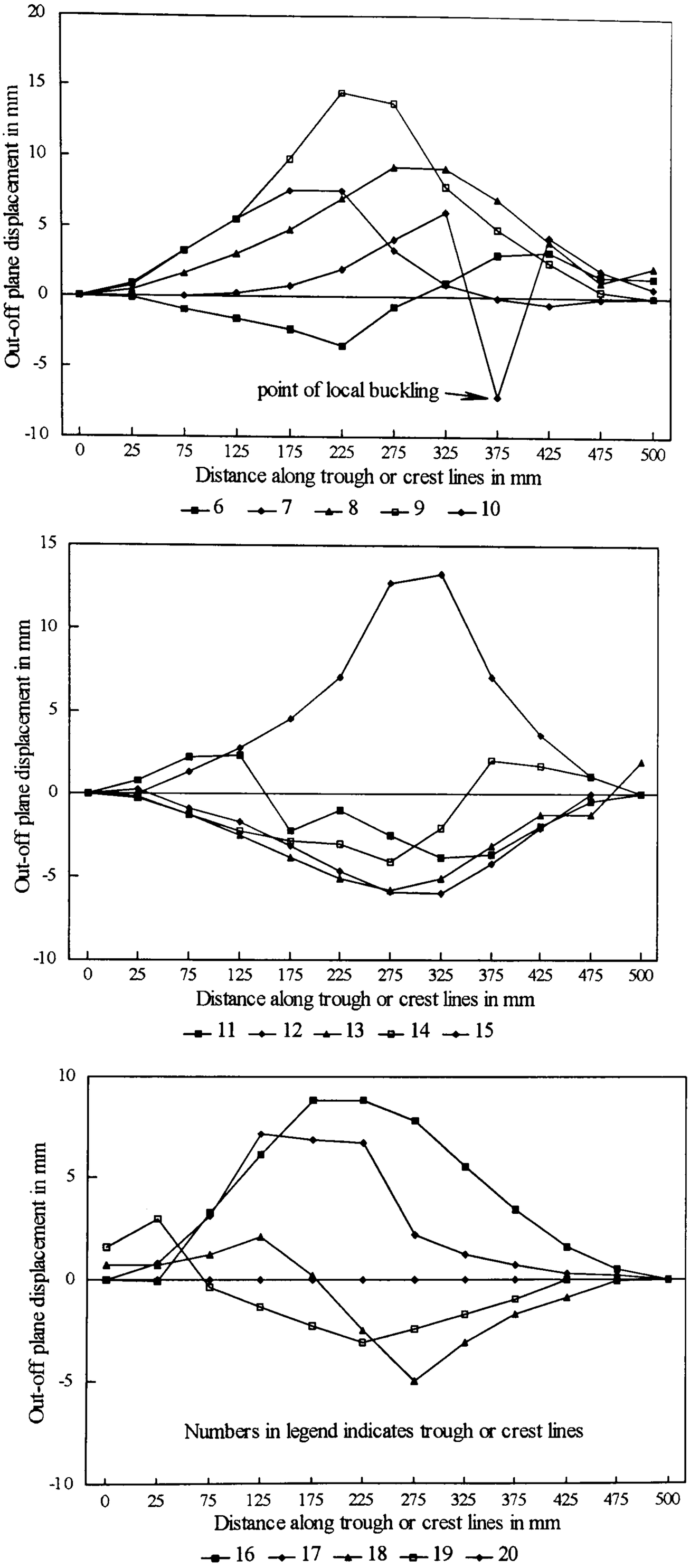

Figure 5.13: Buckling of sheeting in test 1

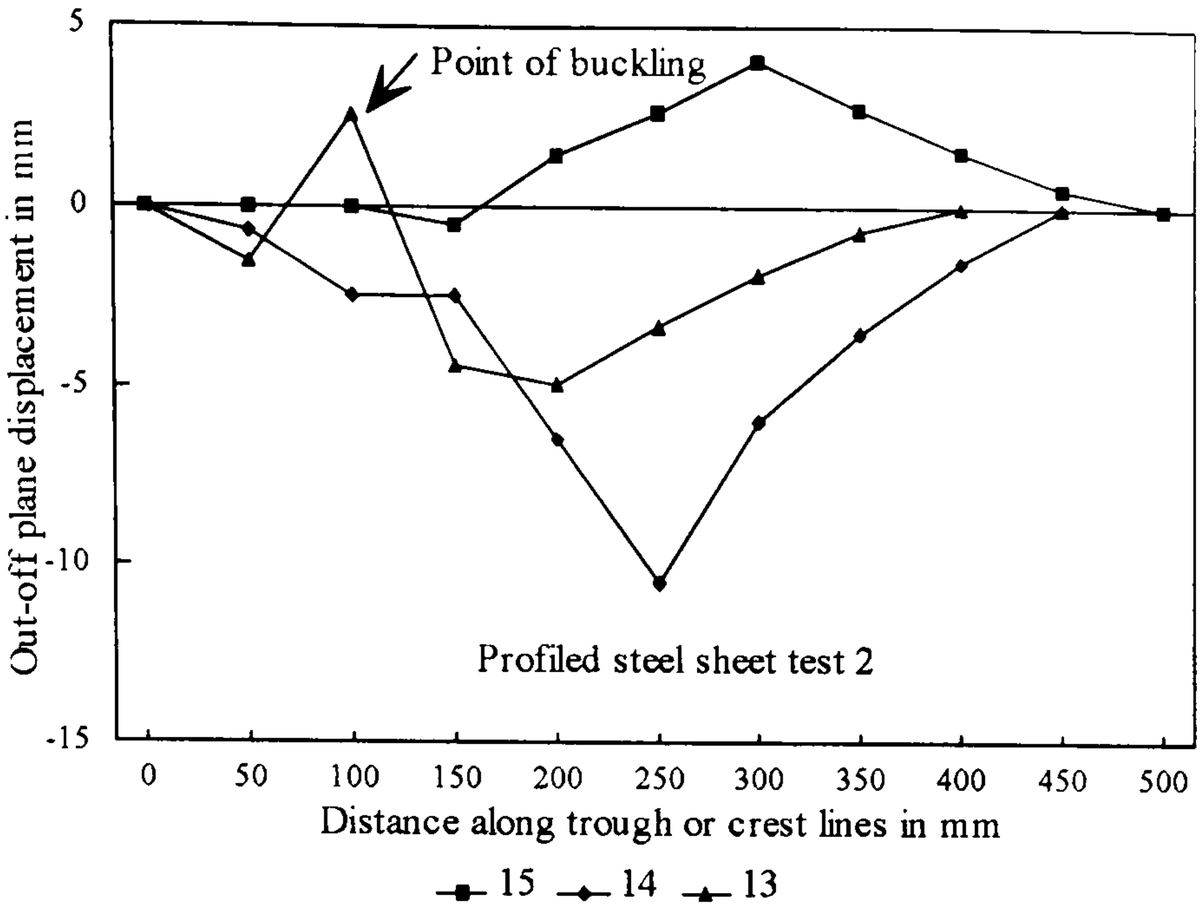

Figure 5.14: Buckling of sheeting in test 2

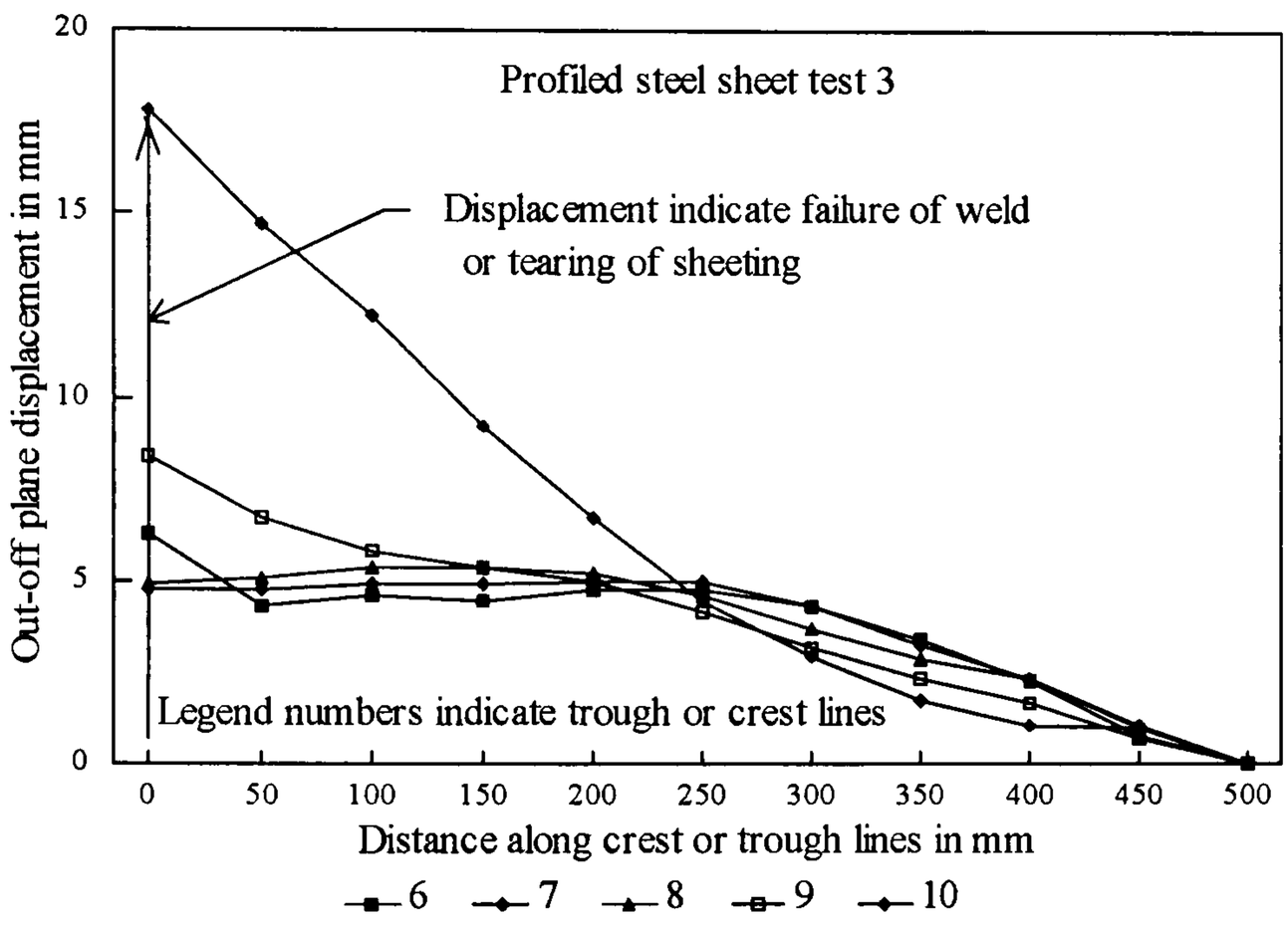

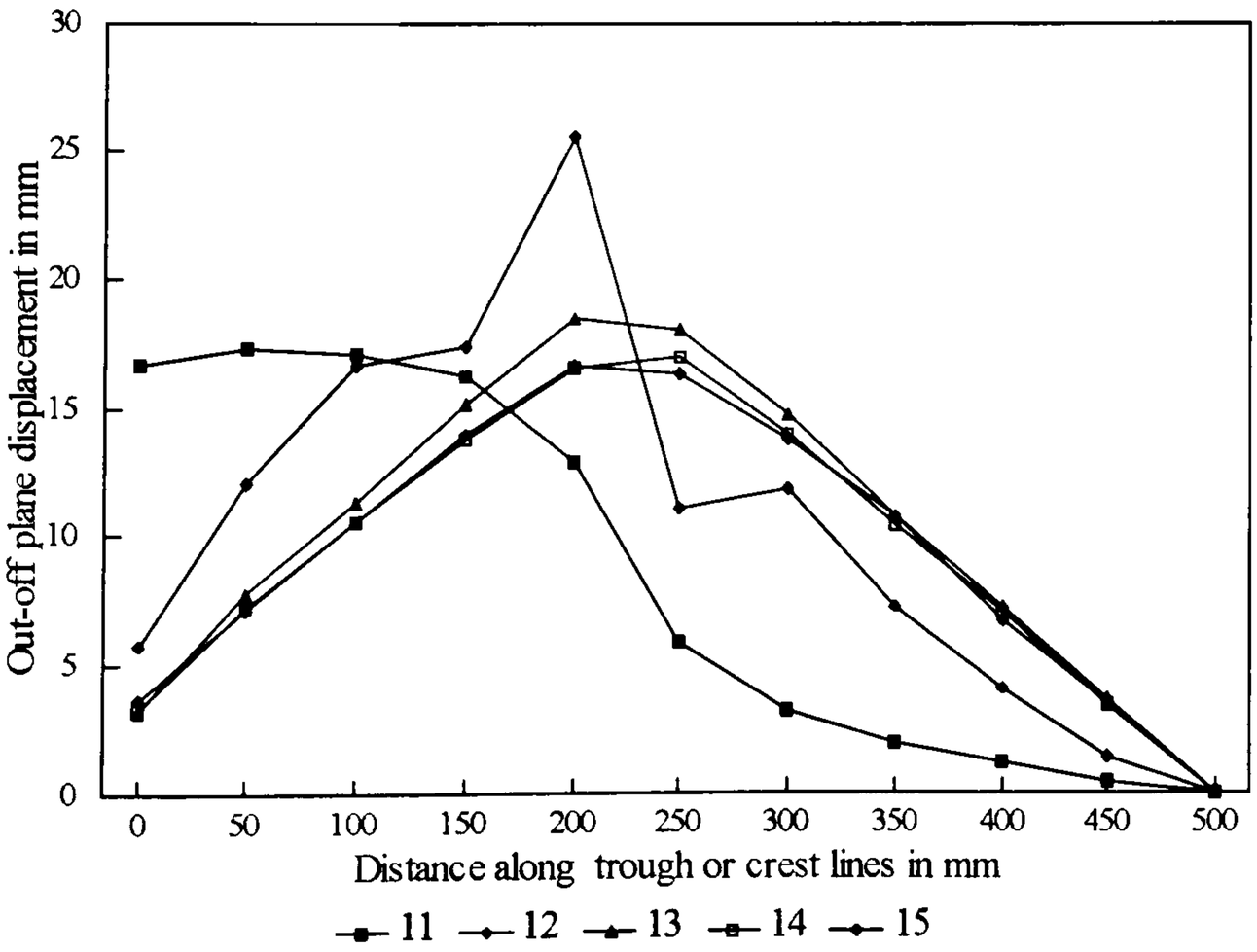

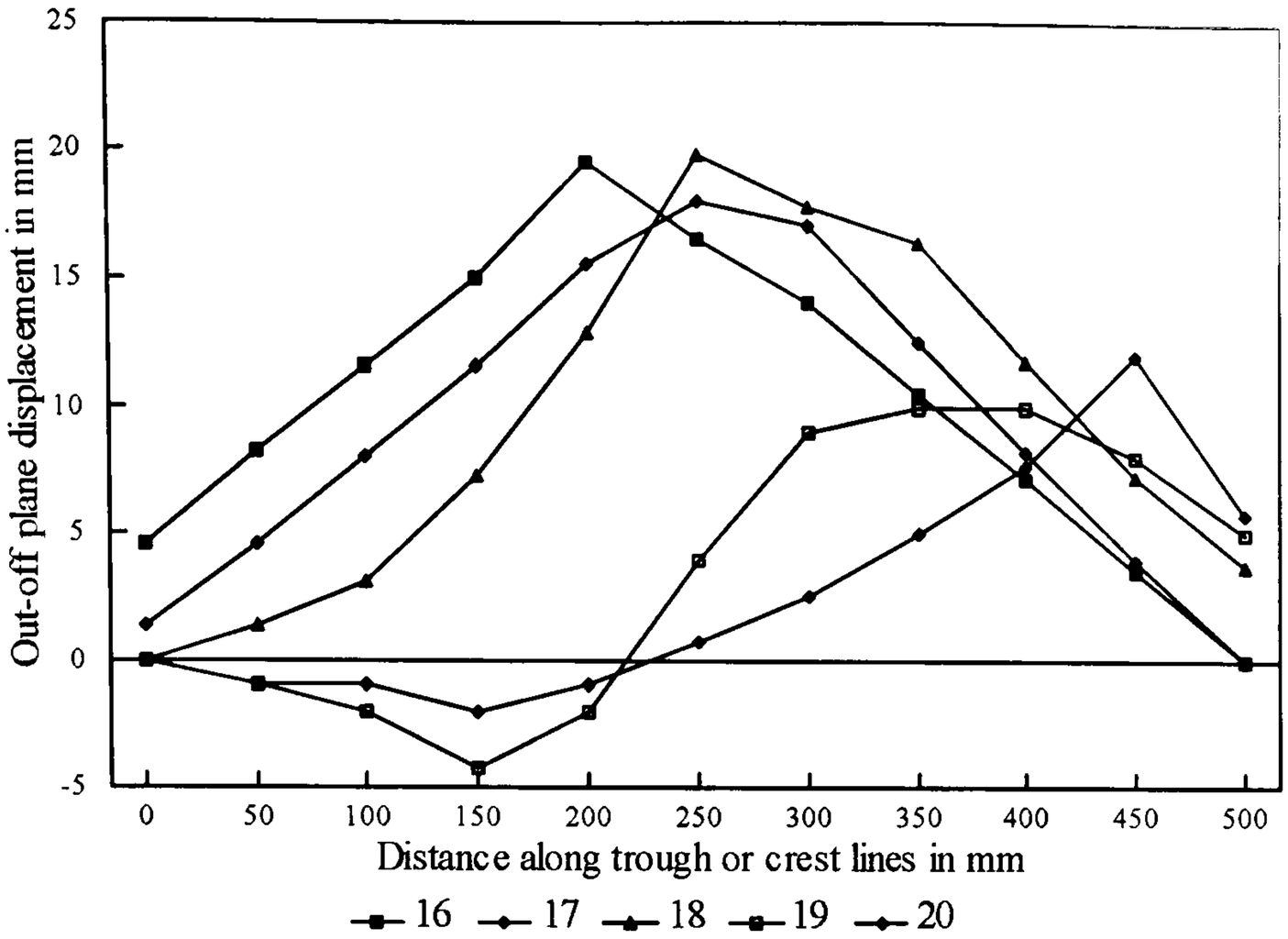

Figure 5.15: Buckling of sheeting in test 3

Test 3

The buckling mode of trough or crest lines is shown in figures 5.15. Most of the buckles are half waves except 19 and 20. The failure of weld or tearing of the sheeting can be identified from the displacements occurred at 0 and 500mm.

Remarks

The buckling waves are found to be similar apart from the large out of plane displacements due to failure of weld or tearing of sheeting in test 3.

5.4.2.4 Analysis of strain results

Strain along the loaded and off-diagonal

Test 1

The variation of diagonal strain is shown in figures 5.16 . The loaded diagonal is found to be under tension and off-diagonal is under compression throughout the loading history. The tensile strains at gauge locations along the loaded diagonal are more less equal varying linearly up to the buckling load and in the post-buckling stage gauges 2 and 5 are supposed to be yielded. The variation of compressive strain at gauges on the off-diagonal are identical but strain in gauge 11 is higher.

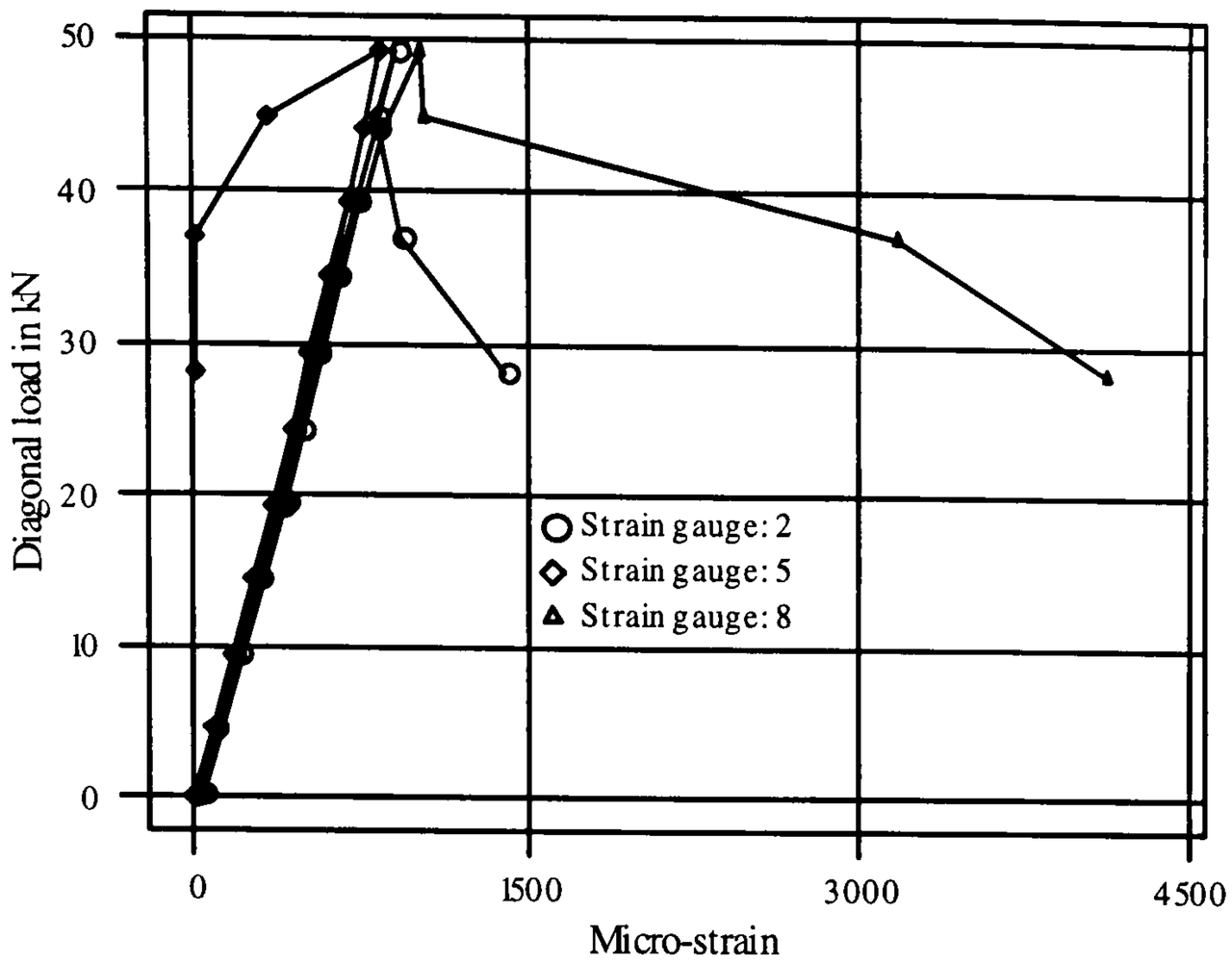

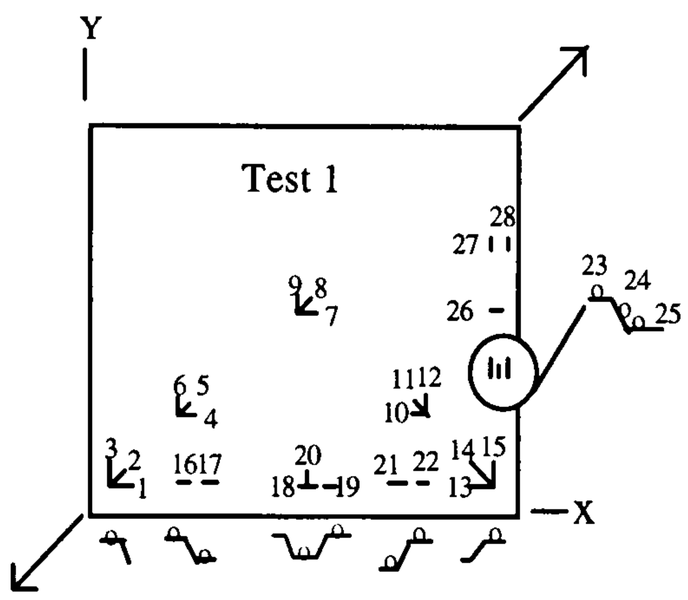

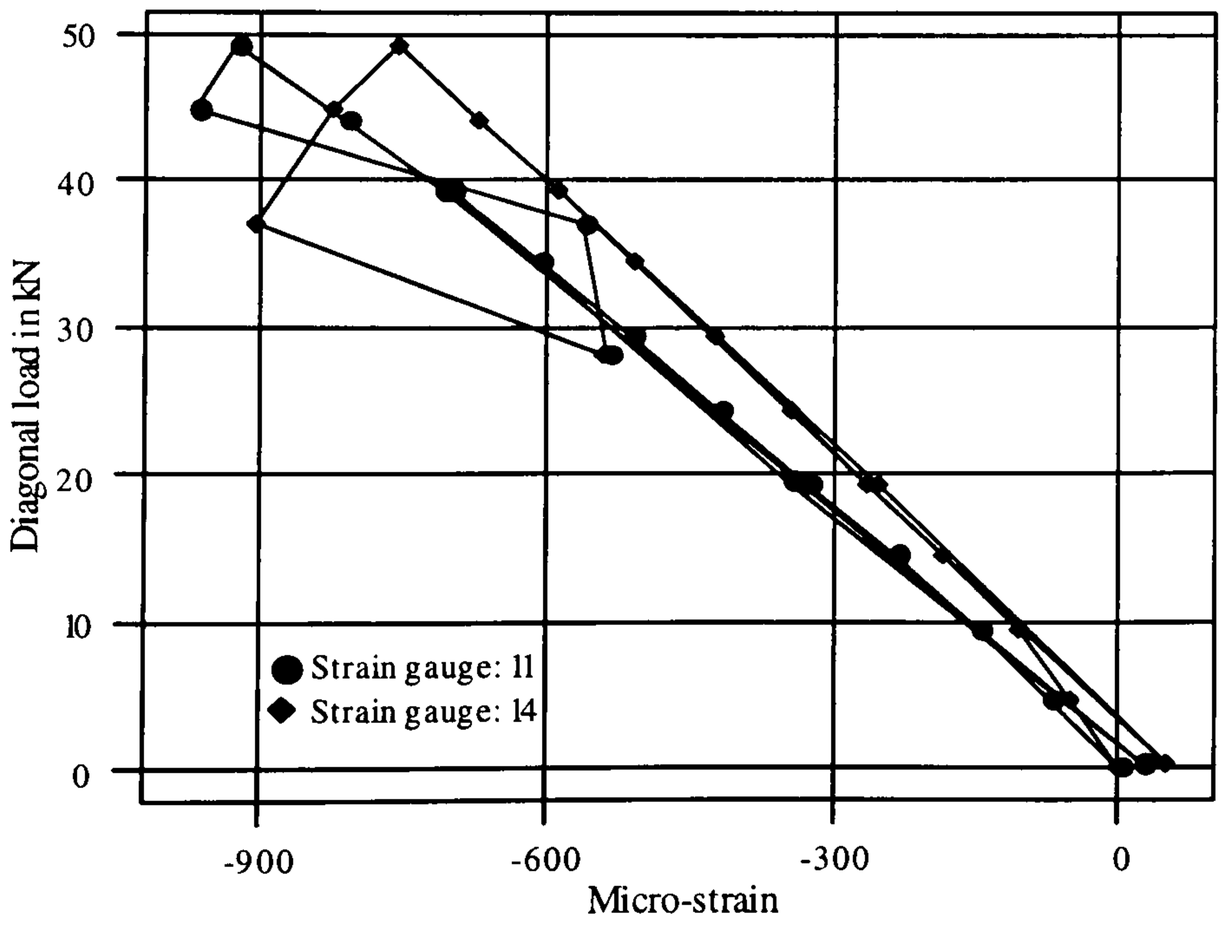

Figure 5.16: Variation of diagonal strains

The variation of principal strain (ε) and principal direction are shown in figures 5.17. Major and minor principal strains are found to be nearly equal for rosette 1 and 4. But for other rosettes the ratio of major and minor principal strain ranges between 1.22-1.65. This may be due to the profile geometry of the panel.

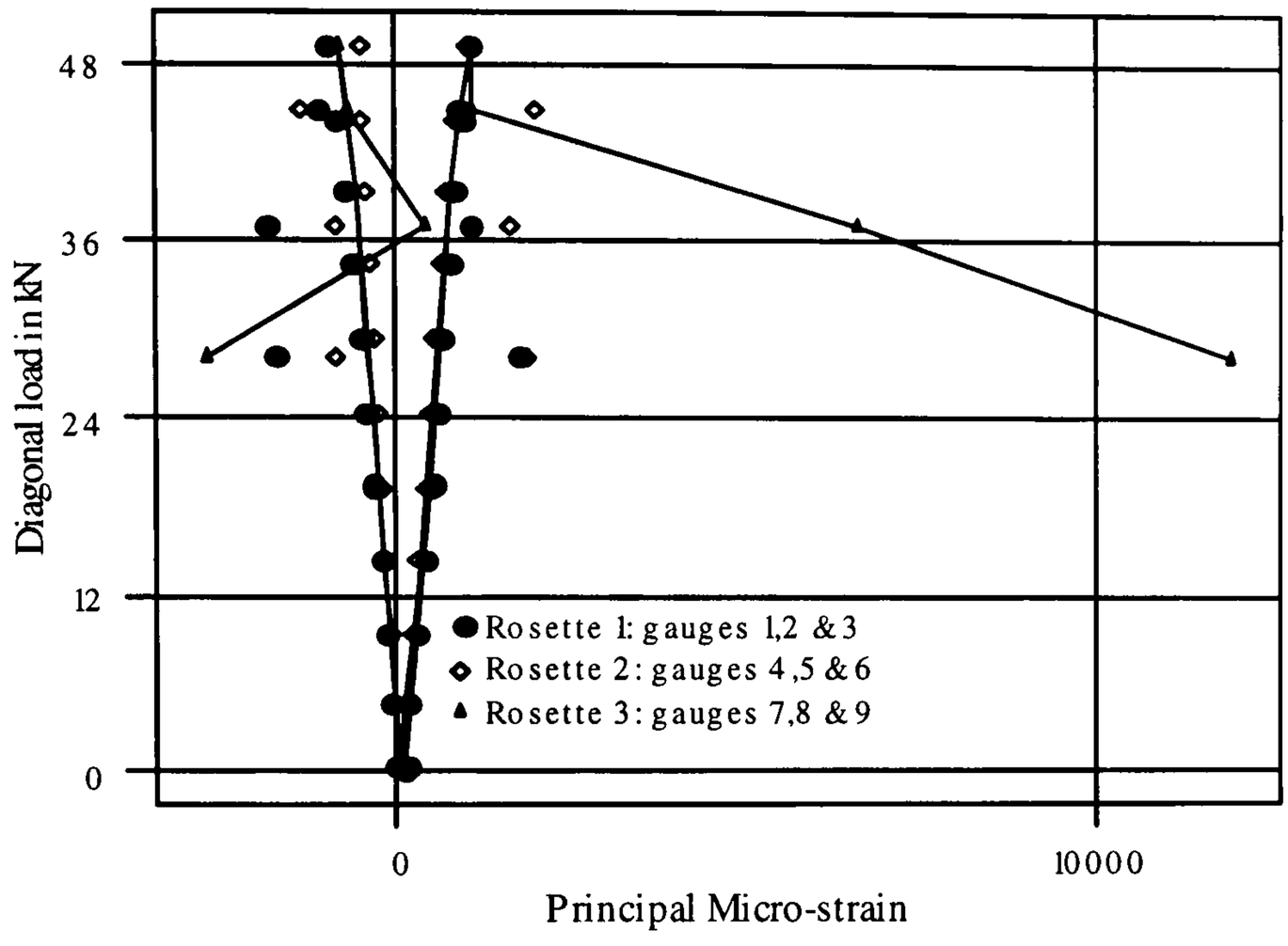

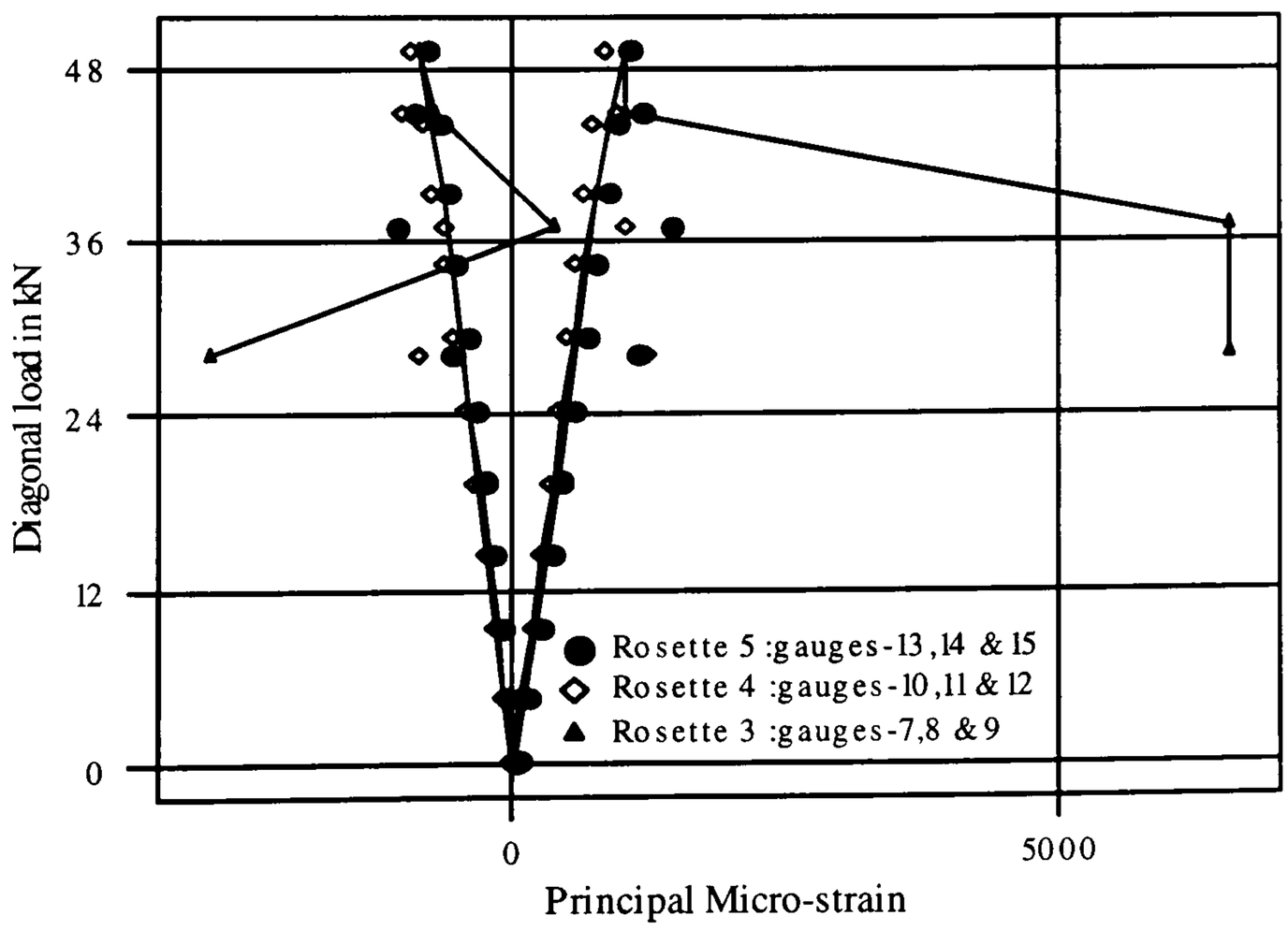

Figure 5.17(a): Variation of principal strains

The principal direction ranges between 34.75-38 degrees for rosette 1, 36.75-40 degrees for rosette-2, 48.5-49 degrees for rosette-3, 41.5 degrees for rosette-4 and 48.5-49 degrees for rosette-5 in the pre-buckling stage.

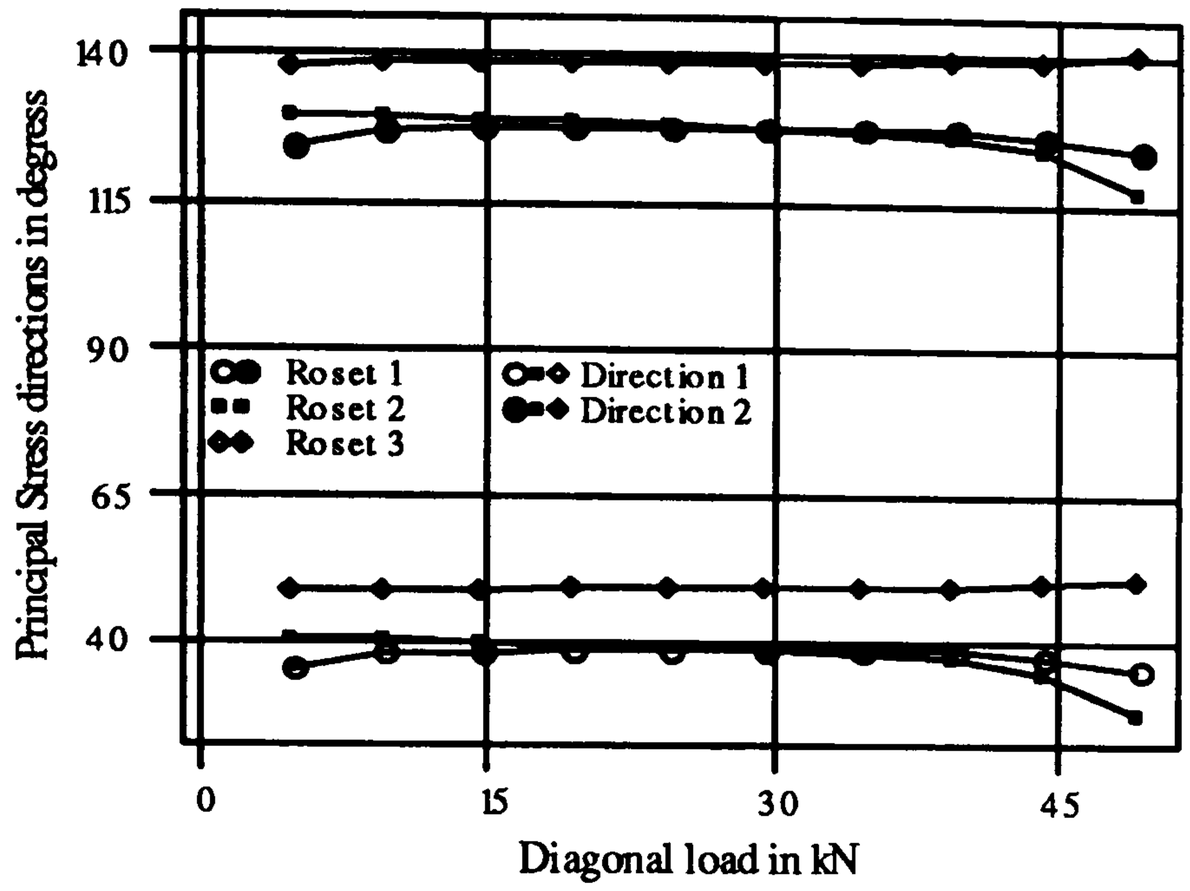

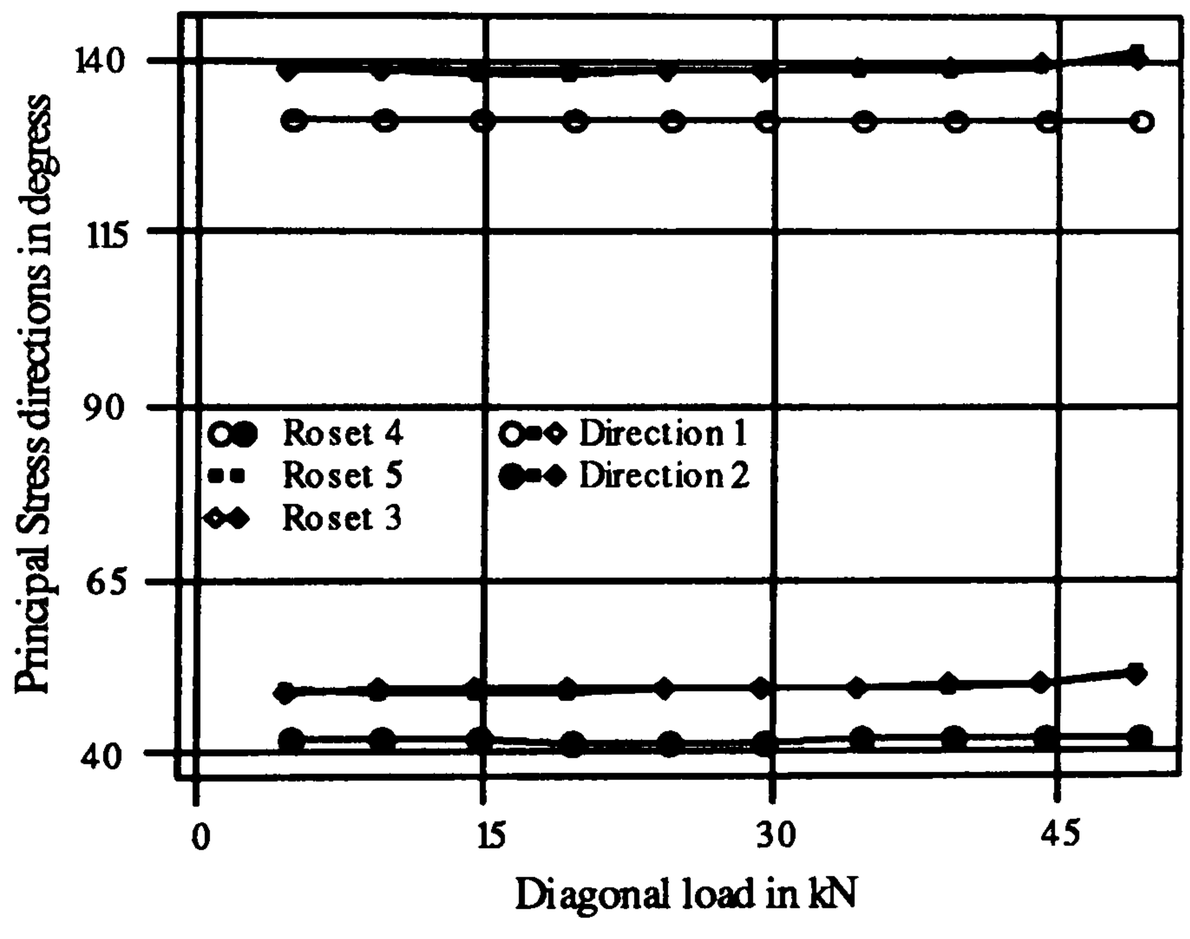

Figure 5.17(b): Principal direction

Test 2

Diagonal strain at gauges 2,10,4,6,11 and 8 on loaded and off-diagonal clearly identify the reversal of strain during cyclic application load as confirmed from the distinctive

hysteresis loops. A few of them are shown in figures 5.18. The two diagonals are found to be oppositely strained in either tension or compression..

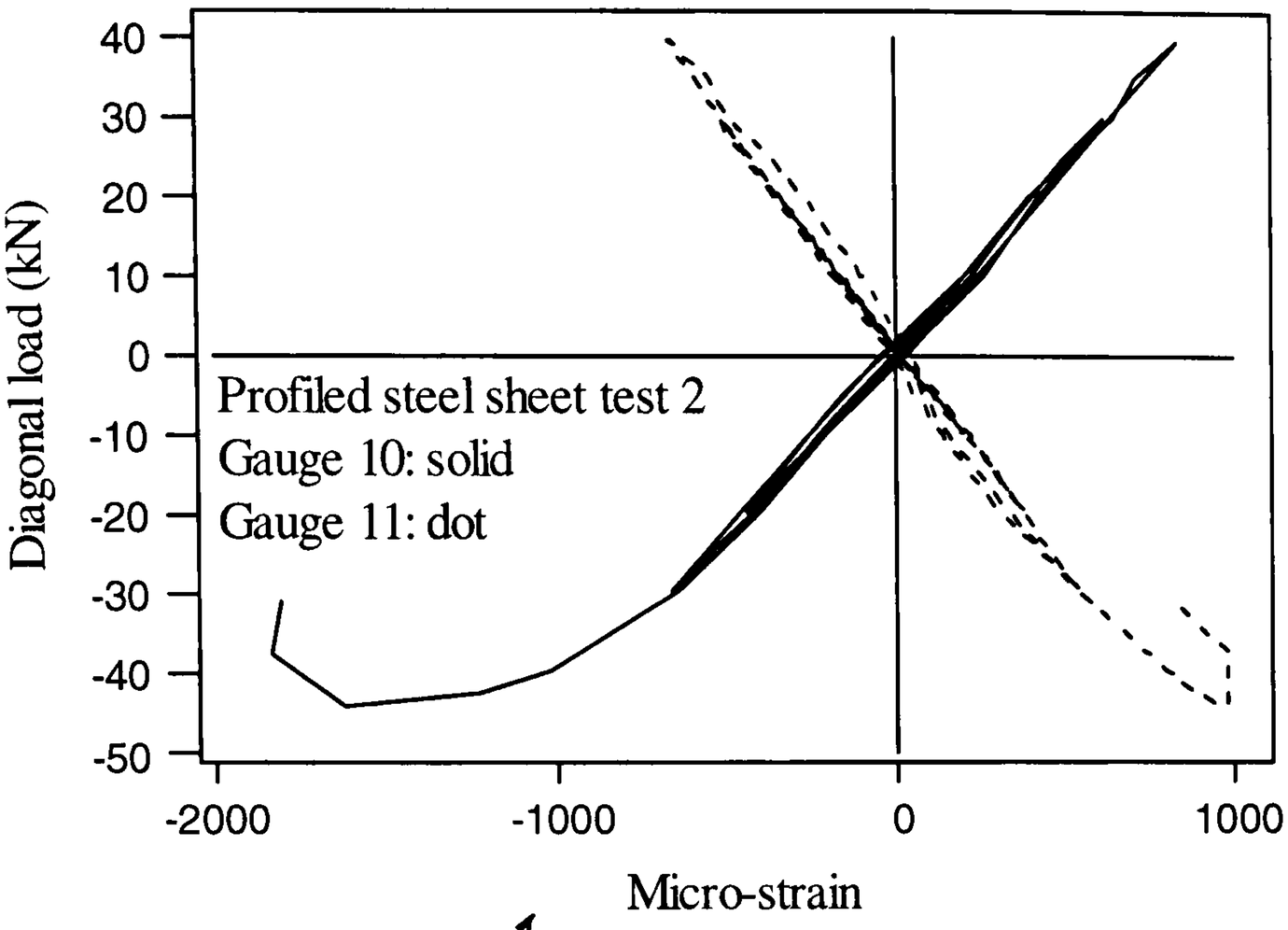

Figure 5.18: Hysteretic loops for the diagonal strains

A typical variation of principal strains under hysteretic load at rosette locations on the diagonals are presented in figures 5.19.

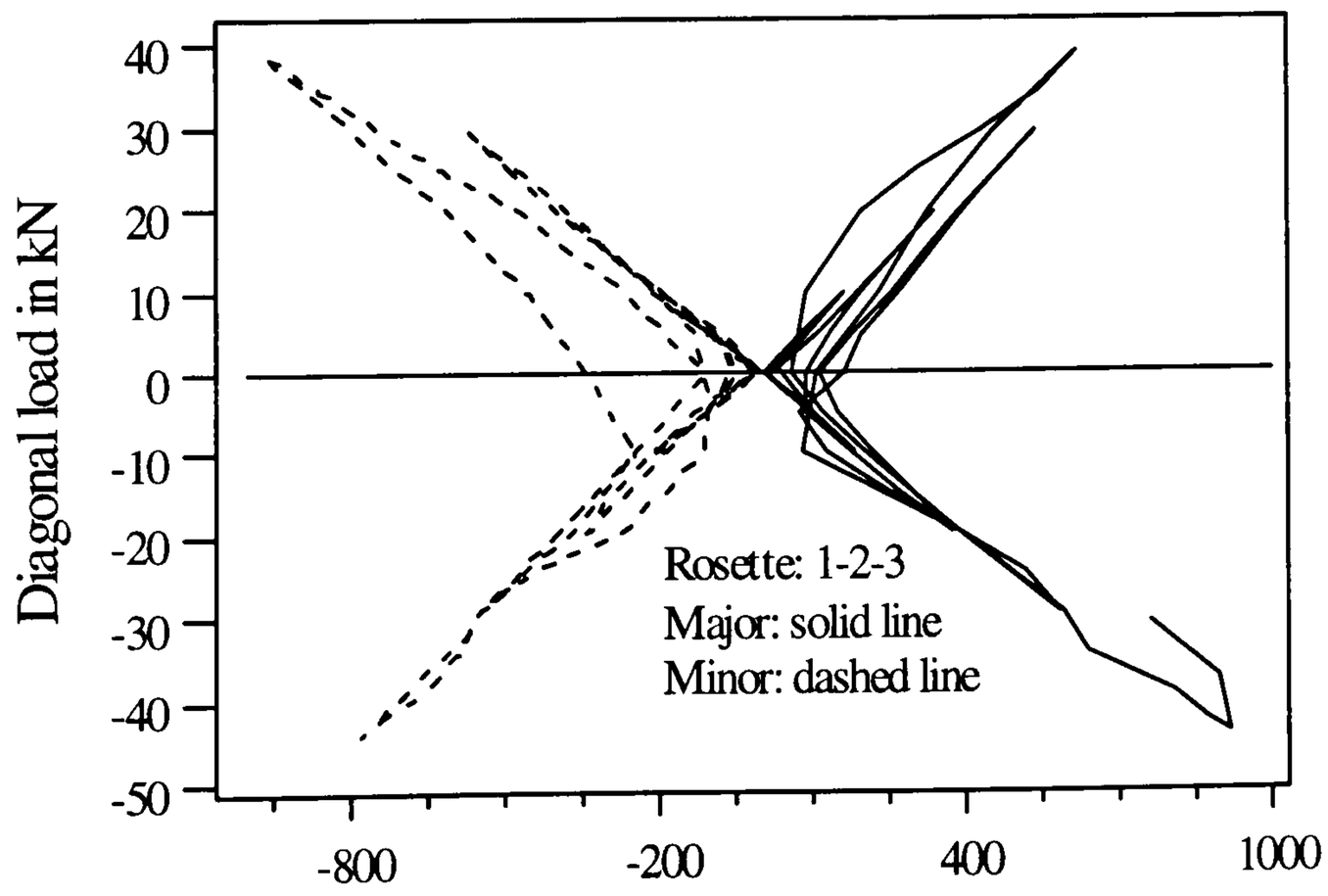

Figure 5.19(a)

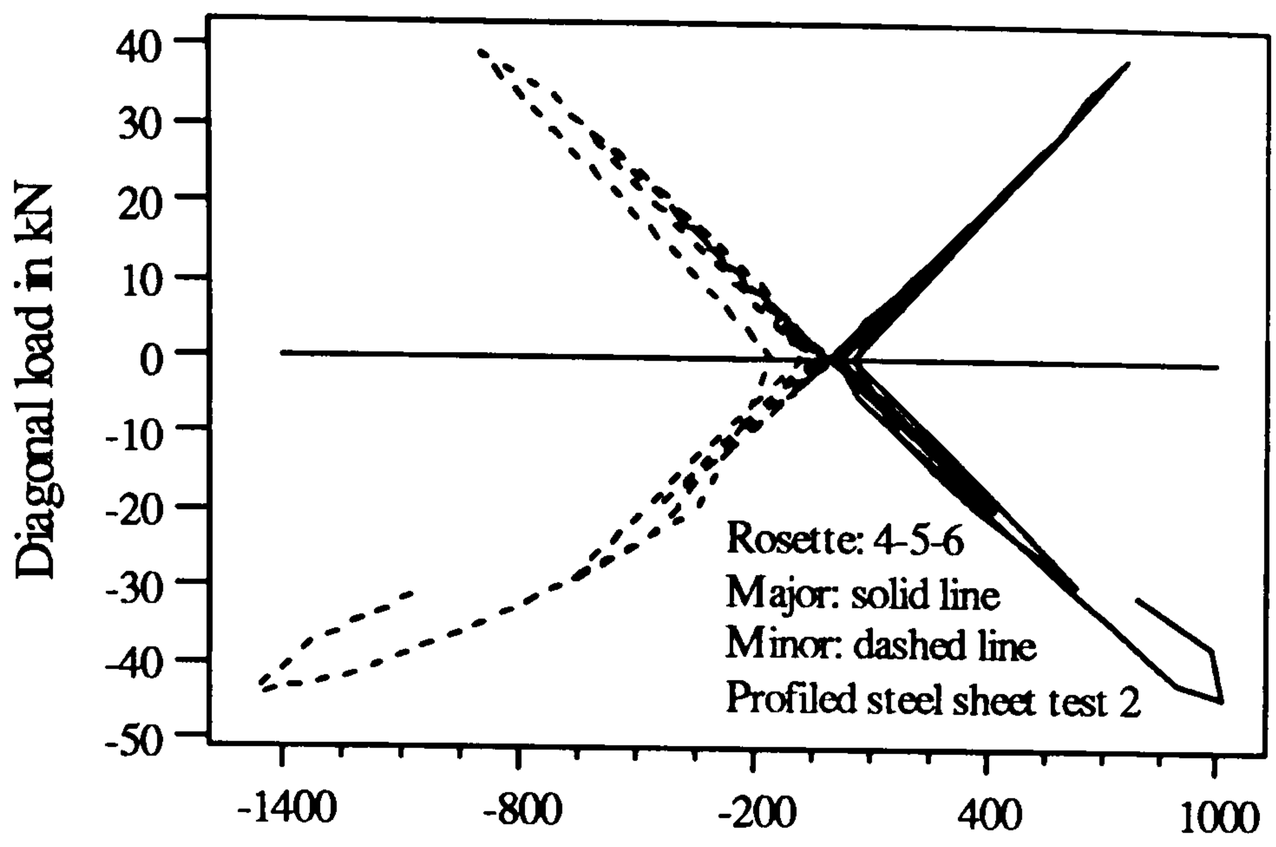

Figure 5.19(b)

Figure: 5.19: Typical variation of principal strain under hysteretic load

The two parts, tension (+ ve) load part and compression (-ve) load part, of major or minor principal strains shown in figures are actually working perpendicular to each other. Residual strains are observed during loading and unloading but the variation can be considered as linear up to the diagonal load of about 30kN. The ratio major (ε_1) and minor(ε_2) principal strains during cycles of loading are tabulated below (table 5.4). The principal strains in rosette 4-5-6 seems to be more or less equal. The hysteretic load seems to have no effect on the range of principal strain ratios.

Table 5.4: Principal strain ratios

Load range	Rosette 1-2-3	Rosette 4-5-6	Rosette 7-8-9
0 to +25 kN	0.76-1.25	0.83-0.96	1.12-1.30
+25 to 0	0.74-1.29	0.87-0.99	1.18-1.44
0 to -30	0.74-1.25	0.92-0.98	0.72-1.01
-30 to 0	0.84 -1.27	0.84-0.93	0.69-0.80

Comparative study

Principal strains and directions from test 1 and test 2 are compared with those from test 3 in figures 5.20 and 5.21. Initial part of the strain curves (up to 30% of ultimate load) from test 3 seems to be in good agreement with test 1 and test 2. After that strains seems to be higher than those from test 1 and test2. But for one of the corner rosette 10-11-12, minor principal strain are in agreement up to the failure load but major principal strains are not in agreement. The figures 5.20 show good agreement of principal strains between test 1 and test 2. The figures 5.21 also show good agreement between principal direction in two tests.

.

This proves the consistency of the tests. But the principal directions (figures 5.21) in panel 3 are not in agreement with those from test 1 and 2. Thus spot welded boundary condition affects the strain conditions within the panel.

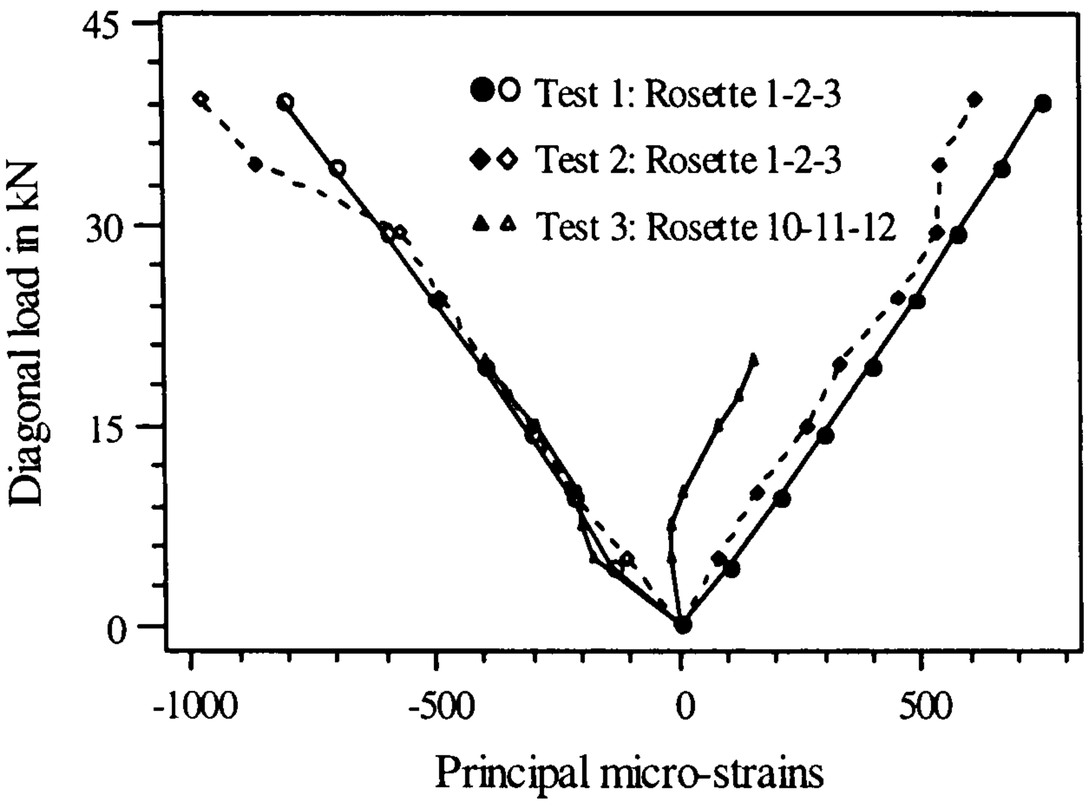

Figure 5.20(a)

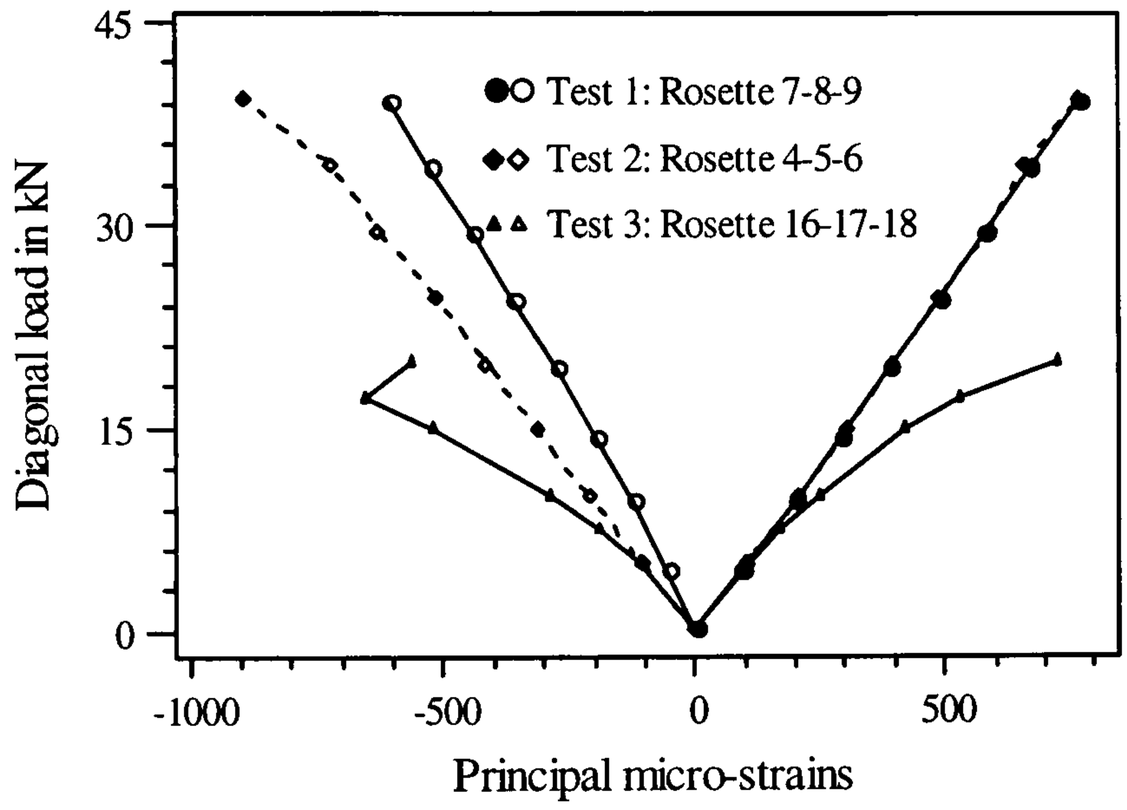

Figure 5.20(b)

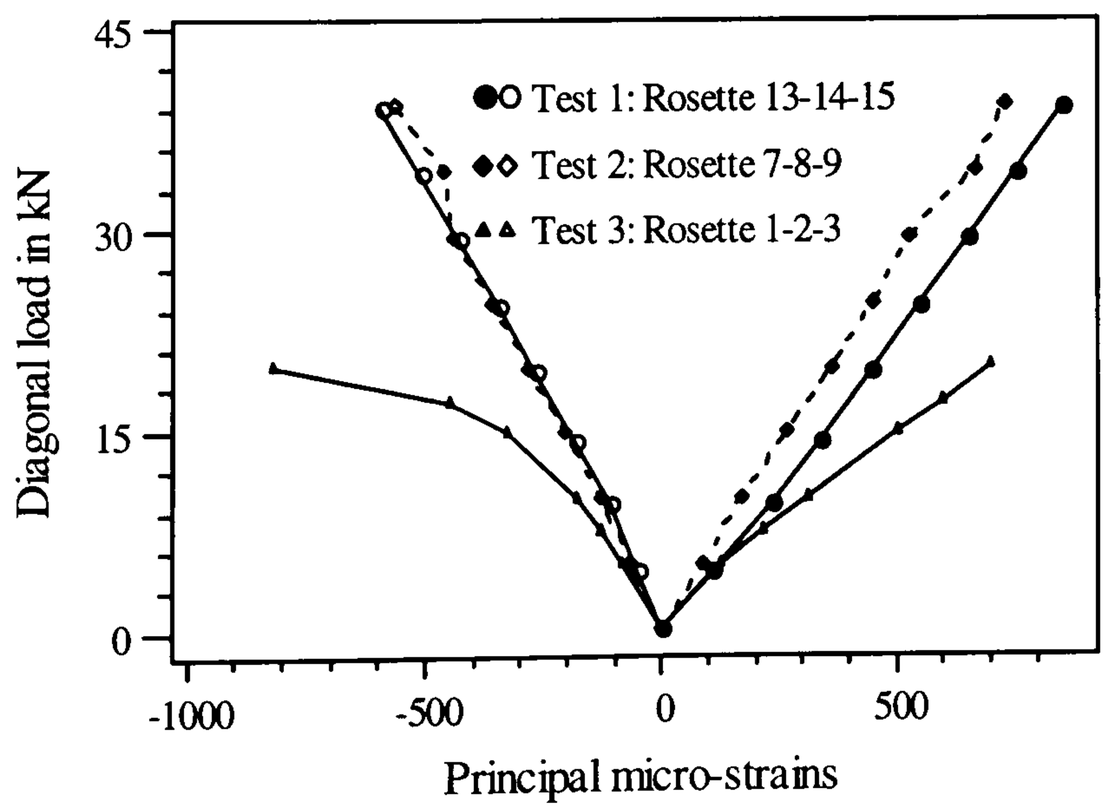

Figure 5.20(c)

Figure 5.20: Comparison of principal strains

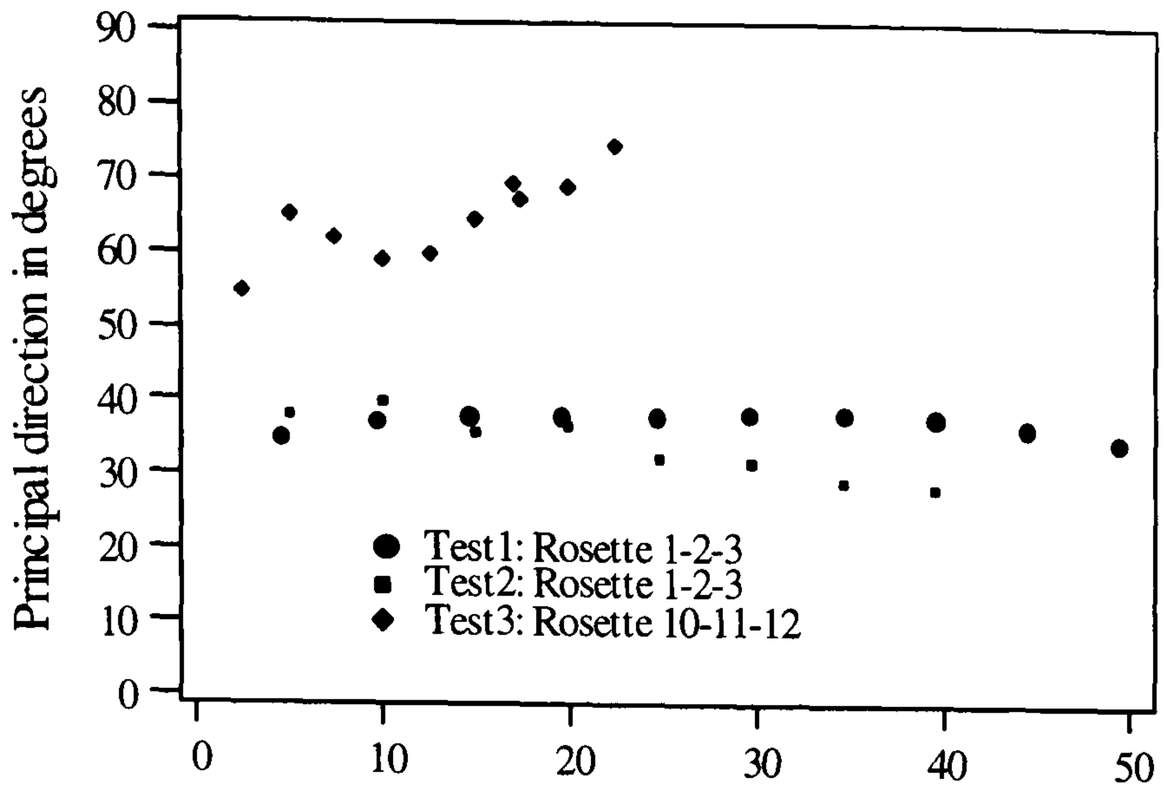

Figure 5.21(a)

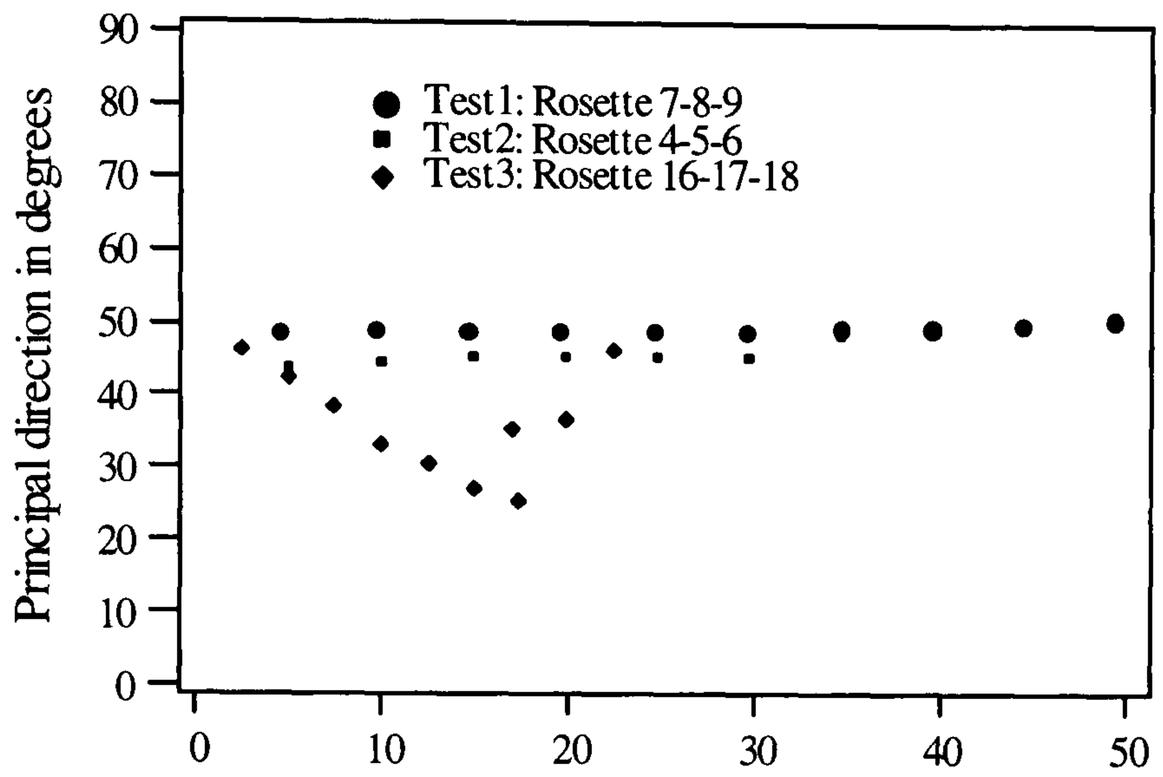

Figure 5.21(b)

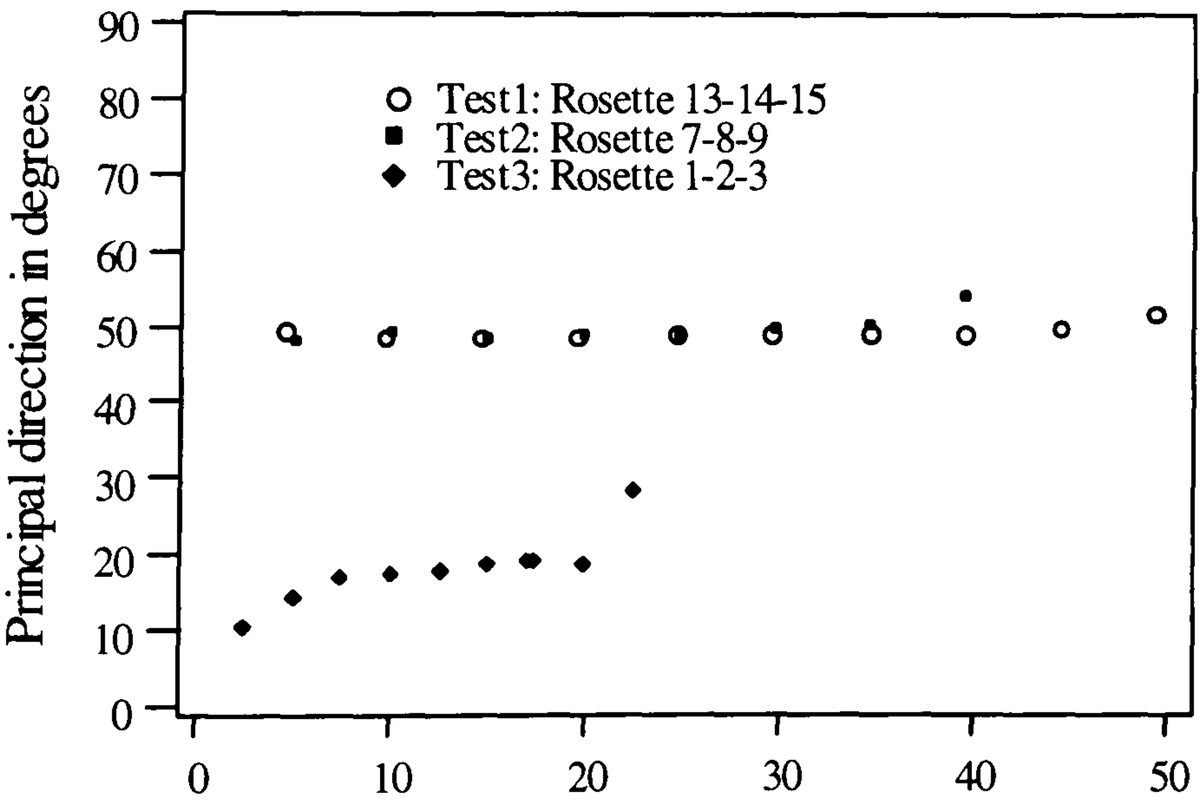

Figure 5.21(c)

Figure 5.21: Comparison of principal direction

Variation of strain along the boundaries

Test 1

Figures 5.22(a) and (b) show the variation of Y and X strains along the profile boundary based on the location of strain gauges. The Y strain seems to be tensile at the loaded corner and compressive at the off-loaded corner with nearly zero values at the centre. X strain seems to be compressive at the loaded corner and tensile at the off- loaded corner. Tension and compression zones have been formed in between them.

The variation of Y and X strains along the plain boundary is shown in figures 5.22(c) and (d). X strain seems to be varied from tension at off-loaded corner to compression at loaded corner with nearly zero values at the centre. The variation of Y strain shows variation from tension to compression at intermediate points.

Test 3

The variation of strain along the plain and profile boundaries are shown in figures 5.22 to compare with those from test 1.

Comments:

Based on gauge strains the variation of X -strain along the profiled boundaries can be qualitatively represented by :

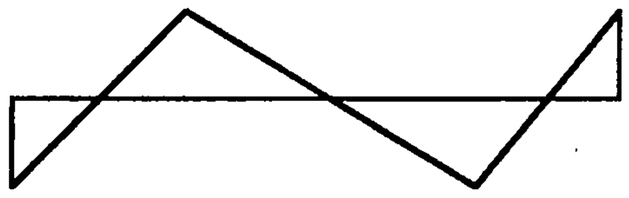

The variation of Y-strain along the profiled boundary and the variation of X-strain along the plain boundary both can be presented as :

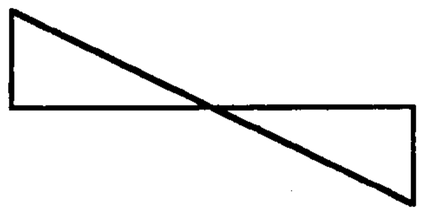

For Y strain along the plain boundary, no such generalised presentaion can be given.

The exact variation of strain can not be represented due to the lines drawn only through the gauge points and position of gauges on top or bottom surface of the sheet may change its sign.

The large strains along the profile boundary in the case of test 3 indicates the initiation of failure at that boundary.

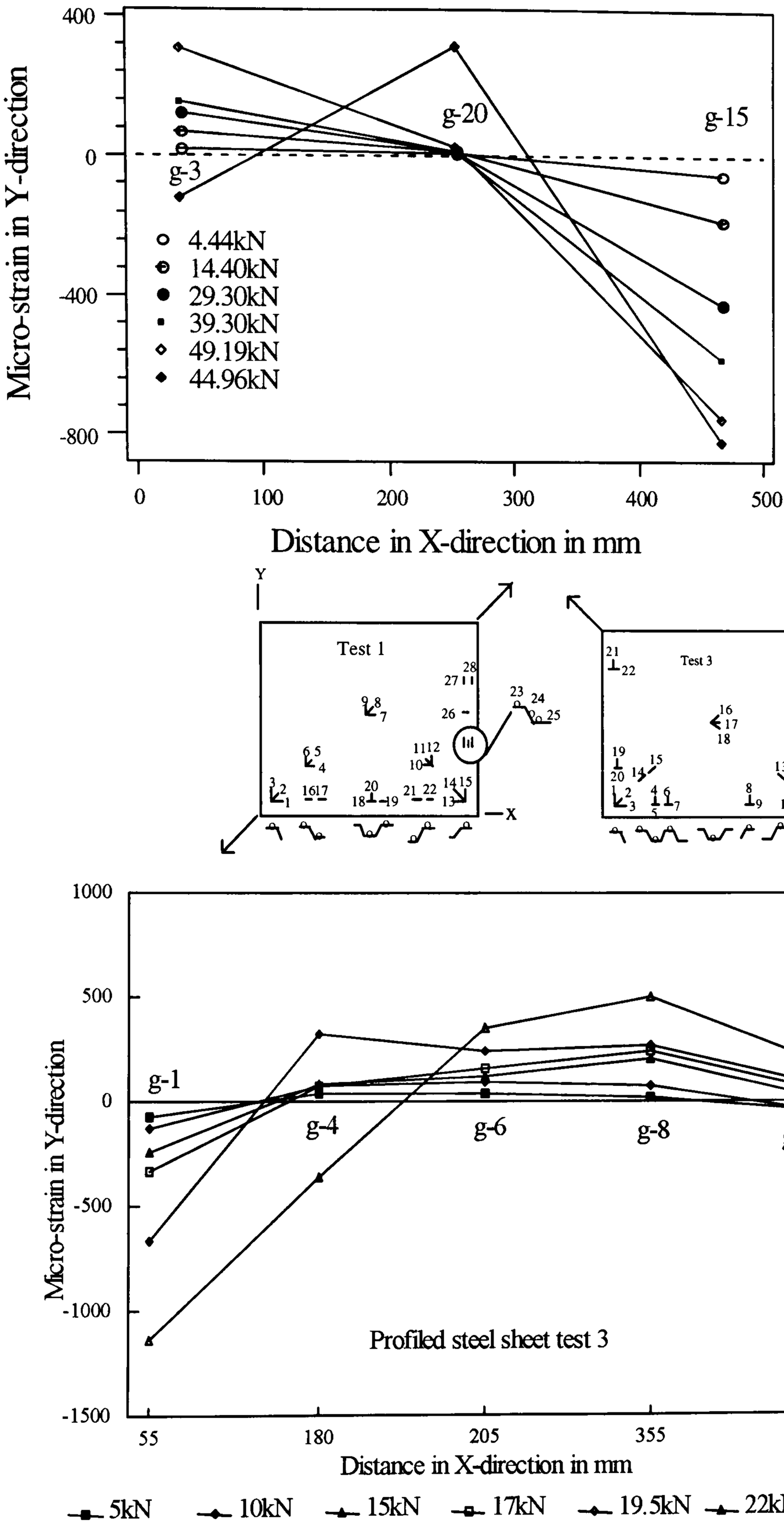

Test1

Figure 5.22(a): Variation of Y-strain along the profiled boundary

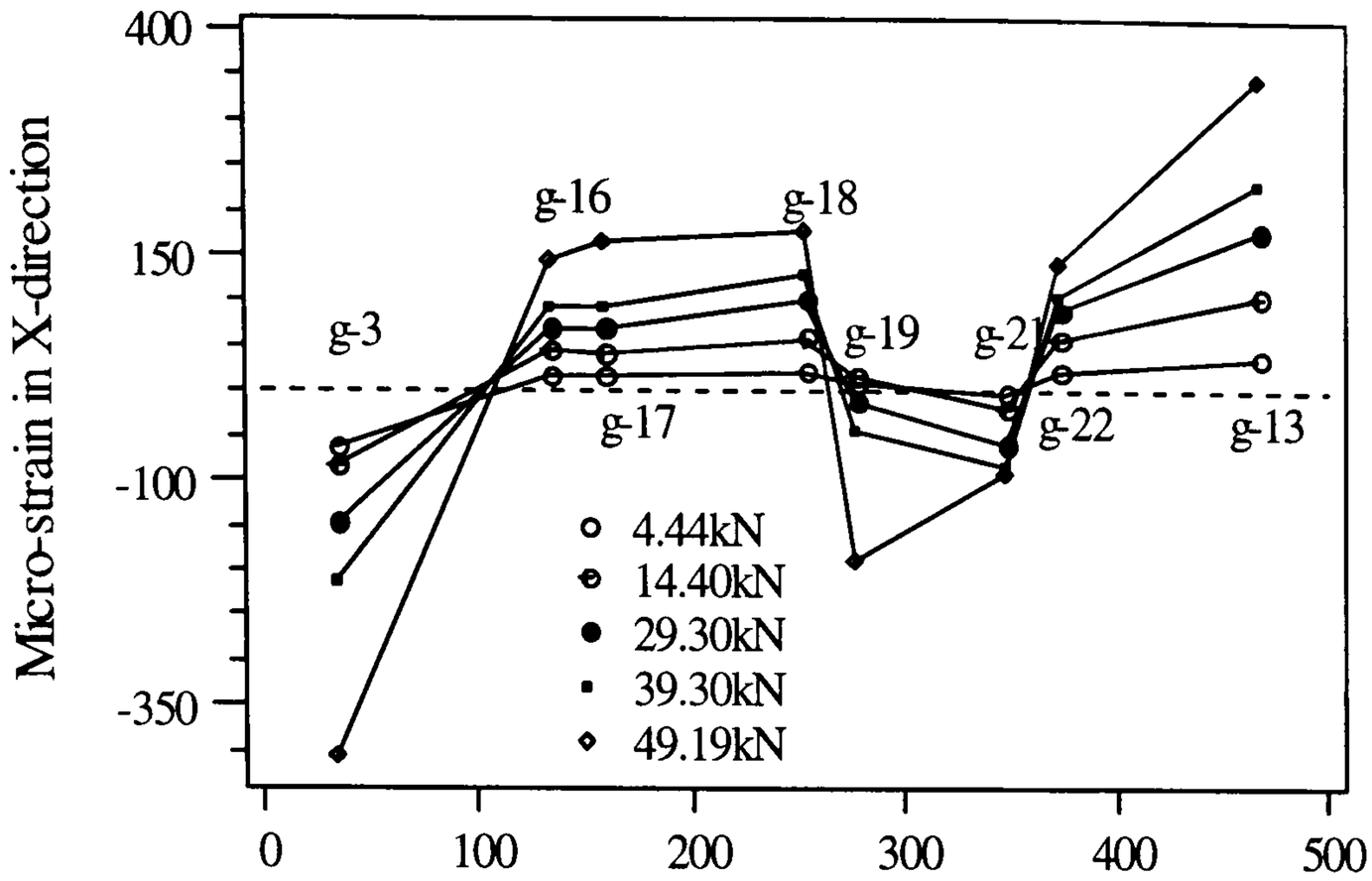

Test1

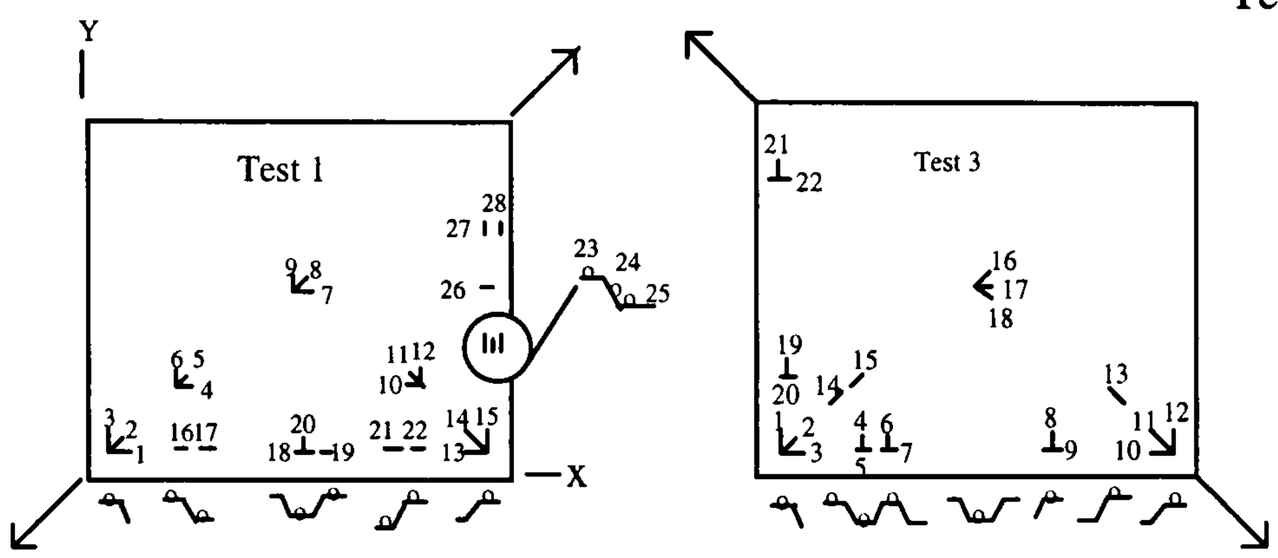

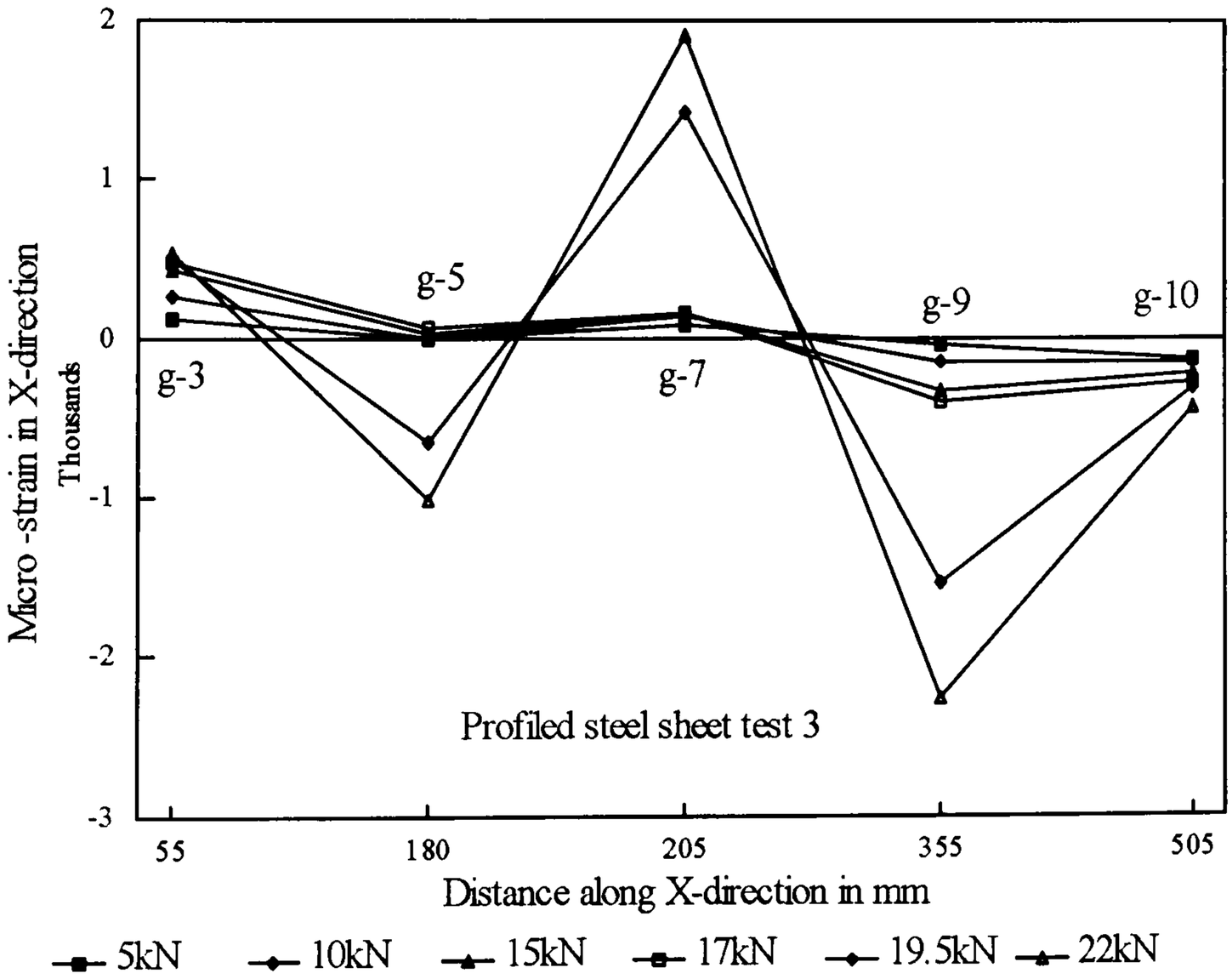

Figure 5.22(b): Variation of X-strain along the profiled boundary

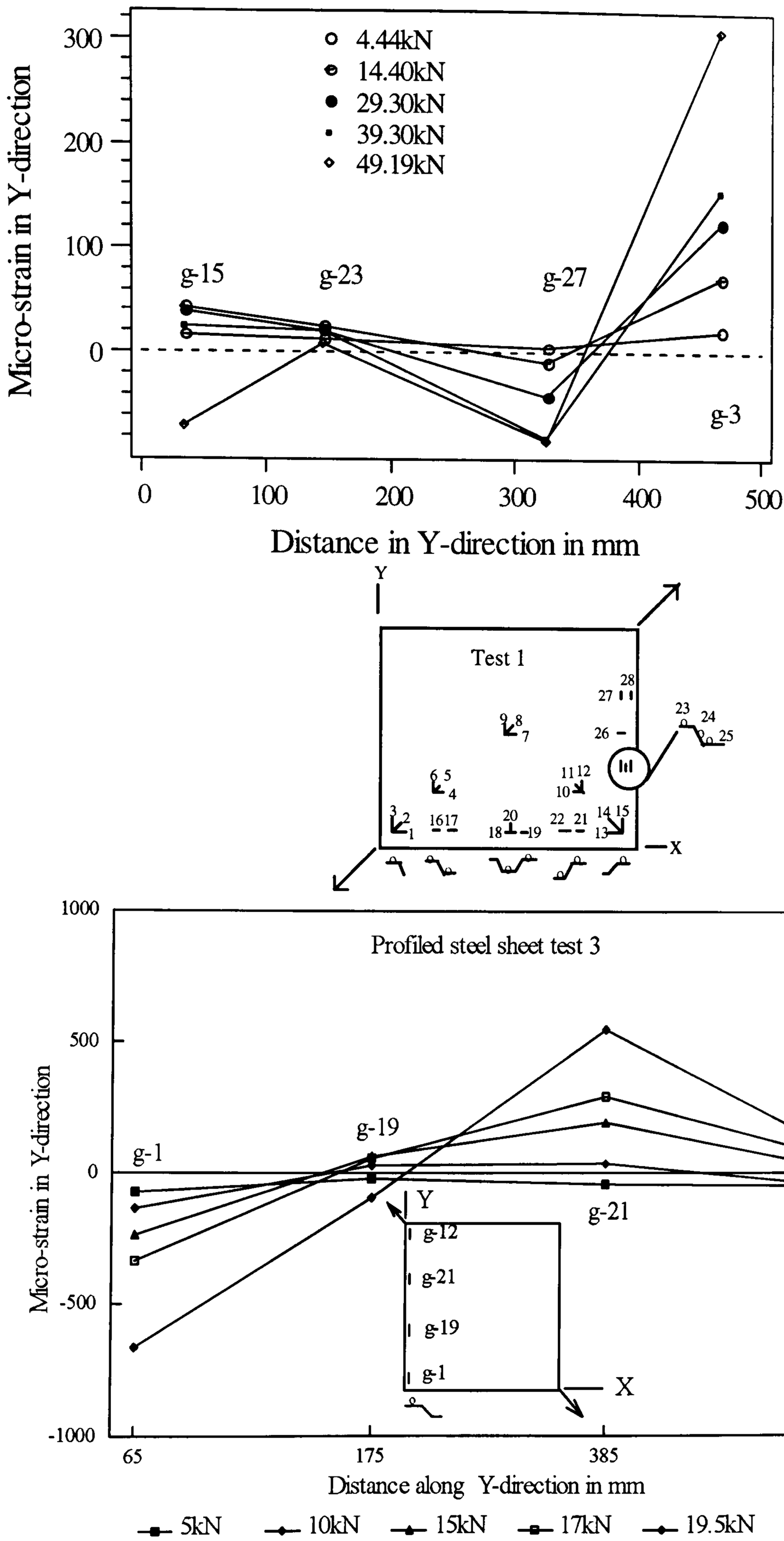

Test1

Figure 5.22(c): Variation of Y-strain along the plain boundary

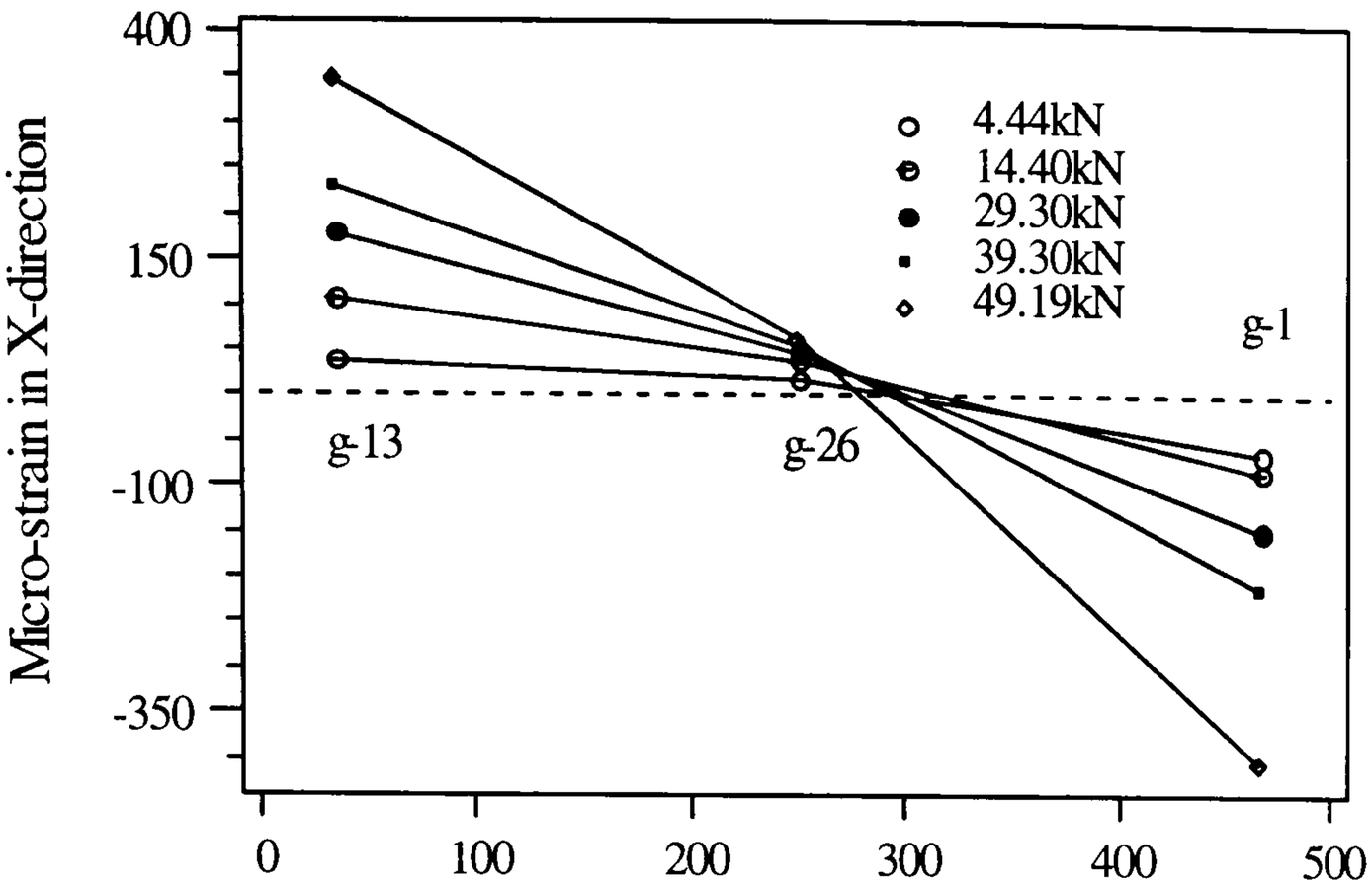

Test 1

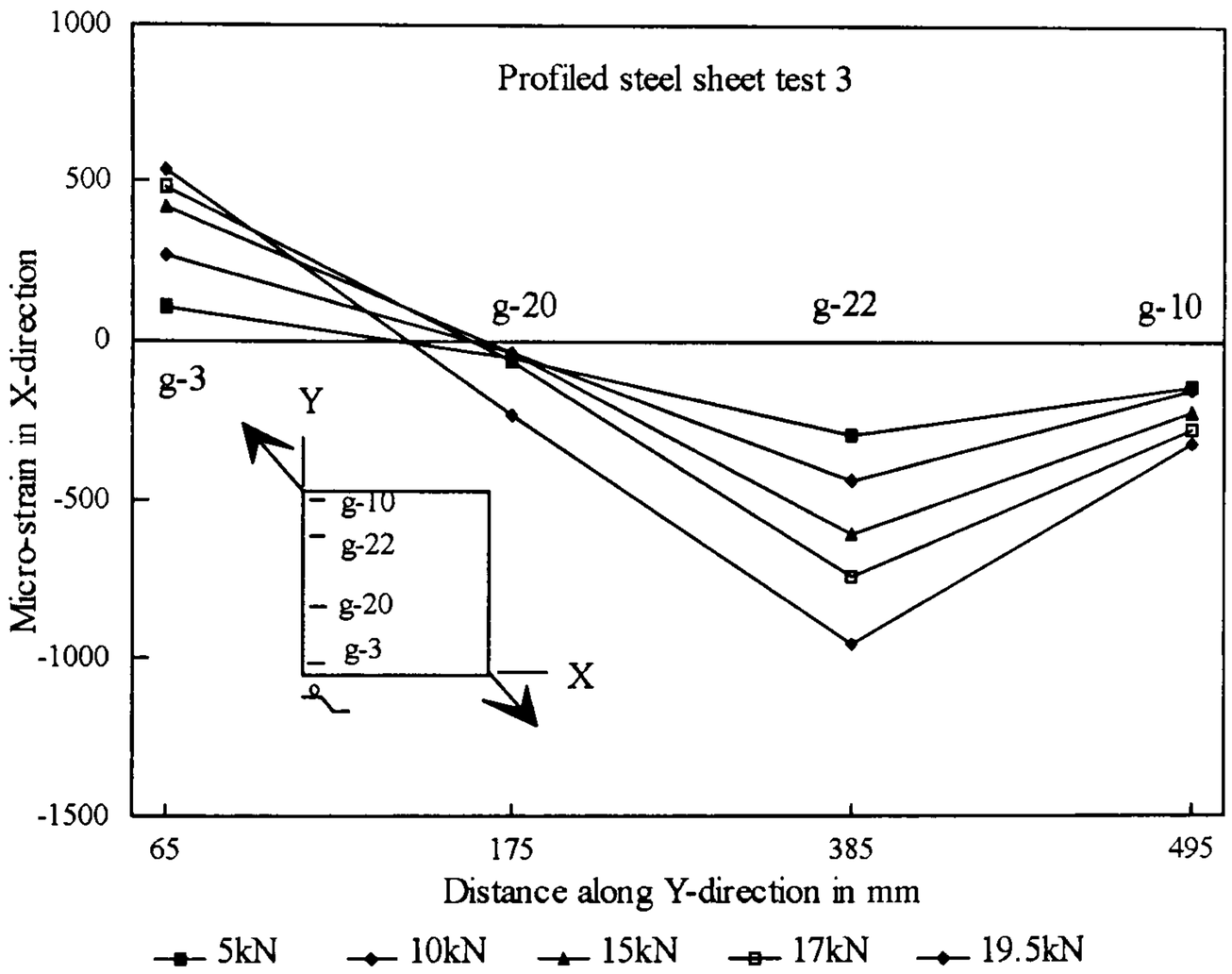

Figure 5.22(d): Variation of X-strain along the plain boundary

5.5 Analytical calculations of model tests

Models for small scale model tests

Small scale model tests were performed simulating two boundary conditions classified as two cases.

Case 1: It represents elemental tests under pure shear where stiffness will be derived only from shear deformation of sheeting. Boundary conditions were such that no bending of profile was allowed. The profiled steel sheeting was manufactured from single piece of flat sheet allowing no seam connections. The connections between

sheet and rigid pin jointed boundary frame of test rig were assumed very rigid satisfying clamped condition at the boundary. Therefore, for case 1, the flexibility equation 5.13 becomes:

$c_s = c_1 = 1/k_S$. .....(5.19)

Small scale Test 1 and Test 2 have been performed simulating case 1.

Case 2: In Test 3 sheet was spot welded to the boundary frame allowing shear deformation of sheeting and bending of corrugation profile. Spot welds connecting the sheet at the centre of trough also contribute to the flexibility. The flexiblity equation 5.13 can be written as :

$c_s = c_1 + c_2 + c_4 = 1/k_S$. .....(5.20)

Analytical models proposed in this section and in section 5.3.2 will be used to calculate the stiffness and strength of the model tests and will be presented in this article.

Analytical flexibilities are tabulated in table 5.5. The stiffness of the panel 3 is found to be almost one third of the test 1 due to the added contribution from bending and crimping of the sheeting. The factor K is calculated for sheeting spot welded or bolted at the centre of the trough to the boundary. The parameter, s, is derived from testing of spot weld specimens described in section 5.4.2.1. There were ten spot weld at each boundary with an average spacing (P_a, P_b) of 54 mm .

Table 5.5: Analytical flexibilities

Test No	Shear	Flexibility	mm/kN	Total shear		Remarks
	Shear deformation c_1	Bending of corrugation profile c_2	Crimping at spot welds c_4	Flexibility c_s mm/kN	Stiffness k_s kN/mm	
1 and 2	0.033	-	-	0.033	30.30	equation 5.19
3	0.033	0.0277 K=0.17188	0.04754 s=0.1233 mm/kN	0.1082 P_a=P_b=54mm average	9.238	equation 5.20

For Test1 and Test 2, buckling will be the failure criteria and equation 5.18 can be used to calculate ultimate load. For Test 3, where spot welds were used as fastener, the weld failure may be a failure criteria and in that case, equation 5.17 can be used to calculate ultimate load. In this case load-deformation response of the spot weld should be determined from sample tests.

Analytical orthotropic constants and ultimate strength of model tests are presented in table 5.6. The factor, β, to be checked from experimental results. The strength of spot

weld where failure was solely due to weld with no tearing of sheeting varies from 1.7 to 2.5 kN as described in article 5.4.2.1 found from sample tests. As a result a range of 17-25kN is suggested and to be compared with experimental results.

Table 5.6: Sheeting constants and strength

Orthotropic constants using equation 5.2 Ultimate shear of Model profile sheeting strength kN					
D_x kN-mm²/mm	I_v mm⁴	D_v kN-mm²/mm	D_{xv} kN-mm²/mm	Buckling Failure(eq. 5.18)	Spot weld failure (eq.5.17)
1.27	398.78	1595.118	2.91	17.23β	17-25kN

5.6. Comparative study of analytical and experimental results

The stiffness and strength from analytical and experiments are compared in table 5.7. The stiffnesses and strengths are found to be in excellent agreement. The strength of the panel 3 is found to be very close to analytical strength calculated using minimum strength of spot weld.

Table 5.7: Comparison of analytical and experimental values

Type	Boundary condition	Shear stiffness kN/mm		Ultimate load in kN		
		analytical	model tests	analytical	model test	β
Test 1	clamped	30.30	28.25	17.23β	29.7	1.72
Test 2	clamped	30.30	26.50	17.23β	28.2	1.64
Test 3	spot welded	9.238	8.935	17-25	17.68	

The analytical model for stiffness can therefore, be accurate enough to be used in design to calculate the stiffness under different boundary condition. The generalised buckling formula can therefore be safely used to calculate the strength of the panels using β=1.00 for simply supported and β=1.72 for clamped condition.

5.7 Efficiency of profiled sheet over plain sheet

The table 5.8 has been prepared based on analytical and experimental results to compare light gauge plain and profile sheeting stiffness and ultimate load. The 99% increase of buckling load is the main advantage of profile steel sheeting which implies a stable behaviour nearly up to the failure load. Considering the post-buckling stiffness of the plain sheet, profiled sheet also provide 25% increase in stiffness almost up to its failure load. All this advantage will need only 15% increase in steel area .

Table 5.8: Comparison between plain and profiled sheet

Type of sheeting	load	kN	Shear stiffness	kN/mm	flat area m^2	Boundary condition
	Buckling	Ultimate	pre-buckling	post-buckling		
plain	0.27	47	35.71	22.7	0.316	clamped
profile	29.7	36.8	30.3	-	0.369	clamped
efficiency	99%	-21.7%	-15% 0 to 0.27kN	25% 0- 29.7kN	14.36%	

5.8 Finite element modelling of profiled steel sheet behaviour

Finite element analysis of the metal deck shear diaphragms were carried out by Nilson and Ammar(1974). They idealised the diaphragm as a plane stress type problem, modelling the profiled steel sheeting by equivalent orhtotropic plane stress element. The purlin and edge members by one dimensional line elements with axial resistance as well as bending. The panels are connected to the purlin and edge members by two dimensional spring elements. The spring stiffnesses were determined experimentally. The elastic analysis of the resulting assemblage provided information on shear flexibility and a conservative estimate of strength. More details finite element analysis of the problem was carried out by Davies (1976,1977). He employed orthotropic plate elements for sheeting, beam elements for purlins or frame and spring elements for fasteners. He also simplified the model further by simulating the flexibility of the sheeting with a series of bars forming a truss and treating fasteners as single lumped elements thus converting the problem into a plane frame.

This article will be devoted to model solely the shear behaviour of profiled steel sheeting under different boundary conditions. Use of 3D shell elements will allow the simulation of profile geometry and it will be possible to look into the development of stress condition in the profiled sheeting along with stiffness and ultimate load.

The study will include the finite element simulation of the model tests and effect of different boundary conditions on certain parameters like K and β using LUSAS. Load-deformation response and strains will be compared with those from model tests.

5.8.1 Finite element modelling details

Idealisation

The model profiled steel sheeting has been idealised with 8 noded 3D-semi loof shell elements (QSL8) having three degrees of freedom at corner nodes. The boundary

frame was represented by semi-loof beam elements with compatible joint elements connecting frame and profiled steel sheet panel. The detail finite element idealisation of the panel with boundary frame is shown in figure 5.23.

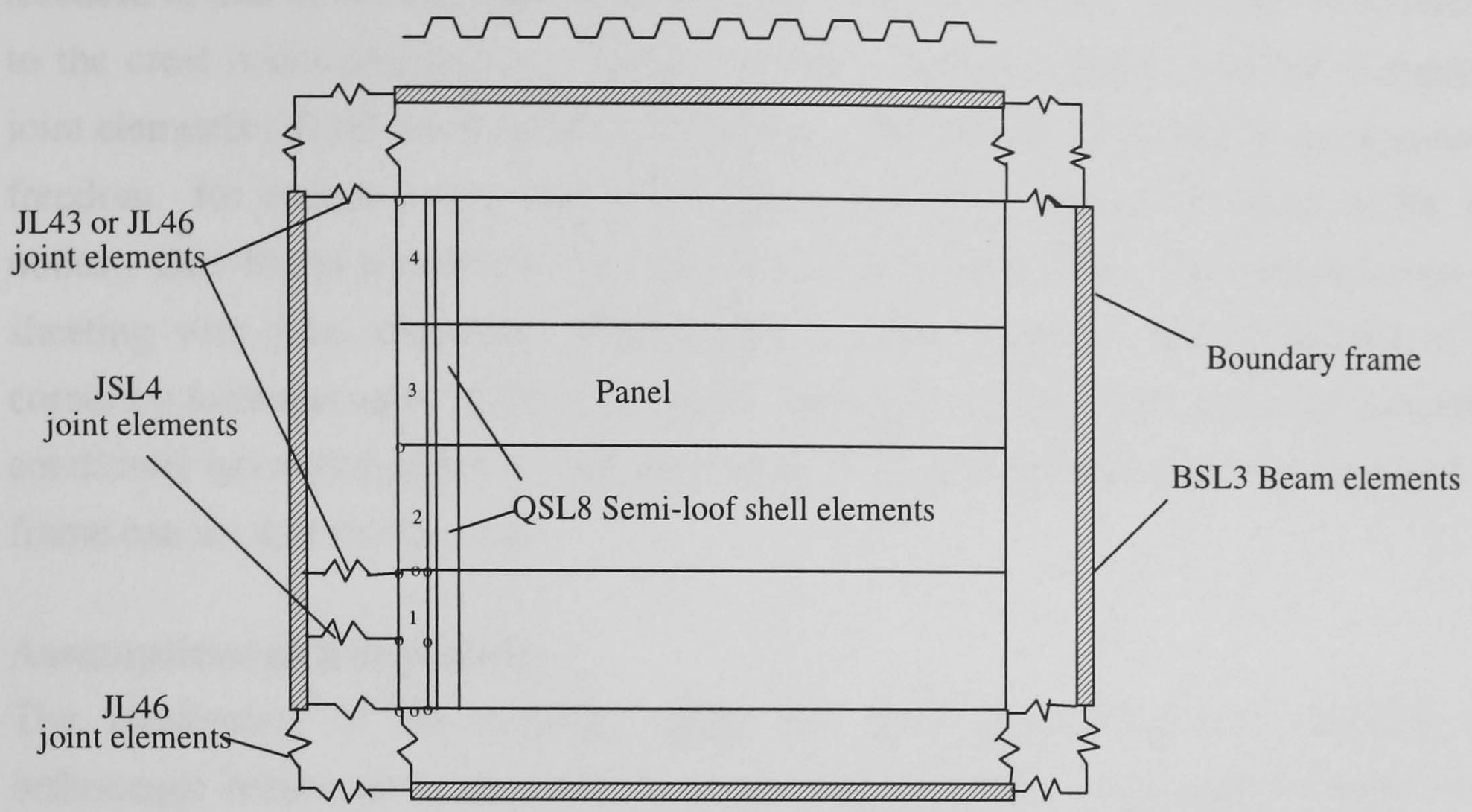

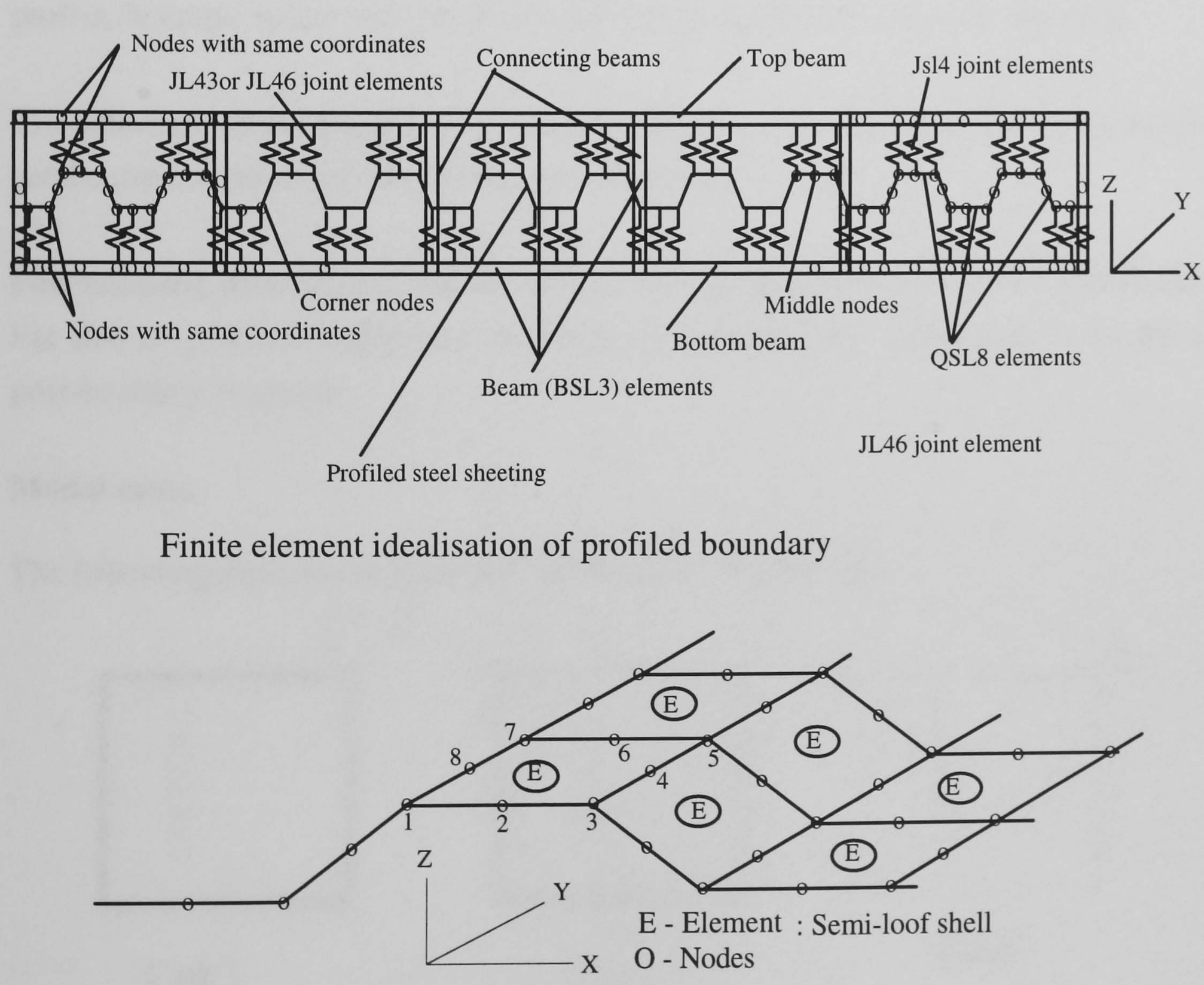

Finite element idealisation of profiled boundary

Profiled steel sheet mesh

Figure 5.23: Finite element Idealisation of profiled steel sheeting

The boundary frame along the profiled boundary is represented by a pair of top and bottom beams connected together by connecting beams. 3D-three noded semi-loof beam elements (BSL3) with six degrees of freedom at corner nodes and 5 degrees of freedom at mid nodes are used to idealise the boundary frame. Top beam is connected to the crest nodes and bottom beam is connected to the trough nodes by compatible joint elements (JL43 joints with three degrees of freedom or JL46 with six degrees of freedom for corner nodes and JSL4 joints with five degrees of freedom for mid nodes). One frame member is used along the plain boundaries and connected to the sheeting with joint elements. The boundary frame members are connected at the corner by joint elements (JL46 joints with six degrees of freedom) and exact boundary conditions have been given so that the hinges can be simulated at the corners and the frame can act as a mechanism.

Assumptions and limitations

The idealisation of the sheeting using 3D elements automatically simulate the orthotropic behaviour of the panel as it takes into account the geometric shape of the profile. Isotropic linear and non-linear material properties are used for sheeting.

The behaviour of the panel can be taken as linear up to the buckling and linear analysis can be used to determine the stiffness of the panel.

Post-buckling simulation of tension field is very difficult to model with LUSAS and it has also no practical implication in design. No attempt has been made to model the post-buckling response.

Model cases

The following simulations have been performed : (figure5.24)

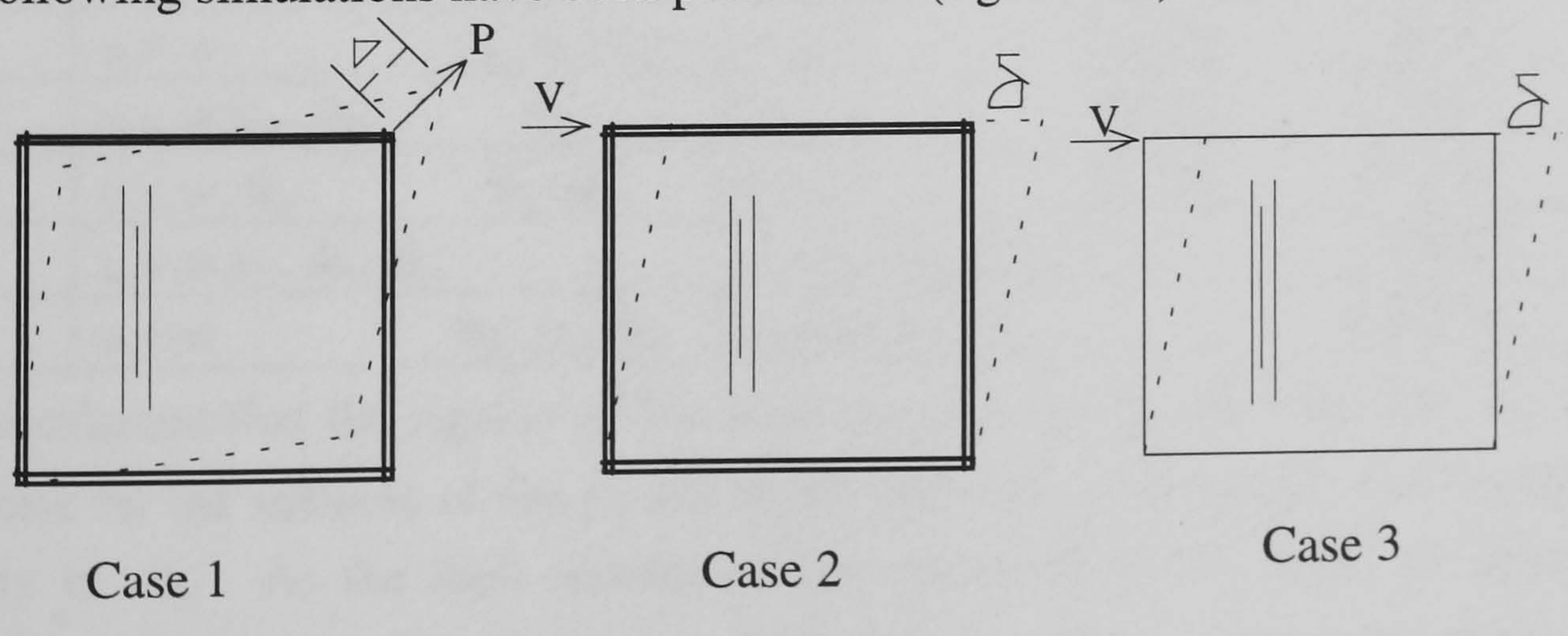

Figure 5.24: Different cases of simulation

Case1: Model test simulation: Actual experimental conditions are simulated to have the P-Δ response and strains within the panel. Non-linear analysis have been performed for two or three load increments just to determine the stiffness and strains. But huge number of elements with a mixture of joint, beam and loof elements needs large number iterations for convergence. As it was intended to determine the pre-buckling stiffness and strain, linear analysis is considered to be sufficient for the purpose. Pre-buckling stiffness from the linear and non-linear analysis was found to be similar and hence for stiffness determination it is economical to use linear analysis.

Case2: Transformed shear simulation with boundary frame: Linear analysis has been carried out to determine the V-δ response of the panel to verify the transformed equation for profiled steel sheet case.

Case 3: Transformed shear simulation without boundary frame: Non-linear analysis of the panel using 3D-semi-loof shell elements are carried out to determine the stiffness and yield load of the panel

Parametric studies

Preliminary analysis has been carried out to determine the effect of mesh refinement on the stiffness of the panel. Study showed that the mesh used for the analysis (164 elements for profiled sheet) can predict stiffness with reasonable accuracy.

The effect of joint element properties on the stiffness of the panel was also studied and summarised in the table 5.9.

Table 5.9: Effect of joint elements

	Joint connecting		Frame and Panel		
Type	Corner nodes JL46		Mid nodes JSl4		Stiffness
	Rigid	Flexible	Rigid	Flexible	kN/mm
1	u,v,w	θ_x ,θ_y, θ_z	u,v,w	θ_1, θ_2	30.12
2	u,v,w,θ_x ,θ_y	θ_z	u,v,w	θ_1, θ_2	30.12
3	u,v,w, θ_z	θ_x ,θ_y	u,v,w	θ_1, θ_2	52.63
4	u,v,w,θ_x ,θ_y, θ_z	-	u,v,w, θ_1, θ_2	-	52.63
5	u,v,w	θ_x ,θ_y, θ_z	u,v,w, θ_1, θ_2	-	30.12

It is confirmed that the rigidity of the joint elements in θ_x ,θ_y , θ_1 and θ_2 has no influence on the stiffness of the panel but the stiffness of the panel is affected by the rigidity in θ_z . As the shell elements representing the panel have no degrees of freedom in θ_x ,θ_y and θ_z , the type 1 ,2 or 3 can be used . Type 1 has been used in the subsequent analysis.

5.8.2 Analysis of FE results & comparison with analytical and model tests

5.8.2.1 Load-deformation response and stiffness

The load-deformation responses of test 1 and those from finite element analysis are shown in figure 5.25. The strength and stiffness are compared in table 5.10. The stiffness from case1 and case 2 are same which indicates the validity of transformed equation 2.1 for the profiled sheet. The stiffness from all three analysis are found to be in excellent agreement with each other. The yield load found from non-linear analysis (case3) is about 12% higher than those from analytical and model test. Therefore, it may be possible to attain the yielding of steel before the shear buckling of the panel by using profiled sheet. However, this is entirely dependent on the boundary conditions which allow the sheeting to fully mobilise and increase the buckling capacity of the sheeting.

Table 5.10 : Simulation of Test 1

Type	Diagonal stiffness kN/mm	Shear stiffness kN/mm	Ultimate shear load kN
Model Test 1	56.5	28.25	29.7 (buckling load)
Analytical	60.6	30.3	29.7
FEA : Case1	60.6	30.3	-
Case2	-	30.3	-
Case3	-	34.5	33.9 start to yield

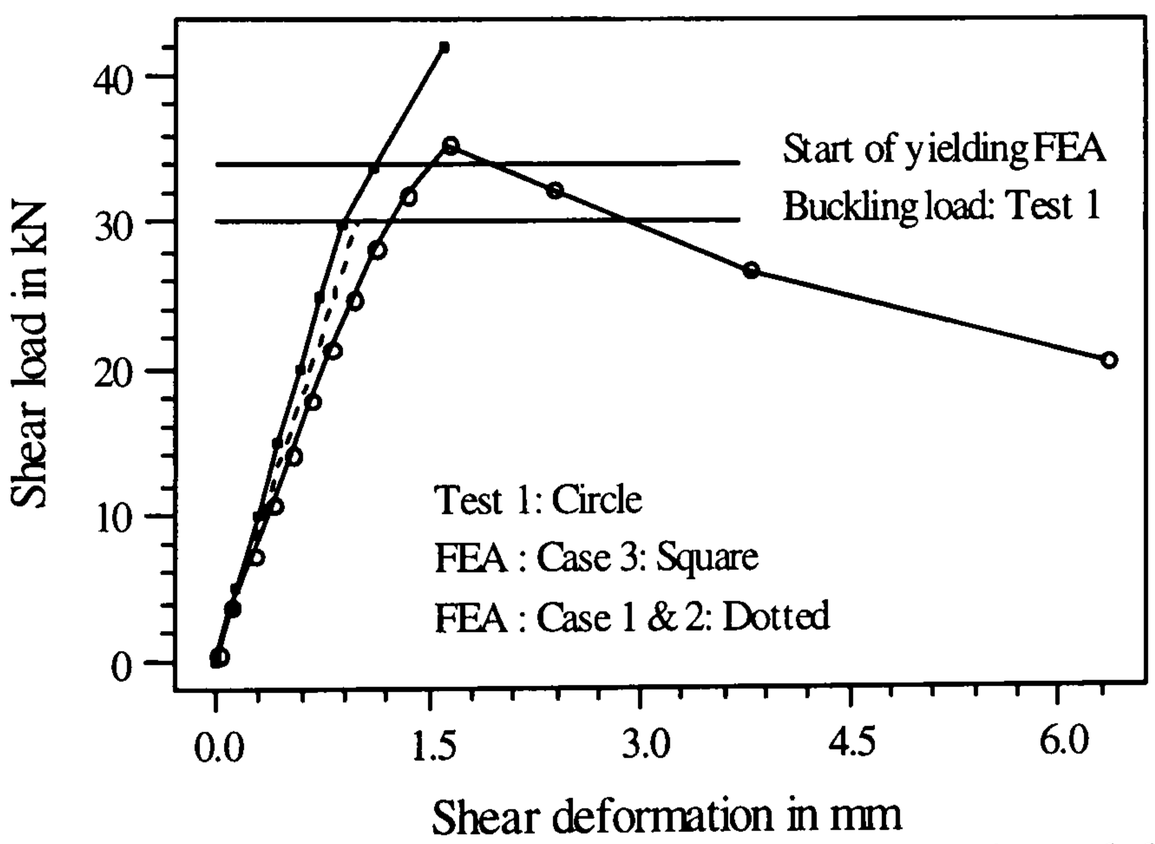

Figure 5.25: Comparison of FEA and model tests

5.8.2.2 Analysis for the factors K and β

The analytical expression for flexibility due to bending or distortion of corrugation profile (c_2) include the factor K, representing the mode of attachment of the sheeting to the frame. The analytical expressions have been suggested for, K, and finite element analysis will be carried out to validate this expressions along with model test

results. Bending and distortional flexibility arises if the centre of shear resistance of the profile is eccentric to the plan of application of the applied shear force and the corrugation is twisted out of shape by its own shear flow. Three mode of attachment will be considered here:

Type1: Clamped condition (model test1 and 2) : The sheeting can be considered to be connected to the frame at both trough and crest lines as shown in figure 5.26(a). The finite element details is shown in figure 5.23. This will allow no bending or distortion of the profile as confirmed from the model test 1 and 2 and also can be seen from the deflected shape of the finite element analysis (figure 5.27(a)). As a result the value of K in this case should be equal to zero. The effect of crimping at the fasteners is zero. The flexibility of the sheeting will be entirely due to shear deformation of the sheeting.

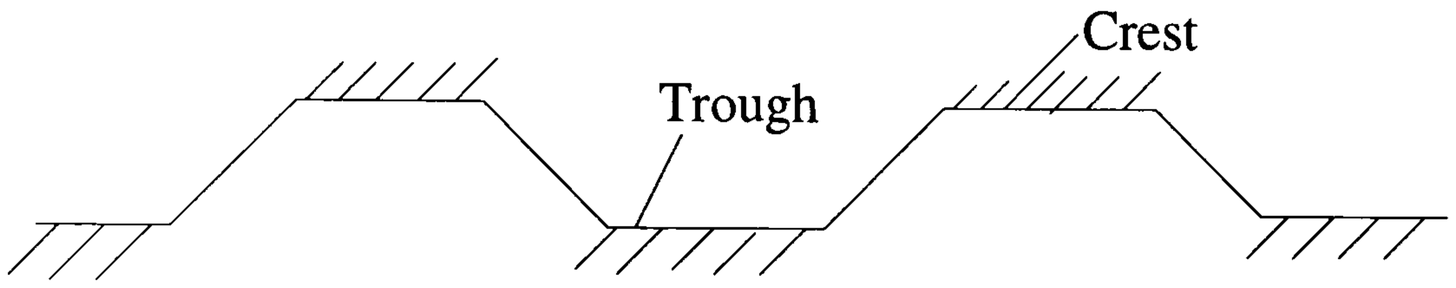

Figure 5.26(a) Clamped at both trough and cest line

Type 2: Welded continuously along the troughs

The finite element idealisation for this case is shown in figure 5.26(b). As the line of application of the shear load is eccentric to the neutral axis of the profile, this will allow bending or distortion of the profile and the factor K will be non zero. The effect of crimping at the fasteners can be neglected.

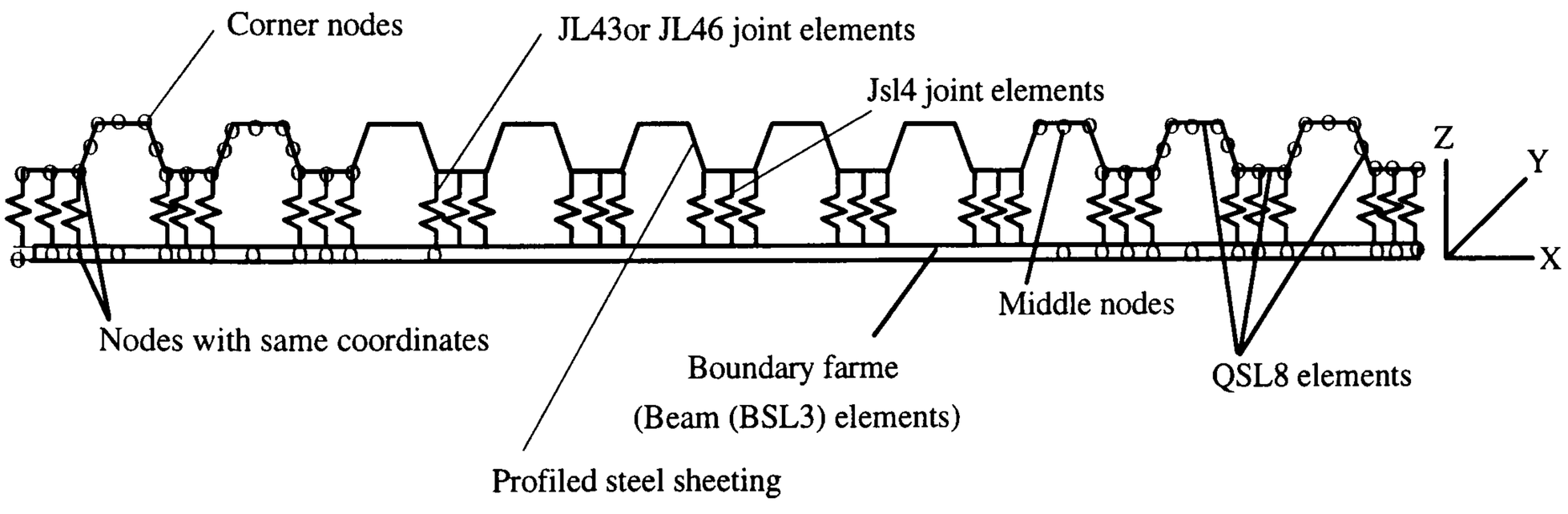

Finite element idealisation of profiled boundary

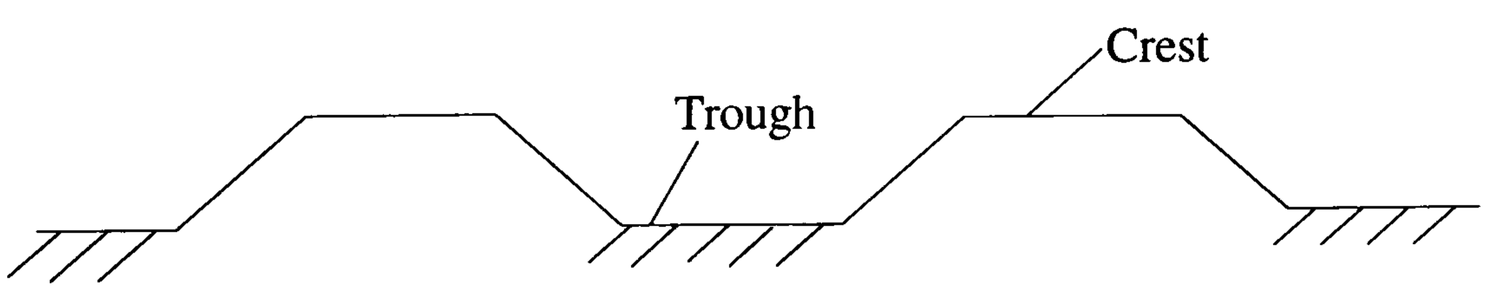

Continously welded along the trough

Figure 5.26(b): Type 2

Type3: Spot welded or bolted at the centre of each trough

The sheet spot welded or bolted to the boundary frame at the centre of each trough representing the model test 3. The finite element idealisation of the panel boundary is shown in figure 5.26(c). This condition will allow shear deformation, bending of profile as well as crimping of the sheeting at spot weld or bolt location as observed from the model test 3. The bending or distortion of the profile can also be seen from the deformed mesh of the finite element analysis shown in figure 5.27(b).

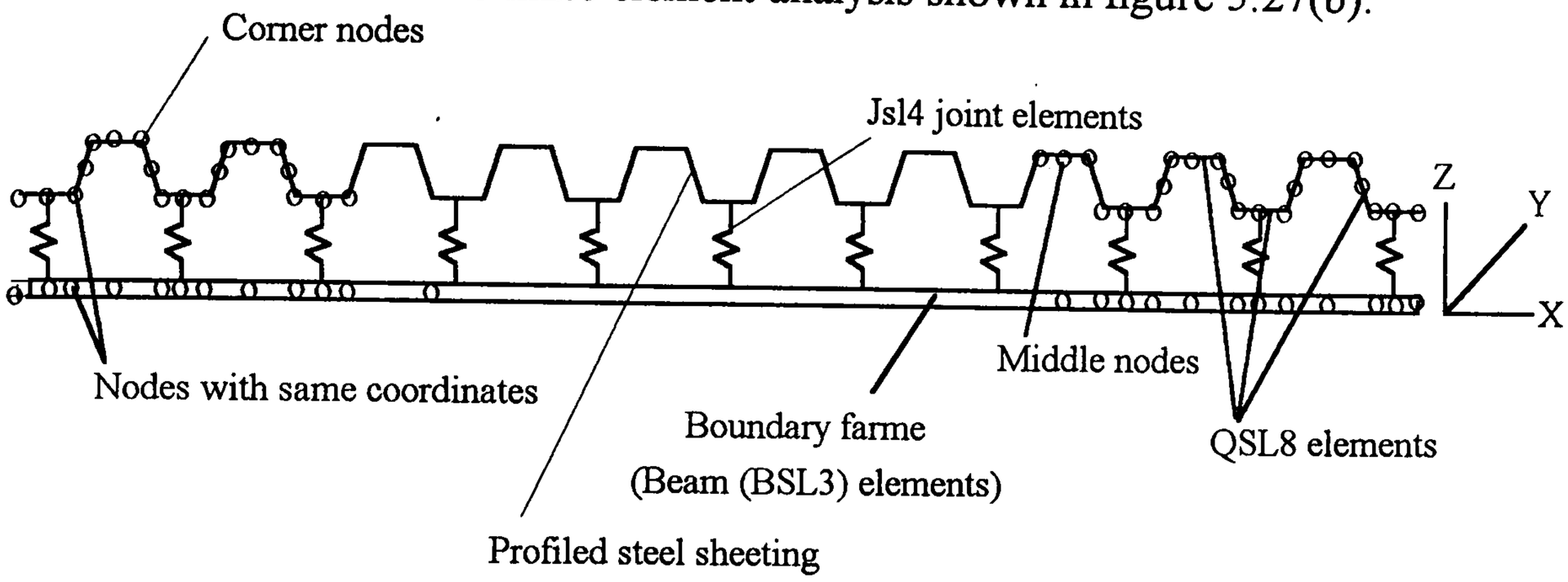

Finite element idealisation of profiled boundary (Test 3)

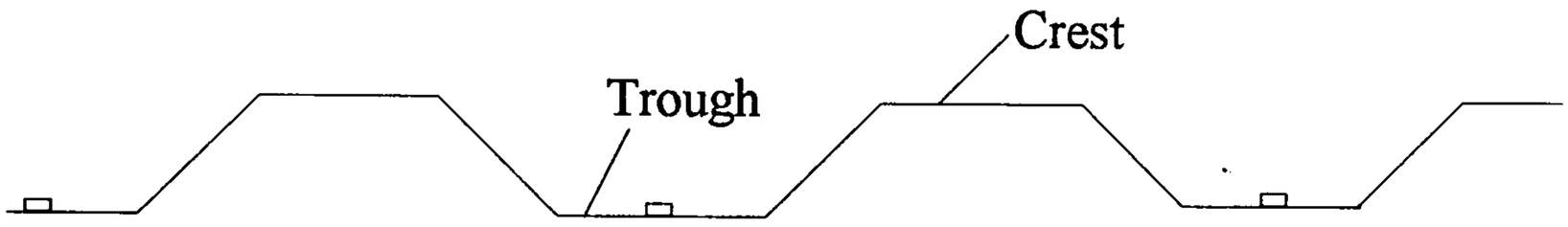

Spot welded or bolted at the centre of each trough

Figure 5.26(c) : Type 3

The table 5.11 summarises the findings of the analysis. The analytical stiffness obtained by using K values derived from analytical expressions (equations 5.8 and 5.9) showed excellent agreement with those from model tests and finite element analysis.

Table 5.11: Comparison of different analysis

	Analysis	Shear Flexibility mm/kN			Total shear		Remarks
		Shear deformation c_1	Bending of corrugation profile c_2	Crimping at spot welds c_4	Flexibility c_s mm/kN	Stiffness k_s kN/mm	K from analytical expression
Type 1	Analytical	0.033	-	-	0.033	30.30	K=0.0
	Test 1& 2	-	-	-	0.0354	28.25	
	FEA	-	-	-	0.033	30.30	
Type 2	Analytical	0.033	0.014	-	0.047	21.27	K=0.0845
	FEA	-	-	-	0.055	18.20	eqn. 5.9
Type 3	Analytical	0.033	0.0277	0.04754	0.1082	9.238	K=0.1719
	Test 3	-	-	-	0.1119	8.935	eqn. 5.8
	FEA	-	-	-	0.1093	9.149	
				s=0.1233 mm/kN	P_a=P_b=54mm average		

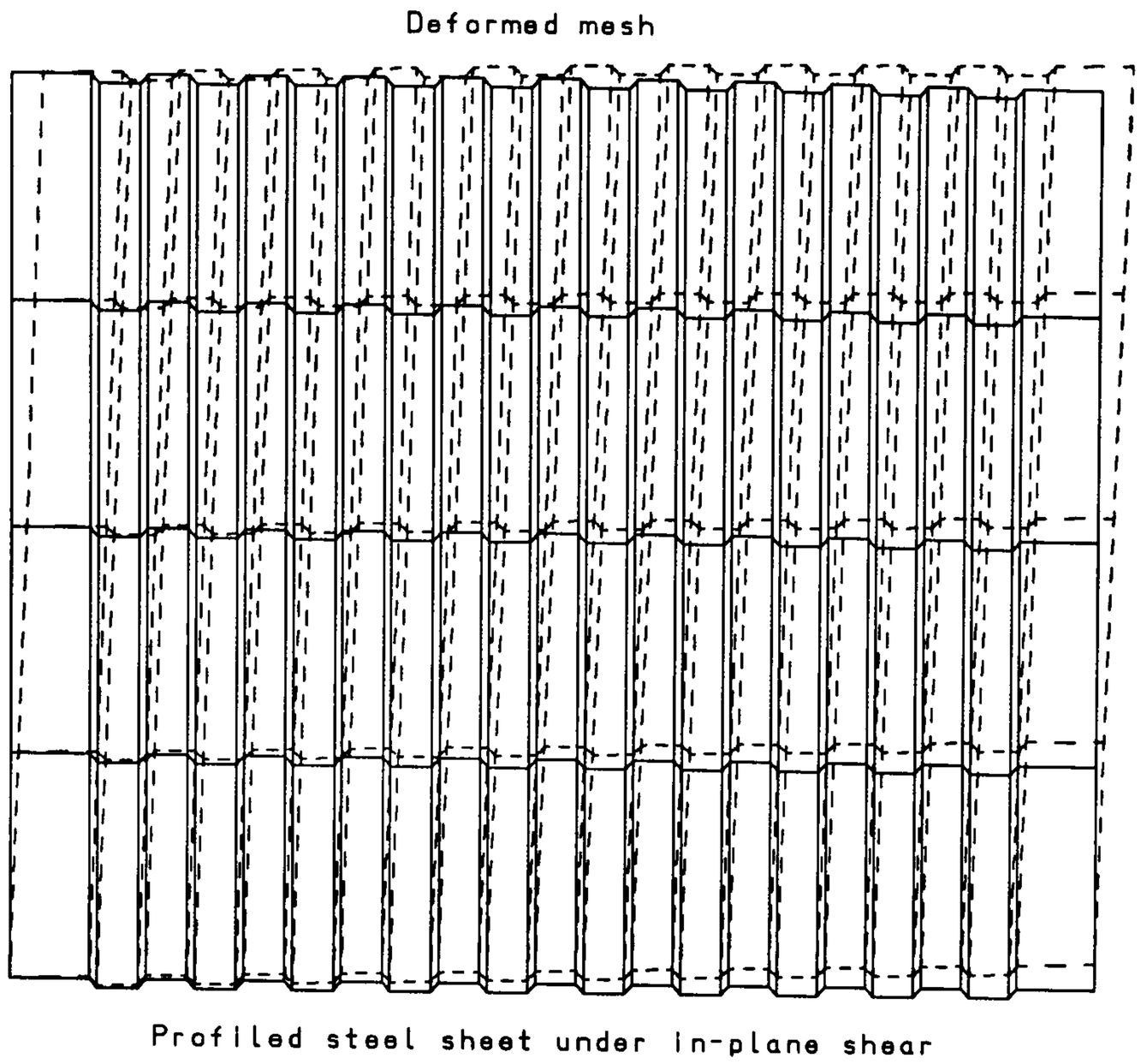

Figure 5.27(a): Deflected shape (Type 1)

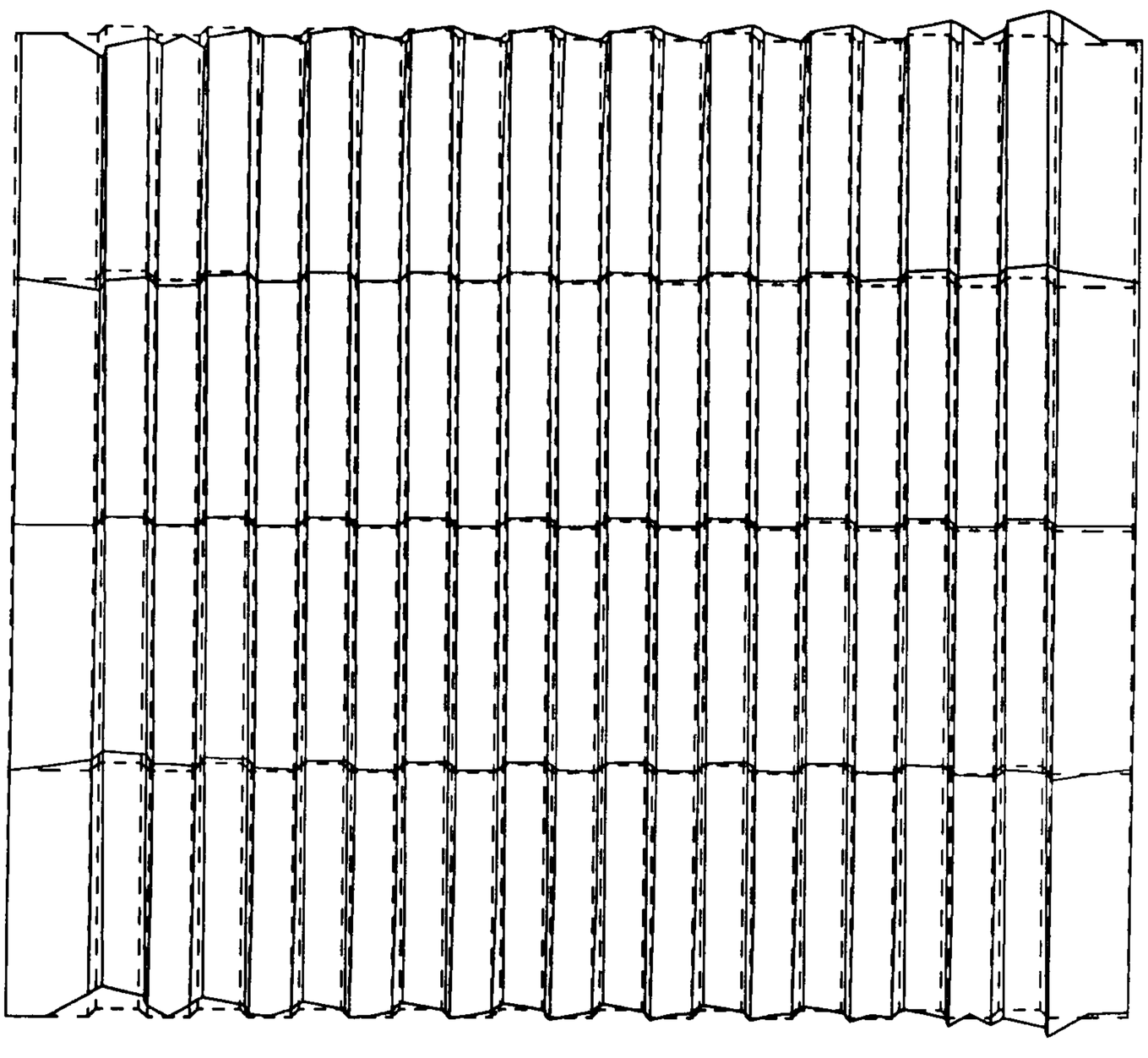

Figure 5.27(b) : Deflected shape (Type3)

This confirms the validation of analytical expressions for determining the value of K. For trapezoidal profiled steel sheeting K=0.0 for clamped, K=0.0845 for continuously welded along the trough and K=0.1719 for sheeting spot welded or bolted at the centre of the trough can be used.

Finite element buckling analysis of the panels were performed with boundary condition type 1, 2 and 3. From the buckling loads of the panels, the values of β were calculated. For boundary condition types 1, 2 and 3, the values of β were found to be 1.72, 1.42 and 1.00 respectively.

5.8.2.3 Analysis of strain

The principal strains from finite element analysis are compared to those at rosette locations of test1 and test 3 in figures 5.28. The principal strains are taken as the average of the nearest gauss point values. For test 1, the gauss point values are found to be reasonably close and there was no problem in taking average of them. The principal strains from finite element analysis are found to be in good agreement with those from test 1.

But for test 3, besides central rosette 16-17-18, the gauss point values are not close enough to average them. The table 5.12 will indicate the divergence of the values. It is interesting to note that the values of principal strains for rosettes 10-11-12 and 1-2-3 are equal and just interchange in two principal direction. This is due to the fact that they are in mutually perpendicular diagonals. The diversity of strain in close gauss points and the difference between major and minor principal strain may be due to the bending and twisting of the profile. The principal strain at central rosette 16-17-18 is compared to that from finite element analysis in figure 5.28(d).

Table 5.12: FEA and Test comparison

Locations	Principal micro-strain Finite element Gauss points		P=5kN analysis		P=5kN Test 3	
Rosette 10-11-12	96	-115	237	-52	185	-62	127	-86
Rosette 1-2-3	116	-96	52	-237	61	-188	-16	-173

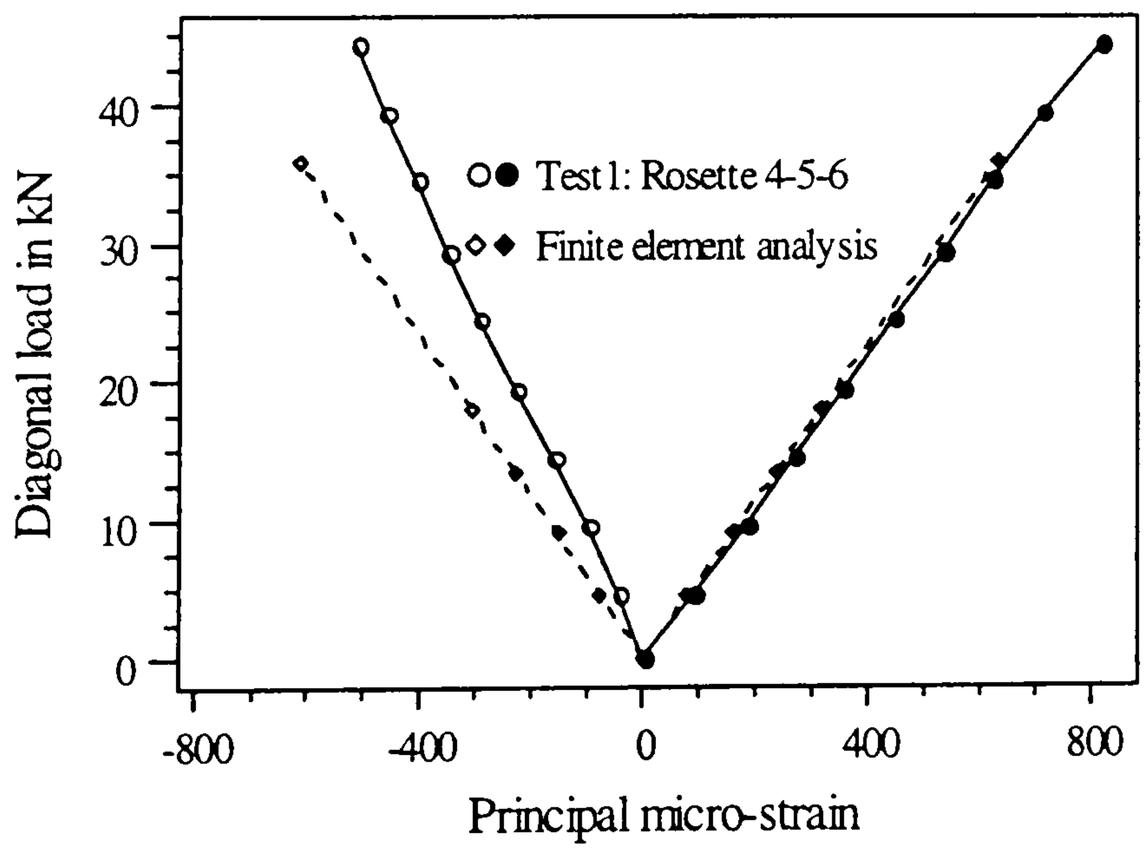

Figure 5.28(a)

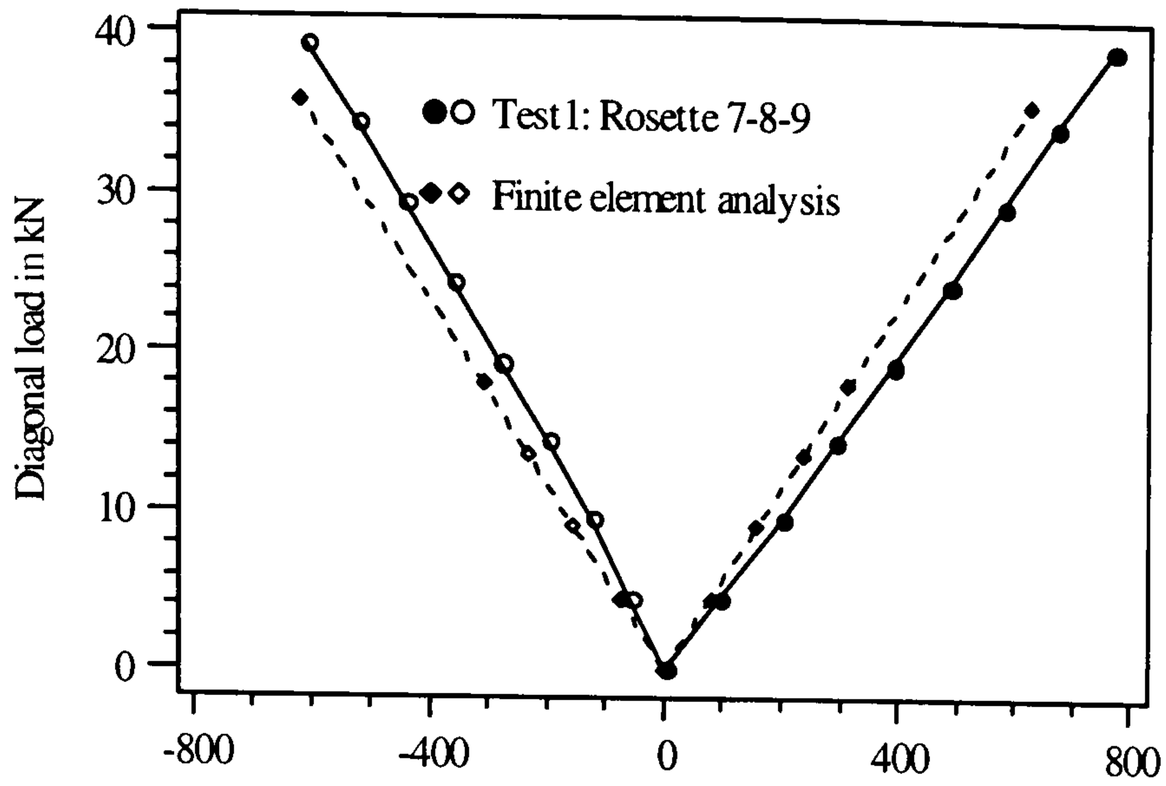

Figure 5.28(b)

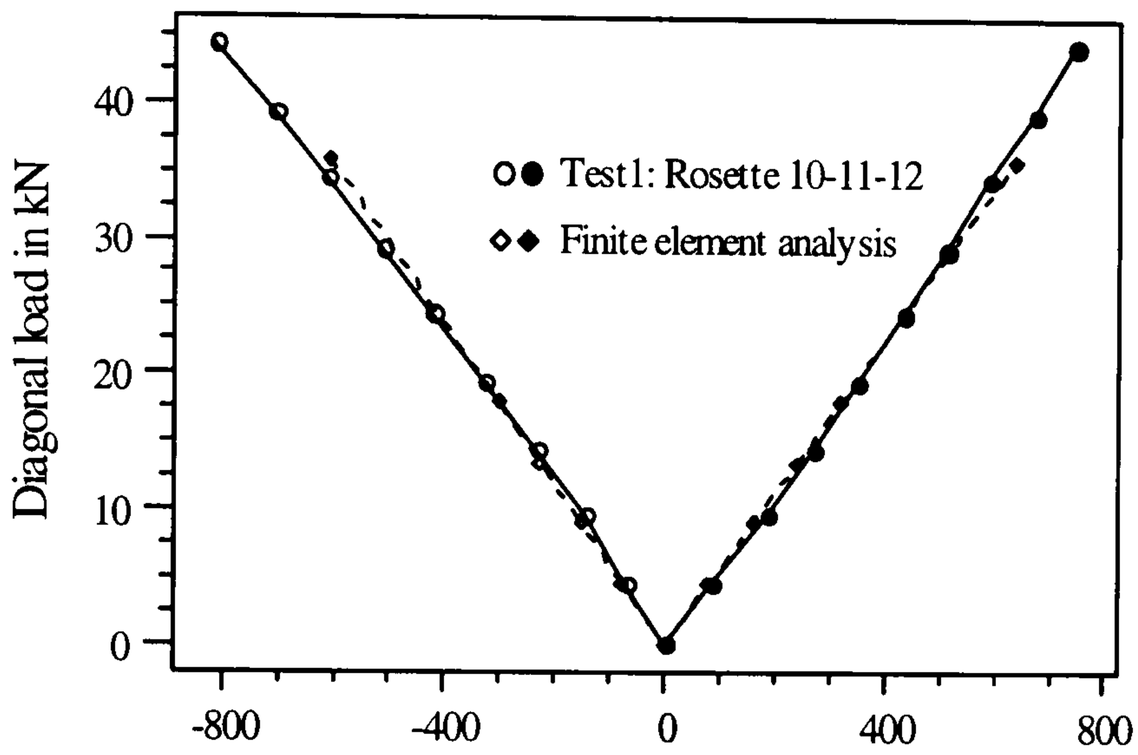

Figure 5.28(c)

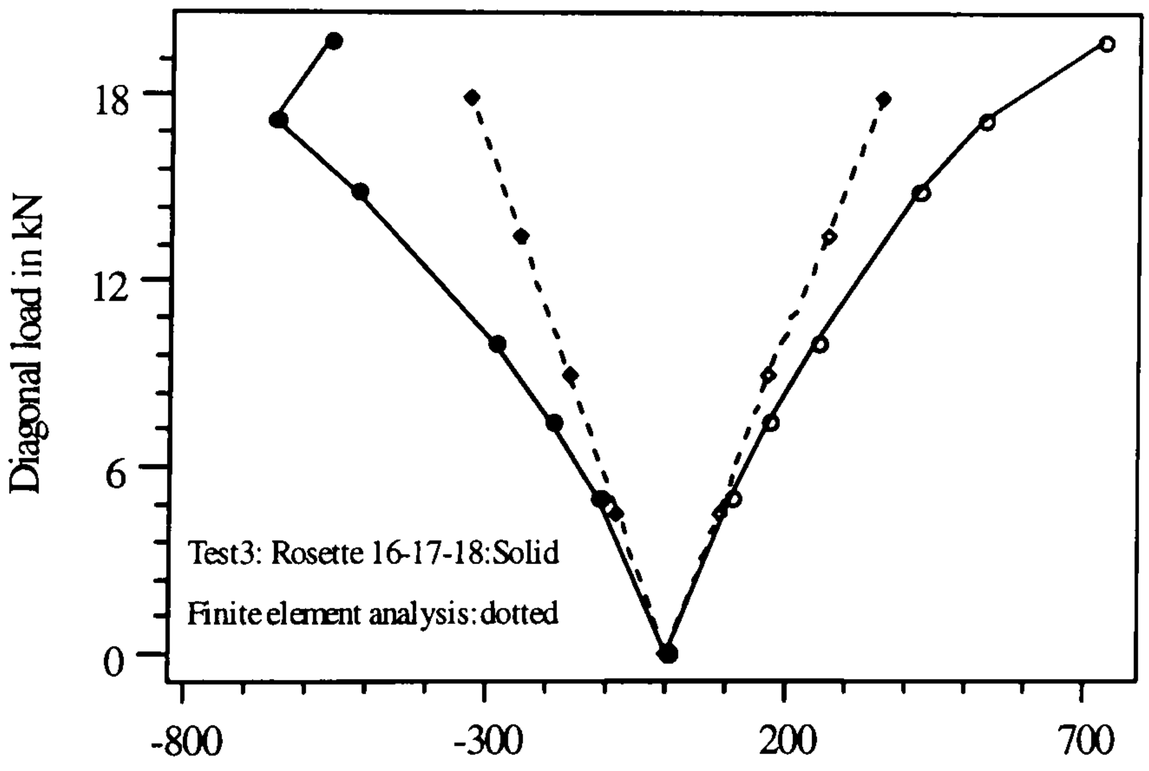

Figure 5.28(d)

Figure 5.28: FEA and Test comparison

The contour diagrams of principal strain and its direction are shown in figures 5.29. The presence of a tension band can be identified from the contour diagram in case of

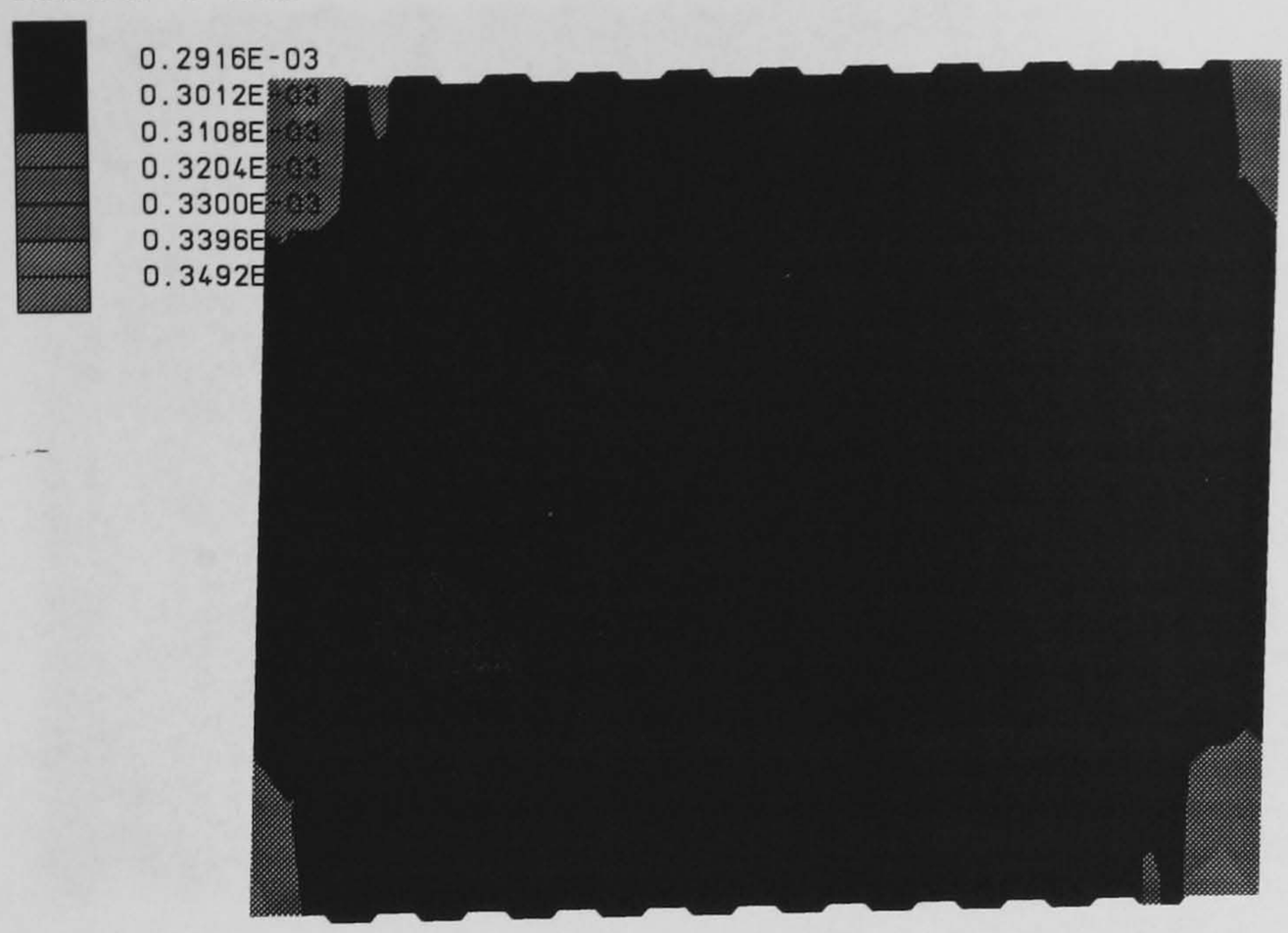

Figure 5.29(a): Contour diagram of maximum principal strain (Test 1 simulation)

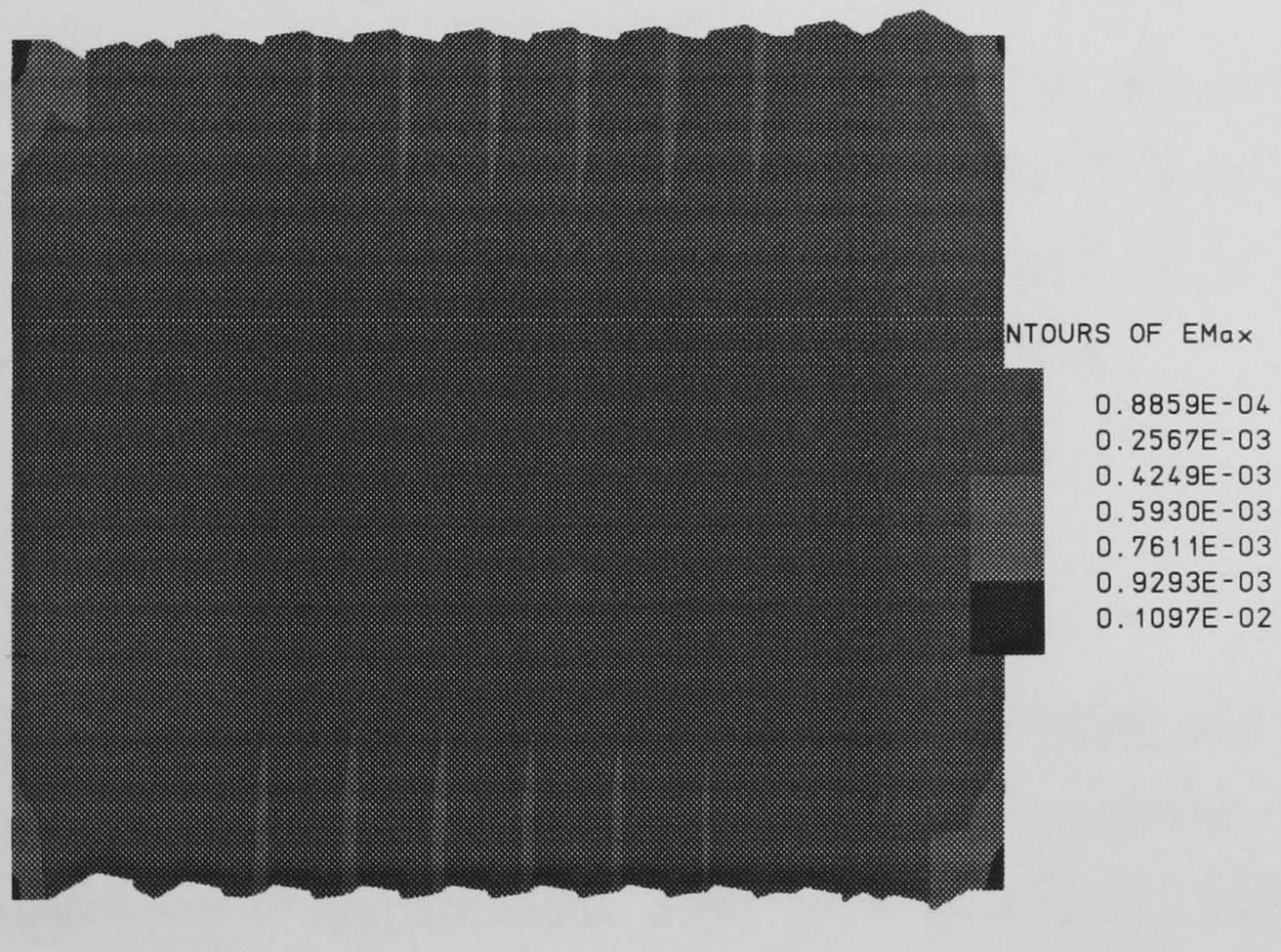

Figure 5.29(b): Contour diagram of maximum principal strain (Test 3 simulation)

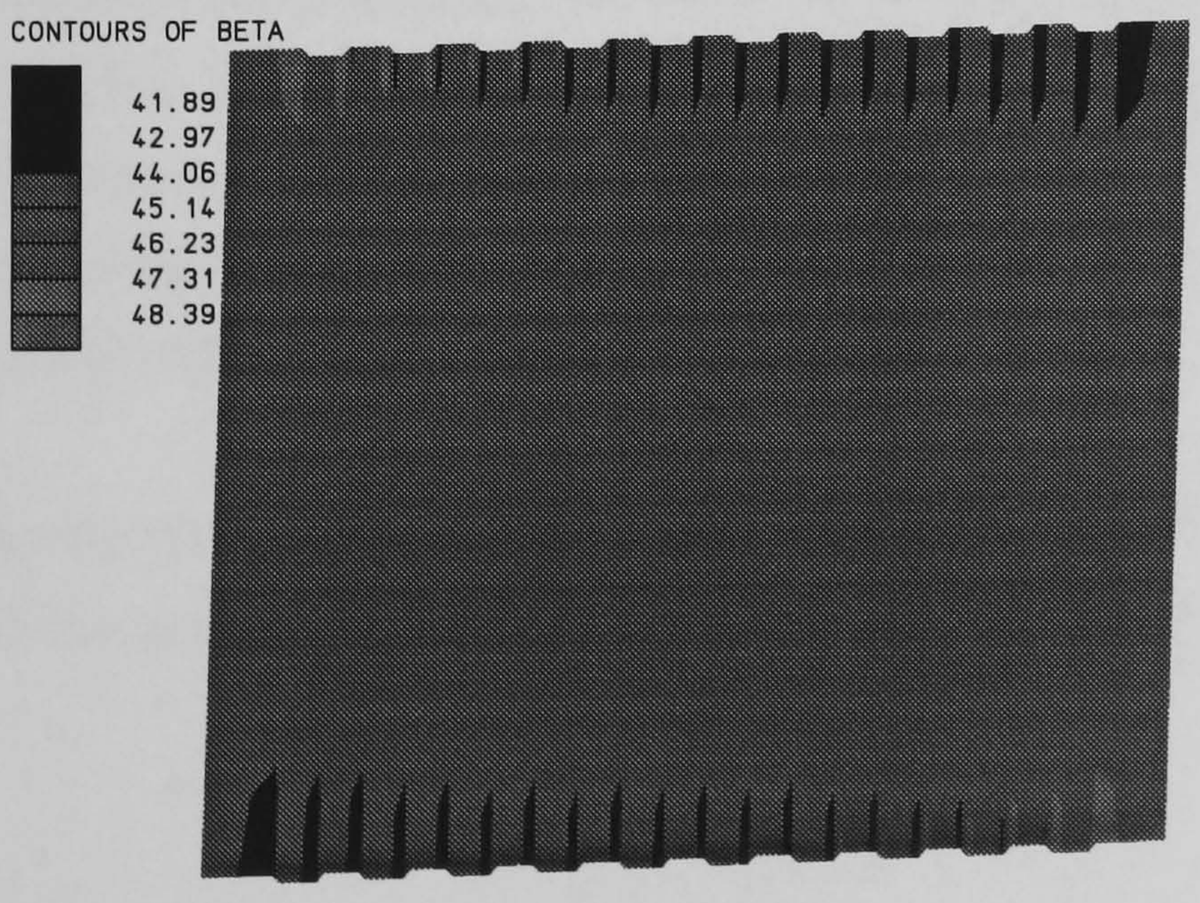

Figure 5.29(c): Contour diagram of principal direction (Test 1 simulation)

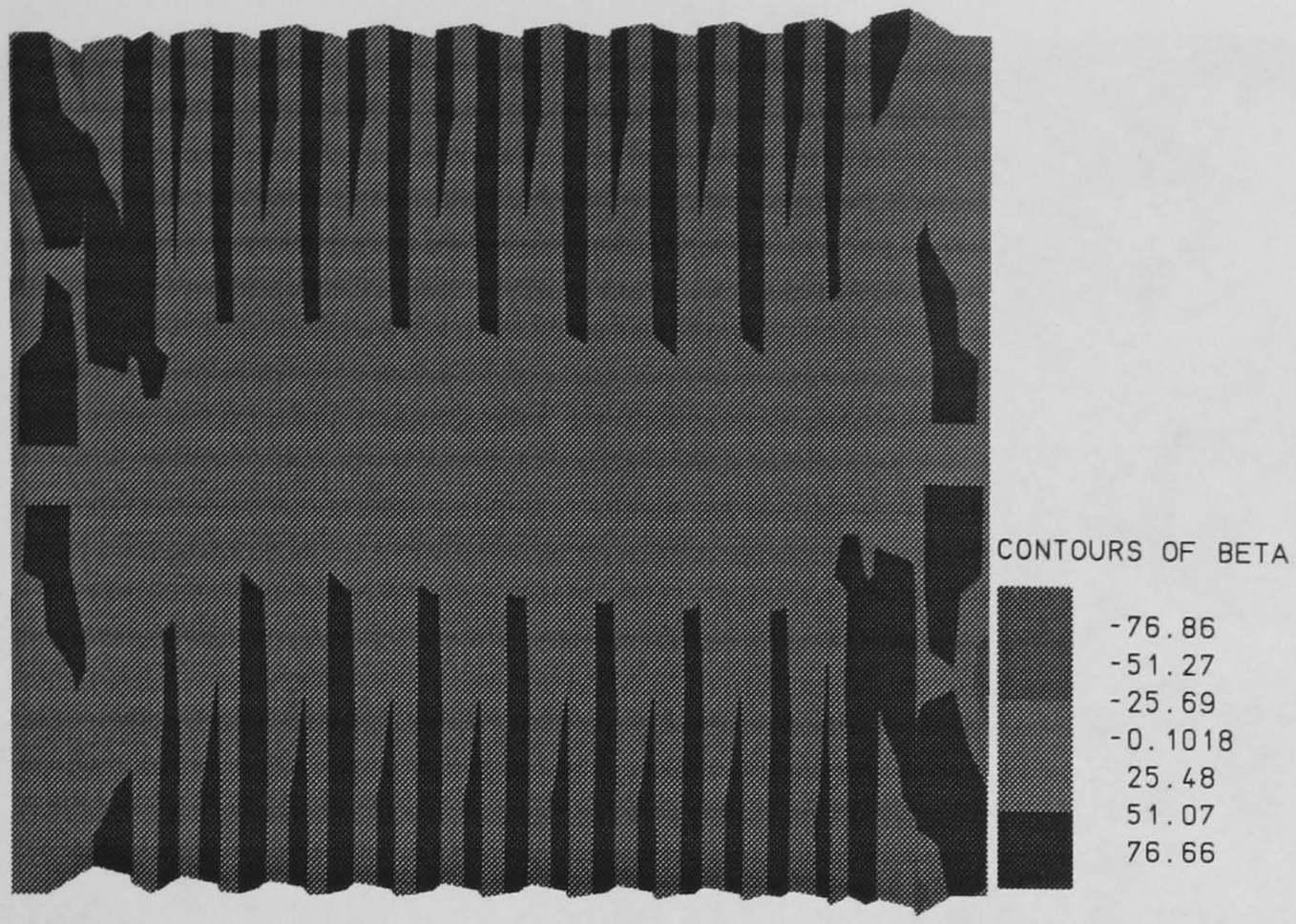

Figure 5.29(d): Contour diagram of principal direction (Test 3 simulation)

test 1. The principal direction ranges between 41.89-48.39 degrees which shows good agreement with test 1. The simulation of test 3 shows large variation in principal direction ranges between 25-75 degrees which is in agreement with test3 where principal direction ranges between 15-70 degress.

5.9 Conclusions

In this chapter the, analytical models for strength and stiffness of the profiled steel sheeting for various boundary conditions are derived. This models are validated by small scale model tests and finite element analysis. Model tests showed reliable and repeatable results with good performance of the shear rig. The stiffness and strength of the profiled sheeting are found to be dependent on the manner of attachment of the sheeting to the boundary frame. The failure of the sheeting is associated with the formation of local buckling and extended tension field. Unstable and very rapid post-buckling behaviour suggested not to use post buckling shear reserves in the calculation of design load.

So far the individual behaviour of the sheeting and concrete core has been covered. In the next chapter, the behaviour of the composite wall will be presented.

Photograph 5.1: Spot welding process

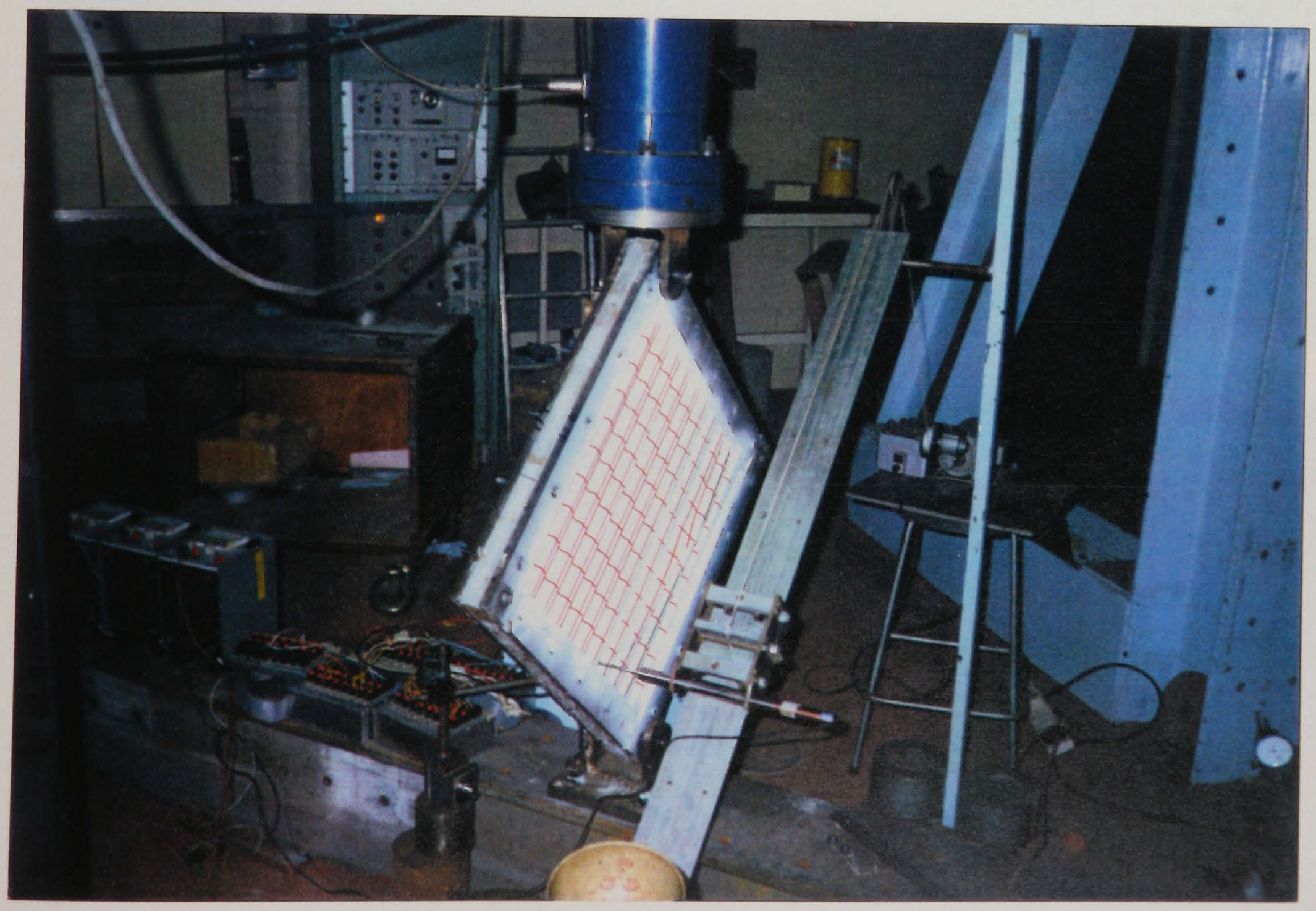

Photograph 5.2: Experimental set-up

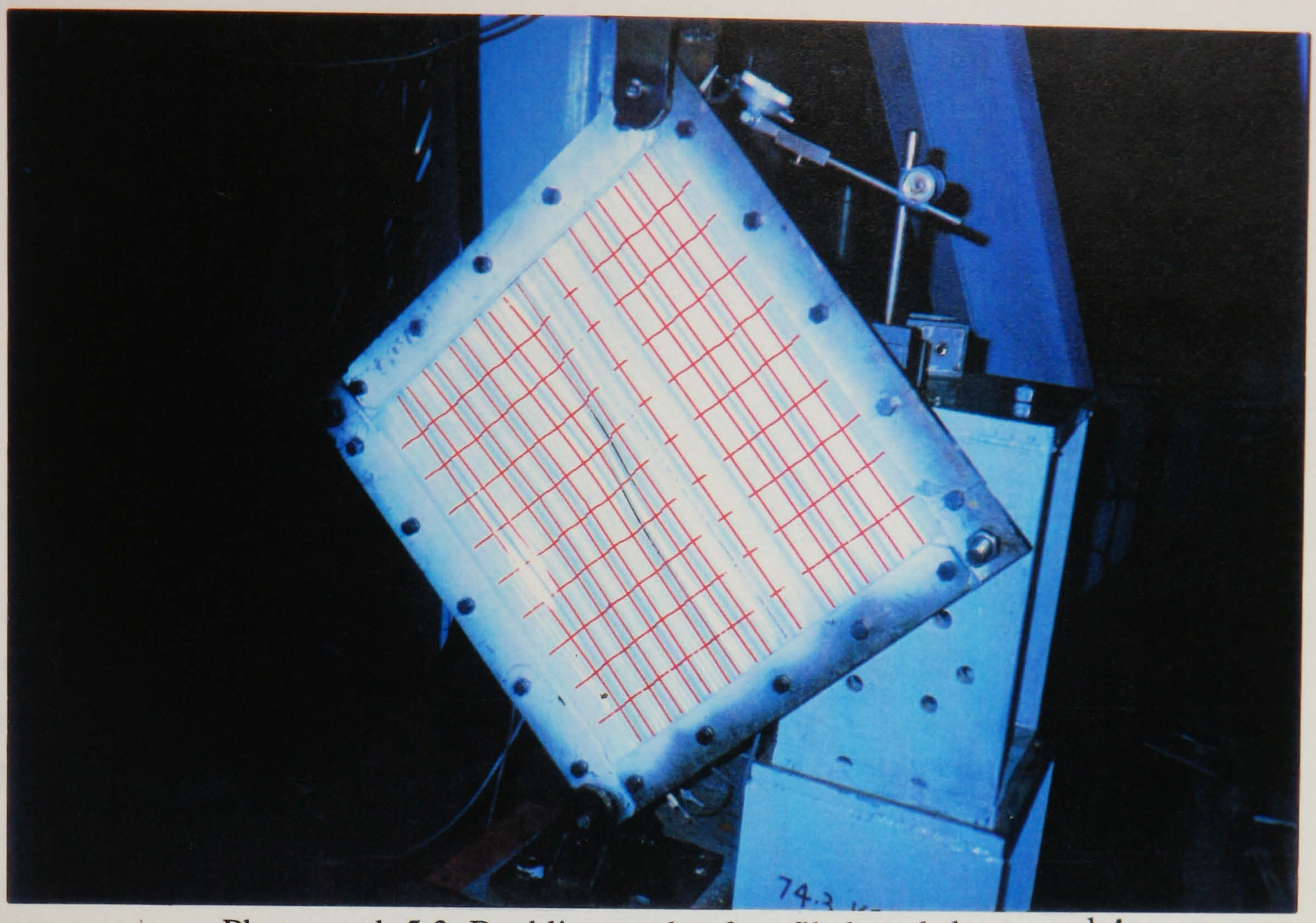

Photograph 5.3: Buckling mode of profiled steel sheet panel

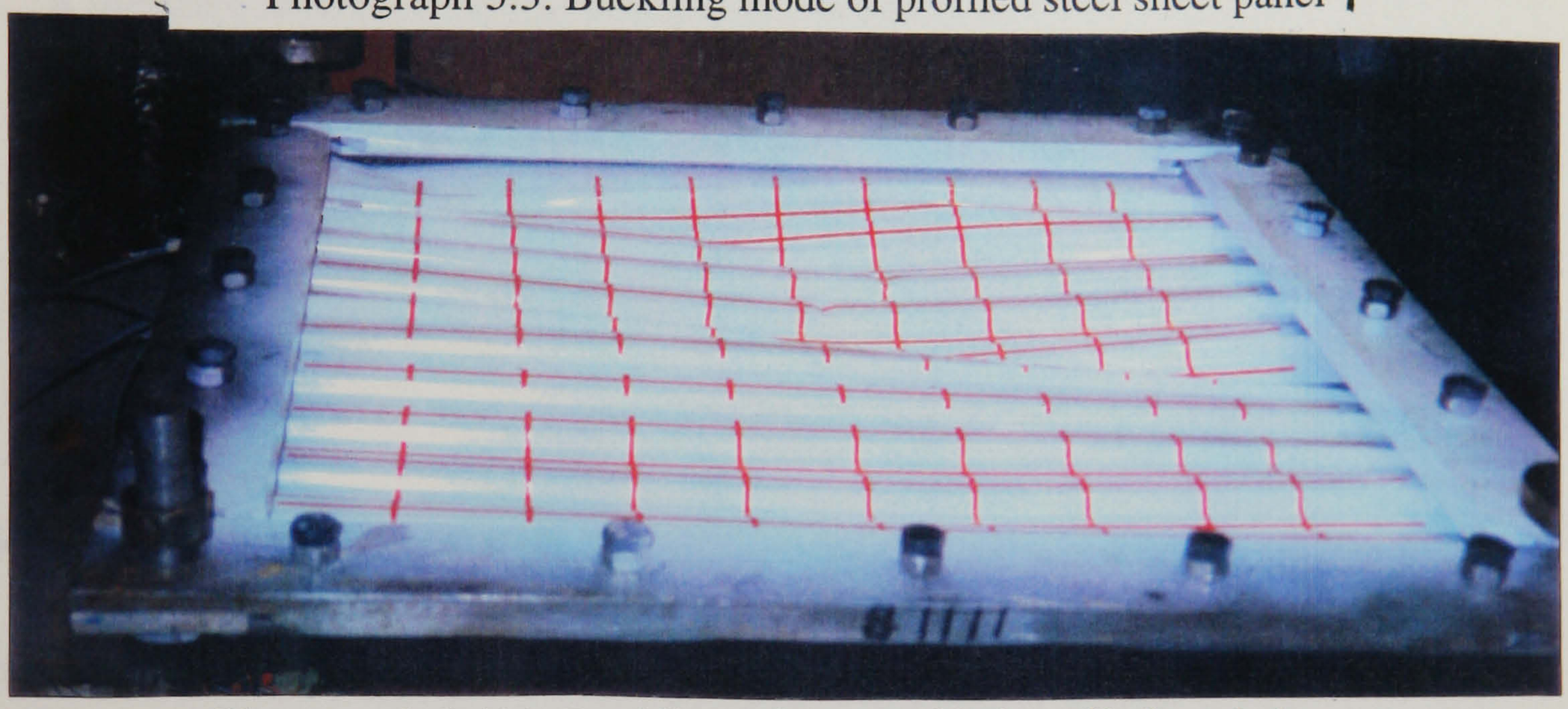

Photograph 5.4(a): Buckling of spot welded profiled steel sheet panel

Photograph 5.4(b): Failure of the panel showing tearing of sheeting

CHAPTER SIX

IN-PLANE SHEAR BEHAVIOUR OF COMPOSITE WALL

6.1 Introduction

The in-plane shear strength and stiffness of the double skin profiled composite wall is very important when they are to be used as lateral load resisting system in steel framed buildings. Design provision for this novel form of construction under in-plane shear does not exist in any specification. Analytical and experimental investigations carried out to study the individual behaviour of the profiled steel sheeting and concrete core were described in previous chapters. This chapter will describe :

- A literature review of the related previous research,
- A description of small scale composite wall model tests and analysis of test results,
- The development of analytical models for the in-plane shear strength and stiffness of composite walls,
- Numerical modelling of the in-plane shear behaviour composite wall using the finite element method and
- Comparison between analysis and experiments and validation of analytical models.

6.2 Review of related research

The idea of the composite walling was originated from the use of profiled steel sheeting in composite construction specially composite slabs. The previous research areas which will provide information on the behaviour of composite walls includes composite slabs, composite slab diaphragms, double skin composite beam columns, steel plated beams and double skin plain and profiled composite walls. A brief description of the previous work exploring the behaviour and identifying the problems that may be related to current research will be highlighted.

6.2.1 Composite slab

Steel framed buildings are typically constructed using steel-deck-reinforced concrete floor slabs commonly referred to as composite slabs. Composite floor system are constructed by fastening sections of cold-formed profiled steel deck to steel framing

members. The connections may be arc-spot welds, screws, powder-actuated pins, air driven pins, welded shear studs, or a combination of these. Seams between adjacent panels may be welded, screw fastened or button punched. A layer of concrete is placed on the deck, with shrinkage and temperature reinforced added. Supplemental reinforcement may also may be added in the positive or negative regions of the slab. Shear transfer needed for composite action between the deck and concrete is established by a combination of chemical or material bonding at the interface, friction and mechanical interlock provided by the shear transfer devices. The shear transfer devices typically consist of embossments of various shapes rolled into the deck profile or re-entrant profile.

Work was begun in the 1950's that led to the acceptance of steel deck as tensile reinforcement (Friberg 1954). The section consisted of a trapezoidal deck section with cold-drawn wires placed transversely to the deck and welded to the deck and was known as 'Cofar'. The required horizontal shear transfer at the deck-to-concrete interface was provided by the transverse wires.

The first steel-deck section with embossments or indentation rolled in to the profile was introduced in 1961 by the Inland-Yerson Co. (Dallire,1971). This Hi-bond floor deck is a trapezoidal profile that uses the embossments as the shear transfer mechanism to achieve composite action.

Bryl (1967) reported an investigation of a number of different steel-deck profiles acting compositely with concrete. Based on numerous test results, Bryl outlined the following important behavioural and design characteristics: i. sudden failure of the slab occurs without the use of shear devices, ii. large plastic deformations are accompanied by considerable increase in load-carrying capacity in the slab with shear transfer devices; and iii. the slab should be analysed as an uncracked composite section with the criteria for concrete bending stress, bond stress and permissible load on shear transfer devices.

Because of the analytical models were not adequate for predicting the strength of composite slabs constructed with embossed decks, the engineers became totally reliant on experimental test programs for strength determinations. This resulted many tests being performed by many different deck manufacturers. In an effort to gain a fundamental understanding of the behaviour of composite slabs and to subsequently develop a general design procedure, the American Iron and Steel Institute (AISI)

initiated an extensive research program at Iowa State University (ISU) in 1967 under the direction of Schuster and Ekberg. Subsequent research were carried out by Schuster (1976), Porter and Ekberg (1971) and Porter and Ekberg (1976) during the course of the project. Design recommendations for composite slabs were developed at ISU in conjunction with an AISI Task Committee. These recommendations formed the basis for the ASCE standard on composite slabs (Specifications 1984) and led to the linear regression method that also forms the basis for the testing requirements included in the British code of practice; B.S.5950 Part 4 (1982).

Related research has also been carried out in Britain by Wright, Evans and Harding (1985,1987) and brief development of the use of composite slab in Britain can be found in their papers.

The most prevalent limit state as identified in past laboratory tests of composite slabs is shear bond which is very much dependent on the geometry, orientation and frequency of embossments. An extensive literature review of the bond in composite slab and mechanism of shear-bond type failure has been presented by Patrick and Bridge (1994). This limit state is characterised by a degradation of the steel-to-concrete interface within the shear span. The shear span is normally defined by the distance from the support to the nearest point load or approximately 1/4 span for a uniformly loaded slab. The steel deck and concrete are then essentially free to slip relative to one another, with only resistance provided by the mechanical interlock due to the embossments. In addition to the horizontal shearing forces, the imposed bending action leads to the vertical separation between steel and concrete.

Wright, Evans and Harding (1985,1987) refer to chemical and mechanical bond in a crude explanation of slab behaviour. They infer that chemical bond may be broken down without flexural cracking and after the initial (end) slip has occurred at the breakdown of shear bond (chemical), the concrete slab separates, lifts and rides over the embossments and collapse occurs. Wright and Evans (1987) stated that re-entrant profile develop longitudinal frictional forces on account of 'vertical bond' and improved friction can be created by rolling embossments in the steel.

Daniels(1988) explained that three different actions resist longitudinal slip, viz.: chemical bond, frictional resistance and mechanical resistance due to physical interlocking of concrete and steel sheeting at embossments. He argued that the term 'bond' should only refer to resistance developed by chemical bond before the initiation

of end slip and frictional and mechanical resistance could both be generally referred to as 'embossment resistance' which was assumed to develop after the initiation of end slip.

Strength expressions based on the shear-bond limit state were originally developed at ISU by Schuster(1976) and are an integral part of the ASCE standard (Specifications 1984). The linear regression method of Code requires a specified series of tests to be carried out for the determination of two factors m_r and k_r expressing the characteristics of a particular profiled sheet. These two factors often thought to represent, the mechanical and chemical bond respectively between steel and concrete. This is however not accurate and these two factors have no physical significance (Wright, Evans and Harding , 1987), but they are important in that they may be used subsequently to determine the ultimate capacity when the same sheet is used for different spans, slab thickness and concrete strengths. The British Standard requires a minimum of six tests to be carried out on representative slabs from which a straight line may be drawn (regression line) as shown in figure 6.1. This line is then adjusted by a reduction of between 10% and 15%, depending on the number of test carried out. Two factors can be taken from this reduced line; the first value m_r represents the slope and the second value k_r represents the intercept. These values of m and k may then be substituted into the empirical expression 6.1 suggested by Porter and Ekberg (1971) to determine the strength of the slab.

$$\frac{V_u s}{bd} = \frac{m_r \rho d}{l'} + k_r \sqrt{f_{cu}} \qquad \text{.....(6.1)}$$

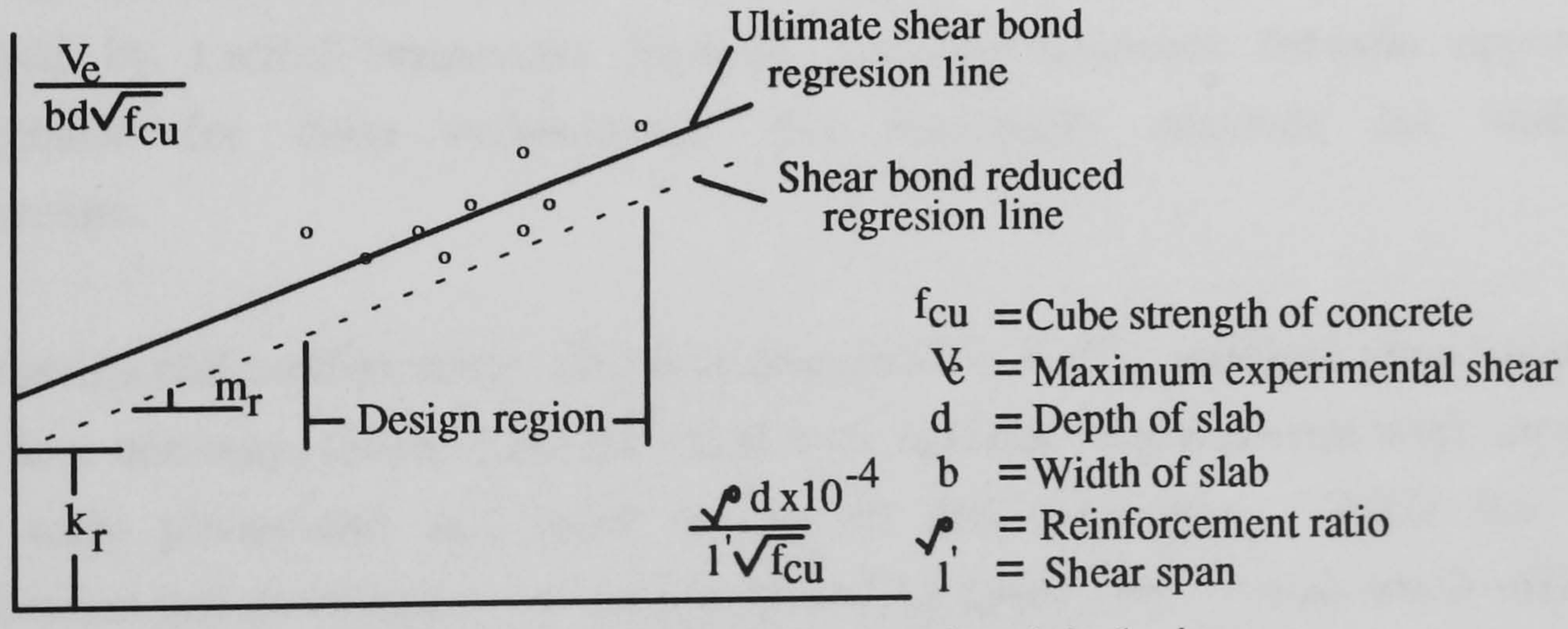

Figure 6.1: Codes method of Composite slab design

Seleim and Schuster (1982) presented a further formula in which the thickness of the sheeting was included, thus further reducing the number of tests required. This formula increases the number of unknown factors to four which have no physical meaning and proves very complex requiring computer statistical packages. Luttrell

and Prasman (1984) proposed a design method which completely removes the requirement for testing. The formula is based on an elastic analysis with four statistical coefficients or relaxation factors, one of these factors being determined empirically from a large number of test results obtained from Luttrell's comprehensive studies over many years. These factors take into account the embossment size and shape, slab dimensions and deck dimensions and have some physical significance. This method is attractive to steel deck manufacturers as it provides a way to predict the performance of a potential new deck profile and embossment pattern without manufacturing and performance testing in advance. However, the accuracy of this method depends on whether the previous test results are entirely representative or not.

Wright, Evans and Harding (1985,1987) carried out over 200 tests on profiled steel sheeting and composite slabs and the results were compared with current design methods. They came out with the following conclusions:
(i) the strength of the concrete did not affect the shear bond strength of the system, providing a minimum concrete strength is achieved, (ii) failure was due to loss of shear bond although yield strains were observed in the steel in some instances, (iii) the depth of embossments had significant effect on the shear bond capacity, (iv) both methods of analysis requiring test information gave accurate prediction of shear bond capacity and additional complexity of the Seleim-Schuster formula does not appear to achieve additional accuracy and (v) the requirement for representative testing appeared unavoidable but decks of similar geometry and indentation might be compared by Luttrell-Prasannam formula. Luttrell-Prasannam formula appeared unacceptable for deep embossments but reasonably accurate for shallow embossments.

The experimental configuration, which is described in ASCE standard (Specification 1984), is a one-way, single-span, provided with nominal reinforcement with support details truly pinned-end and roller having no end anchorage. While the test configuration just described is convenient for testing agency but several details make it non representative of in service composite slabs. The Code assumes that the test results provide lower-boundary estimations of static load carrying capacity. Despite much controversy and criticism, this testing philosophy has stood the test of time. The same design philosophy is used in the British code (Structural, 1982), Canadian (Design, 1988) and Eurocode 4 (1990).

The researcher's were always in search of an alternative to the full-scale testing which take into account the effect of end anchorage, continuos spans, differentiation of ductile or brittle failure and the influence of brittle failure mechanism such as initiation of concrete cracking and chemical debonding. These parameters are not included in the present codes of testing procedures. Daniels and Crisinel (1993) developed analytical models based on partial composite action which fulfils the aforementioned interests and did a good job in modelling the behaviour. These models were dependent on elemental shear bond tests that are used to determine interfacial properties. Pull-out tests were used to determine embossments load-slip behaviour and push-off tests were used to determine end anchorage (provided by shear connector) load-slip behaviour. The results of the elemental tests were substituted into numerical models that require computer-aided solutions for practical applications. The numerical finite element models took account for the non-linear material behaviour and allowed for the effect of slip between the decking and the concrete slab. A typical load-slip behaviour from pull-out test according to Daniels et all (1993) is presented in figure 6.2. Two typical behaviour labelled 'ductile' and 'brittle' are shown. In both behaviours, the chemical bonding is clearly indicated by shear resistance without accompanying slip. Brittle failures are typically associated with decking without embossments or those with small embossments where mechanical and frictional shear resistance are substantially lower than the initial chemical bonding shear resistance. An extensive literature review of these elemental shear bond tests are presented by Patrick and Bridge (1994).

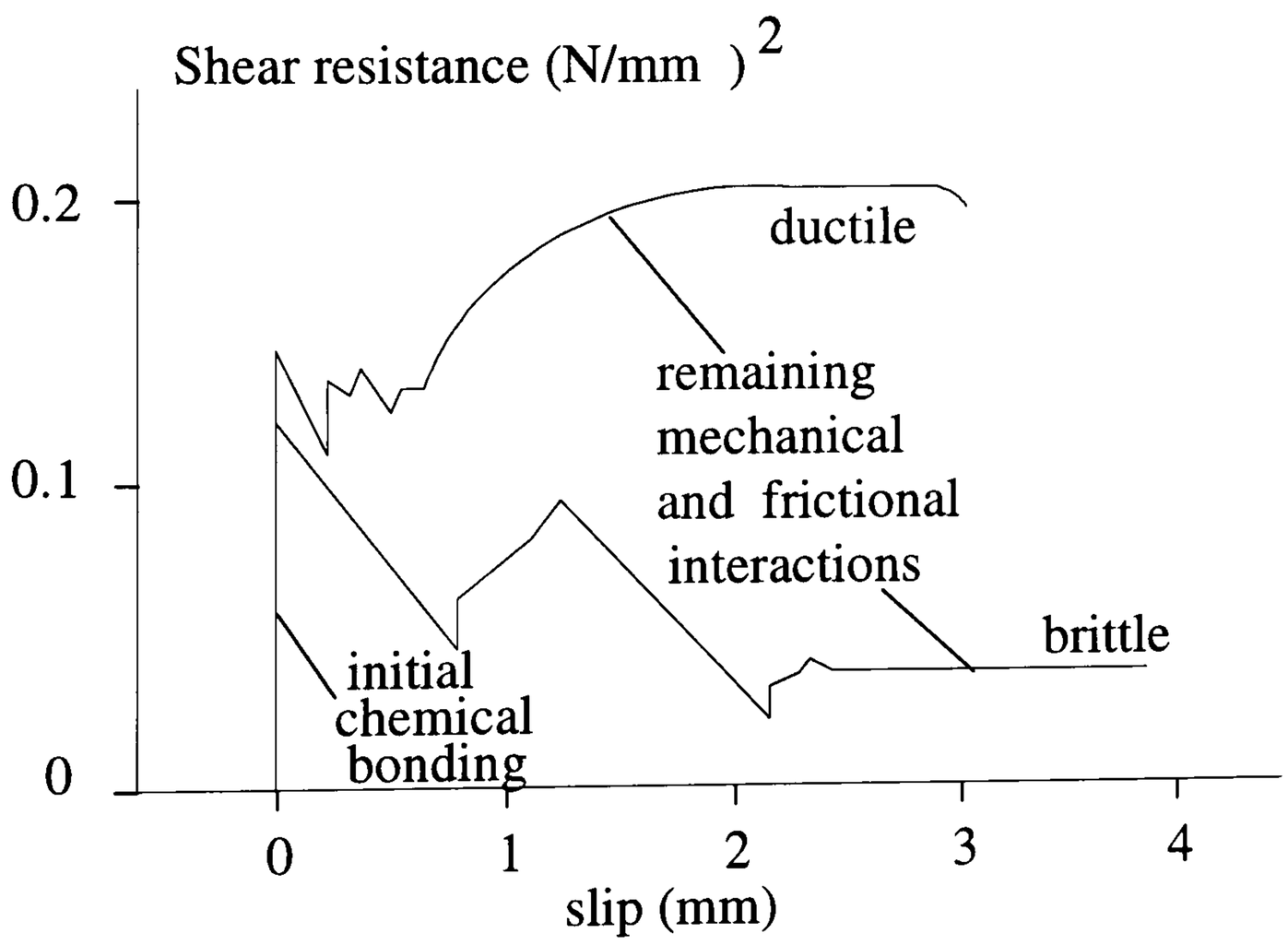

Figure 6.2: A typical load-slip behaviour from pull-out test (Daniels et all,1993)

Easterling and Young (1992) presented an analytical approach for the strength and initial stiffness of composite slabs. The approach is based upon conventional reinforced concrete concepts with elastic principles. Comparison of results from a series of nine experimental composite slab tests that incorporated typical construction details, indicated that design procedures for composite slabs may be developed based on calculations.

A significant series of test results was reported by Roeder (1981). Typical end conditions (shear studs and continuos deck spans) were considered. Although an analytical method was not suggested, the results provide an indication of the conservative nature of the ASCE standard (1984).

Veljkovic (1995) studied longitudinal shear capacity of the composite slabs. The study included the interface performance between sheeting and concrete, full scale composite slab tests and numerical modelling of the slab behaviour using DIANA finite element package. The interface between the sheeting and concrete is modelled using node interface elements. The parameters of the interface elements to represent actual sheet-concrete interface was modelled from the tension-push tests together with push and friction tests.

6.2.2 Composite slab diaphragms

In multi-storey structures, the floor system may be an integral part of the lateral load resisting system in addition to vertical loads and can act as a diaphragm to distribute in-plane loads to adjacent frame or wall. The behaviour of the composite slab as a diaphragm is closely related to the current research of in-plane shear behaviour of composite walls.

A series of nine diaphragm tests with lightweight insulating fill having welded connections were performed by Luttrell (1971) and the results were compared with similar diaphragm without insulating fill. The insulating fill provided an increased warping resistance with connector strength as the controlling limit state. Expressions were developed that correlate diaphragm strength to the number of welds along the edges of the diaphragm.

Four composite diaphragm tests were performed at the University of Salford (Davies and Fisher 1979). Trapezoidal and re-entrant steel deck profiles were used in the study and connected to the perimeter framing members with self-drilling, self-tapping

screws. Equations are presented to determine the strength of the diaphragm based on the strength of the connectors which was the controlling limit state. The expressions were developed based on assumed connector force distribution.

The lack of behavioural understanding and of generally applicable design technique for composite diaphragm was identified by Iyengar (1977). In 1978, the National Science Foundation (NSF) initiated a research project at Iowa State University (ISU) to determine the behavioural and strength characteristics of composite diaphragm. A description of the diaphragm studies prior to ISU research and subsequent research up to 1994 was presented by Easterling and Porter (1994a, 1994b). The predominant limit states in early research by Barnes in 1957,1963 and 1966 (as reported by Easterling and Porter, 1994a) were similar to those described in the ISU studies. Barnes and Associate developed empirical equations for both strength and stiffness of panels that were fastened with arc spot welds. Barnes and Associates reported failure (as reported by Davies & Fisher,1979) in the concrete topping whereas Davies and Fisher (1979) found no distress in the topping. The highest shear in the Davies and Fisher's test was 28.6 kN/mm, whereas in the test of Barnes cracking did not start until a load of 31 kN/mm and failure was delayed until a load of 86.4 kN/mm. The difference in behaviour was clearly a consequence of the relatively high strength of welded connections to the perimeter structures. There was negligible shear strength in the button-punched seam connections.

Experimental results from 32 full-size diaphragm tests having no slab reinforcements and associated elemental push-off tests are presented by Easterling and Porter (1994) including also the experimental limit states, maximum applied load and initial stiffness values. The strength of profiled composite diaphragms is controlled by one of three limit states: diagonal tension failure of the concrete, edge connector failure or shear-transfer mechanism failure. For a given diaphragm, the minimum value of these three is taken as the governing strength. The last two of the diaphragm limit states are a function of force distribution at the perimeter framing members. Analytical expressions strength and elastic stiffness for these limit states have been developed based on results from a non-linear finite element analysis. The following findings can be summarised from this extensive series of tests:

- The results from the experiments confirmed that the shear forces are transferred between the frame members and the concrete slab within a relatively narrow region at the edge of the diaphragm. At locations outside or away from the edge

zone, steel deck contributes little to the diaphragm behaviour. Likewise, the connections outside the edge zone (welds or studs to the edge beams) contribute little to the diaphragm behaviour.

- The use of shear studs restrains the separation between the deck and concrete, therefore, the transfer of shear through the interface is only of interest for composite diaphragms not constructed with shear studs. The steel deck has little influence on the strength or stiffness of composite diaphragms constructed with shear studs.
- The experimental composite diaphragms exhibited brittle inelastic behaviour. The brittle nature of the diaphragm response is not surprising. Each of the three limit states observed in the test program is individually brittle. Diagonal tension strength and shear stud strength, controlled by concrete strength, are both a function of cracking in unreinforced concrete. The deck -concrete interface behaviour is a function of chemical bond which fractures in brittle fashion. The strength of connections made with arc-spot welds in thin -walled steel tends to be limited by tearing of the sheet adjacent to the welds. This results in brittle failure of the connections. Reinforcing of the slab will do nothing to improve the ductility of diaphragms that have strength controlled by either the shear-transfer mechanism or welded connections.
- Only the diaphragms that were connected with arc spot welds showed significant slip between steel deck and concrete. The end slips near the corners exhibited greater increases than those near mid depth. The diaphragm that were fastened using shear studs did not exhibit the separation of the deck and concrete at the interface as long as diagonal tension cracks did not form, the formation of such crack was accompanied by a separation of interface.
- The gravity load influence on the strength and stiffness of the experimental diaphragms appeared to be minimal.

The two dimensional non-linear finite element model developed in this study considered the non-linear behaviour of spot-welds, shear studs and deck concrete interface. The profiled sheet was idealised as equivalent orthotropic flat sheet using linear iso-parametric plane stress elements. The concrete fill was considered as flat plate of average thickness and modelled with iso-parametric plane stress elements. Linear beam elements were used to represent perimeter framing members.

Edge connectors were represented by two one dimensional, lengthless, non-linear, force-displacements elements with one spring parallel to the edge beam and other

transverse. The two elements were independent and this type of modelling ignores interaction in the two orthogonal direction. Analytical weld response curves were formulated based on the information reported by Atrek and Nillson (1976) and Luttrell (1981) along with specification (Specification 1986) values for weld strength. Stiffness and ultimate strength values were determined from this response and incorporated in the spring elements to represent numerically welded connections. The empirical expression for load versus displacement of a headed shear stud embedded in concrete developed by Ollgarrd et all (1971) was used to numerically model the shear stud connectors. The expression was validated by elemental push-off tests conducted as a part of the ISU research.

The deck concrete interface was the most uncertain portion of the model, due to the lack of accurate interfacial data. The load versus displacements relationship was derived from elemental push-off tests (arrangement shown in figure 6.3), performed as part of the ISU research and incorporated in the numerical interface elements. Specimens were constructed to model segments of the diaphragm in which ribs were oriented either parallel (longitudinal shear bond) or transverse (transverse shear bond) to the applied load. The interface was modelled discretely by two one-dimensional, lengthless, non-linear, force-displacement elements similar to edge connections at each locations where the interface was modelled.

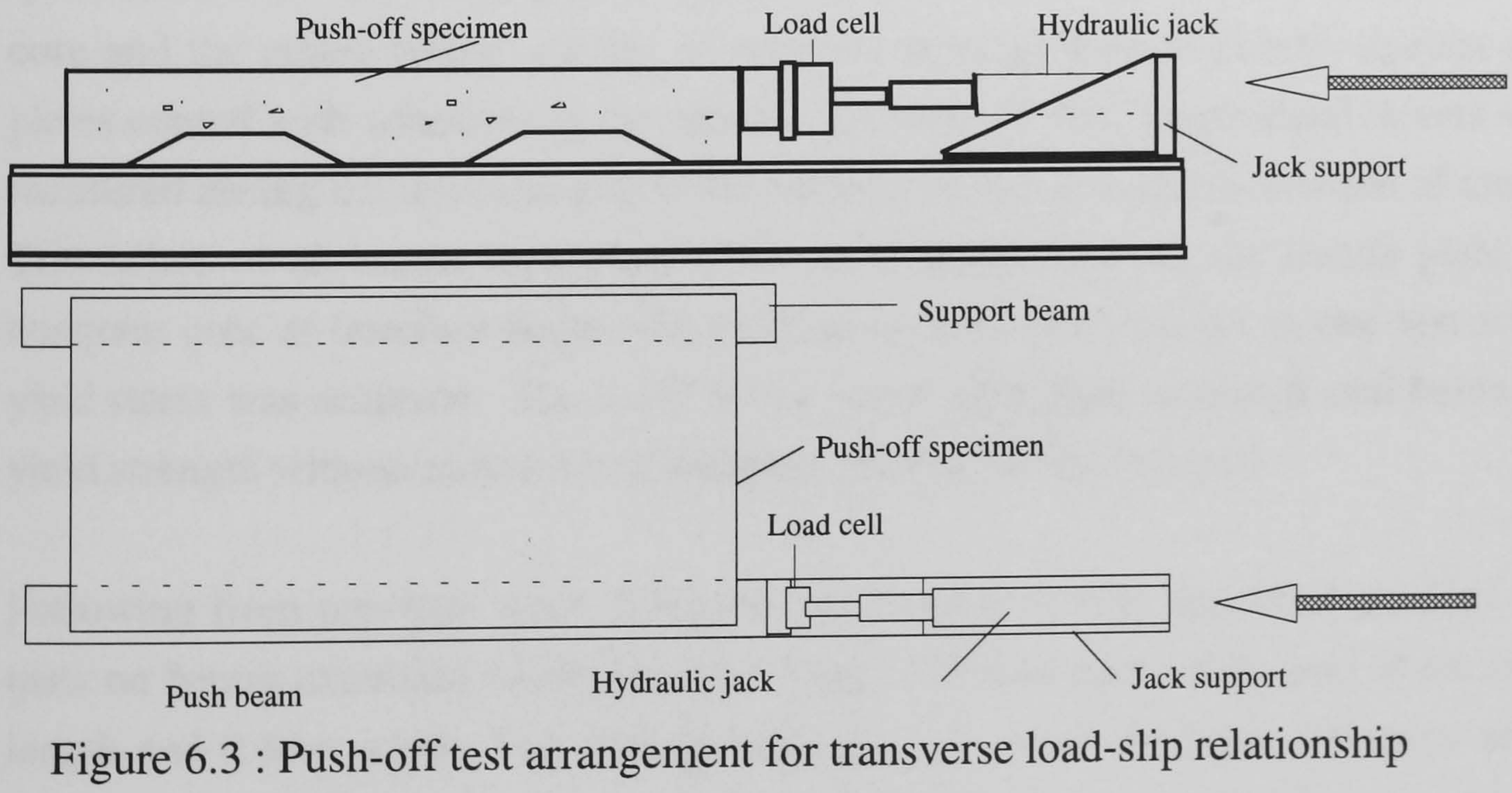

Figure 6.3 : Push-off test arrangement for transverse load-slip relationship

The analytical and experimental strength and stiffness values showed good agreement. The analytical expressions developed for strength and stiffness are a function of cantilever arrangement and they are not directly applicable to other boundary conditions. Attention should be given to the weld and interface models because

general relationships for these elements are not available. Finite element analysis is necessary to determine the edge force distribution for different boundary conditions. Currently available methods to calculate individual weld stiffness or arc-spot welds do not reflect the influence of weld size (Luttrell,1981). This parameter is important as small change in the individual weld stiffness will significantly affect the total diaphragm stiffness.

6.2.3 Steel plated elements

Reinforced concrete beams can be strengthened and stiffened by gluing steel plates to the tension face of the beam. This procedure has been used to repair buildings (Van Gemert 1981) and to strengthen bridges and it has been used in Belgium, France, Japan, Poland, South Africa, Switzerland and United Kingdom (Jones et al 1988). A brief review will be presented here. L' Hermite and Bresson (1967) carried out tests on concrete beams with steel plate bonded by epoxy resins to the tension surface. Tests were also performed on beams constructed by pouring concrete into U-shaped permanent forms coated with epoxy resin.

Solomon, Smith and Cusens (1976) working at the Wolfson Bridge Unit at Dundee University performed a series of flexural tests on double skin slabs and beams and investigated the suitability of the accepted design procedures. Two types of specimens, one where steel plates were glued on both faces of the hardened concrete core and the others where casting of concrete were performed directly against steel plates coated with adhesives in the mould. Deflections and longitudinal strains were measured during the tests along with the notation of location and inclination of cracks. The failure of all beams took place after the slippage between the tensile plate and concrete core at interface before the yielding in steel plate except in one test where yield stress was achieved. The strain in the upper steel plate remained well below the yield strength with no indication of buckling prior to failure reported.

Following from previous work Solomon and Goplani (1979) described a series of 5 tests on beams externally reinforced by a single 1.84mm thick mild steel sheet of 4m length and 0.36m width. The stirrups were also provided, the same thickness as the sheet, and welded to the surface of the sheet. The beams were tested under two point loading and deflection and strains in concrete and steel were recorded during the test. No bond failure at the steel concrete interface or indication of shear cracking within the shear span was observed. All beams collapsed due to failure of the upper concrete in flexural compression following tension yielding of the lower steel sheet.

They concluded that the beams satisfied the ultimate and serviceability requirements and that the main economics of this approach would be in ease of construction and reduction in reinforcing steel and form work.

Mays and Smith (1980) updated work carried out at the Wolfson Bridge Research Unit and confirmed the viability of bonded steel plates as a viable structural option but suggested further work was required on the long term durability and performance under actual traffic conditions.

Ong et all (1982) at the Wolfson Bridge Research Unit noting the low stresses obtained on the upper flanges in the work of Solomon et all (1976) carried out a series of tests using the cast-in-place technique -applying the adhesives to the steel and casting the concrete on top. Different adhesives and mix types were tried on 38 beams and 6 slabs cast. They concluded that provided an efficient bond existed between the concrete and steel both slabs and beams behaved compositely. The long span tests failed in bending with short span tests from shear slip with collapse after the detachment of the concrete from the steel. For optimum strength and ductility a 1mm minimum adhesive thickness was suggested.

MacDonald (1978) reported on a series of four tests on reinforced concrete beams with steel plates bonded to their tension flanges. The tests reacted to the possible use for increasing the load capacity of existing bridges. An interesting results of the experiments was the failure of the beams at al load similar to that of the unplated beams because of horizontal shear forces removing the steel plate at loads below the ultimate unplated beam strength. The variables such as type of resins, thickness of plate, the effect of load cycling had little effect on the load causing plate separation.

Hamoush and Ahmad (1990) examined the debonding of concrete beams strengthened with steel plates applying linear elastic fracture mechanics and the finite element method. The conservation laws were applied to determine the energy release rate at which the crack would propagate and beam failure occur. For undamaged concrete beams the strain energy release rate was negligibly small giving a high interface debonding load. Also, the strain energy release rate reached a maximum value when the length of the interface cracks was equal to the length of the flexural cracks. The adhesive thickness had little effect on the failure load.

Previous experimental tests show the premature failure due to separation between steel plate and concrete referred to as peeling. More recent theoretical research by Roberts and Haji-Kazemi(1989) and experimental tests by Oehlers (1992) show that peeling can be induced by shear forces and flexural forces. Oehlers (1992) studied peeling due to shear forces and interaction between shear and flexural peeling and formulated a design procedure to prevent debonding due to peeling. It is shown that this system is better suited for the strengthening of reinforced concrete slabs than beams.

6.2.4 Double skin composite beam and columns

One of the largest bodies of work investigating the application of double skin composite beams and columns where mechanical devices are used to secure bond between steel and concrete has been performed at the University of Wales College of Cardiff. The system was originally devised for submerged tube tunnels by a team of consultants in Cardiff (Messrs Tomlinson and Partners with Sir Alexander Gibb and Partners). The system proposed by Naraynan et all (1987) consisted of a double-skin steel plated construction secured by welding headed studs at suitable intervals anchored in a concrete infill (see figure 6.4). The spacing of the studs was used to control the local buckling of the steel sheets under loading. The advantages suggested over traditional reinforced concrete tunnels included fabrication in sections, speedier construction and better quality control. Also, in conventional concrete tube tunnels an outer steel layer is required to ensure water tightness but with external steel skin reinforcements this would not be required. Tests were performed on full and half scale models of the tunnel sections.

The half scale tests with a rectangular cross-section 250mm deep x 800mm wide and 4 m long had steel plates 6mm and 3mm thick secured to the outside and inside of the concrete by 6mm diameter mild steel bolts. The failure of the beams in simply supported and cantilevered tests was exhibited by shear cracks developing in the concrete at the quarter span positions with steel plate buckling and yielding accompanied by stud shearing. The full scale double skin composite beams had full size stud connections spaced at 300mm centres. The type of failure is similar to the half scale tests. Naraynan et all concluded that the applications of the system were not limited to submerged tunnels but had wider general applications in construction.

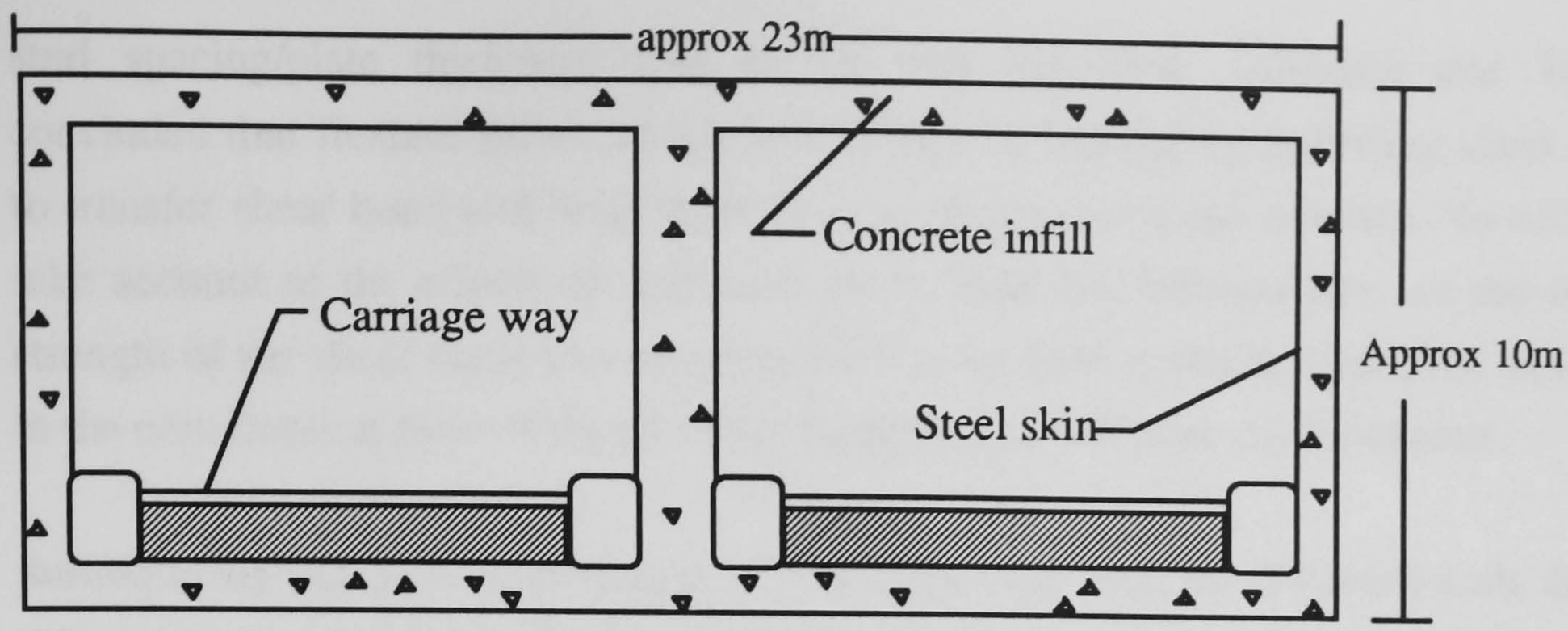

Figure 6.4: Typical tunnel section

Following from this initial work Oduyemi and Wright (1989) reported on an investigation into the behaviour of double sandwich beams. They tested 18 model beams of dimension 150mm x 150mm x 1500mm under two point loading (see figure 6.5) to investigate the effect of overlapping shear studs, steel skin thickness, spacing of top shear connector, amount of bottom shear connector and low concrete strength.

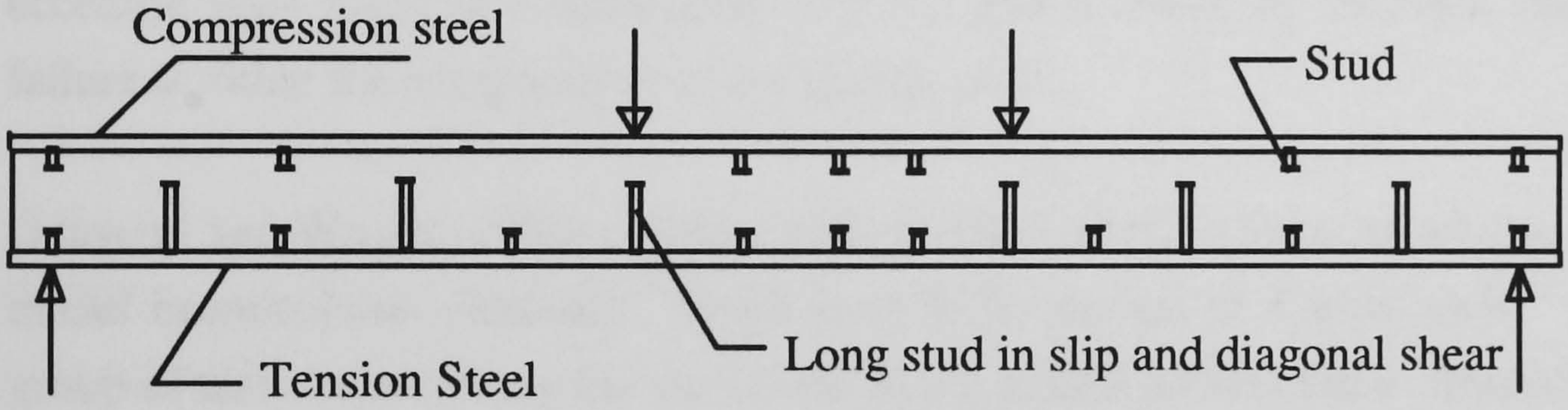

Figure 6.5: Double-skin Composite Beam

The bond between steel plate and concrete was removed by greasing the inside faces allowing the studs alone to take the interface shear. The beams were expected to fail in either flexural, horizontal slip or vertical shear failure. When flexural failure of the beam occurred the deflection was linear up to tensile strength of lower steel. After yielding the beams behaved with a large amount of ductility until collapse produced by concrete crushing. Horizontal slip failure occurred after the flexural cracking of the concrete and an increasing rate of bottom slip. The failure was sudden with shearing of the bottom plate from concrete caused by stud failure. Vertical shear failure occurred in the 'diagonal tension' manner with final collapse when the dowel action capacity of the steel plates was reached. This type of failure was prevented by introducing long studs to provide shear reinforcement. Local buckling of the compression plate reduced the value of ultimate load in some tests and so a maximum

stud spacing/plate thickness ratio of 30 was proposed. Oduyemi and Wright concluded that flexural failure of the beam could be realised by providing short studs to transfer shear bond and long studs to carry diagonal tension stresses. In order to take account of the effects of combined shear, axial and bending stresses the design strength of the shear studs was recommended to be 55% in the tension zone and 80% in the compression zone of the ultimate strength obtained from push-out tests.

Subsequently Oduyemit and Wright (1989) carried out tests on 23 small scale double skin composite columns. The concentrically loaded tests all failed by crushing with plate buckling occurring prior to failure in one test where the ratio of stud spacing/steel thickness was 50. In another test where the stud length/stud diameter ratio was 6 gradual pull-out of the studs occurred followed by immediate collapse. Based on the test observations recommendations were made restricting the stud spacing/steel thickness ratio to 33 and the stud length/stud diameter to minimum of 6. Also suggested for sufficient anchorage was a stud head/shank diameter ratio of 2 and minimum size of stud equal to the plate thickness. Most of the columns tested in the eccentric tests failed in compression with the others failing by interface shear bond failure at either the compression or the tension plate.

Oduyemi and Wright (1990) continued the previous investigations by testing 12 scale model beam/column elements. There were three groups of 4 tests each. The first group of tests investigating the variations in the axial load failed in a flexural manner with cracks appearing at higher load levels for greater axial loads. In the second group, where the spacing between the connectors varied, those tests with the studs closely spaced failed in flexure while the later tests with studs further apart collapsed due to longitudinal shear. In the final group looking at the effect of thickness, the tests with thin plates failed in flexure because of yielding of the steel and the test with thickest plate shear studs failed, before yield, at the steel/concrete interface. The authors concluded that the shear connection at the tension plate was critical in determining the behaviour of the element but with correct design predictable critical loads could be achieved.

Kountoris (1990) produced design charts for the double skin composite elements based on the requirements of BS8110 with modifications to take account of failure at the steel/concrete interface. The design curves showed greater convergence to experimental as the load eccentricity increased probably because flexural rather than axial failure occurred.

Wright, Oduyemi and Evans (1991) described design developments based on the series of tests on double skin beams, columns and beam/columns. The design basis was similar to that of reinforced concrete but with the additional considerations of the possibility of plate buckling and adequate provision of shear connector. The ultimate strength in bending was based on the BS8110 stress block with a partial safety factor of 1.5 on the concrete and 1.15 of the steel strength. These equations assumed full connection between the steel plate and the concrete which require sufficient shear connectors capable of transferring the full yield load to the steel. Design recommendations were made to avoid buckling of compression plate, for basic design shear strength and for combined axial and bending effects.

Oehlers (1992) and Oehlers, Wright and Burnet (1994) described a construction technique (figure 6.6) that uses profiled steel decking as permanent and integral shuttering for the sides and soffits of the reinforced concrete beams. In this form of construction, the profiled sheet is first fabricated into fully braced open box girders as shown in figure 6.6 and reinforcing bars are added as required. The box section can be placed on site with a minimum of additional support, and the concrete can then be poured to form a composite profiled beam. Previous research (Oehlers,1992) has shown that this system has many advantages: the side profiled sheets can substantially increase the flexural strength without loss of ductility and are more ductile than reinforced concrete beams of same flexural strength; the side sheets also increase the shear strength and shear ductility; encasement of concrete reduces shrinkage and creep of concrete, which can reduce deflections by as much as 40% and allow an increase in span/depth ratio of the order of 20%.

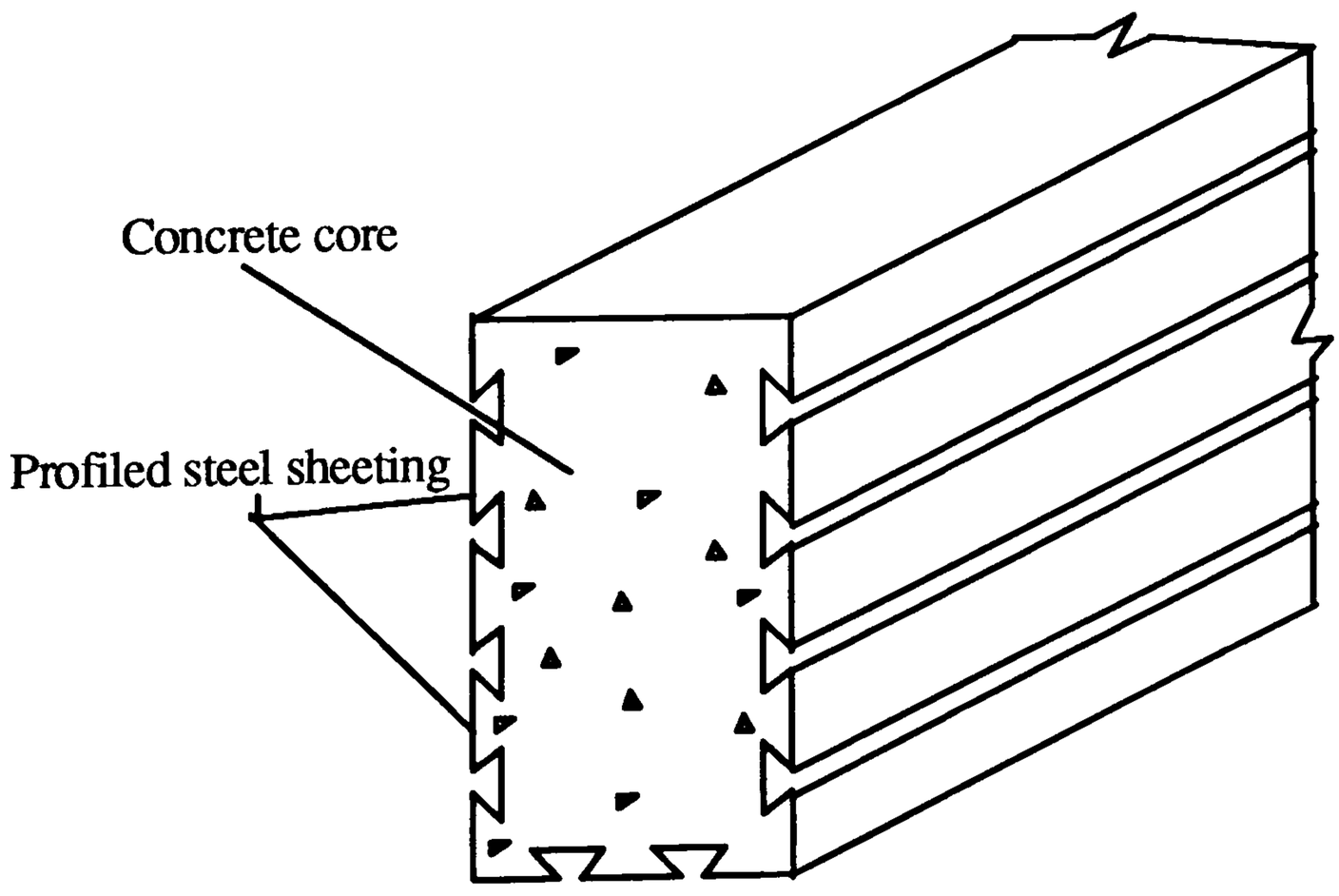

Figure 6.6: Composite Profiled Beam

Oehlers found that the flexural strength of the profiled beams can be affected by the local buckling of the sheet between the ribs of the decking. Oehlers, Wright and Burnet (1994) developed simple design procedures to prevent local buckling of the profiled sheeting before the ultimate strength is reached, and to determine the flexural strength of the beam for various strength of shear bond which allows for the variation in the bond forces at the interface due to slip. They confirmed that the shear bond failure has only a small effect on the ultimate strength.

6.2.5 Double skin composite walls

The idea of using composite steel and concrete walls to resist offshore loads was introduced a decade ago by the Hitachi Shipbuilding and Engineering Company (Adams 1987). Link and Elwi (1995) studied the ultimate and post-peak capacity of composite-steel plate walls subjected to transverse and longitudinal loading. The work is based on a significant research project financed by the Centre for Frontier Engineering Research (CFER). The project investigated simple sandwich walls consisting of double skin steel plates with concrete infill as shown in figure 6.7. The composite action was provided by the internal steel diaphragm plates connecting the two outer skin plates.

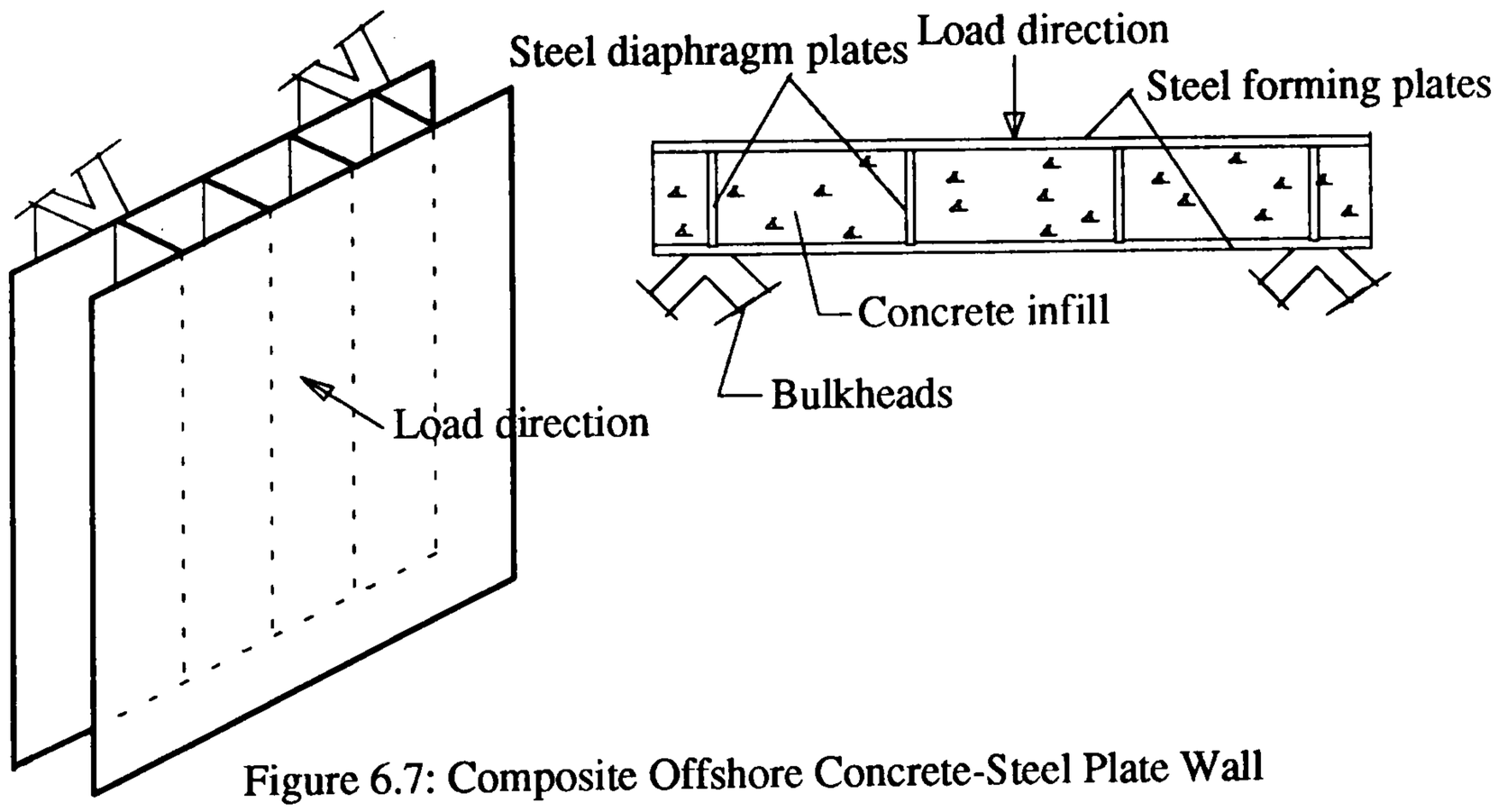

Figure 6.7: Composite Offshore Concrete-Steel Plate Wall

Each span would have 1.0m depth, comprising three or four cells. Steel plate thickness would be of the order of 25mm or more to avoid tearing during major loading events. The main application of these composite walls lies in the design of offshore structures subjected to large forces from wave action or moving ice. A non-linear finite element approach was used to predict ultimate strength, post peak response, modes of failure, load carrying mechanism and stress distribution. The steel-concrete interface was modelled with frictional and contact elements

(Lagrangian multiplier gap elements). Numerical results are compared with experimental results obtained from a variety of wall geometry and loading configurations. The numerical model gave results that were consistent with experimentally observed behaviour. The results showed that the failure mechanism was clearly that of a strut and tie model . The walls exhibited sustained post-peak residual strength for very large deflections which indicates that the ductility requirements can be satisfied.

Yerushalmi (1988) in the United States proposed a form of composite walling known as the ASP Construction System. The development of the system was primarily for use in protective structures from blast resistance and weapons. The proposed wall element consists of exterior steel panels and diagonal interior steel lacing panels with a concrete fill. The ASP wall is erected on conventional concrete foundations with roof slabs constructed using a bottom ASP exterior panel in manner similar to floor decking. The walls vary in thickness from 8 to 16 inches and can be filled with concrete, crushed stone or sand. The main advantages of ASP system according to Yerushalmi are: the potential cost savings compared to equivalent reinforce concrete systems; ASP walls are approximately half as thick as reinforced concrete alternatives; the higher factor of safety compared to reinforced concrete; reinforcement, form work and anti-spalling protection and RF shielding provided in one system and increase in speed of construction and reduction in false work requirements.

Four different types of tests have been performed to assess the ASP performance. Israeli Defence Force tests assessed ASP against fragments generated by near miss air bombs. High resistance to penetration was achieved as spalling of the inside surfaces was prevented by the inner steel surface. Further tests investigated the systems dynamic response, protection against chain detonations and the effects of direct rocket hits where 50 percent less penetration occurred than in massive concrete. Details of the system and the applications are sensitive and detailed results are classified because of the military applications.

The inherent advantages of the use of profiled steel sheeting in composite slabs leads to the concept of current research work on double skin composite wall with profiled steel sheeting with a concrete core. Gallocher (1993) investigated the viability of this novel form of construction and the main aspects of performance considered were:

- The performance of the steel sheeting as vertical form work in construction stage, supported by internal ties and lateral bracing's, subjected to lateral wet concrete pressure and
- The behaviour of the composite walls in the service stage under concentric axial loading with various heights and reinforcing details.

During a pilot study into composite walling, four full scale walls were used to investigate concrete pressures associated with concrete casting. The 150mm thick specimens were formed from 1.0 mm Richard Lees Holorib steel sheeting and grade 30 concrete using 10mm normal weight aggregate. A direct measurement of concrete pressure was obtained by locating a vibrating wire pressure cell approximately 200 mm above the base of 1.9m and 3.4m high walls during the casting process. The pressure was measured as the head of concrete increased during the casting operation. It was found that the lateral pressure envelopes developed by the fresh concrete behind the form work could be conservatively predicted using current U.K. guidance CIRIA(1985). The casting of concrete would be no more difficult than suggested by the test, as the steel sheeting provides reliable form work with little leakage.

Ultimate tests have clearly shown the brittle interface connection between the steel and concrete surfaces. Axial loading causes brittle chemical failure at the interface, with complete loss of bond, without sufficient strain to mobilise the strong ductile force developed by the embossments. Gallocher(1993) derived the following main conclusions from four pilot tests:

- The axial loading of composite wall produces a fundamentally different response than composite slabs. If a rapid distribution of load from the concrete to steel sheeting giving uniform strain distribution is not achieved, concrete crushing at the wall boundaries will result.
- Local buckling of the steel sheeting between the ribs significantly reduces the ultimate capacity of the walls although this may be prevented by reducing the rib spacing or increasing the profile thickness.
- The unrestrained steel boundary conditions requires the addition of internal reinforcement to prevent concrete crushing at the ends. Wire mesh or deformed bars were welded in different tests at the top and bottom. Providing a stronger bond between the steel and concrete at the boundaries increases the load transfer and prevents brittle failure of interface bond.
- If the local buckling is accounted and increased bond provided, the composite walls may be designed as reinforced concrete walls. If this is not the case, they may be designed as plain concrete walls.

Gallocher(1993) also carried out analytical and numerical study to obtain a better understanding of the interface behaviour of composite walls. Linear analytical analysis was performed by constructing one-dimensional linear elastic equations expressed in terms of the axial and lateral displacements in each of the three layers. Solutions were derived for critical buckling load, displacements, slips, stresses, and strains produced by various load boundary conditions. This linear analysis did not include non-linear material and slip relationships which limited their applicability to situations where brittle interface failure occurs particularly in the case of composite walls. However, linear analysis was more suited to composite columns with shear studs where brittle interface behaviour did not appear. Non-linear numerical modelling incorporated non-linear material and interface behaviour and the variation of axial boundary conditions. A computer program, DSCW, in Pascal based on Finite Difference Method was written. The non-linear model proposed by Yam and Chapman (1968) was used to represent the shear-stud behaviour. This model allows the plastic behaviour of the studs to be taken into account once the yielding has occurred. In order to take account of the complicated profiled interface behaviour with the Superholorib profile in the composite wall experiments, a model based on the pull-out tests carried out by Daniels (1988) on Cofastra 40/0.75 with a similar geometry to the Superholorib profile was devised. The model proposed, shown in figure 6.8, consists of 4 straight line sections with an initially high peak obtained from the brittle chemical bond followed by a slight decline and then a steady rise as the ductile mechanical bond from the embossments is mobilised.

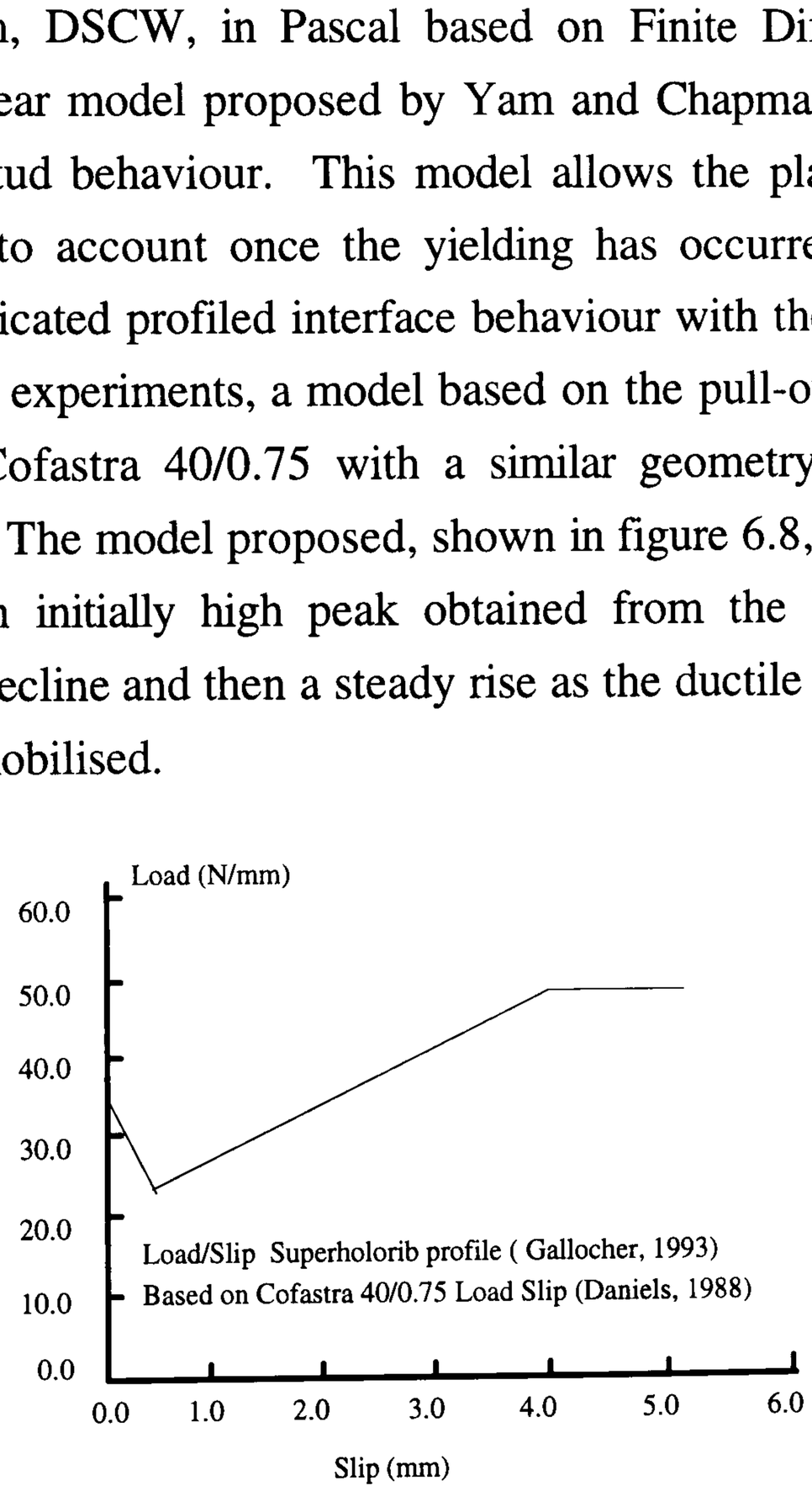

Figure 6.8: Load-slip relationship (Gallocher, 1993)

The performance of DSCW was shown to be particularly accurate when analysing the behaviour of double skin composite beams previously tested by Oduyemi and Wright (1990) but significant differences were found with double skin beam/column results.

Analysis on composite wall results suggested that the program DSCW is unsuitable for analysis, in conditions where a brittle failure occurs followed by a large drop in interface capacity and this was the case in the composite wall tests.

Wright and Evans (1995) carried out 20 full scale wall tests studying the behaviour under axial, eccentric axial and lateral loads. Load was assumed to be carried by both steel and concrete with transfer occurring between the two via embossments. The testing showed that the embossments were not capable of transferring any significant load. To secure the transfer of load, additional shear connection devices at the head and foot of the wall were used. The end shear connector detail is shown in figure 6.9.

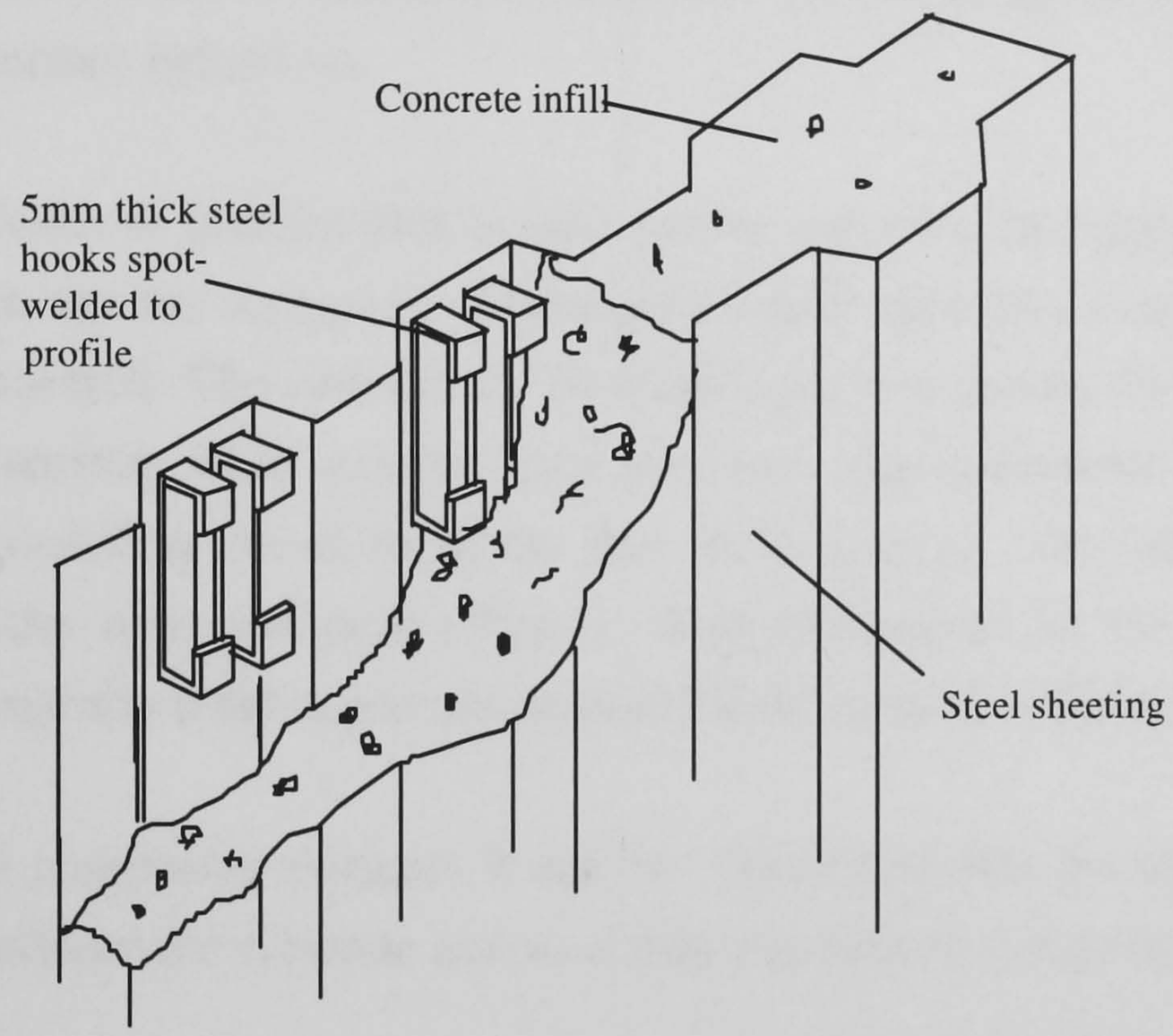

Figure 6.9: Composite wall End shear connector (Wright and Evans,1995)

The steel hooks at the adjacent pair of sheeting are connected together by stirrups welded to them. The information produced during the full scale tests has shown that the reduction in axial capacity (based on cross section area times crushing strength of concrete as assumed for stocky solid concrete wall) is closer to 30% than the nominal 10% allowed to account of imperfection and nominal eccentricity of loading in B.S.8110 (1985). The reasons for this are thought to be associated with local buckling of profiled steel sheeting and the profiled shape of the concrete. Taking into account these factors the following expressions for the axial capacity (P) of composite walls subjected to nominally concentric loading .

$$P = 0.67\alpha f_c A_c + \beta f_b A_{sc}$$

where A_c and A_{sc} are the cross section area of concrete and steel sheeting per unit length respectively, f_c= compressive strength of concrete and f_b= the lesser of the buckling stress and yield stress . The factors α and β vary from 0.6 to 0.9 depending upon the profile geometry.

6.2.6 Review conclusion

The design approach for composite slabs according to current codes of practice is based solely on test results. The shear bond failure is the limiting criteria for the design of composite slabs. The embossments providing mechanical interlock at the interface may govern the ductile and brittle failure of the slabs. Further effort is needed to develop analytical and numerical procedures for the design of composite slabs based on the interface behaviour.

Current codes of practice lack in information regarding the composite floor system as diaphragm and the composite diaphragm research provided useful information for the current research. The strength of the diaphragm was limited by the three limit states: diagonal tension, shear transfer limit state and edge connector limit state. The finite element modelling needs to model the behaviour of the steel -concrete interface based on the elemental push-off tests. Analytical model for the strength and stiffness of the composite diaphragms are derived for the cantilever boundary conditions.

For other composite elements it can be concluded that provided an efficient bond existed between the concrete and steel they can behave compositely.

The behaviour of the composite walls under axial load is quite different than that of composite slab and associated with the difficulty in the transfer of load between the steel skins and concrete core, the buckling of the steel sheeting in the flanges and the reduced capacity of the concrete core due to profiling. The problem of load transfer between the sheet and concrete was overcome by providing additional shear connection devices at the head and foot of the wall. A design method, taking into account buckling in the steel and the reduced capacity of the profiled concrete core has been developed and compares well with the test data.

6.2.7 Thoughts about current research from the literature review

The double skin composite wall with profiled steel sheeting is a new innovation as a structural elements. And as a novel element in construction it needs to explore its

behaviour under practical loading conditions. The behaviour of the wall under axial and, lateral loading conditions have been studied.

The behaviour of the wall under in-plane shear may be dominated by the same problem as in the axial situations. However, the shear behaviour of the wall will be different than axial because the profiled ribs will play an important role in providing mechanical bond as the steel tends to slide over the concrete as chemical bond fails. In this case, the transverse shear bond perpendicular to the profile derived mainly from friction rather than longitudinal shear bond (in case of slab and axial behaviour of wall) play an important role. If it is possible to mobilise fully this transverse shear bond, it is hoped that the composite wall will provide high shear resistance. Numerical simulation of the problem needs the determination of the transverse shear-slip relationship provided by the profiled rib embossed or non-embossed and concrete from push-off or push-out tests.

6.2.8 Focus on Author's study

The study will include the following :

- Small scale model tests providing information on the shear strength and stiffness, strain characteristics within the system, effect of boundary conditions, load transfer along the boundary and overall behaviour of the system including failure mode.
- Analytical model for strength and stiffness of the system which include simple design equations that can be readily used.
- Finite element analysis using package program LUSAS simulating model test conditions and cantilever bending. This will include full composite simulation and simulation with various interface elements.
- The finite element simulation of interface will not be studied too far considering the lack of practical data on the interface behaviour as this is beyond the scope of author's research. The research purely concentrating on this area is currently under progress by other researcher.

6.3 Small scale model tests on composite walls

Six small scale model tests have been performed to study the behaviour under shear loading. Three tests were performed (Test 1, Test 2 and Test 3) on model profiled composite wall where load was applied through both steel and concrete. The test 3

studied the behaviour of the composite wall under hysteretic application of load. The tests 4 and 5 on model profiled composite wall were performed by applying load through concrete only. The test 6 was conducted on model composite wall with plain steel sheeting where load applied through both steel and concrete.

6.3.1 Description and Instrumentation

The models have total dimensions of 620x620mm providing an effective dimensions of 560x560mm between the centre lines of bolts in the test frame members. The panels have a clear internal dimensions of 500x500mm between the frame members. The detailed dimensions of the models for tests 1,2 and 3 are presented in figure 3.2 of chapter 3.

Composite wall model tests 4 & 5

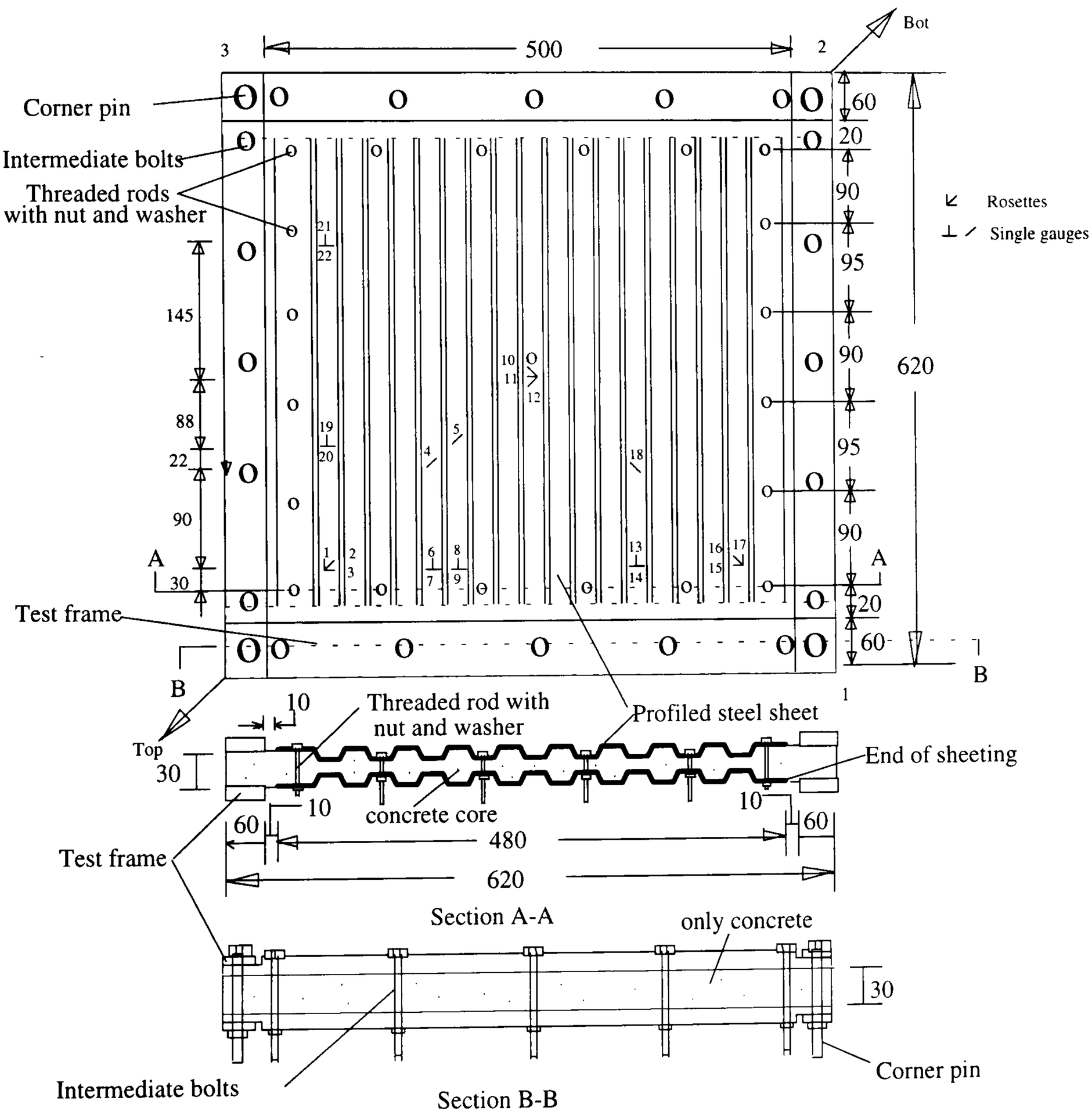

Figure 6.10(a): Details and instrumentation of test panels 4 and 5

The test panels 4 and 5 have some differences in profiled sheeting dimensions compared to those of test 1,2 and 3. As the load will be applied through concrete only, the steel sheeting was not extended beyond the internal edge of the test frame members. A clear distance of 10mm was provided between the boundary of the sheeting and the internal edge of the test frame members which restricted the sheeting size to 480x480mm square. However, the concrete core was extended to full dimensions of 620x620mm which allows the load to be transferred through the concrete only. The details of the test panels 4 and 5 are presented in figure 6.10(a). To secure the connections between the pair of profiled steel sheeting and sheeting to concrete core at the boundaries, threaded screws of 2.5mm diameter with nut and washers having (in case of test 4) or not having (In case of test 5) spacers through the concrete were used. The spacing and location of the threaded screws are shown in figure 6.10(a). The central screw was provided only for securing the alignment of the sheeting's in the mould and was removed before testing.

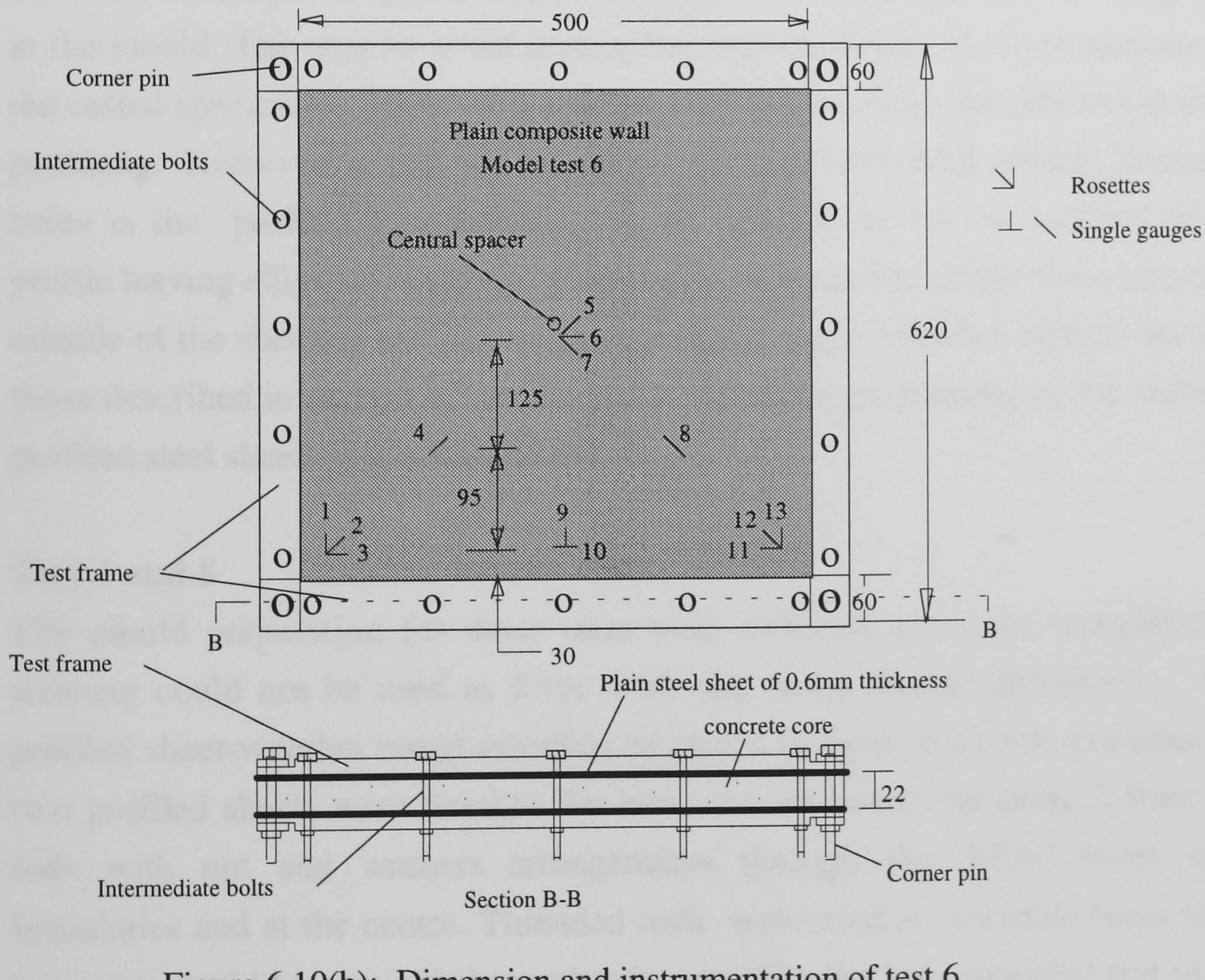

Figure 6.10(b): Dimension and instrumentation of test 6

The over all dimensions of the plain composite wall shown in figure 6.10(b) is similar to those of other tests. The model wall was made from 0.6mm thickness plain sheeting and had an overall thickness of 22mm. A central spacers was used to secure proper

alignment of the sheeting and to help providing lateral resistance of the mould during casting of concrete. Before testing the spacer was removed.

The model tests included the following steps:

Step 1: Manufacturing of the profiled steel sheeting

The manufacturing of the sheeting from flat sheet of 0.45mm thickness is described in section 3.3.5 of chapter 3.

Step 2: Mould preparation

Test 1,2 and 3

This is similar to that of profiled concrete models described in section 4.3 of chapter 4. The pair of profiled steel sheets were drilled to make holes at all intermediate bolts and corner pin locations corresponding to the test frame before being assembled in the mould. This was to avoid drilling through the layers of sheet-concrete-sheet in the casted specimens. Bolts with spacers were used to keep the sheeting in their exact positions. However, it was not possible to provide bolts with spacers through all the holes in the profiled boundaries for some holes to be on the inclined face of the profile leaving elliptical openings. Plastic tape was used to cover those openings from outside of the sheeting and this worked perfectly well. All other aspects are similar to those described in section 4.3 of chapter 4. However, no greasing of the surface of the profiled steel sheeting was carried out.

Test 4 and 5

The mould preparation for these tests were different and quite complicated. The sheeting could not be used as form work due to its shorter dimensions. A special profiled sheet-wooden board assembly as shown in figure 6.11 was constructed. The two profiled sheets were fixed to the two wooden boards by using 2.5mm threaded rods with nut and washers arrangements through the drilled holes along the boundaries and at the centre. Threaded rods were used at alternate holes so that the two parts could be assembled together by inserting the long threaded rod of one part into the opposite empty holes of the other part. The profiled gaps between the sheeting and the wooden board were filled up with 150mm long ply-wood pieces of approximately profiled crossection nailed to the wooden board. The plaster-seal was used at the mouth of each of the plywood filled profile gaps to prevent any leakage during casting.

The sheet-wooden mould assembly was then assembled (as described in section 4.3.1) in the test frame members to complete the mould assembly and is shown in figure 6.12. Absence of profiled boundaries in these specimens made it possible to use all the intermediate bolts with spacers which obviated the need for drilling holes in the later stages.

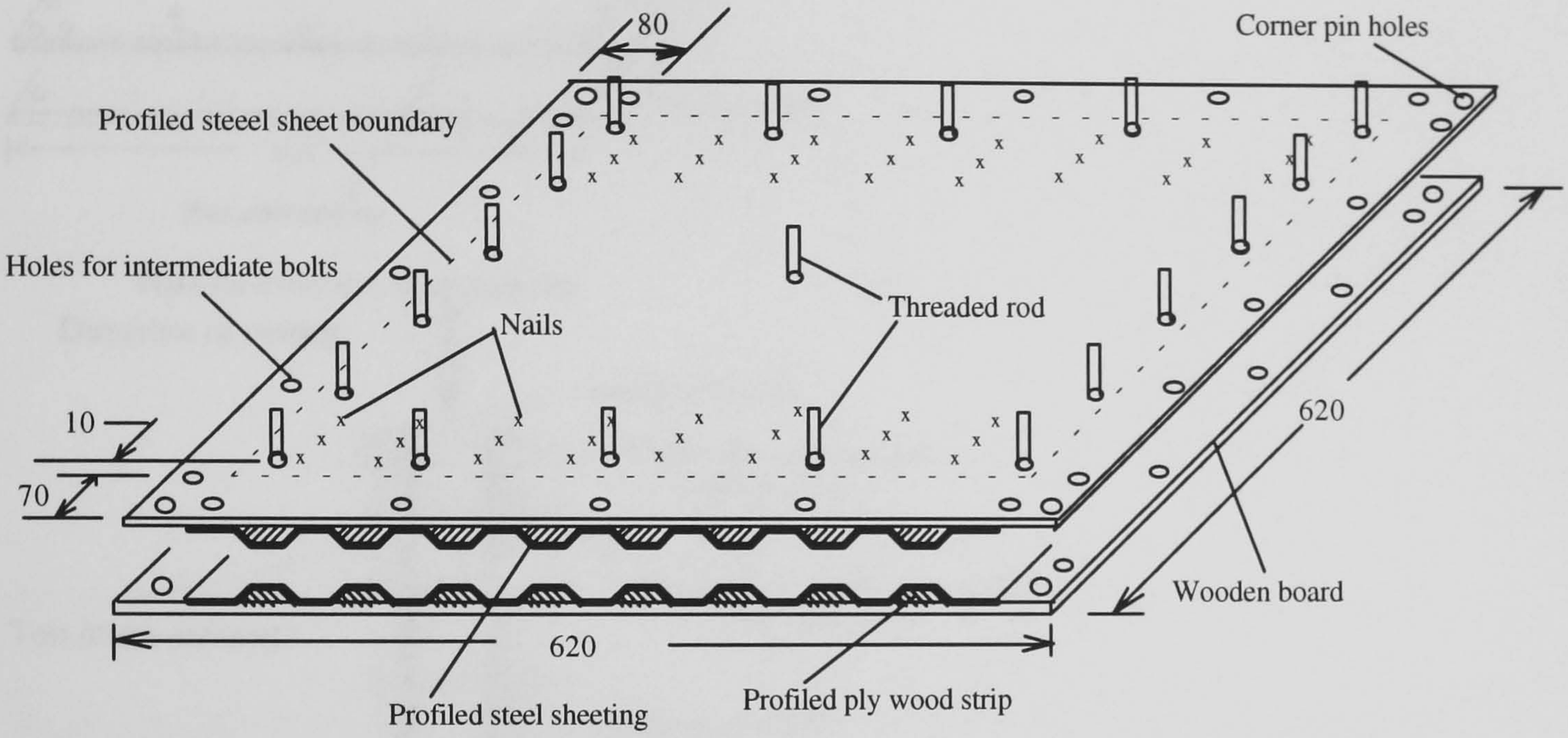

Figure 6.11:Profiled sheet-wooden board assembly

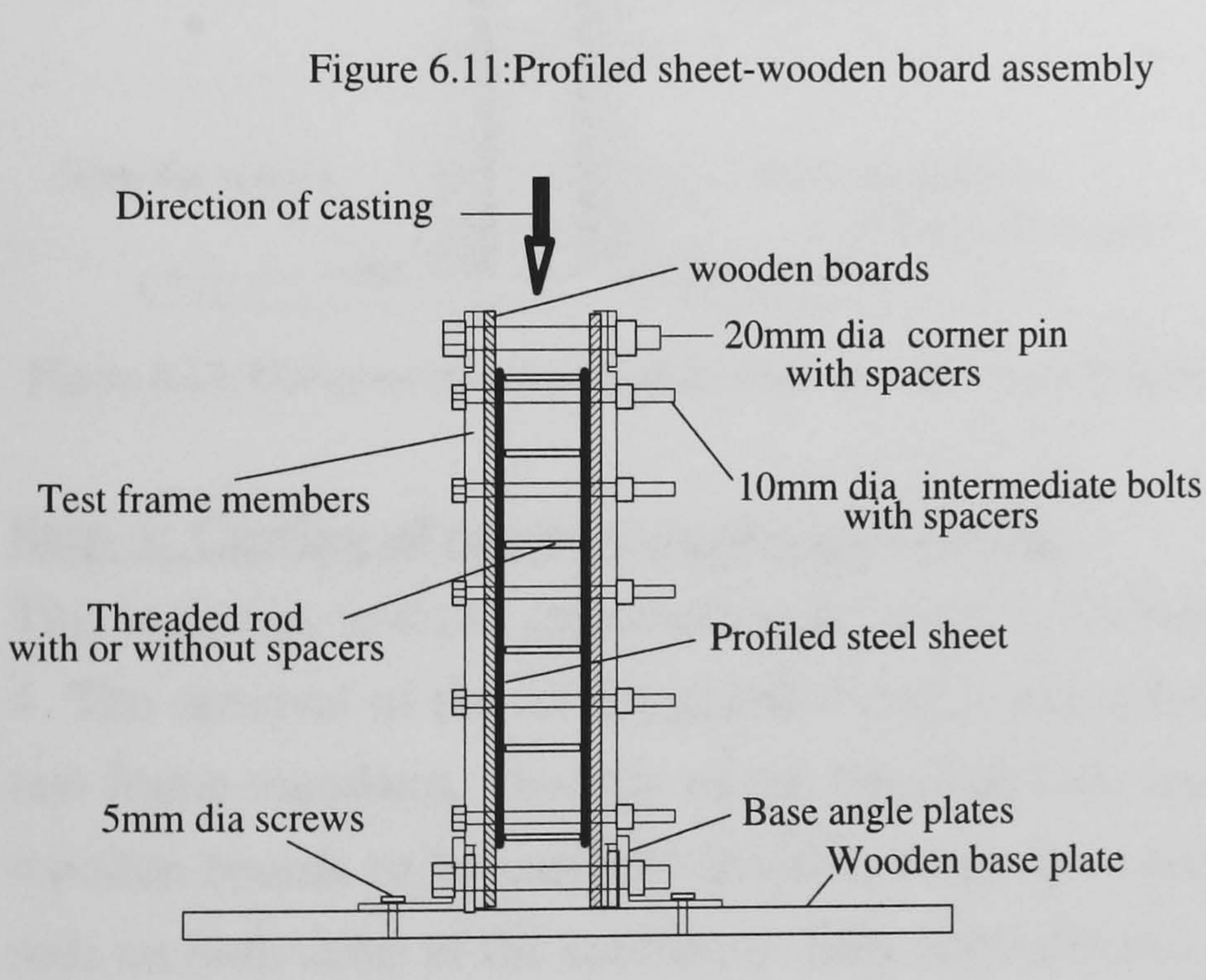

Figure 6.12: Complete mould with profiled sheet-wooden board assembly

Test 6

The mould for casting of model plain composite wall was similar to that of test 1,2 and 3. To prevent buckling of the sheeting during casting of concrete two external wooden boards were used so that they could provide lateral resistance. The mould crossection is shown in figure 6.13. The use of all the intermediate bolts along with spacers, eliminated the drilling of holes in the later stages.

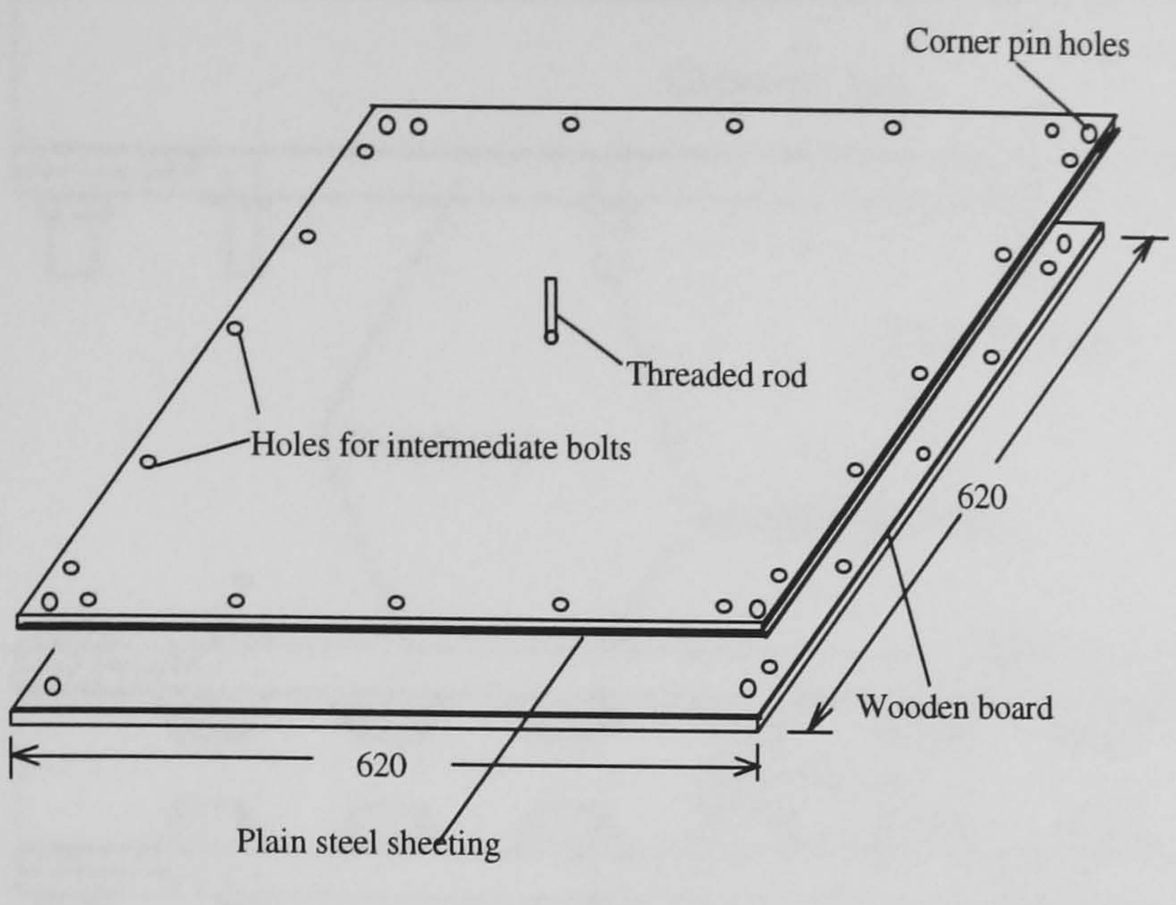

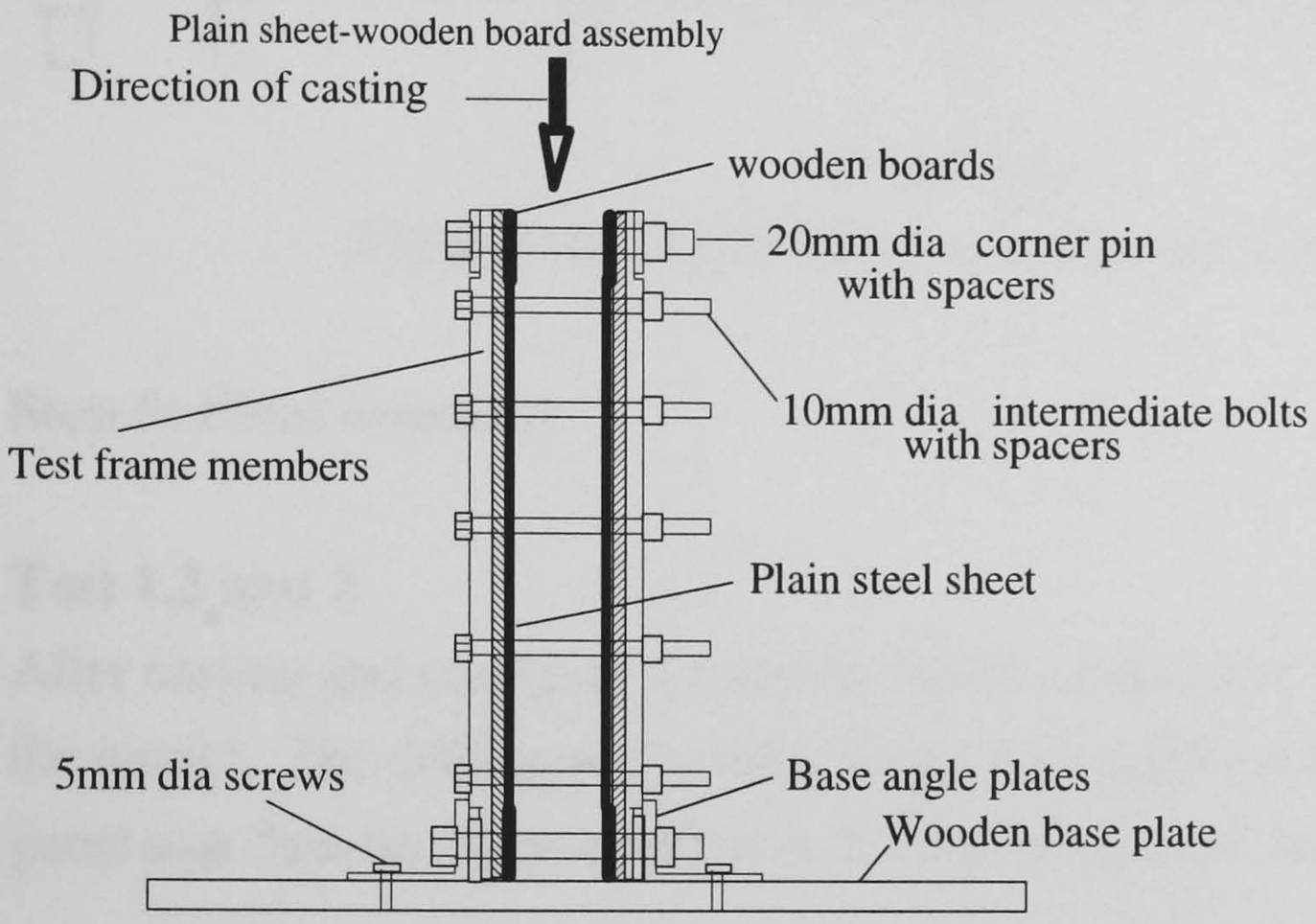

Figure 6.13: Complete mould with plain sheet-wooden board assembly

Step 3: Casting of micro-concrete and curing

This is similar to those described in section 3.5 of chapter 3 and section 4.3 of chapter 4. The removal of the model panels 4 and 5 was a bit difficult. After the removal of test frame members, the nuts of the threaded rods were taken off which allowed the wooden boards to be carefully lifted of from the specimen. The nuts of the threaded rods on both sides of the specimens were replaced and carefully tighted.

Step 4: Casting of Resins

To fill the gaps between profiled boundary of the wall and test frame members as shown in figure 6.14, casting of resin fill has been performed for model tests 1,2 and 3 following the steps and precautions described in section 4.3.4 of chapter 4. However, model tests 4,5 and 6 did not require any casting because they had no profiled boundaries.

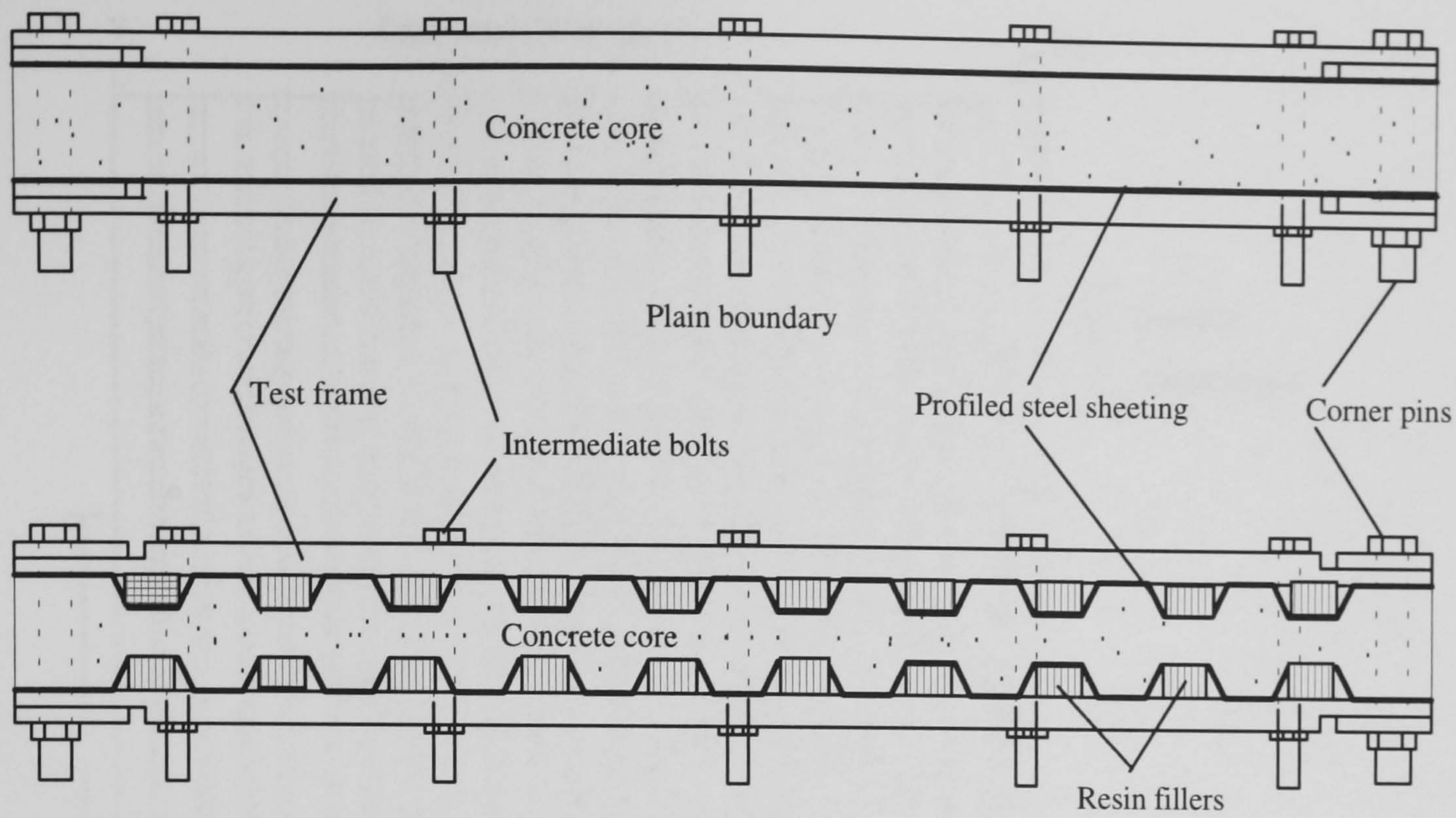

Figure 6.14: Resin fillers in composite wall test 1, 2 and 3

Step 5: Final assemble

Test 1,2 and 3

After casting and curing of the resins, the test frame and the panel was taken out from the mould. The drilling of the holes along the profiled boundary was carried out. The panel was then finally assembled in the similar manner described in section 4.3.5.

Test 4,5 & 6

The panels were directly assembled in the test frame as there was no need of casting resins or drilling of holes. They were assembled in the test frame following the procedure described in section 4.3.5 for plain boundaries of the panel.

Step 6: Instrumentation of the test panels

After complete assemble of the composite wall panels to the test frame, the strain gauges were installed at strategic locations on the steel surface. The details of the strain gauges showing locations and numberings in model tests are shown in figures 6.10 and 6.15. Model tests 4 and 5 have the same details of strain gauging. The strain gauging was done only on one side of the panels.

Step 7: Painting and marking of red line grids

The opposite side was painted white and marked with redline grids to show clearly the buckling and distortion of the profiled sheeting.

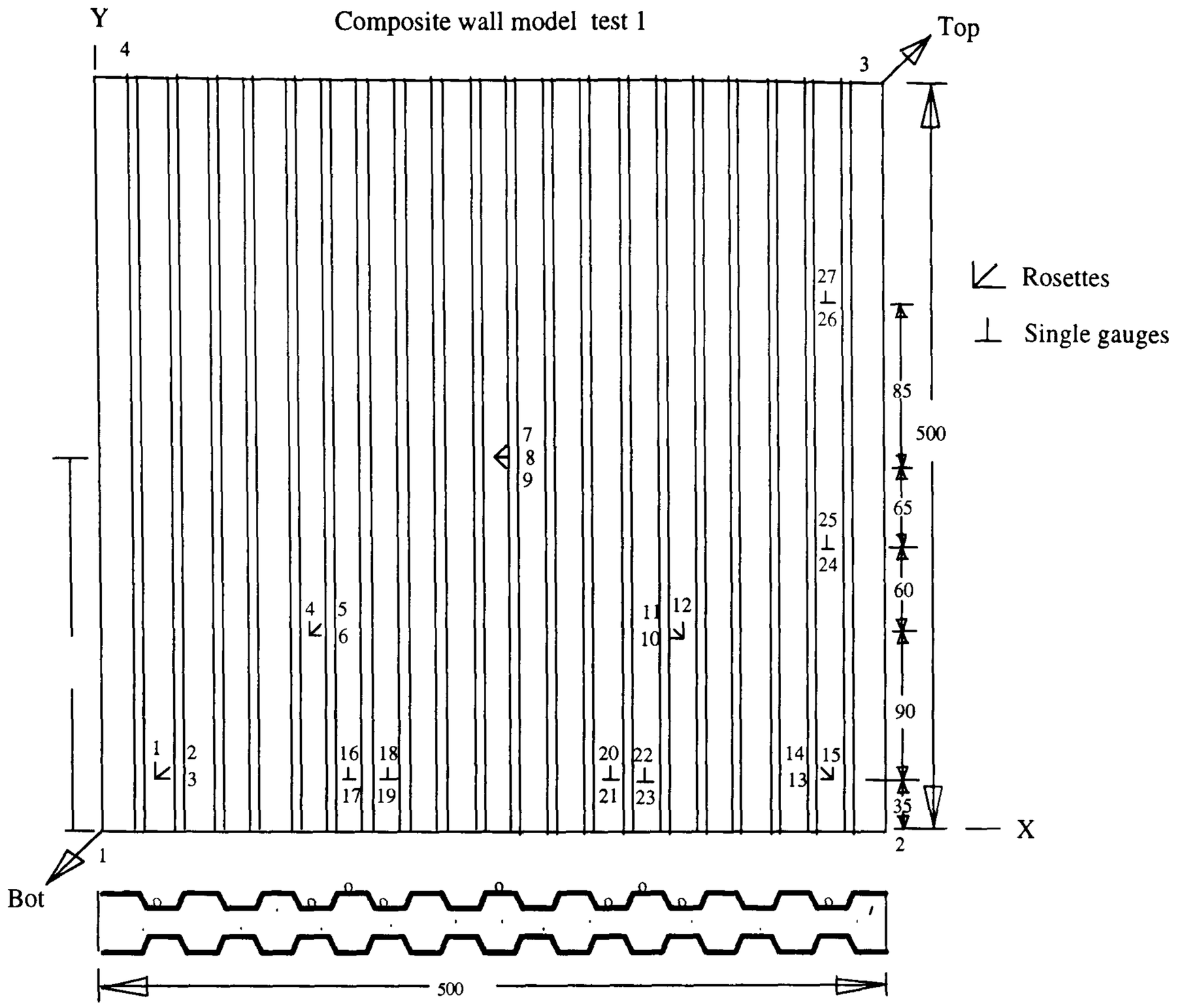

Figure 6.15(a)

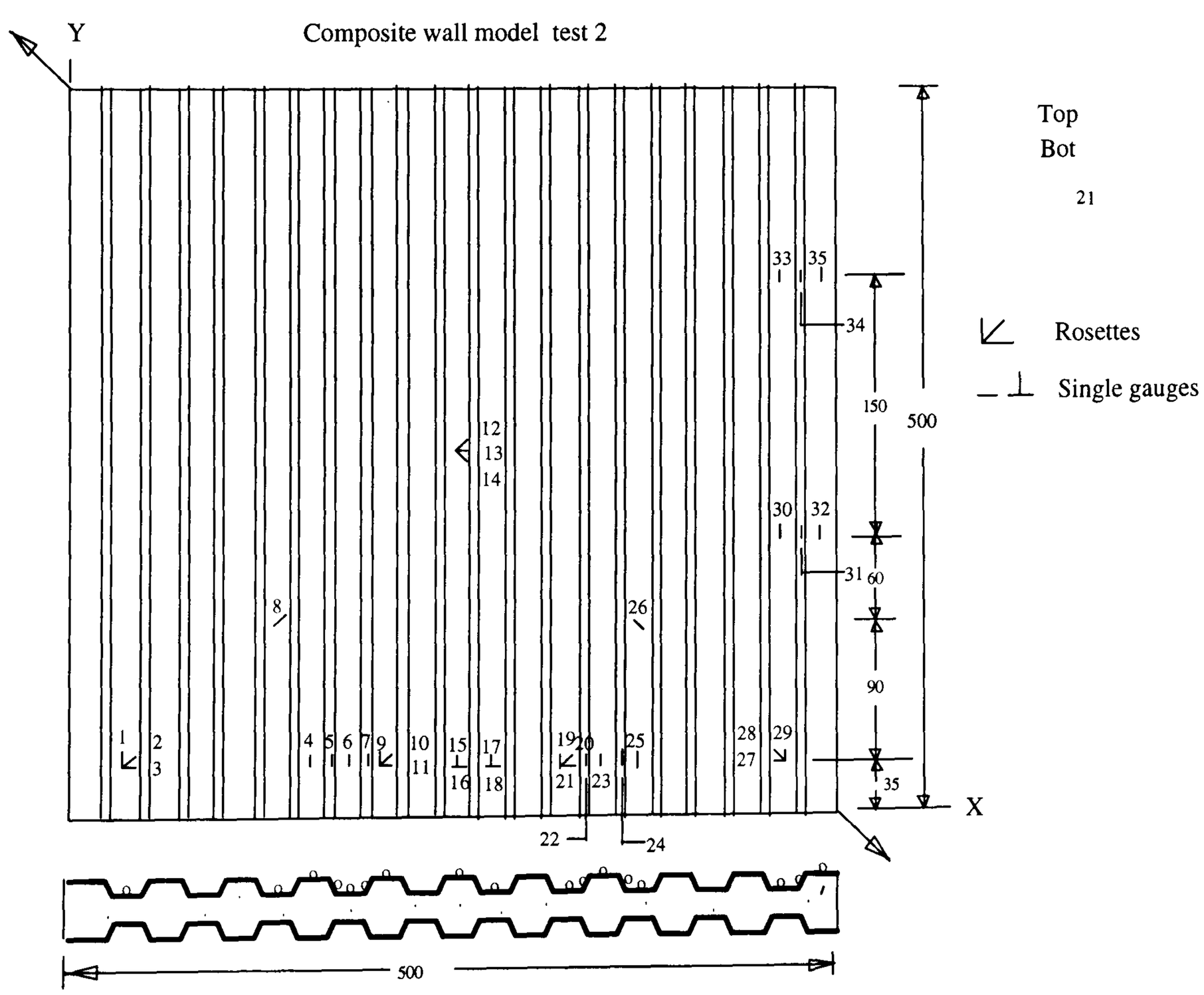

Figure 6.15(b)

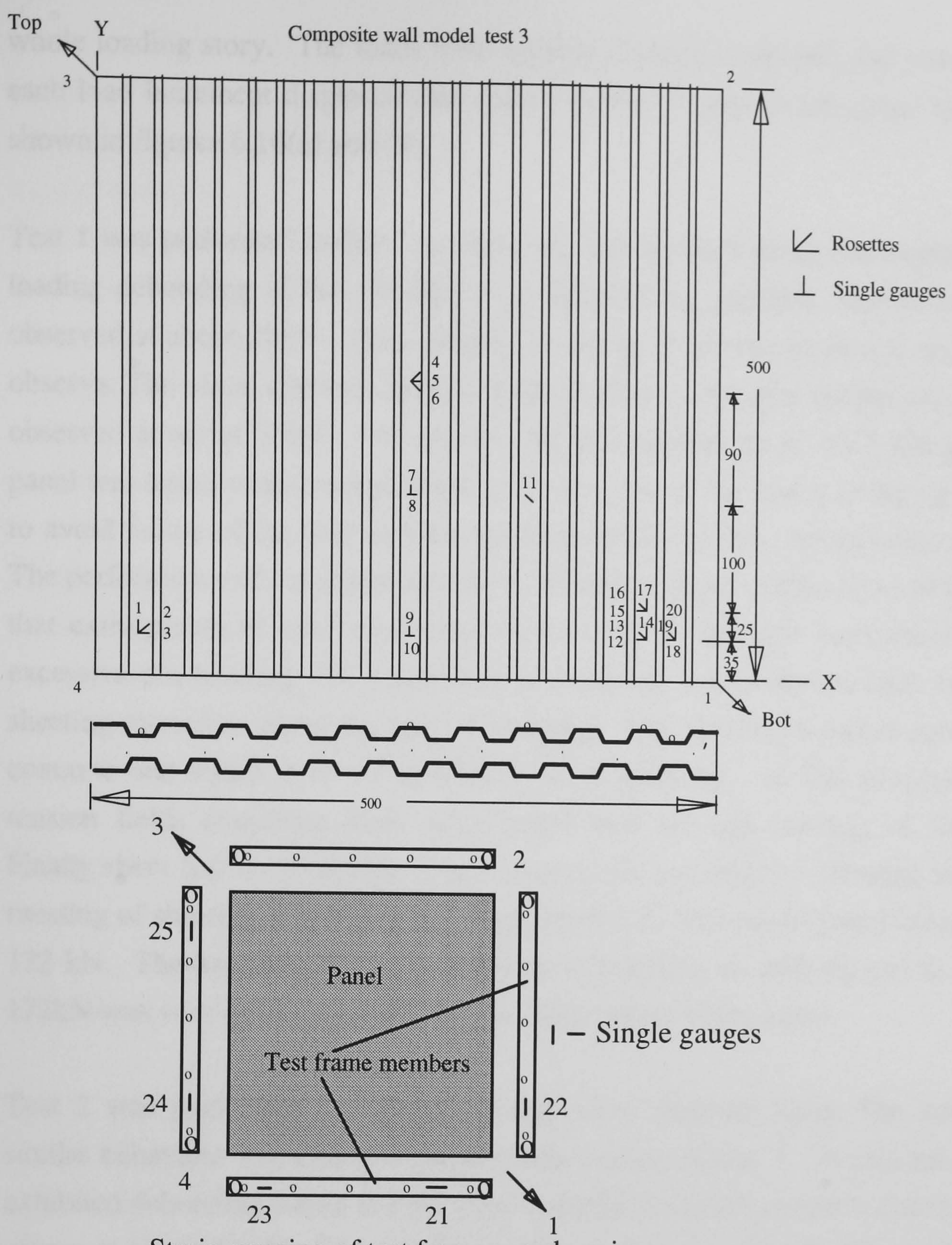

Strain gauging of test frame members in Composite wall test 3

Figure 6.15(c)

Figure 6.15: Instrumentation of composite wall 1, 2 and 3

Step 8: Test set-up

The test set-ups for all the tests were similar to that described in section 5.4 of chapter 5.

6.3.2 Testing and observations

Test 1 and Test 2 (Load applied through both steel and concrete)

These tests were performed by applying tensile or compressive forces along the diagonals of the panel. The loading and unloading were done several times during the

whole loading story. The loads were applied through both steel and concrete and at each load increment displacements were recorded. Load-deformation responses are shown in figures 6.16(a) and (b).

Test 1 was performed initially by applying tensile force along the diagonal. During loading debonding of the sheeting was identified by cracking sounds and was first observed at about 28kN. The concrete cracking in side the panel was not possible to observe. The visual cracking at the boundary of the panel near the loaded corners was observed at about 35kN. The tensile load was applied up to +115 kN and then the panel was tested under compression. This was due to the safety of the rig particularly to avoid failure of the bolts in tension which connected the bottom beam to the floor. The performance of the corner pins was satisfactory up to a load of ±110 kN but after that extra pieces of steel were inserted between the pin and head details to avoid excessive pin bending. No visual sign of buckling was observed until 165kN when sheeting started to show the sign of buckling. The sheeting buckled outward of the concrete and slided over the profiled core of concrete. In this process, it formed tension fields extending over some length and showed twisting of the sheeting. Finally sheet lost its geometry. The failure of the test panel 1 showing buckling and twisting of sheeting is presented in photograph 6.1. The model panel failed at about -172 kN. The transition from the first sign of buckling at -165 kN and its failure at -172kN was very quick resulting into a sudden failure of the panel.

Test 2 was performed by applying compressive diagonal force. The panel showed similar behaviour and failure characteristics to that of test 1. In this case the panel exhibited debonding sound and showed extended boundary concrete cracking near the corner at about 36 kN. The panel started to buckle at about 182 kN and finally failed at about 198 kN.

Test 3: (Hysteretic behaviour)

The boundary condition of this test is similar to that of test 1 and 2. The panel was loaded diagonally under alternate tension and compression to simulate hysteretic effect. The hysteretic application of load was started with tension and then followed by compression. In this way several cycles of loading were applied and the load was increased at an increment of 6 kN in each cycle up to a load of ±60 kN. Beyond 60 kN, the load was increased at an increment of 30 kN to have a total cycle of 14 before the failure of panel. The panel showed boundary corner cracks at about 23 kN and finally failed at about 190 kN. The hysteretic load-deformation response of the

wall is shown in figure 6.16(c). The buckling of sheeting and failure of the panel was similar to those of test 1 and 2. The failed panel is shown in photograph 6.2.

Test 4 and Test 5

The boundary conditions of these tests are different than those of test 1,2 and 3 as the loads were applied through the concrete only. The panels were tested by applying tensile diagonal forces. In the case of test 4, machine fault occurred during the test resulting into a rapid increase in load and gave no chances to record the strain gauge readings. However, it was possible only to record the failure load which was around 58 kN and the associated failure characteristics.

Test 5 was conducted successfully by applying tensile diagonal force. The panel cracked at about 15kN and failed at about 64kN. Both the panels failed with subsequent cracking in concrete and buckling (not so prominent compared to test 1,2 and 3) of the sheeting. The sheeting was distorted at the profiled boundaries where the threaded rods acted as anchor points at the centre of the troughs. In case of test 5 where the threaded rods are in direct contact with concrete, no tearing of the sheeting at rod locations was observed instead the rod sheared off at some corner locations of the panel. In case of test 4 where threaded rods were used through the spacers, the rods were found to be punched through the sheeting. The load-deformation response is shown in figure 6.16(d).

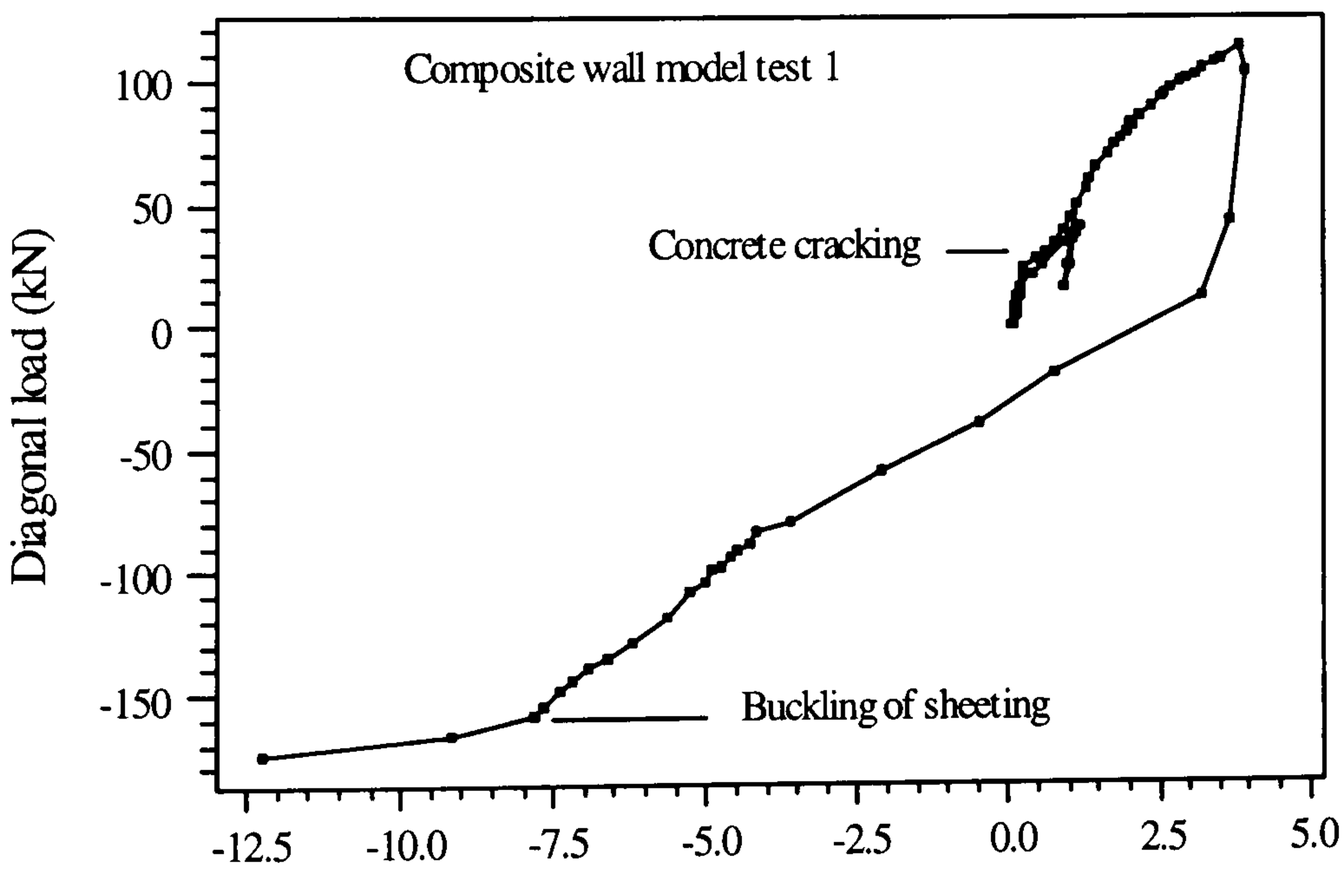

Figure 6.16(a)

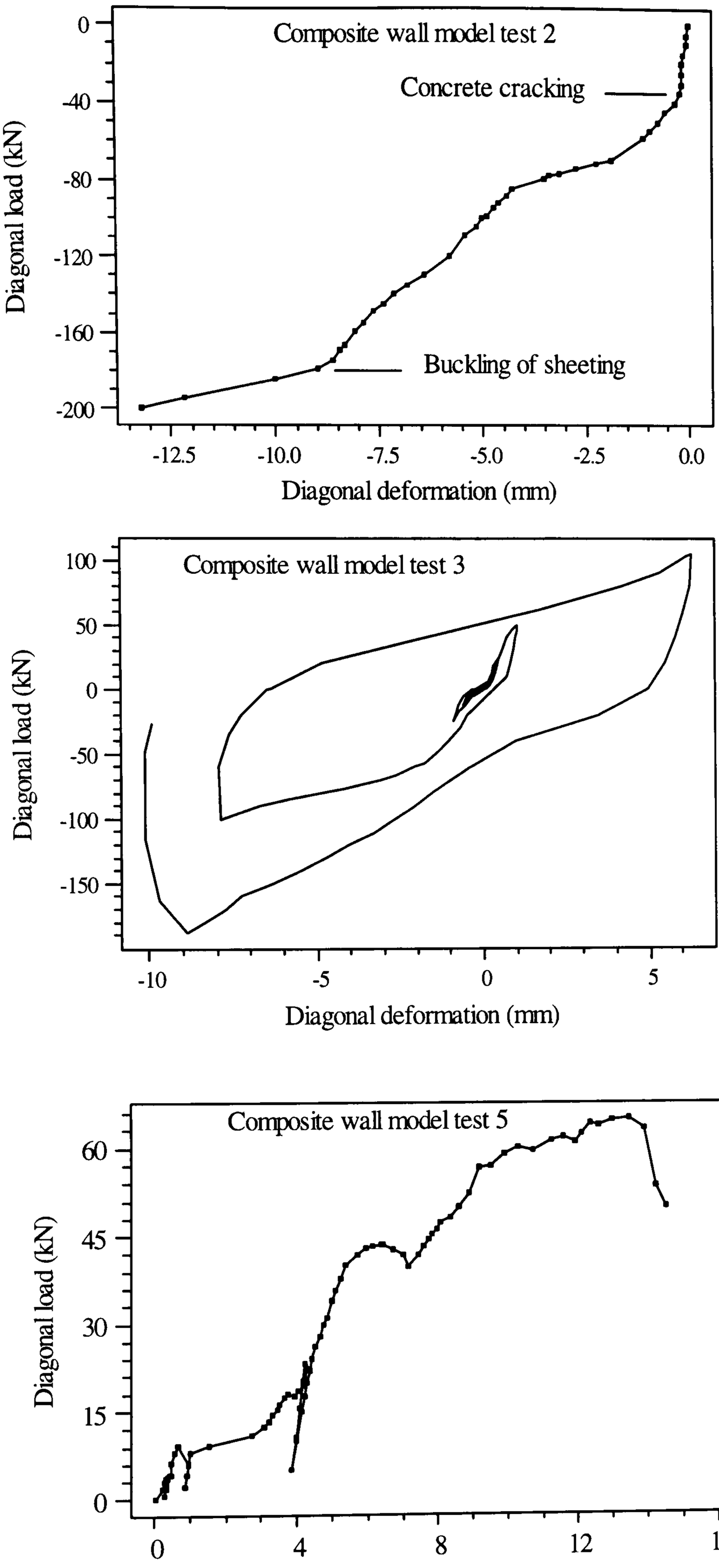

Figure 6.16(b)

Figure 6.16(c)

Figure 6.16(d)

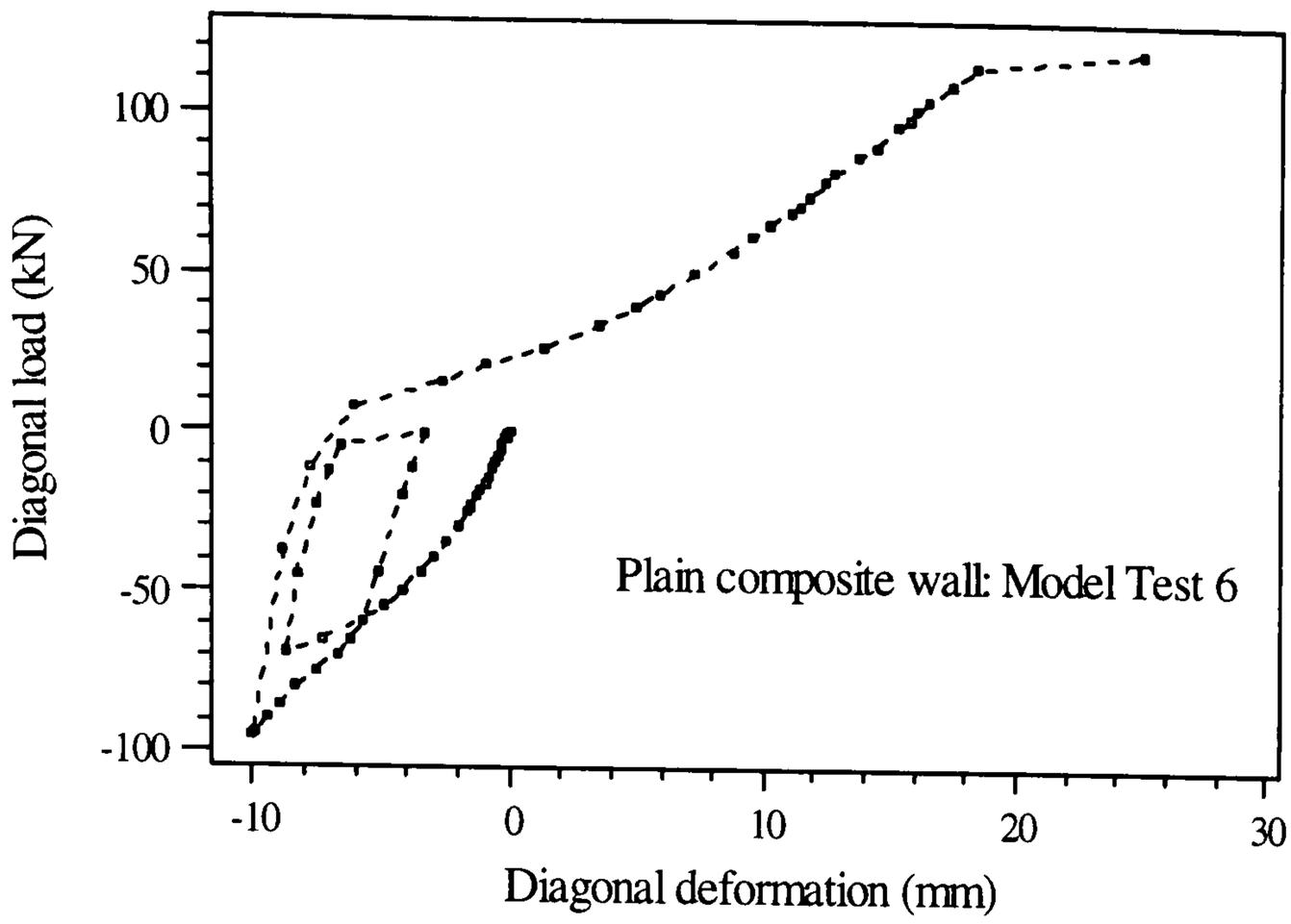

Figure 6.16(e)

Figure 6.16: Load-deformation response of composite wall model tests

Test 6 : Plain Composite wall

The panel was tested by applying compression diagonal force of up to 90kN and then the load was released. The panel was then re-loaded up to a tensile load of 120kN when the sheeting was found yielded. The load deformation response is shown in figure 6.16(e). The concrete cracked at about 20kN. After cracking, a gradual development of tension field in the sheeting was observed. The development of tension field as can be seen in photograph 6.3, mobilised the post-buckling strength of the sheeting and the panel carried a diagonal load of 120kN.

6.3.3 Analysis of failure modes

6.3.3.1 Failure modes of Sheeting

Test 1,2 and 3

The test frame and wall assembly with intermediate bolts and resin filling for test 1,2 and 3 provided full connection between sheeting and concrete at the boundaries. As a result the failure of the composite wall models 1, 2 and 3 occurred through mobilisation of the strength of the steel sheeting. The chemical bond between sheeting and concrete could be considered as negligible. The rigid boundary condition made both sheeting work with concrete core even after cracking of concrete and debonding and consequently proved their ability to resist higher shear loads before failure. The failure was associated with buckling and twisting of the profile with the development of tension fields. The locations of tension fields are shown in figure 6.17 by inspection of the background of red line grids. The extended length of the tension fields varies between 20 to 30% of the total length of the trough or crest lines. The

buckled pattern of sheeting along the trough or crest lines as plotted from out-off plane displacements along central red lines are shown in figures 6.18. They showed similar half buckled waves confirming the outward buckling of the sheeting from concrete.

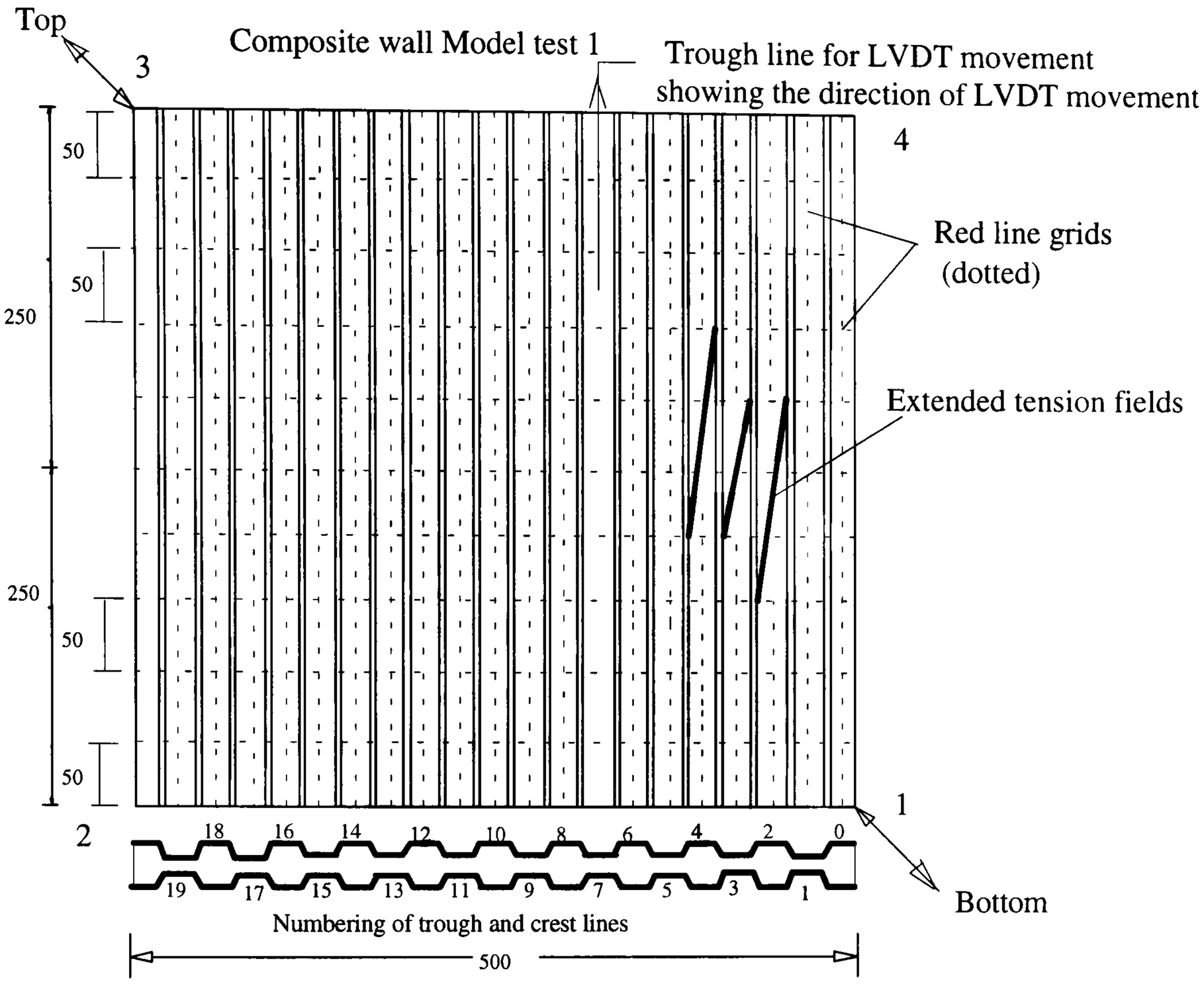

Figure 6.17: Development of tension fields

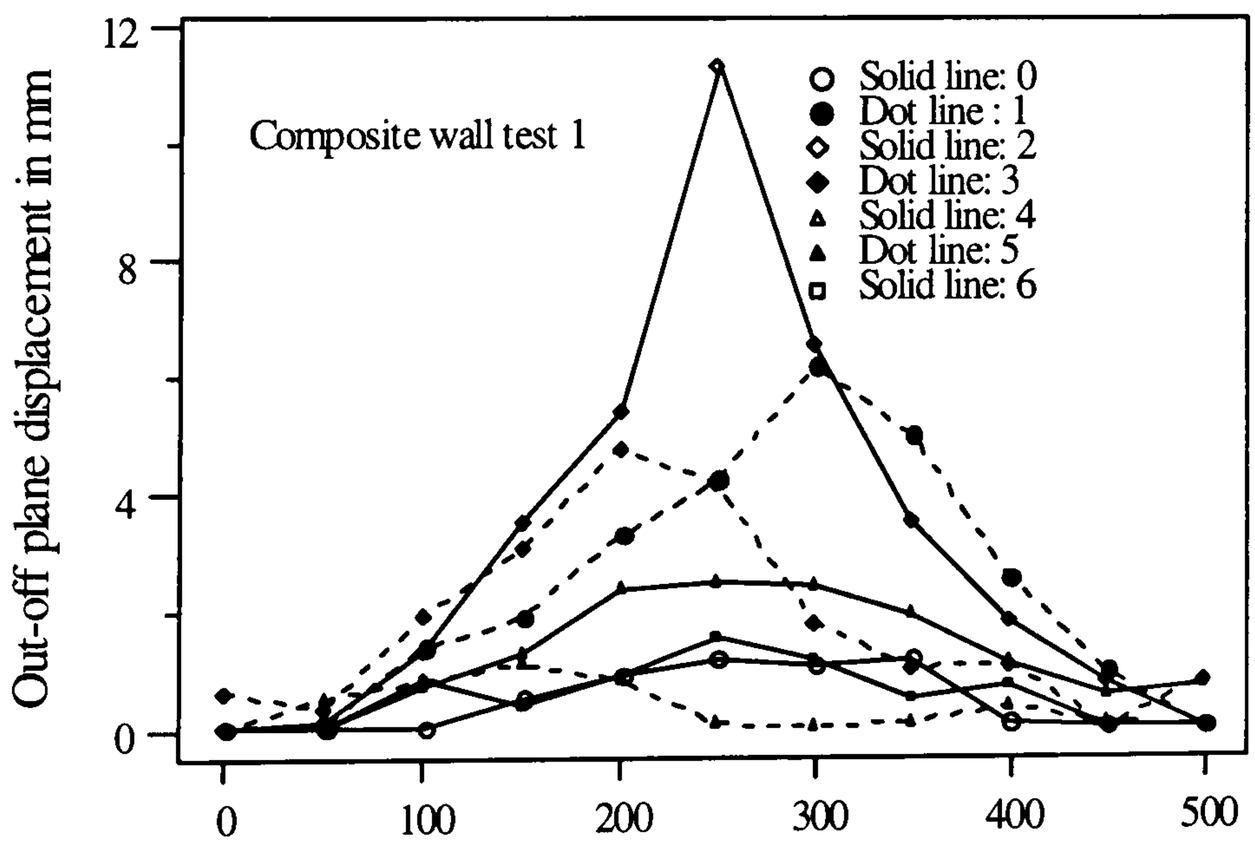

Figure 6.18(a)

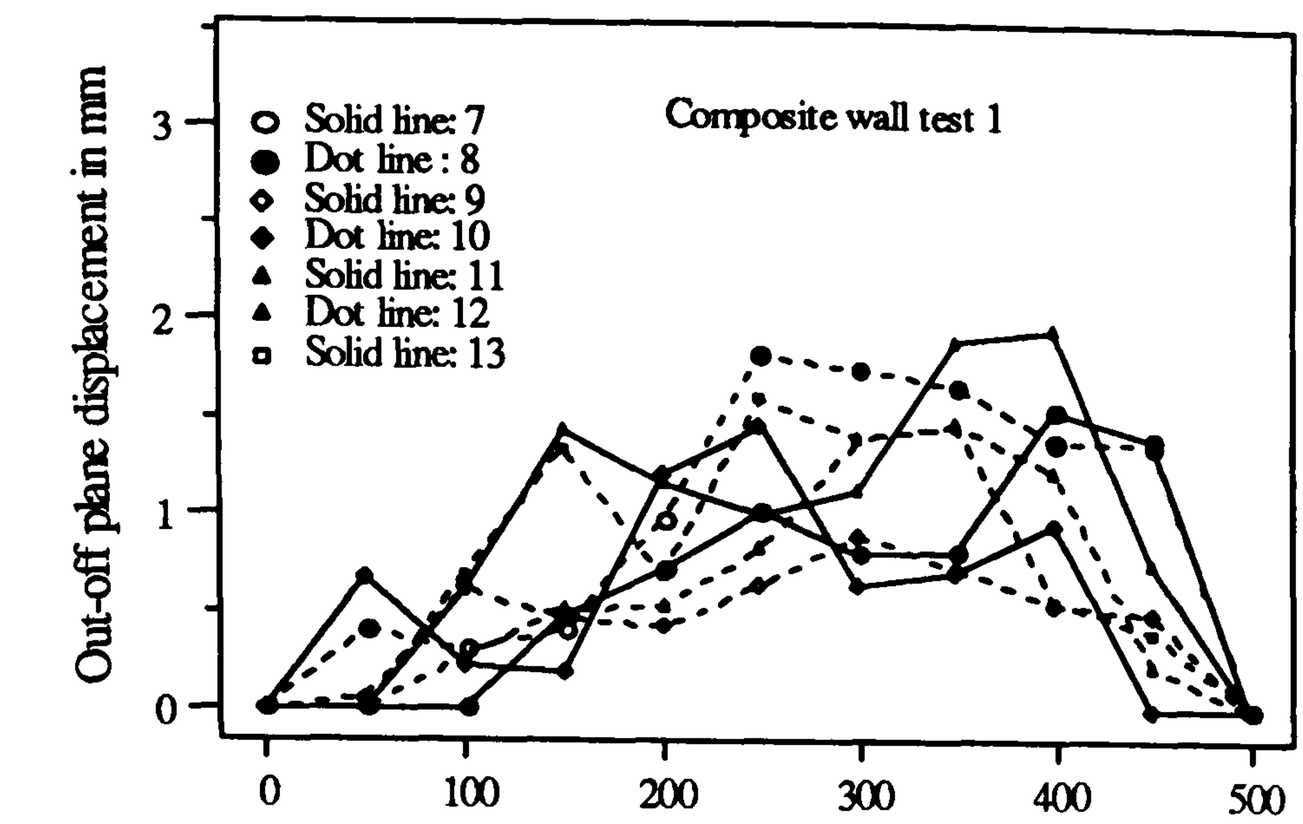

Figure 6.18(b)

Figure 6.18: Buckled pattern of sheeting in test 1

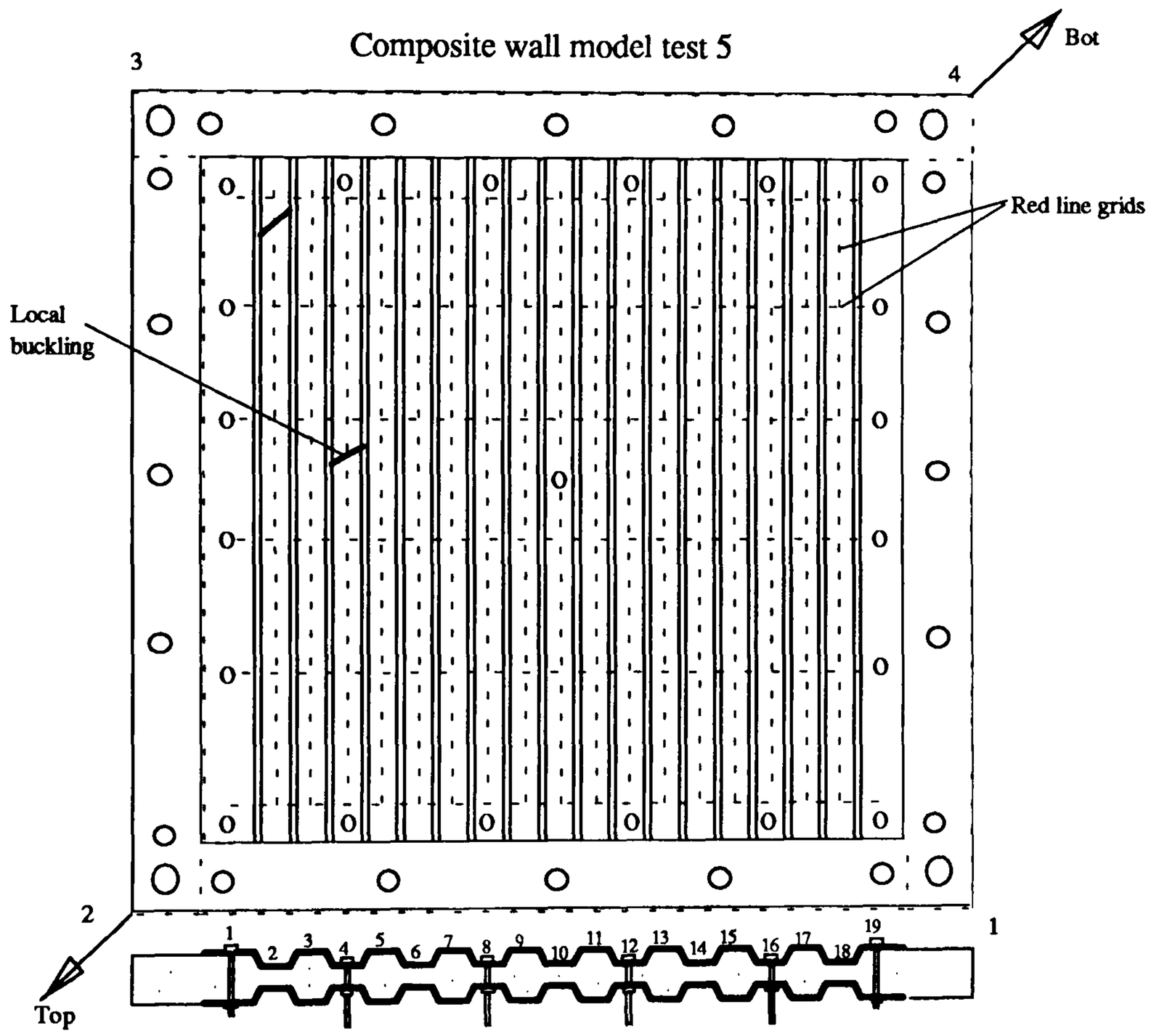

Figure 6.19(a): Location of local buckles

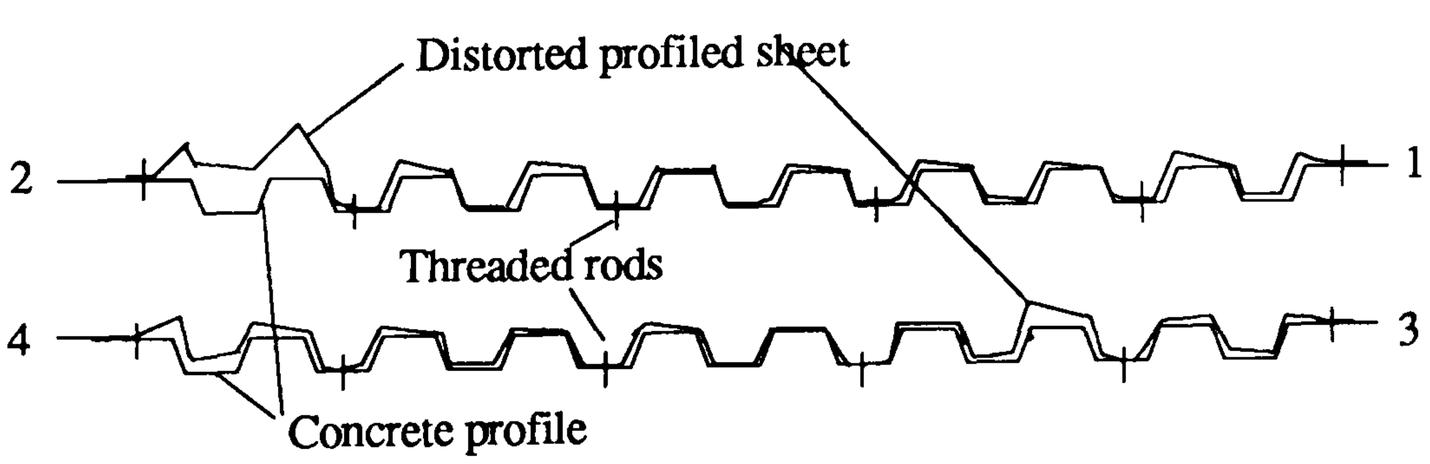

Figure 6.19(b): Distortion of sheeting at the boundary

Test 4& 5

As the loads were applied through concrete, the load was transferred from concrete core to the sheeting. The sheeting was connected to the concrete through the threaded rods at the boundary of the sheeting. The strength of the sheeting was not mobilised and the failure load was governed by the strength of concrete core. The final failure was associated with outward buckling of the sheeting from the core with a few local buckles shown in figure 6.19(a). No tensions fields were developed. The distortion of the profiled steel sheeting at the boundaries is shown in figure 6.19(b). The typical buckled shapes of the trough or crest lines are shown in figures 6.20. They showed identical patterns of the formation of half waves.

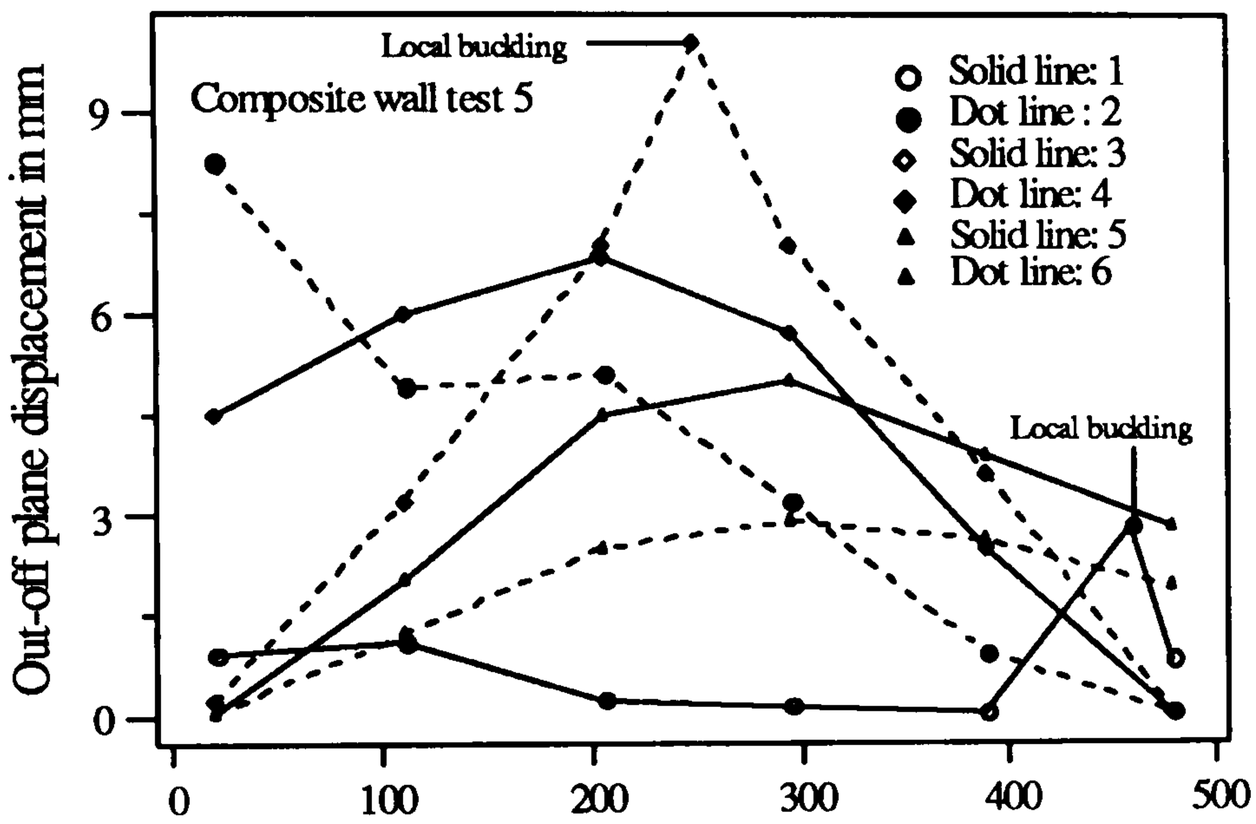

Distance along the profile (mm)

Figure 6.20(a)

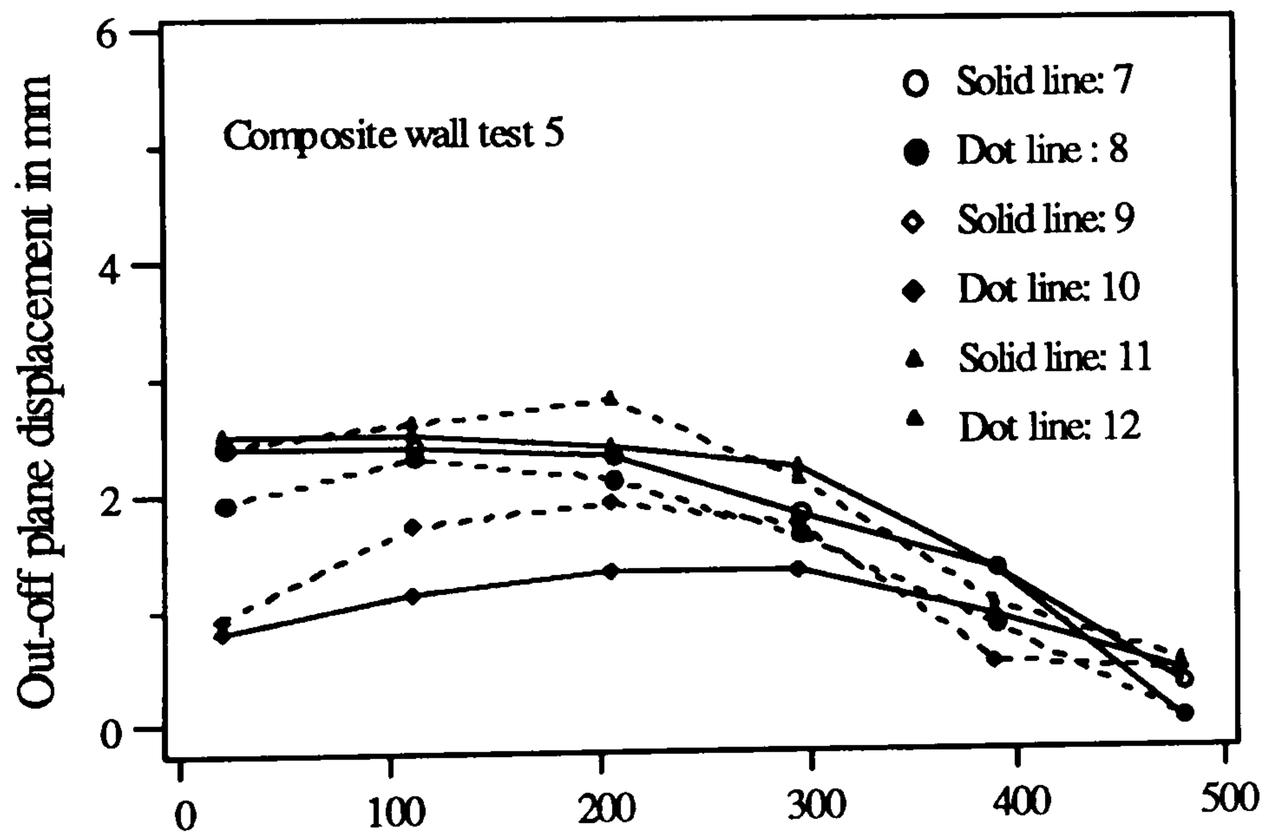

Distance along the profile (mm)

Figure 6.20(b)

Figure 6.20: Buckled pattern of sheeting in test 5

6.3.3.2 Crack patterns in concrete core

The skins of profiled steel sheeting was removed from the failed specimens to reveal the cracking patterns in the concrete core. The photographs 6.4 show the cracking of the composite wall models 1 and 2. The direction of the loading is shown by arrows. Two types of cracks can be classified :

i. Cracks parallel and perpendicular to the loaded diagonal :

Perpendicular cracks were developed due to tensile application load along the loaded diagonal and the parallel cracks were developed due to the application of compressive load along the loaded diagonal. The crack patterns are identical to those of profiled concrete core tests. The formation of diagonal cracks confirmed the formation of diagonal tension failure of the profiled concrete cores.

ii. Cracks along the boundary trough lines:

The trough lines with reduced thickness (almost half compared to crest) along the boundary were the weakest section of the core. These cracks were formed due to shear transfer of load from the adjacent loaded boundary.

The crack pattern for test 5 (shown in photograph 6.5) showed the formation of cracks perpendicular to the diagonal as this panel was tested under tension and confirmed diagonal tension failure.

The cracking pattern shown in photograph 6.6 of plain composite wall core showed the formation of cracks parallel and perpendicular to the loaded diagonal as it was tested under tension-compression load.

Therefore, the crack pattern confirmed the fact that the diagonal tension limit state will be the design criteria for the concrete cores.

6.3.4 Material properties

The micro-concrete properties as found from the cubes and cylinder specimens for the model composite wall tests are presented in table 6.1.

Table 6.1: Micro-concrete properties of model composite walls

Test No.	Wet density	Compressive Strength		Tensile Strength	Age	Ratio
		Cylinder f'_c	Cube f_{cu}	Split cylinder f_t	Days	f'_c/f_t
	kg/m^3	N/mm^2	N/mm^2	N/mm^2		
1	2229	21.00	-	2.35	48	8.94
2	2283	20.00	23.67	2.43	107	8.23
3	2241	24.83	26.73	2.64	55	9.41
5	-	19.10	22.90	2.29	15	8.34
6	-	20.63	22.00	2.03	15	10.16

The model steel sheet properties are similar to those of previous tests on plain and profiled steel sheet panels as presented table 2.1 except for the test 6. A different galvanised sheet of 0.60mm thickness was used which have following properties: Yield strength = 306 N/mm^2; Ultimate strength = 403 N/mm^2; Modulus of elasticity= 200 kN/mm^2 and Elongation=20%.

6.3.5 Load-deformation response and stiffness

The load-deformation responses for model test 1 and 2 and 3 are presented in figures 6.16. The start of concrete cracking and buckling of sheeting are pointed in the figures. After cracking, the stiffness of the panels was greatly reduced but the panels were able to resist large loads before they failed. The load-deformation responses of test 5 and 6 are also presented in figures 6.16. The loads and stiffness values for the model tests are summarised in table 6.2. Test 1, test 2 and test 3 give consistent results with respect to pre-cracking stiffness and ultimate strength of the composite wall. The cracking loads for test 1 and test 2 are very close while the hysteretic test 3 shows a decrease in cracking load by about 20%. The effect of boundary condition simulating load applied through both concrete and steel (Test 1, test 2 and test 3) and load applied through concrete only (test 4 and test 5) is very severe. Tests 4 and 5 show good agreement and confirmed that the steel sheeting did not contribute to the load carrying capacity or stiffness of the wall. These tests suggested that if the load is not applied through both steel and concrete, the wall should be designed as a profiled concrete wall neglecting sheeting contribution.

The hysteretic effects seems to have no effect on the pre-cracking stiffness but 20% decrease in cracking load may be caused by the hysteretic effects.

Table 6.2 : Model test comparison

Test	Pre-cracking stiffness (kN/mm)			Cracking load (kN)			Failure load (kN)		
No	Diagonal	Shear	Ratio	Diagonal	Shear	Ratio	Diagonal	Shear	Ratio
1	496	248	1.00	35	24.75	1.00	172	122	1.00
2	561	280	1.13	36	25.5	1.03	198	140	1.15
3	545	272	1.10	25	17.67	0.79	190	134	1.10
4	-	-	-	-			58	41	0.34
5	260	130	0.524	15	11	0.44	64	45	0.37
6	344	172	0.69	25	18	0.73	120	85	0.70

6.3.6 Strain characteristics

6.3.6.1: Diagonal strains

Test 1 and test 2

The strains along the loaded (gauges 2,5 and 8) and off-diagonal (gauges 9,11 and 14) for test 1 showed similar pattern of variation. All the gauges showed first sign of sudden change in strain within the load range 28-40 kN confirming the cracking of concrete. Typical variation in gauge 5 and gauge11 is shown in figure 6.21(a) and (b).

The typical variation of strain along the loaded (gauges 14,26 and 28) and off-diagonal (gauges 2,8 and 9) for test 2 are presented in figures 6.22(a) and (b). The strain gauges show similar variation of strain along the diagonals with tensile strain along the off and compression strain along the loaded diagonal throughout the loading history. This confirms the mechanism of diagonal tension and compression state within the panel. The lower strains in crest gauges 12 and 14 confirm the presence of higher stress in trough sections. The strains in the diagonals reaches yield only after the initial buckling load (around 180kN).

Test 3 (Diagonal strain hysterisis)

The strains along the loaded (gauges 6,11,16 and 19) and off-diagonal (gauges 2 and 4) under hysteretic load showed similar pattern of hysteretic loops. Again all the gauges showed a change in strain around a load range of 40-45kN from where loops become more clear. The hysteretic loops confirm the mechanism of diagonal tension and compression state within the panel. The typical hysteretic loops for gauges 4 and 6 are presented in figures 6.23(a) and (b) respectively.

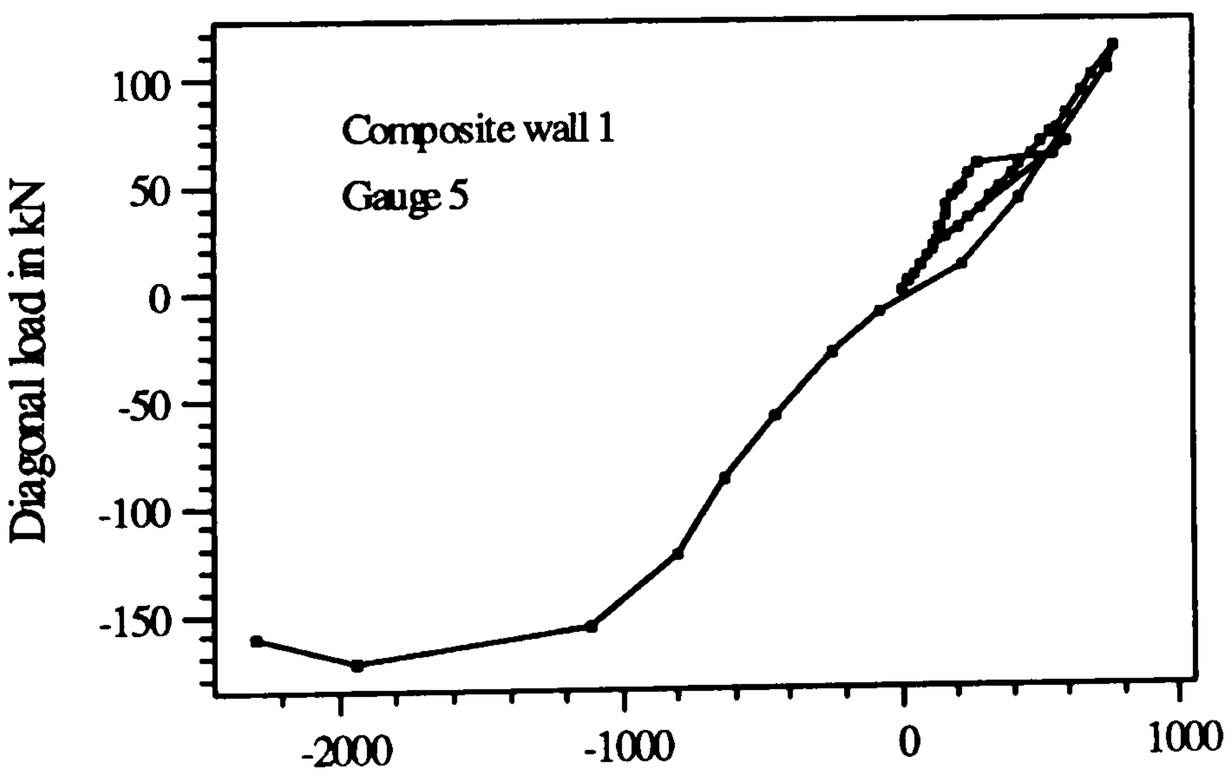

Figure 6.21(a)

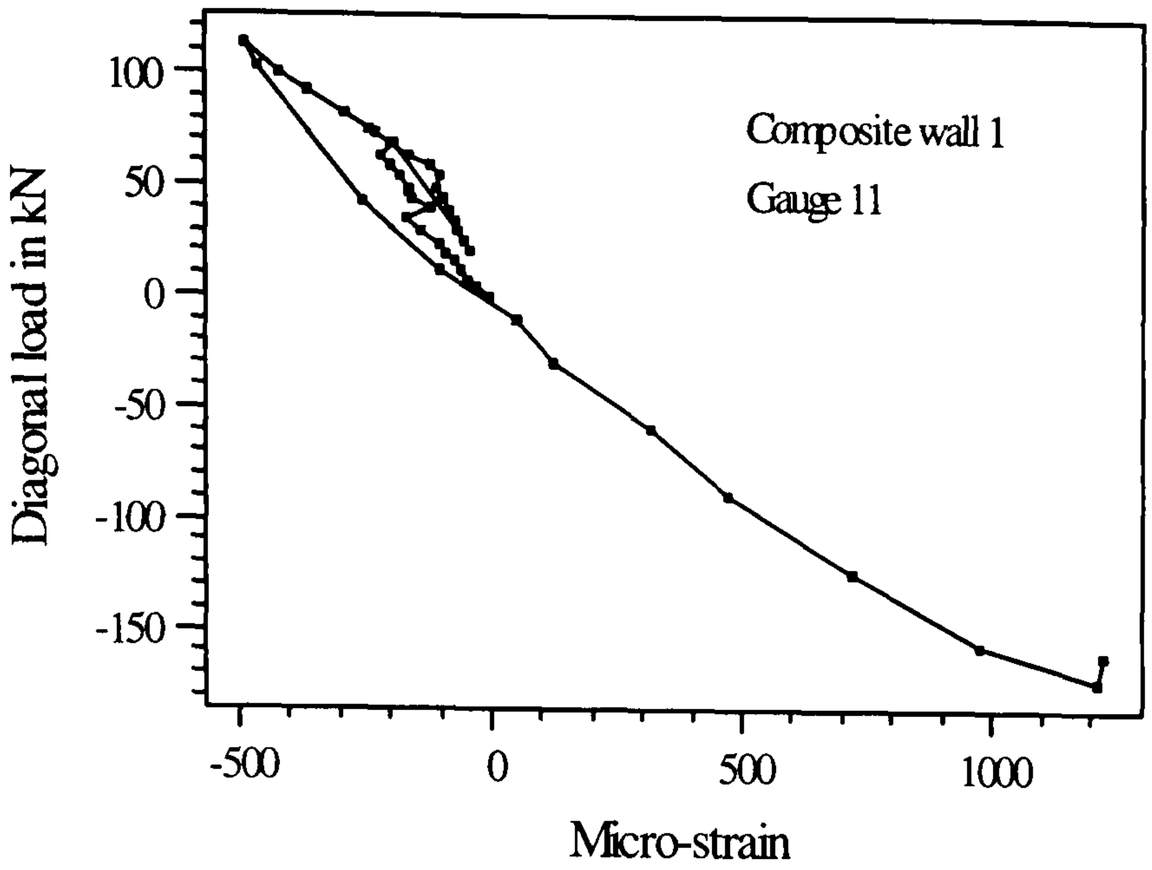

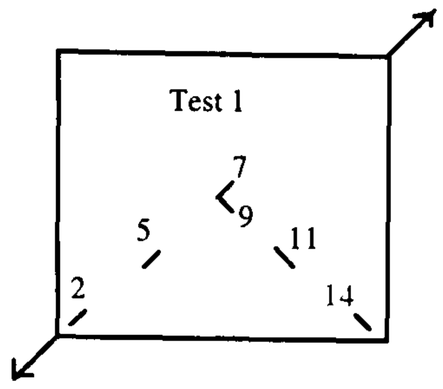

Figure 6.21(b)

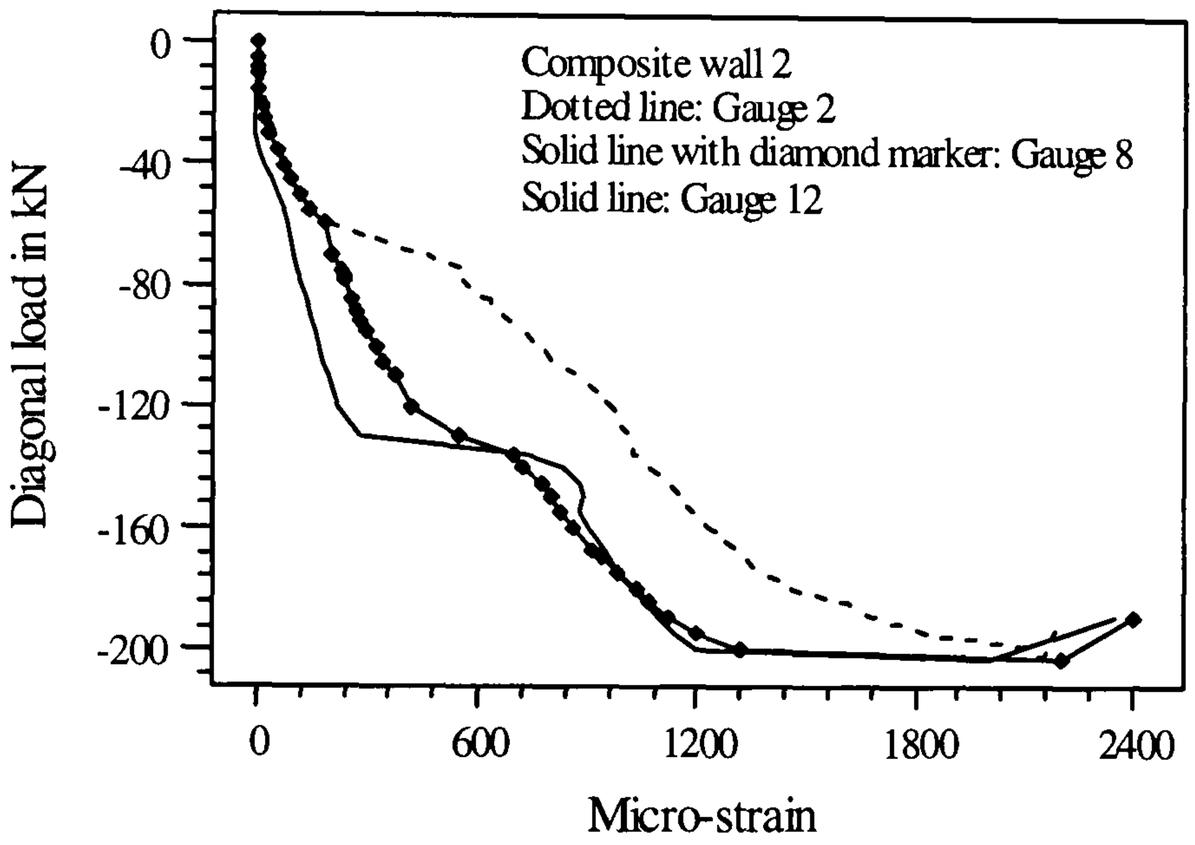

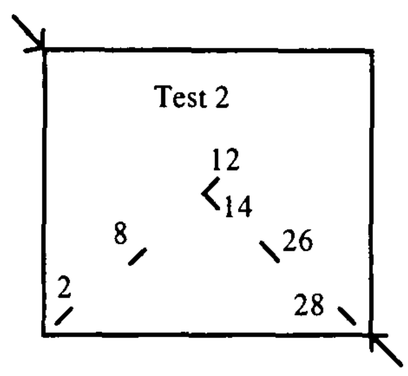

Figure 6.22(a)

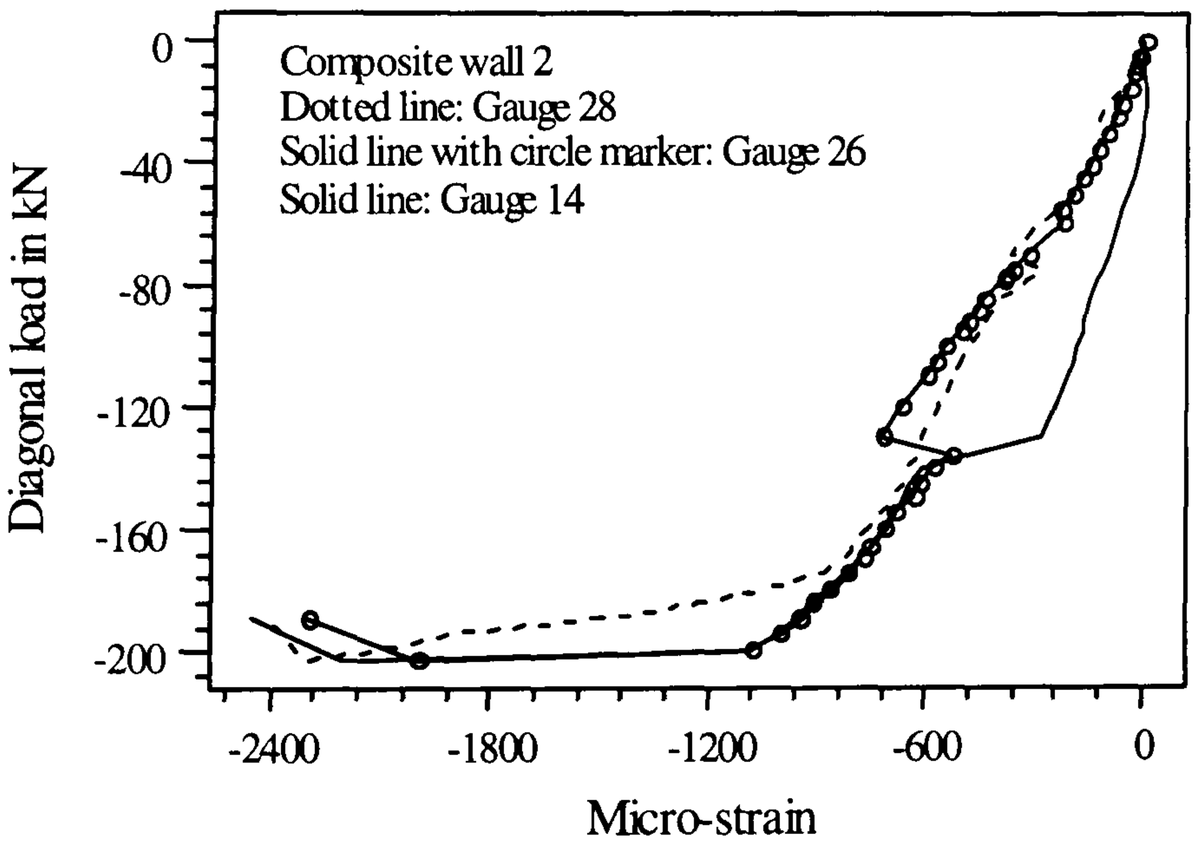

Figure 6.22(b)

Figures 6.21 & 6.22: Variation of diagonal strains in test 1 and 2

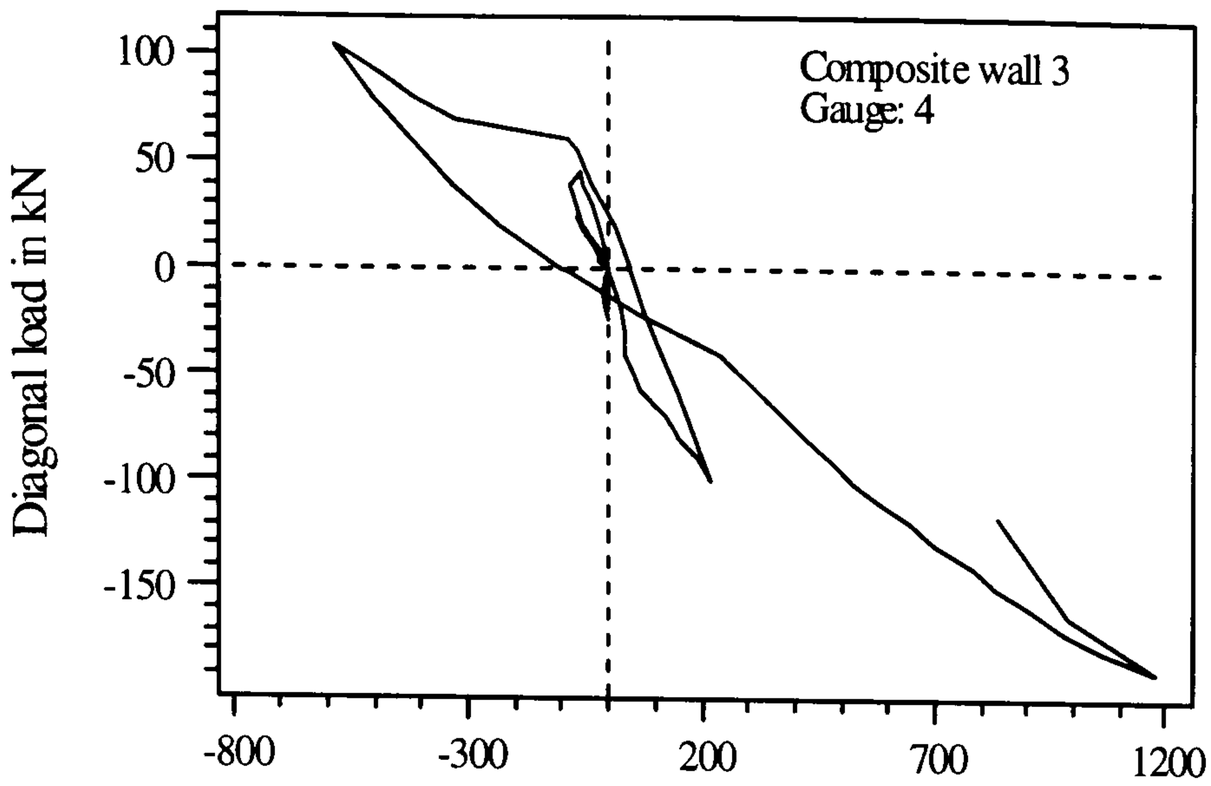

Figure 6.23(a)

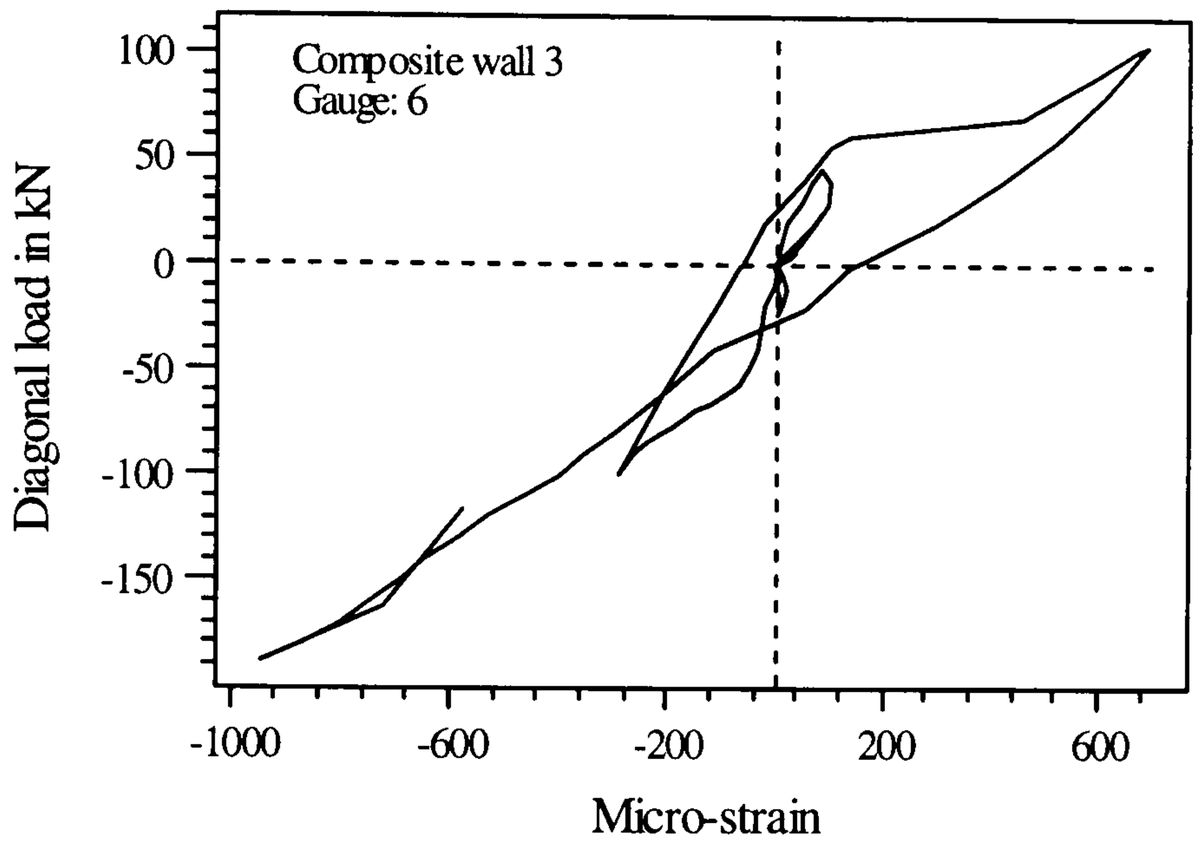

Figure 6.23(b)

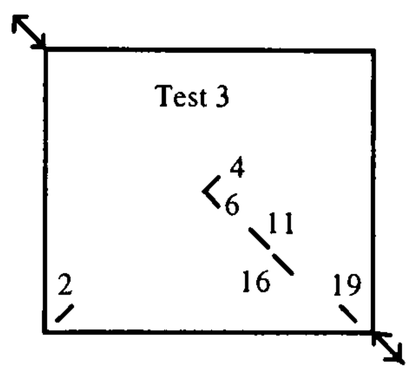

Figure 6.23: Hysteretic loops for diagonal strains in test 3

Test 5: (Effect of mode of load transfer at the boundary)

The variation of strains along the loaded and off-diagonals confirmed that the diagonals were subjected to either tension or compression like the other tests (figure 6.24). The crest sections are found to be less strained compared to the trough section of less thickness as confirmed from the strain at gauge 5 on crest section.

The diagonal strains from test 1 and test 5 are compared in figure 6.24. The strains from both tests show close agreement up to the cracking of panel-5 (14kN) and after that the strains in test panel 5 are higher than those of test panel 1. This confirms that the sheeting is not fully effective when the load is applied through concrete only.

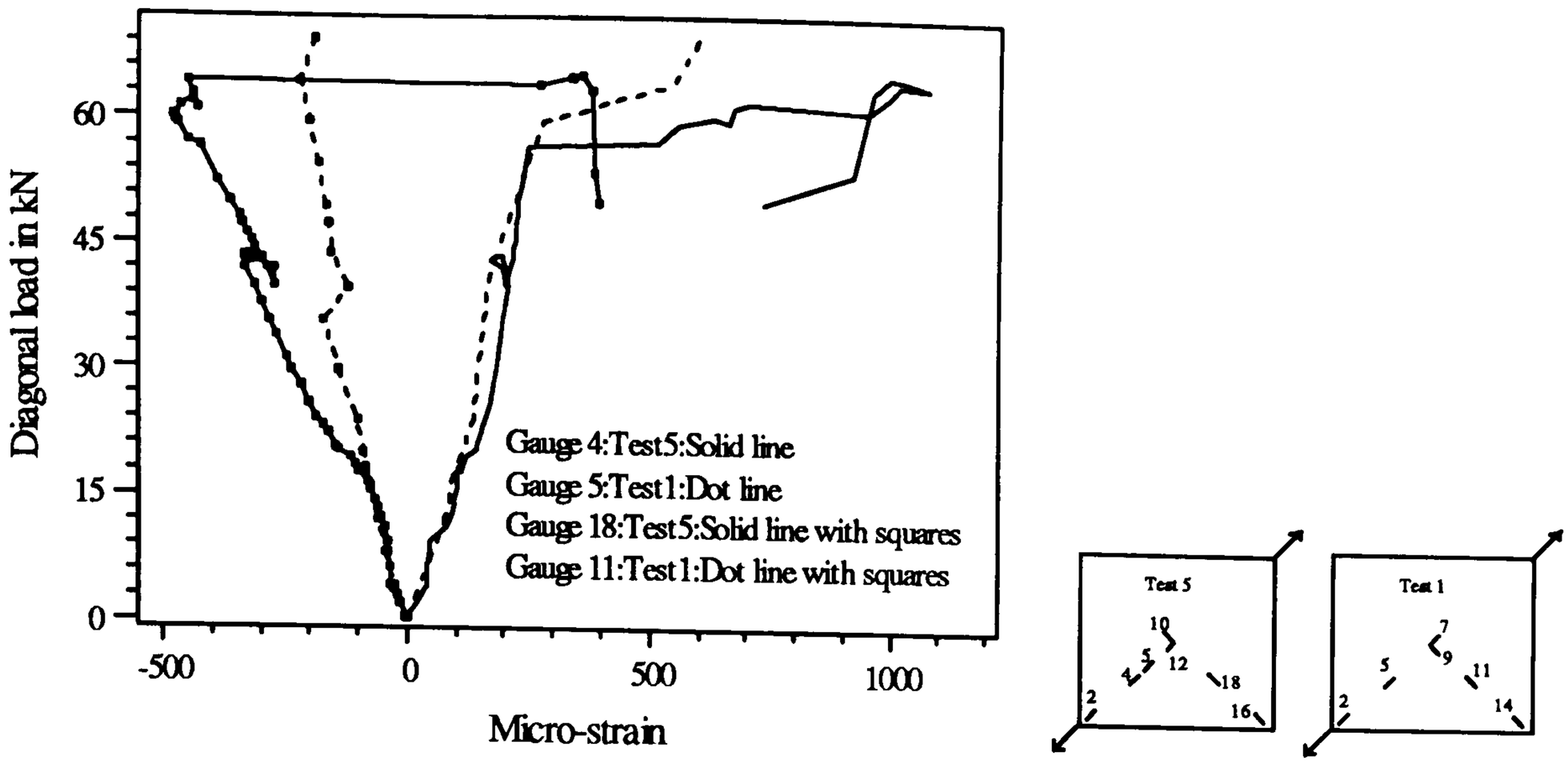

Figure 6.24: Comparison of diagonal strains from tests 1 and 5

Comments

The diagonal strains in all the tests showed identical characteristics with strain conditions changed with cracking of concrete and development of a diagonal tension-compression state in the panels.

The diagonal strains from test 1 and test 5 close agreement up to the cracking load and after that the higher strains were developed in the test panel 5 due to the incapability of the sheeting to share the loads.

6.3.6.2 Principal strains

Test 1 and Test 2

The typical variation of principal strains at rosette locations of panels 1 and 2 are shown in figures 6.25. Similar to the diagonal strains, the variation is marked by the abrupt change in strain at several stages. These may be due to the initial cracking and subsequent progressive cracking of concrete and associated brittle interface between sheeting and concrete. For both walls, the major and minor principal strains at rosette locations seem to be more or less linear up to the cracking of concrete. The strains in the steel reached the yield only after the buckling of the sheeting.

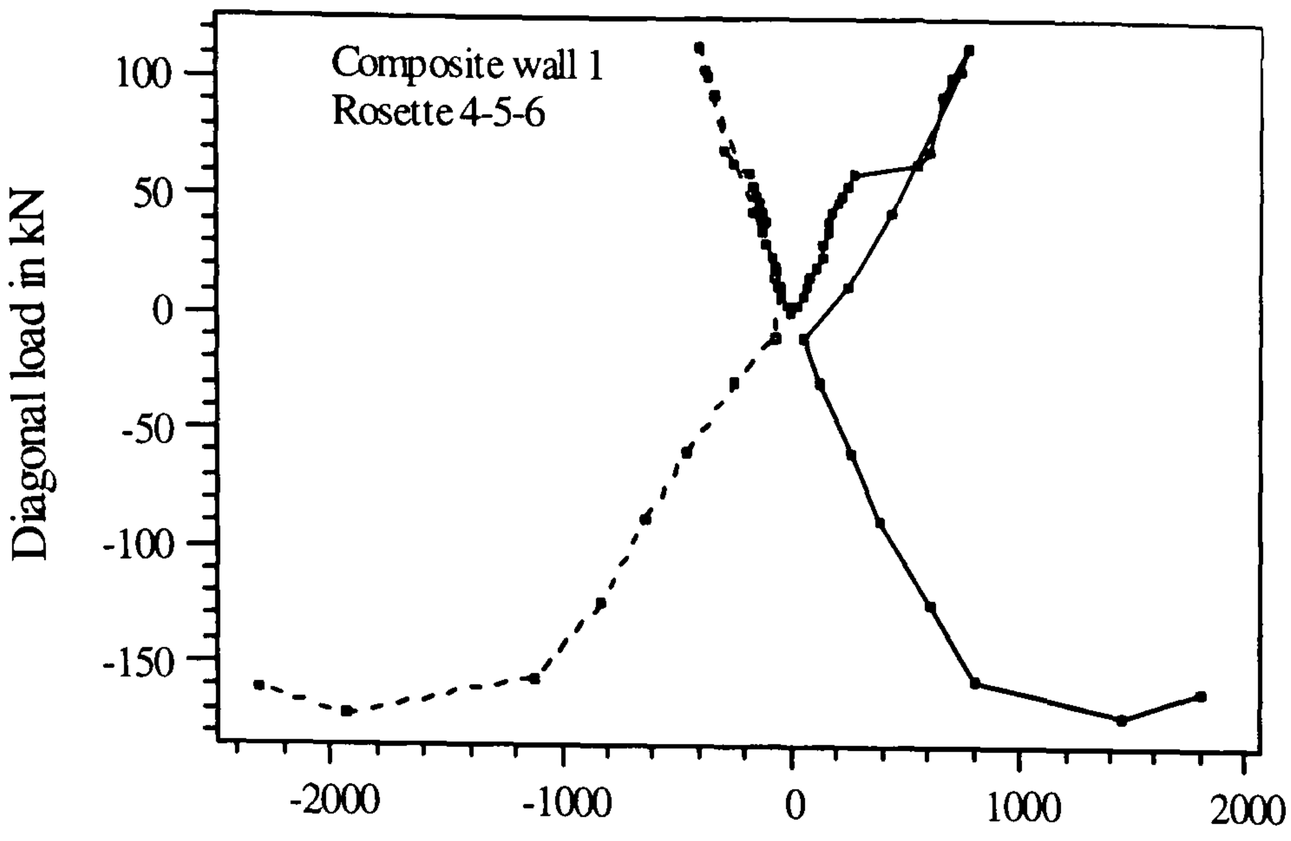

Figure 6.25(a)

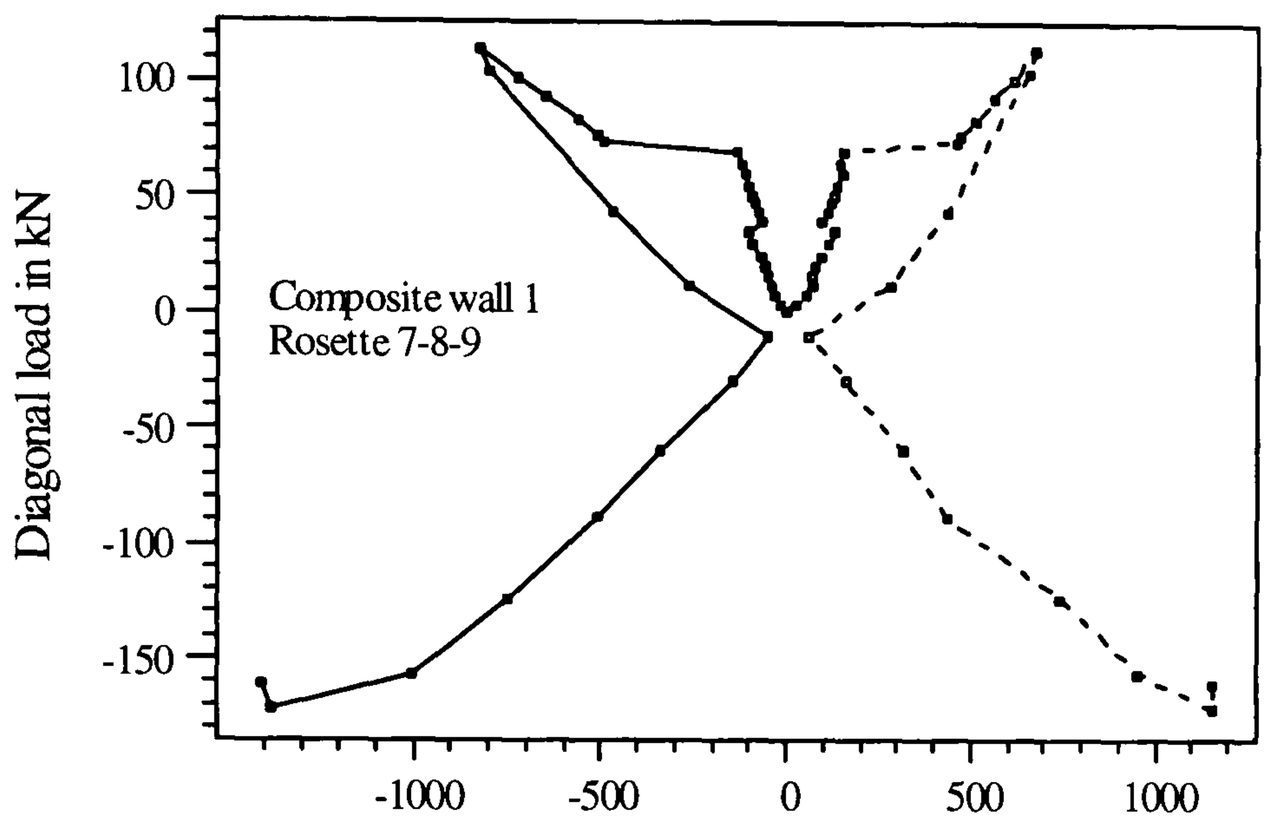

Figure 6.25(b)

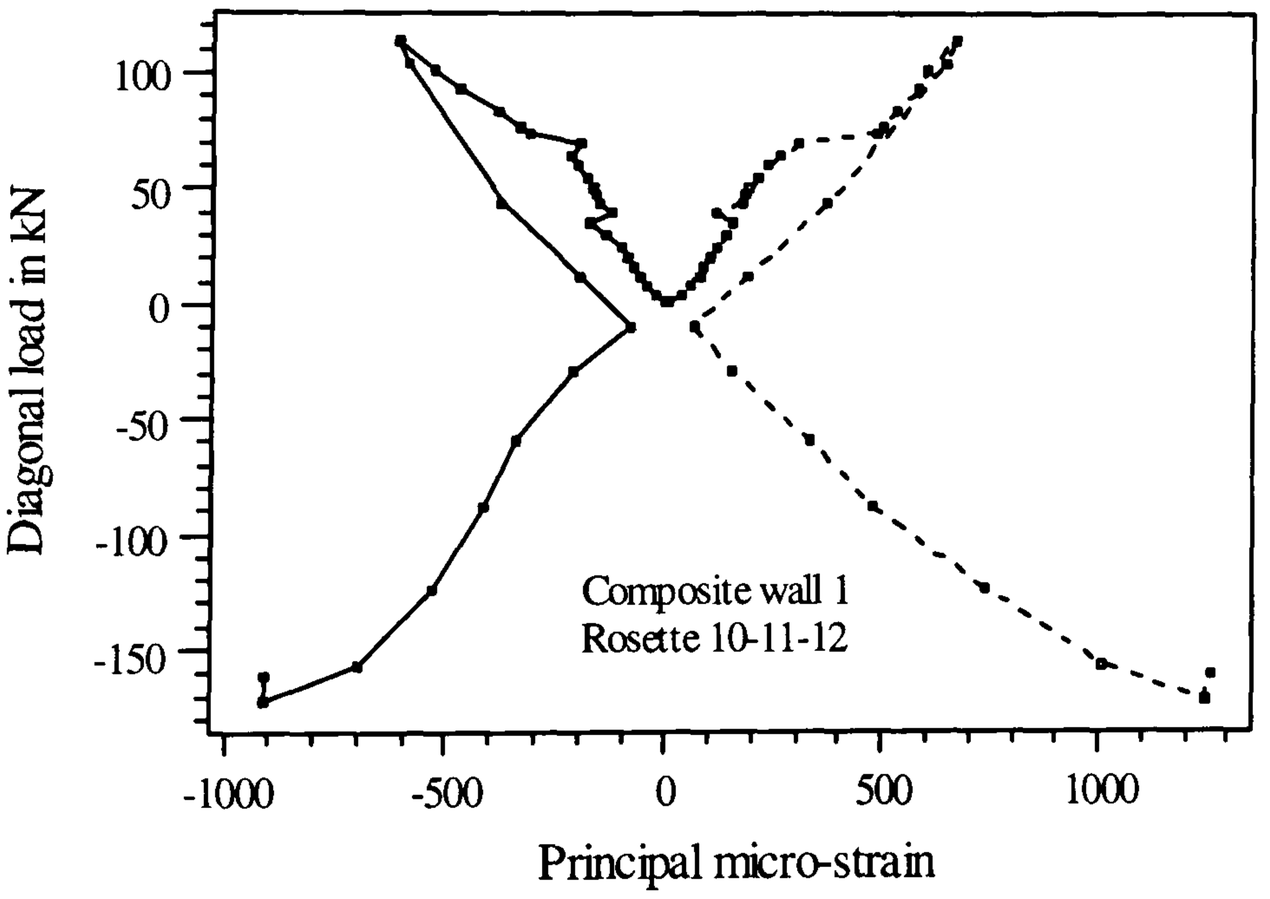

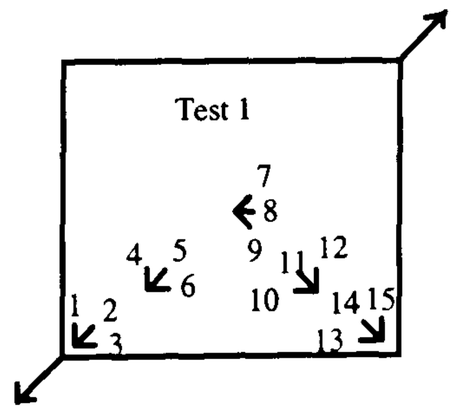

Figure 6.25(c)

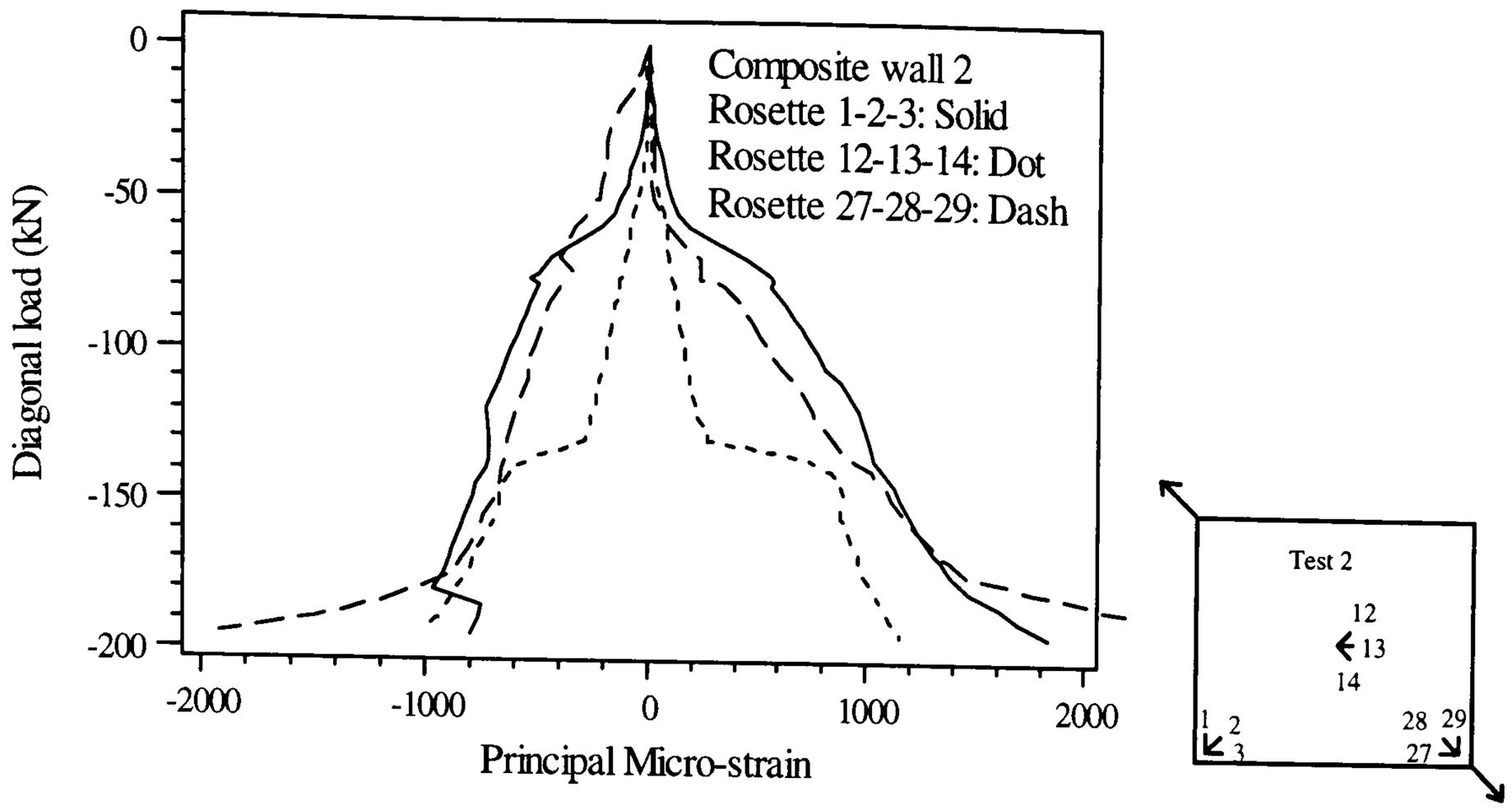

Figure 6.25(d)

Figure 6.25: Variation of principal strains in test 1 and 2

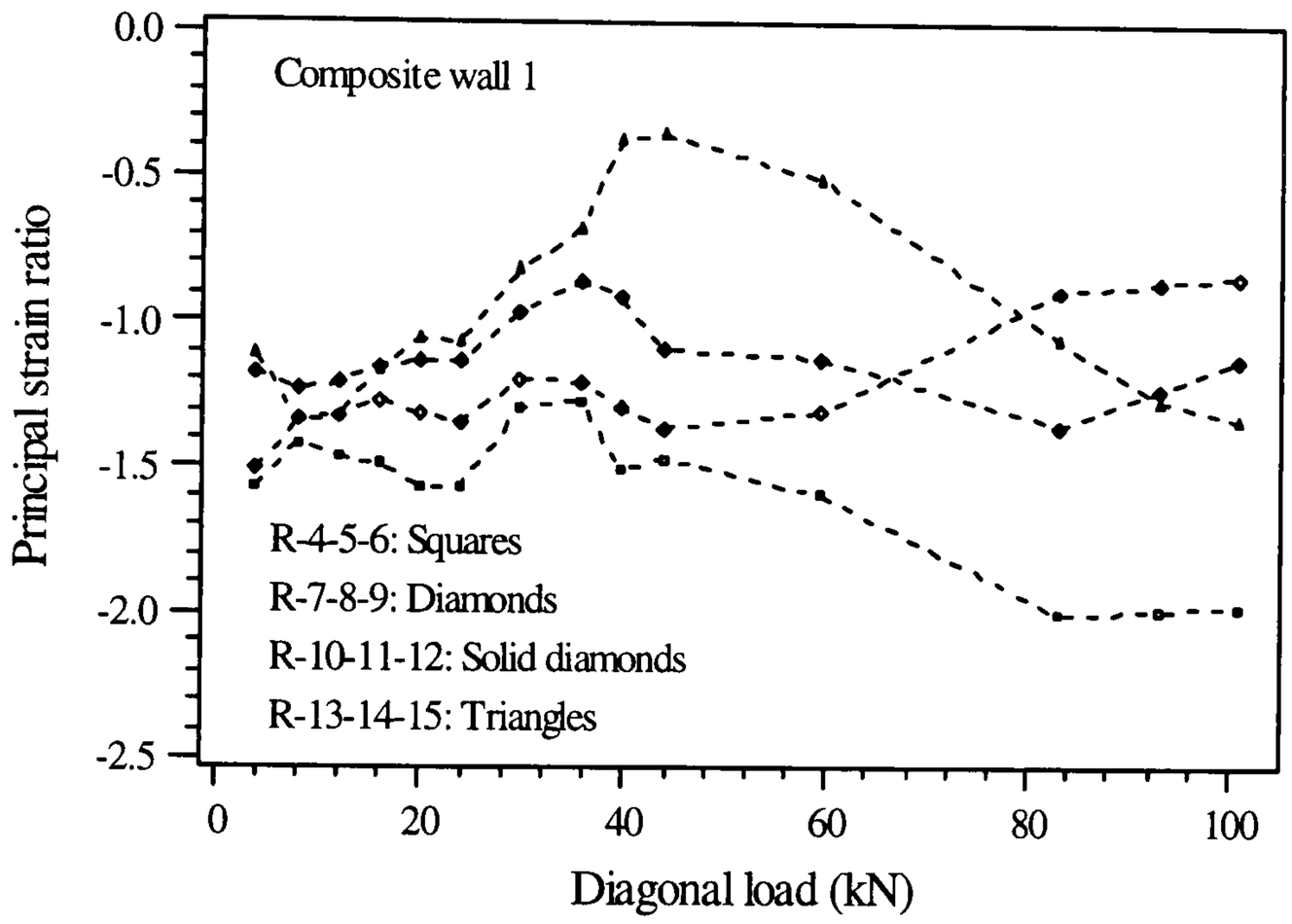

Figure 6.26(a): Variation of principal strain ratios

The variation of principal strain ratios for test 1 are shown in figure 6.26(a). The ratio for loaded corner rosettes (R-1-2-3) are not plotted because of their diversity. The ratio for R-4-5-6 ranges between 1.3 -1.6, for R-7-8-9 between 1.2 -1.4, for R-10-11-12 between 0.9-1.2 and for R-13-14-15 between 0.6-1.1. The diversity of major and minor principal strain seems to be less in the centre rosettes than the corner ones. The variation of principal direction at gauge locations for test 1 is shown in figures 6.26(b) and (c). The principal direction ranges between 16.3 to 44.83 for R-1-2-3, 37 to 44.83 for R-4-5-6, 37.82 to 47.45 for R-7-8-9, 26 to 42.3 for R-10-11-12 and 22.5 to 44.7 degrees for R-13-14-15.

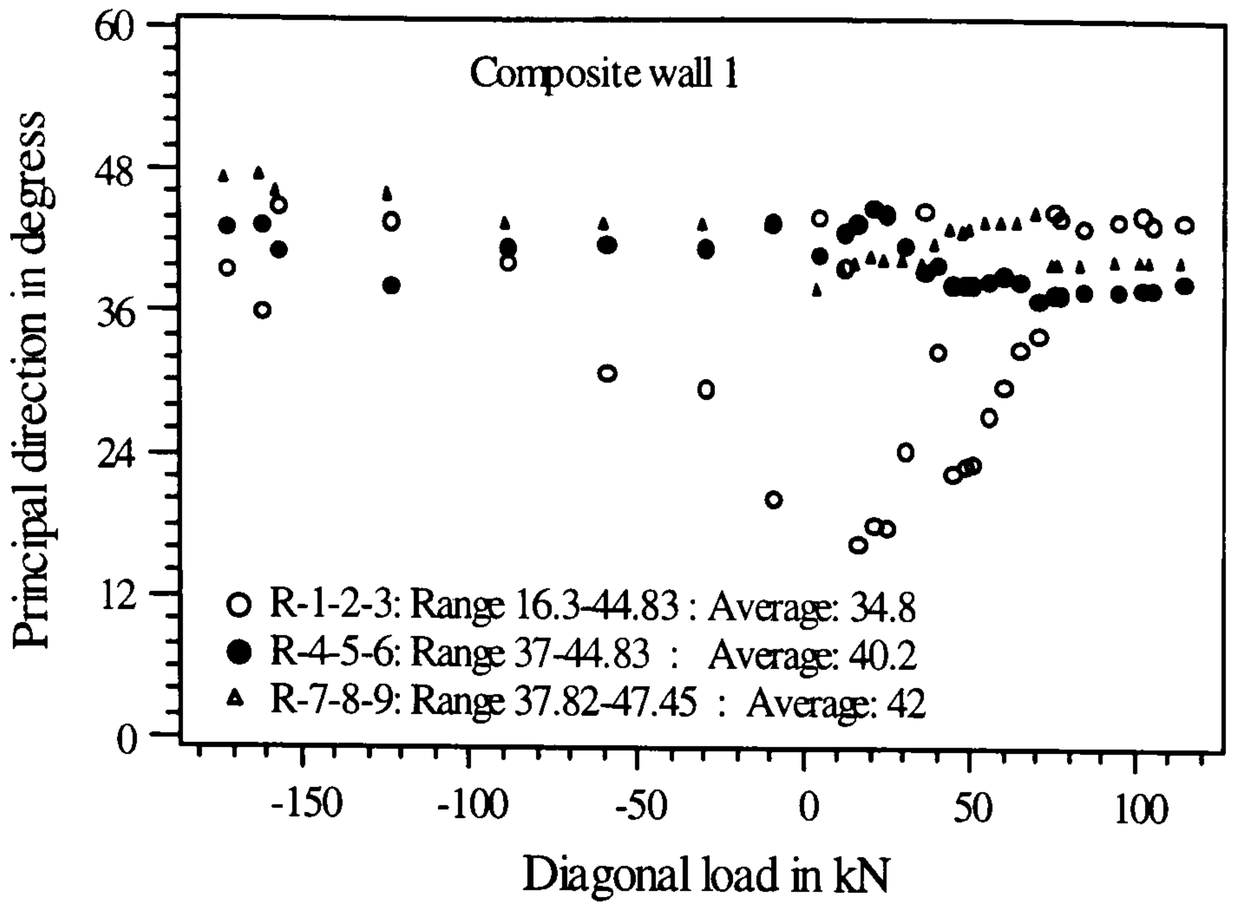

Figure 6.26(b): Variation of principal directions

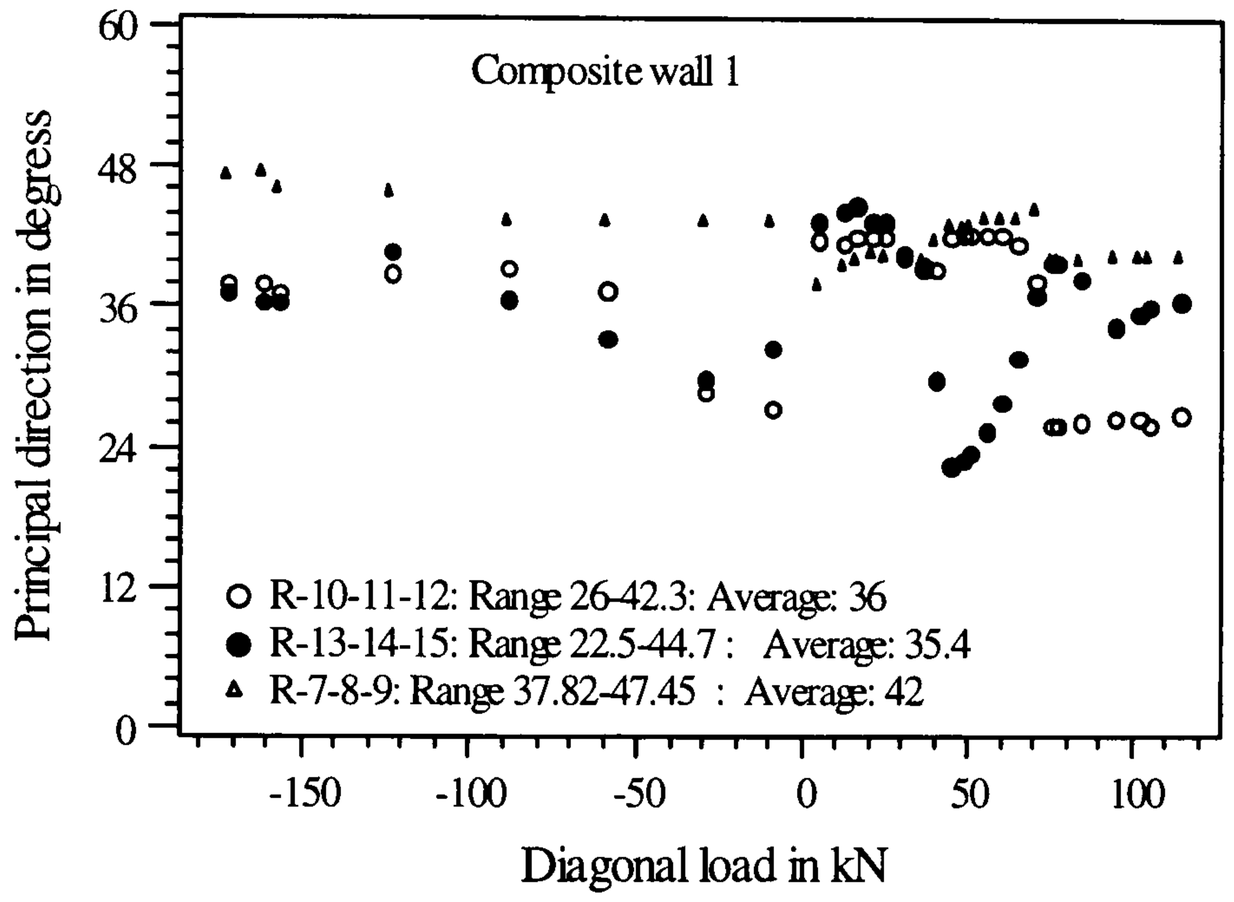

Figure 6.26(c): Variation of principal directions

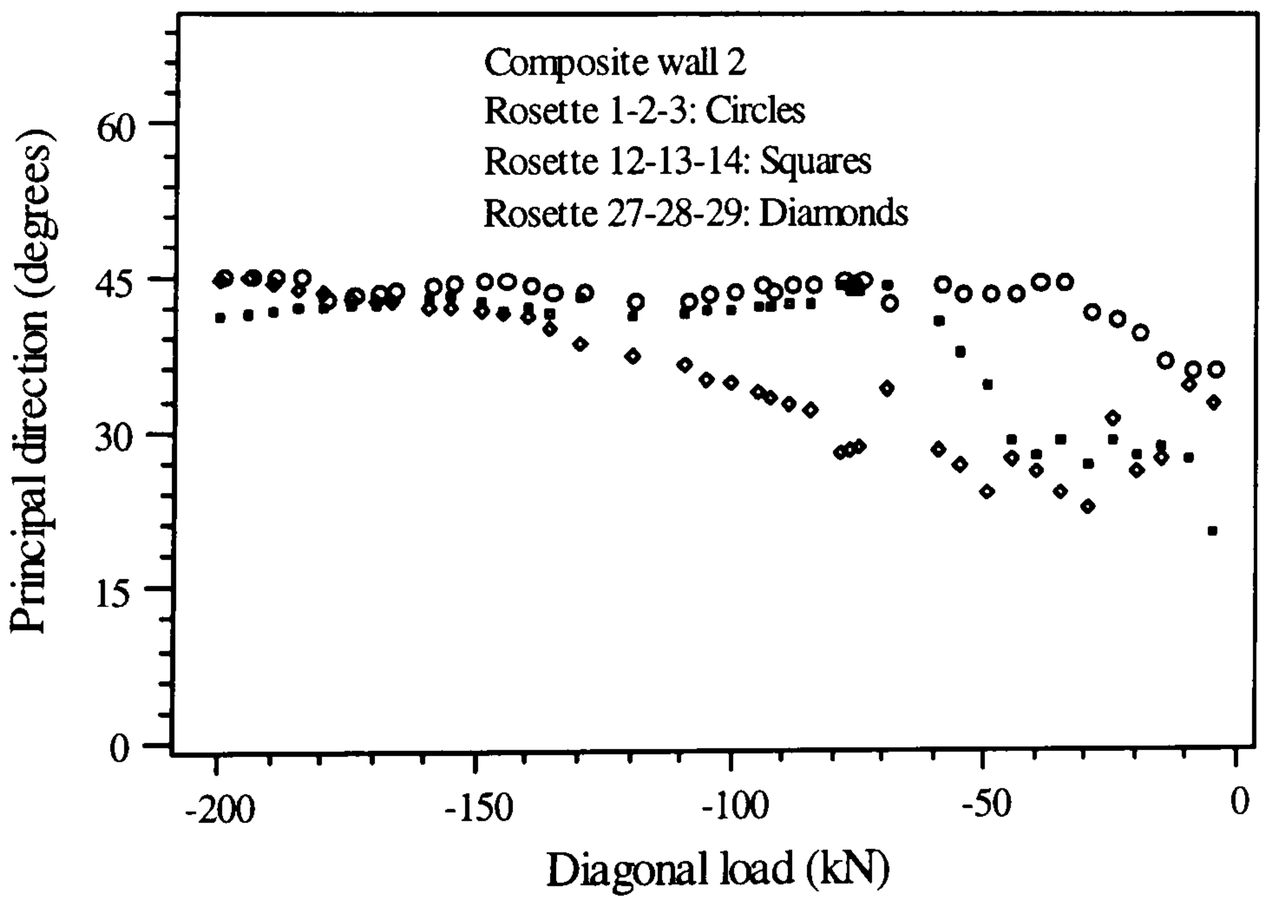

Figure 6.26(d): Variation of principal directions

For test 2 , it is clear that the diversity of major and minor principal strains are higher in the initial pre-cracking stage of debonding but in the post-cracking stage the diversity seems to be reduced. The principal direction diagrams shown in figures 6.26(d) reflects these finding. The lower values of principal directions (21-36 degrees) up to a load of -50kN suggested diversity of major and minor principal strain. The principal direction for R-1-2-3 ranges between 36-45, for R-12-13-14 ranges between 27-42 and for R-27-28-29 ranges between 24-44 degrees.

Test 3 (Hysteretic variation of principal strains)

The typical hysteretic variation of principal strains from test 3 is shown in figures 6.27. The corner rosettes showed much distorted response with higher residual strains than those in the middle of the panel. This may be the consequence of diagonal cracks at the corners.

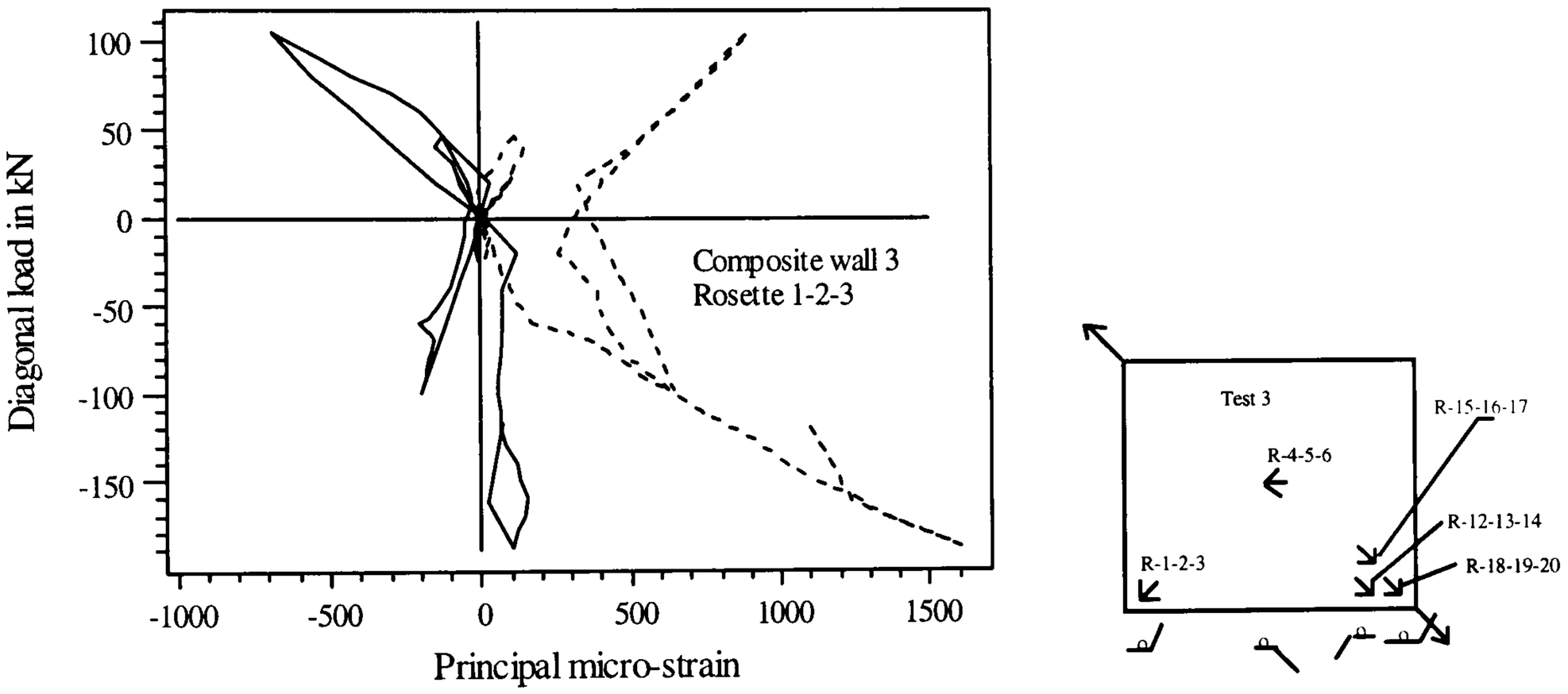

Figure 6.27(a)

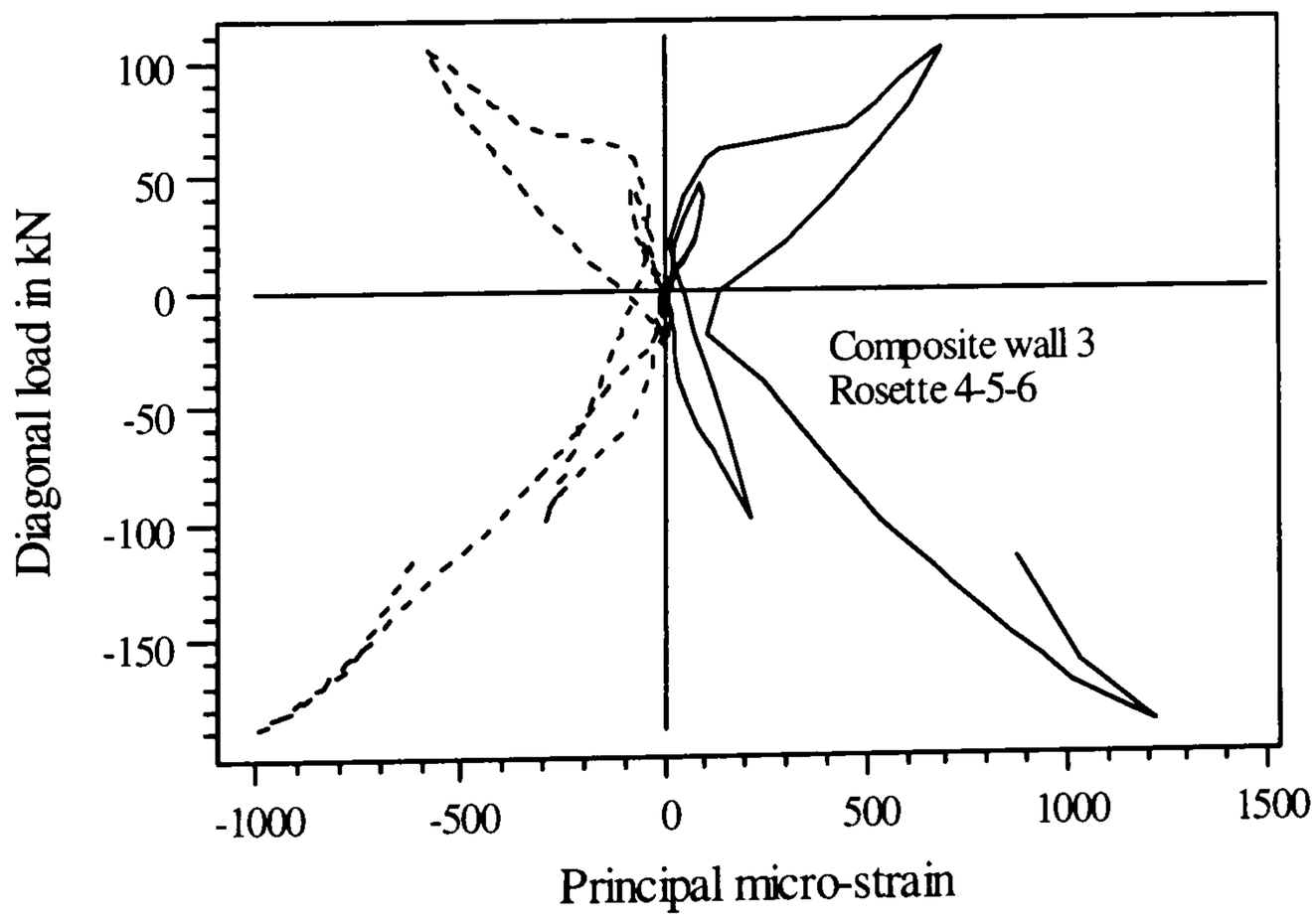

Figure 6.27(b)

Figure 6.27: Hysteretic variation of principal strains in test 3

Comparison between Test 1 and Test 5

The principal strains at rosette locations are compared to those from test 1 in figures 6.28(a) and (b) and found a close agreement up to the cracking load. The strain in panel 5 was greatly increased after the cracking due to the non-effectiveness of the sheeting due to the boundary conditions.

The principal directions at rosette locations are plotted in figure 6.28(c). In the pre-cracking stage, the principal directions in all the rosettes fall within a band of 36-45 degrees but scattered results are found in the post cracking stage like the case of profiled concrete core discussed in chapter 4.

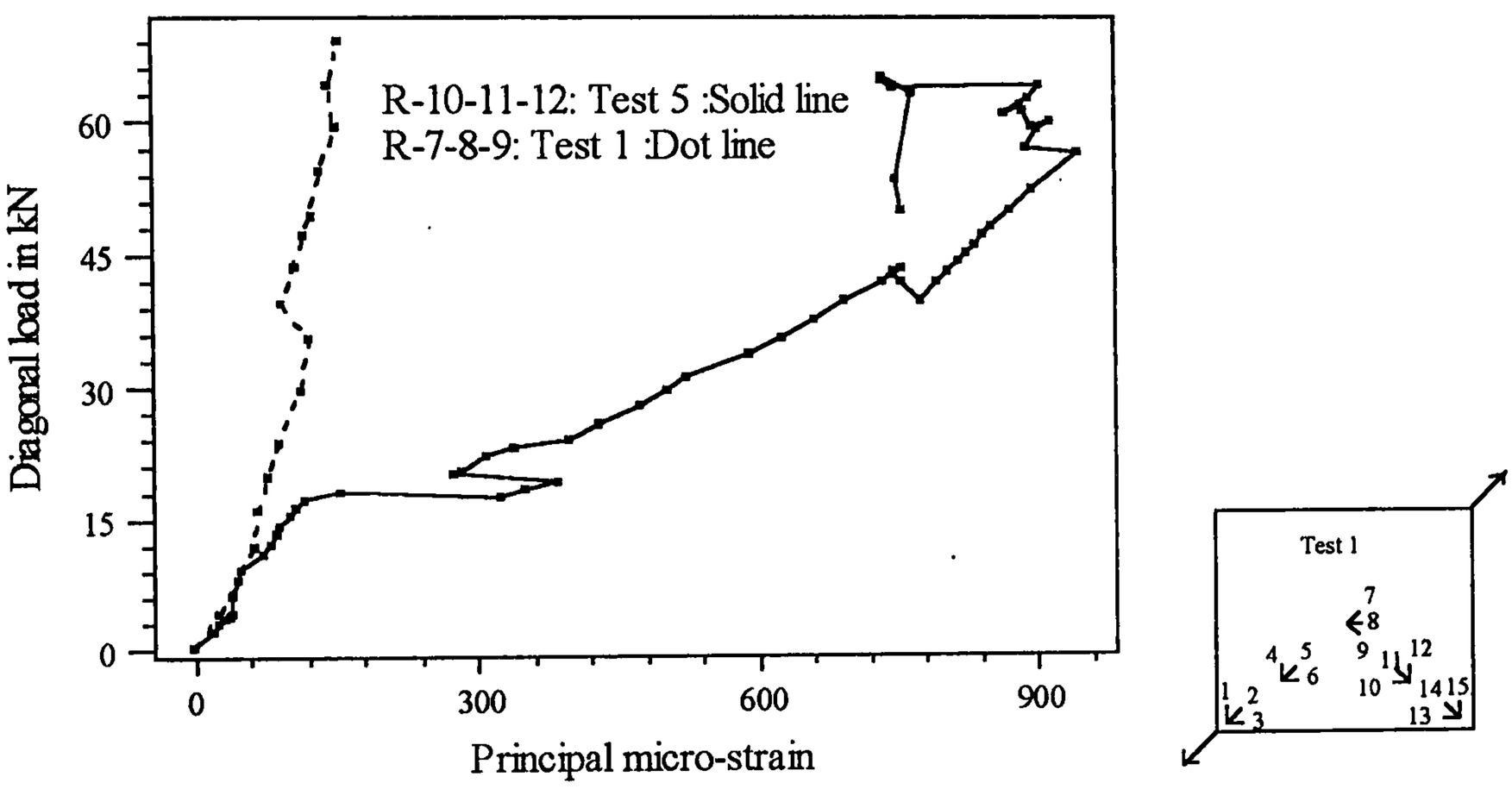

Figure 6.28(a)

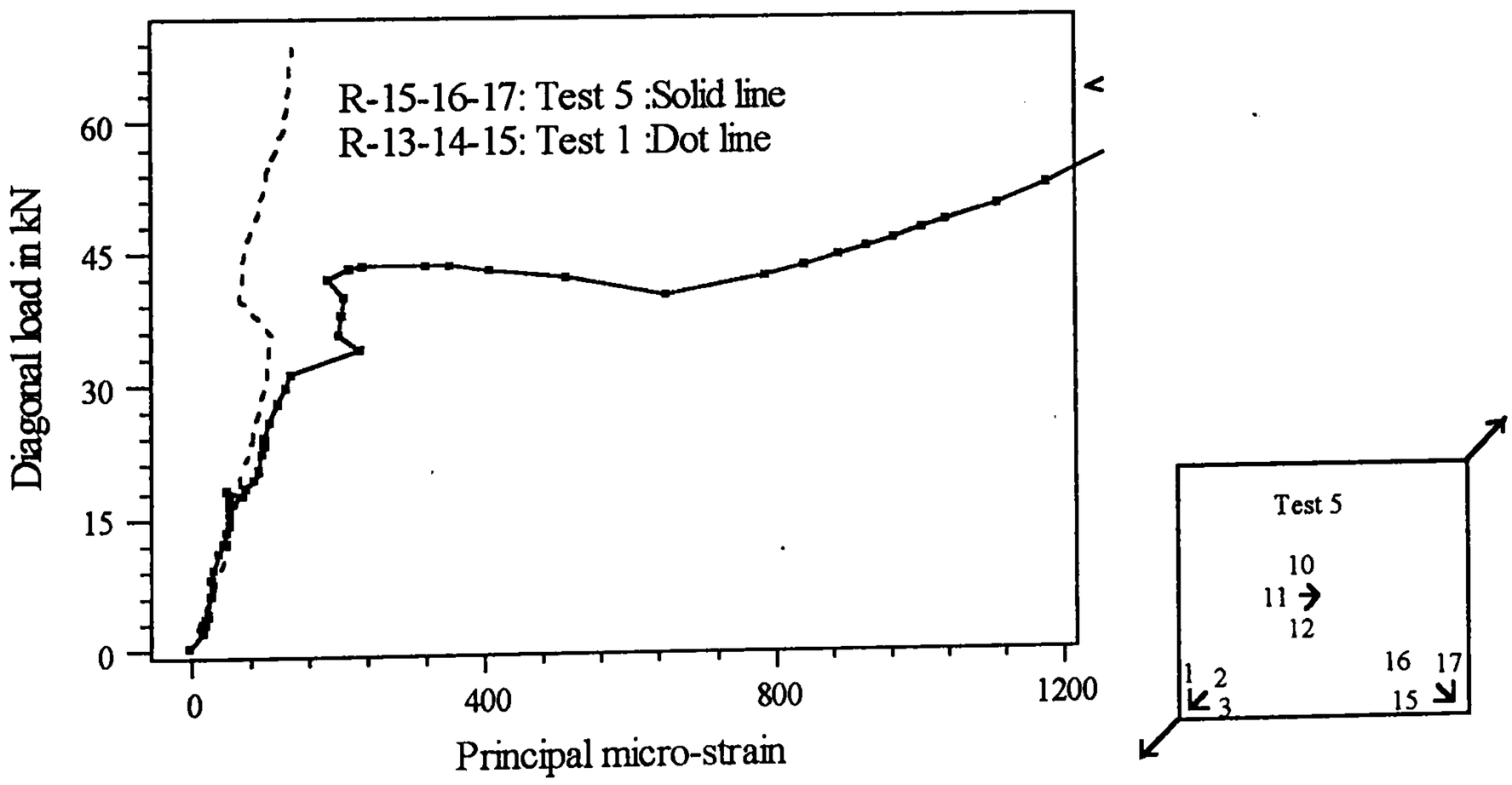

Figure 6.28(b)

Figure 6.28(a) and (b) : Comparison of principal strains from test 1 and 5

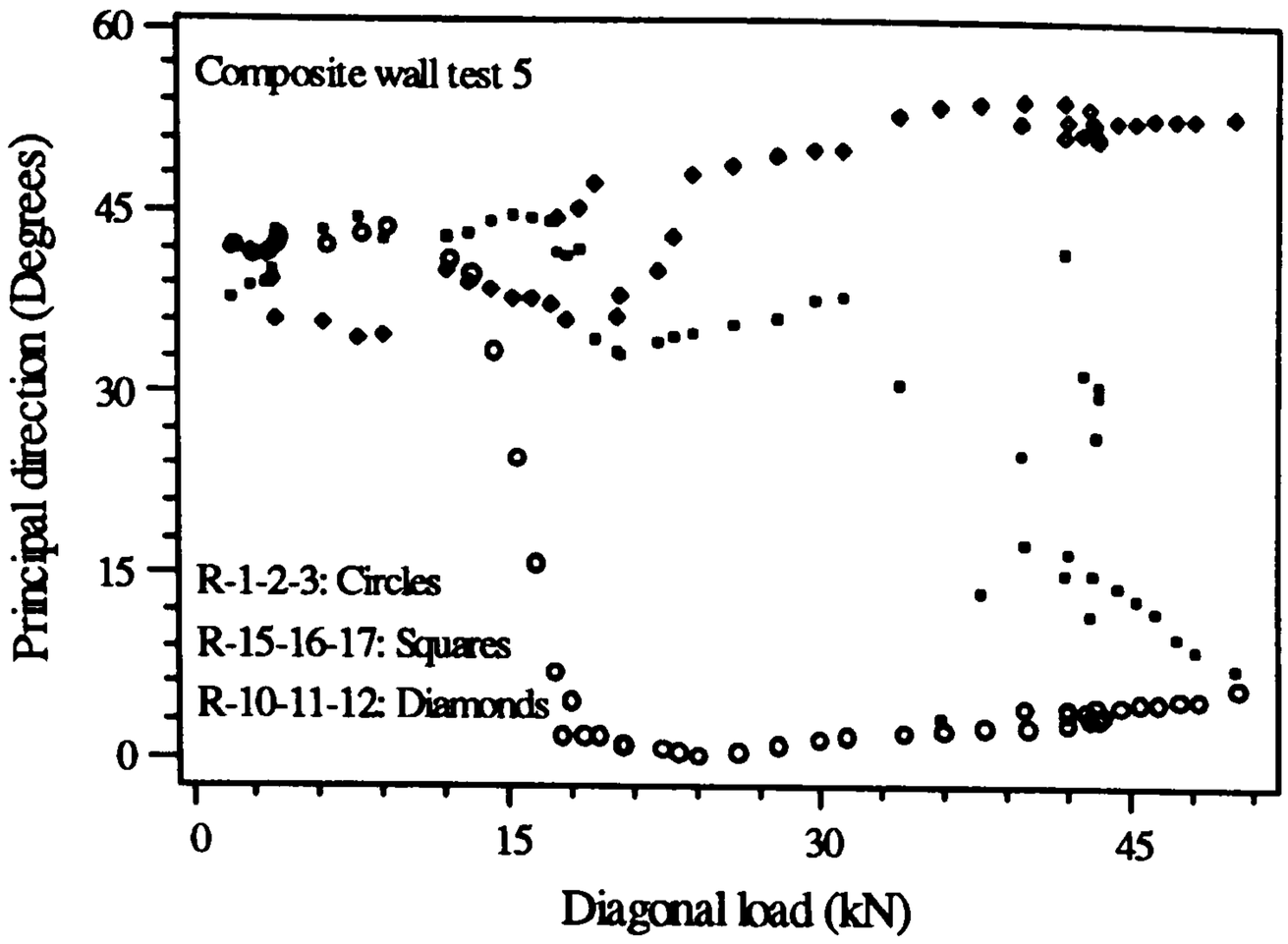

Figure 6.28(c): Variation of principal direction in test 5

Comments:

Up to the cracking of concrete the principal strains in test 1 and test 3 can be considered to be in reasonable agreement as concluded from table 6.3. The strains form test 5 are also tabulated and up to the cracking they are close to those from test 1 and test 3

Table 6.3: Principal strain comparison

Load	Loaded corner rosette			Central rosette			Off-loaded corner rosette		
kN	Principal strains			Principal strains			Principal strains		
	Test 1	Test 3	Test 5	Test 1	Test3	Test5 (crest)	Test 1	Test 3	Test 5
2		20	26		12	19		26	17
4	20	40	46	26	28	38	18	41	27
8	55	51	51	45	37	53	37	46	35
12	76	59	214	62	42	79	51	51	45
18	81	86	430	67	64	153			
20	88	-	863	79	-	386	68	87	91
30	110	121	-	113	94	-	99	156	-
40	623	146	-	93	102	692	68	211	206

The principal strain at rosette locations confirmed that the yielding of steel commences only after the buckling of sheeting. The principal directions are affected by the process of interaction between sheeting and concrete which included debonding and cracking of concrete. The lower values (24-30 degrees) are found in the initial stages of debonding and cracking. In the post-cracking stages the principal directions are found to be ranged between 39-45 degrees.

6.3.6.3 Variation of strains along the boundaries

Adjacent trough and crest section

The strain transfer through the web of the profile at the plain boundary is shown in figures 6.29. Gauges 30,31,32 and also gauges 33,34, 35 showed identical variation of Y-strain throughout the loading history. All the gauges were initially under compression and in the latter stages were subjected to tension. The web strain in Y-direction is consistent with those of adjacent trough and crest strain and follow the pattern of tension -compression similar to them. The strain values were dependent on the thickness of the wall in the sections and as a result crest and web strains were less than those at troughs.

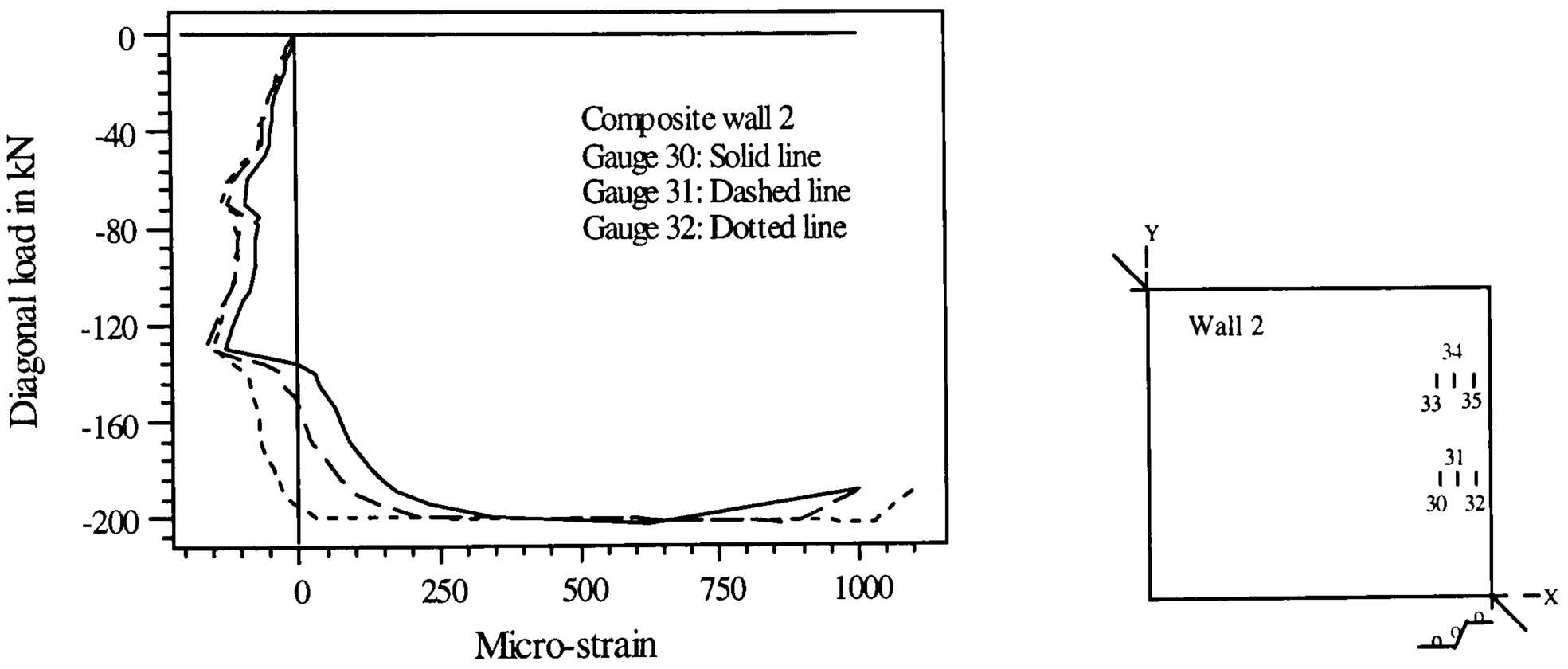

Figure 6.29(a): Y -strain transfer through the web at plain boundary

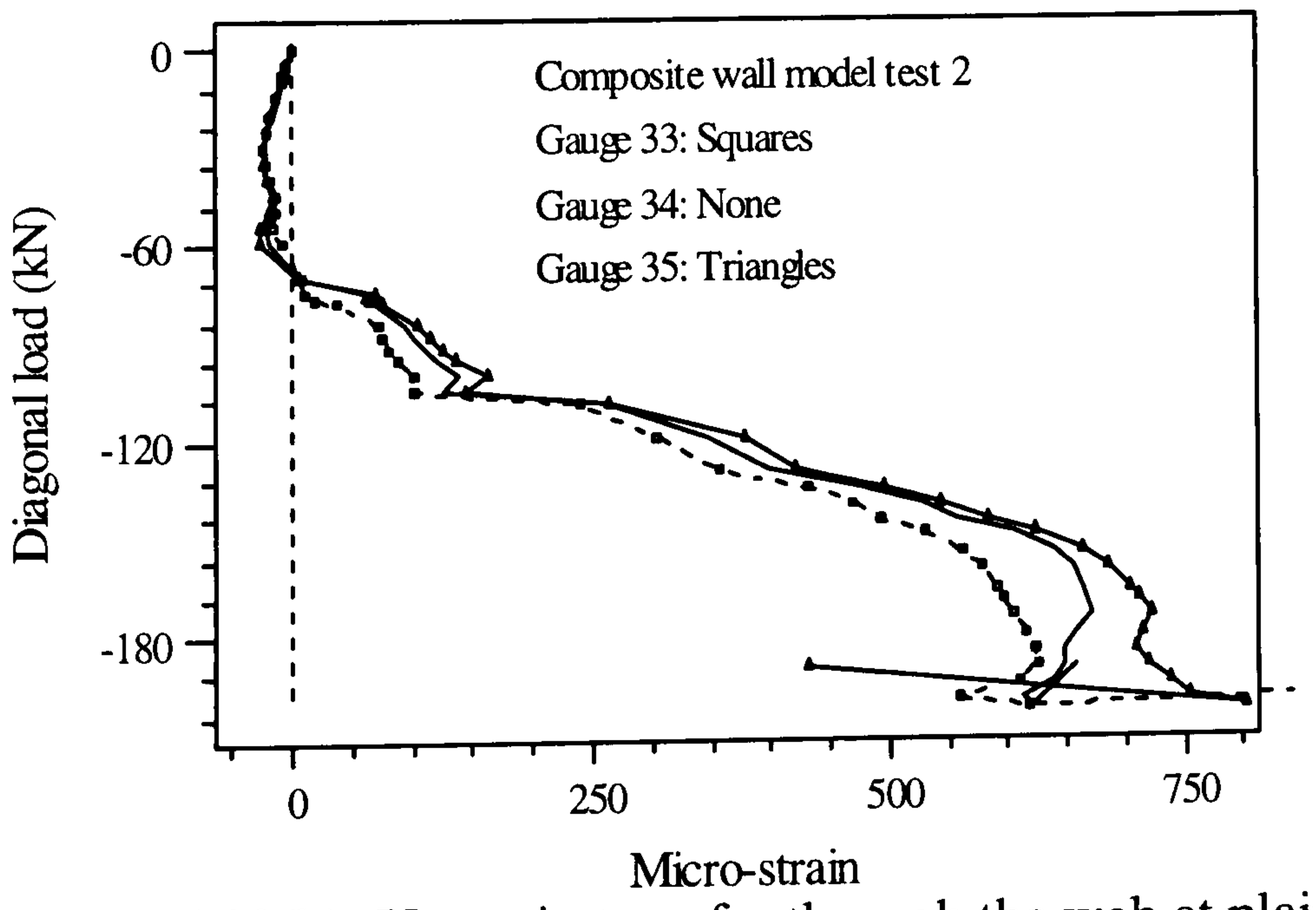

Figure 6.29(b): Y -strain transfer through the web at plain boundary

X and Y strain along the boundaries

Test 2

The variation of Y-strain along the profiled boundary from test 2 is shown in figures 6.30(a) and (b). The pre-cracking variation shown in figure 6.30(a), initially showed tensile strain but after that the strain at loaded end strain was found to be in compression. The figure revealed some information on the strains in a profile sections and it pointed out that the crest may be strained higher (as in gauge 6) in Y-direction than the trough and web sections and it may be a function of the position of the profile in the boundary. However, strain values showed a pattern of variation. But in the post-cracking stage (figure 6.30(b), strains did not follow any definite pattern.

The pre-cracking variation of X-strain along the profiled boundary is shown in figure 6.30(c). The variation can be considered as tension at the corners with compression in the middle region of the boundary. However, this may not be valid in the post-cracking and final stages (figure 6.30(d)). The X-strains seem to be higher in the trough sections than those at crest sections.

The pre-cracking variation of Y-strain along the plain boundary is dominated by compression (figure 6.30(e)). However this was not followed in the post-cracking stages(figure 6.30(f)).

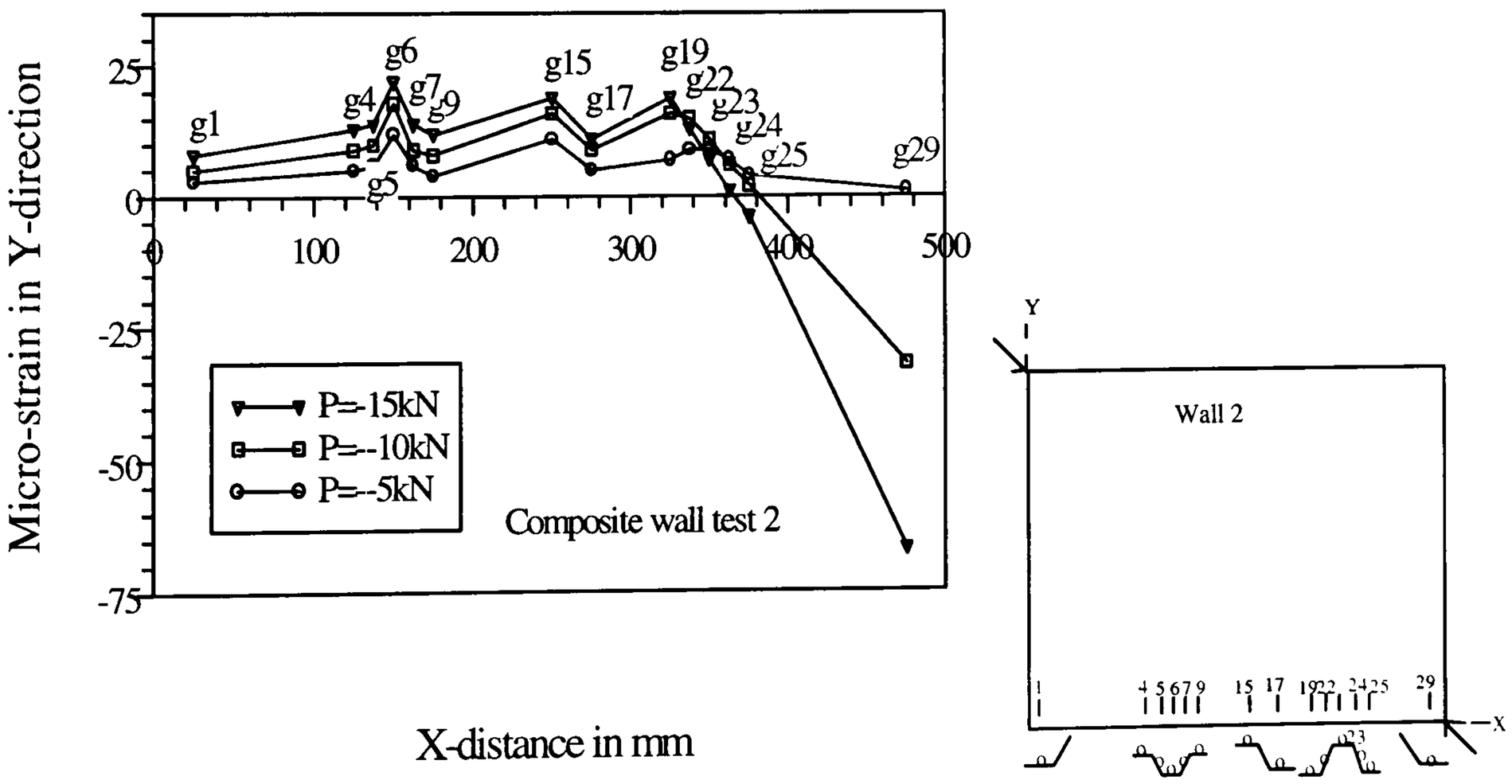

Figure 6.30(a): Variation of Y-strain along the profiled boundary

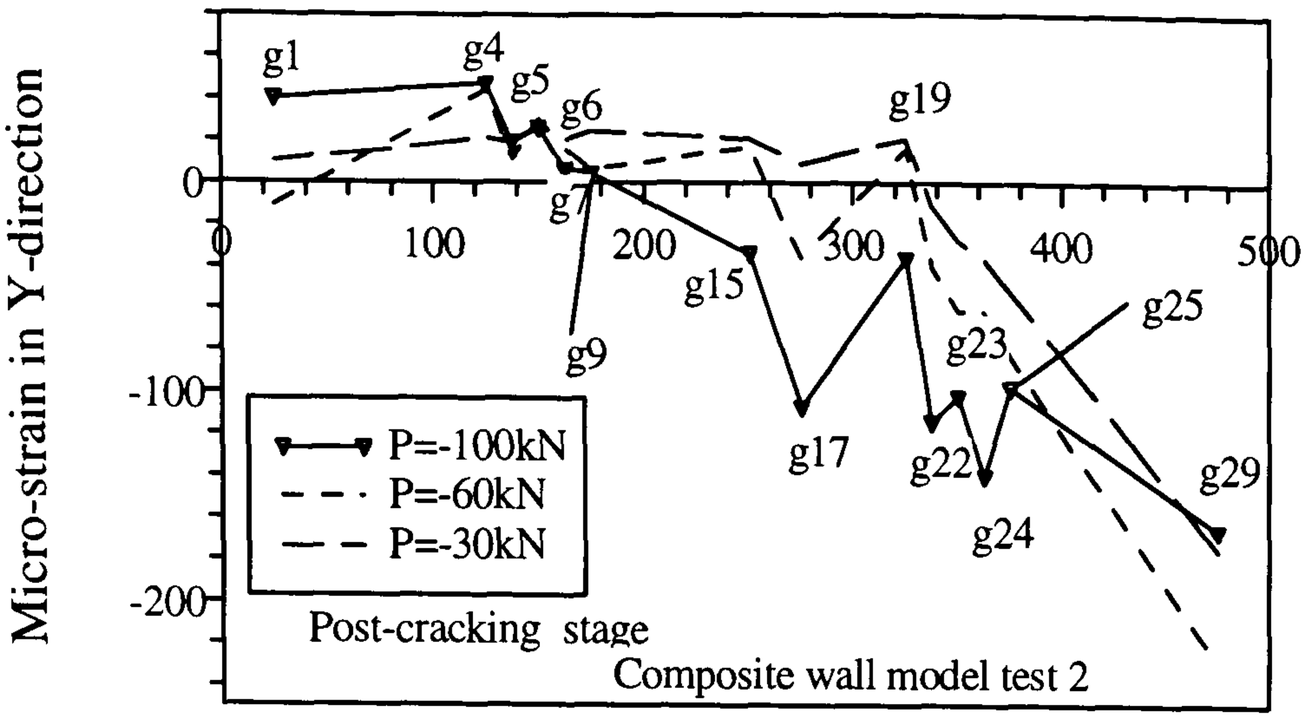

X-distance in mm

Figure 6.30(b): Variation of Y-strain along the profiled boundary

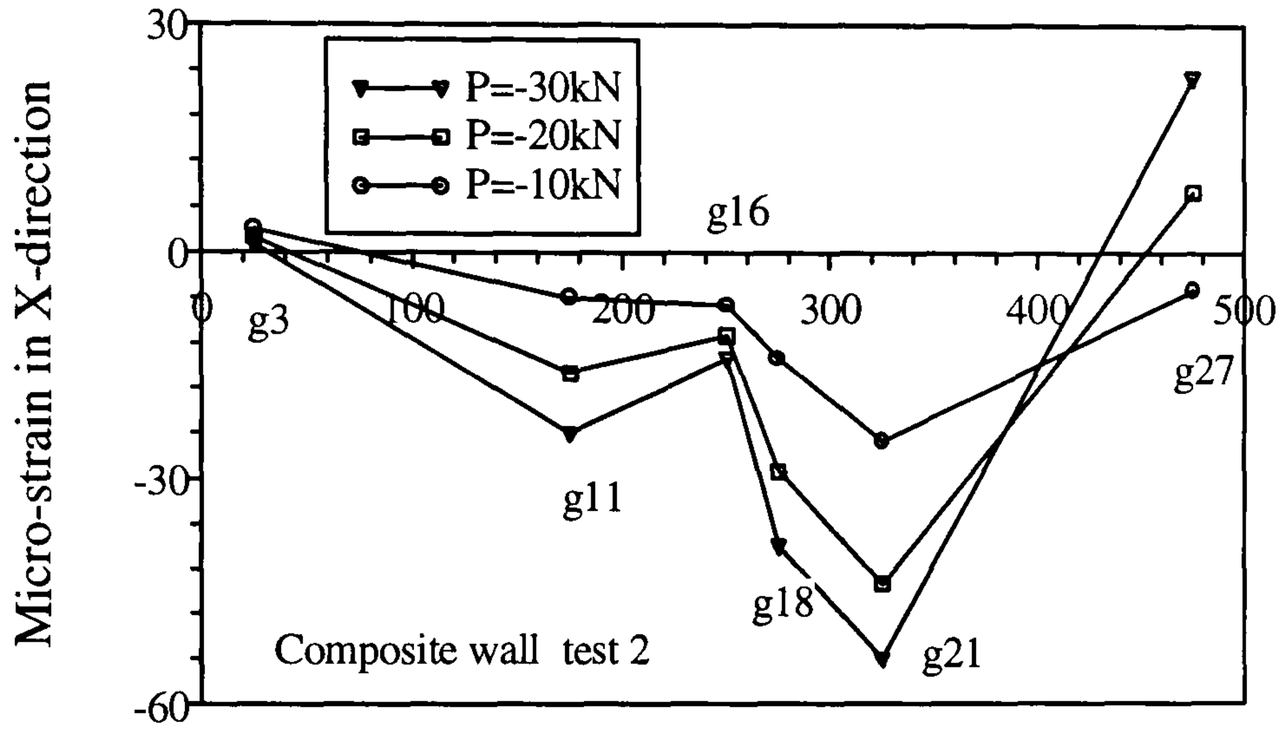

X-distance in mm

Figure 6.30(c): Variation of X-strains in the profiled boundary

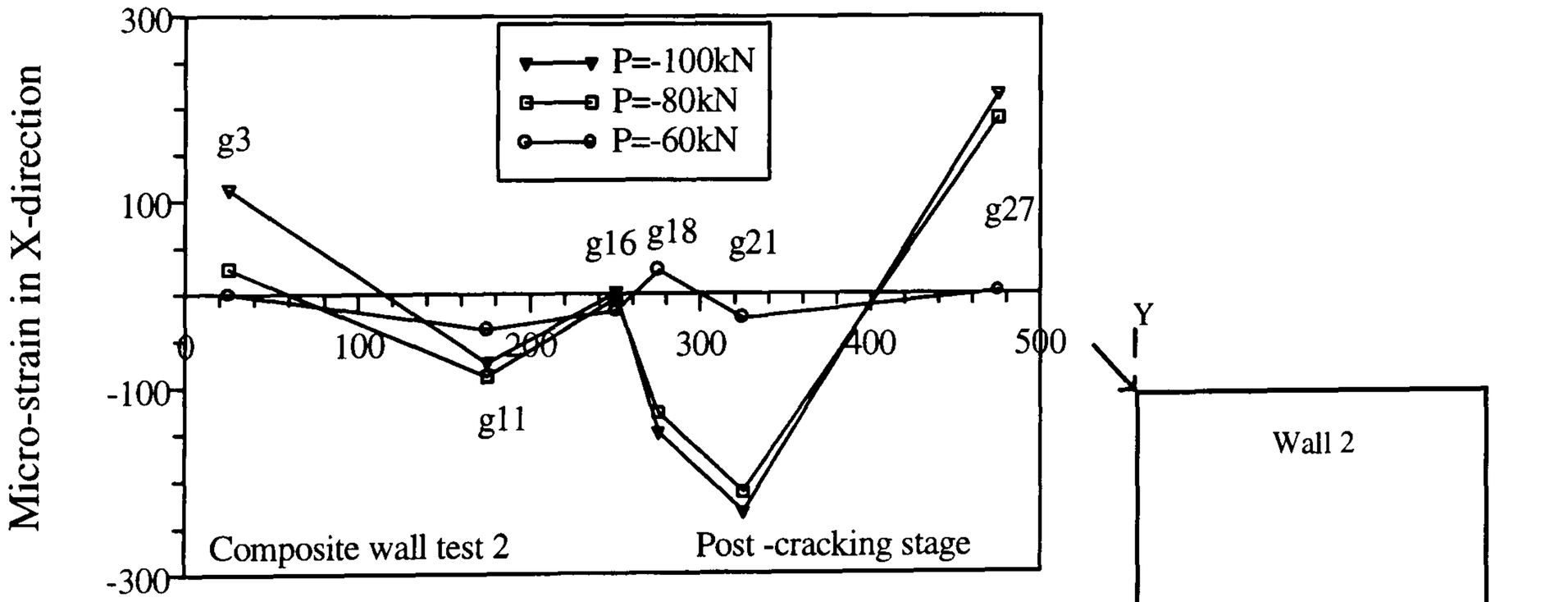

X-distance in mm

Figure 6.30(d): Variation of X-strains in the profiled boundary

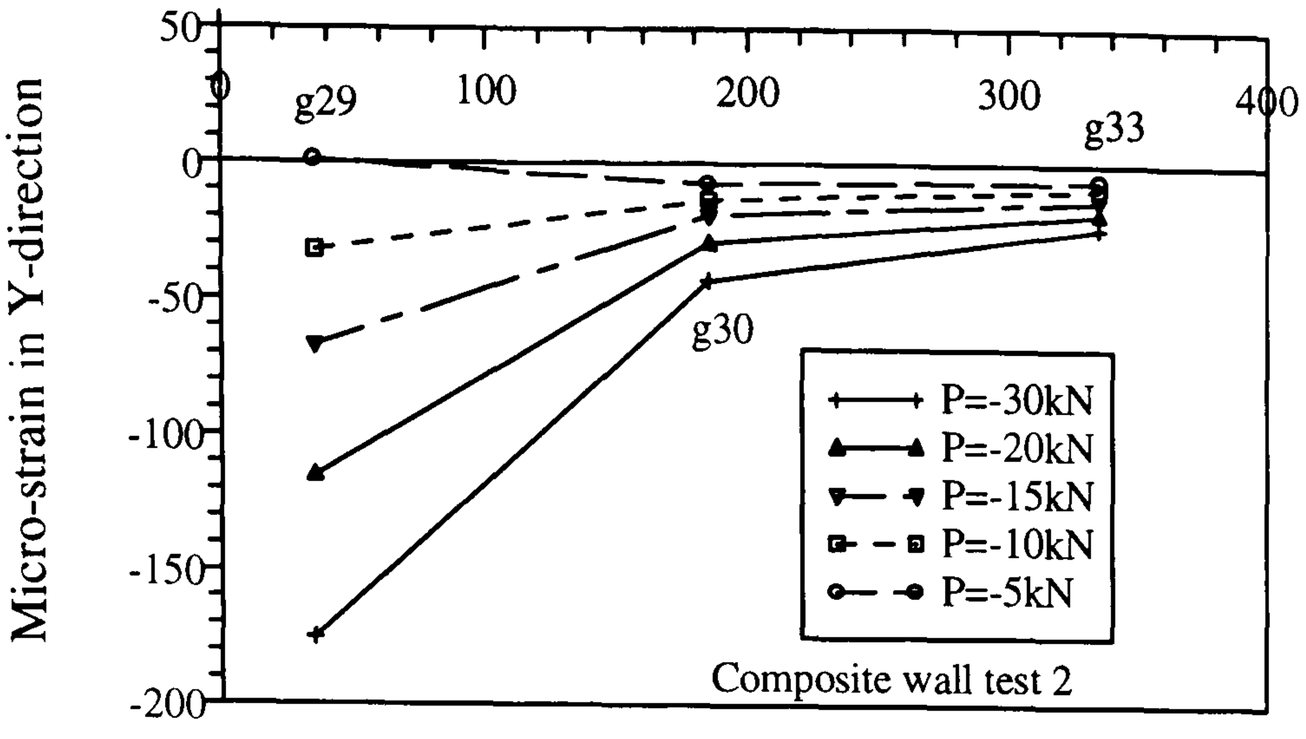

Figure 6.30(e): Variation of Y-strain along the plain boundary

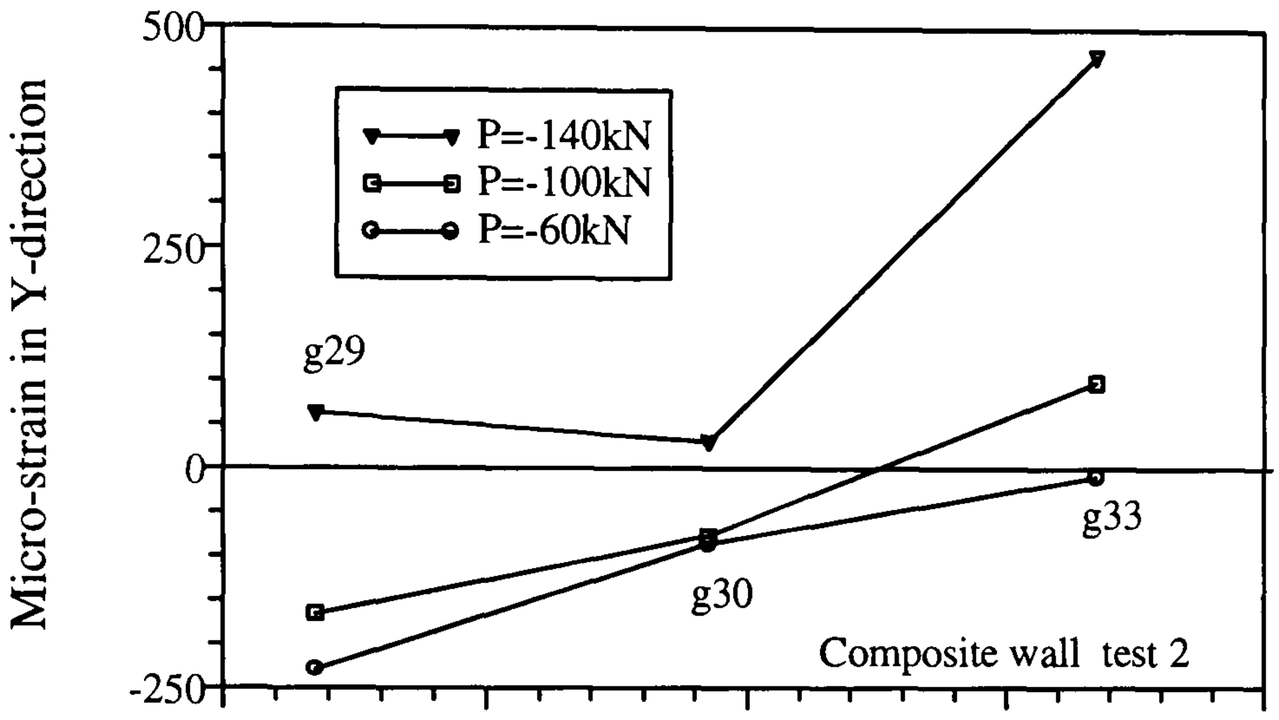

Figure 6.30(f): Variation of Y-strain along the plain boundary

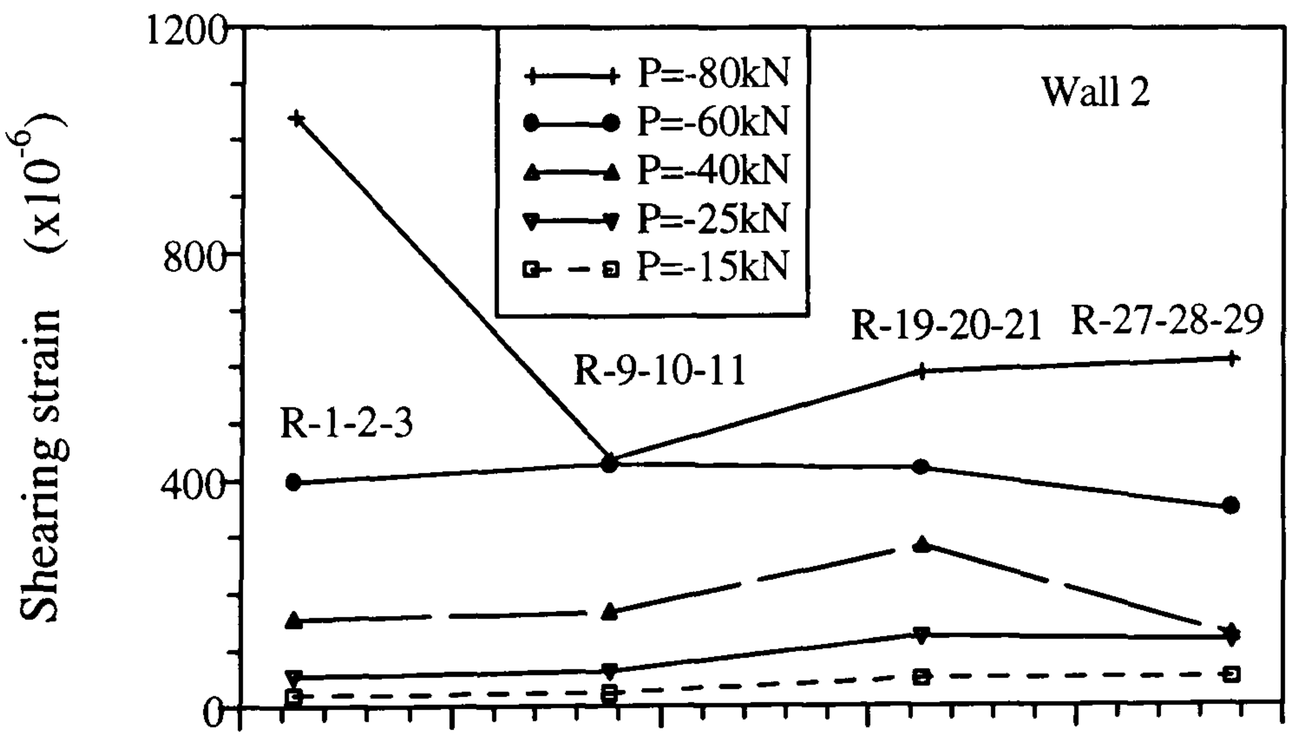

Figure 6.30(g): Variation of shearing strain along the profiled boundary

The variation of shearing strain along the profiled boundary as calculated from the boundary rosettes are presented in figure 6.30(g). In the pre-cracking stage the shearing strain at the loaded corner is found to be higher than the off-loaded corner. In the latter stages, the situation is changed.

Test 1

The variation of Y-strain along the profiled boundary is shown in figure 6.31(a). The figure confirms the presence of higher strain in the crest section (g-16 and g-22) as was found in test 2 besides the higher thickness in this sections. The variation of x-strain is shown in figure 6.31(b), which can be considered to be identical to that of test 2 with higher strain in the trough sections. But in this case the variation curve is reversed as the test was conducted under tensile diagonal load.

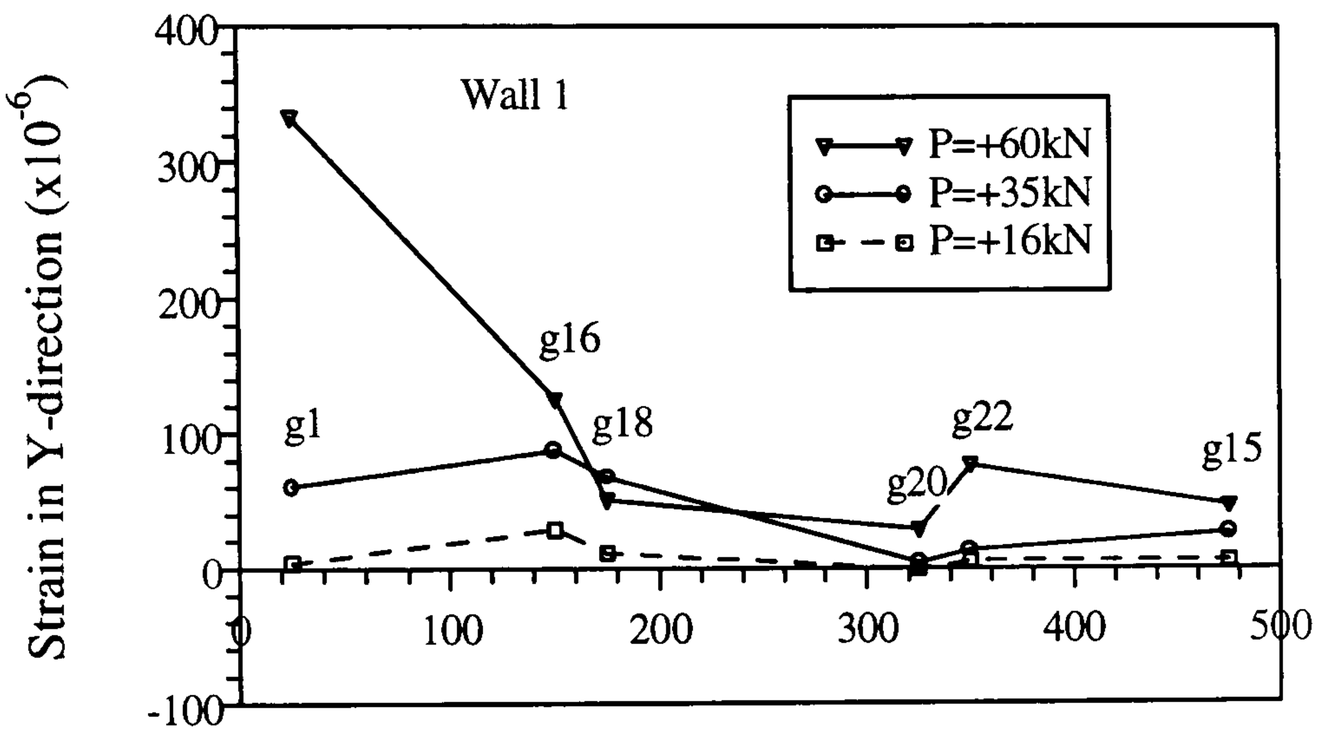

Figure 6.31(a): Variation of Y-strain along the profiled boundary

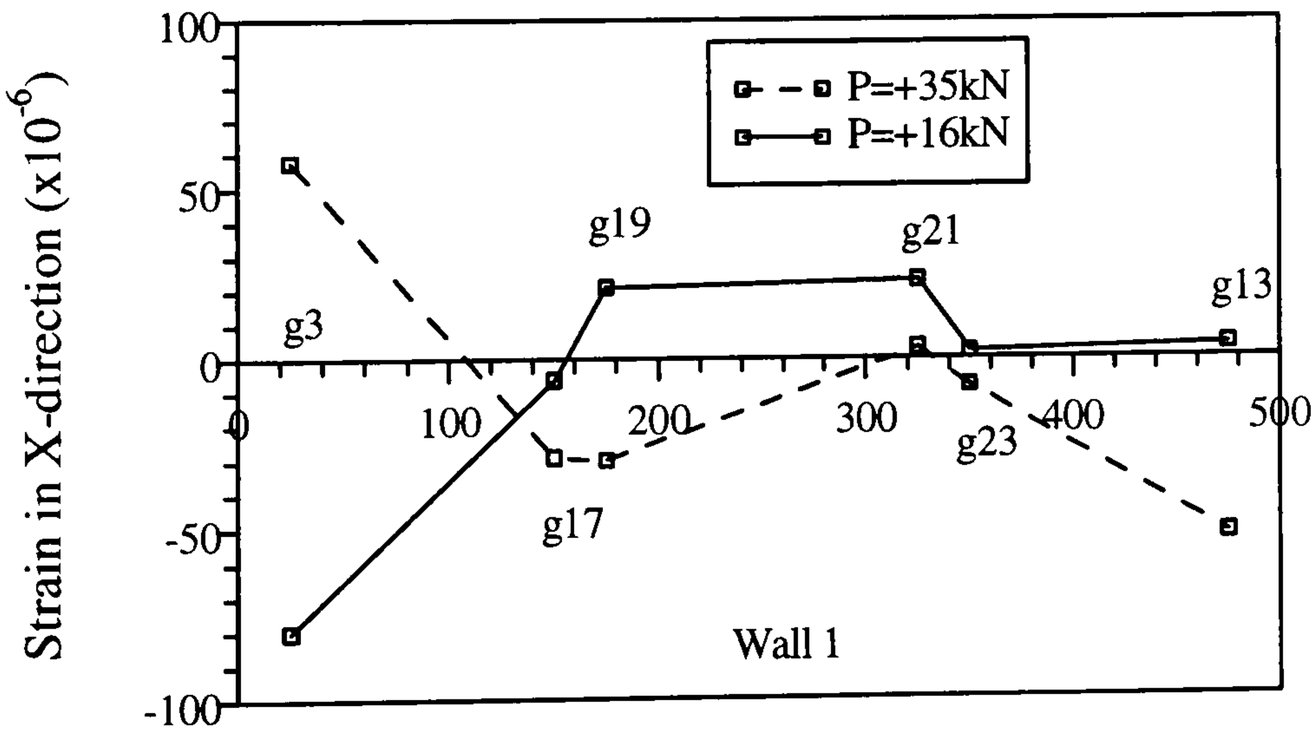

Figure 6.31(b): Variation of X-strain along the profiled boundary

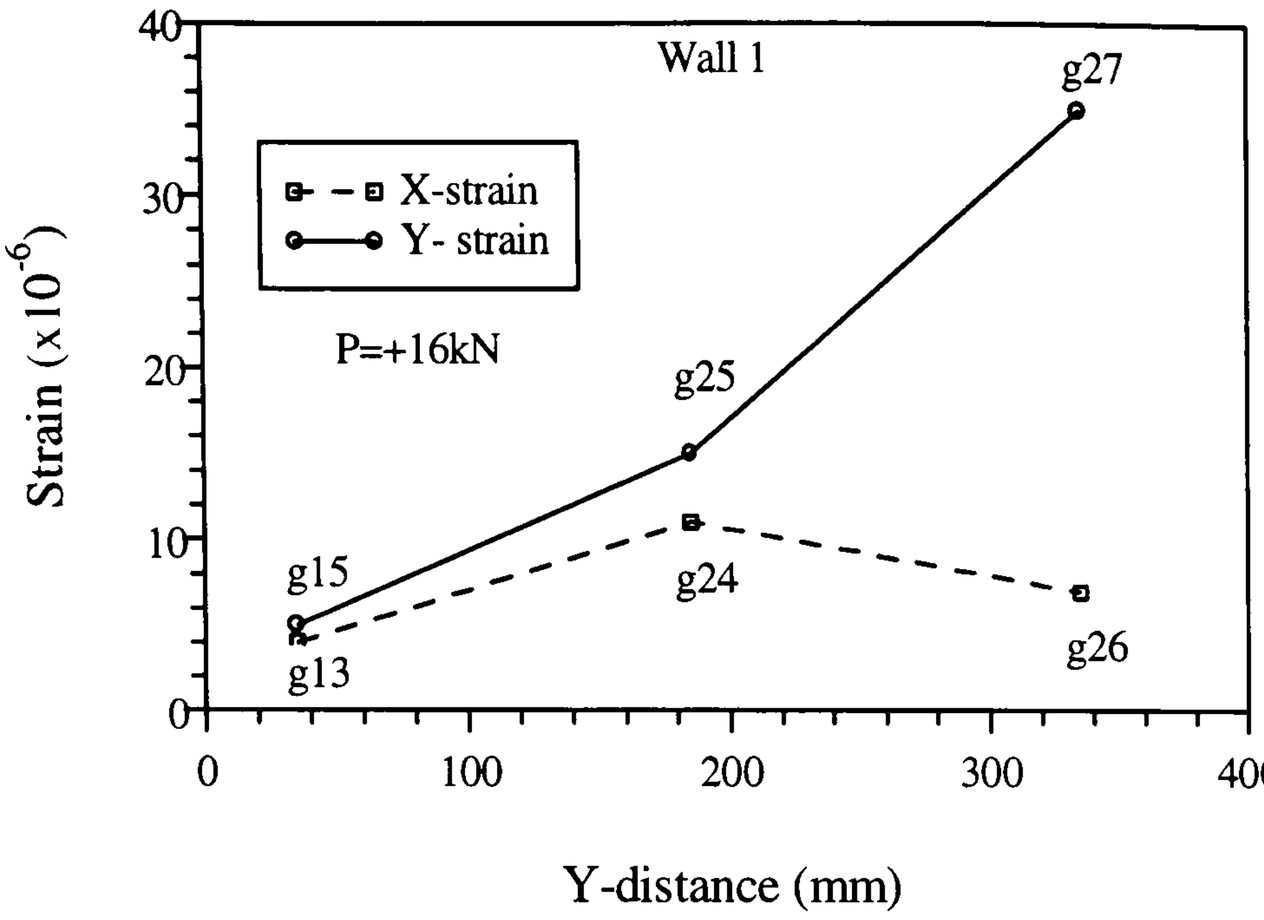

Figure 6.31(c): Variation of X and Y strain along the plain boundary

The pre-cracking stage variation of X and Y-strains along the plain boundary is shown in figure 6.31(c). The pattern of Y-strain is similar to that of test 2 but opposite. The strain is tensile (compression in case of test 2) with higher strain in the off-loaded corner just like the test 2. The X-strain shown in figure 6.31(c) is tensile throughout the boundary with higher values at the centre.

Test 5

The variation of X and Y strains along the profiled boundary is shown in figure 6.31(d). The Y-strain at crest section (g-8) is found to be higher than that of trough section (g-6) similar to walls 1 and 2. The pattern of variation of X-strain is also found to be similar to that of wall 1 and 2 with higher strain in trough section (g-7) than that of crest section (g-9). The pattern of variation of X and Y strains along the plain boundary as shown in figure 6.31(e) is also similar to those of wall 1 and wall 2.

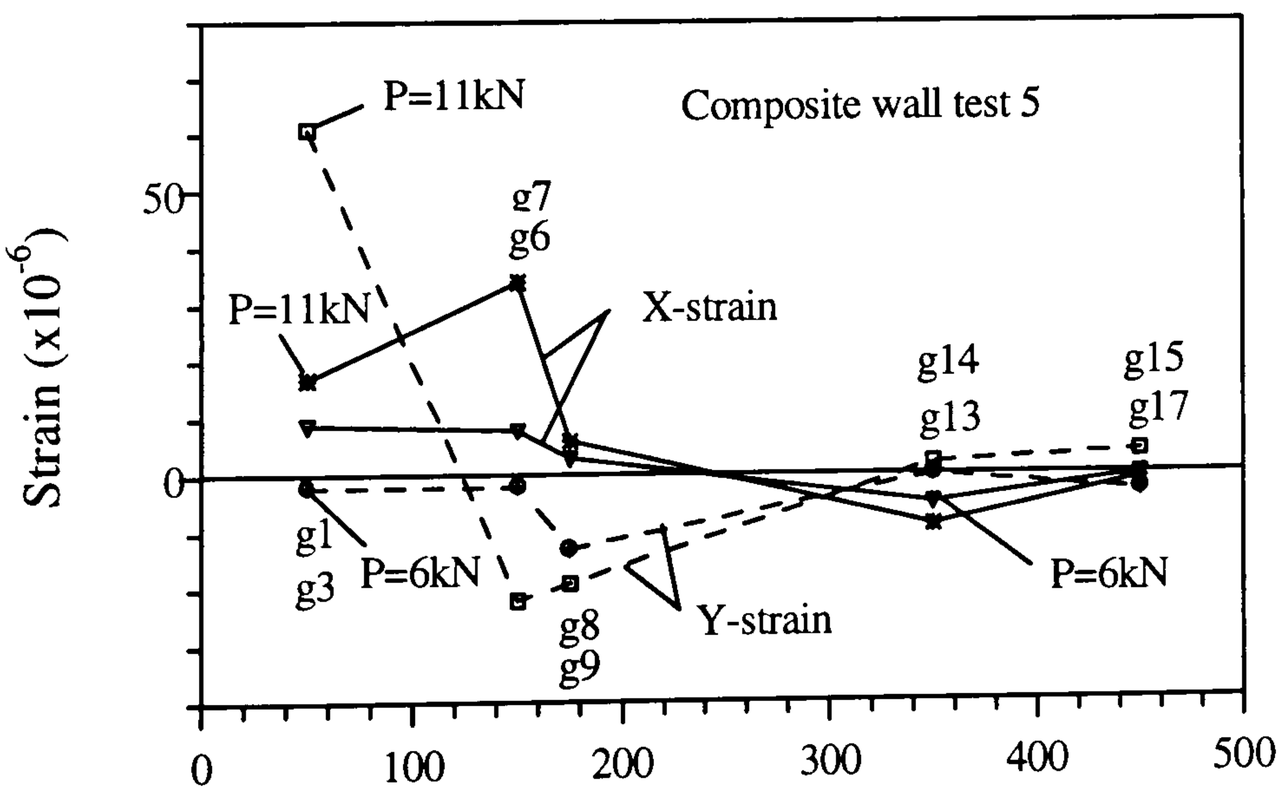

Figure 6.31(d): Variation of X and Y-strains along the profiled boundary

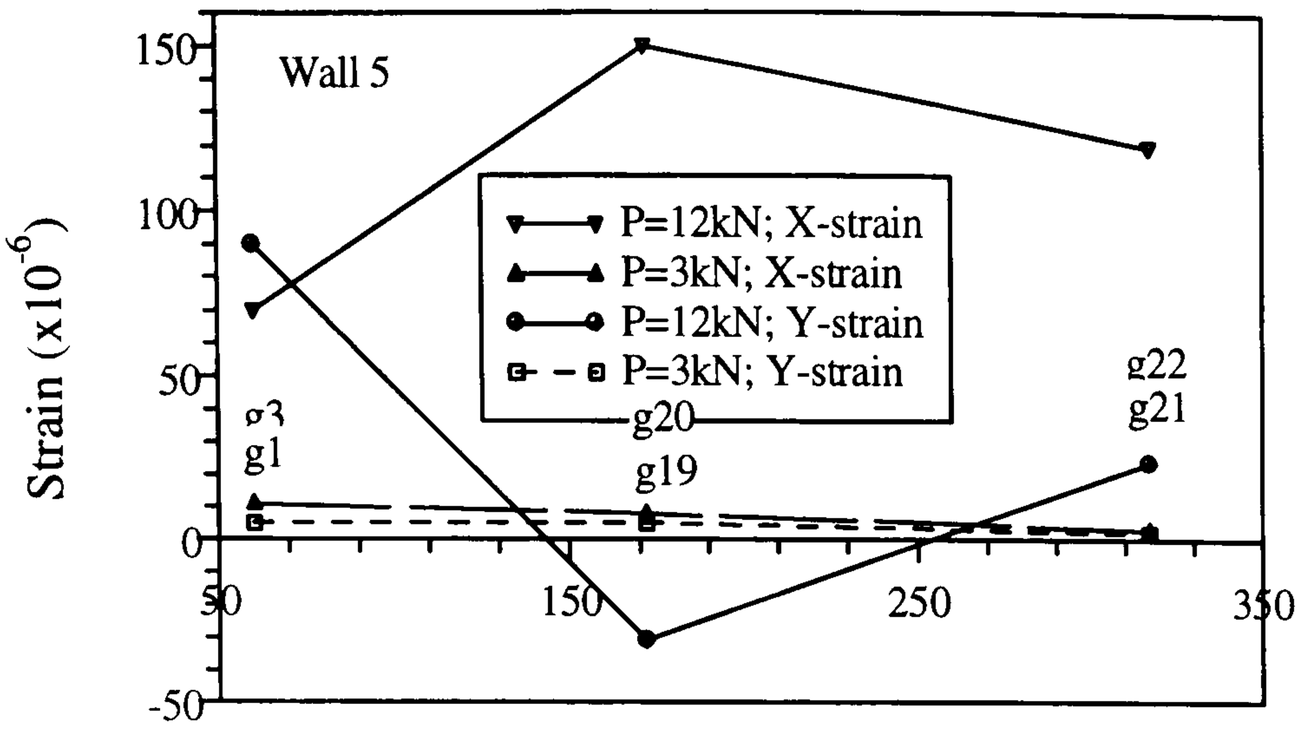

Y-distance (mm)

Figure 6.31(e): Variation of X and Y-strains along the plain boundary

Comments on boundary strains from test 1, test 2 and test 5

The test 1 and test 2 showed identical variation in boundary strains. It is possible to provide a general pattern of variation of boundary strains in the pre-cracking stage for test 1, 2 and 5 and this is drawn, qualitatively, in figure 6.31(f). The Y-strain along the profiled boundary is independent of the thickness of the section and showed higher strain than the trough sections. The strain in the web follow the pattern of adjacent crest and trough strain. While the X-strain in the trough sections were found to be higher than those at crest sections. The presence of trough and crest sections actually affects the strain condition in the profiled boundary. The post-cracking strain distribution for both plain and profile boundaries as shown in figure 6.31(f) does not follow any definite pattern. However, the main limitation is that the patterns are solely based on the strains at gauge locations.

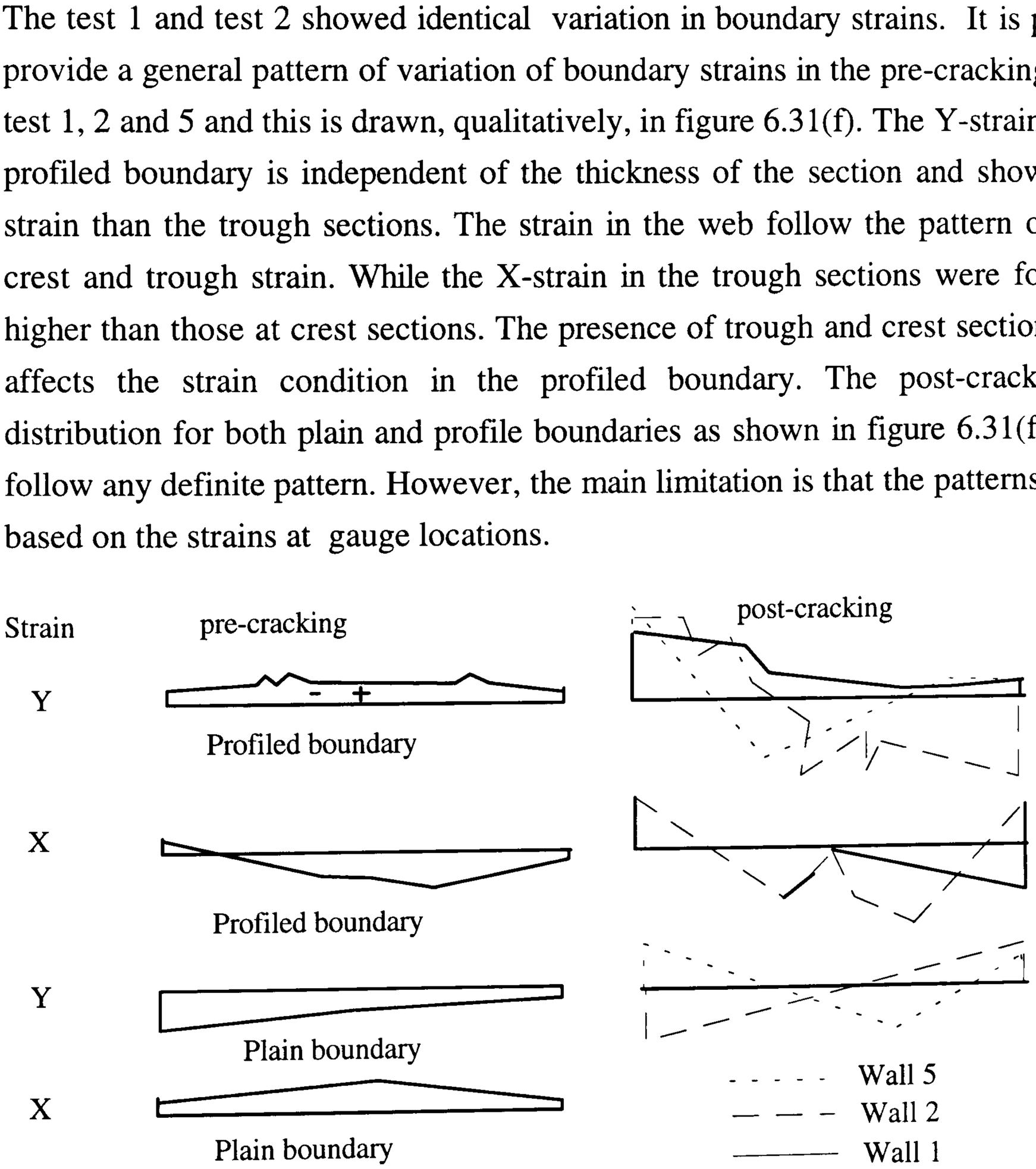

Figure 6.31(f): Qualitative variation of boundary strains

Strain condition at loaded corner

The strain condition in the loaded corner from test 3 is shown in figure 6.32. The corner rosette 18-19-20 showed higher principal strain than the other adjacent rosettes in the crest section. This trough section at the boundary is critical for the development of the initial cracking. However, all the close rosettes in the loaded corner showed identical pattern of variation in principal strains.

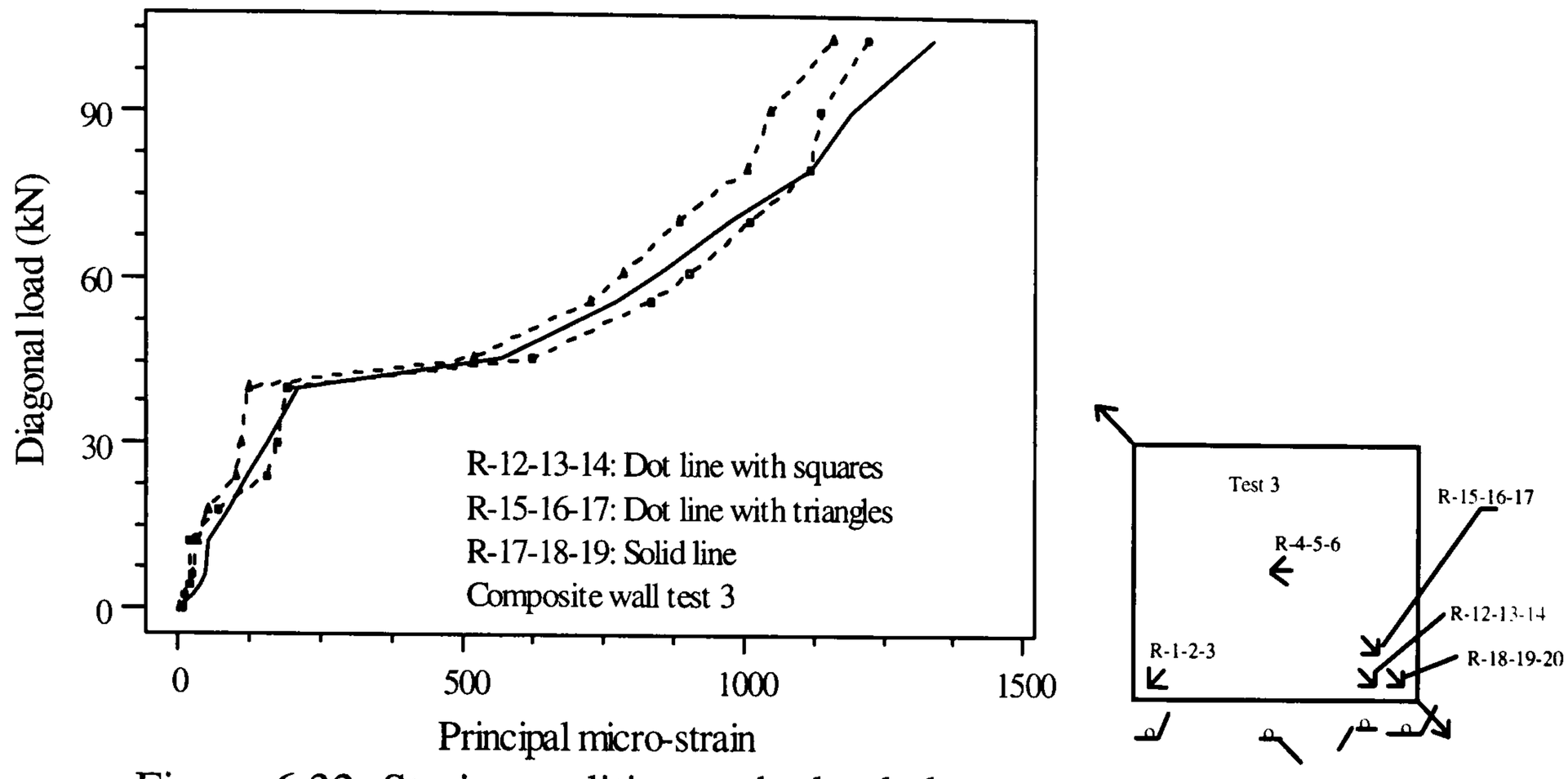

Figure 6.32: Strain condition at the loaded corner

Test frame behaviour

The behaviour of the test frame was investigated by putting strain gauges at critical location of the frame in composite wall test 3. The variation of axial strain as found from the gauges is presented in figure 6.33. The strain in gauges (g21, g22 and g23) at the loaded corner as shown in figure is very close confirming the equal distribution of axial forces to the test frame members.

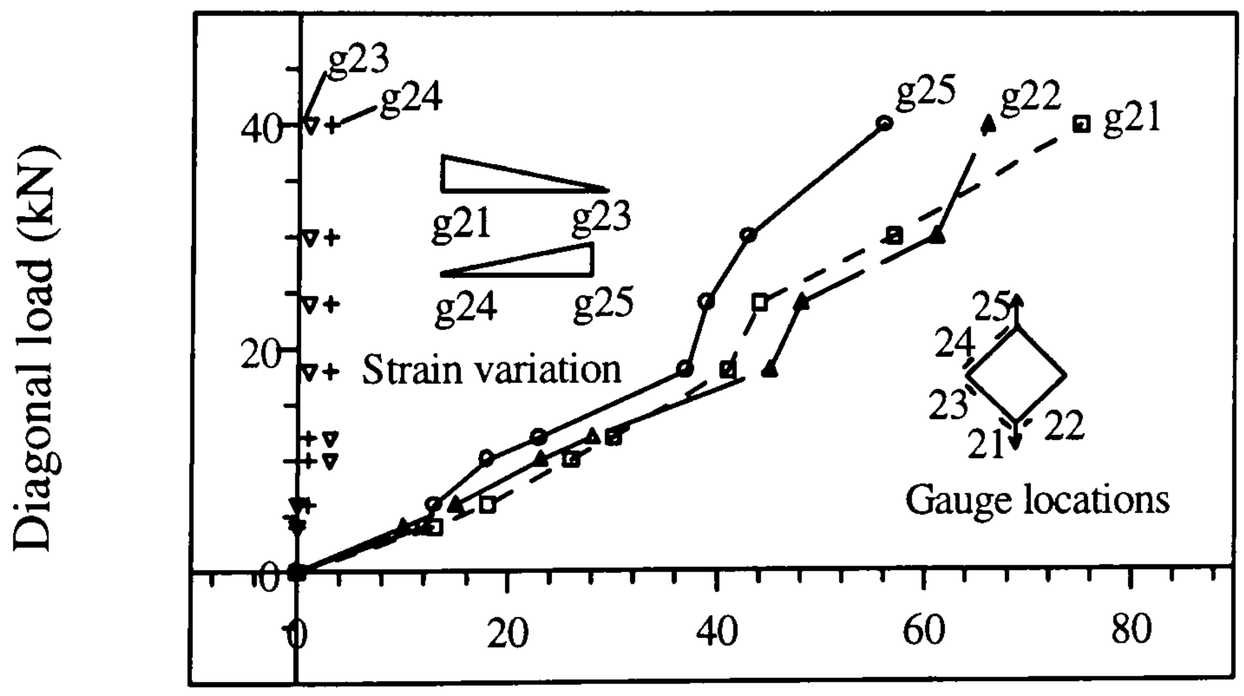

Figure 6.33: Strain condition in Test frame

The strain in the off-loaded corner gauges are very small which confirms the zero axial load condition in the corner. This confirmed that the frame was capable of transferring all the load to the wall panel. The variation of strain as well as axial forces in the frame member will be triangular with maximum value at the loaded end and zero values at the off-loaded end as shown in figure 6.33. The similar variation was confirmed in chapter 3 from finite element simulation of the test frame with plain concrete panel (figure 3.8(b)). This findings confirmed the performance of the shear rig as satisfactory.

6.3.6.4 Behaviour of sheeting and concrete core in composite wall

The behaviour of the sheeting and concrete core in composite wall is assumed to be quite different than the individual behaviour due to their mutual interaction. This will be now discussed on the basis of load-deformation response, mode of failure, out-off plane displacements and strain conditions from model tests.

Load-deformation response

The load deformation responses of the sheeting, profiled concrete and composite wall are superimposed in figure 6.34(a). The composite wall shows higher stiffness and strength than its composite components. The response is much more ductile than individual concrete core and sheeting in a sense that it allows much more deformation than the individual sheeting and concrete. However, the failure of the composite walls is sudden and associated with the buckling of sheeting. The stiffness and ultimate load values are compared in table 6.4. The cracking load of concrete is increased by about 40% for the test 2 representing considerable interaction between sheeting and core. The failure load of composite wall is around 30% higher than the summation of failure load of pair of sheeting and concrete core. And the composite walls have the stiffness 22% higher than the summation of individual stiffness of sheeting and concrete core.

Table 6.4: Comparison between sheeting, concrete core and composite wall

Diagonal	Sheeting	Concrete core	Wall	
			Pair of Sheeting	Concrete core
Stiffness kN/mm	56.5	294	496	
Failure load, kN	52	48	198	
Buckling load, kN	42	-	182	
Cracking load, kN	-	22	-	32

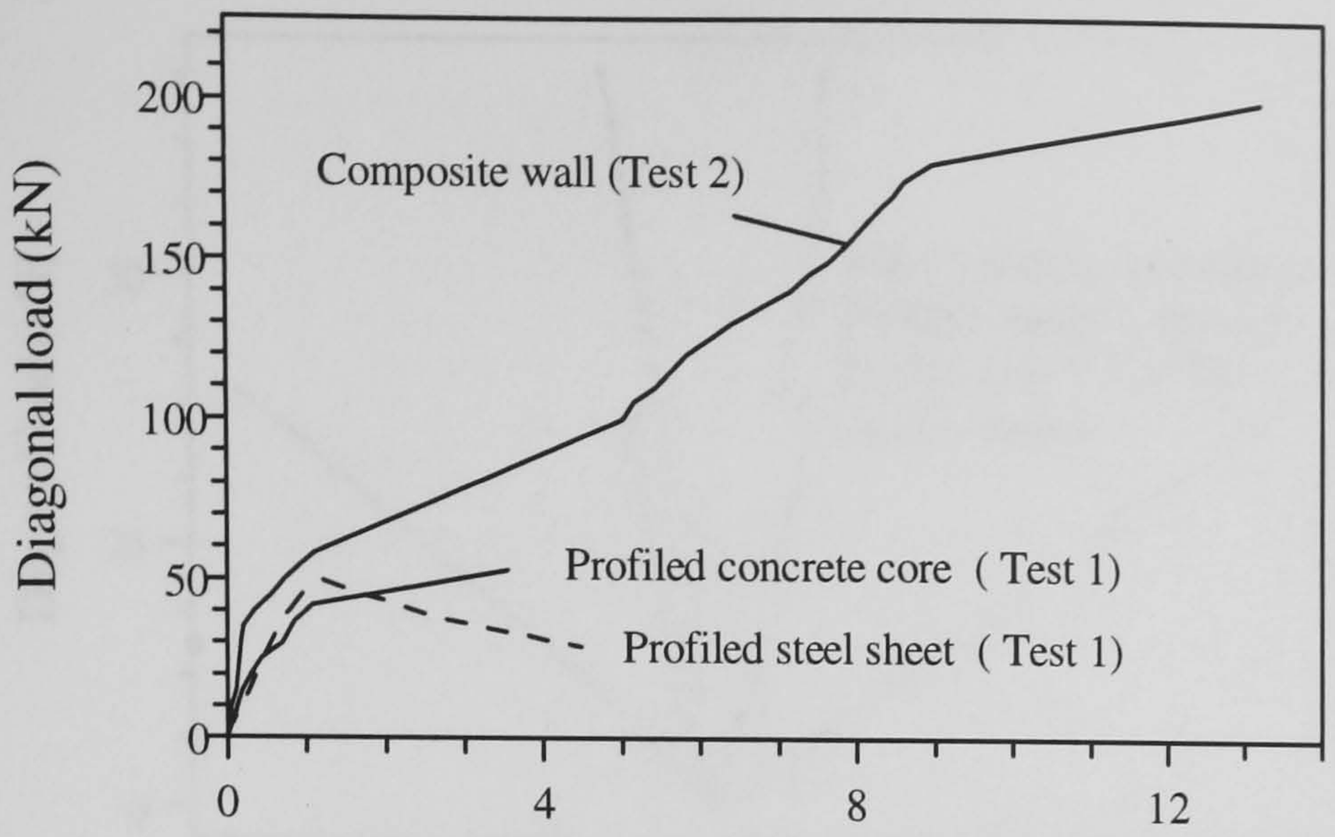

Figure 6.34(a): Comparison of load-deformation responses

Strain conditions

The principal strains at central and corner rosettes are compared in figures 6.34(b) and (c). The strain in composite wall is initially close to the concrete core strain which represents composite action between sheeting and concrete core. After that the strain lies in between the strains in concrete and sheeting but more inclined to the concrete strains. This may happen due to the possible debonding of the sheeting from concrete. And at this stage, the gauges represent the strains in the sheeting as they are instrumented on the steel surfaces. The strains in concrete can not be truly ascertained in this stage . The fact that the strains less than those in profiled sheeting confirms that some sort of partial interaction occurs between sheeting and concrete. The values of principal strains up to the cracking of concrete and buckling of individual sheeting are presented in table 6.5.

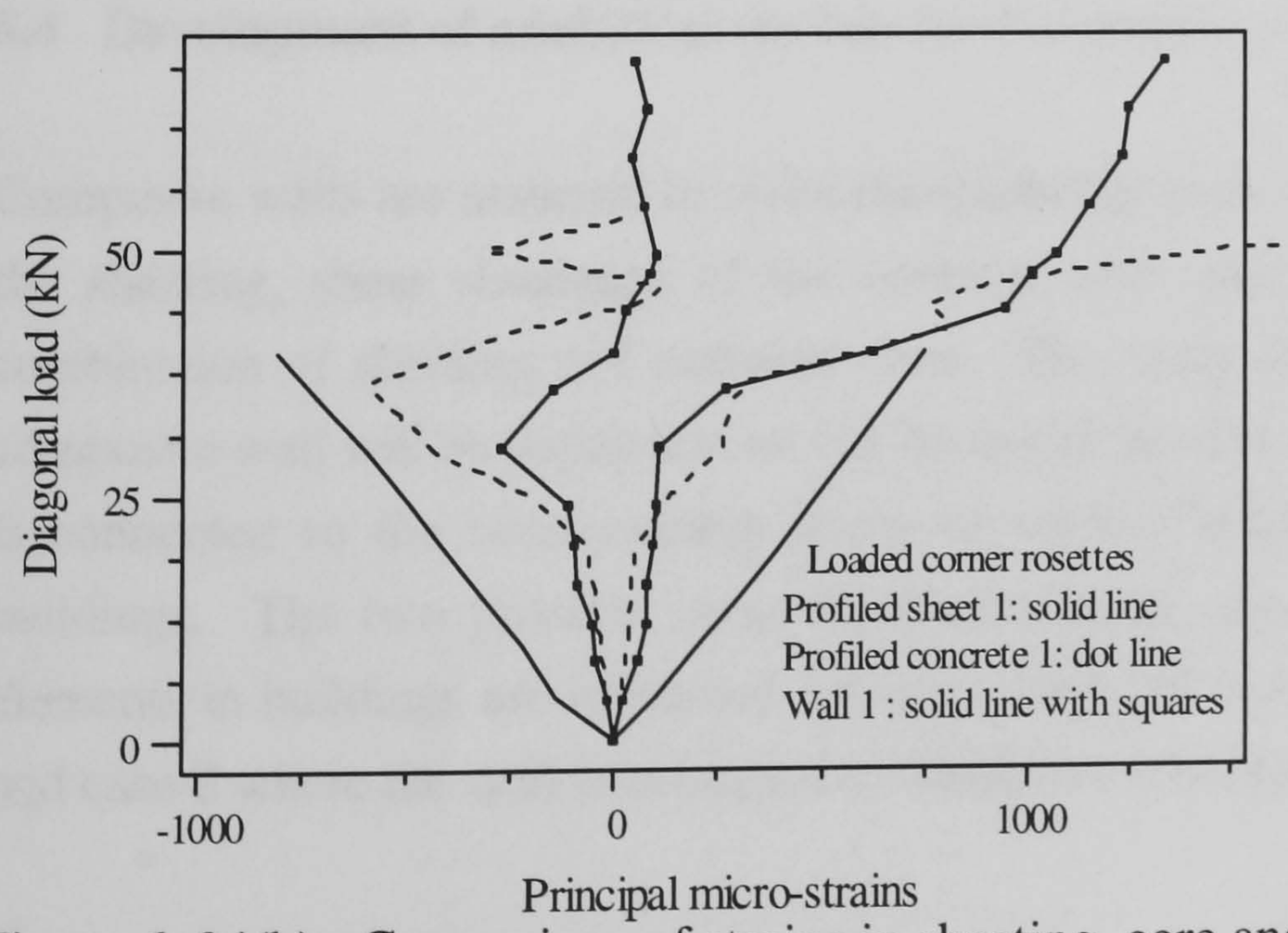

Figure 6. 34(b): Comparison of strains in sheeting, core and composite wall

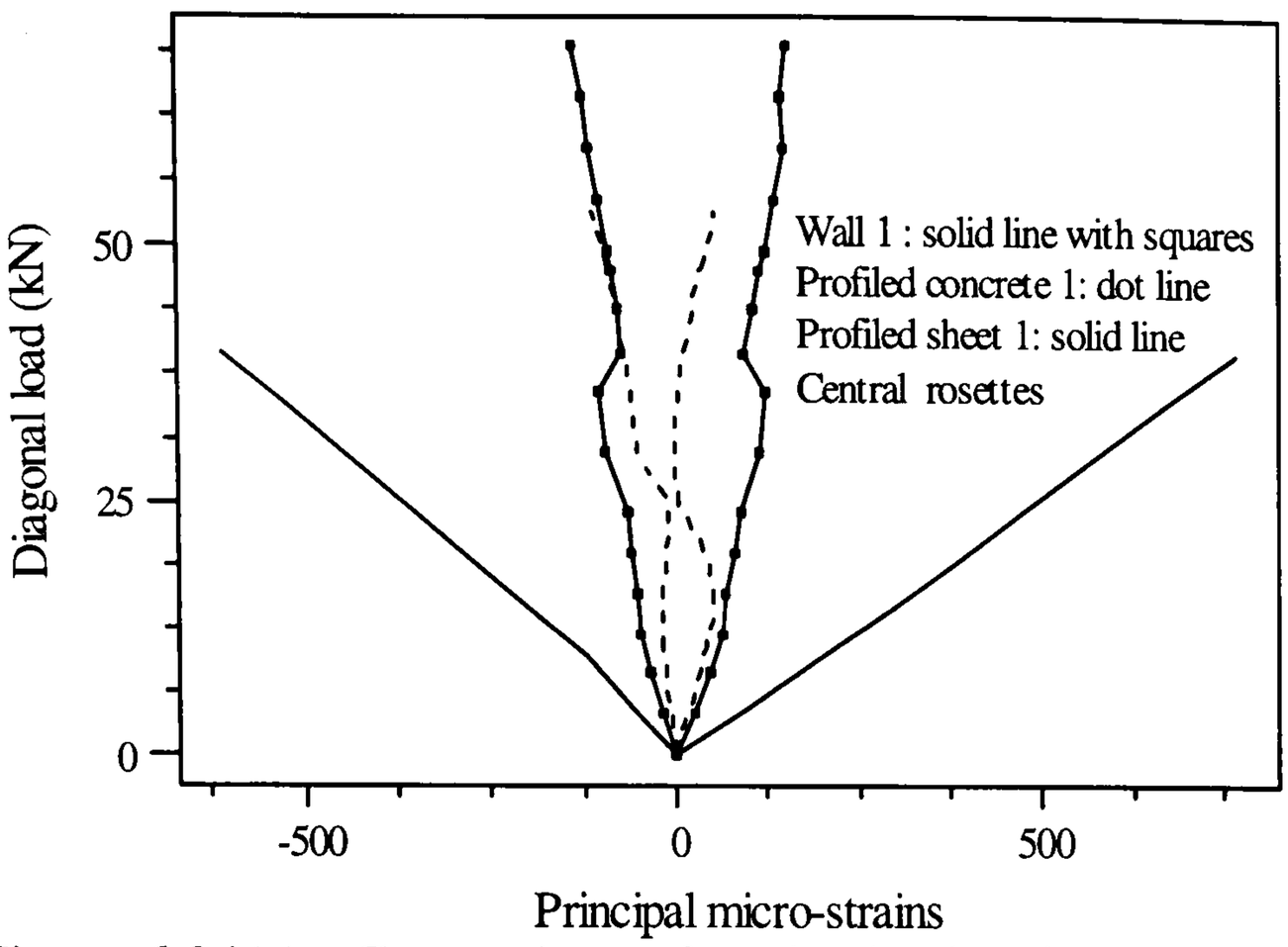

Figure 6.34(c): Comparison of strains in sheeting, core and composite wall

Table 6.5: Principal strains in sheeting, concrete core and composite wall

Load	Loaded corner rosette			Central rosette			Off-loaded corner rosette		
kN	Principal strains			Principal strains			Principal strains		
	Wall 1	Concrete	Sheeting	Wall1	Concrete	Sheeting	Wall1	Concrete	Sheeting
4	19,-20	19,-21	89, -128	26,-17	23,-14	92,-58	18,-16	20,-22	92,-52
8	55,-48	35,-40	170, -185	45,-33	58,-44	175,-121	37,-28	28-35	190,-110
12	76,-51	40,-48	253, -263	62,-47	21,-46	252,-180	51,-38	37,-34	262,-140
20	88, -99	54,-69	393,-404	79,-60	94,-94	388,-278	68,-64	49,-39	441,-268
30	110,-270	--	574,-596	113,-93	------	576,-441	99,-120	-----	647,-429
40	623, -5	--	749,-807	93-72	------	764,-608	68,-183	----	849,-594

6.4 Development of analytical models for Composite wall

Composite walls are assumed to resist shear loading in three ways: shear resistance of the sheeting, shear resistance of the concrete core and shear resistance from the combination of sheeting and concrete core. The shear stiffness and strength of the composite wall will be dependent on the boundary conditions, especially how the wall is connected to the beam-column frame or other components of the steel frame buildings. The two possible cases in connection of using composite wall as shear elements in buildings are identified. Case 1 where the wall is subjected to shear only and case 2 where the wall is subjected to cantilever bending as shown in figure 6.35.

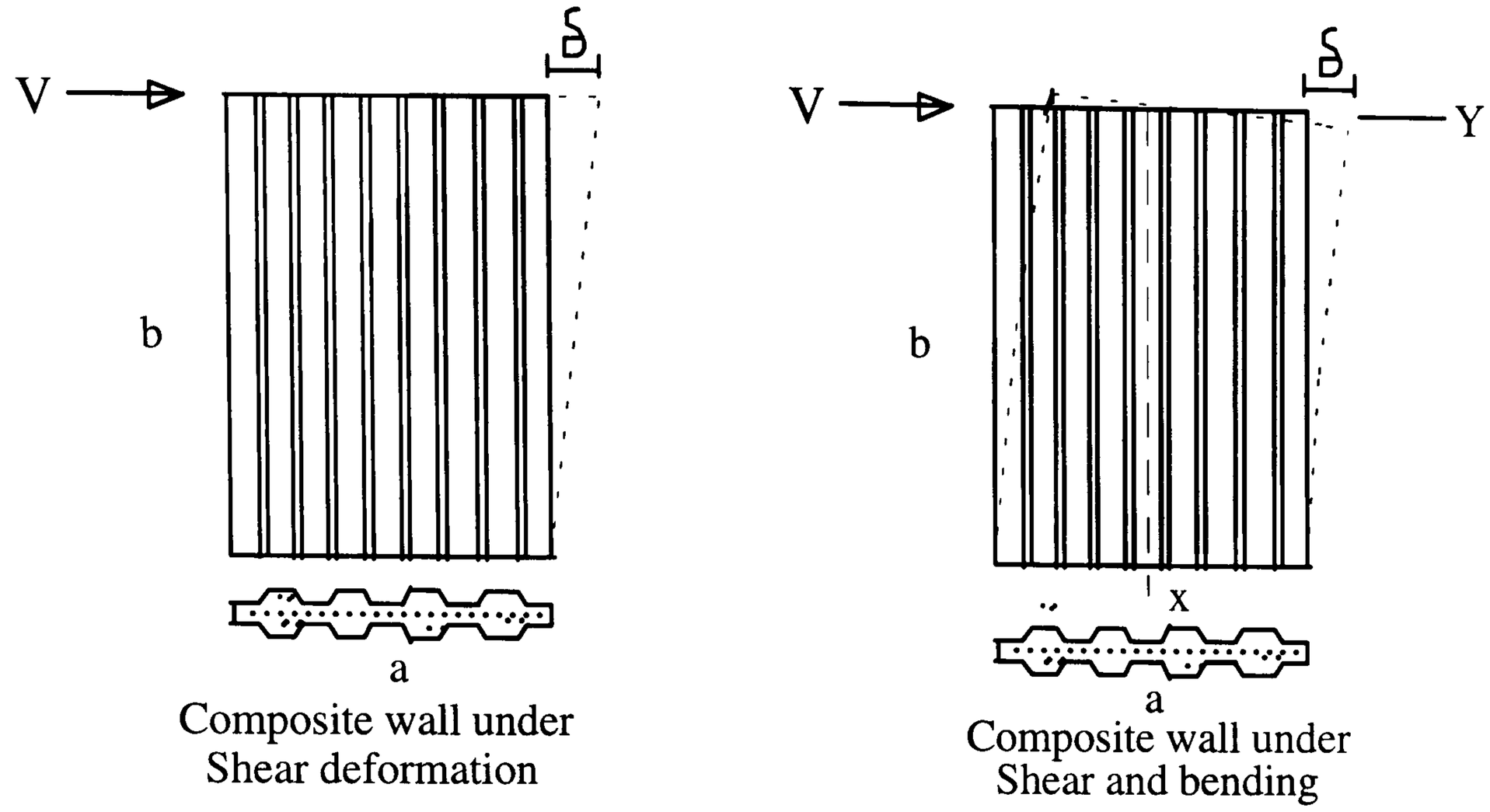

Figure 6.35: Composite wall under in-plane loads

This article will describe analytical models for the determination of stiffness and strength of the composite wall from the individual strength and stiffnesses of sheeting, concrete core and from the interaction between these. The analytical expressions will then be verified with model tests and finite element analysis in the later sections and some practical design recommendations for certain parameters will be highlighted.

6.4.1. Analytical model for the stiffness of the composite wall

An analytical model for the stiffness of the composite wall is presented by Wright, Hossain and Gallocher (1994). The full development of the model will be presented in this section.

6.4.1.1 Stiffness of the profiled concrete core

Shear stiffness of concrete core

The shear stiffness of the profiled concrete core is derived in section 4.6 of chapter 4 applying strain energy approach. The profiled concrete core was considered as a concrete core of rectangular cross section having an equivalent average thickness of t_{eq} . The shear flexibility (c_c) and stiffness (k_c) was expressed as :

$$c_c = \frac{1}{k_c} = \frac{2b(1+\upsilon_c)}{E_c a t_{eq}} \quad \text{.....(6.2)}$$

Shear plus bending stiffness

The differential equation for the case of composite wall subjected to shear and bending as shown in figure 6.35, can be found in Timoshenko and Goodier (1982) when the concrete is considered to be elastic.

$$\frac{\delta^4\psi}{\delta x^4}+2.\frac{\delta^4\psi}{\delta x^2\delta y^2}+\frac{\delta^4\psi}{\delta y^4}=0 \quad \text{.....(6.3)}$$

By taking stress function,ψ, in the form of a polynomial of the form :

$\psi=\frac{Bxy}{3.2}+\frac{Dxy^3}{3.2}$, the stress conditions for the problem can be satisfied as :

$$\sigma_x=\frac{\delta^2\psi}{\delta y^2}=Dxy \quad ; \ \sigma_y=\frac{\delta^2\psi}{\delta x^2}=0 \ \text{ and } \ \tau_{xy}=-\frac{\delta^2\psi}{\delta x\delta y}=-B-\frac{Dy^2}{2} \quad \text{.....(.6.4)}$$

Now at y=±0.5a , shearing stress, τ_{xy}= 0 and at the loaded end sum of the distributed shearing force must be equal to zero ;$-\int_{-a/2}^{a/2}\tau_{xy}dy=V$. Applying these two boundary condition in equation 6.4 leads to the values of constants as : B=3V/2a and D= -12V/a^3. Substituting the values of B and D in equation 6.4 and introducing moment of inertia Ic of concrete the stress values can be expressed as :

$$\sigma_x=-\frac{Vxy}{I_c}; \quad \sigma_y=0 \ \text{ and } \ \tau_{xy}=-\frac{V}{8I_c}(a^2-4y^2)$$

Transformation of stress to strain leads to the following equations:

$$\varepsilon_x=\frac{\sigma_x}{E_c}=\frac{\delta u}{\delta x}=\frac{Vxy}{E_cI_c} \ \text{ and } \ \varepsilon_y=\frac{\upsilon\sigma_x}{E_c}=\frac{\delta v}{\delta y}=\frac{\upsilon Vxy}{E_cI_c} \quad \text{.....(6.5)}$$

$$\text{and also} \ \gamma_{xy}=\frac{\delta u}{\delta y}+\frac{\delta v}{\delta x}=\frac{\tau_{xy}}{G_c}=-\frac{V(a^2-4y^2)}{8I_c} \quad \text{.....(6.6)}$$

Integration of equation 6.5 gives the values of u and v as :

$u=-\frac{Vx^2y}{2E_cI_c}+f(y)$ and $v=\frac{\upsilon Vxy^2}{2E_cI_c}+f_1(x)$; The values of u and v are then substituted in equation 6.6 to get :

$$\gamma_{xy}=\frac{-Vx^2}{2E_cI_c}+\frac{df_1(x)}{dx}+\frac{\upsilon Vy^2}{2E_cI_c}+\frac{df(y)}{dy}-\frac{Vy^2}{2I_cG_c}=\frac{-Va^2}{8I_cG_c}$$

$$= \quad F(x) \quad + \quad G(y) \quad = K$$

The values of f(y) and f_1(x) can be obtained from the above equation with the association of some other constants d,e,g and h. Putting f(y) and f_1(x) in the expressions of u and v leads to the following equations:

$$u=-\frac{Vx^2y}{2E_cI_c}-\frac{\upsilon Vy^3}{6E_cI_c}+\frac{Vy^3}{6I_cG_c}+ey+g \ \text{ and } \ v=\frac{uVxy^2}{2E_cI_c}+\frac{Vx^3}{6E_cI_c}+dx+h \quad \text{.....(6.7)}$$

Applying four boundary conditions to equation 6.7, the values of the constants d,e,g and h can be obtained. After that the deflection at the point of application of in-plane shear load can be obtained as:

$$\delta = \{v\}_{y,x=0} = \frac{Vb^3}{3E_cI_c} + \frac{Va^2b(1+\upsilon_c)}{4E_cI_c} \quad \text{.....(6.8)}$$

The flexibility of concrete core (c_C) or stiffness (k_C) can then be formulated as :

$$c_c = \frac{1}{k_c} = \frac{\delta}{V} = \frac{b^3}{3E_cI_c} + \frac{a^2b(1+\upsilon_c)}{4E_cI_c} \quad \text{.....(6.9)}$$

where V= applied shear load, δ= shear deformation, E_C= modulus elasticity of concrete, a= width of the wall , b= height of the wall , υ_C= poisson's ratio of concrete and I_C= moment of inertia of concrete core. The first term in equation 6.9 represents bending flexibility and the second term represents shear flexibility.

The equation 6.9 is derived for a concrete core of rectangular cross section. Therefore, the profiled concrete core should be transformed into an equivalent concrete core of rectangular cross section having an equivalent thickness t_{eq}. The equivalent thickness can be obtained as $t_{eq} = \frac{Volumeofconcrete}{ab}$, and can be taken as the average thickness of the wall. Therefore, moment of inertia of the concrete core, $I_c = \frac{t_{eq}.a^3}{12}$.

Comments

The equation 6.9 can also be expressed as $c_c = \frac{1}{k_c} = \frac{4}{E_c t_{eq}}\left(\frac{b}{a}\right)^3 + \frac{3(1+\upsilon_c)}{E_c t_{eq}}\left(\frac{b}{a}\right)$ which revealed that bending flexibility is proportional to $(b/a)^3$ while the shear flexibility is proportional to (b/a) . It means that the bending flexibility is more sensitive to slenderness than shear flexibility. The influence of shear flexibility is negligible when b/a ratio is greater than 4. Both equation 6.2 and 6.9 are valid for linear that is pre-cracking stages of concrete.

6.4.1.2 Stiffness of profiled steel sheeting

Shear stiffness

The profiled sheet stiffness in composite wall can be derived from the stiffness of the individual profiled sheet considering the boundary conditions described in detail in chapter 5. The main differences between profiled steel sheeting used for composite walls and that used for roof diaphragms have been pointed out to be that the shear flexibility of the sheeting is the displacement per unit shear load applied normal to the profile rather than parallel to it and that the wall panels are attached to the frame at the boundary.

As described in section 5.3.1, the total shear flexibility of the profiled sheet, c_s, can be taken as the summation of components of the various factors involved. The main components considered are due to : shear deformation of sheet (c_1), bending or distortion of corrugation profile (c_2), axial deformation of the beam-column frame (c_3) and local deformation of sheet at the sheet-frame and seam connections(c_4 and c_5).
Therefore, $c_s = c_1 + c_2 + c_3 + c_4 + c_5 = 1/k_S$. The full derivation of analytical expressions of all these components are given in section 5.3.1.
Now for the case of composite wall, the following reasonable assumptions can be made:

- The confining effect of the concrete eliminates the distortion or bending of the sheeting, and therefore, c_2 , may be neglected . This is reasonable as confirmed from the model tests. However, if the boundary conditions allow bending and distortion then it should be included in the flexibility equation.
- At seams between adjacent steel sheets for practical construction, the concrete carries almost all the shear force and therefore, c_5 , may be ignored.
- If the beam-column frame is considered to be very rigid and this may be the practical case, the axial deformations of the beam-columns can be considered negligible which eliminates the factor c_3 .

Therefore, the stiffness, k_S , of the sheeting in composite wall can be approximated as

$c_s = c_1 + c_4 = 1/k_S$. .....(6.10)

If the connection details are such that the local deformation of sheeting is not allowed in sheet-frame fasteners than the factor c_4 can be omitted and in that case the stiffness of the sheeting can be written as :

$$c_s = \frac{1}{k_s} = c_1 = \frac{2\alpha b(1+\upsilon_s)}{E_s a t_s} \quad \text{.....(6.11)}$$

Stiffness of sheeting under bending plus shear

The stiffness or flexibility of the sheeting in this case will be similar to that of concrete core and the equation 6.9 can be modified to as :

$$c_s = \frac{1}{k_s} = \frac{\delta}{V} = \frac{b^3}{3E_s I_s} + \frac{3\alpha b(1+\upsilon_s)}{E_s a t_s \alpha^2} \quad \text{.....(6.12)}$$

The second term of the equation representing shear contribution is similar to that of expression c_1 and for trapezoidal profiled steel sheeting it produces flexibility's of about 18% higher than that from pure shear case.

6.4.1.3 Stiffness of composite wall

a. Composite wall under pure shear

In this case composite wall undergoes pure shear deformation only and this was the case of all the small scale model tests. The boundary frame is considered to be formed infinitely rigid elements pinned together at the corners and induces pure shear on the infill panel. No bending or distortion of the corrugation profile was allowed due to boundary condition and also the infill concrete will act as a stiffeners keeping the flat cross section of the steel sheets to remain flat. This was confirmed from the model tests where sheet distortion was found to occur at the ultimate stages of loading associated with buckling of the sheeting. Therefore, in this case the stiffness of the composite wall will be derived from the shear deformation of sheeting (equation 6.11), shear deformation of concrete core (equation 6.2) and from their degree of composite connection. The total summation of flexibility's (c_t) and stiffnesses (k_t) of the double skins of sheeting and concrete core is :

$$k_t = \frac{1}{c_t} = 2\left(\frac{1}{c_s}\right) + \left(\frac{1}{c_c}\right) = 2k_s + k_c = \frac{2E_s a t_s}{2\alpha b(1+\upsilon_s)} + \frac{E_c a t_{eq}}{2b(1+\upsilon_c)} \quad \text{.....(6.13)}$$

Composite stiffness

For full composite action, the shear force will be distributed between the steel sheeting and concrete according to the requirements of strain compatibility. Let us consider that the shear wall is subjected to a unit shear load and as a result undergoes a shear deformation of λ. Let the load carried by the individual steel sheeting be V_S and the load carried by concrete be V_C. Then they should satisfy the equation :

$$2V_S + V_C = 1 \quad \text{.....(6.14)}$$

Then the shear deformation in sheeting will be :

$$\lambda = \frac{2\alpha b(1+\upsilon_s)}{E_s a t_s} . V_s \quad \text{.....(6.15)}$$

and shear deformation in concrete will be :

$$\lambda = \frac{2b(1+\upsilon_c)}{E_c a t_{eq}} V_c \quad \text{.. .....(6.16)}$$

Equating equations 6.15 and 6.16 gives :

$$V_s = \frac{E_s t_s (1+\upsilon_c)}{E_c t_{eq} \alpha(1+\upsilon_s) + 2E_s t_s (1+\upsilon_c)}$$

Now substituting V_S in equation 6.15 resulted the composite flexibility (c_W) and stiffness (k_W) of composite wall as:

$$c_w = \frac{1}{k_w} = \lambda = \frac{2\alpha b(1+\upsilon_s)(1+\upsilon_c)}{a\left[E_c t_{eq}\alpha(1+\upsilon_s) + 2E_s t_s (1+\upsilon_c)\right]} \quad \text{.....(6.17)}$$

However if the flexibility due to sheet frame fasteners (c_4) need to be included, it should be added to the equation 6.17 to take it into account in the full composite

stiffness of composite wall. The equation 6.17 is similar to the equation 6.13 representing the summation.

The ratio of load shared by steel and concrete can be expressed as :

$$\frac{V_s}{V_c} = \frac{E_s t_s (1+\upsilon_c)}{E_c t_{eq} \alpha (1+\upsilon_s)} \quad \text{.....(6.18)}$$

Analytical calculation of model test shear stiffness are presented in table 6.6, and the relationship between the load carried by steel and concrete is calculated as Vs=0.17Vc.

Table 6.6: Calculation of shear stiffness

	Profiled steel sheeting	Concrete core	Composite wall equation 6.13 or 6.17
Shear stiffness	30	161	221

b. Composite wall under bending and shear (Cantilever action)

In this case, the total flexibility of the profiled steel sheeting will be derived from bending and shear deformation of the sheeting (equation 6.12) . The sheet distortion or bending (c_2) will not occur due to the interaction between concrete and sheeting . The concrete core will under go bending and shear according to the equation 6.9. The summation of stiffness of the sheeting and concrete (k_w)can be written as :

$$k_w = \frac{1}{c_w} = 2\left(\frac{1}{c_s}\right) + \left(\frac{1}{c_c}\right) \quad \text{.....(6.19)}$$

c_S and c_C can be obtained from equation 6.12 and 6.9 respectively.

Composite stiffness

Let us consider the composite wall subjected to unit shear load and under goes a deformation of λ. If the concrete and steel take a load of V_C and V_S respectively than

$$2V_S + V_C = 1$$

The deformation in sheeting can be expressed from equation 6.12 as:

$$\lambda = \left[\frac{b^3}{3E_s I_s} + \frac{3b(1+\upsilon_s)}{E_s a t_s \alpha}\right].V_s = \Pi.V_s \quad \text{.....(6.20)}$$

and the deformation in concrete can be expressed from equation 6.9 as

$$\lambda = \left(\frac{b^3}{3E_c I_c} + \frac{a^2 b(1+\upsilon_c)}{4E_c I_c}\right).V_c = \Gamma.V_c \quad \text{. .....(6.21)}$$

Equating the equations 6.20 and 6.21 , gives : $V_s = \frac{\Gamma}{\Pi + 2\Gamma}$; Substituting V_S in equation 6.19 , resulted the composite flexibility(c_W) and stiffness (k_W) of the composite wall as:

$$c_w = \frac{1}{k_w} = \frac{\Pi.\Gamma}{\Pi + 2\Gamma} \quad \text{.....(6.22)}$$

The values of Γand Π can be obtained from equations 6.19 and 6.20.
The flexibility due to sheet-frame fasteners can be added if required to the equation 6.22 to include the effect.
The ratio of load shared by steel and concrete can be expressed as :

$$\frac{V_s}{V_c} = \frac{\Gamma}{\Pi} \quad \text{.....(6.23)}$$

6.4.2 Analytical model for the shear strength of composite wall

The strength of the composite wall will be derived from sheeting and concrete core. The shear resistance of the sheeting has been derived for various boundary conditions in chapter 5. The type of failure either buckling of sheeting or failure at sheet-frame connections depends on the boundary conditions. If the sheet-frame connection is sufficiently rigid then the failure will be due to buckling of the sheeting.

For the composite wall in shear, four failure limit states concluded from the model tests can be identified : 1. Diagonal tension concrete limit state, 2. Sheeting-concrete Shear-transfer limit state, 3. Wall-frame connection limit state and 4. Combined wall-frame connection and sheet-concrete interaction limit state.

Diagonal tension concrete limit state

In the model tests, diagonal tension cracks were developed at approximately 45 angle to the boundary of the wall and extended over the wall. As a result the strength of the concrete core was controlled by the diagonal tension failure of concrete. The interface did not degrade significantly until after the diagonal tension cracks occur.

Sheeting-concrete shear transfer limit state

Shear transfer mechanism is a descriptive phrase refer to interface between the sheeting and concrete. This interface consists of chemical bond between sheeting and concrete, mechanical component by the resistance of the embossments and friction at the interfacial surface. If this interface breaks down to the extent that load can no longer be transferred, then the shear-transfer mechanism is considered to have failed. The sheet-concrete shear transfer was only due to chemical bond as no embossments were present in the model sheets. Therefore, their contribution can be omitted in the case of the model tests. The friction between profiled ribs of concrete and steel play an important role in the post cracking stages. But the interaction between sheeting and concrete seemed to be dependent on the boundary conditions.

Wall-frame connection limit state

A connection failure can limit the strength of the composite wall. If the connection The rigid connections can mobilise the full strength of steel sheeting even after the concrete cracks. This happened in case of model tests where strong connection was provided through both sheeting and concrete. The walls were capable of taking high shear loads even after cracking of concrete and finally failure occurs due to buckling and sliding of the sheets over the concrete profile. In the model tests where the connection to the frame was given only through the concrete, the ultimate load was controlled by the concrete strength and sheet was found not to be effective.

Combined Wall-frame connection and sheet-concrete interaction limit state

The actual post-cracking behaviour of the wall was a combined phenomenon of wall-frame connection and sheet-concrete interaction. The boundary condition was rigid enough to induce the failure in the wall panels. The boundary conditions increase the sheet-concrete interaction by keeping sheet-concrete-sheet sandwich intact until buckling of the sheeting commences. This is the practical case of using such walls in conjunction with the building frame to increase the shear resistance of the frame. Where the frame failure is not expected and the failure of the infill wall governed the design.

Practical consideration

To mobilise the full steel-concrete interaction:

- The boundary connection of the wall either to the frame or slab should be provided through both sheet and concrete.
- Connections should be rigid enough to induce failure in the wall panel.
- If the failure is wanted in the boundary connections, it is necessary to provide connections rigid enough so that composite wall strength is higher than the diagonal tension limit strength of the concrete. In this case, it will at least include some % of post-cracking interaction between sheeting and concrete.

Based on the above limit states identified, the analytical models for shear strength of the composite wall will be formulated.

Shear strength of concrete core

The analytical model for the shear strength of the concrete core has been derived previously in section 3.6 based on bi-axial stress conditions in the concrete. The failure criteria proposed by Kupfer and Gerstle(1973) and Balakrishnan and Murray (1988) were adopted. The full details has been given in section 3.6 of chapter 3. The

model included diagonal tension limit state which is the normal phenomenon in pure shear condition. The analytical model derived for a plain concrete panel in section 3.6 has been adopted for profiled concrete panel in section 4.6 of chapter 4 with some modification to take into account profiled cross section. The model includes the idea of transforming the profiled concrete core into an equivalent plain concrete core of rectangular cross-section having an average thickness of t_{eq}. This simplified the problem and was used by Davies and Fisher (1979) and Easterling and Porter (1994) successfully in analysing steel-deck-reinforced concrete diaphragms.

The shear strength of the profiled concrete core (V_c) based on Kupfer and Gerstle (1973) can be written as (equation 4.2) :

$V_c = \frac{at_{eq} f_c^{'} \cdot f_t^{'}}{f_c^{'} + f_t^{'}}$, by converting the cylinder strengths to cube strengths the expression can be re-written as :

$$V_c = 0.074 at_{eq} \cdot f_{cu} \quad \text{.....(6.24)}$$

Shear strength or capacity of profiled steel sheeting

The ultimate shear resistance of the sheeting was derived in section 5.3.2 for failure in the sheet-frame fasteners (equations 5.16 and 5.17) and also for elastic buckling mode of failure in case of rigid connections (equation 5.18).

For the case of buckling mode of failure, the general critical buckling formula suggested by Easely (1975) based on othotropic model as proposed in section 5.3.2 as equation 5.18 can be used. Based on equation 5.18 the shear resistance of the sheeting can be written as :

$$V_s = 36\beta \frac{D_x^{1/4} D_y^{3/4} a}{b^2} \quad \text{.....(6.25)}$$

where β is a co-efficient ranges between 1.00-1.72 dependent on boundary conditions. For simply supported β =1.00 and for clamped conditions β= 1.72 can be used. Due to the very sudden transition (snap-through) to tension field action and the substantial increase in associated deformation, post-critical shear reserves are not included in the proposed models. This reflects the observations of Gachon (1986), Luo(1995), Luo and Edlund (1995), Author's model tests and the recommendations of the ASCE-AASHTO Task Committee (ASCE-AASHTO,1977).

Shear resistance of composite wall

Model tests on profiled steel sheet, profiled concrete and composite walls have revealed that the ultimate shear capacity of the composite wall can be conservatively

obtained from the summation of individual shear resistance of sheeting and concrete core. The ultimate shear resistance of the composite wall can be derived as :

$$V_w = 72\beta\frac{D_x^{1/4}D_y^{3/4}a}{b^2} + 0.074at_{eq}f_{cu} \quad \text{.....(6.26)}$$

The first term in equation 6.26 represents sheet resistance (from equation 6.25) and the second term represents profiled concrete core resistance (from equation 6.24). The equation 6.26 can be used to compare the shear resistance of model tests.

Limitations and assumptions

The equation 6.26 reflects the wall-frame connections and sheet-concrete interaction limit state. The rigid wall frame connections cause the sheeting to buckle after a long interaction process in the post-cracking stage and it was reasonable to take the buckling capacity of the sheeting with some reservation. The possible increase in core capacity and possible increase in resistance of the sheeting due to contact with concrete are not taken into account . This makes the equation 6.26 conservative. The influence of local buckling is not included as it is not found important in pre-buckling stages of the sheeting and in the case of composite wall.

Shear strength of the test models

The shear strength of test models are calculated on the basis of average strength of concrete in model tests and presented in table 6.7. The ratio of minimum failure load from model tests and the analytical failure is around 0.76. This will provide a factor of safety of around 25-30 %. The equation 6.26 can therefore, safely be used in design.

Table 6. 7 : Shear strength

	Profiled steel sheet Equation 6.25, β=1.72 , kN	Concrete core Equation 6.24 kN	Composite wall Equation 6.26 kN	Model tests kN	Ratio
Shear strength	31	30	92	122	0.76

6.5 Finite element modelling of composite wall

The finite element modelling of individual shear behaviour of profiled steel sheeting and profiled concrete core has been described in detail in chapter 4 and 5. This chapter will focus the detail modelling of the composite wall including shear stiffness, shear

plus bending stiffness, strength and strain characteristics within the system. The analysis can be divided into four categories:

Analysis of composite wall assuming full composite action using layered semi-loof shell elements. This will include model test simulation as well as general behaviour of composite wall under pure shear and shear plus bending.

Analysis of composite wall using interface layers between concrete and steel using layered semi-loof shell elements. This will include the effect of interface properties on the strength and stiffness of the composite wall.

Analysis of composite wall using joint elements connecting steel and concrete layer. The model test condition will be simulated on an elemental analysis to analyse the effect of boundary conditions and interface properties on the stiffness of composite wall.

Analysis of composite wall using 3D non-linear interface elements in between concrete and steel. The effect of in-plane and out-off plane shear modulus of interface elements will be studied.

6.5.1. Model test simulation

The model tests simulated pure shear behaviour of the composite wall. It was possible to simulate the whole test frame assembly including boundary frame and panels in the finite element model test simulation of profiled concrete core (chapter 4) and profiled steel sheeting (chapter5). However, for the composite wall case, simulation of boundary frame was not possible due to the following limitations:

The 3D, 8-noded QSL8 semi-loof shell elements allow the provision of different layers and in each layer different properties can be given using the option of composite material in LUSAS. Therefore, it is possible to model profiled concrete and steel using QSL8 semi-loof shell elements as composite layers. The simulation of boundary frame with semi-loof beam elements (BSL3) and joint elements to connect the frame to the wall as described in chapter 4 and 5 have no provisions for composite properties. This miss-matching of material properties did not allow the program to run. Therefore, it was decided to model the composite wall alone without boundary frame using only the semi-loof shell elements.

With the use of proper boundary conditions, it was possible to simulate the pure shear conditions in the panel. A typical finite element idealisation of the composite wall with 164 elements using semi-loof shell elements is presented in figure 6.36. Only symmetric half of the wall was modelled. The steel and concrete are represented as different layers of the element. The following problems and limitations are identified during the analysis:

i. Model test simulation needs a large number of elements with composite properties which faced convergence problem in non-linear analysis specially with interface layers between steel and concrete.

ii. The convergence problem and execution time leads to analyse the composite wall with only two profiles later to have some parametric study.

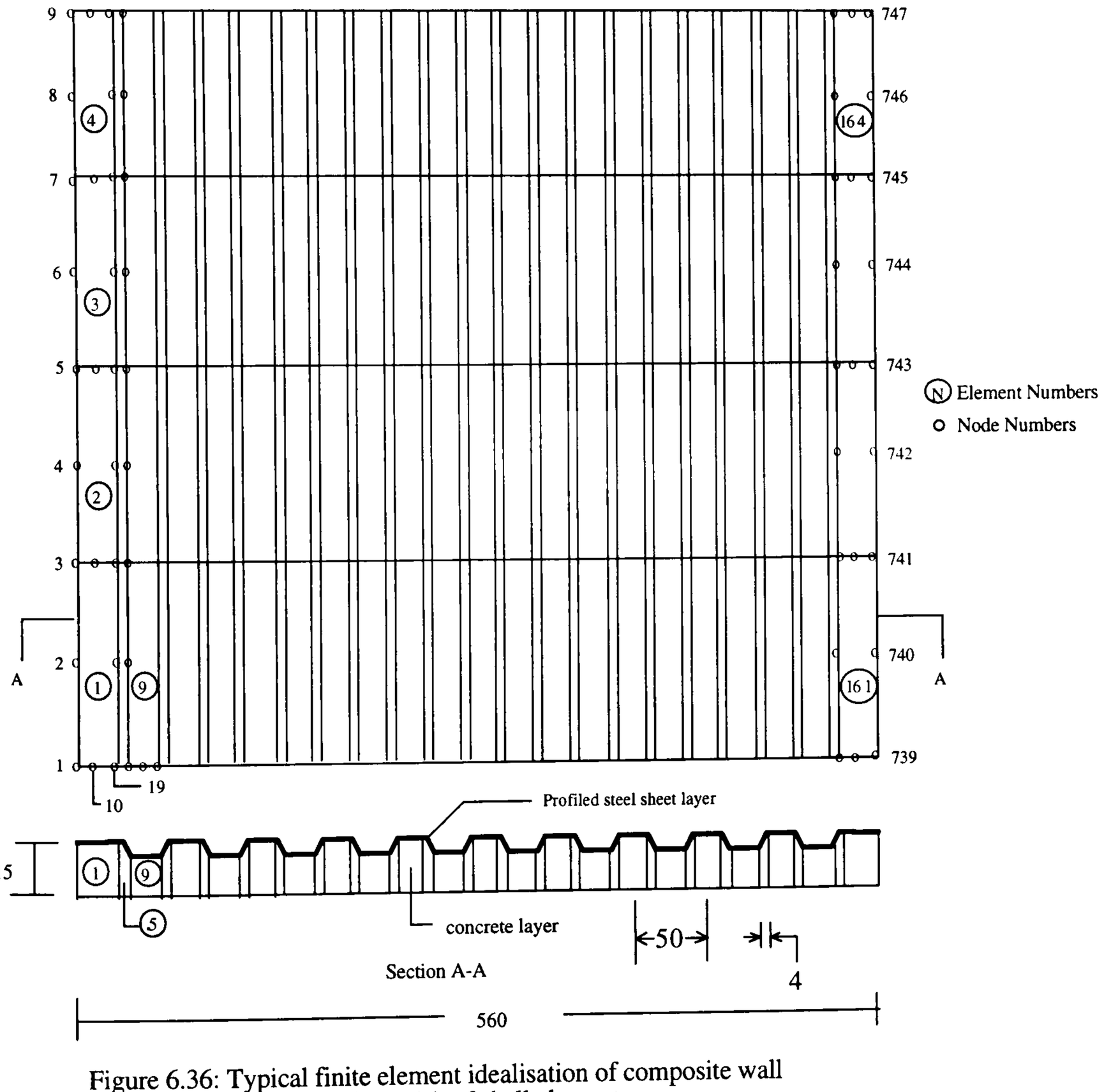

Figure 6.36: Typical finite element idealisation of composite wall with semi-loof shell elements

.

Mesh optimisation

A parametric study had been performed by varying the number of elements and it was found that the stiffness is not so sensitive to the mesh refinement. Mesh having 164 elements provided reasonable results in stiffness and strength and therefore adopted in model test simulation.

Model test simulation type 1

In this full composite simulation, shear load-deformation response of the composite wall was obtained by allowing the wall to undergo shear deformation as shown in figure 6.37(a). The full wall was simulated and load was applied at the top nodes in the form of prescribed displacement. Non-linear finite element analysis provided shear load, V, and corresponding shear deformation, δ, at each load increment. Complete shear load deformation response was obtained with cracking of concrete and yielding of steel layers. The non-linear run was carried out up to the yielding of steel.

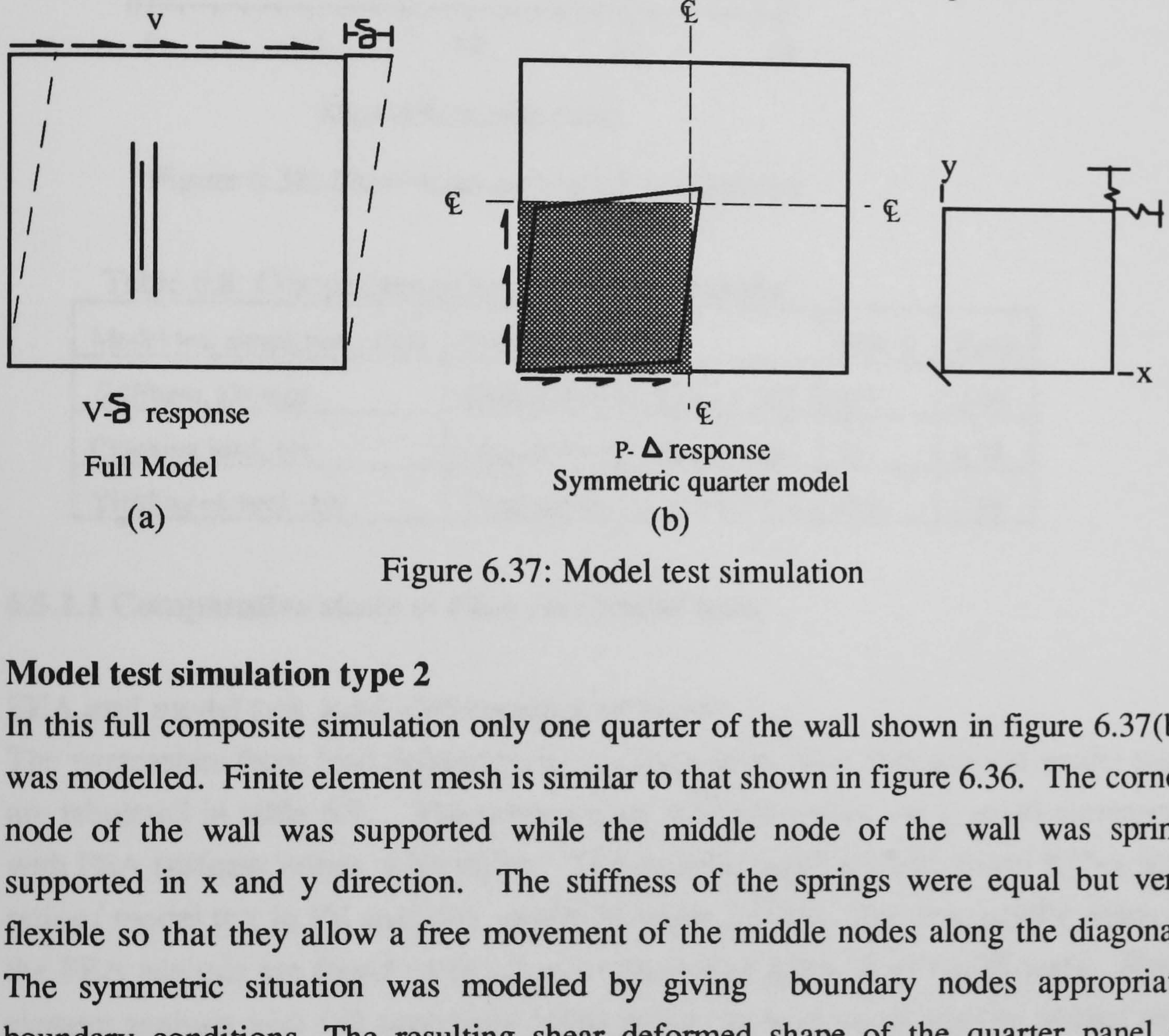

Figure 6.37: Model test simulation

Model test simulation type 2

In this full composite simulation only one quarter of the wall shown in figure 6.37(b) was modelled. Finite element mesh is similar to that shown in figure 6.36. The corner node of the wall was supported while the middle node of the wall was spring supported in x and y direction. The stiffness of the springs were equal but very flexible so that they allow a free movement of the middle nodes along the diagonal. The symmetric situation was modelled by giving boundary nodes appropriate boundary conditions. The resulting shear deformed shape of the quarter panel is shown in figure 6.37(b). The loads are applied in increment along the boundaries and resulting diagonal load versus diagonal deformation response was obtained.

The shear load deformation response from two type of simulation are compared in figure 6.38. They showed almost similar response. The stiffness and strength values are compared in table 6.8 and are found to be in good agreement.

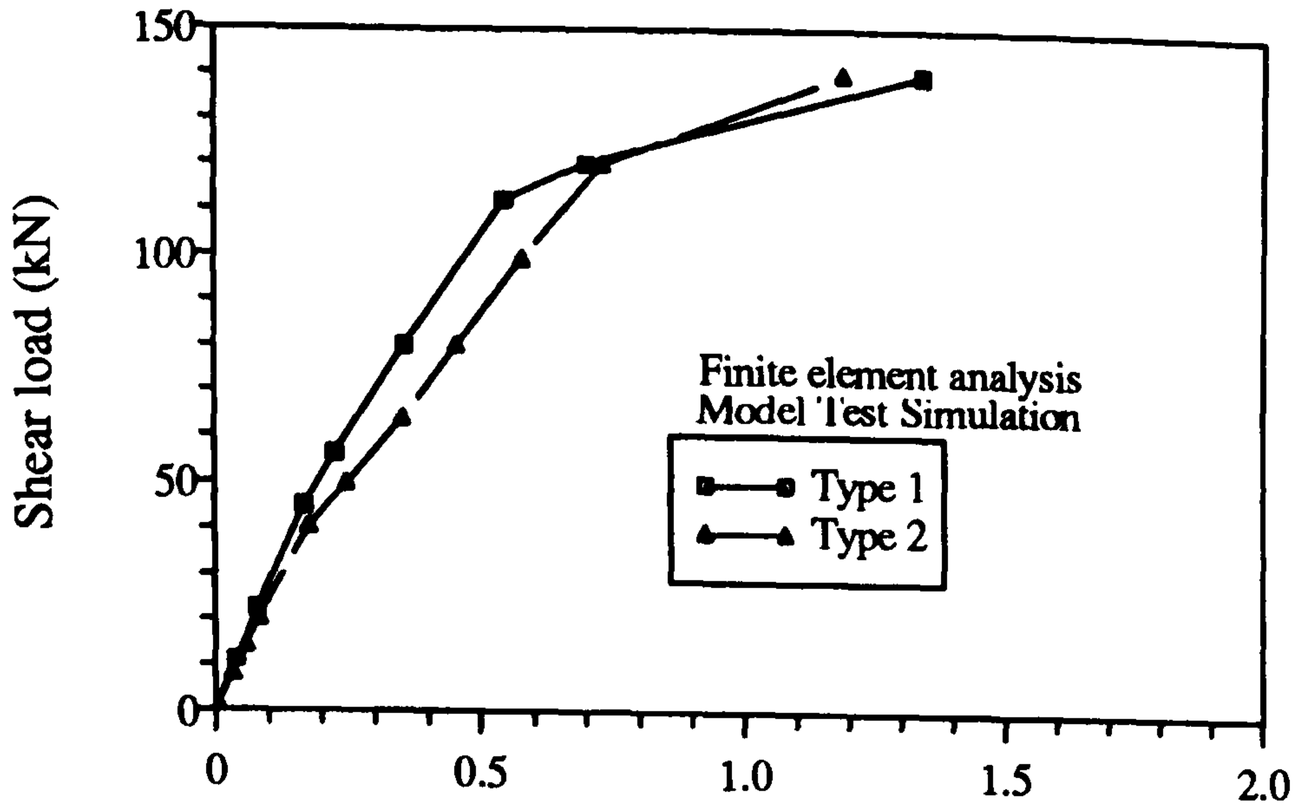

Figure 6.38: Shear-load deformation responses

Table 6.8: Comparison of model test simulations

Model test simulation , FEA	Type 1	Type 2	Ratio
Stiffness, kN/mm	Diagonal =536; Shear = 268	284	0.86
Cracking load, kN	Diagonal = 40 ; Shear = 28	32	0.88
Yielding of steel , kN	Diagonal = 170; Shear = 125	135	0.93

6.5.1.1 Comparative study of FEA and Model tests

FEA and model test load -deformation response

The parameters from load deformation responses from finite element and model tests are tabulated in table 6.9. The pre-cracking stiffness values are in good agreement with FEA stiffness values a bit higher. The cracking loads are also found higher with ratios (model test to FE analysis) ranges between 0.8-0.9. The first yielding loads of the FEA analysis are found to be close to the failure loads from model tests. Finite element analysis with full composite action seems to be good enough to predict pre-cracking and ultimate load of the composite wall although it is not possible to match complete load-deformation response as shown in figure 6.39. The test load-deformation response showed large displacement following the cracking in concrete compared to finite element response. This is obvious due to the full composite modelling in FEA compared to the model tests where after cracking a lot of aspects such as interface separation and sliding of the sheeting against concrete and formation diagonal cracks instead of descrete cracks at gauss points in FEA model, makes the situation further away from the full composite action.

Table 6.9: Comparison of FE analysis and model tests

	FEA analysis			Model tests			
	Type 1	Type 2	Average	test 1	test 2	test 3	Average
Stiffness, Diagonal	536	568	552	496	561	545	534
kN/mm Shear	268	284	276	248	280	272	267
Cracking load, Diagonal	40	45		35	36	25	
kN/mm Shear	28	32					
Yielding load , Diagonal	170	190		172	198	190	
kN Shear	125	135		failure loads			

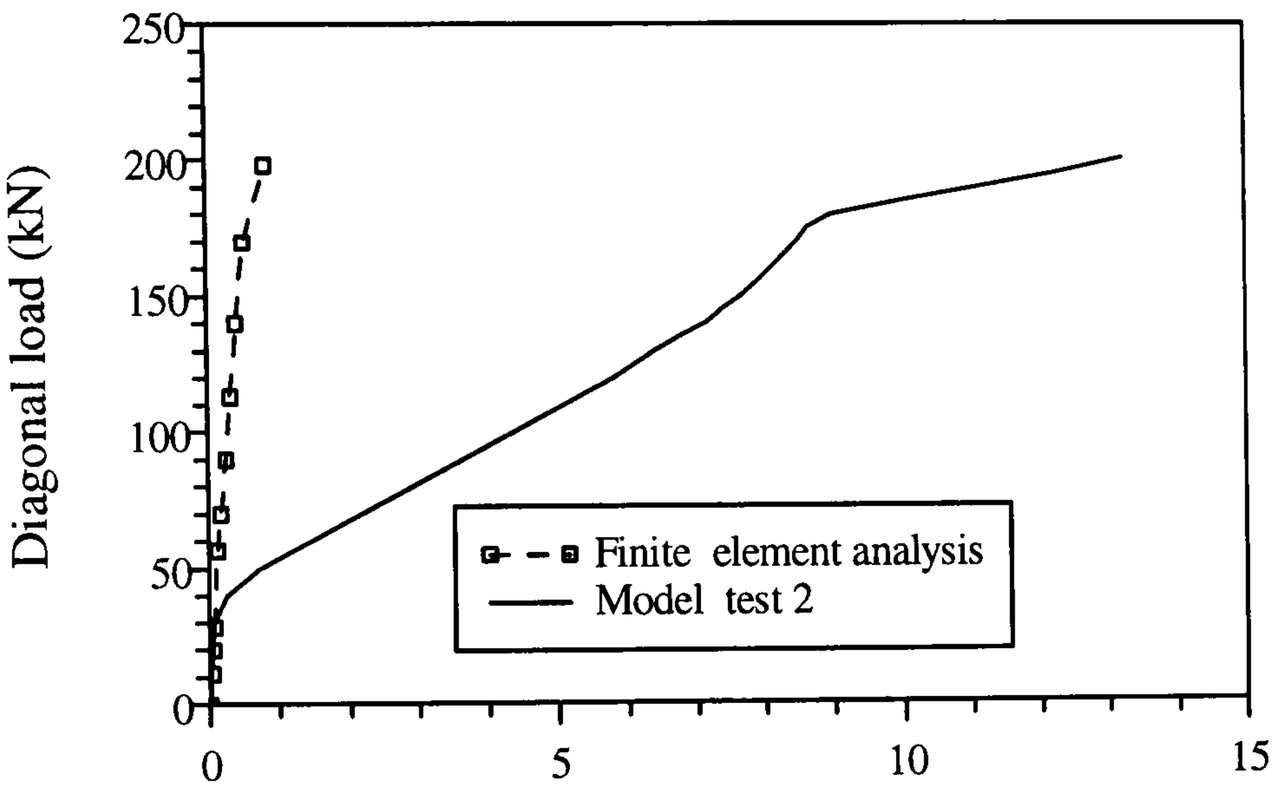

Figure 6.39: Load-deformation responses from FE analysis and model test

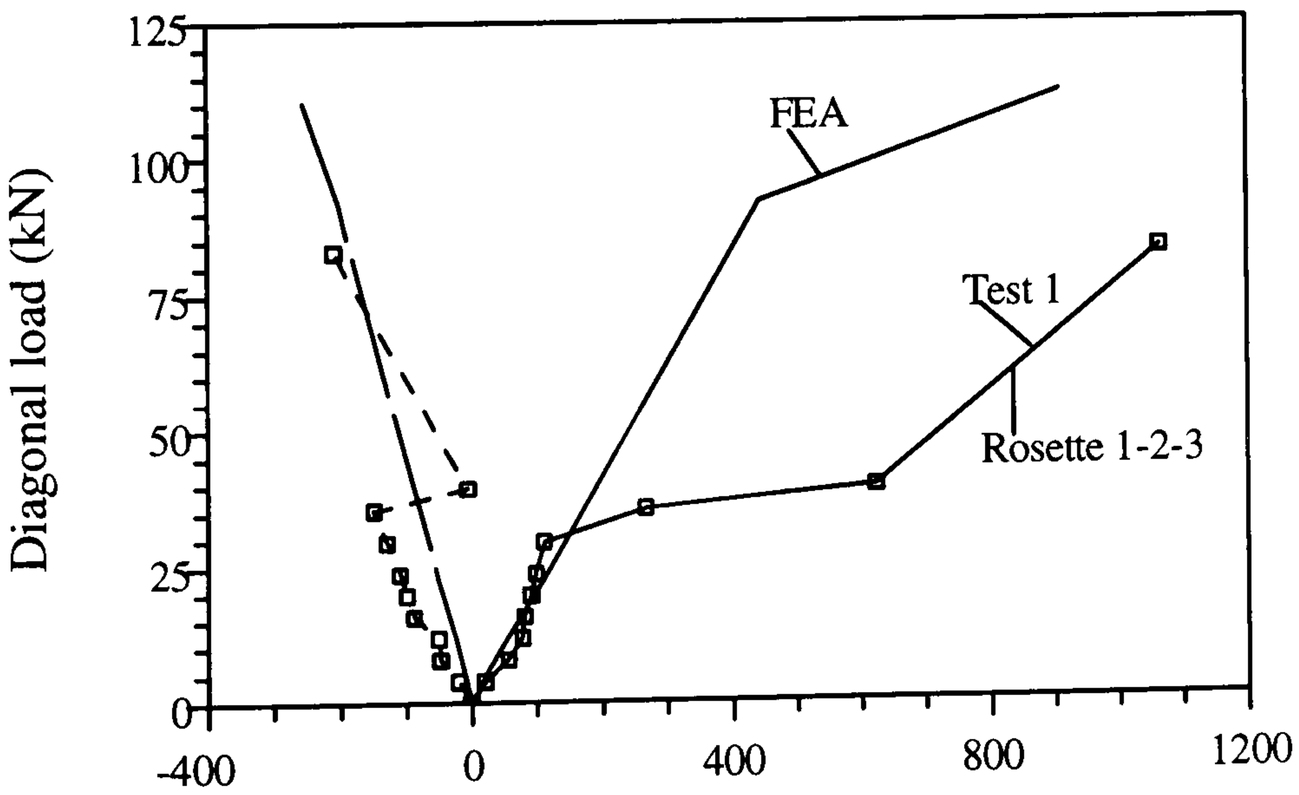

Figure 6.40(a)

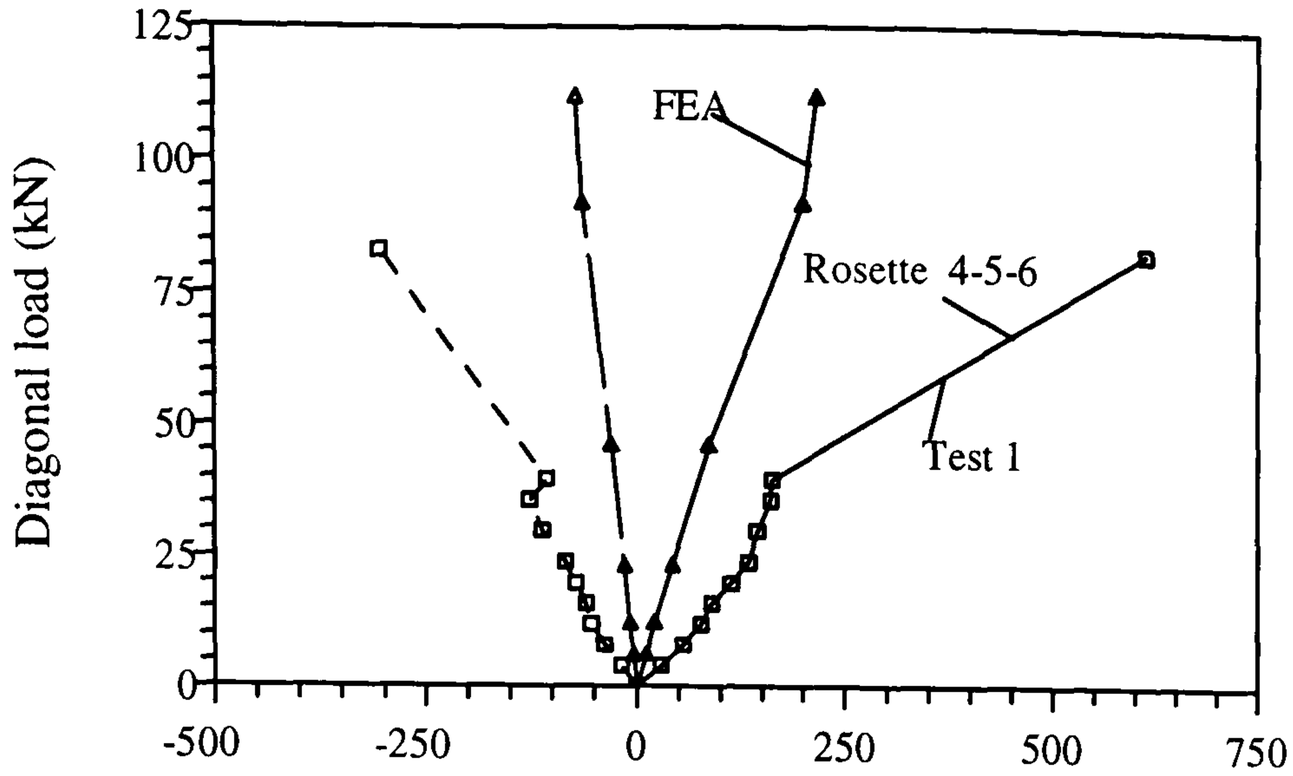

Figure 6.40(b)

Figure 6.40: Comparison of strain from FE analysis and model test

Strain analysis (FEA and Model tests)

The symmetric quarter simulation allows the comparison of principal strains along the diagonal of the panel. The principal strains are compared in figures 6.40. The strains from finite element analysis are found to be less than those from model tests. This is reasonable because of the full composite action in finite element analysis. Therefore, it will be not possible to fully model the strain compatibility between model tests and full composite finite element analysis. It needs to numerically model the interface in finite element analysis simulating actual interface properties in composite wall.

6.5.1.2 Comparative study of FEA , Analytical and Model Tests

The shear stiffness and ultimate load from different analysis will be now compared and presented in tables 6.10. Excellent agreement in individual stiffnesses of sheeting and concrete core are found between different analysis. The finite element and model test results confirmed that the shear stiffness of composite wall is 20-24% higher than the individual summation of stiffnesses of profiled concrete core and profiled steel sheeting.

Table 6.10(a): Shear stiffness

Shear stiffness	Analytical	Finite element	Model test
Profiled steel sheet	30.3	30	28.25
Profiled concrete	161	164	147
Sum of stiffness (pair of sheet +concrete)	221.6	224	204
Composite wall	221.6 equation 6.17	276 Full composite	267

Table 6.10(b): Shear strength

Shear stiffness	Analytical	Finite element	Model test
Profiled steel sheet	31	30.3	29.7
Profiled concrete	30	30	33
Sum of stiffness (pair of sheet +concrete)	92	90.6	93
Composite wall	92 equation 6.26	130 Full composite	122

The equation 6.17 can safely be used in the design calculation of shear stiffness of composite wall. Shear strength values showed excellent agreement between different analysis. The equation 6.26 will provide a factor of safety of around 1.25 and can therefore be safely used in design.

6.5.2 Parametric finite element study

In this section, the different type of finite element analysis on composite wall will be described. The composite wall dimensions were reduced so that the program can be run with no convergence problems, less execution time and provide easier mesh generation.

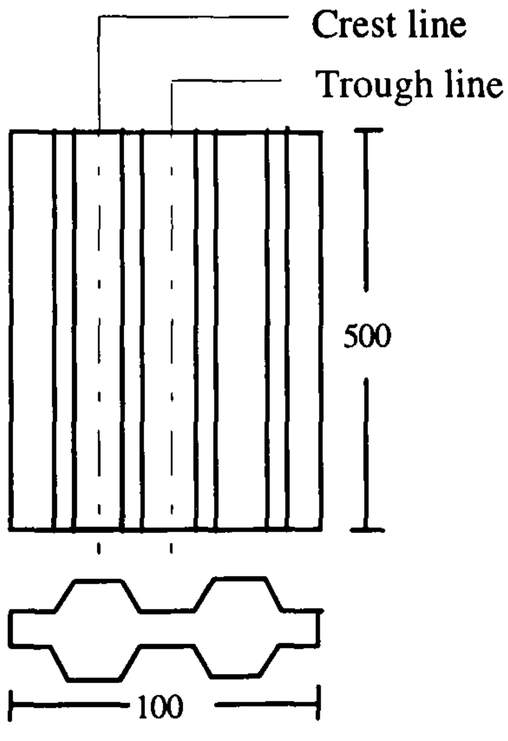

Figure 6.41: Composite wall with two profiles

6.5.2.1 Composite wall under cantilever bending

Finite element analysis has been carried out to verify the analytical stiffness equation 6.22, derived in section 6.4 for wall under bending plus shear. Full composite analysis with QSL8 elements with steel and concrete layers allows symmetric half thickness of the whole wall. The mesh is similar to that shown in figure 6.36, with fewer elements needed for smaller walls with only two profiles (figure 6.41). The linear and non-linear analysis of the composite wall including also individual modelling of the profiled steel sheeting and concrete core have been carried out for stiffness determination.

The stiffness values are tabulated (table 6.11) for comparison. The finite element stiffness of individual sheeting represents approximately the stiffness under cantilever bending due to the fact that the distortion of the sheeting was not allowed under the boundary conditions provided. The individual stiffness values are found to be in excellent agreement. The composite stiffness under bending plus shear (FEA) is found to be 25% higher than the individual summation of stiffness of sheeting and concrete core. The equation 6.22 can safely be used in design.

Table 6.11: Analytical and Finite element stiffness

	Analytical	FEA	Ratios
Profiled concrete	0.79 (equation 6.9)	0.78	1.01
Profiled steel	0.205 (equation 6.12)	0.21	0.98
Sum	1.20	1.20	1.00
Composite wall	1.20 (equation 6.22)	1.60	0.75

6.5.2.2 Modelling of composite wall with interface elements

In this section, composite wall will be modelled using interface elements between sheeting and concrete. The effect of interface properties on the stiffness, strength and strain characteristics of composite wall will be examined. This analysis will not be done in depth because that was not considered to be within the scope of the thesis.

i. Composite layer Analysis

In this case an additional layer will be provided in between steel and concrete as shown in figure 6.42.

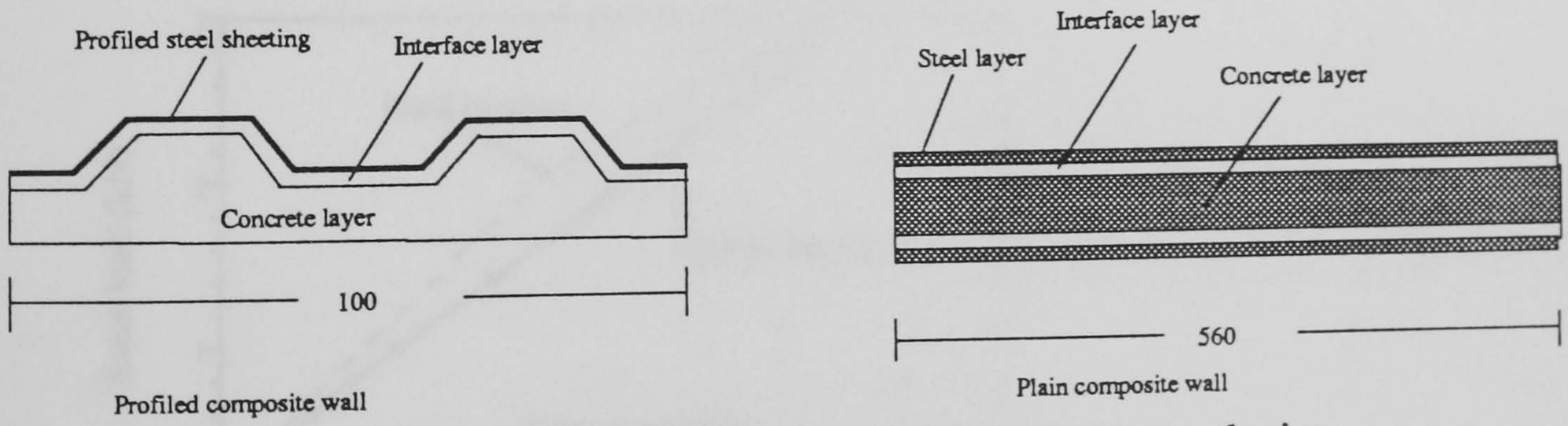

Figure 6.42: Provisions of interface layers in FE analysis

Properties of the interface layer can be changed by changing its material properties (like modulus of elasticity, poisson's ratio, uni-axial yield strength etc.) to study the effects on stiffness, strength and strain condition in steel and concrete layers. Parametric studies have been performed to study the effect of these material

properties on composite actions. The modulus of elasticity and poisson's ratio have little influence on composite action. But the value of uniaxial yield strength of interface layers can change the composite action. Providing very low values of the yield strength means that the interface layer will yield very quickly and allow a flexible interface in the later part of the loading history.

Profiled composite walls

Two extreme cases were considered in the analysis, one with very rigid interface providing full connection and the other very flexible interface providing almost no connection between sheeting and concrete core. Composite walls with rigid and flexible interface layers are modelled for both pure shear and cantilever bending actions (Boundary conditions shown in figure 6.43(a)). The resultant load-deformation responses are shown in figures 6.43(b) and (c). The stiffnesses are found to be reduced with flexible interface layers. But the effect is more pronounced in case of cantilever action where stiffness is reduced by about 18% (table 6.12). The load deformation response also showed an increase in shear deformation in case of flexible interface. However, it seems to be that cracking and yielding load is not affected .

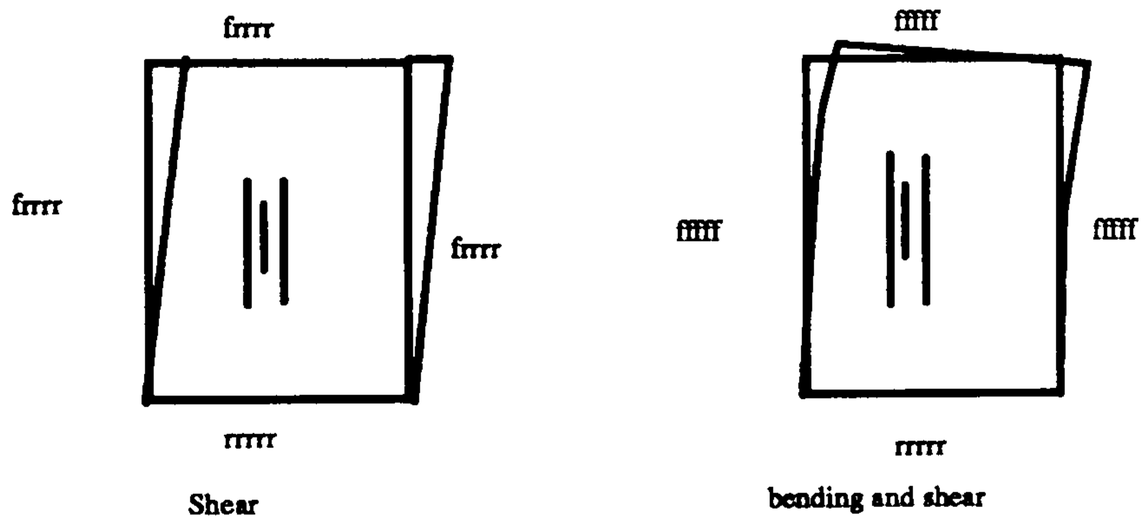

Figure 6.43(a): Boundary conditions

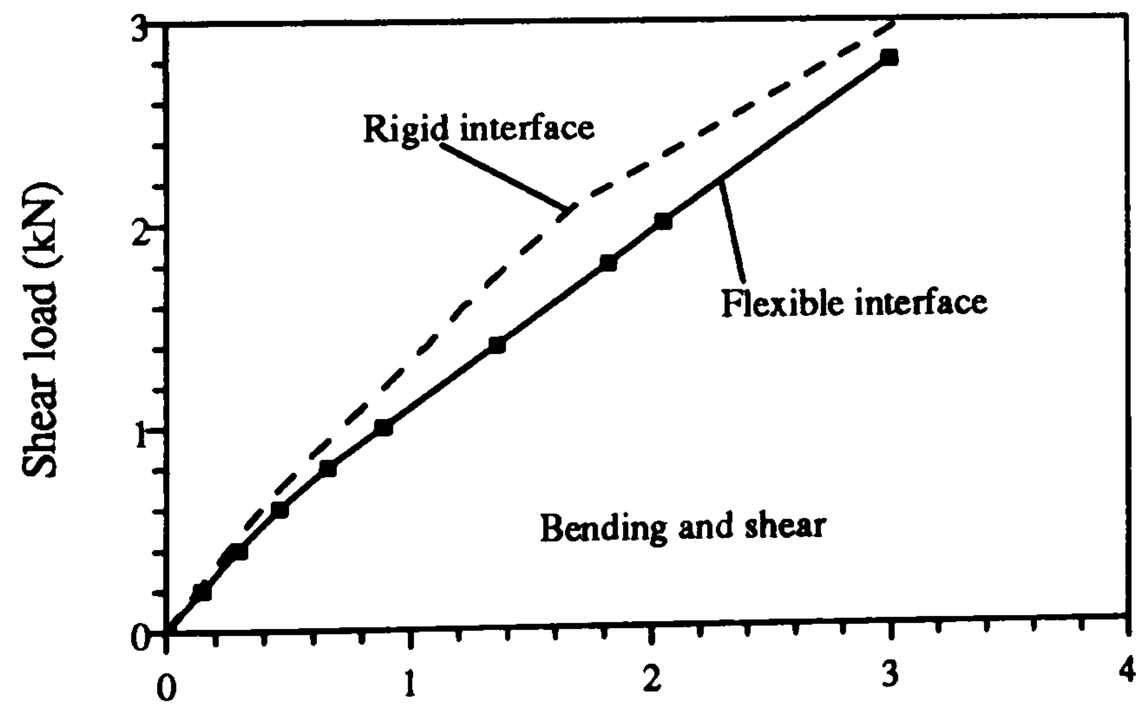

Figure 6.43(b)

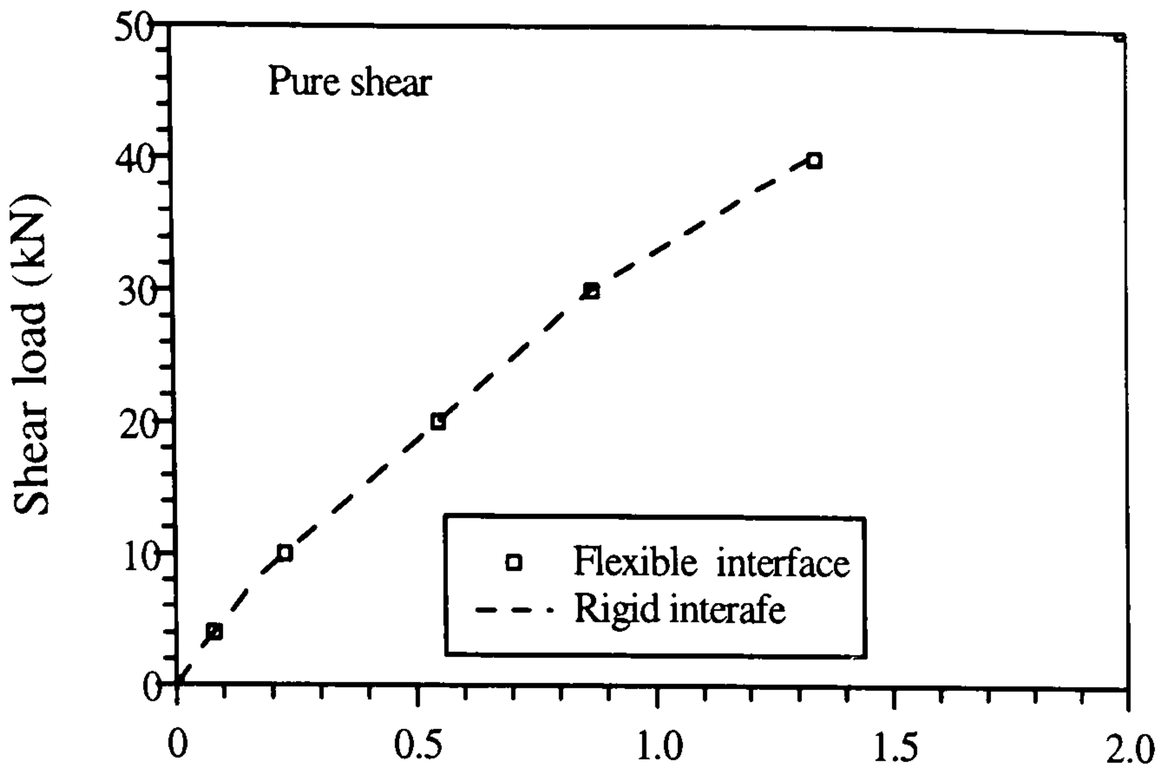

Figure 6.43(c)

Figure 6.43(b) and (c): Effect of interface on load-deformation response

Table 6.12: Effect of interface on the stiffness and loads

	Shear case		Cantilever case	
	Rigid	Flexible	Rigid	Flexible
Stiffness , kN/mm	50.91	50	1.605	1.37
Cracking load, kN	10	10	0.2	0.2
Yield load, kN	40	40	1.9	1.9

The variation of principal strain along the trough and crest profile lines as indicated in figure 6.41, are shown in figures 6.44 for shear case with rigid and flexible interfaces. The pre-cracking strains in both steel and concrete layers are found to be nearly same.

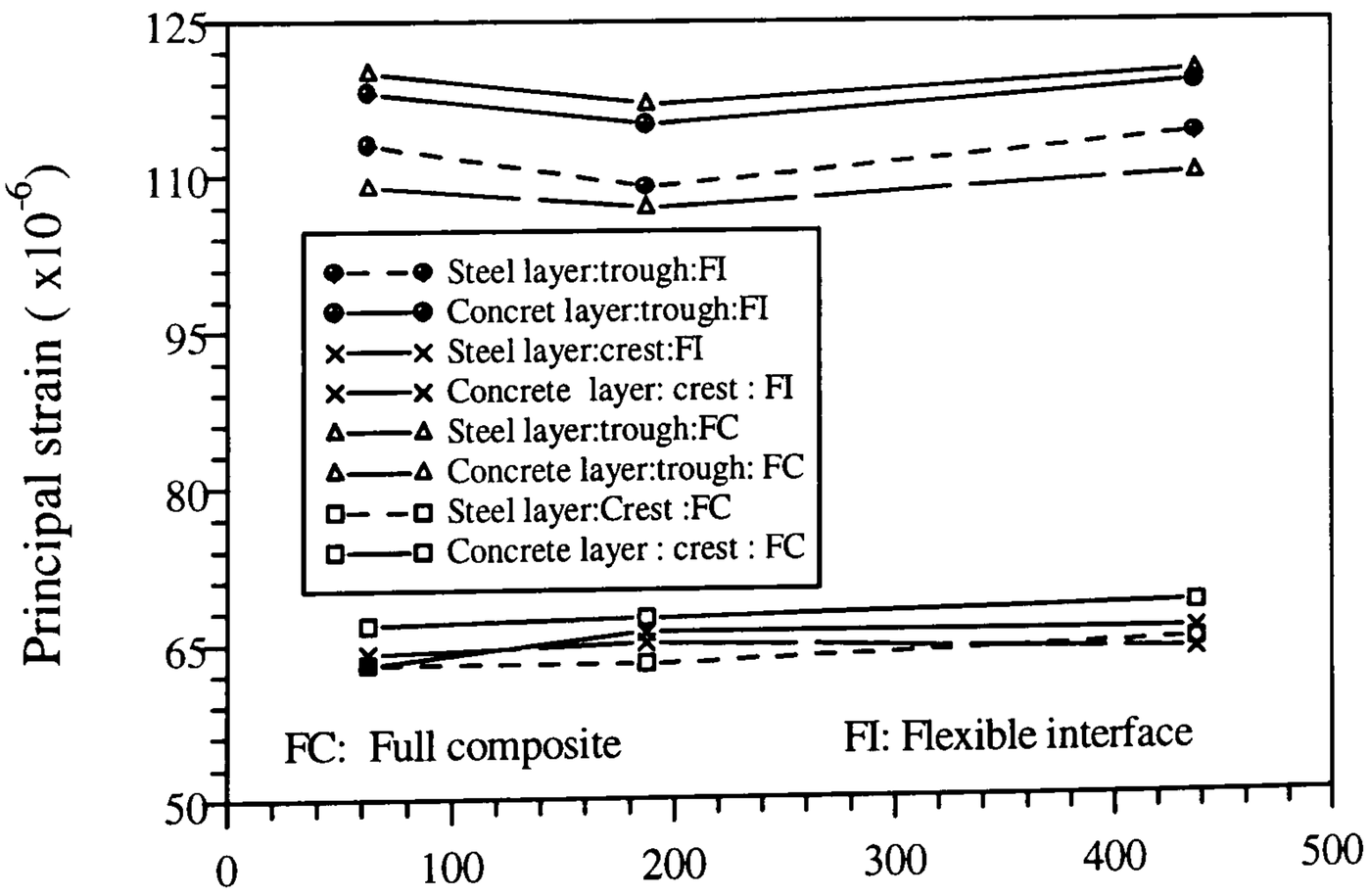

Distance along the profile (mm)

Figure 6.44(a)

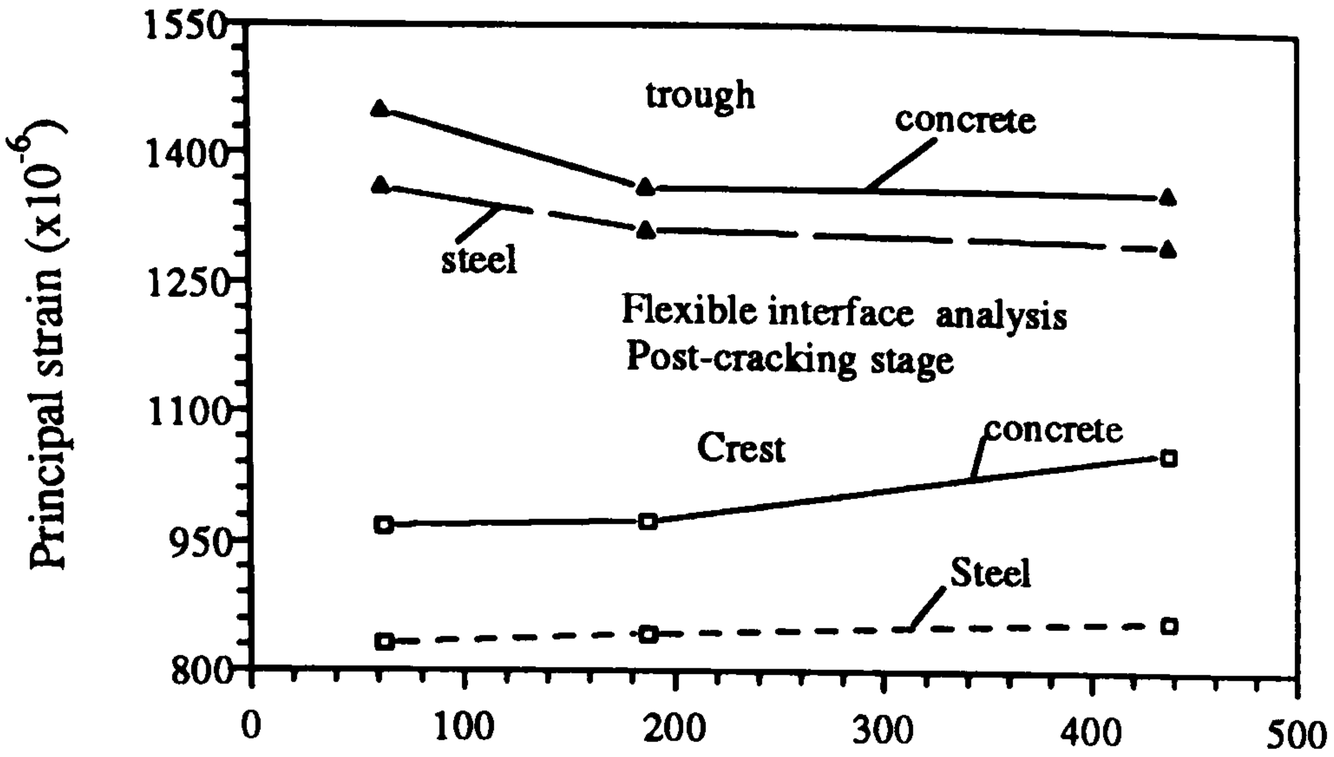

Figure 6.44(b)

Figure 6.44: Variation of principal strains

The strains along the profile are also found to vary uniformly. The trough sections are strained higher than crest sections. In the post-cracking stage, as shown in figure 6.44(b), the strains in concrete and steel layer differs and the difference was found to be higher in case of flexible interface than rigid. The similar behaviour is found in case of cantilever situations.

This composite layer analysis has some limitations. As one element represents all the layers of steel-interface-concrete with same nodes representing all the layers, it will be not be possible to have physical separation between the layers. Therefore, actual interface behaviour may not be simulated only by changing the interface layer properties.

Plain composite wall

The modelling of a plain composite wall is less complicated due to its geometry. Model test 6 has been performed on plain composite wall with 0.55 mm thickness plain sheeting and 22mm thick concrete core. The layer sequence in finite element modelling is shown in figure 6.42. Full wall was modelled with QSL8 elements and three layers of steel-concrete-steel are assigned in the composite material model. The model test conditions are simulated similar so that diagonal load-deformation response can be obtained. Full composite non-linear analysis is performed which allows concrete cracking and yielding of steel.

The principal strains from finite element analysis are compared to those from model test rosette locations at loaded corner (R-1-2-3), at centre (R-5-6-7) and at off-loaded corner (R-11-12-13) in figures 6.45(a), (b) and (c). The strains are plotted up to a load of 95 kN from the model test. The initial strains are found to be close

particularly for the centre rosette. But in the post cracking stage the strains in model test are found to be higher than those from FEA analysis.

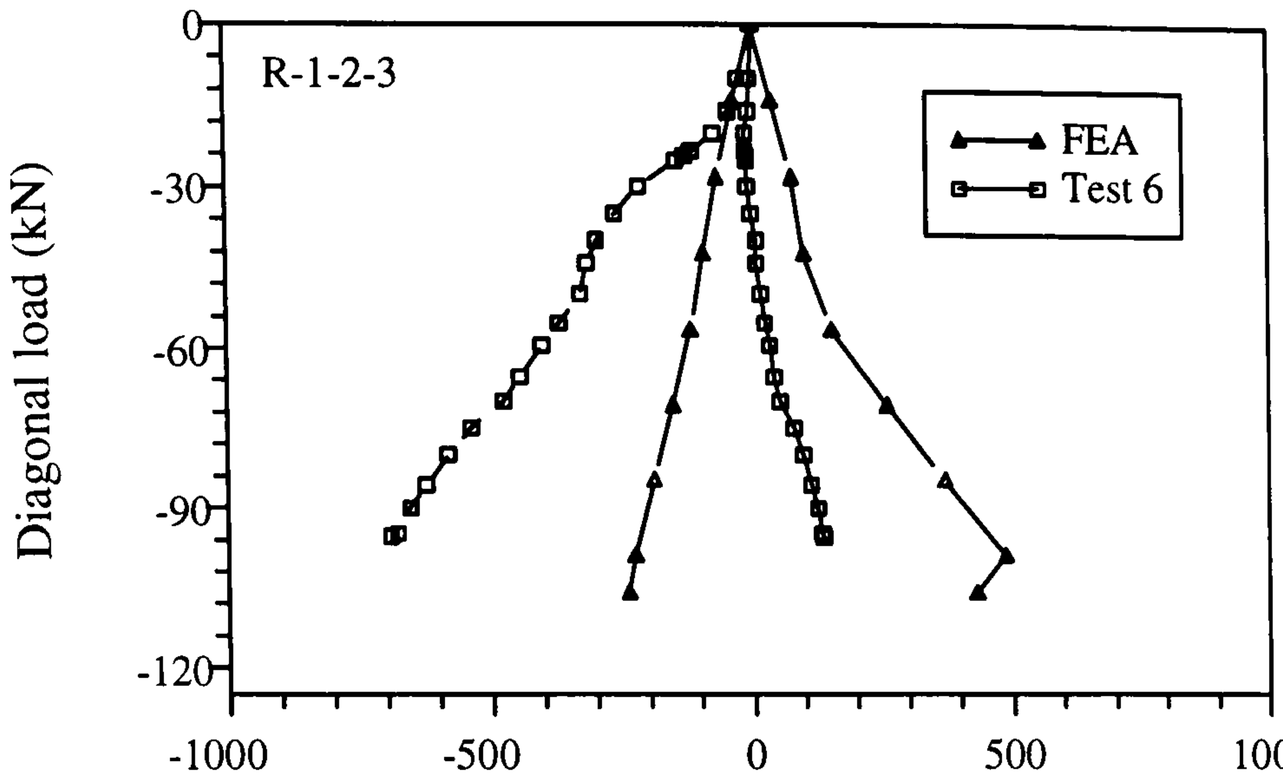

Figure 6.45(a)

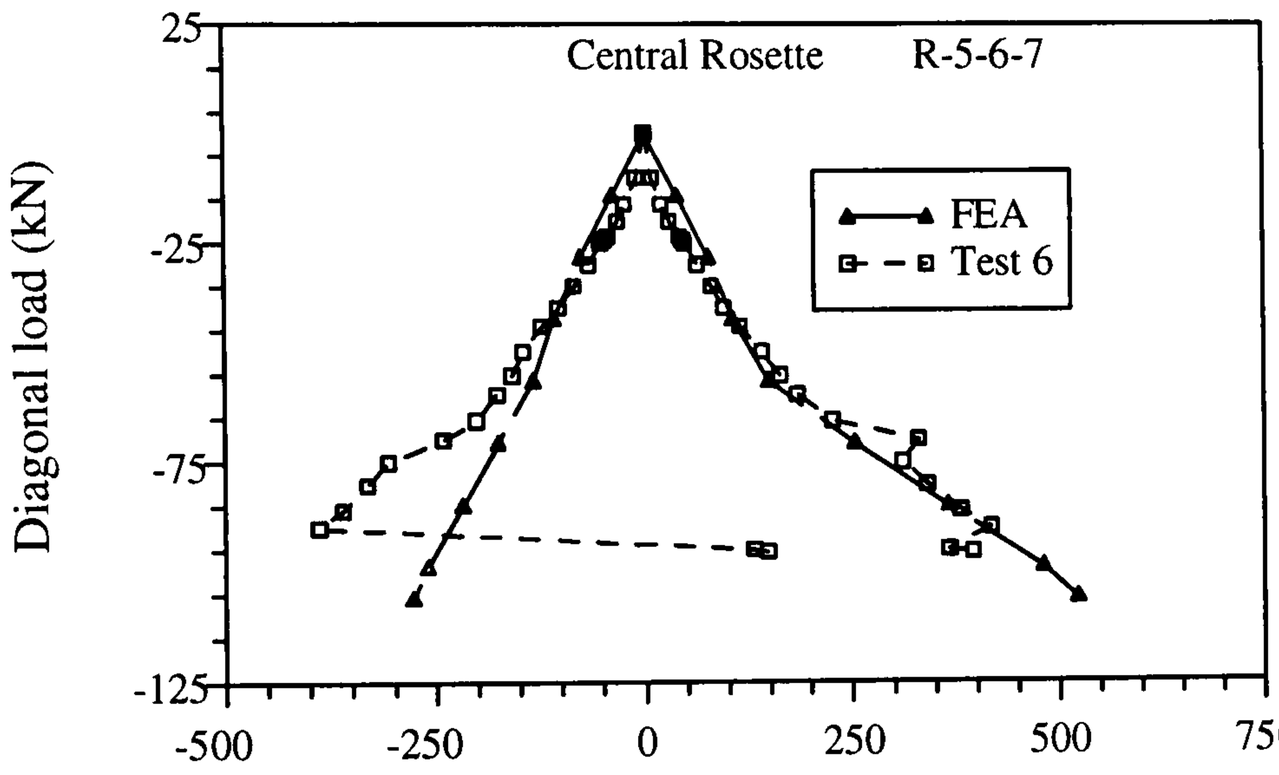

Figure 6.45(b)

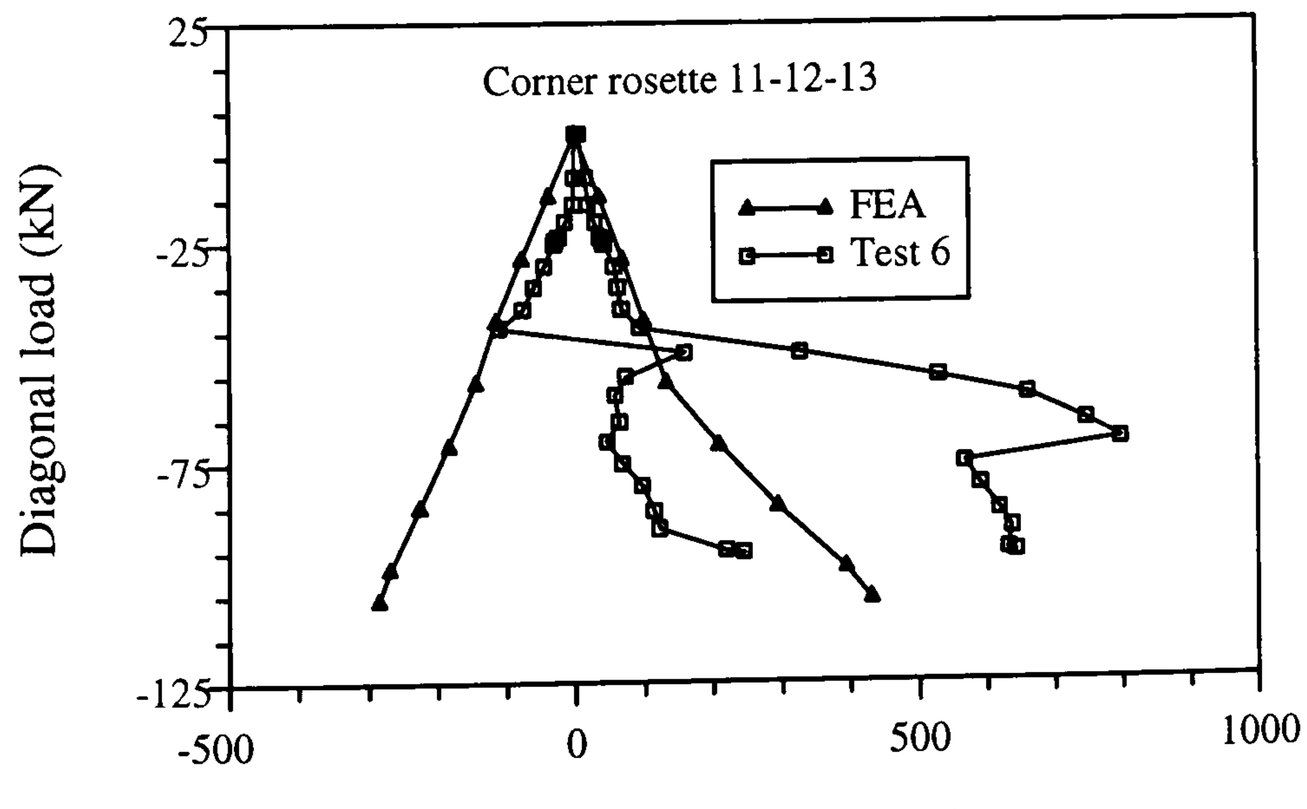

Figure 6.45(c)

Figure 6.45(a), (b) and (c): Comparison of strains

The principal directions are also compared (figure 6.45(d)) where the centre rosette shows good agreement to the finite element analysis.

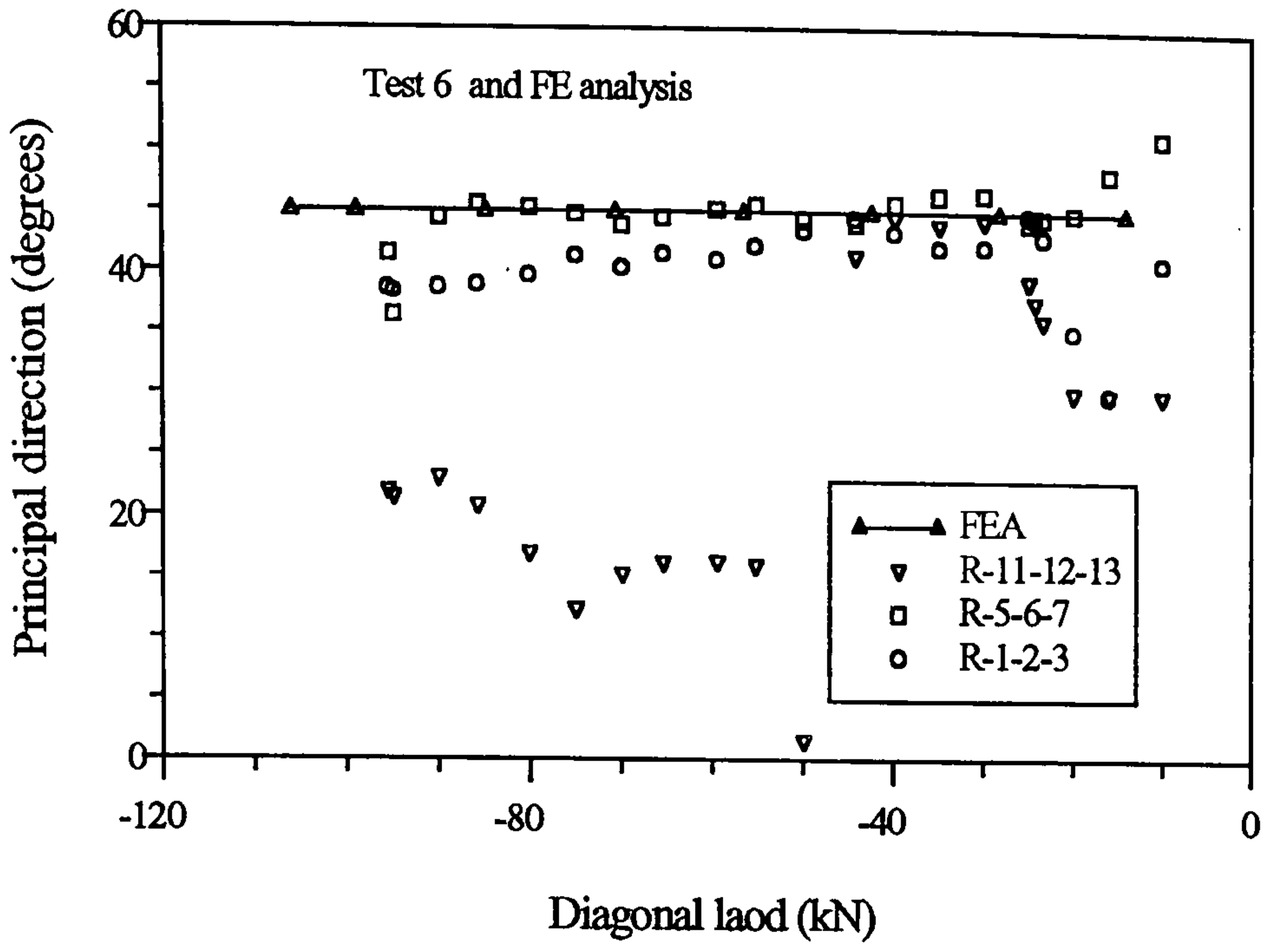

Figure 6.45(d): Comparison of principal directions

To determine the stiffness of the plain composite wall, the equation 6.17 can be modified as:

$$c_w = \frac{1}{k_w} = \frac{2b(1+\upsilon_s)(1+\upsilon_c)}{a\left[E_c t_c(1+\upsilon_s)+2E_s t_s(1+\upsilon_c)\right]} \qquad \text{.....(6.27)}$$

The equation 6.27 considered the pre-buckling stiffness of the sheeting and leads to the analytical stiffness (Table 6.13) of the wall which is around 40 % higher than the model test. The equation 6.27 is therefore, modified to take account of post-buckling stiffness of the sheeting (as the buckling load is very small for the thin sheeting, 4.87kN for model sheeting) as the sheeting may be buckled at a very low load in the composite wall. The post buckling stiffness has been derived in chapter two in the form of equation 2.13 which when incorporated in the equation 6.27, gives the modified stiffness equation to be as :

$$c_w = \frac{1}{k_w} = \frac{2b(1+\upsilon_c)}{E_s a t_s(1+\upsilon_c)+E_c a t_c} \qquad \text{.....(6.27(a))}$$

The modified stiffness showed good agreement between finite element analysis which is around 26% higher than the model test stiffness.

The shear resistance of the plain composite wall can also be derived based on the concrete capacity and the capacity of the plain sheeting considering the full mobilisation of tension field capacity. This may be applied for the model test condition where the development of the tension field was observed with subsequent yielding of the steel sheets. The shear capacity of the wall can, therefore, be written as: $V_w = f_y a t_s + 0.074 b t_{eq} f_{cu}$ .....(6.28)

Table 6.13, compares the shear stiffness and strength values of the plain composite wall from different analyses.

Table 6.13: Shear stiffness and resistance of plain composite wall

Plain composite wall	Model test	Analytical	Finite element
Shear stiffness, kN/mm	172	270 (eq. 6.27) 232 (eq. 6.27(a))	230
Shear resistance, kN	85	119 (eq. 6.28)	90, start of yielding

ii. Elemental simulation with joint interface

An elemental simulation with square panel of 100x100 mm is carried out to model actual model test conditions. The reduced dimensions of the model allows fewer elements needed to simulate steel, concrete, interface and boundary frame members. The detail finite element idealisation is presented in figure 6.46. This time separate QSL8 semi-loof shell elements are used to represent steel and concrete layers but the nodes (for example 1, 96 and 234) have the same co-ordinates. The steel and concrete layers are connected to each other by joint elements (JL46). The boundary frames are simulated with semi-loof beam elements (BSL3) and connection to either sheeting or concrete or both can be made using joint elements.

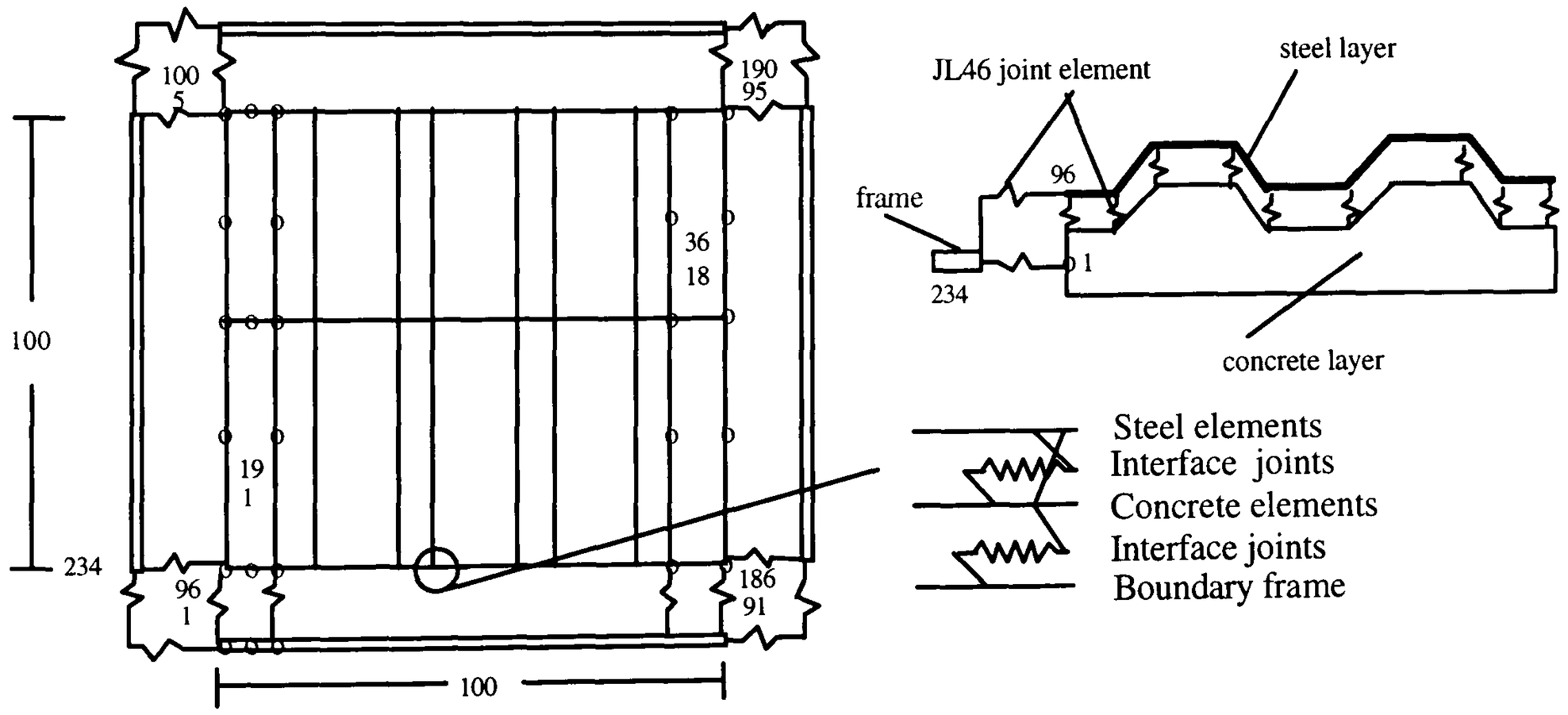

Figure 6.46: Elemental simulation with joint interface

This analysis has the limitation of geometric arrangements of the sheeting and concrete core layers as the layer sequence is not defined. But despite this limitation it can simulate a comparative boundary condition effects on stiffness. Diagonal or shear load can be applied through the frame and corresponding deformation can be obtained. Load can be applied through concrete only (removing joint elements which

connect frame and sheeting) or through both concrete and steel. Due to the practical problems of modelling of actual interface with joint elements (which needs much further studies to co-relate joint properties with actual interface condition and currently this is beyond the scope of this study), extreme cases of full connection (providing very rigid joints) and no-connection are studied. The connections between the frame and sheeting and concrete are made very rigid.

The effect of boundary conditions on the stiffness of the composite wall are summarised in table 6.14. The stiffness is found to be not affected by the sheet-concrete connections provided they both have full connection to the boundary frame.

Table 6.14: Effect of boundary connections and interface

Load applied through	Sheet-concrete connection	Sheet-concrete-boundary connection	Stiffness kN/mm	Ratios
Sheet +concrete	full	both	299	1
Concrete	full	only concrete	277	.92
Sheet+concrete	no	both	299	1
Sheet	full	only sheet	275	0.91

iii. Elemental simulation with 3D interface

In this non-linear analysis, steel and concrete layers are represented by 3D semi-loof shell elements (QSL8) as before but elemental nodes have different co-ordinates. The steel and concrete layers are, therefore, completely separate as the nodes are specified at the centre lines of each of the concrete and steel layer as shown in figure 6.47(a).

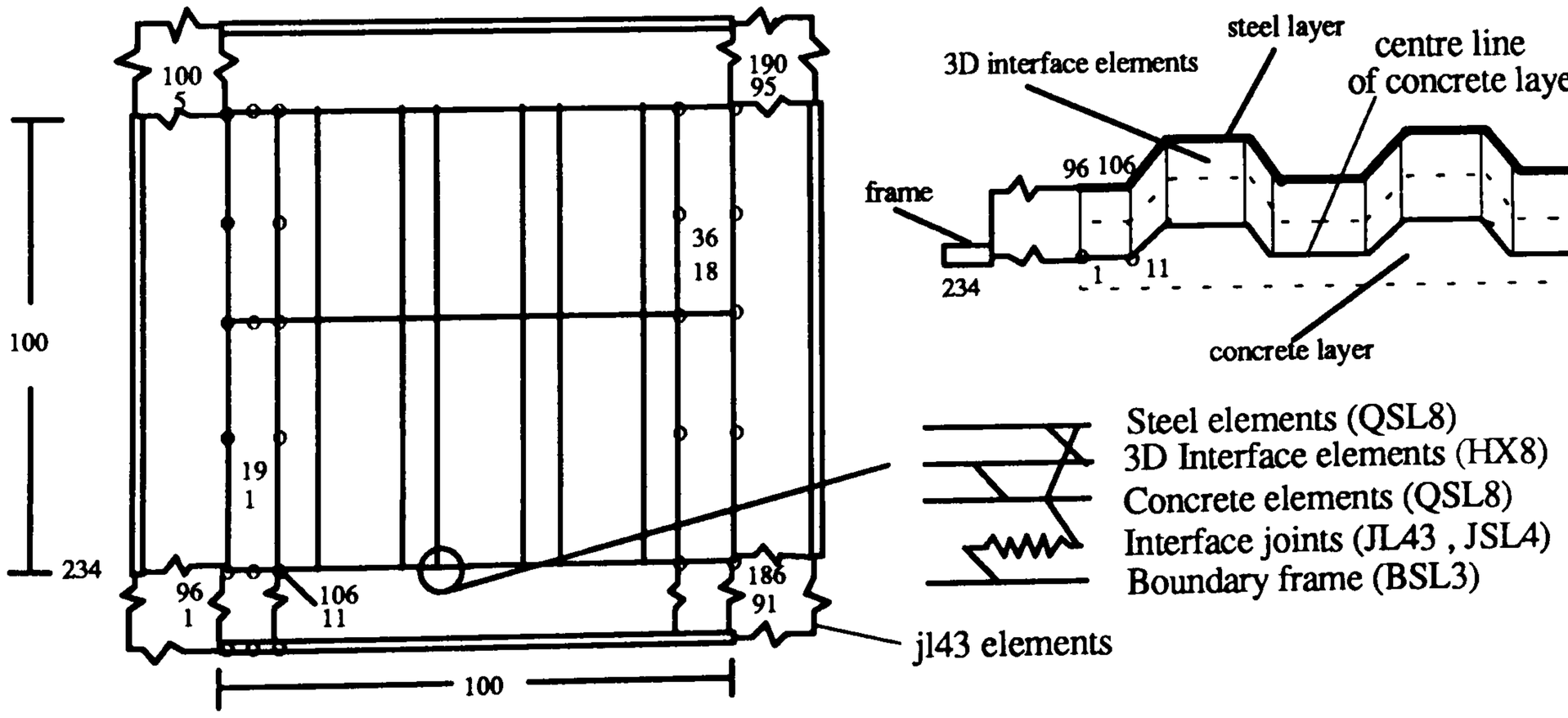

Figure 6.47(a): Elemental simulation with 3D interface

In between the two layers (between the centre lines of the layers), 3D-8 noded interface solid elements (HX8) having 3 translational degrees of freedom (u,v,w) at each node are used as interface elements. The HX8 interface elements connected the steel-concrete layers (QSL8 elements) at corners nodes as these nodes have three translational degrees of freedom (u,v,w) like HX8 elements. Therefore, compatibility of the two different type of elements at nodal points are satisfied.

In the simulation of model test conditions, the boundary frame is modelled with semi-loof beam elements (BSL3 elements) and the connections between frame-sheeting-concrete are provided by JSL4 joint elements for middle nodes and JL43 joint elements for corner nodes to satisfy the compatibility of nodal degrees of freedom. As the joint elements can be used to connect nodes having same co-ordinates, it is necessary to use two frame beams connected together by connecting beams for joining both steel and concrete layers to the frame when load was applied through both steel and concrete. However, for the case of load applied through concrete only, one frame beam is necessary. The detail connections in profile and plain boundaries are shown in figures 6.47(b).

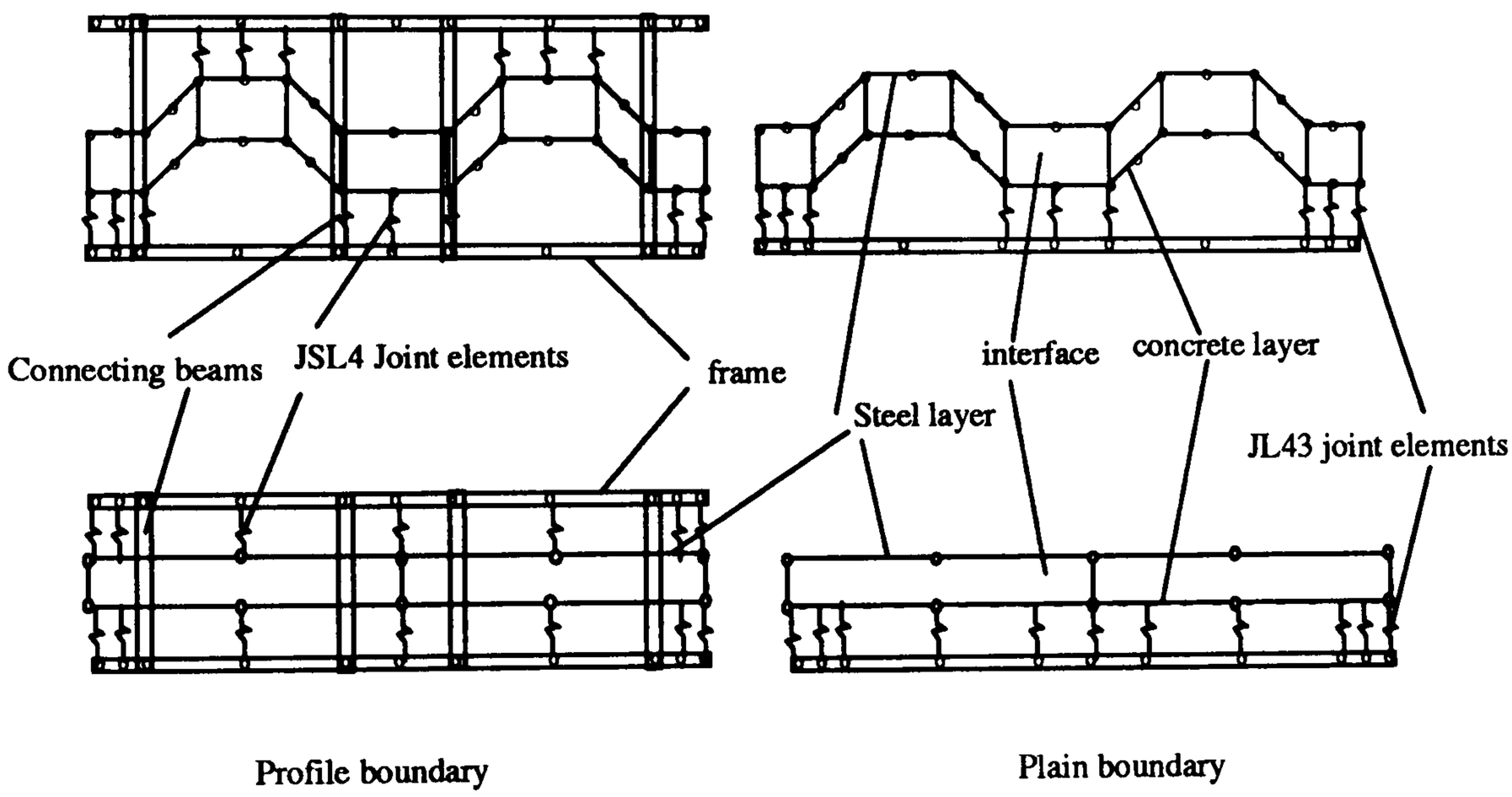

Figure 6.47(b): Detail connections in plain and profiled boundaries

Three separate cases (figure 6.47(c)) are considered : Case1: Pure shear simulation with out boundary frame, Case2: Shear simulation with boundary frame and Case 3: Model test simulation. The following findings including problems can be summarised:

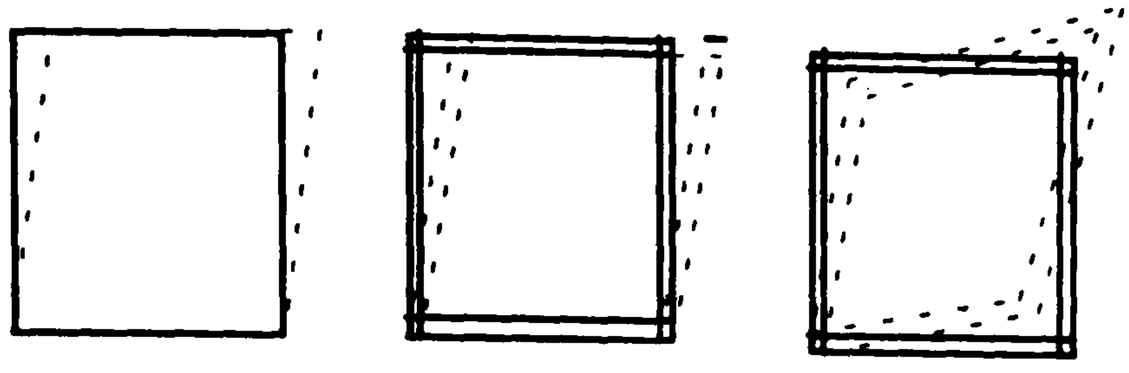

Figure 6.47(c): Types of simulations

Case 1: For this case, the properties of interface layer influenced the behaviour. The non-linear interface elements used needs to provide the following main properties: modulus of elasticity in and out-of plane (E_{in}, E_{out}), shear modulus (G_{in} and G_{out}), poisson's ratio, cohesion, friction angle and uni-axial yield stress. The shear condition was simulated by applying equal prescribed displacement at the top nodes for both steel and concrete. The distortion of steel layer is found to be influenced by G_{out}. As the value of G_{out} changes from 0.1 to 30, the out-off plane Z-displacement of the sheeting is found to be decreased. However, the effect of G_{in} and G_{out} on the stiffness was not so pronounced. The ultimate load of the panel could not be estimated as the program did not converge after cracking of concrete and before that it showed no sign of steel yielding.

Case 2 and Case 3: The analysis was performed for the cases of load applied through concrete plus steel as well as through concrete only. Both cases showed similar problem of convergence only after few increments allowing only to the determination of stiffness. The effect of G_{in} and G_{out} is on the stiffness is shown in figure 6.48. It is found that the stiffness values seem to be not affected by the in-plane and out-of plane shear modulus.

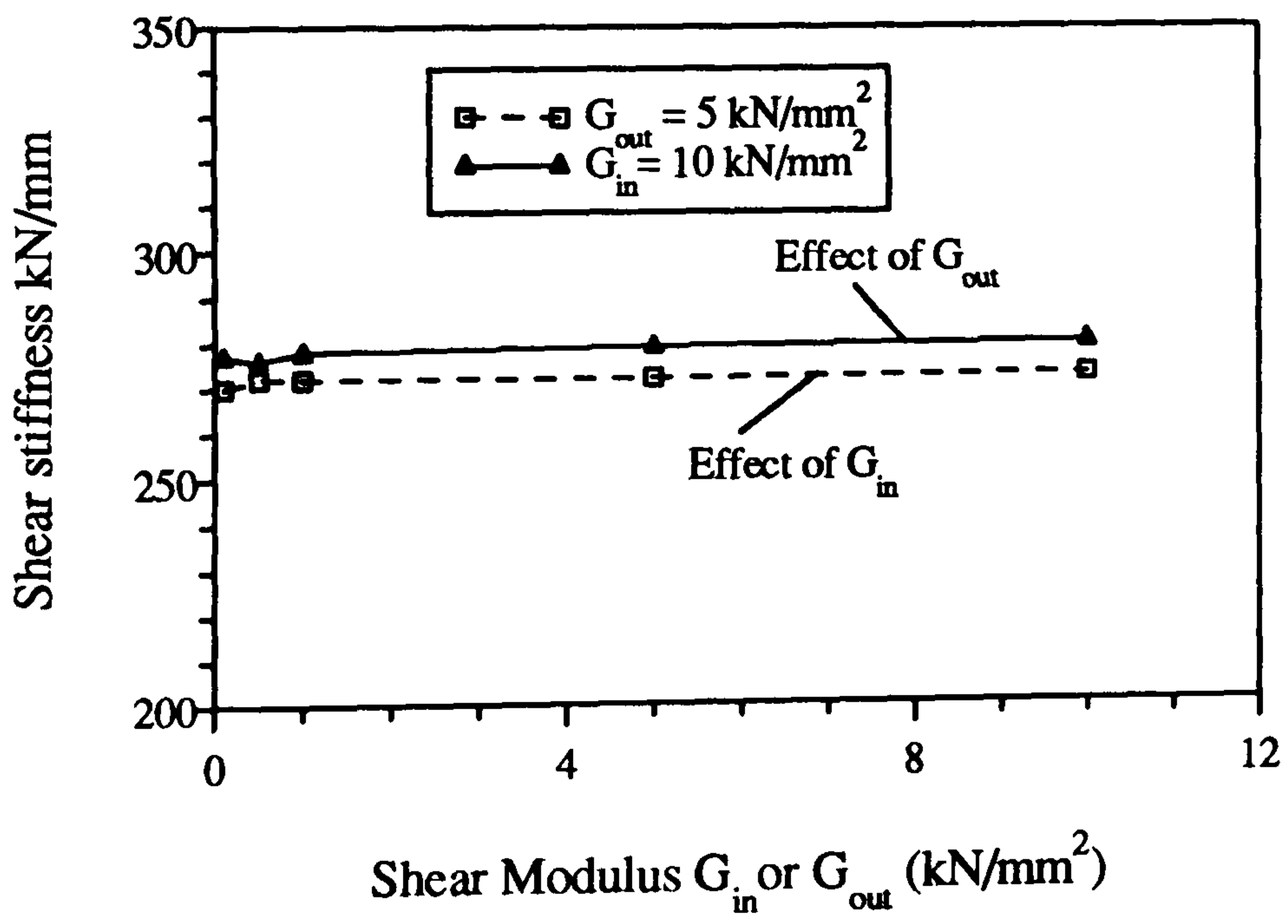

Figure 6.48: Effect of interface shear modulus on stiffness

The effect of load transfer through both steel and concrete and concrete only on stiffness (table 6.15) is also not pronounced although the first condition shows higher values.

Table 6.15: Effect of boundary conditions on stiffness

Load applied through	Interface Gin Gout kN/mm^2	Sheet-concrete-boundary connection	Stiffness kN/mm
Sheet +Concrete	10 1	Both	282
Concrete	10 1	only concrete	273

Comments:

The composite wall analysis with interface elements provided only an outline of the use of available options in the proprietary finite element program LUSAS. More detailed investigations are possible with the modelling of interface elements that co-relate the practical situations in actual steel-concrete interface in composite wall. Further investigations are needed to model this interface properties to make a co-relation between experimental interface properties and 3D finite element interface properties.

6.6 Summary

From the literature review it is identified that the longitudinal shear bond at the interface governs the ultimate failure load of composite slabs. For the case of composite wall under axial load, the embossments were not capable of transferring any significant amount of load and additional shear connections devices are required at the head and foot of the wall to mobilise the load transfer to the greater depth of the wall. In the case of in-plane shear, the situation is much better than the axial case as confirmed from the model tests. From the model tests without embossed sheeting, it was found that the composite wall can provide strength and stiffness higher than the summation of the individual contributions from the sheeting and concrete core. The development of diagonal tension was confirmed from the strain analysis. The failure of the wall was associated with buckling and also with the development of tension fields. The buckled patterns of the sheeting showed the formation of half waves. The effect of boundary conditions and load transfer mechanisms were studied and boundary conditions were found to be very important. Analytical models for the strength and stiffness of the composite wall were derived and validated by model tests and finite element analysis.

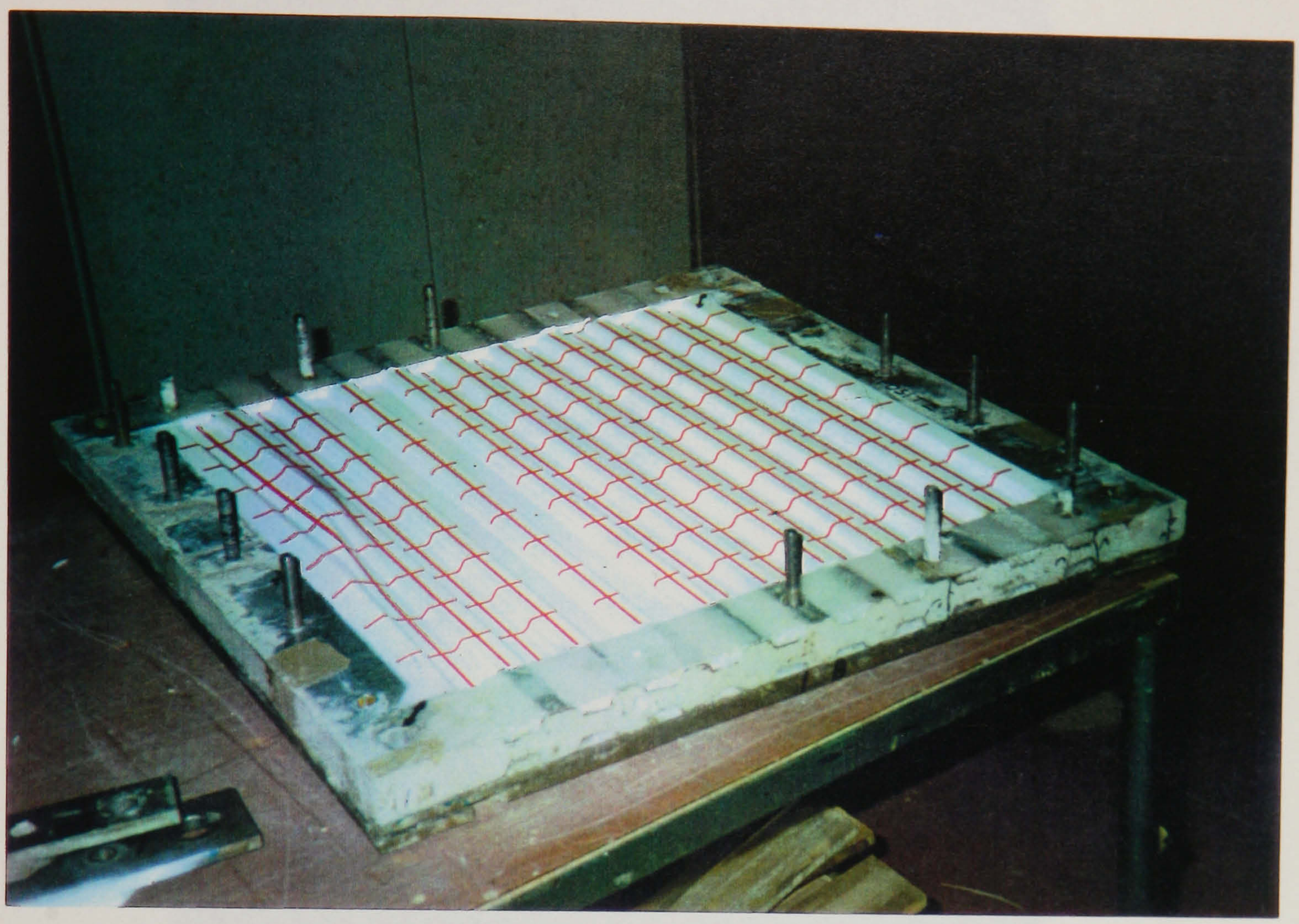

Photograph 6.1: Failure of composite wall 1

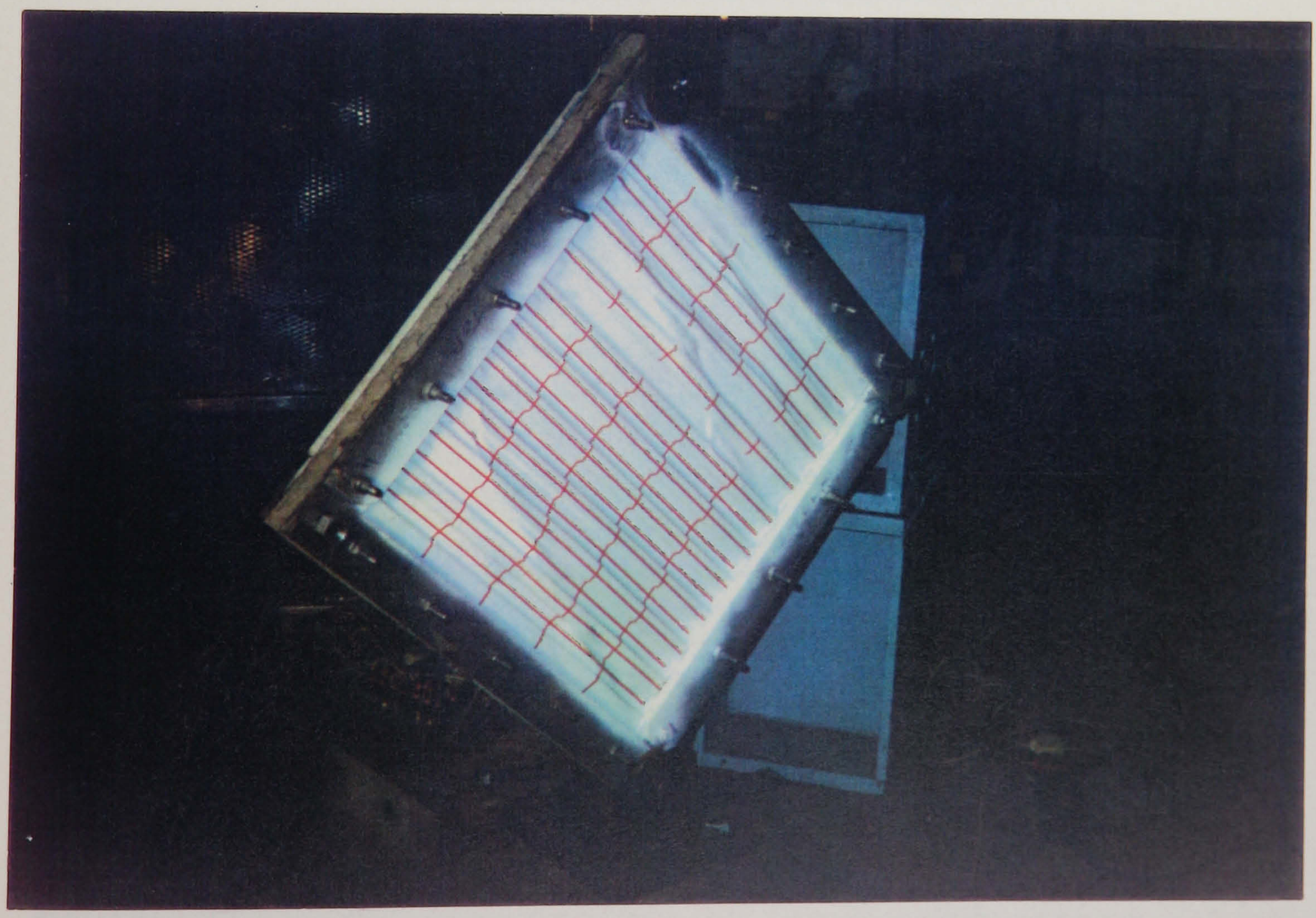

Photograph 6.2: Failure of composite wall 3

Photograph 6.3: Development of tension field in plain composite wall

Photograph 6.4(a): Cracking in concrete core (Test 1)

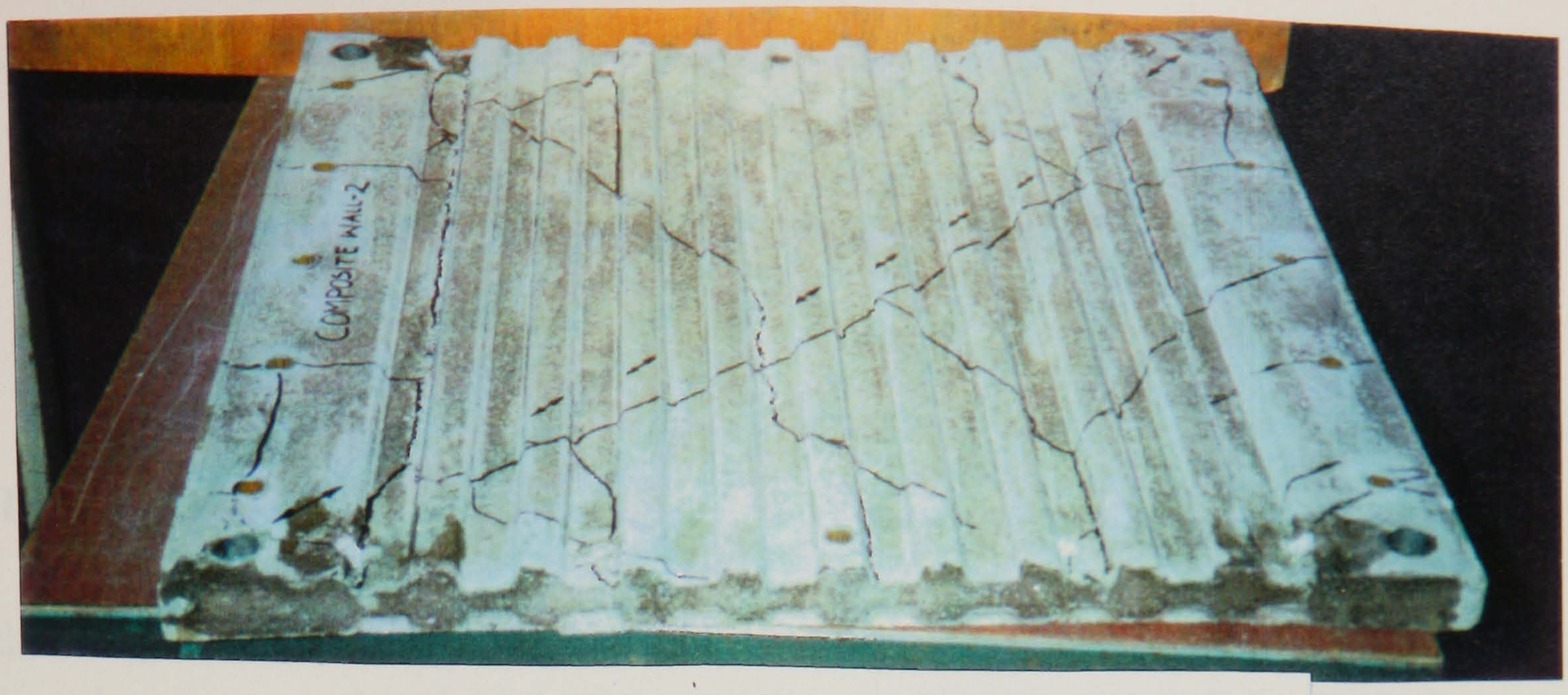

Photograph 6.4(b): Cracking in concrete core (Test 2)

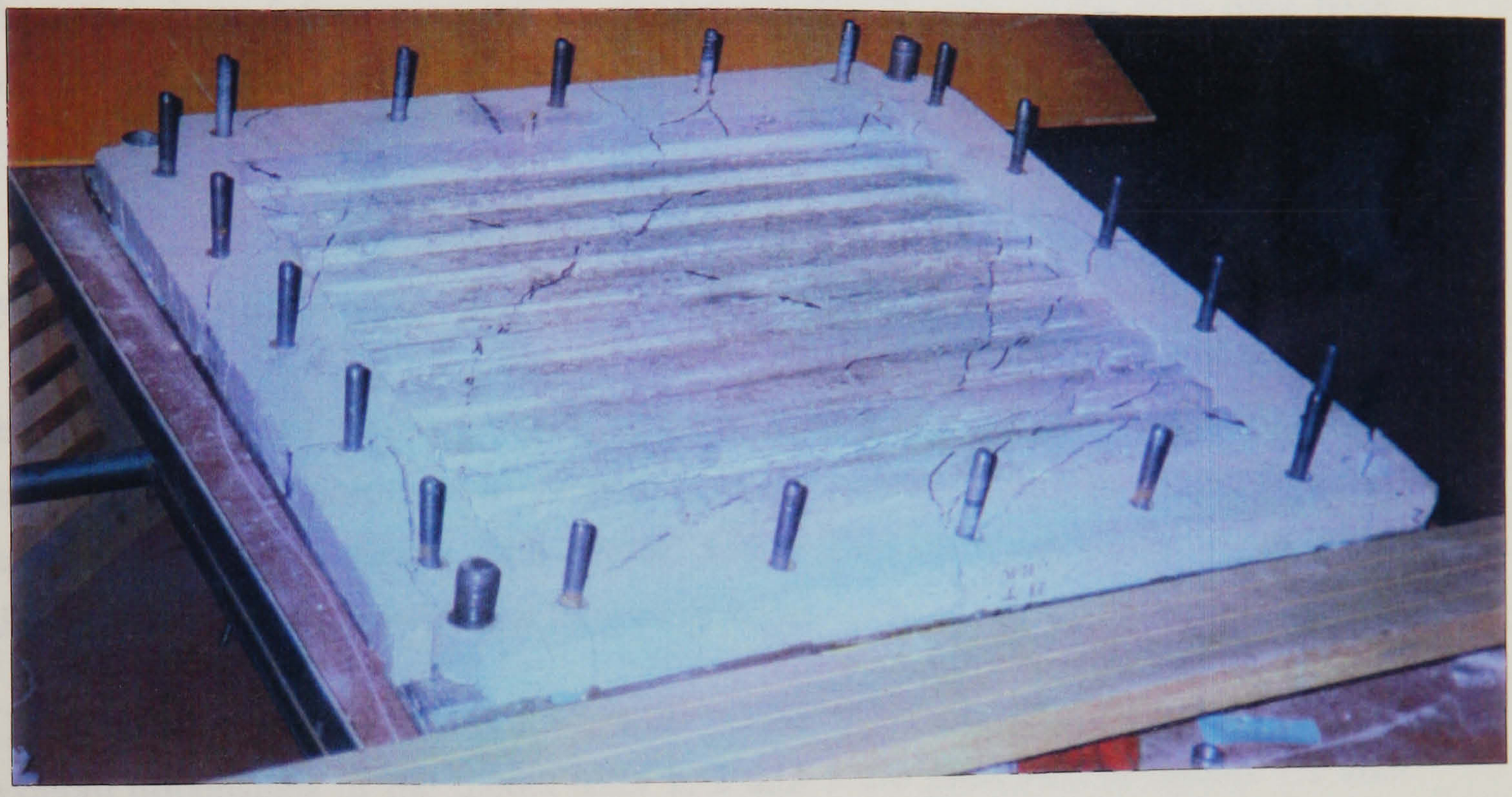

Photograph 6.5: Cracking in concrete core (Test 5)

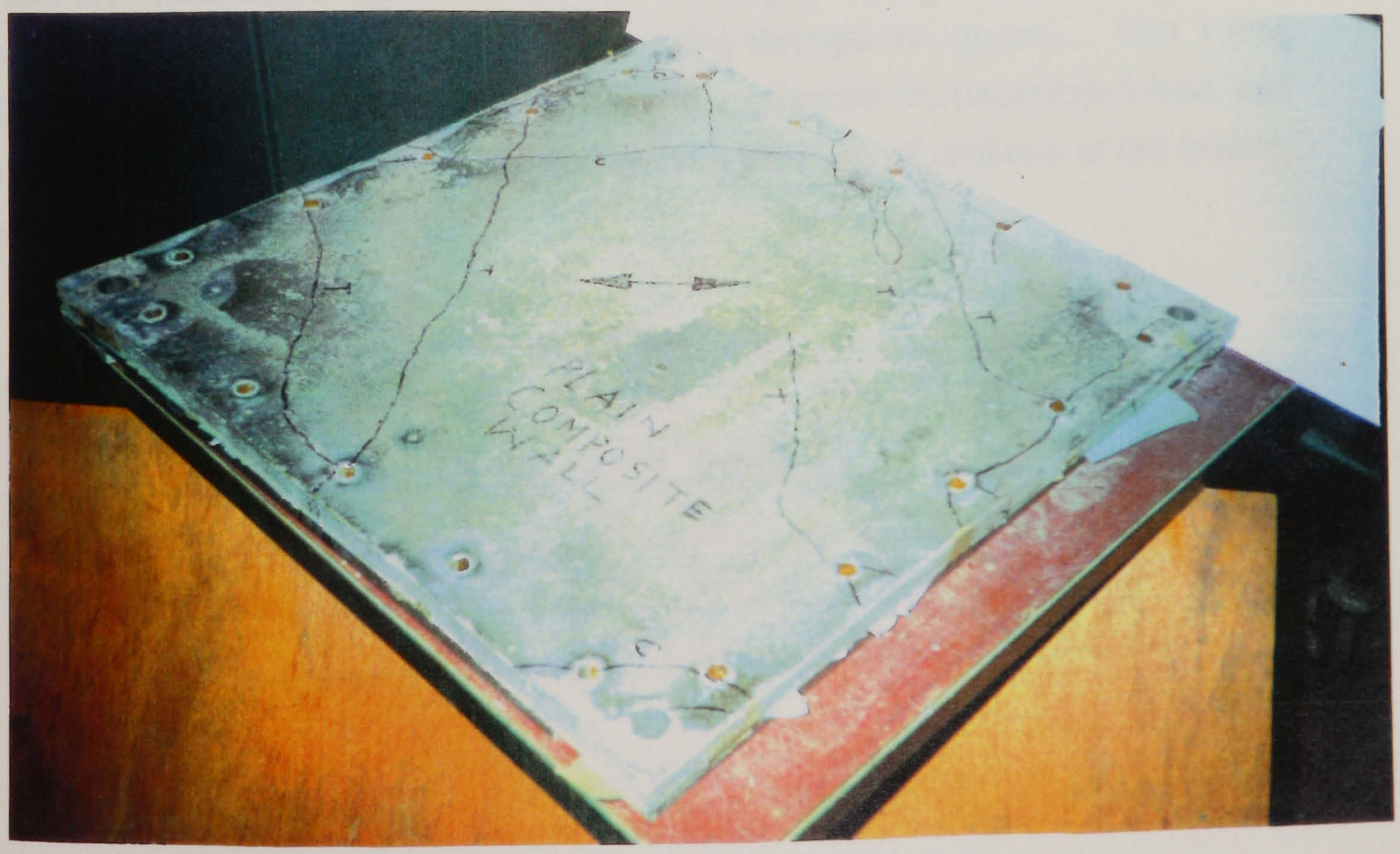

Photograph 6.6: Cracking in concrete core (Test 6)

CHAPTER SEVEN

COMPOSITE WALL AS BEAM ELEMENTS

7.1 Introduction

In this chapter, the behaviour of the composite wall as simply supported beams subjected to a concentrated load at the centre span allowing the wall to undergo bending and shear deformation will be described. Small scale model tests have been performed to investigate the behaviour along with analytical and finite element analysis.

7.2 Small-scale model tests

Three tests have been performed with different span-depth ratios. The tests provided information on load-deformation response, strain characteristics including flexural, shearing and principal strains, and overall failure characteristics of the walls. The model tests will be described in the following steps:

7.2.1 Dimension and instrumentation

The detail dimensions of the model tests 1, 2 and 3 are presented in figures 7.1 and 7.2 and also tabulated in table 7.1 Pairs of sheeting were connected together at the ends and at the centre by threaded rods passing through the spacers. Test 1 was performed without bearing plates at the point of application of concentrated load and as a result the panel suffered bearing failure with crushing of concrete at the loading point.

Table 7.1 : Dimension of the model test walls

Test No	Effective span b in mm	Depth, a in mm	Width crest trough	b/a	Bearing plate
1	590	250	30 14	2.36	no
2	590	240	30 14	2.46	yes
3	590	140	30 14	4.21	yes

To avoid the bearing failure at the point of application of load in model tests 2 and 3. the loaded point was strengthened by using bearing plates in the concrete connecting the sheeting by threaded rods with nuts and washers as shown in figure 7.1 and 7.2.

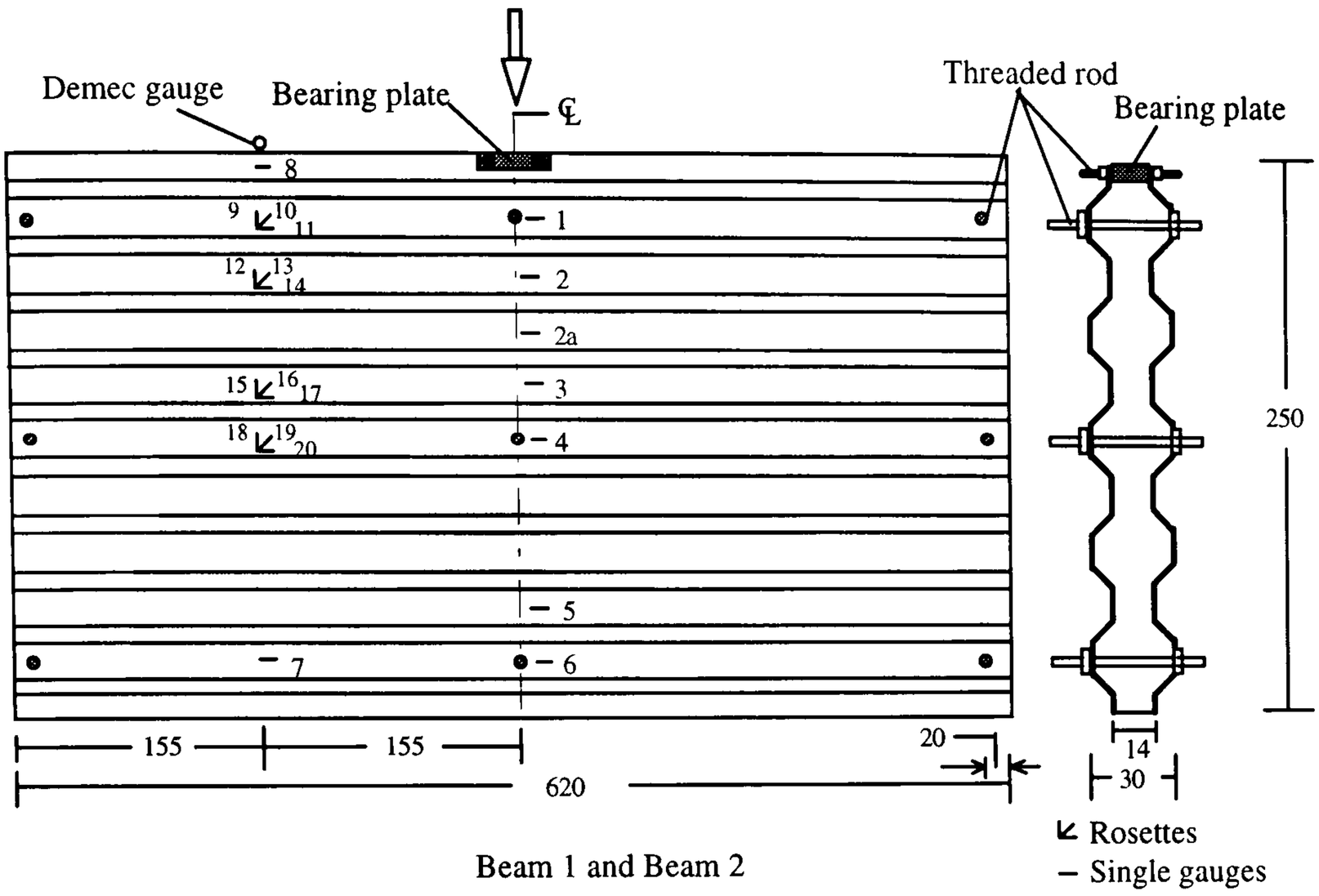

Beam 1 and Beam 2

Figure 7.1: Beam 1 and Beam 2 details

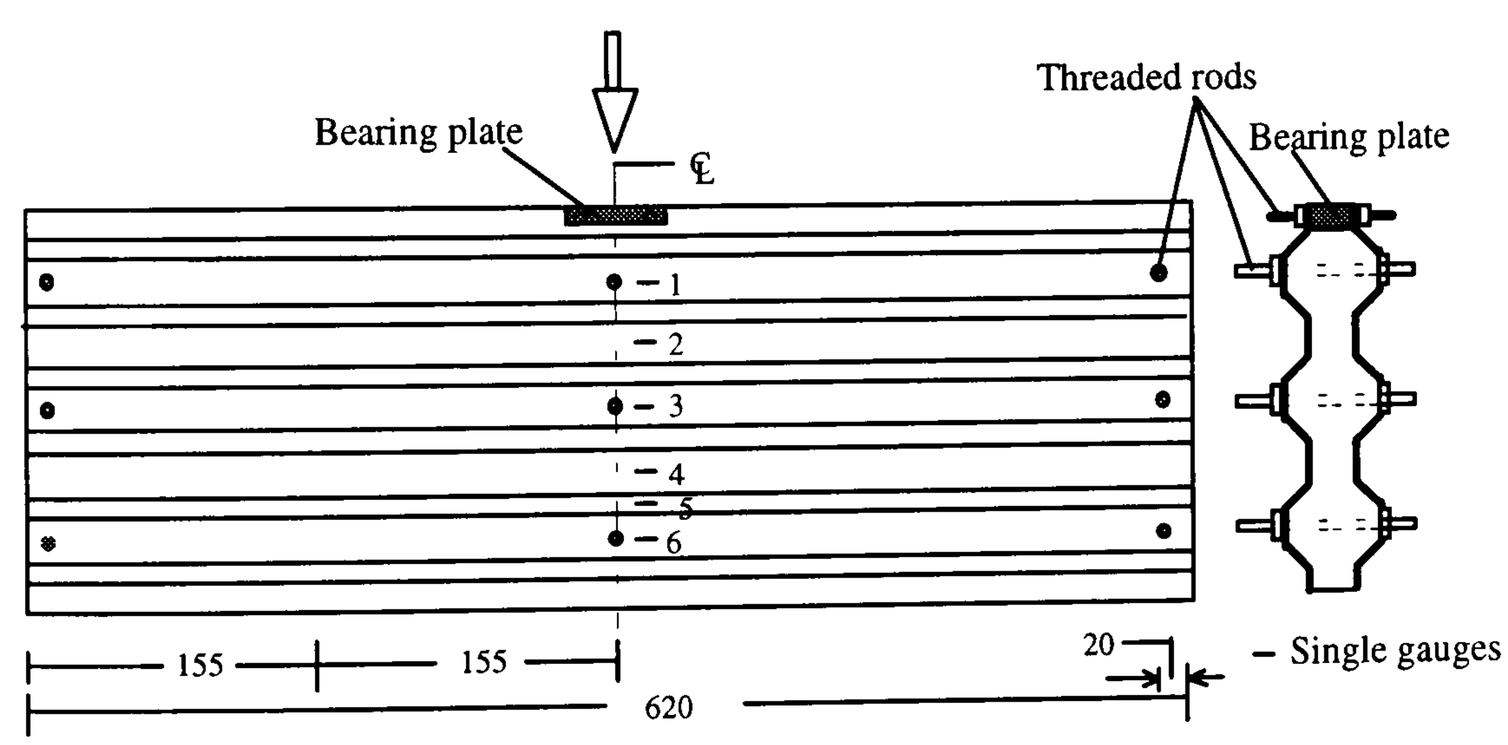

Beam 3

Figure 7.2 : Details of beam 3

7.2.2 Casting of micro-concrete

The steel sheets were connected together using all the threaded rods at the centre and ends maintaining correct spacing with the help of spacers. The sheeting assembly was then placed on a wooden mould having a wooden base and side boards as shown in figure 7.3. The process of casting and curing was similar to those described in earlier chapters.

7.2.3 Instrumentation

The location of strain gauges for test 1 and test 3 are also shown in figures 7.1 and 7.2. The strain gauges were installed on the steel surface. Due to smaller model thickness, it was not possible to install any concrete gauges in concrete. A demec gauge was installed in the concrete in test 1 as shown in figure 7.1 to monitor the concrete strain but the strains monitored were not found satisfactory. In test 2 no strain gauges were installed.

7.2.4 Experimental set-up

The schematic of the experimental set-up is shown in figure 7.4. Model walls were placed in between the guide angles which provided lateral supports to keep the wall in vertically upright position and prevented any tilting. Paddings were used in between the specimen and the guide angles. The assembly of guide angles and roller and pin supports were fabricated on an I-beam base strengthened by stiffening plates. The specimens were then tested by applying concentrated load using the small hydraulic cylinder having a capacity of 25 kN of the DARTEC machine. Dial gauges and LVDT were used to measure central deflection. The strain and displacements were recorded by the computer aided data acquisition system.

7.3 Test observations

The tests were performed by applying a concentrated load on the mid-span of the simply supported composite wall beam specimens. The load was increased incrementally and at each load increment the strains and displacements were recorded. The variation of central deflections from test 1 and 3 are shown in figures 7.5.

Beam 1 suffered local crushing of concrete just at the point of concentrated load at about 4.5 kN which cause an increase in deflection in the load-deflection curve. The beam was then unloaded and then reloaded. The reloading branch shows a gradual increase in load up to 9 kN when the beam is supposed to develop major crack. Finally, the beam failed at about 16kN with the subsequent development of cracks at the mid span, near the support and by crushing of concrete at the loaded point. The failed beam is shown in photograph 7.1. The loading roller was punched into the beam causing the profiled steel sheeting to buckle outward and twist directly beneath the loading point. As a result, the central top threaded rod beneath the loading point punched through the sheeting. The separation of the sheeting was started from the

centre and extended towards the ends. Buckling and twisting of the sheeting was restricted to the compression zone directly beneath the loading point.

The local crushing at the loaded point was avoided in beam test 2 and 3. Due to malfunctioning of the loading machine it was not possible to record the load-deflection curve for beam 2 but the sample failed at about 15kN due to cracking at mid span and local bearing at the supports.

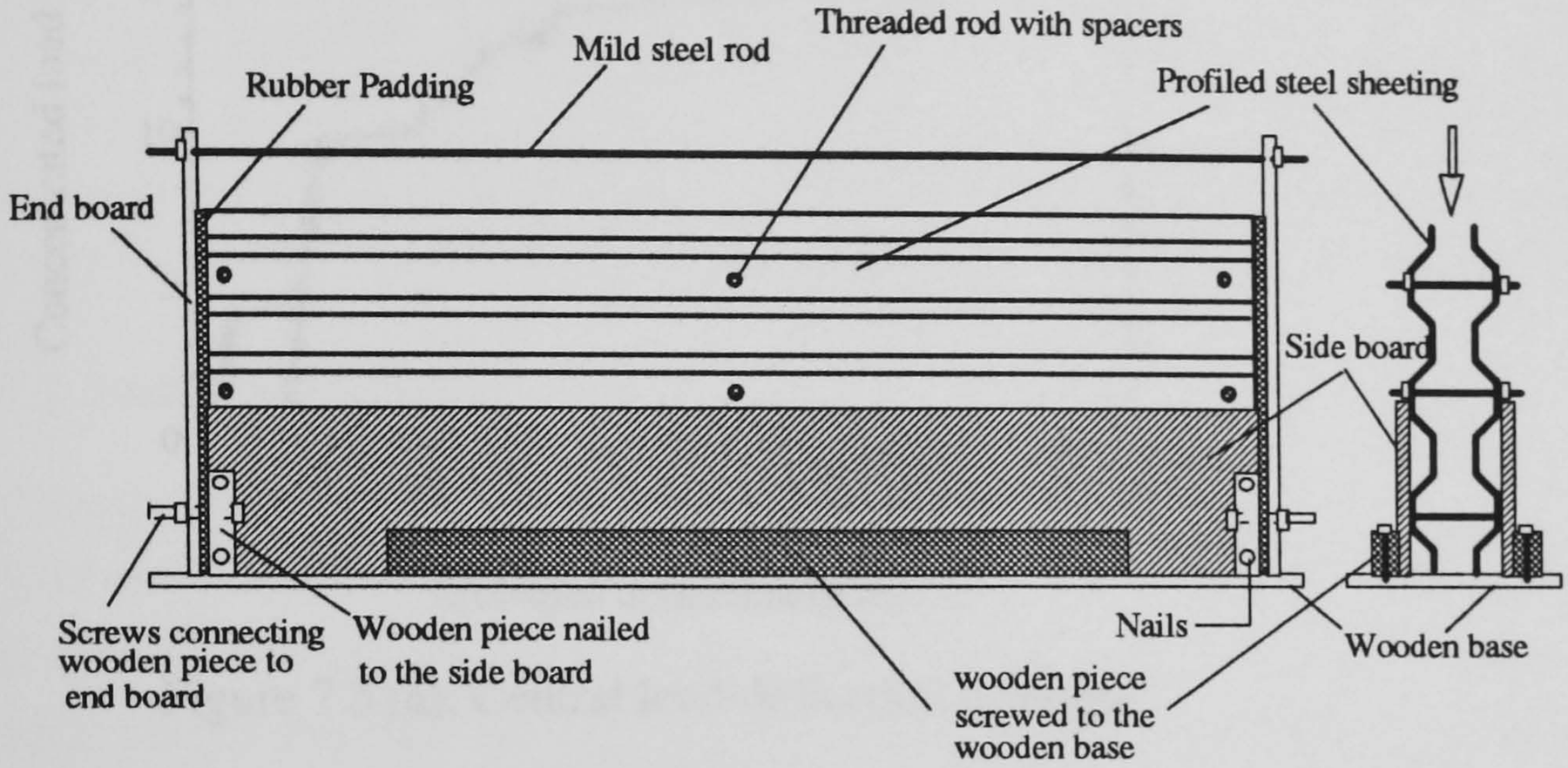

Figure 7.3: Mould assembly

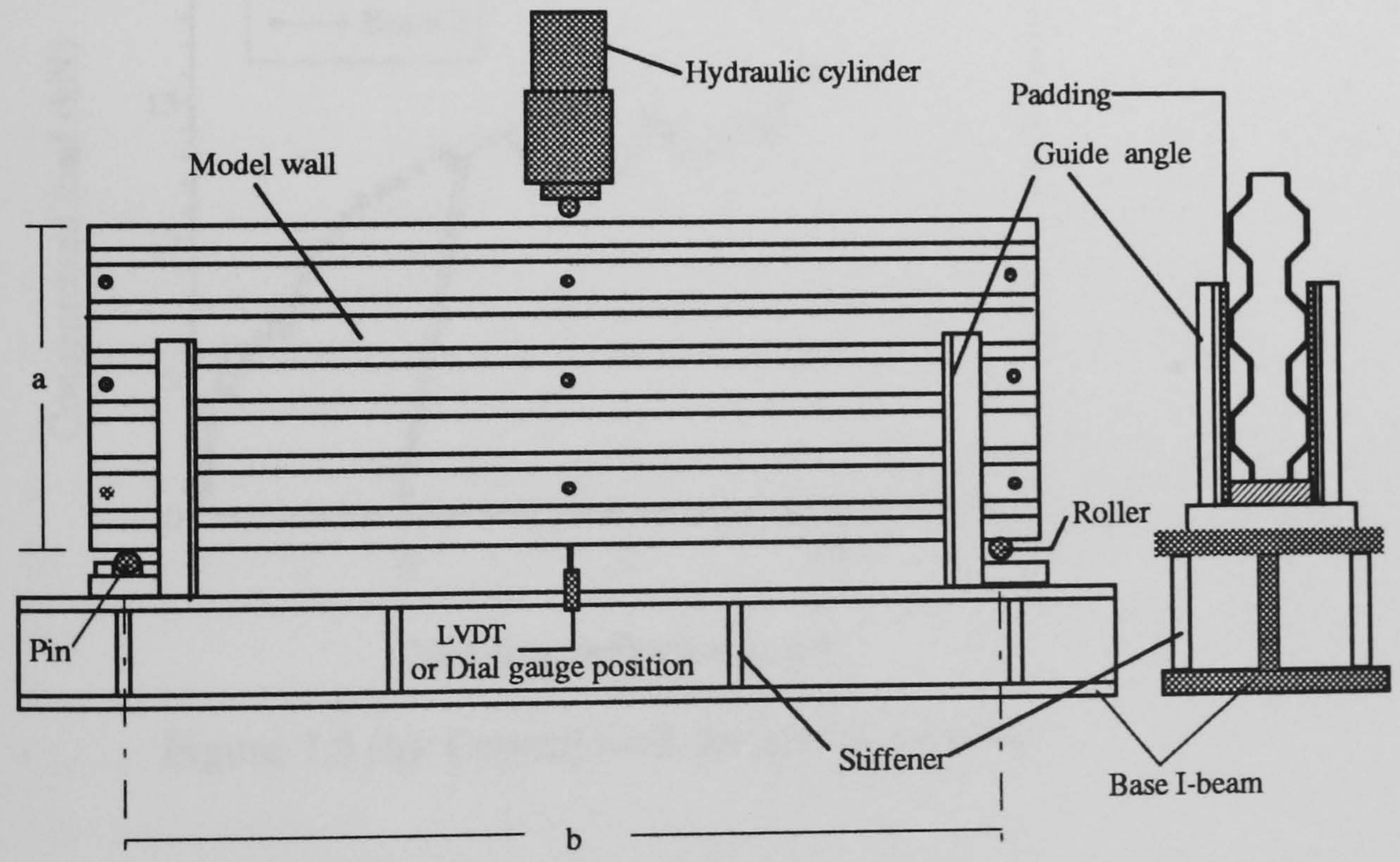

Figure 7.4: Schematic of beam test set-up

The load-deflection curve for beam 3 shows a gradual increase in deformation up to the point of cracking at about 4kN and then the load again increased until the specimen failed at about 14kN. Although the local crushing at the point of applied

load was avoided, another problem arised with the association of bearing failure of concrete and distortion of sheeting at the supports in the final stage. However, for the current research the tests provided valuable information on general behaviour and strain conditions.

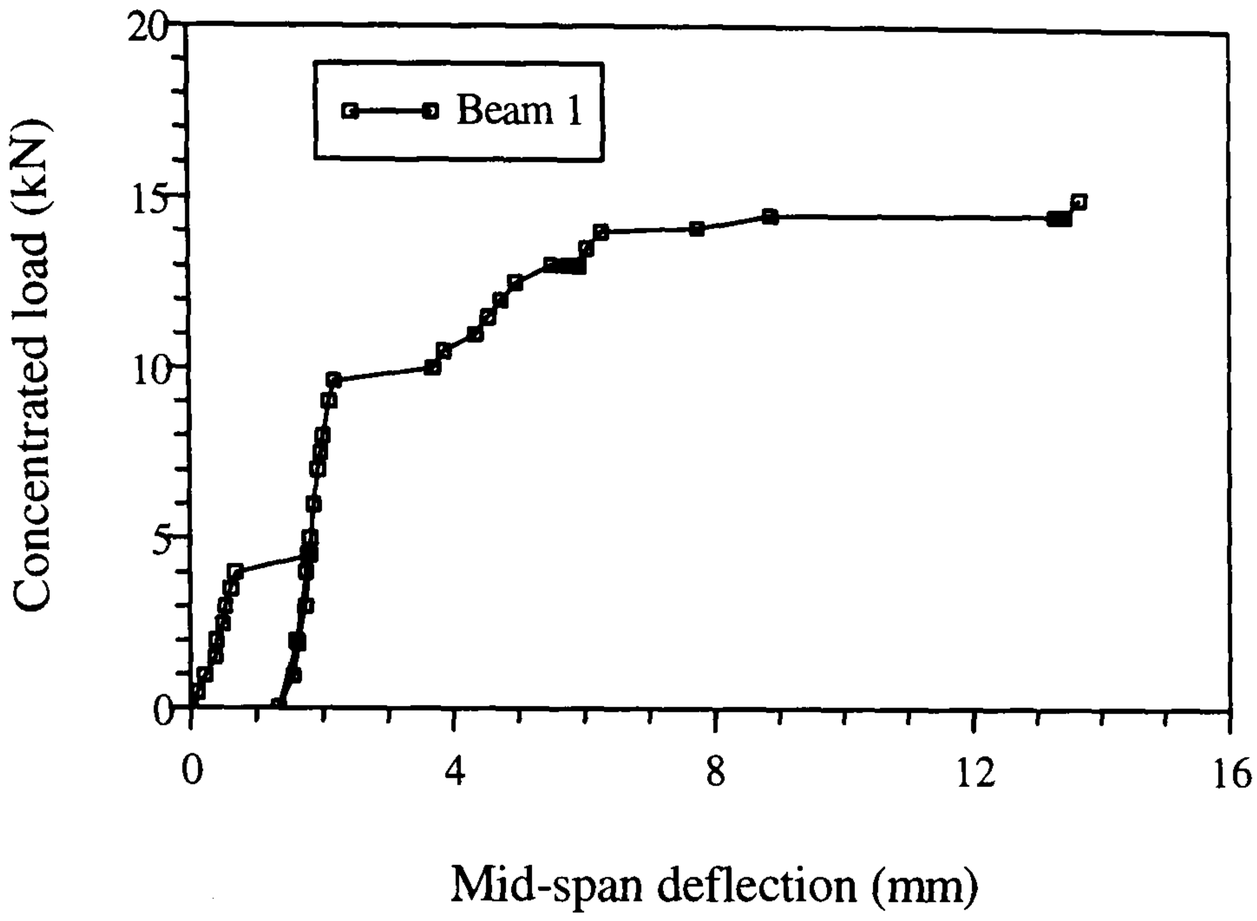

Figure 7.5 (a): Central load-deflection response

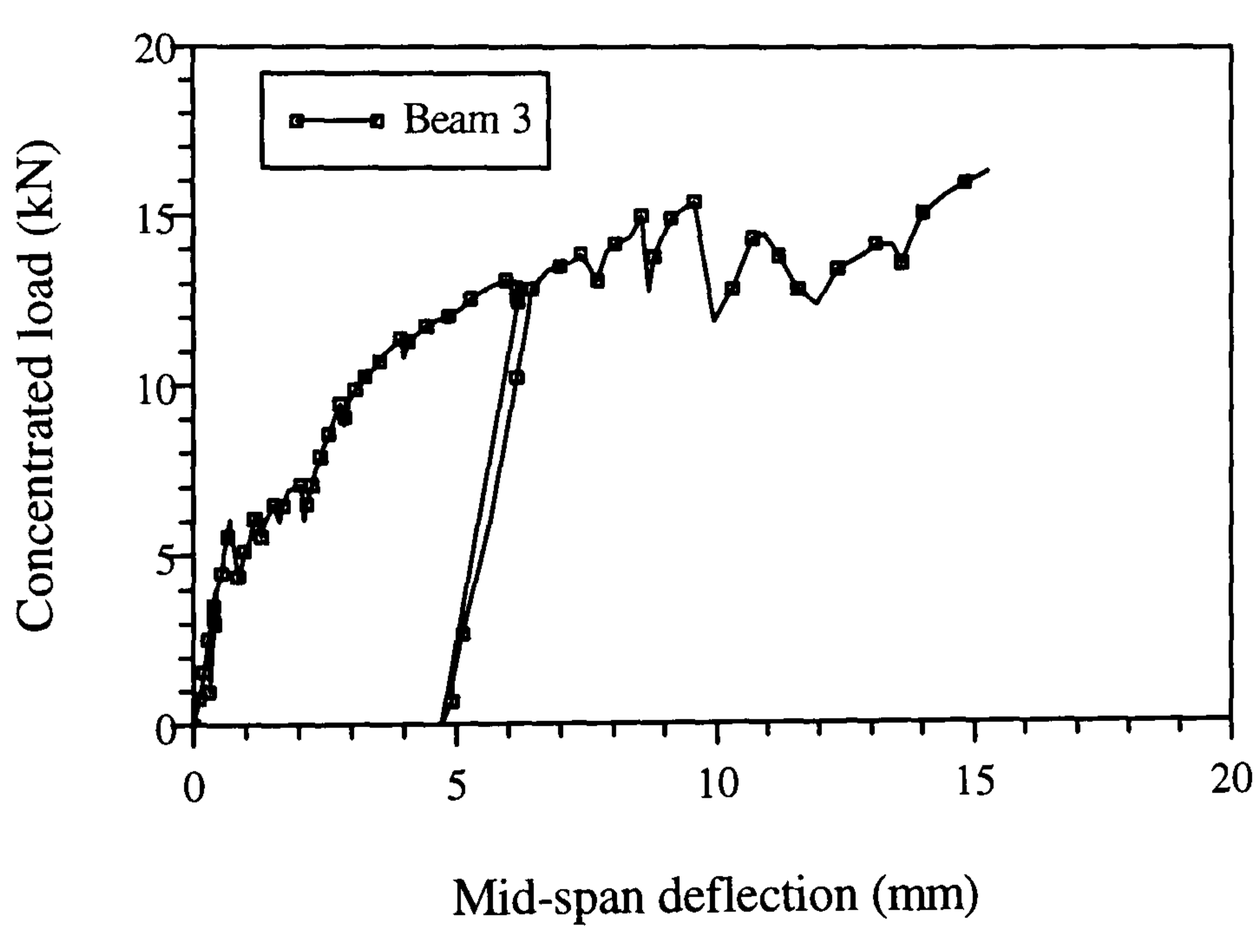

Figure 7.5 (b): Central load-deflection response

7.4 Analysis of failure modes

The crack patterns in concrete core of test 1 and test 3 are shown in photographs 7.2. The full extension of central flexural cracks indicated the flexural modes of failure. The cracks near the supports may be a consequence of shear crack or a bearing

failure at the supports. Therefore, the failure load may be governed by either flexure or shear or bearing modes.

The material properties for concrete in the model test are tabulated in table 7. 2 .

Table 7. 2 . Concrete properties : Beam tests

Test No.	Wet density	Compressive Strength Cylinder f'_c	Cube f_{cu}	Tensile Strength Split cylinder	Age Days	Ratio f'_c/f_t
	kg/m^3	N/mm^2	N/mm^2	N/mm^2		
1	2260	17.70	17.20	1.782	36	9.93
2	2253	20.63	23.67	1.88	34	10.97
3	2241	21.00	25.90	1.94	19	10.82

7.5 Analysis of strains

Flexural strains

The variation of flexural strains across the depth of the beam 1 at mid span in the pre and post cracking stages is shown in figures 7.6. The variation is similar to that of ideal beams with maximum stresses at the top and bottom fibres with zero values at neutral axis. The flexural strain in the bottom fibre exceeds the concrete tensile strain (0.00015) at about 4.5kN.

The variation of flexural strains for beam 3 is shown in figure 7.7, and represented similar behaviour like test 1. In this case, the bottom fibre strain seems to exceed the tensile cracking strain of concrete at about 2 kN. The tensile strain at g-6 (near the bottom fibre) exceeds the yield strain of steel at around 14 kN.

After cracking, the position of zero strain for both beams started to change gradually its position and moving towards the compression zone as identified from figure 7.6 and 7. 7.

Flexural strain at quarter span

The variation is similar to that of mid span (figure 7.8(a)) and it is clear that the strain at crest section (g-11) is lower than that at trough section (g-14) although g-11 is furthest from the neutral axis. Therefore, the strain variation is affected by the profiles shape of the cross section. The flexural strains at mid and quarter span are compared for beam 1 in figure 7.8(b). The strain at quarter span is lower than those at mid span as usual.

Principal strains

The variation of principal strains is shown in figure 7.9. Comparing the strains at trough and crest sections, it seems to be that the strains are higher near the neutral axis than those away from the neutral axis. The principal directions are found to be increased from the outer fibres (around 4 degree) towards the neutral axis (around 42 degree) (figure 7.10).

Shearing strain

The variation shown in figure 7.11 confirms that the shearing strain is zero at the outer fibres and maximum at the neutral axis. The variation is not a parabolic one due to the profiled shape of the cross section. The trough section are strained higher than the crest section with higher thickness.

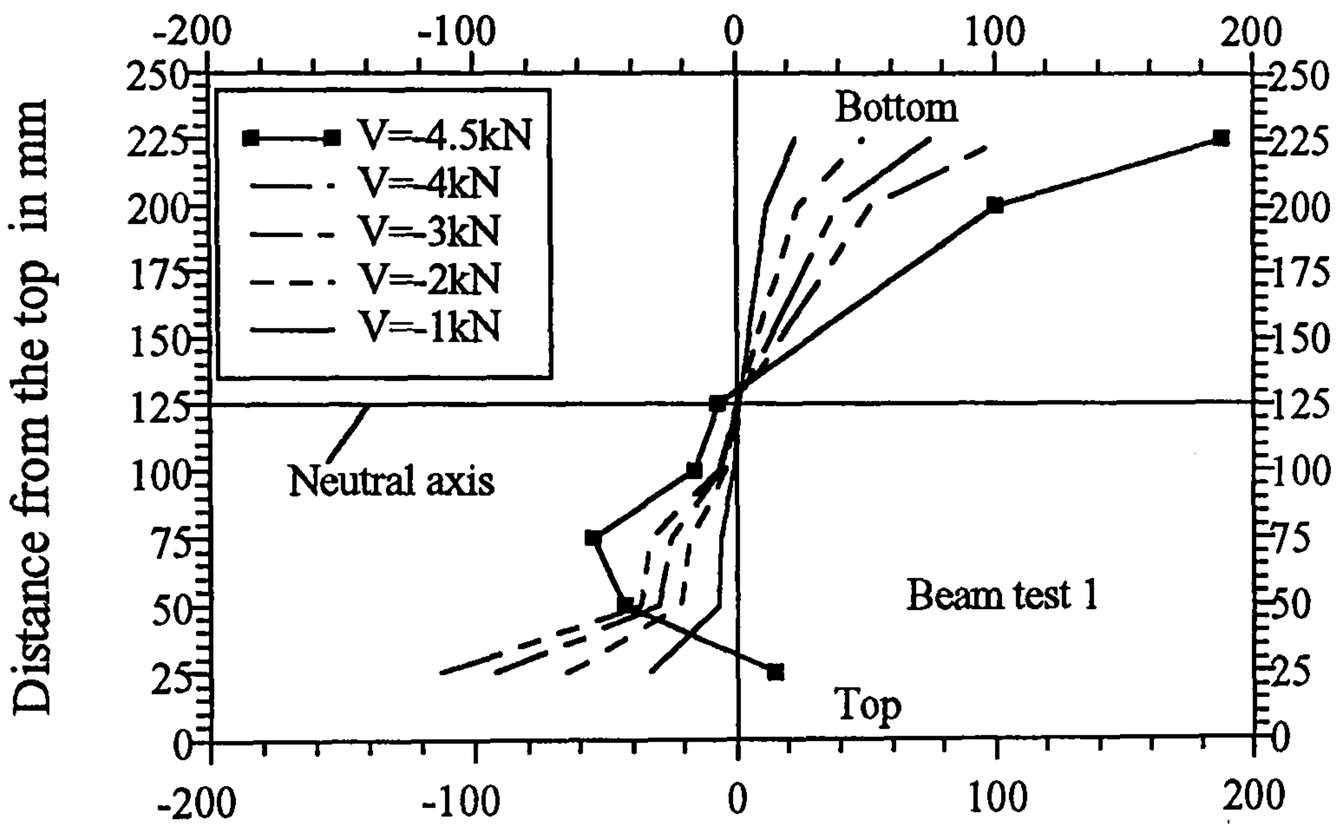

Figure 7.6(a)

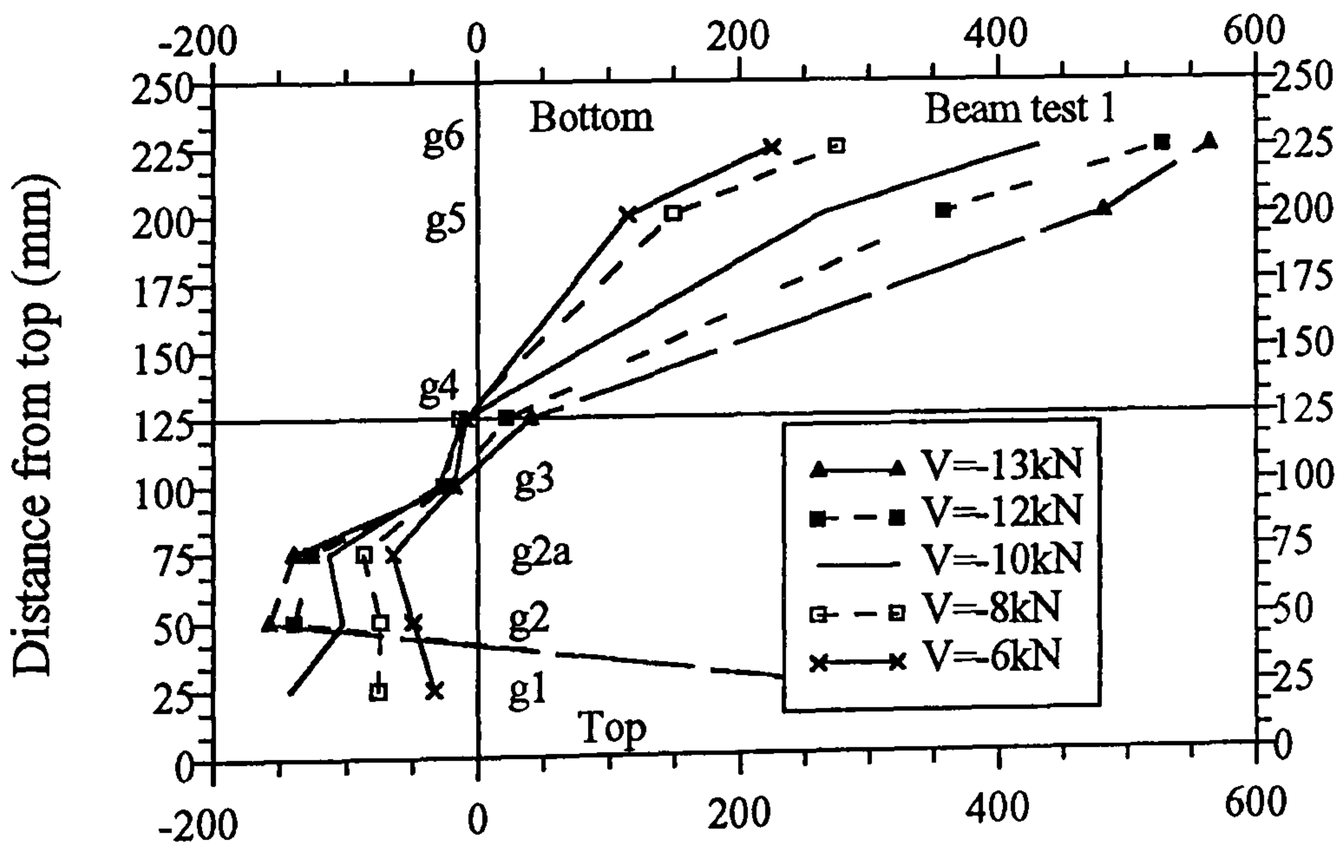

Figure 7.6(b)

Figure 7.6: Variation of flexural strains

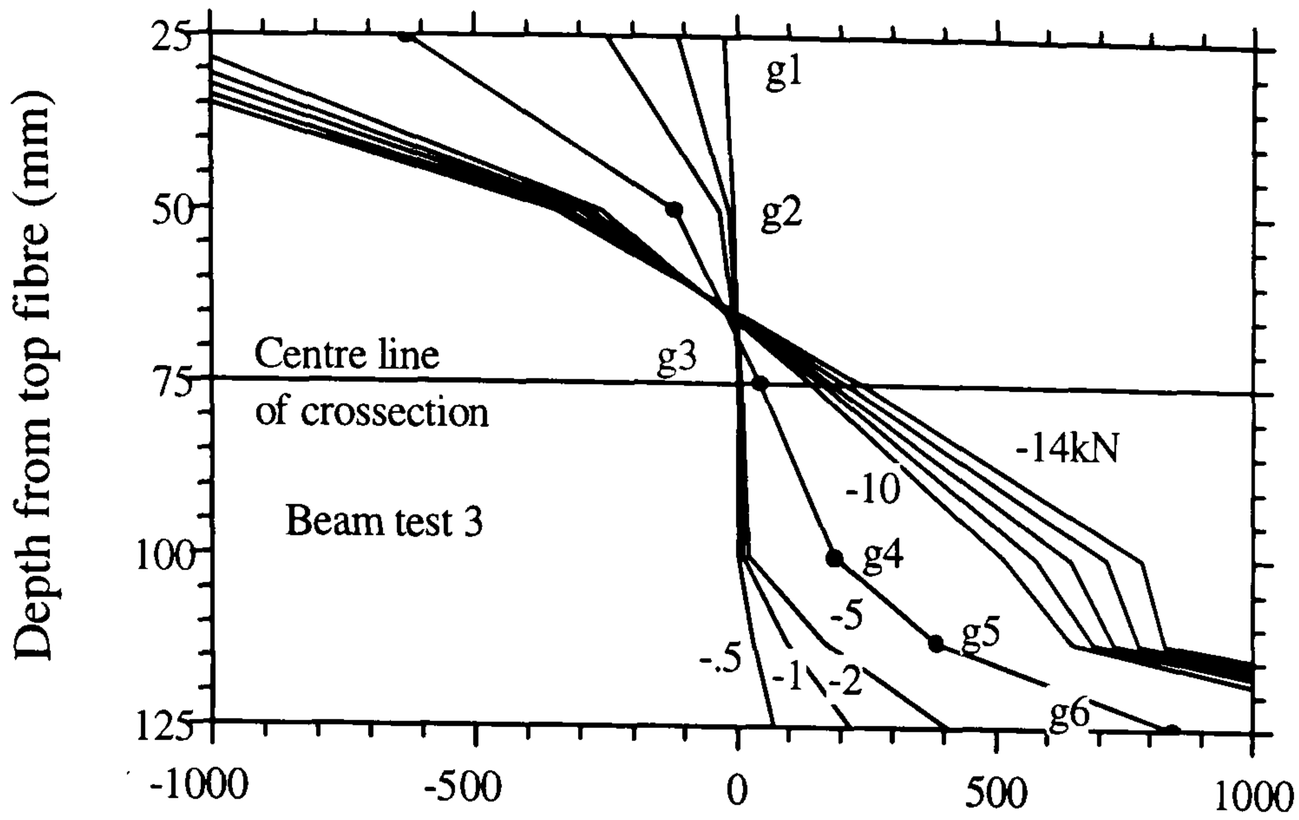

Figure 7.7: Variation of flexural strains

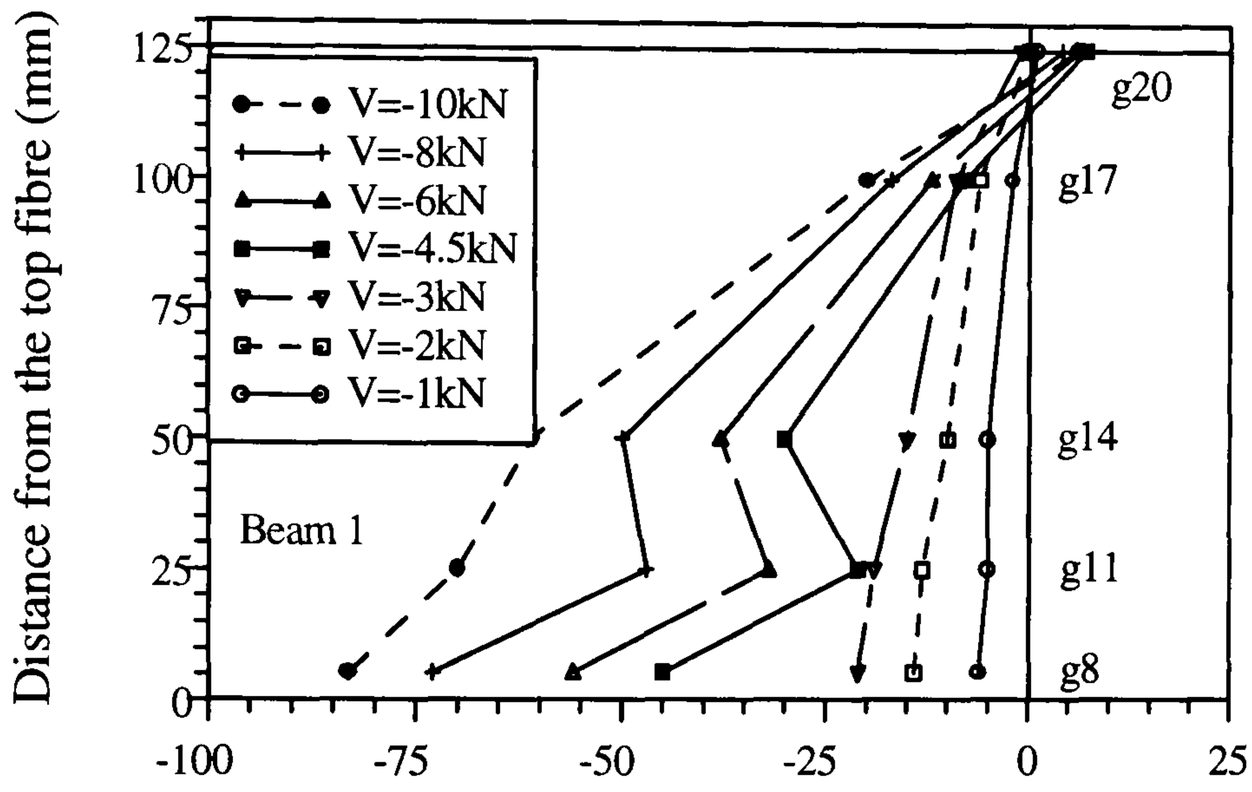

Figure 7.8(a)

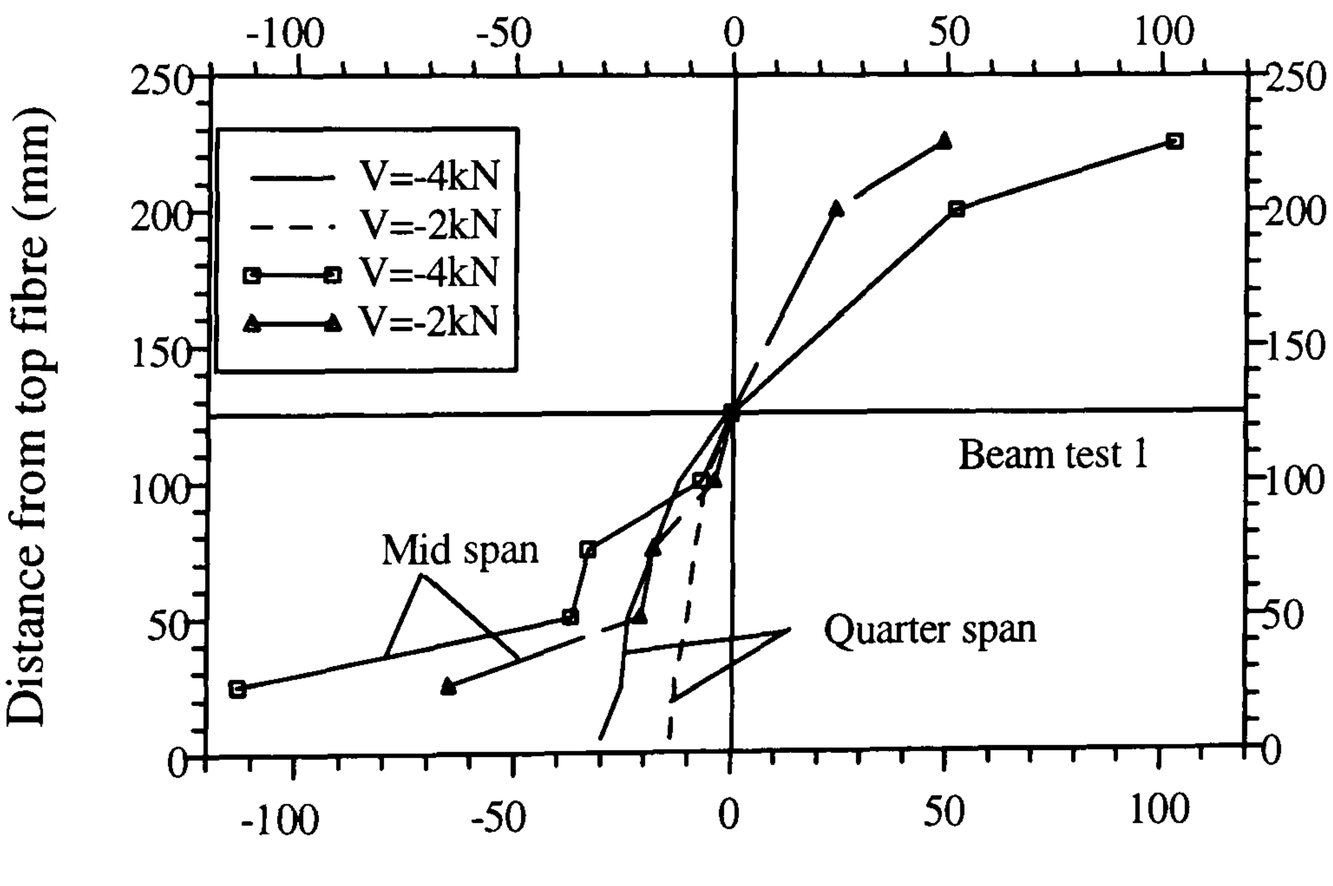

Figure 7.8(b): Mid and quarter span comparison

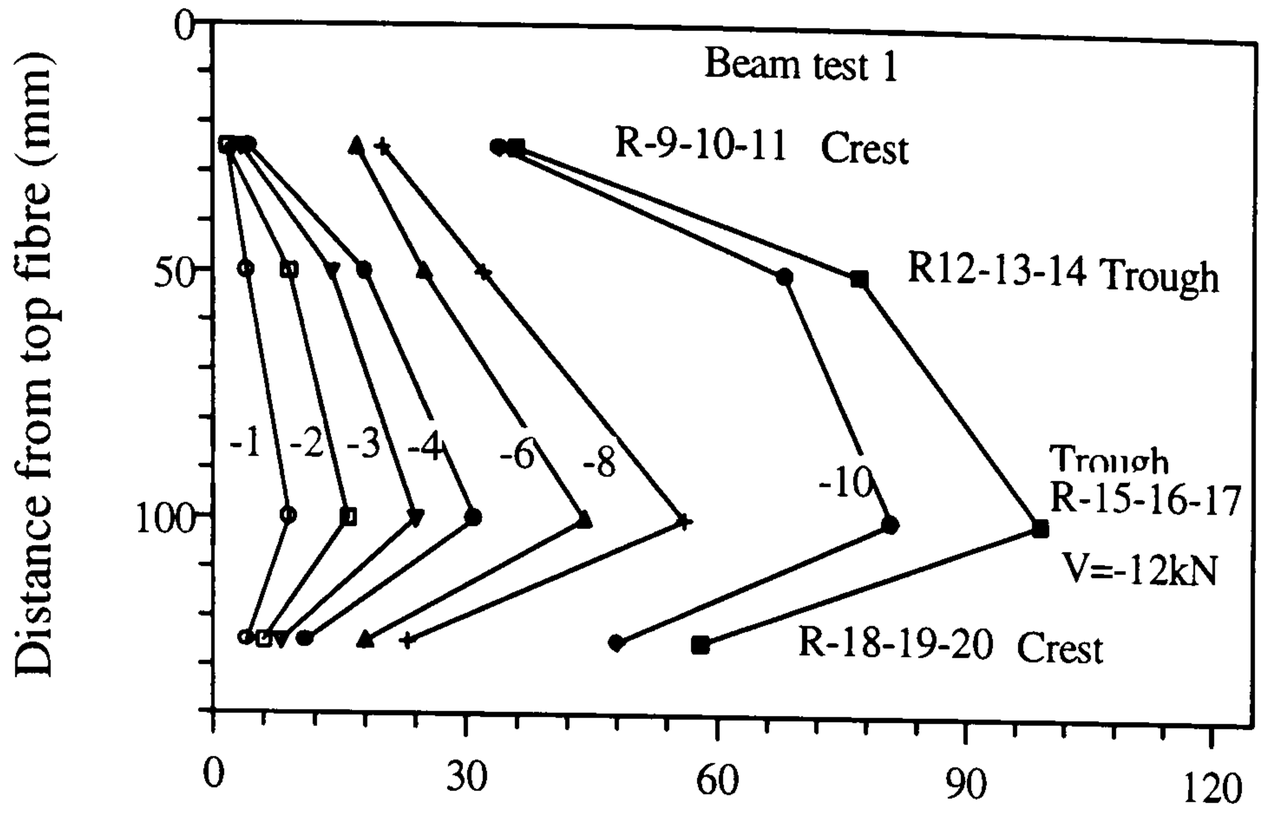

Figure 7.9: Principal strain variation

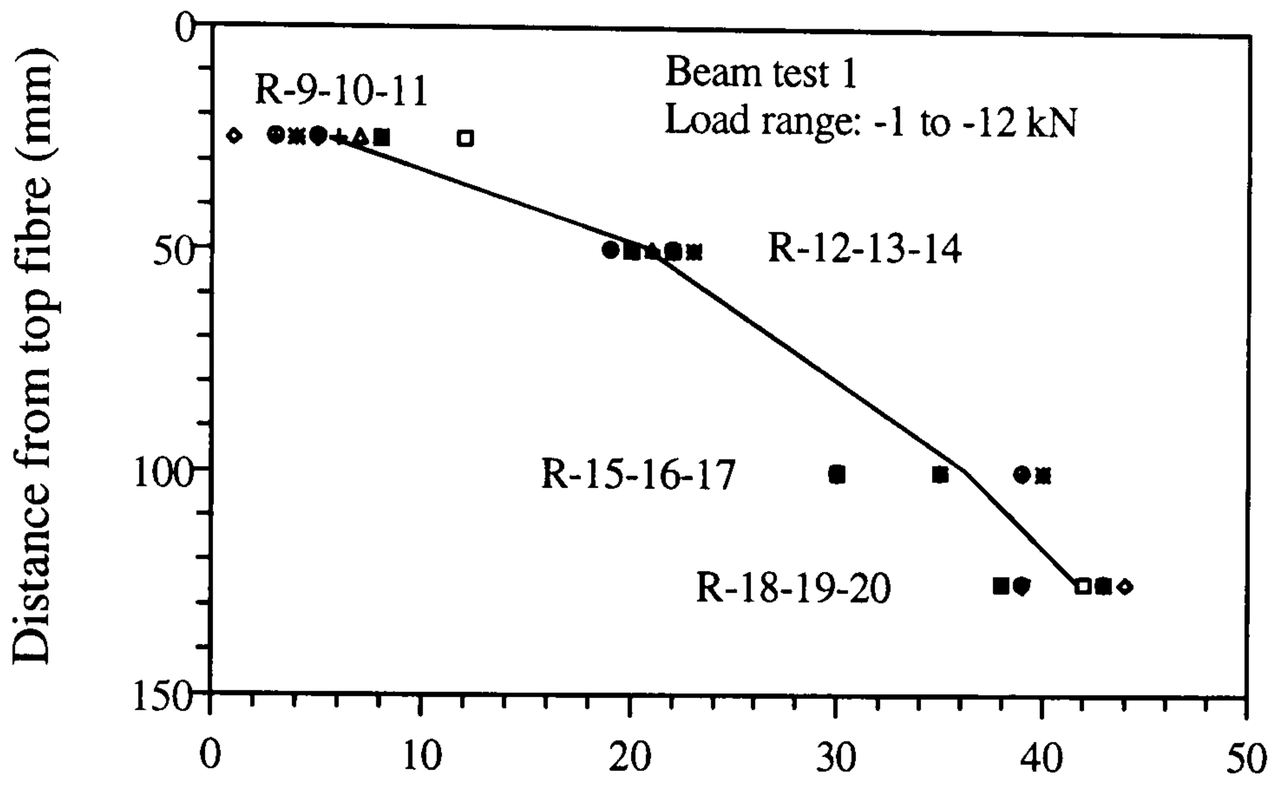

Figure 7.10: Principal direction variation

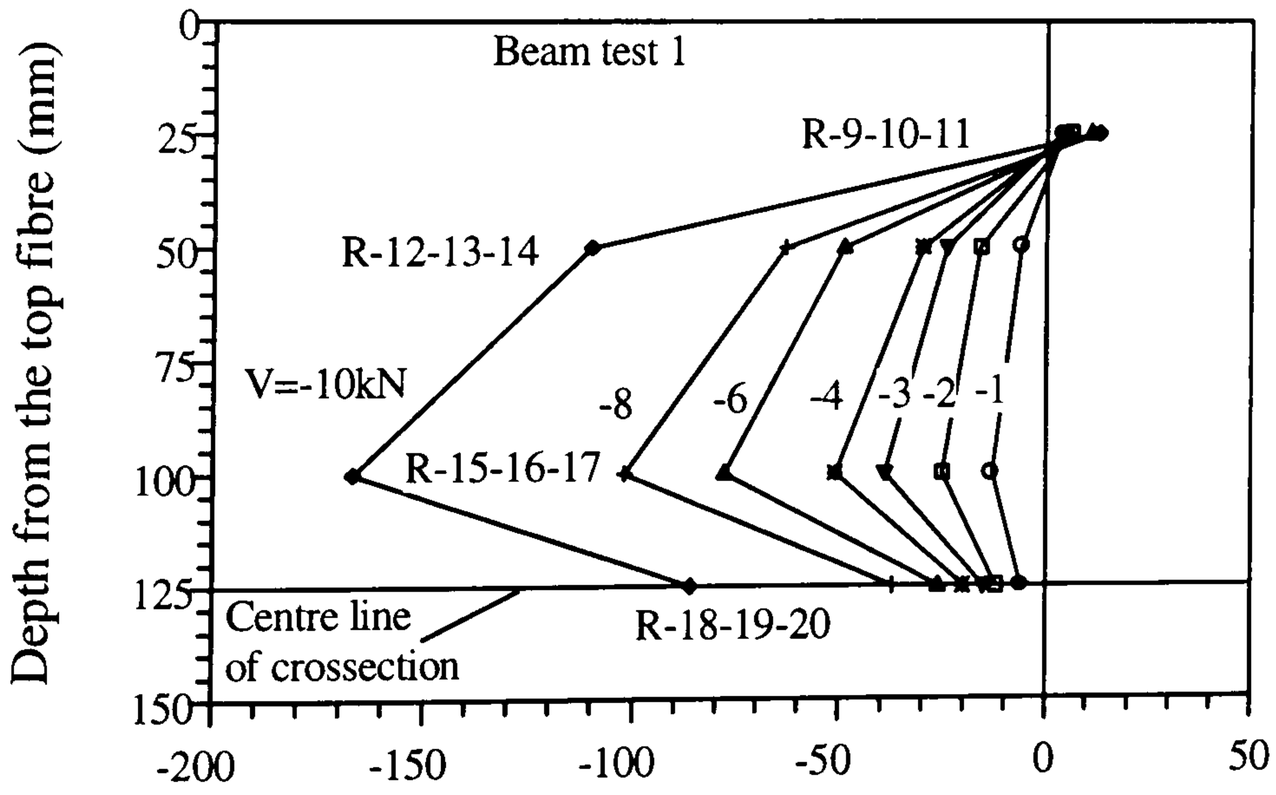

Figure 7.11: Variation of shearing strain

7.6 Analytical investigations

The strength of a beam may be governed by the flexure, shear, diagonal splitting or by bearing at the supports. The mode of failure is a function of the dimensions of the beam such as span/depth, shear span/depth, depth/thickness (slenderness) ratios and also on the reinforcement in the beam. According to the CIRIA Guide 2 (1977), if the span/depth ratio of a simply supported beam is less than 2 the beam should be considered as deep beam. According to this recommendation, the model beams 1, 2 and 3 do not fall into the deep beam category.

7.6.1 Analytical model development

The composite wall beam element as shown in figure 7.1 can be simplified according to Oehlers, Wright and Burnet (1994) as an equivalent rectangular beam as shown in figure 7.12. The effective width of the beam t_{eqc} can be taken as the width of a rectangular block that encloses the same area as the profiled beam. The equivalent thickness of steel can be calculated from

$$t_{eqs} = \alpha t_s \quad \text{.....(7. 0)}$$

where α is the ratio of developed length of the profile to is projected length.

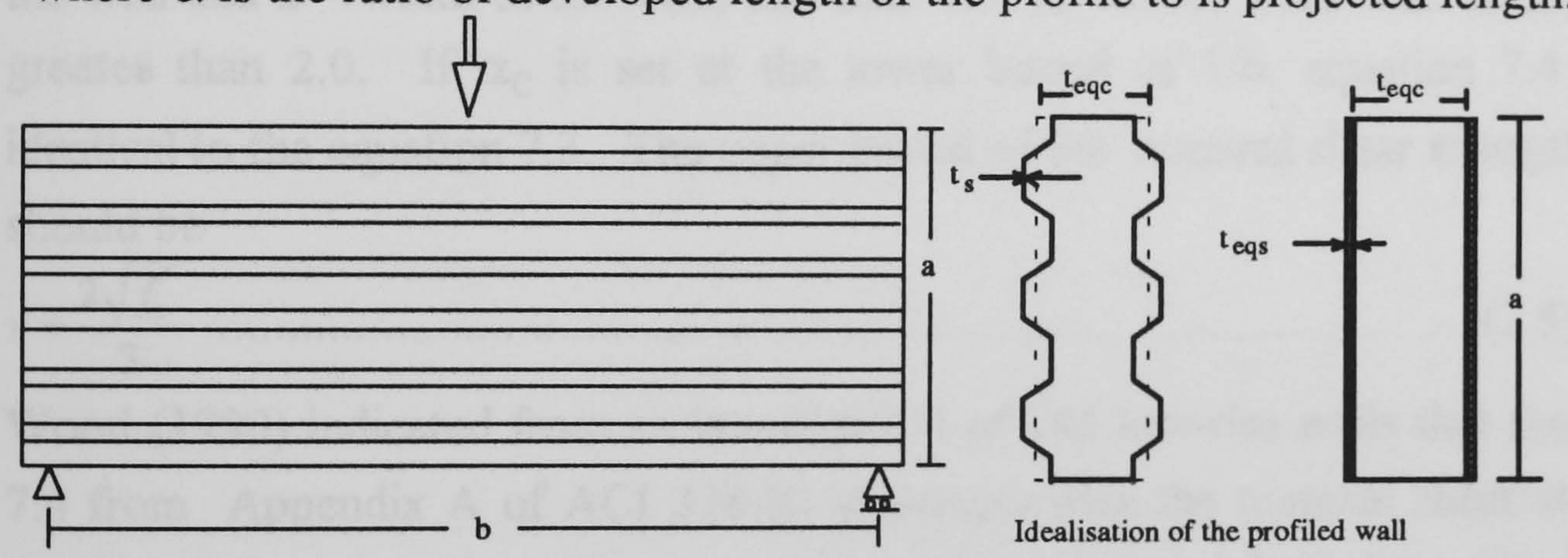

Figure 7.12: Equivalent rectangular beam

7.6.1.1 Model for Shear strength

Existing equations

The truss analogy was developed around the turn of the Century (Wood, 1990), as a means of relating the applied shear to the tensile stresses in the web reinforcement of reinforced concrete beam. The beam is idealised as a truss, where the bottom chord represents the longitudinal reinforcement, the top chord represents concrete in compression zone, compression web members by concrete in the web and the tension web members by the stirrup. The relationship between the average shear stress in the beam, v, and the tensile stress in the vertical web reinforcement f_v, assuming the angle between the longitudinal axis and the compression strut as 45^0, can be written as:

$v = r f_v$ .....(7.1)

where r is the web reinforcement ratio. The equation 7.1 is latter modified to take account the contribution of uncracked concrete in the compression zone and deviation of the direction of diagonal compression from 45^0 in actual situation as :

$v = C + rf_v$ .....(7.2)

where C is the concrete contribution dependent on the quality of concrete and amount of web reinforcement.

The simplest expression similar to equation 7.2 given in ACI 318-83(1983) for calculating the nominal unit shear strength of beams subjected to flexure and shear is :

$$v_n = \frac{\sqrt{f_c'}}{6} + \rho_n f_y \quad \text{in MPa} \qquad \text{.....(7.3)}$$

where v_n is the nominal unit shear strength, ρ_n is the reinforcement ratio for the vertical web reinforcement and f_y is the yield stress of the vertical web reinforcement. The nominal shear strength of walls presented in Appendix A of ACI 318-813 is closely related to the nominal shear strength beams defined in equation 7.3

$$v_n = \alpha_c \sqrt{f_c'} + \rho_n f_y \qquad \text{.....(7.4)}$$

where α_c varies linearly from 0.25 for walls with an aspect ratio of b/a (b= height of the wall and a = width of the wall) less than 1.5, to 1/6 for walls with an aspect ratio greater than 2.0. If α_c is set at the lower bound of 1/6, equation 7.4 becomes identical to the equation 7.3. The upper bound of the nominal shear strength of walls should be

$$v = \frac{2\sqrt{f_c'}}{3} \qquad \text{.....(7.5)}$$

Wood (1990) indicated from an investigation of 143 low-rise walls that the equation 7.4 from Appendix A of ACI 318-83 underestimates the nominal shear strength of lightly reinforced walls. The suggested shear strength of the low rise reinforced concrete walls is of the form :

$$v = 0.5\sqrt{f_c'} \quad \text{.....lower bound}$$
$$= \frac{5}{6}\sqrt{f_c'} \quad \text{..... Upper bound} \qquad \text{.....(7.6)}$$

Model for composite wall beam

The equation 7.4 may be used to determine the shear resistance of the profiled composite wall beam by using the upper and lower bound values of shear tress suggested by ACI 318-83 and Wood (1990). The main problems associated with the composite wall or beam is the degree of compositeness of sheeting and concrete and the role of sheeting as web reinforcement resisting diagonal tension. Assuming full composite action and considering the cross section of the wall or beam as an

equivalent concrete, the shear resistance V_{wb} of the profiled composite wall or beam element can be written as:

$$V_{wb} = va\left[t_{eqc} + 2nt_{eqs}\right] \quad \text{.....(7.7)}$$

The values of v can be taken from equations 7.5 and 7.6.

Comparison between analytical and model tests

Analytical and test shear strength values are compared in table 7.3. The beam1 with an aspect ratio of 2.4 is more likely to be dominated by shear behaviour, however model test shear is close to the lower bound values from ACI 318-83. No definite conclusion can be drawn whether the shear capacity of the composite wall beams can be estimated by using equation 7.7 from the model tests. The bearing failure at the loading point and support may affect the ultimate load of the beam 1. The upper bound shear strength of ACI 318-83 and Wood (1990) underestimate the in-plane shear resistance of the composite wall and seems to be not suitable for composite wall.

Table. 7. 3. Comparison of analytical and test shear strength

	Shear in kN		Shear in kN		Shear kN	Shear resistance,kN	
	Analytical eqn.7.7 ACI 318-83		Analytical eqn.7.7 Wood (1990)		Beam test shear at support	Wall (chapter 6) Test	Analytical eqn. suggested
	lower	upper	lower	upper			
Beam 1	5.56	22.22	16.68	27.8	7.75	-------	----------
Beam 3	3.39	13.5	10.17	16.95	7.5	------	.....
Wall	13.9	55.5	41.6	69.00	----	122	92

7.6.1.2 Model for flexural strength

An analytical model will be developed based on the model proposed by Oehlers, Wright and Burnet (1994) for profiled box section composite beams. Let us consider the profiled beam shown in figure 7.12. The design point is taken as the position of maximum moment at mid span at a distance b/2 from the end of the beam. Up to the limit of generated interface bond force not exceeding the interface bond strength, the composite beam will exhibit full interaction and there will be no slip across the steel-concrete interface. The same strain distribution will exist in sheeting and concrete with neutral axis of both steel and concrete section N coincident to each other as shown in figure 7.13(b). If the maximum moment capacity is reached without the interface bond force exceeding the interface bond strength then the beam exhibits full composite action or full interaction.

But in reality, it is difficult to have full interaction in case of composite wall beam. The wall beam exhibits partial interaction with slip occurring across the interface due to the interface bond force exceeding the interface bond strength. As a result, there will be a step change , ε_{sl} between the strain in sheeting and concrete as shown in figure 7.13(c). The position of the neutral axis for concrete N_c will be different than the steel sheeting N_s. According to Oehlers (1992), the slip strain is assumed to be constant throughout the depth of the beam which leads to a uniform slip at the ends.

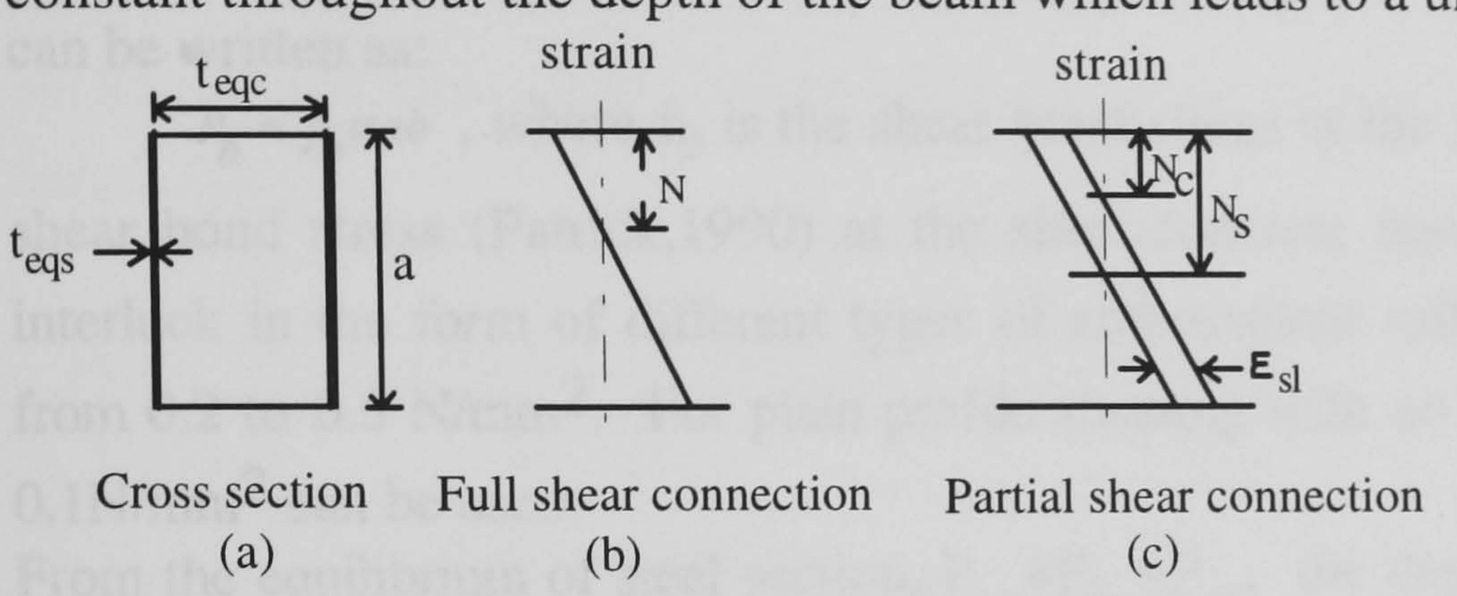

Figure 7.13 : Strain distribution in full and partial shear connection

The flexural strength of the composite beam can be determined by considering the distribution of forces in concrete and steel sections. The distribution of forces in individual concrete and steel sections is shown in figure 7.14 .

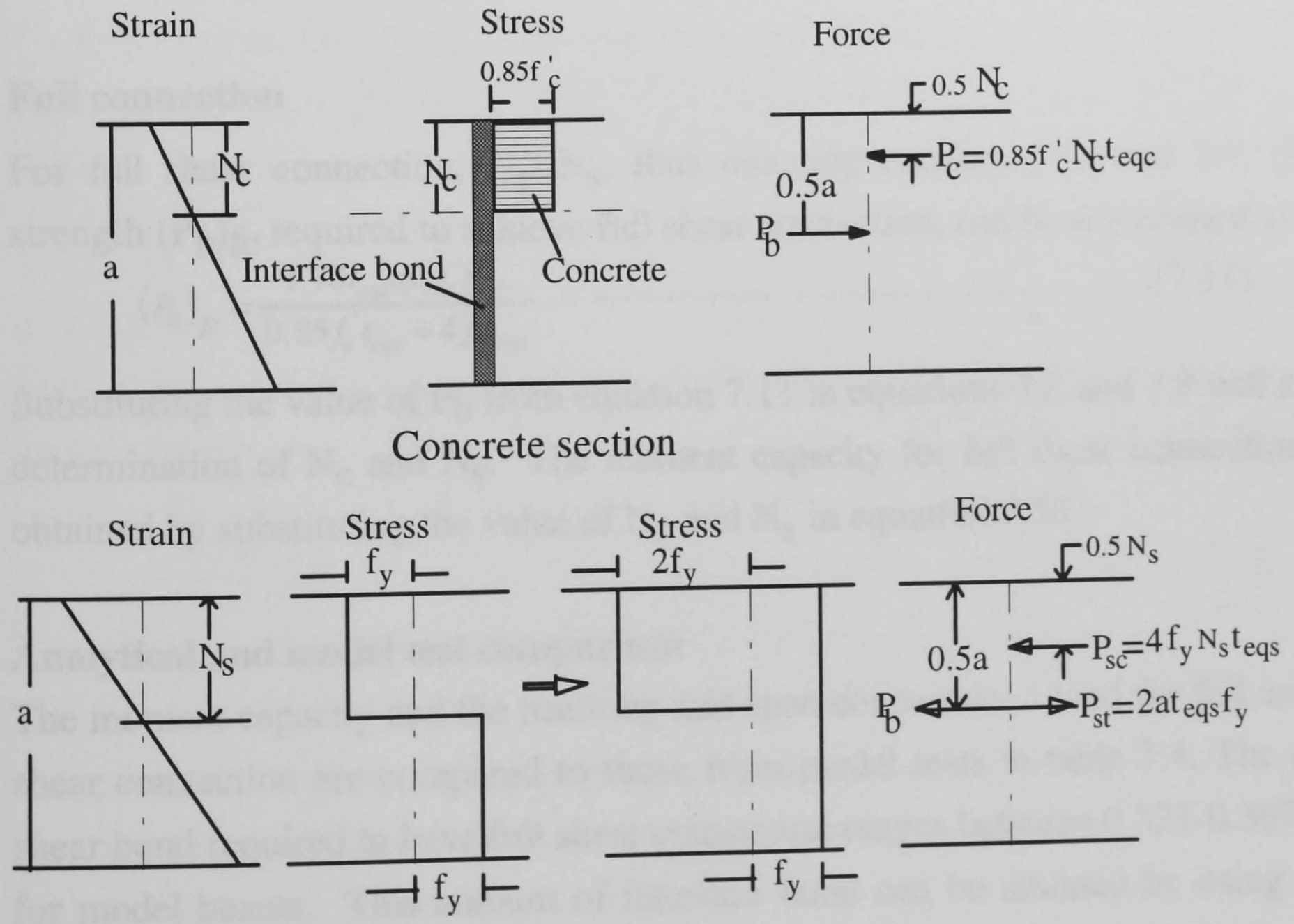

Figure 7.14: Distribution of forces

Partial shear connection

For partial shear connection, $N_C \neq N_S$. Considering the equilibrium of forces in concrete

$P_c = P_b$, the expression for N_c can be written as:

$$N_c = \frac{P_b}{0.85 f_c' t_{eqc}} \quad \text{.....(7.8)}$$

The interface bond force at mid span of the beam derived from interface bond stress can be written as:

$P_b = f_b \alpha a b$, where f_b is the shear bond stress at the interface. The maximum shear bond stress (Patrick,1990) at the sheet-concrete interface due to mechanical interlock in the form of different types of embossment rolled into the sheet ranges from 0.2 to 0.5 N/mm^2. For plain profile sheeting with no embossments, a value of 0.1N/mm^2 can be used.

From the equilibrium of steel section, $P_{sc}+P_b = P_{st}$; the depth of the neutral axis N_s can be derived as:

$$N_s = \frac{2 t_{eqs} a f_y - P_b}{4 f_y t_{eqs}} \quad \text{.....(7.9)}$$

The moment capacity of the composite profiled beam with partial interaction can be determined from the expression :

$$M_{pc} = f_y t_{eqs} a^2 - 2 f_y t_{eqs} N_s^2 - 0.425 f_c' t_{eqc} N_c^2 \quad \text{.....(7.10)}$$

Full connection

For full shear connection, $N_C = N_S$, thus equating equation 7.8 and 7.9, the bond strength $(P_b)_{fc}$ required to achieve full shear connection, can be determined as

$$(P_b)_{fc} = \frac{1.70 t_{eqs} a f_y f_c' t_{eqc}}{0.85 f_c' t_{eqc} + 4 f_y t_{eqs}} \quad \text{.....(7.11)}$$

Substituting the value of P_b from equation 7.11 in equations 7.8 and 7.9 will allow the determination of N_c and N_s. The moment capacity for full shear connection can be obtained by substituting the value of N_c and N_s in equation 7.10.

Analytical and model test comparison

The moment capacity and the resulting mid span concentrated load for full and partial shear connection are compared to those from model tests in table 7.4. The interface shear bond required to have full shear connection ranges between 0.327-0.367 N/mm^2 for model beams. This amount of interface bond can be attained by using sheeting with embossments as confirmed by Patrick (1990). Analytical calculations are performed with interface shear bond of 0.1 N/mm^2 which is typical for plain sheeting

as used in model tests. The moment capacity is not found to be sensitive to the interface bond stress.

The beam 1 with a depth to span ratio of about 2.36 failed at a load which is only one third of the analytically determined capacity. It signifies that the beam can not achieve its moment capacity and failed either by shear or by bearing.
Beam 3 with a depth to span ratio of about 4.25 shows good agreement with the analytical capacities which signifies that the beam attained its full flexural capacity before failure.

Table 7.4: Analytical and Model test comparison

Test no	Analytical Full connection			Analytical Partial connection			Test Load V kN	Ratio of loads
	Moment kN-mm	Load kN	Shear bond required	Moment kN-mm	Load kN	Shear bond assumed		
Beam 1	8151	54	0.327	7874	52	0.1	15.5	.29-.30
Beam 3	2634	17.56	0.367	2494	16.6	0.1	15.7	.89-.95

7.6.1.3 Load-deflection response

To determine the load versus mid span defection, the beam is considered as elastic and section . The moment of inertia I_{com} of the equivalent section can be derived as:

beam cross section shown in figure 7.12 is transformed into an equivalent concrete

$$I_{com} = \frac{t_{eqc}.a^3}{12} + \frac{2nt_{eqs}a^3}{12} = \frac{a^3}{12}\left[t_{eqc} + 2nt_{eqs}\right] \quad \text{.....(7.12)}$$

where n is the modular ratio .
The linear load-deflection relationship for the simply supported profiled wall beam can be written as :

$$\frac{V}{\Delta} = \frac{48E_cI_{com}}{b^3} \quad \text{.....(7.13)}$$

where V is the concentrated load and Δ is the deflection at mid span.

Stiffness (V/Δ) values from model test, analytical and finite element analysis are compared in table 7.5. Model test beam 3 showed lower stiffness values compared to the other but seems to be in good agreement which means that for flexure dominated beam, the equation 7.13 seems to be good. The beam test 1 is not compared because the load-deflection response is affected by the bearing failure at the point of concentrated load and at the supports.

Table 7.5 : Stiffness values

kN/mm	Analytical eqn 7.13	FEA	Beam 3
V/Δ , Beam 3	37.50	44	29
V/Δ, Beam 1	173	122	---

7.7 Finite element analysis

The composite wall beam elements were idealised in a similar manner as described in section 6.5 of chapter 6. 3D semi-loof shell elements (qsl8) with three degrees of freedom (u,v,w) at corner and five degrees of freedom at mid nodes (u,v,w,θ_1,θ_2) were used to model the composite wall. The steel and concrete were represented as different layers of the elements and symmetric half thickness of the beam were simulated. Analysis performed was non-linear providing cracking and yielding of steel layers. The simulated boundary conditions were simply supported and the concentrated load at mid span were applied at the top mid span nodes or distributed equally among the nodes along the mid span. The full composite analysis was performed in the simulation of model test 1 and 3.

The load-defection response at mid span for beam 1 and 3 from finite element analysis is shown in figure 7.15. For beam1, load was applied concentrated at the top mid node as a result the deflection at the top node is much higher than the bottom node in the post-cracking stage as shown in crack pattern in figures 7.16. The difference in the top and bottom node deflection decreases as the depth of the beam decreases. However, the discrepancy in the top and bottom node deflections was avoided by distributing the load among all the nodes along the centre span as shown in the cracking diagram of beam 3. The non-linear program ran until the step reduction process made the load increment very small and up to the non-convergence. Experimental mid deflections are found to be higher than the finite element analysis as they are affected by the deformation of beam on the support.

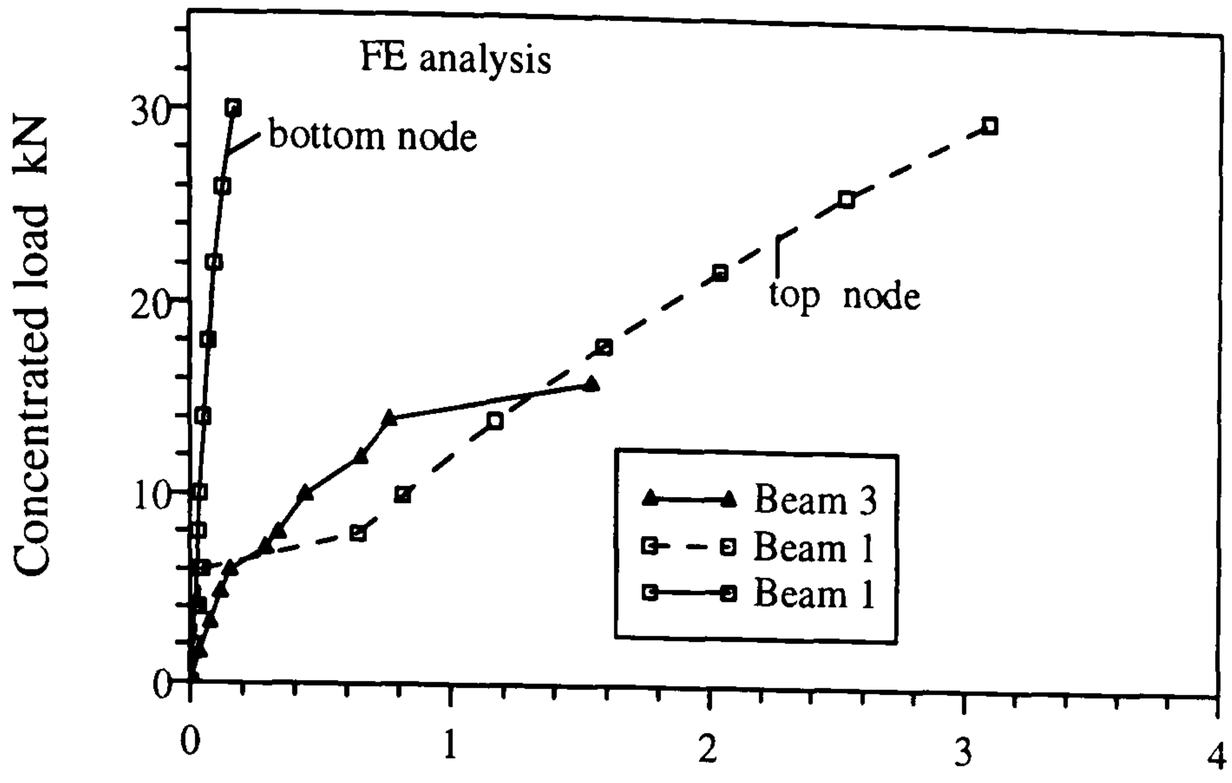

Figure 7.15: Finite element load-deformation response

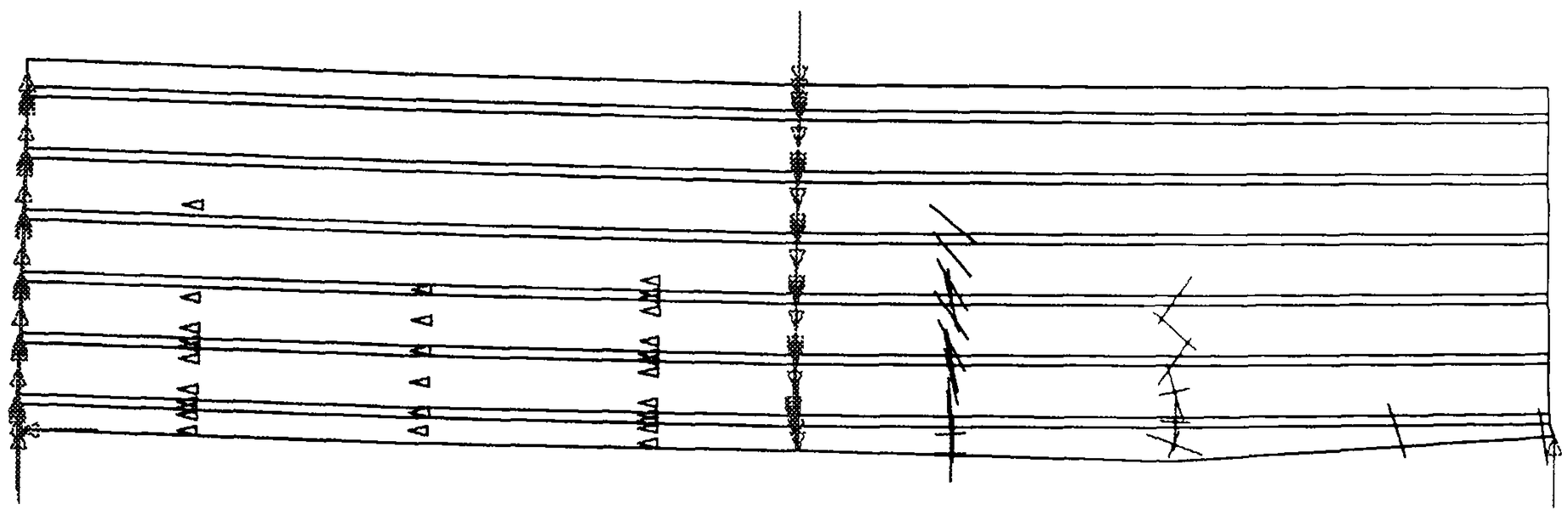

Figure 7.16(a) : Beam 3 : Crack pattern

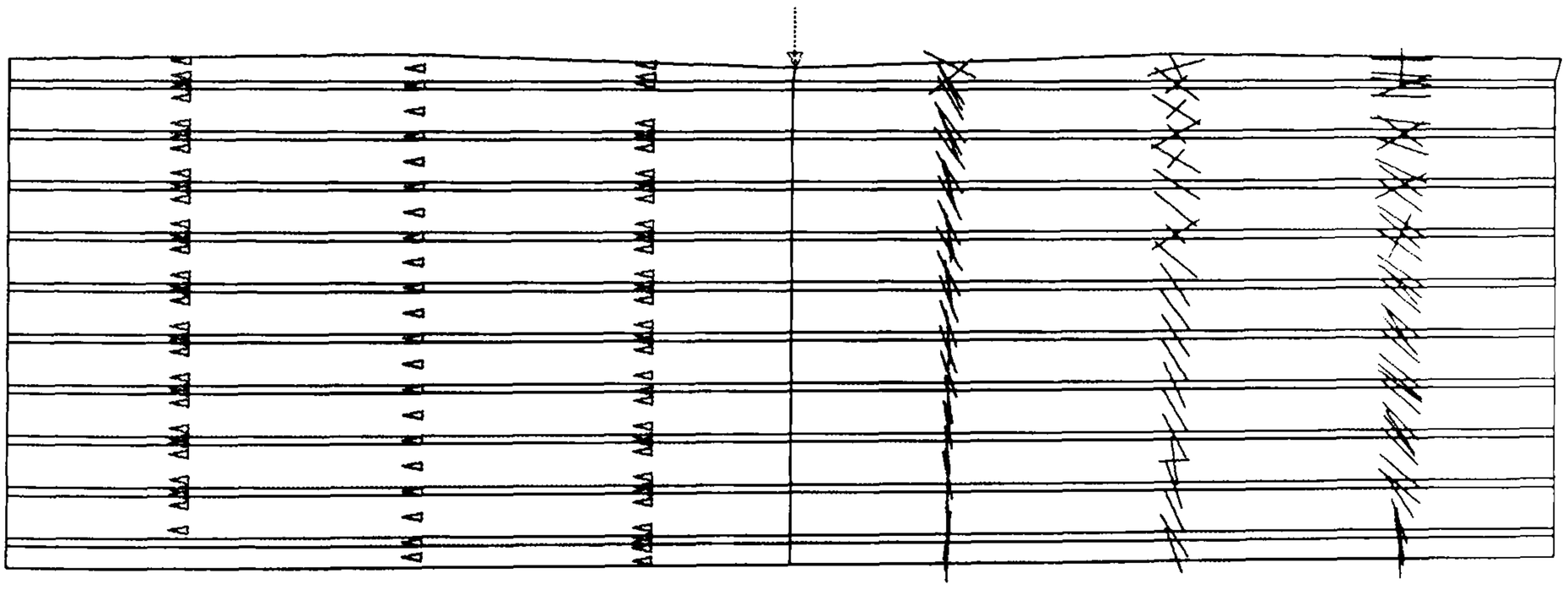

Figure 7.16(b) : Beam 1 : Crack pattern

The variation of shearing strain as found from the finite element analysis (shown in figure 7.17) is similar to those from model test with high strain at trough section having a general pattern of zero at the outer fibre and maximum at the centre of the beam.

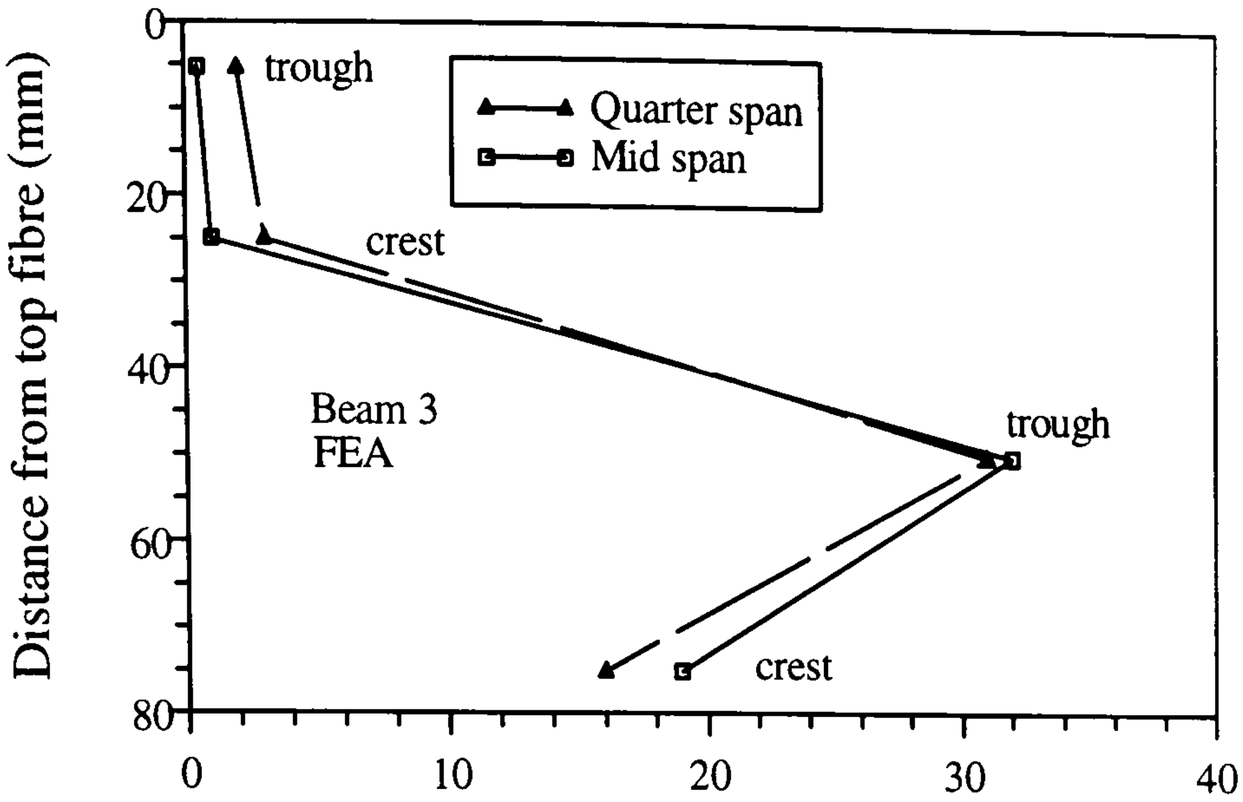

Figure 7.17: Variation of shearing strain

The variation of principal direction (figure 7.18) as found from finite element analysis is also similar to that found in model test with direction gradually increases from outer fibres towards the centre up to around 50 degrees. This trend can also be observed in the principal direction diagram shown in figure 7.19.

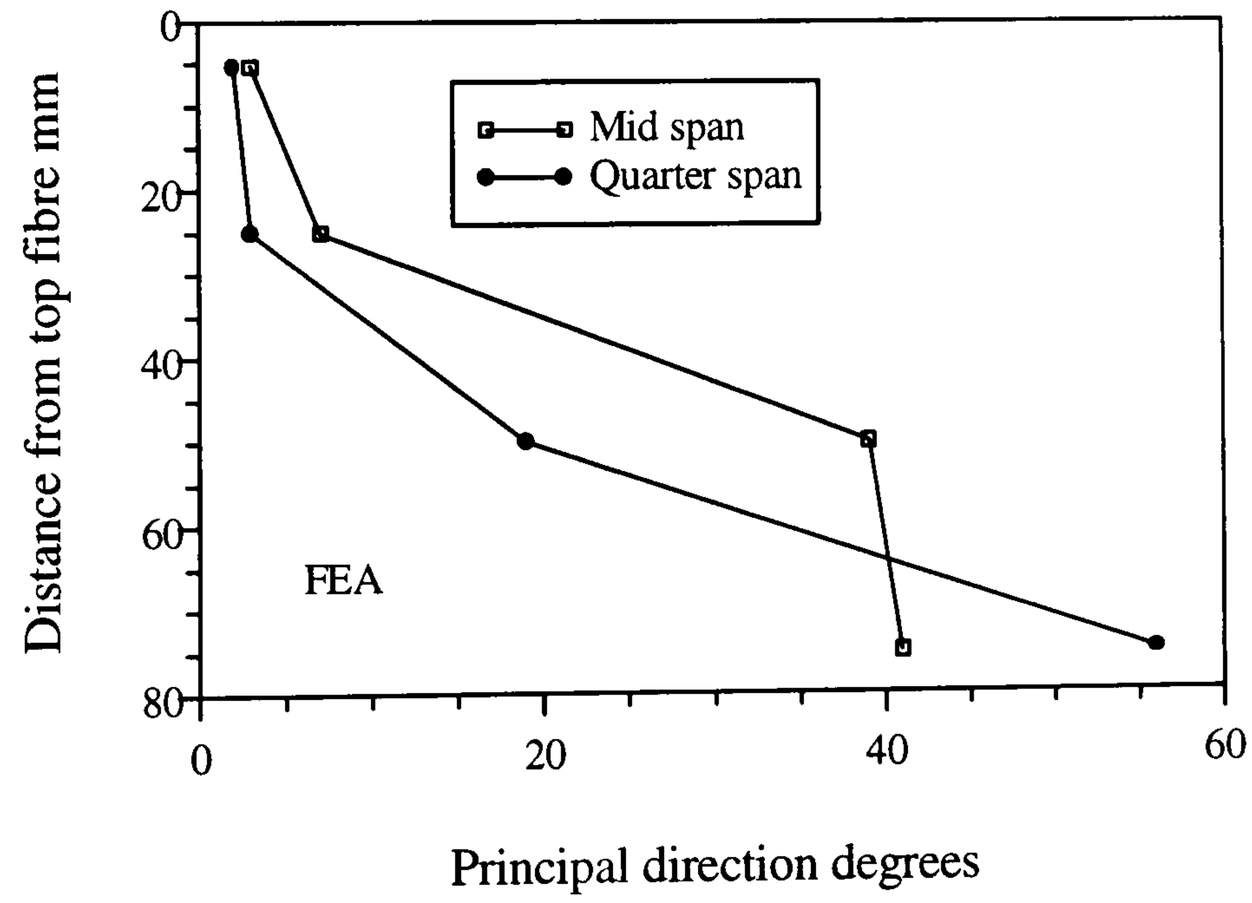

Figure 7.18: Variation of principal direction

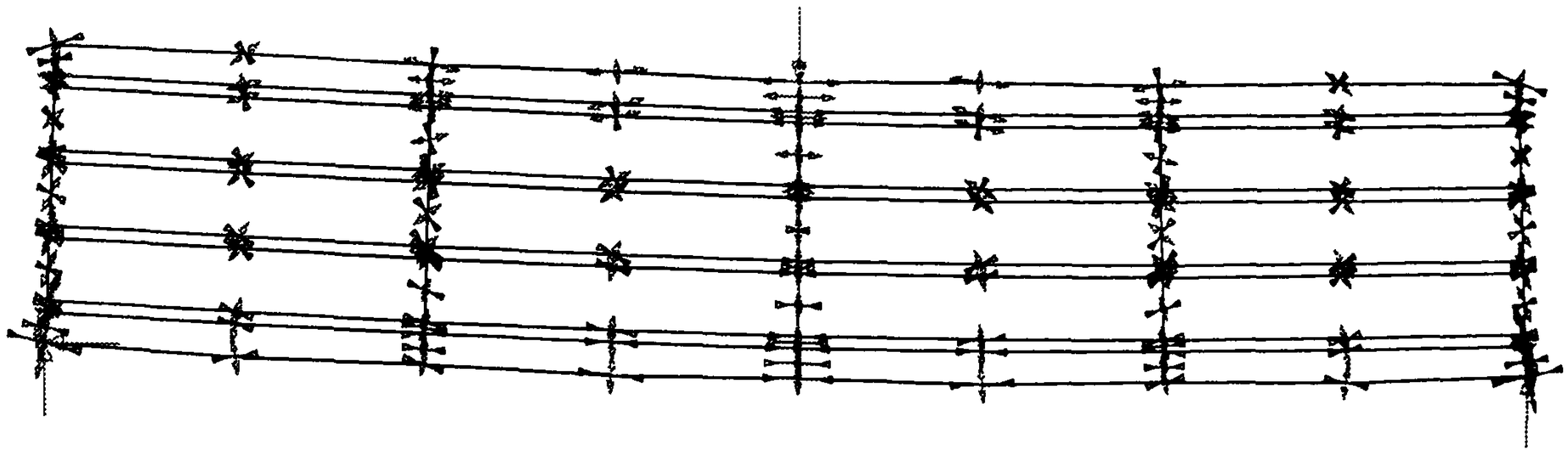

Figure 7.19: Principal direction diagram

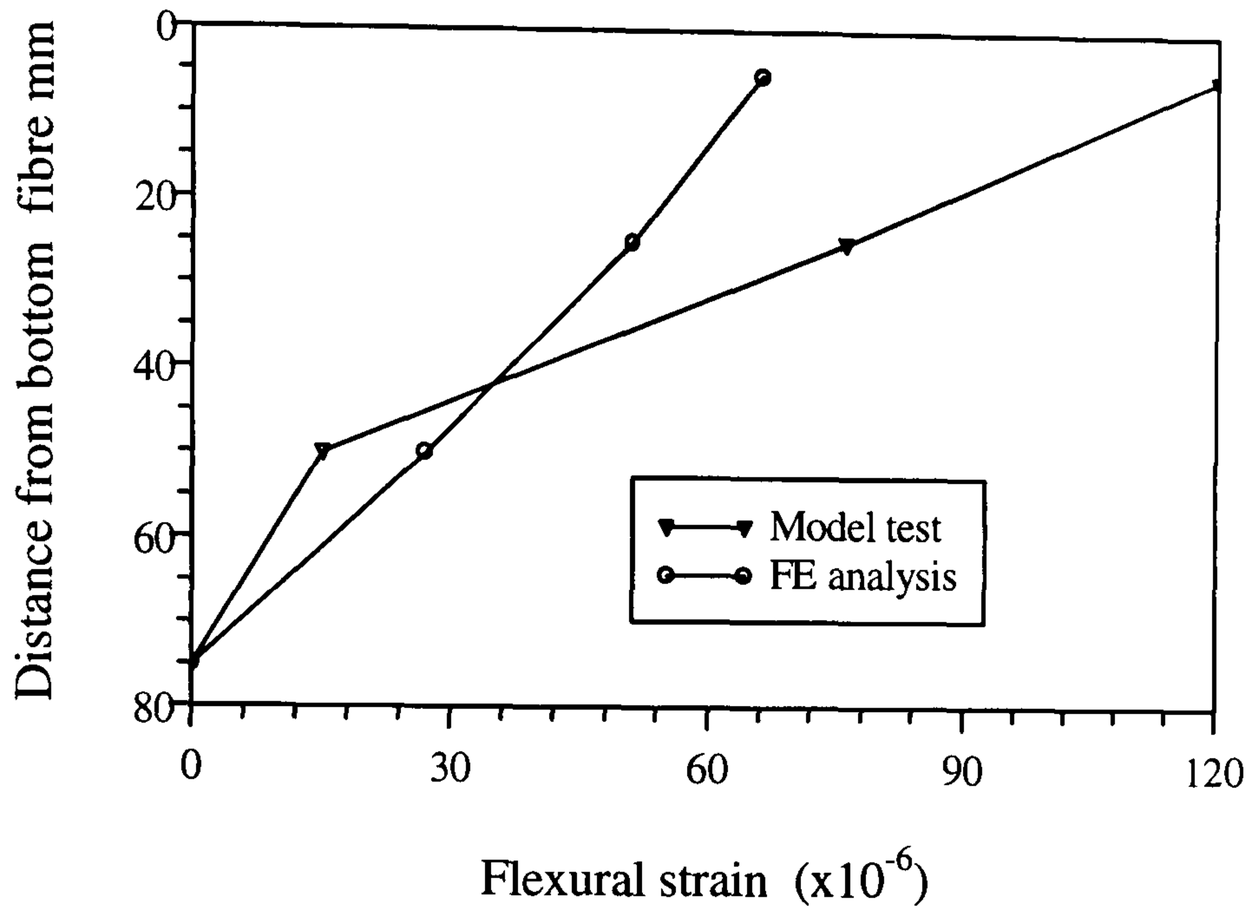

Figure 7.20: Comparison of FE and Model test

The variation of flexural strain along the depth of the beam from finite element and model test is compared to each other in figure 7.20. The model test showed higher strain in most of the gauge points. This is found to be reasonable as the model beams did not behave as fully composite.

7.8 Summary

The small scale model tests described the behaviour of the wall as a beam with distribution of strains within the beam. The model beams suffered bearing failure at the loaded point and at the support, these problems should be avoided in the future tests. Analytical models for the shear and flexural strength of the composite wall beam have been derived. However, for the composite wall beams no definite conclusions can be drawn for the shear strength due to the limited test results. The strains from model tests are compared to those from finite element analysis and they showed similar pattern of variation.

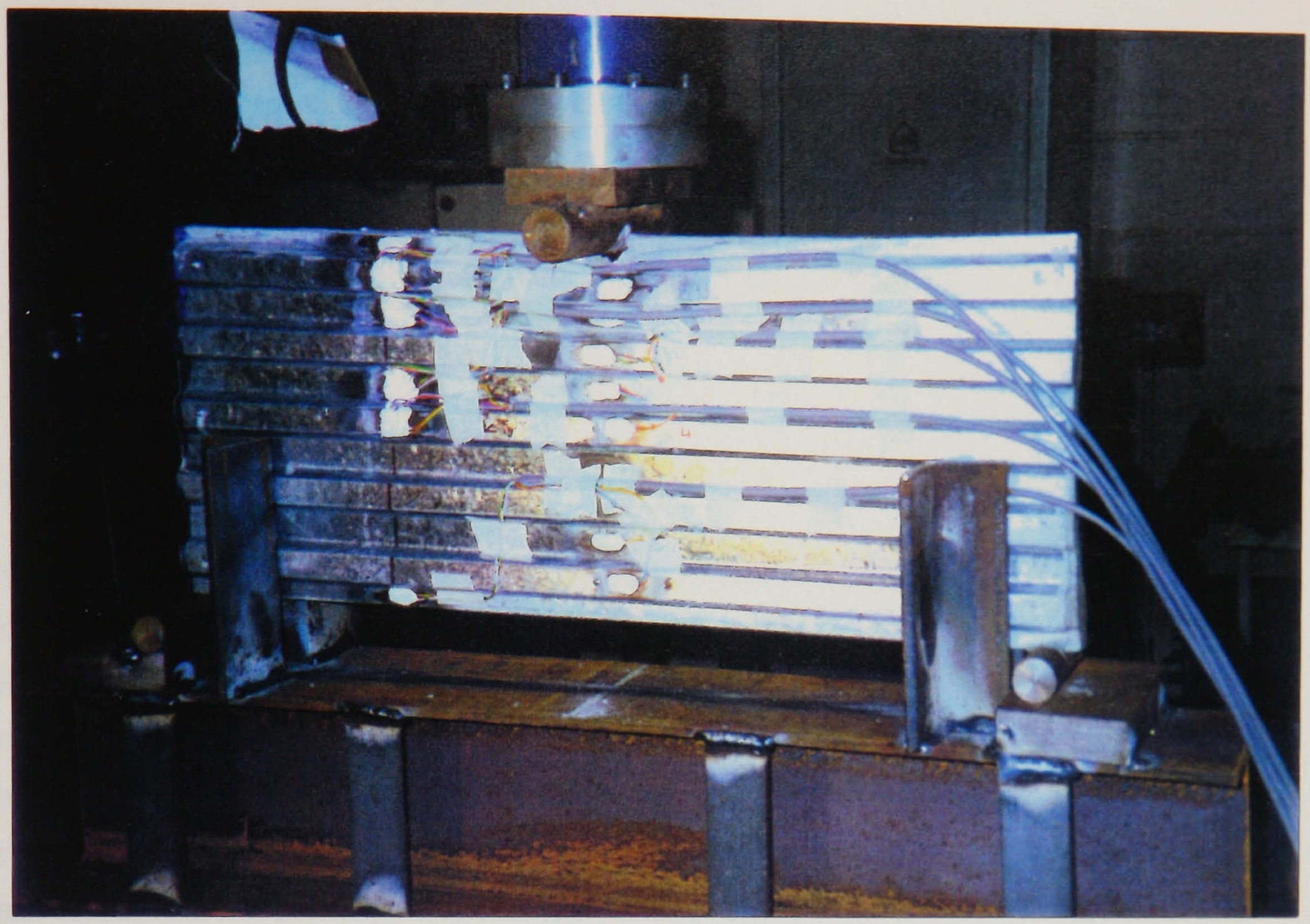

Photograph 7.1: Failed composite wall beam 1

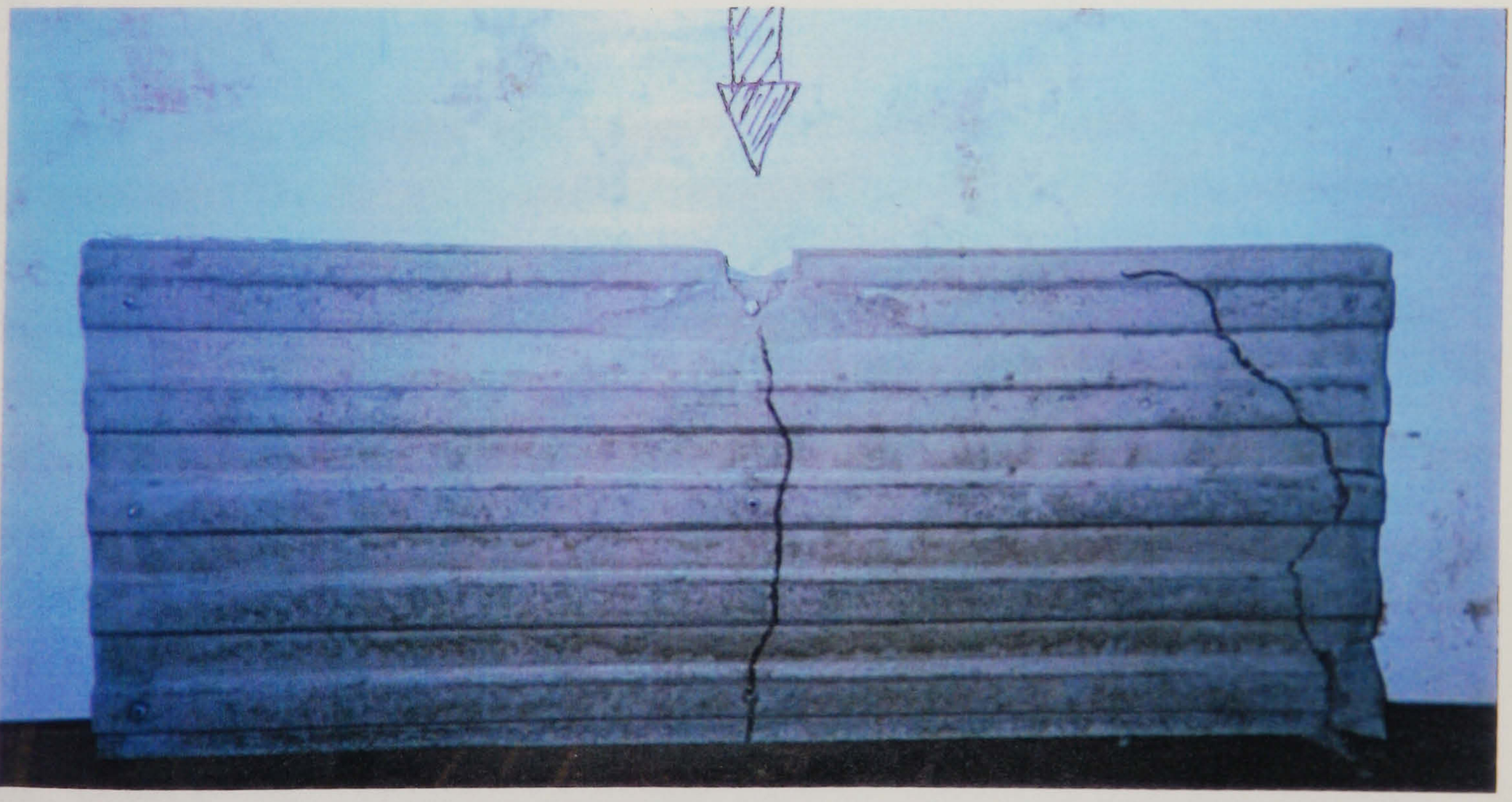

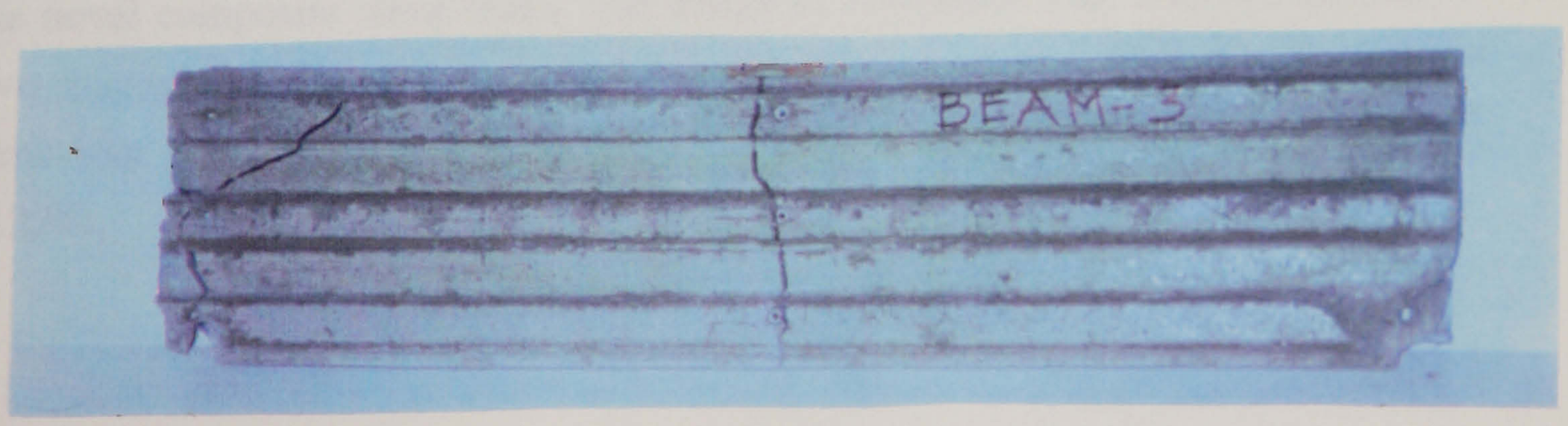

Photograph 7.2: Cracking of concrete in composite wall beams

CHAPTER EIGHT

DESIGN AND APPLICATION OF COMPOSITE WALLING AS SHEAR ELEMENTS

8.1 Introduction

Composite walls are specially thought to be applicable as shear or core walls in steel frame buildings. In many of these structures, the beams and columns are assumed pinned with lateral stability and wind resistance provided by the core walls of concrete. In the use of a composite wall the profiled steel sheeting is fixed at the same time as the main steel is erected and therefore provides temporary bracing to wind and destabilising forces during construction. In this chapter, design of composite wall in construction and service stages will be described along with a practical example.

8.2 Design

The design criteria associated with composite walling includes axial, lateral and in-plane resistance. The current research is concentrated on the in-plane shear resistance of the wall. This may be a case where the wall is used in conjunction with a steel frame in steel frame building where the wall resists only the shear with frame taking the bending loads. In this case we can call the wall as framed shear wall where in plane shear resistance play an important role. Such an application of composite walling in a typical steel framed building is shown in figure 8.1 where profiled composite slabs and composite beams may also be used as structural elements.

Shear wall in buildings must have sufficient strength and stiffness to resist the in-plane loads. Consequently a method for prediction for the stiffness and strength is vital for the novel composite shear walls. The design of composite wall will be described in two stages: (a) Construction stage and (b) Service stage. Full details of these behaviour is presented in chapter 5 and 6 and also presented by Hossain and Wright (1995).

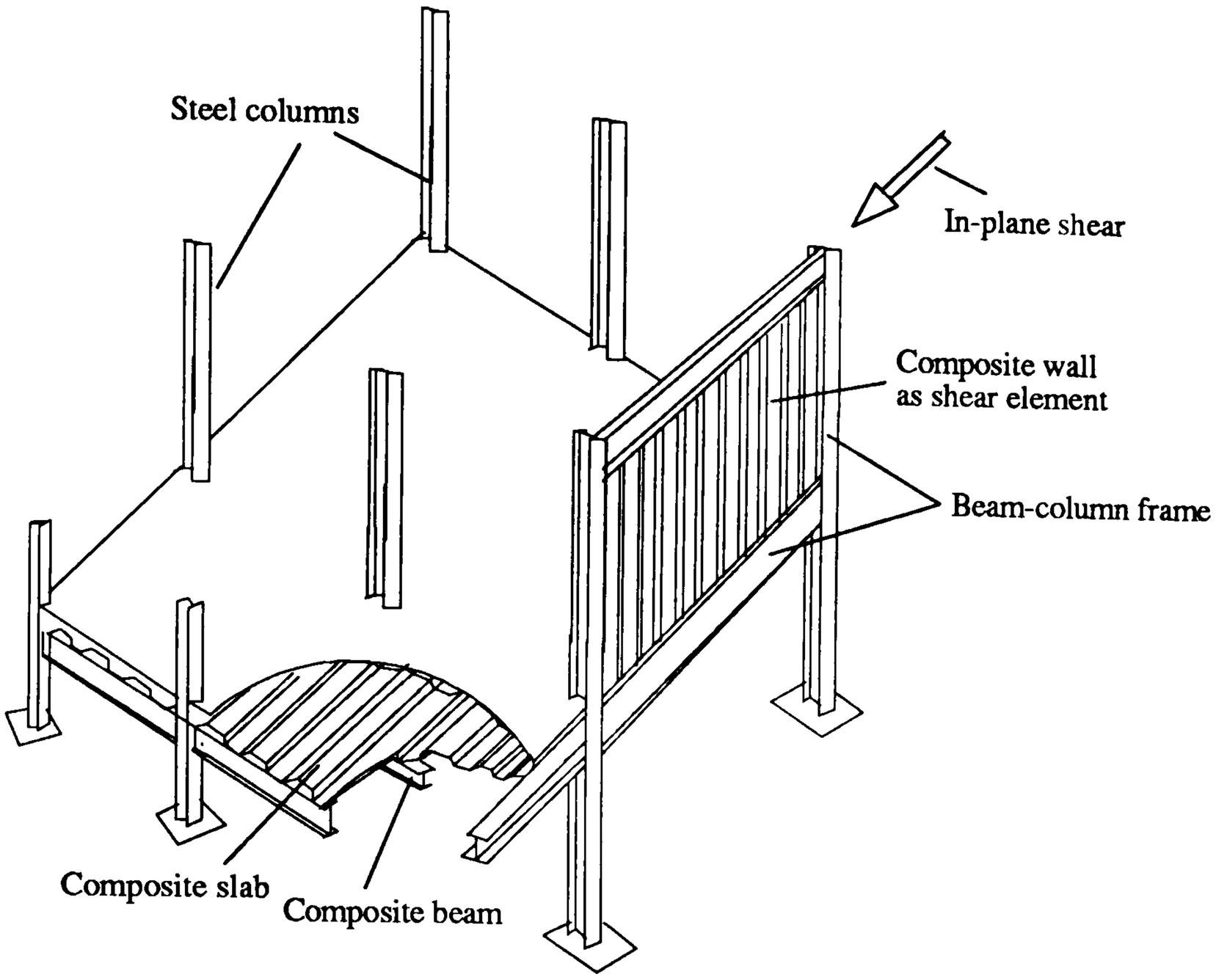

Figure 8.1: Typical application of composite wall in steel-frame buildings

a. Construction stage behaviour

It is envisaged that the steel sheeting alone will provide temporary resistance to in-plane loading from wind and stability loads during the construction. From chapter 5, it is clear that the behaviour of the panel of sheeting within the steel frame will depend on the manner of attachment of the sheeting to the surrounding frame.

Shear stiffness

The shear stiffness (k_s) or flexibility (c_s) of the profiled steel sheet panels will be based on the contribution from sheeting (c_1: shear and c_2: bending or distortion), boundary frame (c_3), sheet-frame fasteners (c_4) and seam fasteners (c_5) as presented in equation 5. 4 of chapter 5:

$$c_s = c_1 + c_2 + c_3 + c_4 + c_5 = 1/k_s \quad \text{..... (8.1)}$$

The expressions for all these components are derived in section 5.3.1 and can be used in design if necessary. For the practical case, building frame may be considered as rigid with axial deformation negligible, the term c_3 can be neglected. The equation 8.1 can simplified as :

$$c_s = \frac{1}{k_s} = c_1 + c_2 + c_4 + c_5 = \frac{2\alpha b(1+\upsilon_s)}{E_s a t_s} + \frac{144 K h^3 l^2}{E_s t_s^{\,3} abd} + \frac{2s}{a^2}\left[P_a a + P_b b\right] + \frac{bs'p'}{aa_0} \quad \text{.....(8.2)}$$

The equation 8.2 can be further simplified. The use of single profiled steel sheeting instead of a number of sheets seamed together will omit the seam fastener contribution c_4. In the case of continuous sheet-frame connections like continuously welded or fixed along the both trough and crest lines instead of descrete connections (spot welded or bolted at each or alternate troughs) will minimise the contribution c_5. In profiled sheet model tests 1 and 2, these two conditions were satisfied. The simplified flexibility equation for this condition becomes :

$$c_s = \frac{1}{k_s} = c_1 + c_2 = \frac{2\alpha b(1+\upsilon_s)}{E_s a t_s} + \frac{144 K h^3 l^2}{E_s t_s^3 abd} \quad \text{.....(8.3)}$$

The factor K represents the mode of attachment of the sheeting to the surrounding. The values of K which is related to profile geometry can be calculated using the equations 5.8 and 5.9 of chapter 5 for various boundary conditions. If the sheet is welded to the frame members at the centre of valley the value of K can be obtained from :

$$K = \frac{(d+2h)(d^2 - 3ld + 3l^2)}{12hd^2} \quad \text{.....(8.4a)}$$

If the sheet is continuously welded along the lower face or just at the toes, K , can be expressed as

$$K = \frac{2l+3h}{12(l+6h)} \quad \text{.....(8.4b)}$$

The equations 8.4(a) and 8.4(b) are found to be reliable as confirmed in chapter 5 by the author. The values of K for trapezoidal profile can be taken from Hossain and Wright (1995) as in table 8.1 :

Table 8.1. Values of K for various boundary conditions

Boundary conditions	K
Welded continuously along the trough	0.0845
Clamped	0
Bolted or spot welded at the centre of the trough	0.1719

The value of K is dependent on the geometric dimensions of the profile and the values for fastener in every trough or in alternate troughs related to different geometric dimensions of the profile can be obtained from Davies and Bryan (1982).

Shear resistance

As described in chapter 5, the shear resistance of the sheeting in construction stage may be governed by the (a) failure at a line of seam fasteners, (b) failure of connections between sheeting and frame, (c) shear buckling of sheeting and (d) gross

distortion or collapse of the profile at the end of sheeting. Equations 5.16, 5.17 and 5.18 are presented in section 5.3.2 of chapter 5 for modes a, b and c respectively and reproduced here as :

Strength due to seam fasteners : $V_u = F_s . b/p'$ .....(8.5a)

Strength due to sheet-beam or sheet-column fasteners:

$V_u = F_{sb}.a/p_a = F_{sc}.b/p_b$.. .....(8.5b)

For shear buckling mode: $V_u = 36\beta \frac{D_x^{1/4} D_y^{3/4} a}{b^2}$ .....(8.5c)

Failure mode 'd' is based on plastic collapse of the extreme end of the profile but failure can't occur until the mechanism has spread some distance into the profile. The mode is much more critical for sheeting fastened in alternate troughs than for sheeting in every trough. To avoid the possibility of gross distortion or collapse of the profile at ends, the maximum shear force should not exceed according to Davies and Bryan (1982):

$0.9 t_s^{1.5} a f_y / d^{0.5}$ ..... for fastener at every trough

$0.3 t_s^{1.5} a f_y / d^{0.5}$ ..... for fastener at alternate trough .....(8.5d)

The minimum shear resistance derived from these four modes of failure can be taken as the shear resistance of the sheeting in the construction stage.

The ultimate shear resistance of the sheeting is derived in section 5.3.2, (assuming no fastener and end distortion failure), to be as the critical buckling load (equation 5.18) and can be expresses as:

$V_u = 36\beta \frac{D_x^{1/4} D_y^{3/4} a}{b^2}$ in which $1 \le \beta \le 1.90$ .....(8.6)

where β is a coefficient dependent on boundary conditions. The values of β suggested for different boundary conditions as discussed in chapter 5, can be tabulated as :

Table: 8.2 : Values of β for different boundary conditions

Boundary conditions	β
Simply (welded at the centre of trough)	1.00
Clamped (continuously welded along both trough or crest line)	1.72
Welded continuously along the trough	1.42

For design shear capacity of the sheeting, Davies and Bryan (1982) suggested a 25% reserve of safety due to the sudden failure associated with shear buckling mode of failure. Therefore, allowing a 25% reserve of safety, the equation 8.6 can be modified to give design shear resistance (V_{design}) as:

$$V_{design} = 28\beta \frac{D_x^{1/4} D_y^{3/4} a}{b^2} \quad \text{.....(8.6a)}$$

The equation 8.6a is valid for fastener at every trough (β=1.0) but for fastener at alternate trough (β=1.0) the equation 8.6a should be further reduced by 50% (Davies and Bryan (1982).

b. Service stage behaviour

In the service stage, the shear resistance of the sheeting will be derived from the shear resistance of the pair of sheeting, concrete core and interaction between the two. The expression for the shear stiffness of the composite wall is derived in equation 6.17 and represented here:

$$c_w = \frac{1}{k_w} = \frac{2\alpha b(1+\upsilon_s)(1+\upsilon_c)}{a\left[E_c t_{eq}\alpha(1+\upsilon_s)+2E_s t_s(1+\upsilon_c)\right]} \quad \text{.....(8.7)}$$

The ultimate shear resistance of the composite wall according to equation 6.26 of chapter 6 can be written as :

$$V_w = 72\beta \frac{D_x^{1/4} D_y^{3/4} a}{b^2} + 0.074 a t_{eq} f_{cu} \quad \text{.....(8.8)}$$

The equation 8.8 already includes a 25% reserve of safety as confirmed from the model tests. If the failure of connections (wall-frame and seams in sheeting) are not desired, sufficient and proper connections should be secured.

The seam failure is unlikely to occur in the case of composite wall. At seams between adjacent steel sheets, the concrete carries almost all the shear force. This is confirmed from the composite slab diaphragm tests by Davies and Fisher (1979). The seam connections can be provided by mechanical clinching, button-punched or combination of either of the two with spot weld.

As confirmed from the model tests, the wall-frame connection is very important to mobilise the full strength of composite wall. It will be preferred to connect the composite wall to the frame through both concrete and sheeting if practical construction detail allows. The sheeting may be either welded, bolted or screwed to the frame. But proper connections between pair of sheeting and concrete core specially at the boundaries should be secured. This can be provided by steel hooks spot welded to the pair of sheeting at the boundaries tied together through concrete.

8.3. Design example

As a simple design example, we shall now calculate the ultimate strength and stiffness of the composite wall in a steel frame building (framed shear wall) in service and construction stages. The detail dimension of the composite wall is shown in figure 8.2. The profiled steel sheet considered here is the trapezoidal Steel Construction Institute generic profile as used in prototype composite wall described in chapter 3. Sufficient fasteners are used to avoid fastener or sheet distortion failure in both construction and service stages. The wall has the following material properties:

Modulus elasticity of concrete: $E_c = 20kN/mm^2$

Modulus of elasticity of steel : $E_s = 200kN/mm^2$

Poisson's ratio of concrete: $\upsilon_c = 0.18$

Poissons ratio of steel: $\upsilon_s = 0.25$

Concrete cube strength $f_{cu} = 30N/mm^2$

Boundary conditions:

The sheeting is considered to be connected to frame by either of the three ways:

Case 1: Bolted or spot welded to the boundary frame at the centre of every troughs

Case 2: Continuously welded at the trough

Case 3: Clamped

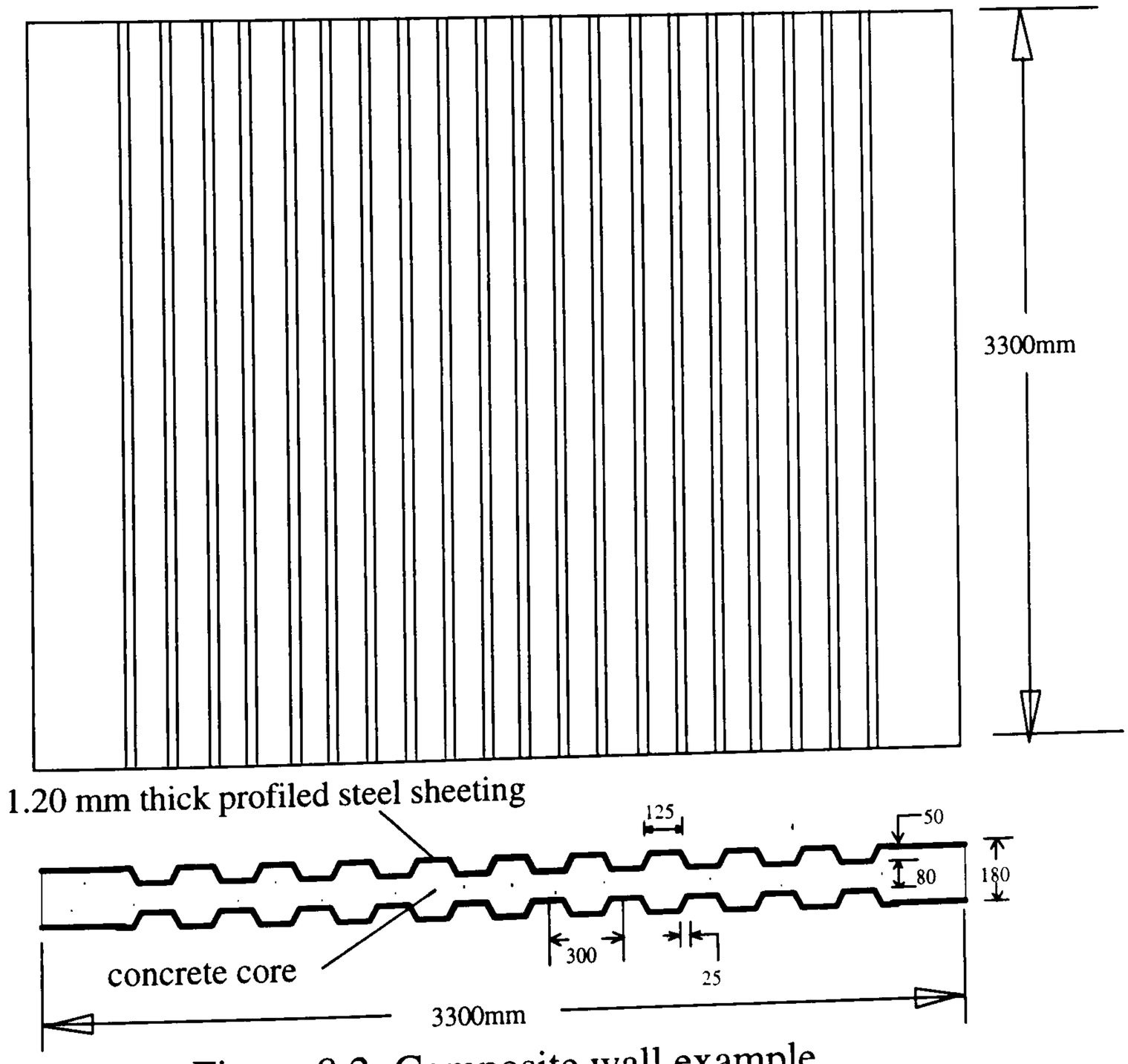

Figure 8.2: Composite wall example

Design:

Step 1: Calculation of profiled steel sheet parameter

a=b= 3300mm, t_{eq}= 130mm, D_x= 23.88 kN-mm^2/mm and

D_y= 2076016 kN-mm^2/mm

i. Construction stage behaviour

Step 2: Calculation of flexibility (f_s) stiffness(k_s) of profiled steel sheeting

Using design equations 8.3 neglecting fastener contributions for simplification

Shear contribution, flexibility = 0.0125625 mm/kN ; stiffness =80 kN/mm

Bending or distortion contribution, flexibility = 0.358K ; stiffness 1/ 0.358K

The total stiffness of a single sheeting , flexibility, f_s or stiffness k_s :

f_s=1/ k_s= 0.0125625 + 0.358K

for case1: Spot welded or bolted at the centre of the trough

From table 8.1,using K=0.1719 : f_s= 0.0125625 + 0.0615=0.074 mm/kN and stiffness, k_s = 13.5 kN/mm

for case 2: Continuously welded along the trough, from table 8.1: K= 0.0845

Flexibility, f_s= 0.0125625 + 0.030=0.0428 mm/kN and stiffness, k_s=23.5 kN/mm

for case 3: Clamped condition, from table 8.1, using K=0.0

flexibility, f_s= 0.0125625 mm/kN and stiffness, k_s= 80 kN/mm

Summary of stiffness (k_s) of sheeting

Case	k_s,for single of sheeting kN/mm	k_s for pair of sheeting, kN/mm
1	13.5	27
2	23.5	47
3	80	160

Note: For simplicity of the problem, the flexibility due to fastener contributions are not included in this example. The stiffness of the sheeting in the construction stage including fastener contributions can be calculated with no difficulty using equation 8.2 if data for the connection parameters are available.

Step 3: Calculation of ultimate shear strength (V_u) of the sheeting

Assuming shear buckling mode of failure and using equation 8.6

V_u= 4349400 βa /b^2 =1318β kN

Shear strength (V_u) of the sheeting , kN

Case	β	Single sheeting , V_u	Pair of sheeting, $2V_u$
1	1.00	1318	2636
2	1.42	1872	3744
3	1.72	2267	4534

ii. Service stage

Step 4: Calculation of shear stiffness of composite wall (k_w)

Using equation 8.7; k_w=1262 kN/mm

Step 5: Calculation of shear strength of the composite wall (V_w)

Using equation 8.8 ; V_w= 2636β+ 31746f_{cu}

Using table 8.2 for the values of β, ultimate shear resistance can be obtained as:

Case 1: V_w= 2636+ 952=3588 kN or 1000 kN/m width of the wall

Case 2: V_w= 3743+ 952=4695 kN or 1422 kN/m width of the wall

Case 3: V_w= 4534+952=5486 kN or 1829 kN/m width of the wall

8.4. Composite shear wall in practical building

A typical composite shear building subjected wind load has been taken to carry out some parametric studies. The typical dimensions of the building is shown in the figure 8.3. The composite walls are placed in the steel-column frames in each storey. The frames are considered as pinned allowing the wall to resist total in-plane shear loads at each storey storey level.

A wind pressure of 1kN/m^2 which approximately represent a wind velocity of 128 km/hour is applied to the building. The exact wind pressure can be calculated for the particular conditions of a building using Uniform Building Code (1985) and B.S. CP3 (1972). All other dimensions of the wall and material properties are similar to the design example (figure 8.2)

The variation of in-plane shear along the height of the building is also shown in the figure 8.3. The wall panel in the lower storey will be subjected to higher in-plane shear and critical for the design.

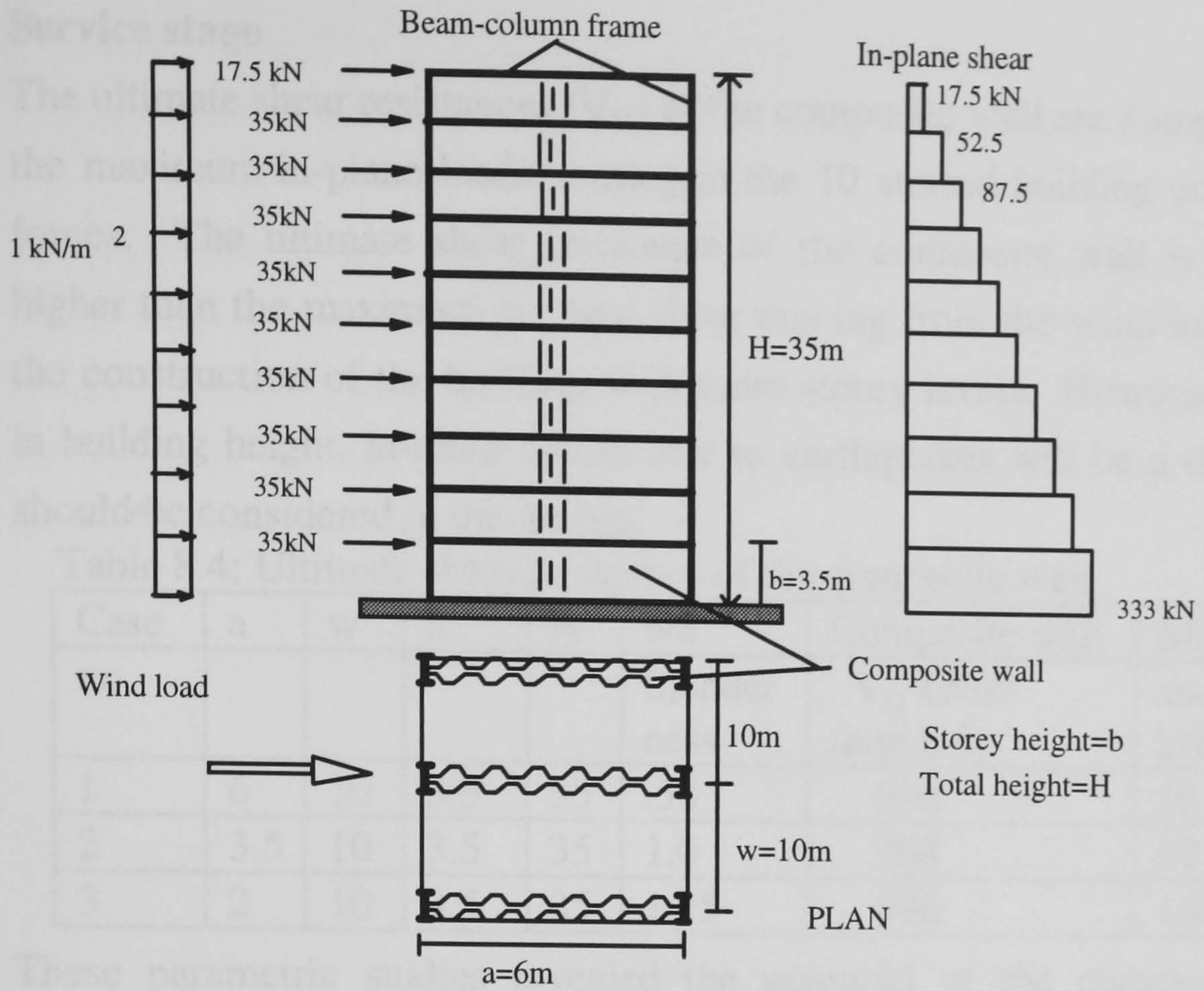

Figure 8.3: Typical composite wall building subjected to wind load

Construction Stage

In-plane shear resistance will only be derived from the sheeting. The shear resistances of the sheeting having fasteners at every troughs are tabulated in table 8.3. The shear resistance of the sheeting is very high particularly for the panels with b/a ratio less or equal to 1.0. For slender panels with a/b ratio equal to 3, the shear resistance is found to be less than the maximum shear developed in the building due to wind. However, in no case, will the maximum shear at the base of the building be a design criteria for the shear resistance of the sheeting in the construction stage. This is due to the construction sequence of the building. The sheeting at the lower storey will be fixed to the frame first and concrete will be cast to have composite wall situation before the subsequent build up of the next storeys. Again, the slenderness for the framed composite wall panels for the practical cases may not be greater than 2. There is no doubt that the sheeting will provide sufficient in-plane shear resistance during construction stage .

Table 8.3: Shear resistance of sheeting in the construction stage

Case No	a in m	w in m	b in m	H in m	b/a	Single sheeting V_{design} (kN) (eqn.8.6(a))	Pair of sheeting V_{design} (kN) eqn.8.6(a))	Maximum shear kN
1	3.5	10	3.5	35	1.0	932	1864	333
2	3.5	10	7	35	2.0	233	466	333
3	3.5	10	10.5	35	3.0	104	208	333
4	6	10	3.5	35	0.58	2130	4260	333

Service stage

The ultimate shear resistances (V_u) of the composite wall are compared in table 8.4 to the maximum in-plane loads coming in the 10 storied building example due to wind forces. The ultimate shear resistance of the composite wall is found to be much higher than the maximum in-plane shear coming from the wind load. This will allow the construction of the building with more storey levels. However, with the increase in building height, in-plane forces due to earthquakes will be a dominant factor and should be considered in the design.

Table 8.4: Ultimate shear resistance of the composite wall

Case no	a	w	b	H	b/a Slenderness	Composite wall V_u kN/m (eqn.8.8)	Maximum shear kN/m
1	6	10	3.5	35	.58	998	55
2	3.5	10	3.5	35	1.0	998	95
3	2	10	3.5	35	1.75	998	167

These parametric studies revealed the potential of the composite walls as shear elements in buildings.

8.5 Other potential applications as shear elements in buildings

The composite wall elements can be used to form core walls in association with steel frame to resist in-plane loads. A schematic of the composite wall core assembly in steel frame building is shown in figure 8.4.

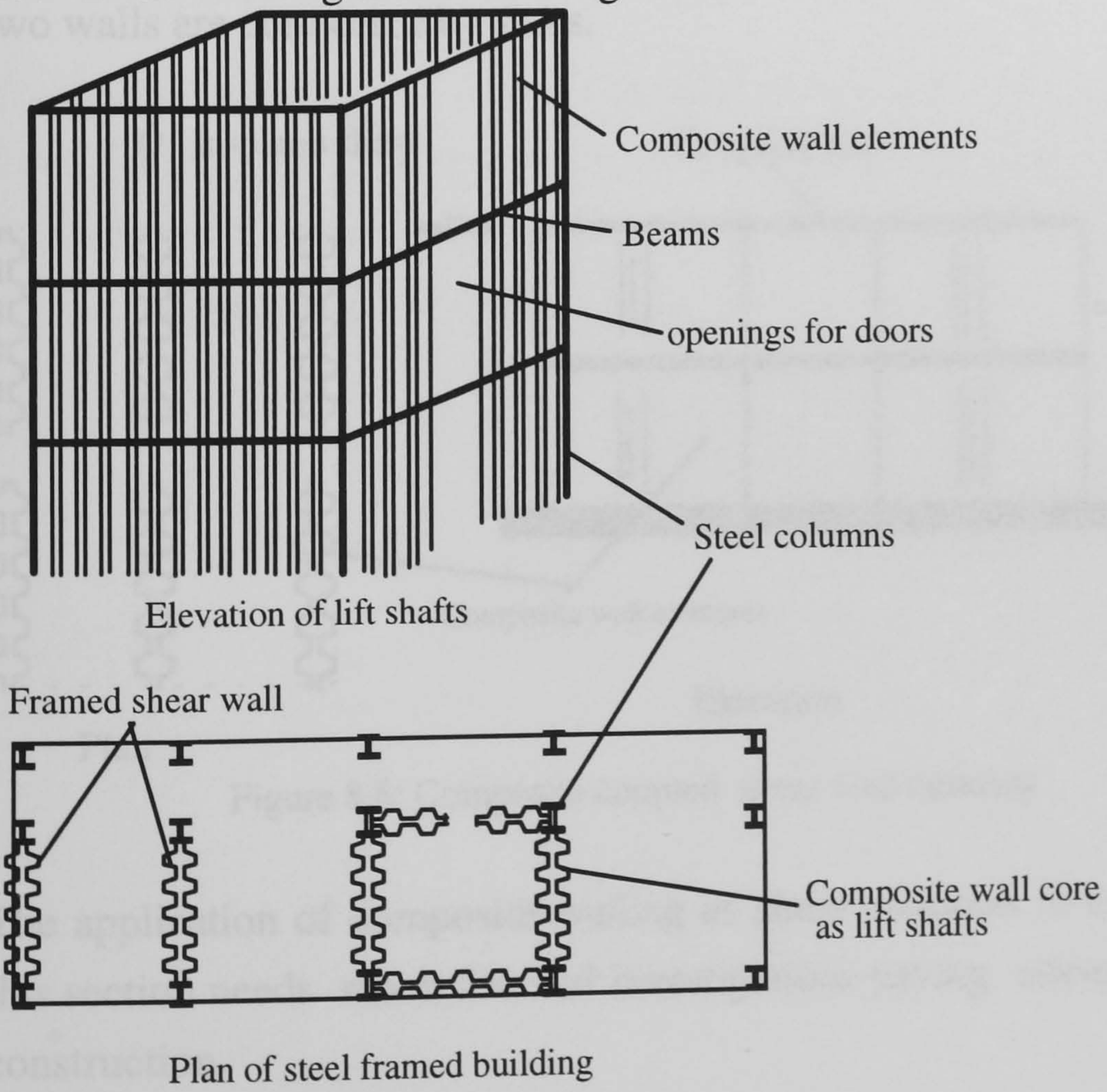

Figure 8.4: Composite wall core assembly in steel frame building

Cores are formed by placing composite wall in the frame. In this case core will resist lateral loads from both direction. Core openings can be provided with no difficulty.

They can also be used as a shear wall connecting directly to the slab as in single storey shear wall or in coupled shear wall building. A single storey coupled shear wall building is shown in figure 8.5. Where in plane loads due to wind will be transmitted from slab to the wall which may be subjected to shear or shear plus bending effects according to its slenderness.

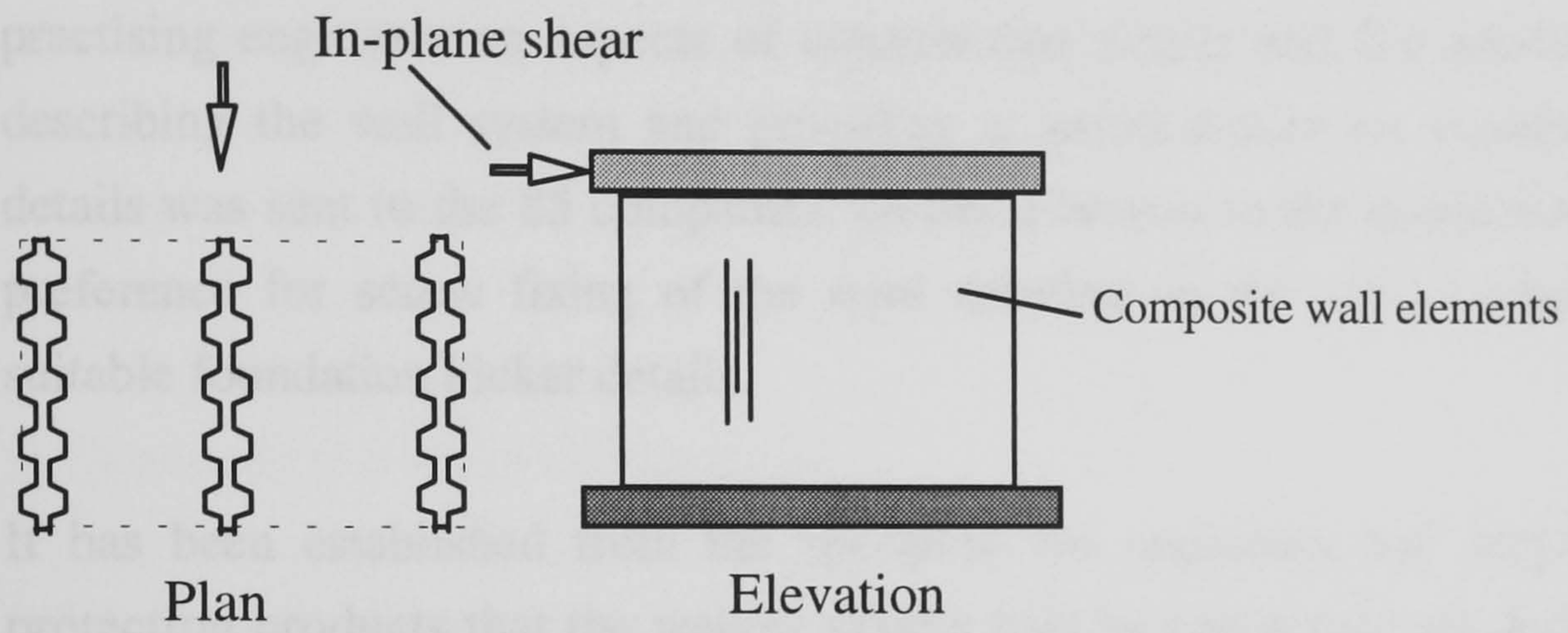

Figure 8.5: Single storey composite shear wall building

A schematic of composite coupled shear wall building is shown in figure 8.6 where two walls are connected by slabs.

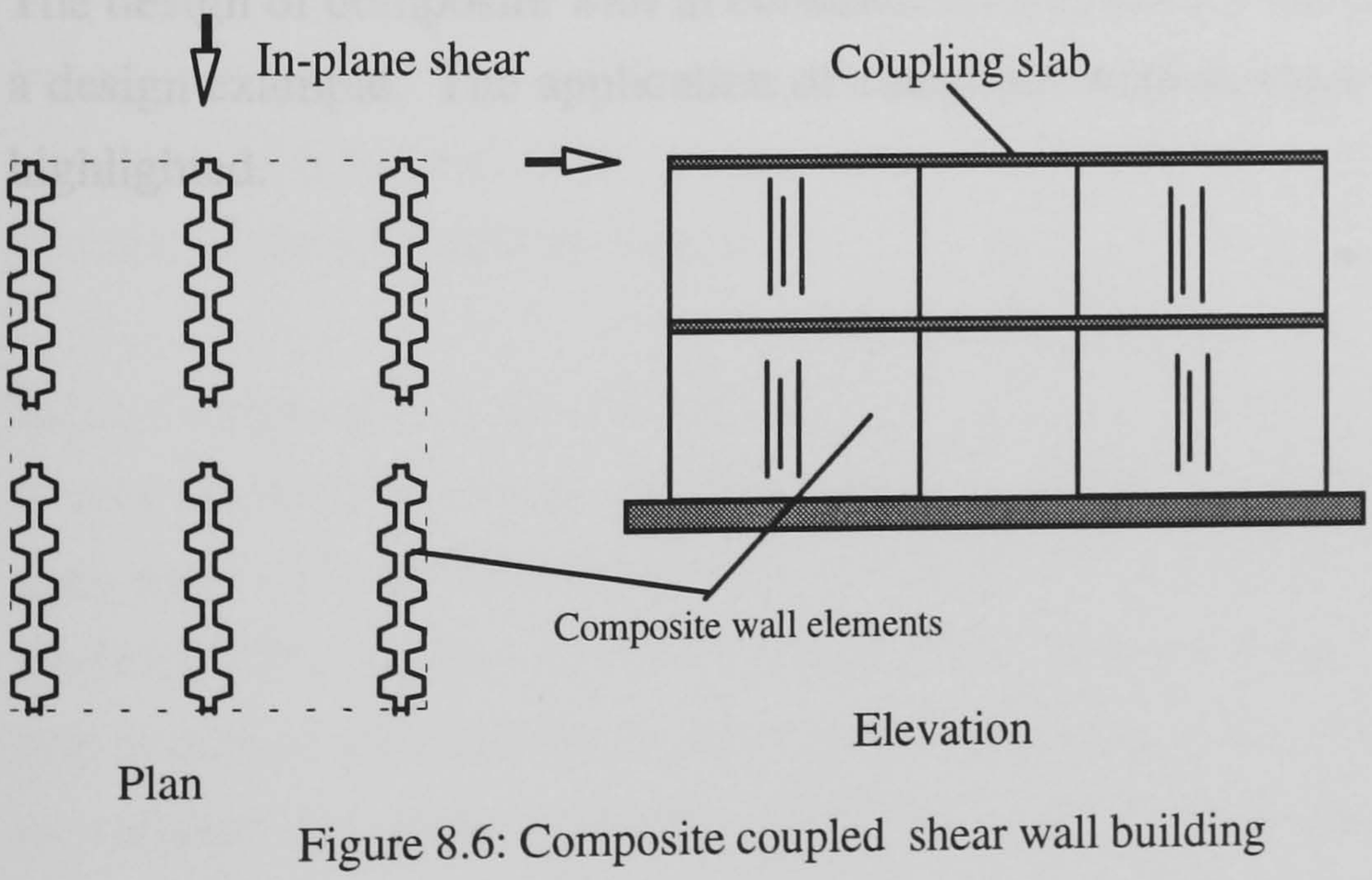

Figure 8.6: Composite coupled shear wall building

The application of composite walling as shear elements in buildings as mentioned in this section needs much detailed investigations paying attention to the practicality of construction.

8.6. Practical construction and connection details

As we have seen in previous sections, the behaviour of the composite wall is affected by the boundary connections either to the frame or to the slabs. The study of connections is vital for the future use of the composite wall in building. This needs the study of full scale composite walling with practical connection details to the boundary frame. This was beyond the scope of the authors research.

Wright and Evans (1995) carried out a survey which included consultation with practising engineers on aspects of construction details and fire resistance. A survey describing the wall system and providing a questionnaire on possible construction details was sent to the 85 companies. Detailed answer to the questionnaires showed a preference for screw fixing of the steel sheeting to the steel frame and identified suitable foundation kicker details.

It has been established from the specialist fire engineers and supplier of the fire protection products that the walling system may be conservatively designed as a solid concrete wall.

8.7 Conclusions

The design of composite wall in construction and service stage is described along with a design example. The application of composite wall as shear elements in buildings is highlighted.

CHAPTER NINE

CONCLUSIONS

9.1 Introduction

This thesis has studied the in-plane shear behaviour of composite walls to explore the potential use of the system as shear elements in buildings. This concluding chapter will summarise the major findings of the earlier chapters and proposals for future investigations.

9.2 Summary of main conclusions

9.2.1. Introduction

The proposed composite walling system was introduced in chapter 1. The overall advantages of the composite walling were highlighted including the decreased construction time, combined permanent form work and reinforcement, shear bracing actions in construction stage and weight reductions. The main design criteria under axial, lateral and in-plane loads are pointed out. The significance of the in-plane shear behaviour of the composite wall as a potential application of the wall as shear elements is described. The chapter concluded with the aim of the thesis and brief content of the subsequent chapters.

9.2.2. Design of a shear testing rig

It was essential to design and fabricate a shear rig to carryout the model tests under pure shear. The rig developed was economical as it utilised the existing facilities like the DARTEC machine with the loading frame in the Structural engineering laboratory. The details of the shear rig is presented. A plain flat sheet was tested under pure shear to validate the performance of the shear rig. The rig demonstrated its ability to simulate pure shear and the panel failed with the development of tension field. The stiffness and strength of the test sheet when compared to those from analytically derived equations and finite element analysis showed reasonable agreement. The main conclusions are:

The performance of the rig was satisfactory as confirmed from the validation tests and subsequent tests carried out in the latter stage.

It is suggested that the rig has the potential to carry out tests on many types of panels, such as, wood based, cement based, and composite panel products.

9.2.3 Small scale modelling of composite walling with micro-concrete

Small scale modelling of composite walling using profiled steel sheeting and micro-concrete was described. The selection of a gap graded micro-concrete was the result of an extensive literature review of the micro-concrete properties and micro-concrete used by previous researchers. The properties of micro-concrete such as compressive to tensile strength ratios, E-values and density from model tests were compared to those of normal concrete to check whether the micro-concrete can simulate the behaviour of full-scale concrete. The model profiled steel sheeting was manufactured in the house from thin plain sheet of 0.45mm thickness using a fly press designed and fabricated specially for that purpose. It was tried to use a sheet of thickness conforming to the scale models. But it was not possible to have a sheet of 0.36mm required according to the model scale. As a result a locally available sheet of 0.45mm thickness was considered to be satisfactory. The performance of the micro-concrete was tested by using a plain micro-concrete panel. The following main conclusions can be drawn from this chapter:

The performance of the micro-concrete was found to be satisfactory.

It is concluded that the behaviour of the chosen micro-concrete can be numerically modelled by using shear retention factor and softening parameter within the range 0.25-0.4 and 20-30 respectively.

Analytical model for the shear strength and stiffness of the plain concrete panel was derived and found to provide satisfactory agreement when compared with the test and finite element results.

9.2.4. Behaviour of profiled concrete cores under in-plane shear

Five small scale model tests were carried out along with the numerical and analytical studies.

The model tests provided consistent and repeatable results.

The model tests validated analytical approaches. The analytical models can safely be used to predict the stiffness and strength of the panels.

The trough sections of the profile were found to be stressed higher than those of crest sections.

The development of a diagonal tension and compression along the diagonals of the panel is confirmed from the model and FE analysis. The principal direction ranges between 42-46 degrees in the pre-cracking stage and 38-55 degrees in post cracking stage.

The crack pattern in the failed model panel and FE crack pattern showed reasonable agreement.

Pre-cracking stiffness of the panel seems to be not affected by the hysteretic application of the load as confirmed from the model tests and FE analysis.

Hysteretic effect reduces the cracking and ultimate load by 30% and 20% respectively.

Good co-relation between FE analysis and model tests regarding strain conditions within the panel and boundaries especially in the pre-cracking stage was found.

9.2.5. Study of the in-plane shear behaviour of the profiled steel sheeting

Three small scale model tests were carried out with clamped and spot welded boundary conditions. Two tests with clamped conditions showed buckling failure while the other one with spot welded boundary failed due to the failure of spot welds and subsequent tearing of the sheeting at the location of spot welds.

Model tests showed reliable and repeatable results with good performance of the shear rig.

The stiffness and strength of the profiled sheeting is found to be dependent on the manner of attachment of the sheeting to the boundary frame which agrees with the findings of previous investigations. It is found from the study that the strength and stiffness of the spot welded panel becomes half and one third respectively of the clamped panel.

Analytical models for stiffness and strength of the profiled sheeting with different boundary conditions are developed. Good agreement between analytical and model tests confirmed that the proposed models can safely be used in design.

The failure of the sheeting is associated with the formation of local buckling and extended tension field with subsequent bending and twisting of the profile which leads to the loss of profile geometry.

The direction of the tension field tends to follow the direction of principal stress.

The length of the extended tension field is found to be higher (maximum up to 70% of the total length of the profile) in spot welded test panels than those from clamped test panels(maximum 35%).

Most of the buckles formed at failure of test models are found to be half waves. But the formation of some full waves in few heavily distorted crest or trough lines are also observed in the model tests.

Unstable and very rapid post-buckling behaviour suggests that it is unwise to use the post buckling shear reserves. The design ultimate load is based on the buckling load. This will provide a factor of safety of 1.20 in the case of clamped panels.

The generalised buckling formula suggested for calculation of strength, needs the use of specific values of, β, to take into account the effect of different boundary conditions. The value of ,β , ranges between 0-1.80. From model tests, it is confirmed that for simply supported cases β=1.00 and for clamped condition β=1.72 can be used.

Analytical equations derived for the calculation of the boundary co-efficient ,K, can be used safely in design to calculate the flexibility due to bending and distortion of corrugation profile as confirmed from model tests, analytical and finite element analysis.

The effect of hysteretic load on ultimate strength of the clamped panels is unclear although a 12% reduction in strength was found.

The stiffness calculated from tension and compression branch of hysteresis loops differ by about 24% which may be due to hysteretic effect. The tension stiffness is found to be in excellent agreement with that from static test under tension.

Boundary conditions affect the strain condition within the panel.

The finite element model proves to be very effective in simulating different boundary conditions.

9.2.6 In-plane shear behaviour of composite wall

Five small scale model tests were carried out to study the in-plane shear behaviour of composite wall.

Model tests provided excellent demonstration of the shear behaviour of composite walls. There was good agreement between load-deformation response, stiffness and strain conditions.

From the model tests without embossed sheeting, it was found that the composite wall an resist high in-plane shear load. The shear resistance of the wall was approximately 25% higher than the summation of individual capacities of the concrete core and sheeting. There is full mobilisation of resistance due to concrete and sheeting by providing only sufficient connections at the boundary.

Full mobilisation of steel and concrete capacity leads to the development of simple design equation for shear resistance of the wall without the need to consider variable conditions due to interface.

The effect of hysteretic load on the pre-cracking stiffness is negligible. But 20% decrease in cracking load may be a consequence of the hysteretic effects.

The strain condition along the loaded and off-diagonal and cracking pattern in concrete confirmed the development of diagonal tension in the panels.

The general pattern of variation of strain along the boundary is identified for pre-cracking stages based on model tests. The post-cracking variation showed no definite pattern for the model tests.

The transfer of load to the wall along the boundary depends on boundary connections. For full mobilisation of steel-concrete capacity effective boundary connections will be required. In the absence of effective connections along the boundary, the stiffness and ultimate load of the wall should be calculated based on only concrete capacity when the load is applied through concrete only.

The analytical models derived for the strength and stiffness of the composite wall are found to be safe when compared with the model tests and finite element analysis.

The stiffness of the composite wall is found to be around 24% higher than the individual summation of stiffness of the sheeting and concrete core.

9.2.7 Composite wall as beam elements

The flexural strength of the composite wall beam can be estimated by analytical models provided the interface bond stress is known.

The variation of flexural and shearing strain across the mid span section are similar to the reinforced concrete construction except that the trough sections are strained higher than the crest sections.

9.2.8 Design and application of composite shear wall

A simple design method for the determination of shear stiffness and strength of the composite wall in service and construction stages is described which can be safely used in design.

The composite wall has good potential to be used as shear elements in buildings.

9.3. Future Study

It is the belief of the Author that the work in this thesis provides a platform for the understanding of the behaviour of composite wall under in-plane shear. In the Author's opinion, the following areas need further research:

The boundary conditions of the wall as identified by the author are important factors affecting the behaviour of the system. The model tests secure full connections

between sheeting and concrete at the boundaries. It will be interesting to test full scale composite wall under in-plane loads in a building frame with practical connection details. At the beginning of this work, the author submitted a proposal to carryout a full scale testing at the Building Research Establishment's Cardington building frame, but the proposal was dropped due to lack of financial assistance. The full scale test with embossed sheeting may further improve the shear capacity of the wall.

It will be interesting to carry out some tests on composite wall with openings as a consequence of the pierced shear wall or opening in core walls for service.

The behaviour of composite wall under bi-axial stress condition may be the another area of research.

The behaviour of the composite wall under fire condition can be another area of research.

The numerical simulation needs the determination of interface properties from transverse push-off tests. It will be helpful to do push-off tests with various profiles to establish load-slip relationship which can be implemented in the numerical simulation of the wall behaviour. It will be desirable to investigate this aspect.

The use of composite wall in building needs the study of practical connection details at the frame, slab or foundation. This study should include the practicality of construction considering concrete casting, fixing of the sheeting and use of pre-cast composite walls. The detailed feasibility study is needed to sort out the practical problems associated with this type of construction.

Finally, the economy may be a factor in the application of the composite walling. A cost comparison should be made between composite wall and traditional reinforced concrete walls, considering the various factors affecting the overall construction cost. There must be some justification for the system, considering the total cost related to its performance to get a market in the construction industry.

REFERENCES

ACI 318-813 (1983), Building Code Requirements for Reinforced Concrete ACI Committee 318, ACI, Detroit, 111pp.

ACI Committee 444 (1979), Models of concrete structures- State -of- Art, Concrete International: Design and Construction, V.1, No.1, Jan. pp.77-95

ACI Committee 318 (1989), Building Code Requirements for Reinforced Concrete and Commentary, (ACI 318-89/318R-89), American Concrete Institute, Detroit.

ACI Structural Journal (1991), Nov-Dec., Recommendation for the Use of Models.

ACI, SP-73 (1982), Dynamic Modelling of Concrete Structures, Detroit, pp.242.

Adams, P.F.(1987), Steel-concrete composite structural system, POAC, 87, 9th International Conference on Port and Ocean Engineering under Arctic conditions, Fairbanks, Alaska, 1-2.

AISI (1967), Design of Light gauge Steel Diaphragms.

ASCE-AASHTO Task Committee(1977), Curved I-girder bridge design recommendations, Journal of the Structural Division, ASCE, ST5, pp-1137-1168.

ASCE A7-88 (1982), Minimum Design Loads for Buildings and Other Structures, New York, Sections 6.1 and 6.4.

Atrek, E. and Nilson, A.H.(1976), Non-linear finite element analysis of light gauge steel shear diaphragms, Structural Engineering Rep.No.363, Cornell University, N.Y.

Australian Code (1974), Building Code Requirements for Concrete, (AS1480/1974).

Balakrishnan, S. and Murray, D.W. (1988), Strength of reinforced concrete panels, Canadian Journal of Civil Engineering, 15, 900-911.

Basler, K. (1961), Strength of plate girders in shear, Journal of the Structural Division, ASCE, ST7, part1, pp.151-180, October.

British Code of Practice for Bridges, BS 5400: Part I (1984), Section 8.6, British Standard Institutions, London.

British Standard Institutions (1985), BS 8110, Structural use of concrete, London.

BS 5950, Part 1 (1988), Introduction to Steel work Design, The Steel Construction Institute, UK.

British Standards Institution (1984), BS 5950, Structural Use of steel work in Buildings, Part4 , London.

British Standards Institution (1972), CP3: Chapter V: Part 2: Wind loads, London.

Bryan, E.R. and El-Dakhakhni, W.M (1968a), Shear of corrugated decks: calculated and observed behaviour, Journal of Institution of Civil Engineers, Vol.41, Nov, pp.523-540.

Bryan, E.R. and El-Dakhakhni, W.M (1968b), Shear flexibility and strength of corrugated decks, Journal of Structural Division, ASCE, Vol.94, ST11, November, 2549-2579.

Bryan, E.R. and El-Dakhakhni, W.M. (1964), Shear of thin plates with flexible edge members, Journal of Structural Engineering, ASCE, Vol.90, August, pp.1-13.

Bryl , S., (1967), The Composite Effect of Profiled Steel Plate and Concrete in Deck Slabs, Acier Stahl Steel, October, 1967.

BS 5950 (1982), Structural use of steel work in buildings: part 4, code of practice for design of floors with profiled steel sheeting, British Standard Institute, London, England.

Canadian Sheet Steel Building Institute (1988), Design criteria for composite slabs, CSSBI, Willodale, Canada.

CEB-FIP Model Code (1978)

CIRIA Report 108 (1985), Clear C.A. and Harrison, T.A., Concrete Pressure on Form work, London, 32 pgs.

CIRIA Guide 2 (1977), The design of deep beams in reinforced concrete, Ove Arup, London, January.

Clark, L.A.(1980), Crack Similitude in Reinforced Micro-concrete, Reinforced and Prestressed Micro-concrete Models, Edited by F.K. Garas and G.S.T. Armer, The Construction Press, Lancaster, pp.77-84.

Dallaire, E.E.(1971), Cellular Steel Floors Mature, Civil Engineering, ASCE, Vol. 41, No. 7 , July, 1971, PP. 70-74.

Daniels, B.J.(1988), Shear Bond Pull-out Tests for Cold-Formed -Steel Composite Slabs, Publication ICOM 194, Ecole Ploytechnique Federale de Lausanne, June, 1988.

Daniels, B.J., Crisinel, M. (1993), Composite Slab Behaviour and Strength Analysis, Part i : Calculation procedure and Part ii: Comparison with test results and parametric studies, Journal of Structural Engineering, ASCE, vol 119, No.1 Jan, pp-16-49.

Davies, J.M. and Fisher, J. (1979), The diaphragm action of composite slabs, Proce. Institution of Civil Engineers, London, England, 67 (Part2) 891-906.

Davies, J.M. (1976), Calculation of Steel Diaphragm Behaviour, Journal of Structural Division, ASCE, Vol. 102, No. ST7, July, pp.1411-1430.

Davies,J.M. (1977), Simplified Diaphragm Analysis, Journal of Structural Division, ASCE, Vol. 103, No. ST11, Nov., pp.2093-2109.

Davies, J.M. (1976a), Light gauge steel folded plate roofs, The Structural Engineer, Vol.54, No. 5, May.

Easely, J.T. and McFarland, D.E. (1969), Buckling of light-gage corrugated metal shear diaphragms, Journal of Structural Division, ASCE, Vol. 95, No, ST7, July, pp. 1497-1516.

Easely, J.T. (1975), Buckling Formulas for corrugated metal shear diaphragms, Journal of Structural Division, ASCE, Vol.101, No, ST7, July, pp. 1403-1417.

Easely, J.T. (1977), Strength and Stiffness of corrugated metal shear diaphragms, Journal of Structural Division, ASCE, Vol.103, No. ST1, pp. 169-180.

Easterling, W.S. and Young C.S. (1992), Strength of Composite Slabs, Journal of Structural Engineering, ASCE, Vol. 118, No. 9, Sep. pp. 2370-2389.

Easterling, W.S., Porter, M.L. (1994a), Steel-Deck-Reinforced Concrete Diaphragms I, Journal of Structural Division, ASCE, Vol. 120, No.2, February, pp. 560-576.

Easterling, W.S., Porter, M.L. (1994b), Steel-Deck-Reinforced Concrete Diaphragms II, Journal of Structural Division, ASCE, Vol. 120, No.2, February, pp. 577-596.

ECCS-Technical Committee (1986), "Behaviour and Design of steel plated structures", Edited by P. Dubas and E. Gehri, ECCS- Technical Committee 8, and Technical Working Group 8.3, Publication No. 44.

Ekberg, C.E. and Schuster, R,M. (1968), Floor Systems with Composite Form-Reinforced Concrete Slabs, Final report, IABSE, 8th congress, New York, N.Y., September,1968, pp.385-394.

El-Dakhakhni, W.M. (1976), Shear of Light gauge Partitions in Tall Buildings, Journal of Structural Division, ASCE, Vol. 102, No.ST7, July, 1431-1445.

Euro Code No. 4 (1990), Design of composite steel and concrete structures, part1-general rules and rules for buildings, Revised draft, Issue 1, Commission on European Communities, Brussels, Belgium.

Fazio, P.F., Kinh, HA, and Chockalingam, S. (1978), Strength of cold-formed steel shear diaphragms, Canadian Journal of Civil Engineering, 6, pp-5-17.

Friberg, B.F. (1954), Combined Form and Reinforcement for Concrete Slabs, Journal of the American Concrete Institute, Vol. 50, May, 1954, pp.697-716.

Fujii, Tokio (1968), On an improved theory for Dr. Baslers Theory, Procee. 8th Congress, IABSE, NewYork, September, pp.477-487.

Gallocher, S.C.(1993), The behaviour of composite wall with profiled steel sheeting, PhD Thesis, University of Strathclyde, Glasgow, UK.

Gaylord, E.H. (1963), Discussion on " Shear strength of plate girders", ASCE, ST2, Vol.82, pp.151.

Hamoush, S.A. and Ahmad, S.H. (1990), Debonding of steel plate-strengthened concrete beams, Journal of Structural Engineering, ASCE, Vol.116, No.2, February.

Hlavacek,V. (1968), Shear Instability of Orthotropic Panels, Acta Technica CSAV, Prague, Czechoslovakia, No.1.

Hlavacek, V. (1970), discussion of "Buckling of light-gage corrugated metal shear diaphragms by Easely, J.T. and McFarland, D.E, Journal of Structural Division, ASCE, Vol.96, No. ST3, Proce. Paper 7116, pp-740-743.

Hofbeck, J.A., Ibrahim, I.O. and Mattock, A.H.(1969), Shear Transfer in Reinforced Concrete, ACI Journal, Vol. 66, February, pp.119-128.

Horne, M.R. and Raslan, R.A.S. (1971), A finite Difference approach to Corrugated Shear Panels, Publications Int. Assn. of Bridge and Structural Engineers (31-I), pp.73-91.

Horne, M.R. and Raslan, R.A.S. (1971), An Energy Solution to the Shear Deformation of Corrugated Plates, Publications Int. Assn. of Bridge and Structural Engineers (31-I), pp.51-72.

Hossain, K.M.A. and Wright, H.D. (1995), Composite walling with special reference to the stabilisation of building frames, Proceedings Nordic Steel Construction Conference, pp. 531-538, Malmo, Sweden, June 19-21, 1995.

Hossain, K.M.A. and Wright, H.D. (1994), Use of micro-concrete to simulate in-plane shear behaviour, National Research Workshop on Cement and Concrete, Centre for Cement and Concrete, University of Sheffield, July, 11-12.

Hughes, B.P.(1966), The Deformation of Concrete and Micro-concrete in Compression and Tension with Particular Reference to Aggregate Size, Magazine of Concrete Research, Vol.18, No.54, March, pp.19-23.

Hussain, M.I. and Libove, C. (1976), Trapezoidally Corrugated plates in Shear, Journal of Structural Division, ASCE, Vol. 102, No. ST5, May, 1109-1131.

Iyenger, H.S. (1977), State-of-the -art report on composite or mixed steel-concrete construction for buildings, ASCE, New York

Johnson, R.P.(1962), Strength Tests on Scaled-Down Concrete suitable for Models with Note on Mix Design, Magazine of Concrete Research, Vol.14, No.40, March, pp.47-53.

Jones, R., Swamy, R.N. and Charif, A. (1988), Plate Separation and anchorage of reinforced concrete beams strengthened by epoxy-bonded-steel plates, The Structural Engineer, 66 (5), 85-94.

Kountouris, G. (1990), Design charts for double skin composite elements, Dissertation, University of Wales College of Cardiff, April.

Kulak, G.L. (1986), Unstiffened steel plate shear walls: static and seismic behaviour, Steel structures: Recent research advances and their applications, Elsvier Applied Sciences, London, pp. 561-580.

Kumar,S. and Dupuch,G.W.(1980), BRS Tests on Micro-concrete Models -A Review of the Scaling Aspects", Reinforced and Prestressed Micro-concrete Models, Edited by F.K. Garas and G.S.T. Armer, The Construction Press, Lancaster, pp.27-38.

Kupfer, H.B.and Gerstle, K.H. (1973), Behaviour of concrete under bi-axial stresses, Journal of Engineering Mech. Division, ASCE, 99, pp.852-866.

L' Hermite, R. and Bresson, J (1967), Beton arms d'armatures colles, RILEM colloque International, themr 2, Paris, September.

Lawson, M.R. (1976), Buckling formulas for corrugated metal shear diaphragm, Discussion, Journal of Structural Engineering, ASCE, No. ST5, May, pp.1168-1170.

Link, R.A. and Elwi, A.E.(1995), Composite Concrete-Steel Plate Walls: Analysis and Behaviour, Journal of Structural Engineering, ASCE, Vol.121, No. 2, February,pp. 260-271.

Long,A.(1980), A Review of Recent Developments in Concrete Modelling, Reinforced and Prestressed Micro-concrete Models, Edited by F.K. Garas and G.S.T. Armer, The Construction Press, Lancaster, pp.1-15.

Luo, R. and Edlund, B (1995), Strength of plate girders with trapezoidally corrugated webs in shear or under patch loading, Proceeding Nordic Steel Construction Conference, Sweden, June 19-21, pp.79-86.

Luo, R. (1995), Load -carrying capacity of steel girders and panels with thin-walled trapezoidally corrugated web, Ph.D Thesis, Chalmer University of Technology, Goteborg 1995.

LUSAS (1987), Finite element stress analysis system, FE Analysis limited, LUSAS 87.08, Theory Manual, Section 4, pp. 4.3.1-4.3.13.

Luttrell, L.D. and Prassanan, S. (1984), Strength formulations of Composite slabs, Proceedings Seventh International Speciality Conference on Cold-Formed Steel Structures, University of Missouri at Rolla, 307-326.

Luttrell, L.D. (1971), Shear diaphragms with light weight concrete fill, Proceedings 1st speciality conference on Cold-Formed Steel Structures, University of Missouri-Rolla, Rolla, Mo. 111-117.

Luttrell, L.D. (1981), Diaphragm Design Manual, Steel Deck Institute, Inc., St. Louis.

MacDonald, M.D. (1978), The flexural behaviour of concrete beams with bonded external reinforcement, Transport and Road research Laboratory supplementary report 415, Crowthorne, England.

Maisel, E.(1980), Reinforced and Prestressed Micro-concrete Models, Reinforced and Prestressed Micro-concrete Models, Edited by F.K. Garas and G.S.T. Armer, The Construction Press, Lancaster, pp.17-25.

Majlessi, S., Noor, F.A. and Newman, J.B.(1985), Size Effects in Micro-concrete Beams and Control Specimens, Design of Concrete Structures - The use of Model Analysis, Elsvier Applied Science Publisher, pp.117-128.

Mattock, A.H.(1974), Shear transfer in concrete having reinforcement at an angle to shear plane, in Shear in Reinforced Concrete, Proceedings of the Shear Symposium, ACI, ACI Special Publication SP-42, Vol1, pp. 17-42.

Mays, G.C. and Smith, D.W. (1980), Slab of the future, Concrete, pp-13-16, June.

Muller, R.K.(1985), Micro-concrete for Structural Model Analysis, Design of Concrete Structures - The use of Model Analysis, Elsvier Applied Science Publisher,pp.1-11.

Narayan, N., Wright, H.D., Evans, H.R. and Francies, R.W. (1987), Double skin composite construction for submerged tube tunnels, Steel Construction Today, 1, pp.187-189.

National Building Code of Canada (1985), National Research Council of Canada, Ottawa, Section 4.1.1.4, pp. 20, 153.

New York City Building Code (1985), section C.26-1002.4, p.10-5.

Nilson, A.H.(1960), Shear Diaphragm of Light Gage Steel, Journal of Structural Division, ASCE, Vol.86, No.ST11, Nov. pp. 111-139.

Nilson, A.H. and Ammar, A.R. (1974), Finite element analysis of metal deck shear diaphragms, Journal of Structural Division, ASCE, Vol, 100, No. ST4, April, pp.711-725.

Noor, F.A. and Wijayasri (1982), Modelling the Stress-Strain relationship of Structural Concrete, Magazine of Concrete Research, Vol.34, No.118, March, pp.25-83.

Noor,F.A. and Khalid, M.(1980), Deformed Wire Reinforcement for Micro-concrete Models, Reinforced and Prestressed Micro- concrete Models, Edited by F.K. Garas and G.S.T. Armer, The Construction Press, Lancaster, pp.103-118.

Oduyemi, T.O.W. and Wright, H.D. (1990), The behaviour of double skin composite beam-columns, Report DS3, Univrsity of Wales College of Cardiff.

Oduyemi, T.O.W. and Wright, H.D. (1989), The behaviour of double skin composite columns, Report DS2, Univrsity of Wales College of Cardiff.

Oehlers, D.J. (1992), Reinforced concrete beams with plates glued to their soffits, Journal of Structural Engineering, ASCE, Vol. 118, No.1, pp. 2023-2038.

Oehlers, D.J., Wright, H.D. and Burnet, M.J. (1994), Flexural strength of profiled beams, Journal of Structural Engineering, ASCE, Vol. 120, No.2, February, 378-393.

Oehlers, D.J.(1993), Composite Profiled Beams, Journal of Structural Engineering, ASCE, Vol. 119, No.4, 1085-1100.

Ollgaard, J.G., Slutter, R.G. and Fisher, J.W. (1971), Shear strength of stud connectors in lightweight and normal weight concrete, AISC Engr. Journal, 55-64.

Ong, K.C.G., Mays, G.C. and Cusens, A.R. (1982), Flexural tests on steel-concrete open sandwiches, Magazine of Concrete Research, Vol.34, No. 120, 130-138, September.

Parkinson, J. (1978), Glue solves a sticky problem for Gestetner, New Civil Engineering, 310, (September), 26-27.

Patrick, M and Bridge, R. (1994), Review of Concepts Concerning Bond of Steel Decking, Twelfth International Speciality Conference on Cold-Formed Steel Structures, St. Louis, Missouri, USA, October, 18-19, pp.335-359.

Patrick, M (1990), A new partial shear connection strength model for composite slabs, Journal of Australian Inst. Steel Res. 24(3) 2-17.

Paulay,T. and Loeber, P.J. (1974), Shear Transfer by Aggregate Interlock, in Shear in Reinforced concrete, Proceedings of the Shear Symposium, ACI, ACI Special Publication SP-42, Vol1, pp. 1-15.

Porter, M.L., and Ekberg, C.E. (1971), Investigation of Cold -Formed Steel-Deck Reinforced Concrete Floor Slabs, Proceedings of the 1st Speciality Conference on Cold-Formed Steel Structures, University of Missouri-Rolla, Rolla, Mo, Aug, 1971, pp. 179-185.

Porter, M.L. and Ekberg, C.E. (1976), Design recommendations for steel deck floor slabs, Journal of Structural Division, ASCE, 102(11), pp.2121-2136.

Porter, D.M., Rockey, K.C. and Evans, H.R. (1975), The collapse behaviour of plate girders loaded in shear, The Structural Engineer, No.8, Vol. 53, pp.313-325.

Regan, P.E. (1969), Shear in reinforced concrete beams, Magazine of Concrete Research, Vol. 21, No.66, March, pp.31-42.

Roberts, T.M. and Haji-Kazemi, H. (1989), Theoretical study of the behaviour of reinforced concrete beams strengthened by externally boned steel plates, Procee. Institutions of Civil Engineers, Part 2, 87, 39-55.

Roberts, T.M.and Sabouri-Ghomi, S. (1992), Hysteretic Characteristics of Unstiffened Perforated Steel Plate Shear Panels, Thin Walled Structures,14, pp.139-151.

Roberts, T.M. and Sabouri-Ghomi, S. (1991), Hysteretic Characteristics of Unstiffened Plate Shear Panels, Thin Walled Structures, 12, pp.145-162.

Rockey, K.C., Anderson, R.G. and Cheung, Y.K.(1969), Thin walled structures, their design and use in buildings, Symposium at university College of Swansea school of Engineering, 11-14 Sept, pp.148-163.

Rockey, K.C. and Skaloud, M. (1968), Influence of flange stiffness upon the load carrying capacity of webs in shear, final report, Proc. 8th Congress, IABSE, New York, pp.429-439.

Roeder, C.W. (1981), Point loads on composite deck reinforced slabs, Journal of Structural Division, ASCE, 107 (12), 2421-2429.

Schuster, R.M. (1976), Composite Steel-Deck Concrete Floor Systems, Proceedings of the ASCE , Journal of Structural Division, Vol. 102, No. ST5, May, 1976, pp.899-917.

Selberg, A. (1973), On the shear capacity of girder webs, University of Trondheim.

Seleim and Schuster, R.M.(1982), Composite Floor Slabs, Proceedings of the 6th Speciality Conference on Cold Formed Steel Structures, University of Missouri-Rola.

Solomon, S.K., Smith,D.W. and Cusens, A.R.(1976), Flexural tests on steel-concrete-steel sandwich, Magazine of Concrete Research, Vol. 28, No. 94, 13-20, March.

Sommerville,G., Roll,F. and Caldwell,J.A.D.(1965), Tests on one-twelfth Scale Mancunianway, Technical Report TRA/394, Cement and Concrete Association, London, December.

Specifications for the design and construction of composite slabs (1984), ASCE N.Y..

Specifications for the design of cold formed steel structures (1986), American Iron and Steel Institute (AISI), Washington, D.C.

Swamy, R.N. and Andriopoulos, A.D. (1974), Contribution of Aggregate Interlock and Dowel Action to the shear Resistance of Reinforced Beams with web reinforcement, in Shear in Reinforced concrete, Proceedings of the Shear Symposium, ACI, ACI Special Publication SP-42, Vol1, pp. 129-165.

Swamy, R.M. and Falih, F.M.(1985), Development of a Small Aggregate Concrete for Structural Similitude of Slab-Column Connections, Design of Concrete Structures - The use of Model Analysis, Elsvier Applied Science Publisher, pp.25-37.

Taylor, H.P.J. (1974), The fundamental behaviour of reinforced concrete beams in bending and shear, in Shear in Reinforced concrete, Proceedings of the Shear Symposium, ACI, ACI Special Publication SP-42, Vol1, pp. 221-230.

Van Gemert, D.A. (1981), Repairing of concrete structures by externally bonded steel plates, Procee. International Symposium on Plastics in Mat. and Struc. Engineering, Prague, Czechoslovakia, 519-526.

Vecchio, F. and Nieto, M. (1991), Shear-Friction Tests on Reinforced concrete panels, ACI Journal, Vol. 88, May-June, pp.371-379.

Vecchio, F and Collins, M.P (1986), Modified compression field theory for reinforced concrete elements subjected to shear, ACI Journal, Proceedings Vol.83, No.2, March-April, PP.219-231.

Veljkovic, M (1995), Longitudinal shear capacity of composite slabs, Proceedings Nordic Steel Construction Conference, pp. 547-554, Malmo, Sweden, June 19-21.

Viest, I.M.(1960), Review of Research on Composite Steel-Concrete Beams, Journal of the Structural Division, ASCE, 86 (ST6), pp.1-21, June.

Waldron,P; Pinkney,M.W. and Perry,S.H.(1980), The Construction of a 1/12 th Scale Prestressed Concrete Biufricated Bridge Model ", Reinforced and Prestressed Micro-concrete Models, Edited by F.K. Garas and G.S.T. Armer, The Construction Press, Lancaster, pp.39-52.

Waldron, P. and Perry, S.H.(1980), Small Scale Micro-concrete Control Specimens, Reinforced and Prestressed Micro- concrete Models, Edited by F.K. Garas and G.S.T. Armer, The Construction Press, Lancaster, pp.261-276.

White, R.N. and Sabnis, J.M.(1966), A Bibliography on Structural Model Analysis, Report No.325, Department of Structural Engineering, School of Civil Engineering, Cornell University, Ithaca, N.Y., September.

White, R.N., Sabnis,J.M. and Harries,H.G.(1966), Small Scale Direct Models of Reinforced and Prestressed Concrete Structures, Report No.326, Department of Structural Engineering, School of Civil Engineering, Cornell University, N.Y., Sept.

White, I.G. and Clark, L.A.(1977), Bond Similitude in Reinforced Micro-concrete Models, Proceedings of Research Seminar, Cement and Concrete Association, September, pp.12-15.

Wood S.H.(1990), Shear Strength of Low-Rise Reinforced Concrete Walls, ACI Structural Journal, Volume 87, No. 1, Jan-Feb., pp. 99-107.

Wright, H.D., Evans, H.R. and Harding, P.W. (1985), Composite Floors: Comparisons of Performance Testing and Method of Analysis, IABSE-ECCS Symposium, Luxembourg, 1985, pp.219-225.

Wright, H.D., Evans, H.R. and Harding, P.W. (1987), The Use of Profiled Steel Sheeting in Floor Construction, Journal Construction Steel Research 7, pp 279-295.

Wright, H.D. and Evans, H.R. (1987), Observations on the Design and Testing of Composite Slabs, Steel Construction Today, Vol. 1, pp. 91-99.

Wright, H.D., Oduyemi, T.O.S. and Evans, H.R. (1991), The double skin composite elements, Journal of Constructional steel Research, 19, pp. 111-132.

Wright, H.D., Evans, H.R. and Gallocher, S.C.(1992), Composite walling, Composite Construction II, Engineering Foundation Conference, Missouri, June 14-19 .

Wright, H.D., Hossain, K.M.A., Gallocher, S.C. (1994), Composite walls as shear elements in tall structures, Proce. of papers presented at ASCE Structures Congress XII, Atlanta, GA, USA, April 24-28, pp. 140-145.

Wright, H.D. and Evans H.R.(1995), Profiled Steel Concrete Sandwich Elements for Use in Wall Construction, Proceedings of the Third International Conference on Sandwich Construction, Southampton, 12-15 September, 1995.

Wright,P.J.F.(1952), The effect of the Method of Test on the Flexural Strength of Concrete ", Magazine of Concrete Research, Vol.14, No.11, October, pp.67-76.

Yam, L.C.P. and Chapman, J.C. (1968), The inelastic behaviour of simply supported composite beams of steel and concrete, Procee. Inst. Civil Engrs. 41, pp. 651-683.

Yarushalmi, Y.(1988), Tests performed on the ASP construction system, The ASP Group, Washinton D.C.

Zaras, J., Rhodes, J. and Krolak, M.(1992), Buckling and Post-buckling of rectangular plates under linearly varying compression and shear, Part2- Experimental Investigations, Thin walled Structures, 14 pp. 105-126.

Bibliography

Armer, G.S.T. and Garas, F.K. (1982), Design for Dynamic loading--The Use of Model Analysis, Construction Press, England, pp.360.

Bryan, E.R. (1972), The stressed skin design of steel buildings, Crosby Lockwood Staples, London, England.

Clarke, J.L., Garas, F.K. and Armer, G.S.T. (1985), Design of Concrete Structures, Elsevier Applied Science Publishers, London, 380pp.

Davies, J.M. and Bryan, E.R. (1982), Manual of stressed skin diaphragm design, Granada, London.

Gere, J.M. and Timoshenko, S.P. (1984), Mechanics of Materials, Brookes Cole Engineering Division, ISBN 0-534-03099-8.

Langhaar, H.L.(1951), Dimensional Analysis and Theory of Shells, John Willey and Sons Inc., New York.

Prece,B.W. and Davies,J.D.(1962), Models for Structural Concrete, CR Books Limited.

Sabnis,G.M.; Harries,H.G.; White,R.N. and Mirza, S.M.(1982), Structural Modelling and Experimental Techniques, Prentice-Hall, pp.147-150.

Timoshenko, S.P. and Gere, J.M. (1961), Theory of Elastic Stability, 2nd ed., McGraw Hill International Book Company, New York.

Timoshenko,S.P. and Goodier, J.N. (1982), Theory of Elasticity, McGraw-Hill Book Company.

Uniform Building Code, (1985), International Conference of Building Officials, 5360 South Workman Mill Road, Whitter, CA 90601.

Willems, N., Easely, J.T. and Rolfe, S.T. (1981), Strength of Materials, McGraw-Hill Book Company.